



HIGH-RESOLUTION REMOTE SENSING APPLIED TO MINERAL EXPLORATION IN
AUSTRALIA

VOLUME I

ANDREW R. GABELL

DEPARTMENT OF GEOLOGY AND GEOPHYSICS, UNIVERSITY OF ADELAIDE

April, 1986

A Thesis submitted for the Degree of Doctor of Philosophy

Awarded 12/9/86

TABLE OF CONTENTS

VOLUME I

	Page
ABSTRACT	xiv
STATEMENT OF ORIGINALITY	xvii
ACKNOWLEDGEMENTS	xviii
CHAPTER 1. INTRODUCTION	1
1.1 Background	1
1.2 Aims of the Study	2
1.3 Outline of the Thesis	5
1.4 Method of Study	7
1.5 Definition of Terms	8
PART I. INSTRUMENTATION AND TECHNIQUES	11
CHAPTER 2. THE USE OF REMOTE SENSING TECHNIQUES IN AUSTRALIA	12
2.1 Introduction	12
2.2 The Type of Spectral Information Available for Remote Sensing	12
2.2.1 Electronic processes	14
2.2.2 Vibrational processes in hydroxyl-bearing minerals	15
2.2.3 Vibrational processes in other minerals	18
2.3 Some Examples of Successful Remote Sensing Applications in the U.S.	20

2.3.1	Detection of hydrothermally altered areas in south-central Nevada using Landsat MSS data (Rowan <u>et al.</u> , 1974, 1977)	20
2.3.2	Detection of non-limonitic hydrothermal alteration at Cuprite, Nevada, using aircraft scanner images in the .46 to 2.36 μ m region (Abrams <u>et al.</u> , 1977)	22
2.3.3	Thermal Infrared Multispectral Scanner data from Cuprite, Nevada (Kahle and Goetz, 1983)	23
2.3.4	High-resolution airborne spectrometer data from Oatman, Arizona (Marsh and McKeon, 1983)	23
2.3.5	Identification of alteration mineralogy at Cuprite, Nevada, and sedimentary minerals in the Wind River Basin, Wyoming using airborne imaging spectrometry (Goetz, 1984, NASA, 1985)	24
2.4	The Australian Environment and Problems it Poses for Remote Sensing	25
2.4.1	Development of the weathering profile	26
2.4.2	Alteration and erosion of the profile	27
2.4.3	Remote sensing in deeply weathered terrain	28
CHAPTER 3. HARDWARE UTILISED AND TECHNIQUES USED FOR SPECTROMETER DATA ANALYSIS		33
3.1	Introduction	33
3.2	Hardware	33
3.2.1	The GER Mark II airborne spectrometer	33
3.2.2	Laboratory measurements	35
3.2.2.1	VNIR and SWIR laboratory measurements	37
3.2.2.2	MIR laboratory measurements	39

3.2.3	Image processing system	40
3.3	Analysis Techniques	40
3.3.1	XPUT files	41
3.3.2	XBOSS	42
3.3.2.1	Log residuals	42
3.3.2.2	Log residual images	45
3.3.2.3	Tchebychev analysis	46
	PART II. CASE STUDIES	48
	CHAPTER 4. WEIPA BAUXITE PROVINCE, CAPE YORK PENINSULA, QUEENSLAND	49
4.1	Introduction	49
4.2	Regional Geological Setting	50
4.3	Climate	51
4.4	Previous Geological Investigation	52
4.5	Regional Vegetation Patterns and their Seasonal Variation	55
4.6	Previous Remote Sensing Investigation	56
4.7	Landsat Characteristics of Major Lithologies and Terrain Units	58
4.8	Regional Variations in Landsat Characteristics of Bauxite Plateaux	60
4.9	Detailed Analysis of Weipa Peninsula	64
4.9.1	Hydrology	64
4.9.2	Vegetation	64
4.9.3	Geomorphology	66
4.9.4	Landsat characteristics - dry season	66
4.9.5	Landsat characteristics - wet season	67

4.9.6	Soil geochemistry trends	68
4.9.7	Laboratory reflectance spectra of soils	70
4.9.7.1	VNIR spectra	71
4.9.7.2	SWIR spectra	72
4.9.8	Bauxite drilling geochemistry trends	73
4.9.9	Image display of bauxite geochemistry	74
4.9.10	Landsat/bauxite geochemistry correlation	75
4.10	Significance of Bushfires in Utilisation of Landsat Imagery	77
4.11	Detection of High-Grade Bauxite Areas	78
4.12	Regeneration Studies Using Landsat MSS Data	79
4.13	Summary	80
CHAPTER 5. MT TURNER PORPHYRY COPPER SYSTEM, GEORGETOWN INLIER, QUEENSLAND		83
5.1	Introduction	83
5.2	Regional Geological Setting	84
5.2.1	Host geology	84
5.2.2	Alteration and mineralisation	86
5.3	Previous Remote Sensing Investigation	89
5.4	Laboratory Spectral Measurements	92
5.4.1	Weathering effects	92
5.4.2	Vegetation effects	93
5.4.3	Laboratory spectral types	94
5.4.3.1	Kaolin-type spectra	94
5.4.3.2	Muscovite-type spectra	95
5.4.3.3	Sericite-type spectra	95
5.4.3.4	Mafic-type spectra	96

5.5	Airborne Spectrometer Data	97
5.5.1	Acquisition	97
5.5.2	Analysis of radiance data - 'first-order' effects	97
5.5.3	Analysis of log residual images - 'second-order' effects	99
5.5.4	Classification of log residual data - 'third-order' effects	102
5.5.4.1	Types 1 and 2 spectra	106
5.5.4.2	Type 3 spectra	106
5.5.4.3	Type 4 spectra	108
5.5.4.4	Type 5 spectra	109
5.5.4.5	Type 6 spectra	110
5.5.4.6	Assessment of significance of classification scheme	110
5.5.5	Other analysis-techniques	112
5.5.5.1	Tchebychev analysis	112
5.5.5.2	Band ratios	113
5.6	Correlation between Airborne and Laboratory Spectra	113
5.7	Significant Individual Spectra	116
5.8	Comparison with Silver Bell Porphyry Copper Deposit, Arizona, U.S.	117
5.9	Summary	119
CHAPTER 6. KAMBALDA NICKEL PROVINCE, EASTERN GOLDFIELDS, WESTERN AUSTRALIA		122
6.1	Introduction	122
6.2	Regional Geological Setting	122
6.3	Detailed Geology	123

6.4	Factors Affecting Remote Sensing at Kambalda	125
6.4.1	Weathering Effects on Primary Mineralogy	125
6.4.2	Cultural and Vegetation Effects	129
6.5	Previous Remote Sensing Investigation	130
6.6	Laboratory Spectral Measurements	131
6.6.1	Laboratory spectral types	132
6.6.1.1	Flat spectra	133
6.6.1.2	Variable absorption by water	133
6.6.1.3	2.2 μ m absorption features	134
6.6.1.4	2.3 μ m absorption features	135
6.6.1.4.1	Talc	135
6.6.1.4.2	Chlorite	136
6.6.1.4.3	Amphibole	137
6.6.1.4.4	Mixtures	137
6.7	Spectral Variation of Chlorites	139
6.8	Airborne Spectrometer Data	140
6.8.1	Acquisition	140
6.8.2	Analysis of radiance data - 'first-order' effects	141
6.8.3	Analysis of log residual images - 'second-order' effects	141
6.8.3.1	Type 1 spectra	142
6.8.3.2	Type 2 spectra	143
6.8.3.3	Type 3 spectra	144
6.8.3.4	Type 4 spectra	145
6.8.4	Interpretation of data from flight line K2	145
6.8.5	Significant airborne spectra	147
6.8.5.1	Talc spectra	147
6.8.5.2	Mafic spectra	148

6.8.5.3 Kaolin spectra	148
6.8.6 Distribution of mineralogy interpreted from 'second- and third-order' effects	149
6.8.6.1 St Ives	149
6.8.6.2 Tramways	151
6.8.6.3 Kambalda Dome	151
6.8.6.4 Democrat	152
6.8.7 Other analysis techniques	152
6.9 Comparison of Airborne and Laboratory Spectra	154
6.10 Summary	156
CHAPTER 7. FORTESCUE GROUP BASIC VOLCANICS, HAMERSLEY BASIN, WESTERN AUSTRALIA	160
7.1 Introduction	160
7.2 Regional Geological Setting	161
7.2.1 The Fortescue Group	162
7.3 Metamorphic Setting	162
7.3.1 Zone I - prehnite-pumpellyite zone	164
7.3.2 Zone II - prehnite-pumpellyite-epidote zone	166
7.3.3 Zone III - prehnite-pumpellyite-epidote-actinolite zone	166
7.3.4 Zone IV - actinolite zone (greenschist facies)	167
7.4 Previous Remote Sensing Investigation	167
7.5 Laboratory Spectral Measurements	169
7.5.1 VNIR W (weathered) surface spectra	169
7.5.2 VNIR F (fresh) surface spectra	171
7.5.3 Some comments on SWIR spectra	172
7.5.4 SWIR W (weathered) surface spectra	174

7.5.5 SWIR F (fresh) surface spectra	177
7.5.6 MIR W (weathered) surface spectra	178
7.5.7 MIR F (fresh) surface spectra	178
7.6 Summary	180
CHAPTER 8. PEAK HILL EPITHERMAL GOLD PROSPECT, LACHLAN FOLD BELT, NEW SOUTH WALES	183
8.1 Introduction	183
8.2 Location and Regional Geology	183
8.3 Detailed Geology and Alteration	184
8.4 Laboratory Spectral Measurements - Core Samples	185
8.4.1 Introduction	185
8.4.2 VNIR spectra	187
8.4.3 SWIR spectra	187
8.4.4 Conclusions on data from core samples	189
8.5 Laboratory Spectral Measurements - Surface Samples	189
8.5.1 Introduction	189
8.5.2 VNIR spectra	189
8.5.3 SWIR spectra	191
8.6 The Distribution of Alteration Minerals	193
8.7 The Potential for use of Remote Sensing Techniques at Peak Hill	196
8.7.1 Proximal sensing	196
8.7.2 Remote sensing	197
8.8 Summary	198

PART III. DISCUSSION OF RESULTS AND THEIR IMPLICATIONS FOR FUTURE REMOTE SENSING APPLICATIONS IN AUSTRALIA.	200
CHAPTER 9. TITLE AS ABOVE.	201
9.1 Introduction	201
9.2 The VNIR	202
9.3 The SWIR	204
9.4 The MIR	206
9.5 The Effects of Weathering	207
9.6 The Effects of Vegetation	208
9.7 Scanners or Spectrometers?	209
REFERENCES	213
APPENDICES	

VOLUME II

LIST OF FIGURES
FIGURES

LIST OF TABLES

Table 2.1	Mineralogic information available from remote sensing.	13
Table 2.2	Fundamental hydroxyl absorption features.	17
Table 2.3	Ratios calculated for MSS bands for selected mafic rocks, felsic rocks and alteration minerals (after Rowan <u>et al.</u> , 1977).	21
Table 2.4	Alteration minerals occurring in the southwestern U.S. (after Rowan and Lathram, 1980).	30
Table 4.1	Weipa soil sample grid coordinates and SiO ₂ , Al ₂ O ₃ , TiO ₂ and Fe ₂ O ₃ analyses.	69
Table 4.2	Mean values of various Landsat MSS values and Al ₂ O ₃ , and their correlation coefficients, for Weipa training areas.	76
Table 5.1	Recorded production from mines in the vicinity of Mt Turner (after Baker and Horton, 1982).	88
Table 5.2	Comparison of Mt Turner with the Silver Bell porphyry copper deposit (using data from Baker and Horton, 1982 and Abrams and Brown, 1984).	90
Table 5.3	Second-order effects interpreted from images of Mt Turner airborne log residual data.	103
Table 5.4	Third-order effects interpreted from Mt Turner airborne log residual data.	111
Table 5.5	Bands simulated after examination of images of Mt Turner airborne log residual data.	113A

Table 6.1	Minerals identified by XRD analysis of samples from Kambalda.	128
Table 6.2	Second-order effects interpreted from images of Kambalda airborne log residual data.	146
Table 7.1	Formations of the Fortescue Group (after Hickman, 1983).	162
Table 7.2	Summary of mineralogical variation with metamorphic grade in Fortescue Group rocks (based on data from Smith <u>et al.</u> , 1982).	165
Table 7.3	Summary of the interpretation of laboratory reflectance spectra of samples from the Fortescue Group.	170
Table 7.4	Minerals from the Fortescue Group likely to dominate the SWIR spectrum for different alteration and metamorphic zones.	173
Table 8.1	Minerals identified by XRD analysis in different studies at Peak Hill.	186
Table 8.2	Summary of the interpretation of laboratory reflectance spectra of core samples from Peak Hill.	188
Table 8.3	Summary of the interpretation of laboratory reflectance spectra of surface samples from Peak Hill.	190

LIST OF APPENDICES

- APPENDIX I Clay mineral absorption features in the 0.9 to 1.1 micrometre region and their implications for proximal and remote sensing (Gabell et al., 1985).
- APPENDIX II VNIR laboratory reflectance spectra of soil samples from Weipa.
- APPENDIX III SWIR laboratory reflectance spectra of soil samples from Weipa.
- APPENDIX IV SWIR laboratory reflectance spectra of samples with XRD analyses from Mt Turner.
- APPENDIX V Hull residuals of averaged SWIR laboratory reflectance spectra from Mt Turner.
- APPENDIX VI Correction factors for time differences between flight lines at Mt Turner.
- APPENDIX VII Log residual spectra derived from modelling of mixtures of MT Turner SWIR laboratory reflectance spectra.
- APPENDIX VIII SWIR laboratory reflectance spectra of samples with XRD analyses from Kambalda.

- APPENDIX IX Interpretation of data from flight line K2 - SWIR laboratory reflectance and airborne log residual spectra.
- APPENDIX X VNIR laboratory reflectance spectra of samples from the Fortescue Group.
- APPENDIX XI SWIR laboratory reflectance spectra of samples from the Fortescue Group.
- APPENDIX XII MIR laboratory (laser) reflectance spectra of samples from the Fortescue Group.
- APPENDIX XIII VNIR laboratory reflectance spectra of core samples from Peak Hill.
- APPENDIX XIV SWIR laboratory reflectance spectra of core samples from Peak Hill.
- APPENDIX XV VNIR laboratory reflectance spectra of surface samples from Peak Hill.
- APPENDIX XVI SWIR laboratory reflectance spectra of surface samples from Peak Hill.

ABSTRACT

This thesis aims to identify some of the spectral properties of Australian terrain useful for geology and mineral exploration. To meet this objective, data are examined from five diverse geological environments, all of which are prospective for economic minerals.

To date, most remote sensing research has been undertaken in the southwestern U.S. Because Australia is more extensively and intensively affected by surface weathering than this region, the low-spectral-resolution techniques used successfully in the U.S. will not necessarily produce comparable results in Australia. Therefore, most of the data presented here have high spectral resolution. Notwithstanding the effects of weathering, significant mineralogical information is still available from the measurements acquired from each of the five test sites.

The results from Weipa, the world's largest bauxite deposit, establish a significant correlation between Landsat MSS values and bauxite ore geochemistry. Bauxite ore minerals present in surface soil samples from the area produce distinctive features in high-resolution spectra.

An airborne survey over the Mt Turner porphyry copper deposit shows that muscovite, from the weathering of granites, and sericite, from hydrothermal alteration, can be differentiated on the basis of the relative strengths of their absorption features. Because vegetation is denser over the alteration zone, absorption at $2.2\mu\text{m}$ in the airborne data is stronger over unaltered, but weathered and lightly vegetated areas. This is the converse of most situations in the southwestern U.S.

(e.g. Silver Bell, Arizona) where uniformly sparse vegetation and lack of absorption from unaltered material allow easier discrimination of hydrothermal alteration.

Two minerals not previously reported from the Mt Turner area, viz. talc and topaz, were identified respectively from their airborne and laboratory spectral signatures.

A similar airborne survey over the Kambalda nickel province shows that talc (derived from ultramafic rocks which host the nickel mineralisation) and other minerals can be mapped on the basis of their spectral absorption characteristics. In fact, the distribution of talc is shown to be more extensive than conventionally mapped outcrop and float occurrences indicate, suggesting that significant concentrations persist in residual soils.

Previous work by Smith et al. (1978) on rocks of the Fortescue Group showed that metasomatic alteration of basic volcanics could be detected in some areas using Landsat MSS imagery. This finding was attributed to differences in soil and vegetation development over altered and unaltered rocks, rather than to the spectral properties of the rocks themselves. Measurement of a suite of samples from the area confirms this conclusion, no differences being evident in high-resolution laboratory spectra covering the same wavelength region as Landsat MSS. However, measurements at longer wavelengths allow the identification of the key metamorphic and alteration minerals pumpellyite, epidote, actinolite and chlorite (from the 1.4 to 2.5 μ m region), and of the high silica content of altered rocks (from the 9.14 to 11.25 μ m region).

At Peak Hill a number of hydrothermal alteration minerals (pyrophyllite, muscovite, kaolinite, alunite and jarosite) can be identified from their spectral properties. The surficial distribution of these minerals matches closely the alteration zoning established in a previous study based on XRD analyses of core samples.

Thus, although most of the spectral effects described appear to be weaker in Australian environments (compared to published U.S. examples), significant mineralogical information is still available from high-spectral-resolution measurements. Limited studies involving simulation of broad-band instruments (e.g. Landsat TM) show that at least some of the minerals identified using high-resolution techniques would not have been discriminated with the lower spectral resolution and sensitivity of these instruments.

This thesis contains no material which has been accepted for the award of any other degree or diploma in any University and, to the best of the author's knowledge and belief, this thesis contains no material previously published or written by another person, except where due reference is made in the text.

ACKNOWLEDGEMENTS

The study documented here has drawn on the skill, knowledge and data provided by a number of people.

Professor Peter Ypma undertook the sometimes onerous task of supervision of the project. He has my thanks for the time and attention I received. Many other colleagues at the University of Adelaide provided stimulating discussion and moral support at various stages of the work. Particular thanks go to Dr Yvonne Bone and Mr Mark Hochman, who embarked on their own projects at the same time as the author - it was easier in their company. Thanks are also due to the technical staff of the Department of Geology and Geophysics. Electronics technical officer John Willoughby was sometimes patient and sometimes harried, but always skillful, while helping during the early stages of the project. Dr Graham Staker provided considerable assistance during the author's struggle with the University computer.

Many people from the CSIRO Division of Mineral Physics and Mineralogy have also rendered invaluable assistance. Drs Jon Huntington and Andy Green gave expert guidance and encouragement during the author's period with CSIRO. I am greatly in their debt. Other staff, including geologists Mr Steve Fraser and Mr Chris Horsfall, have provided stimulating discussion on different aspects of this, and other, work. Dr Maurice Craig has made numerous suggestions which I am sure have improved the text. Technical staff Mr Robert Cook and Mr Mike Hornibrook provide a good deal of assistance at various times - Robert by plotting flight line tracks over Kambalda and Mt Turner, and Mike by assisting with measurement of some of the laboratory spectra of samples from Peak Hill, Kambalda and Mt Turner. Dr Terry Cocks was responsible

for converting the SWIR spectrometer for laboratory use, and is thanked for his efforts.

The photography section at CSIRO, comprising Mr Geoff Lane and Mr Chris Taylor, is responsible for the skillful production of most of the photographic products which appear in the thesis. Mr Alan Horne provided the XRD analyses of samples from Weipa and Peak Hill.

A number of organisations and individuals have also contributed to the thesis by allowing access to study areas and, in some cases, unpublished data. Comalco Ltd. provided geochemical data from their drilling program, and assistance during the field work undertaken at Weipa. Drs Jon Huntington and Kerry O'Sullivan (CRAE) accompanied the author on this field visit.

Mr Ian Simon (CRAE) accompanied, and greatly assisted, the author throughout the field trip to Mt Turner. The XRD analyses of Mt Turner samples were provided by AMDEL.

Western Mining Corporation allowed free access to the field areas at Kambalda, as well as the run of their extensive collection of drill core and maps. Geologists Mr Jeff Gresham, Mr Lyle Burgess, Mr David Quick, Mr Mick Elias and Mr Ian Glacken are all thanked for their assistance with, and interest in, the author's work. Western Mining's analytical laboratories at Kambalda provided the XRD data on samples from the area.

Dr Ray Smith, of CSIRO's Division of Mineralogy and Geochemistry, provided samples, mineralogical determinations and invaluable advice for the study of the Fortescue Group. Dr John Eberhardt (of CSIRO's Division of Mineral Physics and Mineralogy, Lucas Heights Laboratory)

kindly undertook the task of measurement of the MIR laser reflectance spectra of the Fortescue Group samples.

Gold Fields Exploration Pty Ltd allowed access to Peak Hill, and provided field support for the author's visit to the area. Dr John Angus, and Mr Murray Hutton (who also provided unpublished XRD analyses of core samples from Peak Hill) are particularly thanked.

Some of this work (at Adelaide University) was undertaken while the author held a Commonwealth Postgraduate Research Award, while much of the remainder was undertaken at CSIRO during research projects supported by the Australian Mineral Industry Research Association (AMIRA). AMIRA also provided much-appreciated financial assistance for the production of the thesis.

Last, but by no means least, I wish to acknowledge the encouragement and assistance received from my family. My parents, and those of my wife, contributed in many ways, not least financially. To my wife Karen, my daughter Cassie and my son Samuel, all of whom suffered increasingly as the work progressed, go my thanks for their love and patience during sometimes trying periods.

CHAPTER 1. INTRODUCTION



1.1 Background

Remote sensing techniques date from the first use of aerial photography and have been widely used in geology for many years, both in Australia and overseas. However, the launch of the first Landsat satellite in 1972 saw a rapid expansion in the use of remotely sensed data. Landsats 1, 2 and 3, with their Multispectral Scanners (MSS), were primarily designed for agricultural applications (Taranik, 1978). But geologists quickly came to appreciate the value of Landsat imagery in their work. The small scale of a Landsat scene makes it particularly useful for regional studies, allowing the detection of large linear features (lineaments) not always obvious on the larger scales of aerial photography. Initially, the analysis of lineaments dominated the literature (NASA, 1972, 1973a, 1973b, 1975), but considerable research into computer manipulation of Landsat data soon showed that it also contained extremely useful spectral information (Rowan et al., 1974, Albert and Chavez, 1977, Lyon, 1977, Rowan et al., 1977, Schmidt and Bernstein, 1977). However, further development of these techniques is limited by the wide band-widths and the small spectral range of the Landsat MSS sensors. For instance, the 2.2 micrometre (μm) wavelength region (where hydroxyl absorption bands can be used to detect clay-rich alteration products) is not covered by the MSS, but proved to be particularly promising for geological applications (Rowan et al., 1977, Abrams et al., 1977).

With this recognition came a shift in emphasis of research from the wavelength regions covered by Landsat MSS data to longer wavelength

radiation. In turn this led to the inclusion of a band in the 2.2 μ m region on the Thematic Mapper instrument of Landsats 4 and 5 (Engel and Weinstein, 1982). Investigations in the 1960s and early 1970s (some pre-Landsat) of spectroscopic techniques suitable for geological remote sensing have provided a solid base for renewed research efforts (see Hunt and Salisbury, 1970a, 1970b, Hunt et al., 1971a, 1971b, 1972, 1973a, 1973b, 1974a, 1974b, 1976a, 1976b, Lyon, 1962, 1964, Lyon and Patterson, 1966).

Australia, with its large area and small population has much to gain by the use of remote sensing techniques. However, there is very little known about the spectral properties of Australian terrain in the region from .4 to 14 μ m. The research reported in this thesis was begun at the University of Adelaide in 1979, and continued at the CSIRO Division of Mineral Physics and Mineralogy (CSIRO/MXY) from 1981, in an attempt to redress this imbalance.

1.2 Aims of the Study

The primary aim is the evaluation of the potential usefulness in Australia of advanced remote sensing techniques in the .4 to 14 μ m wavelength region for mineral exploration. In particular, the effects of Australia's prolonged and complex weathering history, and the unique Australian flora, need to be considered with respect to the applicability of remote sensing. To this end, the techniques used have mainly involved the interpretation of high-resolution spectral data. In this way, the maximum amount of spectral information can be assessed, and the spectral content of lower resolution instruments (e.g. the Landsat Thematic Mapper) can be simulated.

In order to achieve the primary aim of the thesis, data have been examined from a number of test sites around Australia (Fig. 1.1). The test sites have been affected to varying degrees by weathering processes, ranging from the most extreme case of a bauxite deposit (formed by prolonged weathering), to a site with relatively fresh rocks exposed at the surface. Apart from the primary aim, each test site poses its own, more specific, problems related either to observations from previous remote sensing investigations, or to the particular geological environment under consideration. The test sites, with their associated specific aims, are listed below :

1) Weipa, Cape York Peninsula, Queensland - Bauxite Deposit.

Aims include the investigation of patterns recognised on Landsat MSS imagery by previous workers, and their relationship to the geochemistry of the bauxite. The usefulness of both Landsat and high-resolution data for further evaluation of known bauxite, or for exploration for new deposits elsewhere (including overseas), also warrants investigation.

2) Mt Turner, Georgetown Block, Queensland - Porphyry Copper-Type Deposit.

Mt Turner was chosen as a test site to allow comparison of a weathered alteration system from Australia with similar systems from the southwestern U.S., where considerable remote sensing research has been undertaken.

3) Kambalda Region, Eastern Goldfields, Western Australia - Nickel Province.

Kambalda lies in an Archaean greenstone belt, thereby allowing the investigation of remote sensing techniques in ultramafic terrain. The area is also deeply weathered, hence is of major interest considering the primary aim.

4) Fortescue Group, Hamersley Basin, Western Australia - Metamorphosed and Metasomatised Basic Volcanics.

The investigation of the Fortescue Group Volcanics aims to evaluate high-resolution spectral data in an area where metasomatic alteration effects, resulting from burial metamorphism, have been recognised for part of their extent on Landsat MSS imagery. This area also affords the opportunity to study the use of remote sensing as an aid in mapping low-grade metamorphic assemblages of a particular lithology.

5) Peak Hill, Lachlan Fold Belt, New South Wales - Fine Gold Deposit.

Peak Hill is an epithermal gold prospect that displays considerable hydrothermal alteration. It therefore provides a geological environment well suited to assessing the value of high-resolution reflection spectrometry.

These problems were investigated as far as possible within the constraints imposed by the availability of appropriate instrumentation, and time.

1.3 Outline of the Thesis

The thesis is divided into three parts. Part 1 (Chapters 2 and 3) contains a discussion of the problems posed by the Australian environment, analysis techniques, and the instruments used in the course of the project. Part 2 (Chapters 4 to 8) comprises case studies of the test sites, while Part 3 (Chapter 9) discusses the results and implications for future remote sensing studies in Australia.

The first chapter of Part 1 (Chapter 2) discusses in some detail the nature of the problem posed by Australia's long and complex weathering history. Chapter 3 describes the image processing system and the instrumentation and analysis techniques for high-resolution spectral data. High-resolution spectra of field samples have been measured in the laboratory, for all five study areas, and from aircraft for two test sites. They were analysed at the CSIRO/MXY at North Ryde, Sydney.

Part 2 begins with Chapter 4, dealing with data from the area on Cape York Peninsula, North Queensland, which includes the world's largest bauxite deposit at Weipa. Previous work by the CSIRO (Huntington et al., 1982) resulted in the recognition of regular colour variations in Landsat imagery of the Weipa region. These colour variations are evaluated and compared to trends in geochemical data from the area. Some high-resolution spectral data measured in the laboratory are also included, but it was not possible to acquire high-resolution airborne data in this area. The author believes this to be the first study of this type of geological environment that utilises high-spectral-resolution data.

Chapter 5 contains high-spectral-resolution data from a 1982 airborne survey, and laboratory measurements of samples from Mt Turner. The spectral effects due to weathering and to hydrothermal alteration are similar. These effects are compared to those described from remote sensing studies over alteration in the southwestern U.S.

Chapter 6 presents similar high-resolution data from the Kambalda region. To the best of the author's knowledge, this represents one of the first detailed high-spectral-resolution remote sensing studies undertaken in ultramafic terrain.

Laboratory data on samples from the Hamersley Basin are presented in Chapter 7. Previous work by the CSIRO (Smith et al., 1978) using Landsat MSS data has identified variations that can be related to metasomatic alteration of basic lavas of the Fortescue Group in some areas. High-resolution laboratory spectra were measured to assess the cause of the variations seen in Landsat imagery and to investigate the use of other wavelengths to identify alteration minerals from different metamorphic zones.

Chapter 8 presents laboratory data on samples from Peak Hill. Hydrothermal alteration is well characterised due to exploration in the area, affording the opportunity to compare the results from a spectrometer survey to those based on more traditional mineralogical techniques.

In the final chapter (Chapter 9), which constitutes Part 3, the significant points to emerge from the thesis work are summarised, and the implications for future remote sensing applications are discussed.

1.4 Method of Study

It is obvious from the outline above that the scope of this thesis is extremely broad. In carrying out such a wide-ranging study, with the collection of enormous amounts of data, it is unavoidable that some data sets are not analysed to the same degree. It is certainly true that some areas (Weipa, Mt Turner, and Kambalda) have been studied more extensively than the others, and the spectral interval between 1.1 and 2.5 μ m has received much more attention than other wavelength regions.

However, the writer feels that the advantage gained by the examination of a variety of effects capable of detection by remote sensing, in a number of different locations (each having economic relevance) allows a much better evaluation of the general applicability of established remote sensing techniques in Australia. In the process, though, some questions will inevitably remain unanswered.

The approach taken at each study area differs according to the nature of the data available, the type of remote sensing effects being investigated, and the amount of time available for each area. One area, the Fortescue Group of the Hamersley Basin, was not visited in the field, but this is compensated by the detailed information available from previous work (Smith et al., 1978, 1982).

In all cases the geology of the test sites has been established by previous workers, and existing data have been relied upon for the evaluation of remotely sensed data. In three cases (Weipa, Mt Turner, and the Fortescue Group) the writer's work follows study of the areas by CSIRO personnel using Landsat MSS data and widely used interpretation techniques.

The approach at each area therefore started with a literature search covering previous geological and remote sensing investigations. In those areas where high-resolution airborne data were available, these data were processed to a standard format (see Chapter 3), and were interpreted in the light of existing geological information. At least one field trip to each test site (except the Fortescue Group) was then undertaken, and an attempt made to evaluate the variations present in the spectrometer data. At the same time, samples were collected from locations along the flight lines, or other appropriate locations, for further, laboratory, analysis. Investigations in the laboratory comprised measurement of high-resolution spectral data for most samples. XRD analyses of some rock and soil samples, and a few wet chemical and microprobe analyses were obtained from various sources to aid the interpretation.

Unfortunately, no spectral measurements were possible in situ because of the lack of suitable instrumentation.

The complete data set for each area was then evaluated in an attempt to explain the major variations present in the spectral data. For some areas the observed effects were also compared to simulated narrow bands (with the bands selected on the basis of the results for each area) and simulated Thematic Mapper (TM) bands in order to model the performance of multispectral scanners in the Australian environment.

1.5 Definition of Terms

The Manual of Remote Sensing (ASP, 1975, p.206) defines visible radiation as "the spectral interval from approximately 0.4 to 0.7 micrometres (4000 to 7000 Angstroms)", the near infrared as "about 0.7

micrometres (visible red) to around 2 or 3 micrometres", with "the longer wavelength end grading into the middle infrared". The far infrared is assigned the interval from "25 micrometres to 1 millimetre".

However, the Landsat MSS and some other instruments used in collecting data for this thesis have sensitivity ranges in the wavelength region 0.4 to 1.1 μm . For this reason, this interval will be referred to as the visible and near infrared (VNIR).

A second group of instruments has detectors sensitive to wavelengths longer than approximately 1.1 μm , and out to approximately 3 μm (which is then further limited by atmospheric absorption to approximately 2.5 μm). This wavelength region will be referred to as the short wavelength infrared (SWIR), as used by Goetz and Rowan (1981, Fig. 1).

According to the Manual of Remote Sensing definitions above, the middle infrared lies between approximately 3 and 25 μm . Because of overlap of reflected and emitted radiation in the 3 to 5 μm region, and the interference of atmospheric absorption, the 8 to 14 μm region is the one most commonly associated with the middle infrared in remote sensing. Therefore, in this thesis, the term middle infrared (MIR) refers to this portion of the electromagnetic spectrum. The only instrument used to acquire data in the MIR for this thesis detects radiation emitted from a laser source in the wavelength range 9.14 to 11.25 μm .

The term 'proximal sensing' is introduced to cover applications of spectroscopy in the field. The use of field-portable instruments is not strictly 'remote' from the target, but is shown in this thesis to have considerable potential, independent of 'true' remote sensing. The author therefore believes that the use of this term is justified.

Airborne spectrometer data are interpreted in Chapters 5 and 6. The data are presented in three different forms. Firstly, corrected radiance data are dominated by atmospheric absorption features, but also contain some mineralogical (lithospheric) effects. These are defined here as 'first-order effects'. Secondly, the data are corrected for atmospheric absorption and differential illumination (using the log residual process of Craig and Green, 1985), and significant portions of a flight-line are presented in an image format. Changes visible in these images are defined as 'second-order effects'. Finally, individual (log residual) spectra, or the mean of a group of these spectra, can be interpreted to reveal more subtle variations in the data. These variations are defined as 'third-order effects'.

PART I. INSTRUMENTATION AND TECHNIQUES

CHAPTER 2. THE USE OF REMOTE SENSING TECHNIQUES IN AUSTRALIA

2.1 Introduction

The development of remote sensing has been extremely rapid over the last thirteen years, stimulated to a large extent by the huge success of the Landsat Multispectral Scanner (MSS). The MSS can be considered a first-generation remote sensing system. The second generation of sensors, which are now becoming widely available, have been designed for more specific applications. In particular, it is clearly possible to design systems that will be sensitive to certain types of mineralogy.

The range of minerals that can be identified is, of course, limited to those with diagnostic optical properties in the wavelength regions which coincide with 'atmospheric windows' (i.e. a portion of the electromagnetic spectrum where only minor atmospheric absorption occurs - see Fig. 2.1). Between 0.4 and 14 μm , there are three such 'windows', where different types of spectroscopic information are available. These are summarised in Table 2.1. In the VNIR and SWIR regions the energy detected by remote sensing instruments is reflected solar radiation. However, in the MIR solar radiation is minimal and the detectable energy is emission by the target itself.

Although the number of detectable minerals is somewhat limited in practice, some quite subtle discriminations are possible within each wavelength region.

2.2 The Type of Spectral Information Available for Remote Sensing

The spectral reflectance of minerals is affected by two main

Table 2.1 Mineralogic information available from remote sensing

Region	Minerals	Cause of features
VNIR (.4-1.1 μ m)	Iron oxides, sulphates	Electronic processes - charge transfer and crystal field absorption effects
	Phyllosilicates	Vibrational processes - high-order overtones (very weak)
SWIR (1.1-2.5 μ m)	Phyllosilicates, carbonates, some others	Vibrational processes - combinations and overtones of fundamental O-H and C-O features.
MIR (8-14 μ m)	Silicates, carbonates, some other information	Vibrational processes - fundamental vibrations of Si-O stretch, Cation O-H bend and internal modes of the CO ₃ ⁼ group

processes. These are Electronic processes, and Vibrational processes. They are dealt with separately in the following sections. The reflectance spectrum of vegetation, also important in the VNIR and SWIR, is shown in Fig. 2.2.

2.2.1 Electronic processes

Electronic transitions can occur between different energy levels if energy, in the form of electromagnetic radiation, is available for the process. All transition elements (Burns, 1970), can affect the electromagnetic spectrum in this fashion, but iron is by far the most important for remote sensing purposes, particularly in Australia, where iron-rich minerals are widespread as weathering products. Figure 2.3 shows, for a number of iron-rich minerals, the reflectance spectra in the VNIR, where these effects are most important. The broad minima in these spectra, in the 0.85 to 0.95 μ m region, are due to the absorption of energy that enables electronic transitions to occur. The variation in the shape and position of these features is due to the differing ligand, or crystal, fields surrounding the transition elements.

The steep fall-off in reflectance from the visible towards the ultraviolet, however, is caused by absorption due to charge transfer. In this process, absorbed energy promotes the transfer of electrons from one ion to another. For the minerals shown, the transfer occurs between ferric and other ions.

In contrast, rocks not containing iron generally have no characteristic spectral reflectance features in the VNIR.

2.2.2 Vibrational processes in hydroxyl-bearing minerals.

Absorption features can also occur as a result of quantised transitions between the vibrational energy levels of groups of atoms.

In general, vibrational transitions are of three types - fundamentals, overtones, or combination tones. The strongest of these, fundamental absorptions, result from a change in energy from one kind of vibration only - the jump from the ground state to the first excited state. An example of this is the fundamental O-H stretch (denoted ν_{OH}), which occurs near $2.85\mu\text{m}$ (or at a frequency of about 3500cm^{-1} ; see Fig. 2.4a). The fundamental O-H stretch is not utilised for remote sensing because it is in a region of total atmospheric absorption (see Fig. 2.1).

A combination tone occurs when a transition takes place from the ground state to a state whose energy is determined by the sum of the energies of two (or more) fundamental vibrations. This effect is most conveniently treated in terms of the wavenumbers (in cm^{-1}) at which the fundamental vibrations occur, rather than their wavelengths (in μm). Thus, the wavenumber of a combination band can be estimated by adding those of the component fundamentals. An example is the combination band produced by the fundamental O-H stretch (approx. 3500cm^{-1} or $2.85\mu\text{m}$) and the fundamental Al-O-H bend (which occurs near 1000cm^{-1} , see Fig. 2.4b). Addition of these values gives :

$$\begin{array}{r} 3500\text{cm}^{-1} + 1000\text{cm}^{-1} = 4500\text{cm}^{-1} = 2.2\mu\text{m} \\ \text{stretch} \quad \quad \quad \text{bend} \end{array}$$

In fact, the whole wavelength interval between 2.0 and $2.5\mu\text{m}$ is of particular interest because many sharp, highly diagnostic spectral

absorption bands, caused by combinations of bending and stretching vibrations of O-H bands in amphiboles, phyllosilicates and other hydroxyl-bearing minerals, occur in this region (Hunt and Salisbury, 1970, also Figs. 2.5 and 2.6). This wavelength interval is widely utilised in remote sensing because of these features, and because it coincides with an atmospheric 'window' (Fig. 2.1).

An overtone occurs when a fundamental is excited by two or more quanta, so that features may appear at approximately twice (or some integral multiple of) the fundamental frequency (Hunt, 1980). An example is the first overtone of the fundamental O-H stretch (denoted $2\nu_{\text{O-H}}$), which occurs at a frequency of $3500\text{cm}^{-1} \times 2 = 7000\text{cm}^{-1} = 1.4\mu\text{m}$. The $2\nu_3$ overtone of water occurs in the same region, and together they form the $1.4\mu\text{m}$ absorption feature observed in all hydroxyl-bearing mineral spectra (see Figs. 2.5 and 2.6). This feature is also in a region of major atmospheric absorption, so is useful only in laboratory studies.

The second overtone of the fundamental O-H stretch (denoted $3\nu_{\text{O-H}}$) occurs at roughly three times the frequency of the fundamental (approximately $10,500\text{cm}^{-1}$, or $.95\mu\text{m}$), but is much weaker than the first overtone. However, it does occur in a region of only partial atmospheric absorption (Fig. 2.1). Therefore, although it has not yet been utilised for remote sensing applications, there is a possibility of its use (see Gabell et al., 1985, in Appendix I). In exceptional cases the third overtone (denoted $4\nu_{\text{O-H}}$) may also be detectable, near 14000cm^{-1} ($.71\mu\text{m}$, see Fig. 2.7).

Other types of vibration of some interest are the lattice vibrations, where a group of atoms (usually an anion) vibrates as a

single entity against the framework of the lattice (Hunt and Salisbury, 1970). These lattice vibrations can combine with other fundamentals to produce (usually minor) effects in the SWIR.

The frequencies (and wavelengths) of some of the major types of fundamentals are summarised in Table 2.2, below.

Table 2.2 Fundamental Hydroxyl Features

Wavenumber	Wavelength	Cause
1570 - 3400 cm^{-1}	2.7 - 2.9 μm	O-H stretch
1100 - 600 cm^{-1}	9.0 - 16.7 μm	X-O-H bend
900 - 200 cm^{-1}	11.1 - 50 μm	lattice vibrations

The precise position and shape of the vibrational absorption features depend on the number, mass, geometry and values of the interatomic forces of atoms in the immediate environment.

Thus, an O-H group bonded to aluminium (i.e. dioctahedral phyllosilicates) will have a major combination band in the 2.2 μm region, while an O-H group bonded to magnesium (i.e. trioctahedral phyllosilicates) will produce a feature closer to 2.3 μm (Hunt and Ashley, 1979, compare Figs. 2.5 and 2.6). Some minerals (for instance, kaolinite in Fig. 2.5) have a doublet structure caused by hydroxyl groups occupying non-equivalent sites in the lattice, hence vibrating at slightly different frequencies. With measurements of sufficient

resolution, it is therefore possible to derive an enormous amount of mineralogical information from this part of the electromagnetic spectrum.

2.2.3 Vibrational processes in other minerals

The excitation of overtones and fundamental tones of the carbonate (CO_3^{2-}) ion, and hydroxyl groups in some sulphate (SO_4^{2-}) minerals, also produces characteristic absorption features in the SWIR. Spectra of some of the important minerals containing these anion groups are shown in Figs. 2.8 and 2.9.

The most important fundamental vibrations for remote sensing are those of the silicates. Silicon-oxygen vibration fundamentals occur at much lower frequencies than those of the hydroxyls, and coincide with an atmospheric window in the 8 to $14\mu\text{m}$ region. The effects of variation in fundamental vibrations can be detected by measuring either the emittance or the reflectivity of a material. Because the sun emits very little radiation at these wavelengths, reflectivity measurements need to be made with an artificial source (such as a laser).

Figure 2.10 shows some emissivity curves of a variety of silicate samples, and illustrates the systematic migration of emissivity minima in sympathy with the silicate composition of the rocks (after Eberhardt et al., 1984). These minima are called reststrahlen bands. Their precise positions, like those of the hydroxyl features, are controlled by the cation at the second co-ordination position and by bond angles and strengths (Reeves et al., 1975). Figure 2.10 also depicts some laser reflectance measurements for comparison.

Figures 2.11 to 2.14 (all from Eberhardt et al., 1984) depict emissivity curves of a variety of rock types, with laser reflectance spectra of similar materials.

Additional compositional information from low-frequency vibrations (such as those of Al-O and C-O bonds) is also available in the MIR for carbonates, phosphates, sulphates, oxides and hydroxides (Hunt, 1980). Figures 2.15 and 2.16 show laser reflectance spectra of a number of individual minerals, highlighting just some of the mineralogical information available from this spectral region.

2.3 Some Examples of Successful Remote Sensing Applications in the U.S.

The purpose of this section is not to present a comprehensive review of the geological application of remote sensing techniques, but rather to provide a brief summary of a few significant examples of the way that different remote sensing techniques (based on spectral properties) have been applied. This summary will provide some insight into the potential of remote sensing, and build a framework around which an analysis of the possibilities for application of these techniques in Australia can be formulated.

2.3.1 Detection of hydrothermally altered areas in south-central Nevada using Landsat MSS data (Rowan et al., 1974, 1977)

In this study Landsat MSS imagery was used to discriminate most of the major rock types in the region, and to detect and map areas that had undergone hydrothermal alteration. Figures 2.17a,b&c and Table 2.3 (all from Rowan et al., 1974) summarise the VNIR reflectance properties of a number of altered and unaltered rocks of the type found at the test site. In addition, the ratios derived from the spectra (in the wavelength regions covered by the Landsat MSS bands) are shown.

The effects of the reflectance differences on the Landsat MSS (radiance) data are subtle. Individual, enhanced, black and white, single-band images, and enhanced false colour infrared composites derived from them, fail to show any of the altered areas. So, too, do Skylab colour photographs. However, alteration around the Goldfield area, in particular, is visible on enhanced, black and white, MSS 4/5, MSS 4/6, MSS 4/7 and MSS 5/6 ratio images. But, the most effective representation is a combination of MSS 4/5 in cyan, MSS 5/6 in yellow,

Table 2.3 Ratios calculated for MSS Bands for selected mafic and felsic rocks and some alteration minerals (after Rowan et al., 1974).

Sample	Number	MSS 4/5	MSS 5/6	MSS 6/7
MAFIC ROCKS				
Basalt	13	1.05	1.03	1.06
Gabbro	9	1.07	1.01	0.99
Peridotite	8	1.01	1.01	1.05
Serpentinite	15	1.04	1.05	1.07
FELSIC ROCKS				
Rhyolite (pink)	12	0.79	0.92	0.96
Rhyolite (grey)	4	0.96	0.96	0.98
Granite	14	0.89	0.94	0.91
Granite	5	0.97	0.98	0.92
Granodiorite	2	0.92	0.94	0.97
ALTERATION MINERALS				
Limonite (goethitic)		0.61	0.72	0.94
Limonite (hematitic)		0.49	0.85	0.95
Jarosite		0.78	0.99	1.27
Montmorillonite		0.65	0.84	1.07
Alunite		0.66	0.88	0.97
Kaolinite		0.93	0.98	0.99

and MSS 6/7 in magenta using diazo transparencies to produce a colour ratio composite (CRC) image. On this presentation, altered areas appear as green to dark-green and brown to red-brown coloured pixels. In addition, mafic rocks (mainly basalt and andesite) are white, while felsic intrusive and extrusive rocks are pink. Over the whole scene there is a good coincidence of alteration, as depicted by Landsat, with known mining areas. In particular, there is a striking match around the Goldfield area, where alteration has been mapped on the ground in some detail. There are two major limitations of the technique. On the one hand, non-limonitic, altered areas (composed mainly of intensely leached and silicified rocks) are not separable from some silicic tuff and flow rocks. On the other hand, non-hydrothermally-altered, yet iron-rich rocks, are not discriminated from limonitic rocks that have been hydrothermally altered.

2.3.2 Detection of non-limonitic hydrothermal alteration at Cuprite, Nevada, using aircraft scanner images in the .46 to 2.36 μ m region (Abrams et al., 1977)

One of the areas where the Landsat MSS study described above failed to detect altered rocks, because of the absence of limonitic alteration, is the Cuprite mining district. Analysis of .45 to 2.5 μ m field and laboratory spectra showed that iron-deficient opalised rocks have intense OH absorption bands near 2.2 μ m due to their kaolinite and alunite content (Fig. 2.18, from Abrams et al., 1977). In unaltered rocks, this spectral feature is either weak or absent. A CRC image derived from airborne multispectral scanner data in the .46 to 2.36 μ m range takes advantage of the spectral properties of limonitic material in the VNIR (1.6 μ m/.48 μ m and 0.6 μ m/1.0 μ m band ratios) and those of the

clay alteration products in the SWIR (1.6 μ m/2.2 μ m band ratio). In this way nearly all of the altered material was discriminated from unaltered material, and some zoning of the alteration was also detected.

2.3.3 Thermal Infrared Multispectral Scanner data from Cuprite, Nevada (Kahle and Goetz, 1983)

A Thermal Infrared Multispectral Scanner (TIMS) was flown over the Cuprite area in 1983. The TIMS instrument has high radiometric sensitivity (.1 to .3 noise equivalent temperature difference (NE Δ ^oK), at 300^oK). There are six channels in the MIR region (8.2 to 8.6 μ m, 8.6 to 9.0 μ m, 9.0 to 9.4 μ m, 9.4 to 10.2 μ m, 10.2 to 11.2 μ m and 11.2 to 12.2 μ m). The combination of high sensitivity and relatively narrow channels enables a more accurate determination of the spectral properties of materials in the MIR than previous scanners operating in this wavelength region. Based on the positions of reststrahlen minima, (see Fig. 2.10) basalts, unaltered tuffs, carbonates, unaltered sandstones and the altered rocks in the area were all discriminated. However, unlike the VNIR and SWIR data, the MIR discrimination is made largely on the basis of the free silica content of the rocks, thus adding a further dimension to the remotely sensed data acquired in this area.

2.3.4 High-resolution airborne spectrometer data from Oatman, Arizona (Marsh and McKeon, 1983)

Geophysical Environmental Research Inc. of New York (GER) has developed a high-resolution airborne spectrometer, with 512 data channels in the .35 to 1.1 μ m range and 64 data channels in the 1.9 to 2.5 μ m range. The GER instrument was flown over the Oatman epithermal

gold deposit in northwest Arizona. The airborne data were processed to remove atmospheric effects (Figs. 2.19a&b), and a high-resolution, field-portable instrument was used to provide additional data for interpretation. Three different mineralogical zones were distinguished. Strong sericitic signatures were detected in one area and alunitic signatures from another delineating two types of argillic alteration, while various mixtures of illitic, chloritic and kaolinitic signatures were found in an area of mixed phyllic and propylitic alteration (Fig. 2.20). Ground and airborne data correlated well. Specific mineralogies were therefore identified and mapped based on the high-resolution spectrometer data.

2.3.5 Identification of alteration mineralogy at Cuprite, Nevada, and sedimentary minerals in the Wind River Basin, Wyoming using airborne imaging spectrometry (Goetz, 1984, NASA, 1985)

A high-spectral-resolution airborne imaging spectrometer (AIS) has been flown by NASA over Cuprite, Nevada, and the Wind River Basin, Wyoming. A prototype of the instrument was flown in a configuration comprising 32 contiguous bands in the 2.03 to 2.32 μ m region, with 32 pixels across the swath. At Cuprite, the minerals alunite and kaolinite were identified and their distribution accurately mapped by the instrument (Fig. 2.21). In the Wind River Basin, montmorillonite, calcite and dolomite were identified, and their distribution correlated to various sedimentary units (Fig. 2.22).

Thus the AIS is the first instrument operating in the SWIR with the ability to identify minerals coupled with an imaging capability that allows mapping of the two-dimensional distribution of those minerals.

2.4 The Australian Environment and Problems it Poses for Remote Sensing

The geological histories of the United States (where remote sensing techniques have been applied so successfully) and Australia are markedly different. The southwestern U.S., which is the focus for the studies summarised in section 2.3, has a history that includes many intrusive, extrusive and mountain-building events. These events span the time from the oldest recorded rocks in the region, volcanic units some 1800 m.y. old, to Late Tertiary volcanism, with major episodes of igneous activity during the Precambrian, the Mesozoic, and the mid-Tertiary (Titley, 1982). In addition, the climate in North America has been dominated by multiple glaciations since the late Tertiary, with repeated growth and decay of ice-sheets extending as far south as latitude 40° (Andrews, 1970). The overall picture, then, is of a moderately juvenile topography that has existed under conditions non-conducive to extensive chemical weathering.

In contrast, much of Australia, particularly the western two-thirds, has been emergent and stable since Permian times, and thus subject to sub-aerial weathering. The last major (Permian) glaciation was followed by active erosion in the Jurassic and Cretaceous, leading to extensive planation by the mid-Cretaceous (Butt, 1981). A prolonged period of weathering followed, with probably humid and temperate to warm mid-Mesozoic climates becoming sub-tropical to tropical in the Oligocene-Miocene, when lateritic processes dominated. The trend thereafter was to aridity, spreading outwards from the centre of the continent, that has continued to the present (Ollier, 1978). The result is an extensive mantle of weathering products that have been stripped to varying degrees (Fig. 2.23, after Butt and Smith, 1980).

2.4.1 Development of the weathering profile

Weathering profiles can be considered to form progressively, with each horizon forming from a precursor resembling the underlying one (Butt, 1983, McFarlane, 1976, Fitzpatrick, 1980). Under stable conditions conducive to chemical weathering, a full weathering profile may develop with time (Fig. 2.24, from Butt, 1983).

In such a profile, saprolite develops from fresh rock by the loss of mobile constituents, while retaining the texture of the original unweathered material. The loss of primary textures, which usually occurs close to the water-table, defines the top of the saprolite (Butt, 1983). In this zone a considerable amount of chemical activity leads to dissolution of Mg, Ca, Na and K and dissolution and precipitation of Al and Fe. With this activity the destruction of the original rock textures can lead progressively to the formation of a mottled zone, transitional to a zone of retention of Al and Fe, which may show seasonal (pisolitic) concentrations. Above the water-table, where conditions are both acid and oxidising, reworking of the ferruginous zone can leave a zone of residual sand, composed of quartz and the more resistant accessory minerals (Butt, 1983).

Formation of the deep weathering profile is portrayed above, in a simplified way, as a continuous process, with chemical degradation of the rocks, leading to relative depletions and enrichments, being the only process considered. In reality, the processes involved are much more complex, and factors such as climatic fluctuations and epeirogenic movements can affect the position of the water table, and the amount of erosion of the weathering profile. Lateral migratory processes are also important, but have not been considered here.

2.4.2 Alteration and erosion of the profile

In Australia the most important effects on the pre-Miocene lateritic weathering profile were the increasing trend to aridity, and tectonic uplift, particularly in coastal regions. The resulting gradual lowering of the water table has led to the dehydration and hardening of the ferruginous layer (to form duricrusts), and some precipitation of certain components (silica, carbonates, sulphates and chlorides) in topographically low regions (Butt, 1981). It was the combined effects of the trend to aridity and of epeirogenic uplift that has resulted in the partial stripping of the mantle of deep weathering over much of Australia. As stated by Butt (1983, p. 44):

"..... the climatic changes that caused an alteration in the style of chemical weathering also induced vegetational changes and slope instability. Hence, despite the protection offered by duricrust formation, erosional activity increased by headward stream erosion and pedimentation."

An added complication is the transported overburden that commonly overlies the in situ weathering zone. Again, Butt (1983, p. 45) states:

"The greatest thicknesses ... are found in areas of already low relief, particularly the valleys. The sediments of alluvial and colluvial origin consist for the most part of the products or residues of weathering, such as kaolinite, smectites, illites, quartz, Fe oxides, ilmenite and other heavy minerals, plus evaporites such as carbonates, chlorides and sulphates. Some of the sediments are quite old and may have been deposited during the period of deep weathering and hence may themselves have been lateritised. In places, they are almost indistinguishable from the weathered zone on which they have been deposited."

In addition, the arid conditions have allowed increased wind erosion, and aeolian deposits of varying thicknesses are widespread. It is with this complex weathering history in mind that one should undertake any remote sensing investigation in Australia.

2.4.3 Remote sensing in deeply weathered terrain

The weathering process, especially when operating over the periods of time and with the severity that it has in Australia, tends to result in convergent evolution. Bauxites, for instance, have been shown to develop from a variety of quite diverse precursors (Valeton, 1972). In particular, the range of minerals found in a duricrust is quite limited, with iron oxides, quartz and clays (generally kaolinitic, but gibbsitic or boehmitic in bauxites) almost always dominating. Schellman (1979) has reported that the relative amounts of these minerals in a duricrust vary systematically, depending on the composition of the rock type that forms the parent material. This systematic variation can be seen when duricrust compositions are plotted on triangular diagrams with corners represented by the components Fe_2O_3 , Al_2O_3 and SiO_2 (Figs. 2.25a-e).

From a remote sensing viewpoint, it is notable that these weathering products are all theoretically capable of detection (and identification) using their spectral properties. Iron oxides produce absorption features in the VNIR, clays in the SWIR, while quartz has its characteristic reststrahlen minimum in the MIR (see section 2.2). With appropriate high-resolution instruments, it may even be possible to produce diagrams similar to those of Fig. 2.25, using semi-quantitative data obtained from remote sensing alone. If so, some inferences about the composition of the parent material could then be drawn.

However several factors would limit this approach. The amount of absorption of radiation by Fe-oxides has been shown by Buckingham (1981) to be correlated to the percentage of Fe-oxides present, only up to a certain "saturation point". Past this point (about 10% Fe-oxides), the depth of absorption features remains fairly constant. Any spectral

effects due to non-lateritic material (e.g. vegetation) within the field-of-view of the instrumentation would also need compensating.

Despite the effects of convergent evolution, variations in parent lithology, coupled with topographic differences (such as drainage and catenary position) and even regional settings (Butt, 1983), will also all have an influence on the deeper portions of the weathering profile. Therefore, the signal remotely sensed over in situ weathered material will depend on both the nature of the profile, and the level to which it has been eroded. Figs. 2.26a-c (after Butt, 1983) show the composition of a number of profiles that have developed over a variety of rock types in Western Australia.

As is the case for duricrusts, the minerals present in the lower parts of the profile are all amenable to detection by remote sensing, the SWIR region being particularly important for minerals such as talc, serpentine, amphiboles, carbonates, and the clay minerals, kaolinite, vermiculite, smectites and gibbsite. Table 2.4 contains a list of hydrothermal alteration minerals in different categories of altered rocks studied in the southwestern U.S. (after Rowan and Lathram, 1980). Comparison of Fig. 2.26 and Table 2.4 shows that, even from such disparate sources, there are minerals common to hydrothermal alteration and weathering. Furthermore, examination of the SWIR spectra of some of these minerals (Figs. 2.5 and 2.6) shows that they all have absorption minima in the 2.08 to 2.35 μ m region of the spectrum.

It therefore becomes obvious that remote sensing in Australia, particularly the targeting of hydrothermal alteration, is not going to be a simple matter of identifying the presence of absorption features caused by iron oxides in the VNIR, and by clay minerals in the SWIR. It

Table 2.4 Alteration minerals occurring in the southwestern U.S.
(after Rowan and Lathram, 1980)

Propylitic Rocks	Epidote, chlorite, albite, carbonate, montmorillonite, goethite, K-mica, pyrite, zeolites
Argillic Rocks	Montmorillonite, kaolinite, quartz, K-mica, goethite, haematite, jarosite, chlorite, carbonate
Phyllic Rocks	Quartz, K-mica, kaolinite, mixed-layer clays, haematite, jarosite, K-feldspar, albite
Advanced Argillic Rocks	Quartz, pyrophyllite, alunite, kaolinite, opal, K-feldspar, K-mica, haematite, anatase, relict zircon
Opalite	Quartz (opaline), alunite, kaolinite, pyrophyllite, calcite, anatase
Silicified Rocks	Quartz, alunite, kaolinite, diaspore, pyrophyllite, haematite, goethite, jarosite, anatase, rutile, relict zircon, opal, K-mica

follows that the low-resolution techniques used for analysis of remotely sensed data by many workers in the southwestern United States (Rowan et al., 1974, Abrams et al., 1977) cannot simply be transferred for Australian applications.

What is required is the capability to identify the minerals' absorption features, and interpret these identifications in terms of mineral assemblages, and their distribution. For instance, an assemblage consisting of kaolinite, montmorillonite, quartz, K-mica, goethite and haematite taken as indicative of argillically altered rocks could also be indicative of of a saprolite derived from a granitic precursor (Fig. 2.26) or of argillically altered rocks (Table 2.4, also Rose and Burt, 1979). However, the presence of an assemblage containing chlorite and epidote in an adjacent area would warrant the interpretation of the assemblages as argillic and propylitic alteration, respectively.

With one exception, to the writer's knowledge, the only remote sensing (sensu stricto) studies that have led to the direct identification of mineral assemblages have involved the use of high-resolution spectrometers. Most of these studies have resulted from the use of the GER airborne instrument, or NASA's AIS. The exception is a study that involved the use of narrow-band radiometer data acquired from orbit (Goetz et al., 1982). The filters used for this experiment were narrow, and specifically designed for the identification of certain minerals. This success demonstrates the feasibility of using similarly designed narrow-band filters in airborne and other scanners in Australia for the direct identification of alteration, or other, mineral assemblages.

Wherever possible, this study has made use of data from high-resolution spectrometers in order to glean the maximum amount of mineralogical information. However, it is the writer's opinion that the most effective use of remote sensing in this country will also involve the use of imagery. Geomorphological interpretation of the weathered terrain (hence of relative position in a partially stripped, weathered profile) is essential. The two-dimensional view afforded by imagery will also allow a much better appreciation of the distribution of minerals, or mineral assemblages (the value of which is illustrated above). In the case where evaporitic or transported material is being detected, a combination of imagery and spectral properties will also be extremely useful. Not only will a better discrimination of transported and residual material be possible, but some information may be gained about the provenance of the transported material. This has been shown to be the case in two different studies of Landsat TM and airborne TMS data over Death Valley, California, where even the TM's broad-band spectral data allow some inferences to be made about the source of alluvial and colluvial material (Huntington, 1984, Kahle et al., 1984).

To further underline the value of imagery, there have been numerous studies of Landsat MSS data in Australia that have provided useful geological information (e.g. Green et al., 1980) - even with its limitations due to limited spectral range and coarse spectral resolution. One such study appears in this thesis (see chapter 5).

CHAPTER 3. HARDWARE UTILISED AND TECHNIQUES USED FOR SPECTROMETER DATA ANALYSIS

3.1 Introduction

A variety of instruments and techniques was used during the course of this study. Where a technique has been applied at a single test site, an explanation of the technique is usually included in the relevant Chapter. However, the bulk of the information is contained in the present Chapter.

Spectra were acquired in the laboratory on samples from all test sites, using three different spectrometer systems. High-resolution airborne spectra were acquired over two test sites - Mt Turner (Chapter 5) and Kambalda (Chapter 6) as part of a wider survey using a spectrometer system developed by Geophysical Environmental Research, Inc. (GER), of New York.

Software aiding interpretation of these data was developed at the CSIRO/MXY at North Ryde, Sydney.

3.2 Hardware

3.2.1 The GER Mark II airborne spectrometer

During September, 1982 the CSIRO brought to Australia the GER Mark II airborne spectrometer, which was flown over 4 test sites around the country. The data from two of these sites are presented in Chapters 5 and 6.

The GER Mark II instrument was designed and developed at Columbia University, Division of Engineering (Collins et al., 1981), with funding

from the U.S. National Science Foundation. The system design is similar to that of the Mark I system described by Chiu and Collins (1978). In contrast to the Mark I system, solid state detector arrays are utilised in the Mark II instrument. In addition, the Mark II actually consists of two spectrometers operating in the spectral range from .4 to 2.5 μm . A 512 element silicon diode array covers the .4 to 1.1 μm region (.0015 μm channel separation, approximately .0020 μm resolution), and a 64 element lead sulphide array covers the 1.9 to 2.5 μm region (.008 μm channel separation, approximately .012 μm resolution). The arrays are positioned at the exit focal planes of two 275mm focal length spectrographs, and all channels receive the spectrally dispersed bands of energy (from two holographic gratings) in parallel as the field-of-view on the ground is swept along the aircraft track.

The instrument integrates the energy in each band simultaneously over contiguous 20m by 2m areas along the flight path at the nominal altitude of 600m above terrain (Collins et al., 1981). The output from ten such areas is integrated, to produce contiguous 20m square pixels, with the resultant data being stored in a buffer. The data are digitised to 12 bit resolution in real time, and dumped from the buffer onto computer-compatible tape (GER, 1982). The data were calibrated band-by-band by GER for radiance received at the front apertures, and for wavelength by Krypton lamp measurements taken in the air at each site. Location of the spectra on the ground was achieved by simultaneous coverage using 35mm colour photography, the camera being boresighted with the spectrometers.

The parallel input to all channels results in high signal-to-noise ratios and very good resolution of spectral features. The noise

equivalent reflectance difference ($NE\Delta\rho$) is .025% at 2.2 μ m (W. Collins, written comm., 1986), but is highly dependent on wavelength. The trade-off is that the spatial context of the data is lost, because only a single line of pixels is acquired at any one time.

The instrument was mounted over a standard, 18-inch aerial photography port in a twin-engined Cessna 402 operated by Qasco, out of Sydney.

3.2.2 Laboratory measurements

With the exception of the samples from the Fortescue Group (provided by Dr Ray Smith), samples for laboratory spectral measurement were collected by the author from each test site.

The samples from Weipa (Chapter 4) are predominantly soil samples, and are identified by the grid coordinates from which they were collected.

Samples from Mt Turner and Kambalda were collected from selected flight line locations in June and October, 1983, respectively. This activity followed preliminary interpretation of the airborne data. In these areas the sample numbering system is similar. At Mt Turner (Chapter 5) the following information was included:

Flight line identification (e.g. MT1)

Pixel number along the line (e.g. 685)

Sample number collected at that site (e.g.1)

Nature of the sample (S if soil)

Nature of the surface (W for weathered or F for fresh surfaces)

Thus, MT1/685/1 W represents the weathered surface of sample number 1 from pixel 685 of flight line MT1, while MT1/685/1 F represents the "fresh" (actually inner) surface of the same sample. MT1/685/S represents a soil sample from the same location. If more than one spectrum was measured on a particular surface, a distinguishing number was appended.

At Kambalda (Chapter 6) a more detailed description of the sample's nature is included. Hence O denotes an outcrop sample, F float, S, soil and P, the spectrum of a powder used for XRD analysis. Thus, K2/290/F2/W represents the weathered surface of sample number 2 (float) from pixel 290 on flight line K2. K2/290/F2/P is the XRD powder derived from the same sample, and K2/290/S is a soil sample from the same location.

The samples from the Fortescue Group (Chapter 7) retain their original sample numbers, as do the core samples from Peak Hill (Chapter 8), provided by Gold Fields Exploration.

A second suite of samples from Peak Hill was collected by the author during November, 1984. These samples were gathered along two traverses, as well as additional, scattered sites. NT represents the 'Northern Traverse', BBT the 'Bobby Burns Traverse' in the southern part of Peak Hill, and the remainder of the samples are labelled PH (Peak Hill). The sample location, indicated by a number, appears after the traverse notation, and a letter follows when more than one sample was collected from the same site. Finally, as for Mt Turner and Kambalda, a letter, W or F, indicates the nature of the surface being measured. Thus, PH 2C W represents the weathered surface of sample C, site number 2, at Peak Hill.

3.2.2.1 VNIR and SWIR laboratory measurements

Two different instruments were used for VNIR and SWIR measurements, but samples were measured simultaneously (Fig. 3.1). The VNIR instrument is a Tracor Northern spectrometer utilising a 1024 element, solid-state, silicon array (Reticon), owned by the Department of Geology and Geophysics, University of Adelaide. It was linked to a multichannel analyser, allowing simple manipulation (addition, subtraction) and wavelength calibration of the spectra (Fig. 3.2). The wavelength calibration was achieved by measurements of the spectrum of a neon calibration lamp with known emission peaks. The spectra were measured using half the maximum resolution of the instrument (512 channels), which allowed 8 spectra to be stored in the multichannel analyser memory, and gave an approximate channel separation of $.0012\mu\text{m}$, and an approximate spectral resolution of $.002\mu\text{m}$. At least one of the 8 spectra stored in memory was of a reflectance standard. After each set of eight spectral measurements, the instrument was placed in a 'subtract' mode, and dark current was subtracted from each spectrum.

A quartz-halogen projector lamp was used to illuminate the sample at a high angle of incidence. After the lamp had warmed up, the reflectance standard was measured, and the instrument 'exposure time' adjusted until the detectors saturated. The exposure time was then decreased to just below the level of saturation. Thirty scans were acquired for each sample. The scans were summed, and the resultant spectrum stored in memory. These settings were maintained throughout a measurement session.

Data were transferred to an HP1000 minicomputer, via an RS232 link, from the multichannel analyser. A specially designed software package

(XBOSS - see Section 3.3) was used to calculate reflectance relative to the standard. The $NE\Delta\rho$ is estimated (from spectral plots) as being better than .02% at all wavelengths, with maximum sensitivity near the centre of the spectral range (.7 μ m).

The reflectance standard used for both VNIR and SWIR measurements was a pressed polytetrafluoroethylene powder (marketed as Halon). The Halon spectrum is essentially flat in the VNIR with a reflectance greater than 99.3% at the angles of incidence used (Weidner and Haia, 1981), so that reflectance measurements relative to Halon are close to true reflectance values.

The instrument used for SWIR measurements (Fig. 3.3) was designed and built at the CSIRO Division of Cloud Physics by Dr Terry Cocks (now with CSIRO/MXY). Used initially for airborne cloud radiance measurements, it was modified by Dr Cocks for laboratory use. A single lead sulphide detector receives chopped radiation after it has passed through a revolving circular variable filter (CVF). The resolution of the CVF is approximately 1% of wavelength, which is not sufficient to resolve the kaolin doublet at 2.17 μ m and 2.208 μ m (see Hunt and Ashley, 1979), but will produce a shoulder. The spectrum was usually scanned 30 times for each sample (120 scans for some particularly dark samples) with an average 20ms dwell time in each of 128 digitised output channels. This results in an $NE\Delta\rho$ of better than 0.1%, but is highly dependent on wavelength. Those regions of the spectrum affected by atmospheric absorption (near 1.4 and 1.9 μ m) obviously have the highest noise levels.

The output recording medium was a floppy disc driven by an Apple II personal computer. The same computer was used to calculate absolute

reflectance, using the Halon reflectance data from Weidner and Haia (1981). Approximately every sixth spectrum recorded was that of Halon, and successive Halon spectra were ratioed. Any significant deviation from a straight line near 100% reflectance resulted in the repetition of all measurements between the Halon spectra used to produce the ratio. Spectra were plotted using software on the Apple computer, and were also transferred to the HP1000 for any further analysis.*

3.2.2.2 MIR laboratory measurements

The MIR laboratory reflectance spectra were measured by Dr John Eberhardt of the CSIRO Division of Mineral Chemistry using a continuous line-tuned CO₂ laser (Fig. 3.4). The laser oscillates on 128 CO₂ laser wavelengths between 9.14 and 11.25µm (Eberhardt et al., 1984), with the spectral resolution of the system determined by the spacing between laser lines. Coverage between 9.14 and 11.25µm is virtually continuous, with only a small gap between 9.94 and 10.08µm. A rotating mirror sweeps the beam across several specimens in approximately 3ms, and 512 such sweeps were averaged per spectrum. The diffuse reflected signal returns along the same path and is reflected from a ZnS splitter to a lens focussed onto a HgCdTe photoconductive detector with a ~MHz bandwidth (Eberhardt et al., 1984). The instrument is extremely sensitive, with a signal to noise ratio of approximately 10⁵ (or an NEΔρ of .001%). Ground NaCl cold-pressed against filter paper was used as a reflectance standard.

*Some of the laboratory spectral plots have asterisks alongside values on the y-axis. Where this occurs the value shown is a factor of 1,000 greater than the true value.

3.2.3 Image processing system

An HP1000 computer (see section 3.2.2.1) acts as a host to the image processing system used in the analysis of MSS imagery over Weipa (Chapter 4), and in the production of log residual images (Chapters 5 and 6). The image processing system was designed and built by Mr Guy Roberts at the CSIRO/MXY, using CCD460 Fairchild Semiconductor chips for refresh memory (Roberts, 1982). A 51cm Barco high-resolution colour television monitor (model CDCT 2/51-H) is used for output display (Fig. 3.5). There are 8 bits used for red, green and blue colours respectively, with 512 lines and 256 pixels displayed on the screen (Roberts, 1982). Colour images used in this thesis were produced either by photographing the screen, or by writing 3 monochrome images of red, green and blue output individually onto 25cm x 20cm film using a model P1500 PHOTOWRITE manufactured by Optronics International Inc. From these monochrome separates, colour film products were made by commercial photographic laboratories.

3.3 Analysis Techniques

A number of techniques have been developed by members of the CSIRO/MXY Remote Sensing Group for the analysis of high-resolution airborne and laboratory spectra. These techniques have been applied to the analysis of the data presented here, particularly airborne data. The software package is described in detail by Craig et al. (1984), but some aspects relevant to the thesis are noted in sections 3.3.1 and 3.3.2.

3.3.1 XPUT files

An XPUT file is a disc file comprising spectral information and some identifying records. The XPUT file was designed to deal with more than one spectrum of the same sample - for instance VNIR and SWIR laboratory spectra of the same surface, or airborne spectra from the same pixel. Each record in the file has an address comprising a Sample number and a Group number. Sample numbers are sequential and correspond to the actual position (pixel number) along a flight line for airborne data. The unique sample description code (see section 3.2.2) for laboratory data is stored in a corresponding sample header. Group number distinguishes the type of spectral information, with each spectrum contained in a different group. Each group comprises a number of channels that correspond to the output channels of the spectrometer used to acquire the data. Additional groups may be included to hold information derived from the original spectra - for instance simulated values of band ratios - or even non-spectral information such as coded geology.

A typical sample from an airborne data set might have the structure shown in Fig. 3.6. The file therefore includes as many repetitions of this 5-record unit as there are pixels in a flight line.

A set of subroutines collectively known as XPUT performs the functions of transferring spectral data (creating files, reading or writing files, etc.).

3.3.2 XBOSS

All operations with XPUT files are performed through the

controlling program XBOSS. The three menus in Fig. 3.7 show the number and type of operations that can be performed on spectral data. Many of the programs to execute these XBOSS options have been developed in response to requirements outlined by users (such as the author) who are attempting to interpret the data. Some of the procedures relevant to this thesis are described below.

3.3.2.1 Log residuals

The airborne spectra acquired over Mt Turner and Kambalda represent radiance received at the front apertures of the spectrometers. As such, they are dominated by the absorption features of atmospheric gases (Fig. 3.8a&b). In order to remove these effects, and those of terrain brightness (albedo), the log residual technique was developed by Green and Craig (1985, see Figs. 3.8c&d). The concept behind this technique is similar to that utilised by Marsh and McKeon (1985), in their treatment of data from the same instrument over Oatman, Arizona.

A program (XLOG) was written by Dr Maurice Craig. His description of the program (from Gabell et al., 1983) appears below:

PROGRAM XLOG

"Let $X_{i\lambda}$ denote the reading in channel λ at point i of a flight line, and $\rho_{i\lambda}$ the reflectance of the terrain within the sampled 'footprint'. The values of $X_{i\lambda}$ and $\rho_{i\lambda}$ are connected (in one model of the process) by a formula of the type

$$X_{i\lambda} = A_i \rho_{i\lambda} I_\lambda .$$

Here A_i represents factors, such as topographic slope, which influence the angle of illumination and are common for all channels, while I_λ

represents the solar illumination as a function of wavelength.

Suppose there are N channels and M sample points. If we write

$$X_{.\lambda} = M^{-1} \sum_i \log X_{i\lambda}$$

for the (logarithmic) mean spectrum over all samples,

$$X_{i.} = N^{-1} \sum_{\lambda} \log X_{i\lambda}$$

for the mean over all channels of the i-th spectrum, and

$$X_{..} = M^{-1} \sum_i X_{i.} = N^{-1} \sum_{\lambda} X_{.\lambda} = (MN)^{-1} \sum_i \sum_{\lambda} \log X_{i\lambda}$$

for the grand mean, then the quantity

$$Y_{i\lambda} = \log X_{i\lambda} - X_{i.} - X_{.\lambda} + X_{..}$$

provides a transformation of the original data to what we may call the logarithmic residual. This quantity is no longer influenced by solar illumination or topographic variations, i.e., with the obvious definitions of $\rho_{.\lambda}$ etc. we have

$$Y_{i\lambda} = \log \rho_{i\lambda} - \rho_{i.} - \rho_{.\lambda} + \rho_{..}$$

It thus provides a practical invariant measure of the terrain composition.

Program XLOG accepts an input group containing a spectral sequence ($X_{i\lambda}$). A first pass through the file allows accumulation of the mean $X_{.\lambda}$ and also of the standard deviation $S_{.\lambda}$, where

$$(M-1) S_{.\lambda}^2 = \sum_i (\log X_{i\lambda} - X_{.\lambda})^2$$

These quantities produce spectra which are written to specified samples (often the first and second) of an 'output group for residuals'.

On a second pass one computes the logarithmic residual spectra ($Y_{i\lambda}$) and writes them to the same group. At the same time the 'channel mean' $X_{i.}$ and standard deviation $S_{i.}$, where

$$(N-1) S_{i.}^2 = \sum_{\lambda} (\log X_{i\lambda} - X_{i.})^2,$$

are saved in two additional, single-channel output groups.

It is possible to skip either the first or the second pass. Thus, if a common mean for several adjacent flight lines is to be used, one would need the first pass to compute the mean of each flight line separately. The results of the second pass would not be wanted at that time, so it should be skipped. The separate means would then all be overwritten with the common mean (XA option in XBOSS) and XLOG run again. On this occasion there is need only for the second pass, since the results normally derived from the first pass are already in place.

It is clear that, although this process eliminates the effects of solar illumination and slope, the result is not a reflectance spectrum. It does, however, show the difference in reflectance for each sample from that of the 'mean' reflectance term $\rho_{. \lambda}$. If this 'mean' spectrum shows little spectral structure, then the $Y_{i\lambda}$ will be a good approximation to the shape of the reflectance curve."

In practice, the logarithmic mean of a flight line was calculated excluding those areas that are atypical of the geology - shadowed areas, salt lakes, water, etc. The resultant log residuals contain spectral information that can appear very similar to reflectance as measured in the laboratory.

The major difference is that the spectral content of a sample's log residual is relative to the mean reflectance of the flight line, (expressed in logarithmic form), while laboratory reflectance is relative to the reflectance of the standard used. Hence strong absorption by a mineral will produce a negative log residual (Fig.

3.9a), while an absence of the mineral that contributes most to the flight line mean will produce a positive feature at the same wavelength (Fig. 3.9b). Log residuals therefore need to be interpreted with due consideration of the likely content of the flight line mean, an appreciation of which comes only from field observation and laboratory measurements of samples from the flight line.

For the purpose of this thesis, an absorption feature (in airborne data) is defined as a minimum in the negative range of log residual values, whilst a local minimum may have the appearance of an absorption feature, but occurs in the positive range of log residual values. A local minimum in the log residual spectrum may coincide with an absorption feature in the true reflectance spectrum of the same material.

If the flight line has no single strongly contributing mineral (for instance if it covers a great variety of mineralogy, or if most of the flight line contains spectrally flat material), then the log residual begins to look much more like true logarithmic reflectance.

3.3.2.2 Log residual images

Once log residuals have been calculated the spectral properties of material along a flight line can be interpreted. However, in a flight line with as many as 1200 spectra, the individual examination of every spectrum is not feasible. Therefore a technique was used that allows examination of a number of spectra simultaneously. Once again, Marsh and McKeon (1983) used a similar method in the analysis of the Oatman data.

The method involves display of the spectral data on an image processing system (Fig. 3.10). Each sample along a flight line is assigned a horizontal row on the TV screen. Each spectrometer channel is assigned one (or more) TV pixels so that wavelength varies across the screen. The log residual spectra are then colour coded by density slicing into 16 colour levels. The lowest values (lowest log residuals) are dark blue, zero residuals are green, and high values (positive log residuals) are deep red.

Thus blue areas on Fig. 3.10 represent areas of maximum absorption, while red areas represent areas of maximum reflectance. The data generally fall into 'blocks' that have a similar log residual signature. The precise shape and position of absorption features can be determined by averaging the log residual response over each block and plotting the resultant high-resolution spectrum.

3.3.2.3 Tchebychev Analysis.

For some time Tchebychev Analysis has been used for the analysis of spectrometer radiance data (Collins et al., 1981, GER, 1983). The technique involves the representation of a radiance spectrum by linear combination of a number of polynomial functions (see Figs. 3.11a-1). The amount contributed by each function to the reconstruction of the original spectrum is described by the magnitude of its coefficient. In order to reconstruct perfectly a radiance spectrum with 64 channels of data (as for the SWIR data), an expression with 64 terms would in general be required. However, the higher-order terms correspond to high-frequency features (noise), so a considerable amount of information is available by examination of a few lower-order coefficients. In order

to maximise the information content in a single plot, Tchebychev Analysis is usually presented as the magnitude of certain ratios of coefficients along a flight line. The technique has been used in this thesis (see section 5.5.5.1) for the analysis of airborne data.

However, the technique has also been utilised in a different manner for the analysis of VNIR laboratory spectra. Because the high-order Tchebychev polynomials reproduce noise, reconstruction using only lower-order polynomials effectively smooths the spectrum. This is particularly useful for VNIR data, where broad iron oxide absorption features (the most common effects being studied) can be reproduced faithfully. Figures 3.12a&b are a VNIR spectrum, and its smoothed version, respectively.

Once smoothed, the first and second derivatives can be calculated, and the results stored in separate groups of the same XPUT file (see Figs. 3.12c&d). Values of zero for the first derivative correspond to inflection points in the spectrum, while values of zero for the second derivative correspond either to maxima or minima. A program (XNIX, see Fig. 3.7) can be used to list the wavelengths at which zero values occur for each derivative. When applied to a number of samples in the same XPUT file, this method provides a fast, objective and consistent method for determination of the wavelengths of critical features in a spectrum.

PART II. : CASE STUDIES

CHAPTER 4 WEIPA BAUXITE PROVINCE, CAPE YORK PENINSULA, QUEENSLAND

4.1 Introduction

This chapter documents an investigation of the value of Landsat MSS imagery, and the potential of high-resolution spectrometer data, for bauxite exploration and development. The study area, Weipa, lies on the western side of Cape York Peninsula, far northern Queensland, and falling approximately between latitudes 12° to 14° S, and longitudes 141° to $143^{\circ} 20'E$.

The specific aim of this study was to determine whether remote sensing can provide information, important for exploration and development of the deposits, on the location, character and grade of bauxite. For Landsat MSS data, this information includes the differentiation of bauxite plateaux from surrounding terrain, the study of variations within the extensive areas of bauxitisation, and assessment over a large region of environmental factors that might influence the MSS response. For high-resolution data the aim is to identify the bauxite mineralogy through spectral measurements of the overlying soils.

Prior to this study, Landsat imagery of the Weipa area was enhanced by the CSIRO/MXY (Huntington et al., 1982). The considerable areal extent of bauxitisation in the Weipa region is amenable to treatment at the working scales and resolution afforded by Landsat MSS data (the only Landsat data currently available in Australia). This image enhancement revealed some subtle variations within the Landsat data that (qualitatively) correspond to known, broad variations in the bauxite composition.

This study assesses the enhanced imagery in some detail, in the light of these known regional variations. A more quantitative analysis is also undertaken, in a smaller area around Weipa, by comparison of Landsat values to soil geochemistry (derived from surface samples), and ore geochemistry (derived from drilling data).

Theoretically the mineralogy of the bauxite can be determined from high-resolution spectrometer data. The iron oxides present in the area have distinctive signatures in the VNIR, whilst the clay minerals (including the ore minerals gibbsite and diaspore) can be identified from their SWIR responses. A number of soil samples had their spectra measured to test whether the soils overlying the bauxite have detectable characteristic signatures that mirror the underlying ore mineralogy.

The investigation therefore includes the assessment of Landsat and geochemical data, integration of these data, field investigation, photo interpretation, and some VNIR and SWIR spectral measurements of soil samples. Seasonal variations, which influence the Landsat data trends, are also briefly studied using multi-date imagery.

This study is believed to be the first utilising high-spectral-resolution VNIR and SWIR data from a bauxitic environment.

4.2 Regional Geological Setting

Cape York Peninsula comprises a central core of Palaeozoic basement rocks, with Mesozoic and younger sediments dipping gently towards both coastlines. Alumina-rich laterite occurs on the western, more stable, limb of the regional structure. Almost continuous remnants, in the form of discrete plateaux, extend from Vrilya Point in the north to Archer

Bay in the south - a distance of 240 km. The plateaux extend up to 50 km inland from the coast, but seldom exceed about 30 metres above sea level.

The laterite is developed over a succession that includes arkosic sands, clays and siltstones from Jurassic to Tertiary age. In the Weipa region the Mesozoic succession can be reconstructed only from borehole data. Gibson (in Douth et al., 1973) has investigated the subsurface stratigraphy using cuttings and wireline logs of a drillhole and several water-bores in the region. His findings are summarised in Figure 4.1. This figure, and the BMR 1:250,000 scale geology map of the area, show that the aluminous laterite occurs exclusively on the late Cretaceous or early Tertiary Bulimba Formation. Evans (1972) sub-divided the laterite into 4 different groups based on its chemical and physical characteristics (Fig. 4.2).

4.3 Climate

Weipa's climate is hot and monsoonal, with a maximum temperature ranging from 35°C (November) to 30°C (July) and a minimum ranging from 25°C (December-March) to 21°C (July and August).

Bureau of Meteorology figures for the period 1967-1978 show a mean annual rainfall of 1929mm (76") with more than 95% falling November to April inclusive. Little rain (averages of between 1 and 3mm per month) has been recorded for the months June to September.

Residents have noted significant local variations in rainfall. For instance, Comalco records show that there is consistently 10-30% more precipitation at Andoom than at Weipa (M. Goudie, pers. comm., 1981). A

difference of perhaps 130mm (5") per annum has been noted between the western and eastern ends of the Weipa Peninsula (I. Goudie, pers. comm., 1981). This variation may have had a significant effect on the evolution of the bauxite deposits, if similar rainfall patterns existed in the past.

The area is subject to tropical cyclones that can cause considerable damage. According to Coleman (1972), on average one cyclone has been recorded every two years in the 5° latitude by 5° longitude grid centred on Weipa. However, little long-term damage has thus far been recorded, with stripping and even uprooting of trees the major effect.

4.4 Previous Geological Investigation

There is some published work on the Weipa region. H.J. Evans (who originally recognised the extent and significance of the bauxite) has written several papers on the geology (Evans, 1959, 1971a, 1971b, 1975). The CSIRO has contributed with Mineragraphic Investigation Reports 748 to 751 - mainly comparing the heavy mineral composition of different stratigraphic components. Loughnan and Bayliss (1961), Grubb (1971), MacGeehan (1972), and Plumb and Gostin (1973) have also published work on the mineralogy and genesis of Weipa or Aurukun bauxites. These papers present a generally consistent story.

On Weipa Peninsula the stratigraphic succession has been well characterised by shallow borehole drilling (Figs. 4.3 and 4.4). Under the bauxite-laterite lies a highly kaolinitic horizon described as 'stiff silty and sandy clays'. Underlying this rock-type are 'aquifer sands' that comprise up to 90% silica with a kaolinitic matrix.

Examination of the data in the CSIRO Mineragraphic Investigation Reports 748-751 indicates only slight differences in heavy mineral composition between the bauxite and the underlying kaolinitic sandstone ('aquifer-sands'). An interpretation by Edwards (1957, p. 3) based on the weathering texture found within an outcrop at 'Weipa Camp', indicates that the kaolinitic sandstone was probably originally derived from "granitic pebbles in an arkosic matrix". Thus it is inferred that the bauxite formed along with the kaolin from an arkosic portion of the Bulimba Formation during the weathering cycle.

Loughnan and Bayliss (1961), on the other hand, suggest that the kaolinitic sandstone is a primary rock type presumably unrelated to the Bulimba Formation, and that, given ideal conditions, the bauxite could have developed from a rock with its present chemistry. Their calculations were based on an estimate of the amount of silica that would have to have been removed, and they indicate that a stable geologic and climatic environment could have formed the deposits now present over a period of 50 million years - placing the latest possible commencement of bauxitisation at Lower to Middle Tertiary.

The author believes that this length of time need not be invoked if the bauxite has formed from an arkosic portion of the Bulimba Formation.

Evans (1975) also expresses the opinion that a Tertiary 'arkose' is the parent material of the bauxite. However, he incorrectly quotes Edwards (1957), stating that the basal nodular bed consists entirely of bauxite-coated fragments of the underlying sediments, and that the arkosic texture of the original beds is preserved in many of the pisolites of the bauxite horizon. In fact, Edwards only commented on relict textures within the kaolinitic sandstone.

Although differing slightly in details, these interpretations all imply that the lateritisation process must have been a long-term, stable one, capable of producing an in situ bauxite. Grubb (1971) agrees with this view in stating that "the Weipa bauxites have had a relatively uncomplicated history of meteoric leaching", and that "evidence of the relatively quiescent conditions is also revealed by the significant diminution of 'B' and 'C' concretionary horizons ...". However, on the basis of some heavy mineral observations he also states that "...it is probable that this again reflects the slightly differing lithology of both the bauxite parent rock and the porous sand clay horizon, which now underlies the pisolitic bauxite zone", which could mean that the kaolinitic sandstone is not the parent material, and therefore that the bauxite is not 'in place'.

Plumb and Gostin (1973) also discuss the possibility that the bauxite is detrital in origin, with an easterly provenance. The vast extent, lithological uniformity and the loose pisolitic nature of the majority of the bauxite are characteristics that might be explained at least as well by a sedimentary, rather than an in situ, origin. There are also several textural characteristics of the bauxite pisolites that could be indicative of a detrital origin (Plumb and Gostin, 1973, p. 41). However, laboratory investigations by these workers, and the work of MacFarlane (1972), showed that most of the contentious textures have also been observed in indisputable in situ positions. Other aspects contra-indicative of a detrital origin are the distribution of aluminous laterite only on the Bulimba Formation, the need for transport over at least 30 km, and very probably further (at least beyond the present limit of bauxite). Soft pisolites are unlikely to survive intact transported over such distances, and incorporation of rock fragments

from other sources would also be expected. Most of the observed indications of transport of pisolites could be explained either by vertical movement during the downwasting process, or by local lateral movement.

As Smart (1977) points out, most evidence on the origin of the bauxite therefore points to lateritic weathering of an originally arkosic Bulimba Formation. Furthermore, this was probably under climatic and groundwater conditions likely to be slightly different from the present. The change of bauxite formation conditions seems indicated by the present reduced vegetation compared with the much denser vegetation that would be necessary to produce the reducing environment necessary to induce bauxite formation (Petersen, 1971). The previous existence of such vegetation is indicated by remnant patches of dense rainforest in the Andoom area, and to the south of Weipa Peninsula.

Whichever process is responsible for bauxite formation, authors are unanimous in their conclusion that a closely controlled set of climatic and geomorphic conditions must have persisted over an unusually long period of time.

4.5 Regional Vegetation Patterns and their Seasonal Variation

The only major published work on vegetation in the vicinity of Weipa is by R.L. Specht et al., (1977). They defined ten major ecosystems in the Weipa area (Fig. 4.5), with the distribution of different vegetation units closely matching the major geological/geomorphological terrain units (see section 4.7 for description).

In general, the bauxitic plateaux are mapped entirely as open-forest comprising Eucalyptus tetradonta with subordinate E. polycarpa. The only exceptions are where creeks dissect the plateaux or patches of swampy land exist within plateaux.

E. tetradonta (or Darwin Stringybark) is one of the most widespread eucalypts in Northern Australia, found throughout an area stretching from the Kimberley region in Western Australia through to Cape York Peninsula. This tree thrives in bauxitic/ironstone soils, with considerable moisture storage capacity within the root zone, and, on Weipa Peninsula, excess water draining into an underlying aquifer. Fine roots penetrate deeply (probably 10 metres) enabling exploitation of water stored during summer rains. An indication of the resultant vegetation vigour is given by the monthly values of the Moisture and Net Photosynthetic Indices shown in Fig. 4.6. This cycle greatly affects the reflected infrared radiance measurements as detected by Landsat (see Section 4.9).

There is a major change in vegetation type as one moves eastward off the bauxite plateaux and onto the 'breakaway' country where considerable erosion has stripped the bauxite/laterite to expose the underlying Cretaceous soils. These often waterlogged, mottled, yellow earths support an E. confertiflora, E. cullenii and E. polycarpa population co-dominant in a woodland formation (Specht et al., 1977).

4.6 Previous Remote Sensing Investigation

The Landsat MSS imagery used in this analysis was produced by the CSIRO/MXY Remote Sensing Group as part of AMIRA Research Project

77/P85. Figures 4.7, 4.8 and 4.9 were produced before the author's involvement in the project.

All of these figures were produced, using standard image processing techniques, from a dry-season Landsat image acquired on 26th July, 1973 (WRS path 105, row 69, scene no. 9036-00004). Figure 4.7 is a simple linear stretch utilising statistics from a sub scene of the image. Figure 4.8 is the optimum enhancement produced in the early stages of the study, and is a result of histogram normalisation of bands 4,5 and 7 to a Gaussian distribution. The subscene statistics used for the production of this image exclude the sea and cloud cover, and are based largely on the area immediately around Weipa Peninsula (see overlay).

The last image produced by the CSIRO is specifically designed to enhance the vegetation over Weipa Peninsula. The technique of Rouse et al. (1974) was adopted, whereby point transformations are applied to Landsat MSS data, producing the vegetation index (VI) and transformed vegetation index (TVI). The VI is defined as

$$VI = \frac{MSS7 - MSS5}{MSS7 + MSS5}$$

In order to avoid negative values, and the possibility that the variance of the ratio would be proportional to the mean values (a Poisson distribution) Rouse et al. further defined

$$TVI = \sqrt{VI + 0.5}$$

The VI may be calculated from bands 7 and 5 or 6 and 5. In this case bands 7 and 5 were used (as shown above) and hence the notation TVI7. Figure 4.9 is a representation of TVI7 over Weipa Peninsula.

The TVI7 was calculated for most of the Cape Weymouth scene and smoothed with a 3-by-3 low pass filter to accentuate any regional trends. The image was then density sliced, displayed on the image processing system monitor, and photographed to produce Fig. 4.9.

Of particular significance are the images in Figs. 4.8 and 4.9, because they first allowed recognition of a qualitative relationship between Landsat image colour variation and bauxite grade, so providing the starting point for the investigation detailed in this thesis.

4.7 Landsat Characteristics of Major Lithologies and Terrain Units

The following units and their sub-divisions can be differentiated in the Weipa area

1. 'Older' basement
2. Cretaceous basement
3. Tertiary bauxite/laterite plateaux
4. Quaternary and younger deposits
 - (a) coastal sands and dunes
 - (b) tidal mud flats
 - (c) alluvium along streams and in swamps

Most of these features can be identified on all of the Landsat products shown here (including imagery from both wet and dry season) due to subtle tonal changes and textural variations between terrain units. However, the contrast between these units is considerably greater on the optimally enhanced dry season image (Fig. 4.8).

The linearly stretched Landsat sub scene (Fig. 4.7) is dominated by red tones due to the abundance of vegetation. Mangrove swamps and heavily vegetated watercourses obviously are the deepest red, but paler reddish tones are evident on the bauxite plateaux. Little detail is discernible in or between plateaux, with a relatively uniform spread of colour. Paler, yellow-green tones define the low ground where Tertiary laterite has been stripped and Cretaceous glauconitic sands and silts remain. The observed spectral differences between these two units is probably largely due to species variation (see Section 4.5) causing vegetation reflectance differences, with, perhaps, a lesser component contributed by the geology. However, textural differences between plateaux and 'breakaway' country are largely due to geology, and contribute strongly to the overall perception of differences between the terrain units. Older basement appears in the NE corner of the sub scene (under moderate cloud cover) as a slightly redder-toned, more rugged area. Bushfire scars are very prominent, with generally a large areal extent and tones ranging from dark to pale green. Most of the large scars are on the low 'breakaway' ground, with only a few, smaller, scars clearly evident on the bauxite plateaux. Easily distinguished by their higher reflectance in all bands are Quaternary alluvial soils developed along streams draining the area and in swamps, together with the plastic clay soils forming tidal mud-flats and coastal sands and dunes.

It is also notable that a wet-season image (Fig. 4.10), with a linear stretch similar to that in Fig. 4.7, shows much less variation between terrain units. More luxuriant vegetation (predominantly grasses) tends to 'even out' the differences. Surface water is also more obvious and more widespread, appearing as dark patches near the centre of Weipa Peninsula.

As noted in section 4.6, histogram normalisation provides the optimal image enhancement. Much more detailed differences become apparent, not only between terrain units, but also within individual units (see Fig. 4.8).

The mangrove swamps, patches of rain forest and heavily vegetated creeks remain a brilliant red, but the bauxite plateaux are transformed into various shades of green combined with a diversity of red tones that appear to vary regularly in some areas. Much more internal variation is therefore evident within the bauxite/laterite coastal zone.

The low, Cretaceous ground contrasts much more sharply with the bauxite plateaux, and also shows much more internal variation than the other images. In the south-central part of the image the Cretaceous areas show as pale pinks and tans grading to a bright, light green tone to the east, and to darker greens interspersed with pale patches further to the north.

Bushfire scars are somewhat enhanced, and show a variety of shades from a pale blue-green to a dark, almost black green. Differences between bushfire scars probably reflect either a difference in intensity (resulting in varying amounts of damage to pre-existing foliage) or a difference in age (resulting in varying amounts of regrowth) or both.

4.8 Regional Variations in Landsat Characteristics of Bauxite Plateaux

Within the area covered by the Cape Weymouth scene the bauxite/laterite can be divided into a discrete number of blocks, with slightly different Landsat characteristics from block to block (see overlay to Fig. 4.8).

The southernmost block (7 on Fig. 4.8) south and east of the Watson River (6) has been characterised by Evans (1975) as a mixture of "pisolitic bauxite laterite" with "non-bauxitic, earthy, high silica, ferruginous laterite". The area is probably the palest in tone, and least green in colour. In places its appearance is similar to the adjacent Cretaceous material, consistent with its low rating as a bauxitic area.

All other areas on the Cape Weymouth scene have been described by Evans as "strongly pisolitic bauxitic laterite", although there are significant regional variations in the ore chemistry. The Pera Head block (5) shows a gradational change in chemistry (decrease in aluminium and iron, and increase in silica) to the north on a regional scale (pers. comm., Comalco personnel, 1981). This major change in chemistry seems to be mirrored by the enhanced Landsat data, the Pera Head block changing from dark greens, with a mixture of reds in the north, to much lighter tones, with less red, closer to the Watson River in the south. The colours of the Pera Head and the Hey Point (4) blocks are rather patchy, and the corresponding bauxite grades have been similarly described by Comalco personnel (pers. comm., 1981).

There is also a gradational change in the Pera Head and Watson River blocks' Landsat responses, which become lighter green southwest from the escarpment towards Aurukun and the Gulf of Carpentaria. This change parallels a drop in elevation of the plateau surface.

The Weipa Peninsula (3) also displays a regular colour variation, but from west to east in this case. Close to the mine area the image is a dark green but, the further east, the higher relative contribution from the band 7 component, produces a redder image. A colour composite

of bands 4, 5 and 6 shows the same effect to a different degree (see Fig. 4.11). This variation is paralleled by a progressive increase in elevation of the plateau from 20 m at Weipa airport to 66 m at the eastern end of the Peninsula at the 100,000 E grid position. These effects will be discussed further in the following section.

The Andoom area (2) has a much more even spread of colour, and overall appears to be less red than all the other blocks. Variations are mainly due to either swampy ground or bushfire scars. Evans noted an appreciable difference in the iron content of the bauxite, with up to 16% at Andoom compared to around 7% near Weipa (Evans, 1972, p. 962). The result is a reddening of the Andoom bauxite, compared with the Weipa bauxite, visible to the naked eye in hand specimen. On a field-visit to the area, the forest on Andoom seemed to the author to be more open than that on the Weipa Peninsula and further south. If this is so then a higher degree of exposure of a redder soil might help explain the high Landsat band 5 (greener) response compared to the Landsat band 7 response, relative to other areas. The low band 7 response may also be caused by lower vegetation vigour as a result of the soil chemistry.

Andrews (pers. comm., 1982) notes that the Andoom area is wetter than the Weipa Mine area, which suggests ground water table differences. Certainly the Andoom area has more swamps and low lying terrain that could be having an influence on vegetation type or condition. Andoom is typically lower (a maximum of 20 m) than the Weipa Peninsula.

It is interesting to note that the topographically lowest areas (the western end of Weipa Peninsula and Andoom) have the 'greenest' (largest contribution by band 5) colours on the enhanced Landsat image

(Fig. 4.8). Some relationship between topography, drainage, water table and vegetation condition may well be influencing the Landsat response of these areas.

To the northwest of Andoom karst-like features are evident and are surrounded by colours similar to, or paler than, those at Andoom. Valentin (1959) suggests that these features result from collapse after the removal of silica by groundwater. Grimes (1974) has described similar depressions in the western Carpentaria Basin, and ascribes them a similar origin. To the east of this area is the Palm Creek block (1), which shows similar Landsat characteristics to the southern portion of the Hey Point block. Again according to Evans, the material here is still strongly pistolitic bauxite laterite, but not far to the north the classification changes to "partially eroded cemented ferruginous pisolitic laterite, bauxitic in places". Once again it seems likely that the Landsat characteristics are changing in sympathy with the laterite chemistry.

The changes noted could be reflecting primary variations (as in the possible explanation of 'greenness' at Andoom as being due to more exposed and redder soil). Alternatively, they could be secondary variations (such as vegetation differences) related to the laterite chemistry. Either is possible in all areas where the amount of red varies in the image. The latter possibility will be discussed further in section 4.9.

4.9 Detailed Analysis of Weipa Peninsula (Area 3 on Fig. 4.8)

4.9.1 Hydrology

On the open forested bauxite plateau at Weipa, little surface runoff is observed. Rainfall infiltration is rapid even in the wet season, with excess water draining into the shallow aquifer underlying the bauxite zone (see Figs. 4.3 and 4.4). With progression of the wet season the water table rises, eventually saturating overlying clays and bauxite/ironstone over large areas. Coffey and Hollingsworth (1971) have shown that the amount the water table rises is dependent upon but not equal to the rainfall. In fact, the rise is proportional to the rainfall in excess of 42 inches. The water table reaches its maximum height at the end of the wet season (in March or April), then gradually falls, reaching its lowest level by January before recharge.

There is a certain amount of seepage during the wet season into surface swamps and various streams that dissect the bauxite mass. Grubb (1970) suggests that these conditions are conducive to the mobilisation of iron into a ferruginous laterite, rather than bauxite. Nevertheless the hydrologic conditions presently in existence may have some relationship to the trends in Landsat imagery. This is almost certainly the case for wet-season imagery (see Section 4.9.5).

4.9.2 Vegetation

Although Specht et al (1977) mapped almost the entire Weipa Peninsula as a uniform vegetation type (Figure 4.5), optimally enhanced Landsat imagery has shown variations within the plateau. The author believes these variations are due to the vegetation cover.

An extremely good indicator of the biomass variation (TVI7) over Weipa is shown in Fig. 4.9. The west-to-east changes on the Weipa Peninsula (also seen in the colour composites) and the changes across the edge of the plateau (north to south) are easily seen in this image. The TVI highlights the west-to-east variation in green biomass, but does not explain it.

Detailed field data should throw some light on the vegetation distribution. To this end the author conducted a traverse along the peninsula by road, taking photographs at regular intervals in an attempt to pinpoint the types of variation being reflected in the Landsat data. An aerial survey was also undertaken for the same purpose, with 35mm photographs being taken from the plane window. Analysis of these photographs, and of a false colour infrared photographic survey flown by Qasco in 1970, has failed to show any obvious trends that would explain the patterns seen in the Landsat imagery. It should be noted that Specht et al (1977, p.33) said :

"It may be debated whether the flora of the E. tetradonta open forest developed over bauxite is different from that developed over lateritic ironstone. No detailed studies have so far been made in Cape York Peninsula on this subject but the broad-scale survey by Pedley and Isbell (1971) indicates that no striking differences may exist between the flora of the two soil types. This general conclusion is supported by detailed studies on the E. tetradonta open forest in NE Arnhem Land, N.T. (Specht 1958a and 1958b)".

Nevertheless the patterns on the TVI and on the histogram normalised image show beyond doubt that there is some sort of variation in the vegetation. That the nature of this variation has not yet been recognised merely points only to its subtlety.

4.9.3 Geomorphology

Two facets of local geomorphology are of some interest. The first of them involves a reassessment of data originally presented by Evans (1975). Figure 4.12a shows the original interpretation of local variations in ore thickness as a complex pattern of structural features. Areas where the greatest thickness of ore had accumulated were thought to be fold hinges. A more likely explanation (K. O'Sullivan, pers. comm., 1982) of the observed variation involves occupation by the bauxite of an older drainage pattern (Fig. 4.12b). As local geochemical variations are related to ore thickness (op. cit.), a closer examination of the data may throw more light on the mechanism of bauxite formation.

Secondly, the unusual drainage patterns surrounding the Weipa Peninsula (see Fig. 4.8), and the interpretation of linear features in some of the imagery (see overlay to Fig. 4.13) are worthy of mention.

A more detailed investigation of these facets may aid in unravelling the history of block movements in the region.

4.9.4 Landsat characteristics - dry season

Comparison of Figs. 4.13 and 4.14 illustrates the wide colour variation that can be seen in optimally enhanced imagery of the Weipa Peninsula, and the difference between imagery from dry and wet seasons.

The semi-continuous tonal variation from west to east (Figs. 4.8 and 4.13) must be explained in terms of variation of band 6 and/or 7 response. The factor most likely to influence these bands is vegetation. Possible causes for the observed phenomenon include a

change in species distribution from west to east, a change in vigour of essentially a single species (perhaps relating to the soil geochemistry), tree density, crown size/maturity or the density of undergrowth.

Section 4.9.2 established that there was no obvious variation in species distribution on Weipa Peninsula. Similarly, no obvious change in tree density, crown size or maturity could be established from colour IR aerial photography or field examination. Variation in the vegetation vigour, or the density of undergrowth, are therefore more likely explanations of the phenomenon.

Close examination of the dry-season imagery also shows a second regular variation in tonal patterns on the bauxite plateau. Around the edges of the bauxite is a fringe of brighter red, rapidly falling off towards the centre of the peninsula. This is a common effect at the edges of a laterite, where break-up of the hard surface facilitates water movement and new soil development. In the case of the Weipa Peninsula, a shallow aquifer is closer to the surface here as well, resulting in a more accessible water supply. A combination of these factors results in denser, more vigorous vegetation along the plateau border.

4.9.5 Landsat characteristics - wet season

An optimally enhanced wet-season image of the Weipa Peninsula is shown in Fig. 4.14. It is clear that the regular west-to-east variations noted in the previous sections are not repeated. Instead of the gradational change in tone from one end of the peninsula to the other, there is a heightening of the plateau-edge effect noted in the

dry-season imagery. The borders of the plateau appear to be deeper in colour and they form a much broader red zone, with more obvious gradation into a central, greener area. The effect is also obvious in a colour ratio composite (Fig. 4.15), and can be adequately explained by looking at variations in the level of the water table. Comparison with Fig. 4.16 shows that the greener areas correspond to areas of greatest average wet-season water table rise. It is possible that the phenomenon being observed is one of moisture stress on the vegetation, with the more broken and better drained ground at the edges of the plateau better able to cope with the high rainfall, resulting in 'healthier' vegetation and higher infrared signatures. It should be kept in mind, however, that this is a subtle effect seen only on enhanced images. There is obviously a major difference at Weipa in the vigour of vegetation between seasons. The more luxuriant growth present during the wet season appears to mask the subtle, west-to-east variations observed on dry-season imagery.

4.9.6. Soil geochemistry trends

Evans (1975, p.962) noted the existence of a "broad regional decrease in alumina and increase in silica eastward from the coast ...". This statement, along with the trends observed on enhanced Landsat imagery, prompted the present study. A limited soil-sampling program was carried out, during August, 1981, to test whether this trend occurs on the surface. Twenty-two samples, mostly collected on an east-to-west traverse along the Weipa Peninsula, were analysed for silica, alumina, titanium and iron. Sample locations and analytical results are presented in Table 4.1 and Figs. 4.17 to 4.20.

Table 4.1 Weipa soil sample grid coordinates and SiO₂, Al₂O₃, TiO₂ and Fe₂O₃ analyses.

Grid Coords.		SiO ₂	Al ₂ O ₃	TiO ₂	Fe ₂ O ₃
E	N				
2W	35	19.7	35.3	2.18	24.00
12	10	32.3	36.5	1.98	6.50
18	10	39.8	35.4	1.82	4.66
21	32	31.3	37.1	2.04	7.05
24	10	30.8	39.6	2.10	5.65
28	10	48.6	29.3	1.82	4.58
32	10	46.6	23.3	1.32	6.30
36	10	45.1	29.1	1.54	3.60
40	10	30.6	40.1	1.95	8.85
46	10	51.0	25.8	1.59	4.00
50	10	48.7	27.2	1.46	4.40
50	20	54.7	21.5	1.41	2.72
50	30	60.8	12.3	0.65	16.50
54	20	64.7	17.0	1.20	2.65
64	18	65.4	17.3	1.26	2.34
64	20	49.5	26.7	1.38	4.68
66	20	49.7	26.1	1.51	3.96
70	20	55.6	22.4	1.23	6.35
74	20	49.7	27.4	1.56	4.94
78	20	58.6	20.4	1.44	3.86
82	20	82.1	7.9	0.79	1.33
90	35	50.9	25.3	1.37	4.88

Figure 4.17 shows that silica increases, and Fig. 4.18 that alumina decreases, moving from west to east. Titanium soil values (Fig. 4.19) also indicate a general decreasing trend from west to east along the peninsula. The iron values are presented as percentage Fe_2O_3 and these also show a slight trend in the same direction (Fig. 4.20). All of these trends are compatible with increased leaching of residual soil towards the west.

Given that one might expect a larger contribution from green (band 5) and a smaller contribution from red (band 7) with an increasing amount of iron in the soil, it is possible that the image colour variation along Weipa Peninsula might be due, at least in part, to the observed variation in iron content. The soil geochemistry data presented here do not exclude this possibility, but a more detailed study would be required to confirm it (see section 4.9.7.1).

Whilst only the largest trees may be rooting in the ore horizon (and thereby affected by its geochemistry), the existence of geochemical variation at the surface means that the explanation of the observed variation in the Landsat imagery should also consider the effects of the rest of the vegetative cover.

4.9.7 Laboratory reflectance spectra of soils

The soil samples referred to above were also measured for their VNIR and SWIR reflectance in the laboratory. Representative examples appear with the text, but all spectra appear in Appendices II (VNIR), and III (SWIR).

The geochemical analyses of surface soil samples allow discernible trends to be established from west to east along the peninsula. Because these analyses were based on major element composition this trend was thought likely to be mirrored in the mineralogical composition of the samples, hence in their spectral reflectance curves. The mineralogy of bauxites - iron oxides, kaolinite, gibbsite, boehmite and quartz - is amenable to spectral measurement, with iron oxides producing absorption features in the VNIR (Fig. 2.2), and kaolinite and gibbsite known to produce features in the SWIR (Figs. 2.5 and 4.21). Boehmite could not be isolated for spectral measurement, nor could its SWIR spectrum be found in the literature. However, Farmer (1974) presents IR absorption data for boehmite which shows that it has two features in the ν_{OH} region (3283 and 3087cm^{-1}), and a single OH bending feature at 1160cm^{-1} . Combination of these features could be expected to produce its strongest absorption near the wavelengths $2.25\mu\text{m}$ (similar to gibbsite) and $2.35\mu\text{m}$. Because the SWIR spectra presented here are likely to result from the combined influence of gibbsite and boehmite, features in the 2.25 to $2.28\mu\text{m}$ region will therefore be attributed to 'bauxite minerals'. Quartz will produce spectral features in the MIR, but facilities were not available for these measurements at the time of the study.

4.9.7.1 VNIR spectra

Representative examples of VNIR laboratory spectra of Weipa soils appear in Figs. 4.22a-c. Most of the soil samples are grey in colour, presumably because of contained humic material, but a few have a pale red colour. All samples contain some pisolites. A magnet was passed over each sample, showing that all samples also contain some magnetic

material. Therefore, the iron content of each sample (determined by wet chemistry, and expressed as Fe_2O_3) will not be a true indication of the haematite or goethite content, and thus may not directly relate to the depth of absorption in the .85 to .90 μm region. If the magnetic material is magnetite, the most likely effect on the VNIR spectrum will be a reduction of the reflectance at all wavelengths (see Hunt *et al.*, 1971a).

In fact, most of the samples measured show no iron absorption features at all (Fig. 4.22a). A few samples (those containing greater than about 6% Fe_2O_3) show very weak absorption features in the .87 μm region (Fig. 4.22b). In contrast, a sample of cemented pisolites from Andoom exhibits strong haematitic absorption near .88 μm (Fig. 4.22c). Therefore, except in those rare cases where concentrations of haematite-rich pisolites occur at the surface, the contribution by soils to the observed trends in Landsat values at Weipa (greenness of the image) is likely to be negligible. Insufficient data are available to draw the same conclusion about the Andoom area.

4.9.7.2 SWIR spectra

The majority of the SWIR laboratory spectra show the characteristic minimum, near 2.27 μm , of the bauxite minerals (see Fig. 4.23a). This is quite an unusual wavelength, most hydroxyl-bearing minerals absorbing at wavelengths just longer than 2.2 or 2.3 μm . Therefore, in this environment, the presence of these absorption features is diagnostic, and likely to be of considerable use in an exploration program.

In addition, all of the SWIR spectra measured show 2.2 μm absorption features. Most are too weak to be identified, but the strongest are

indicative of kaolin (Fig. 4.23b). Figure 4.23c depicts the most common type of SWIR laboratory spectrum of the Weipa soils. In these cases, weak absorption features at both wavelengths are present, indicating a probable mixture of kaolin and bauxite minerals. The bauxite 'signature' is likely to originate from the pisolites, whilst the 2.2 μ m absorption is more likely to be due to the finer-grained soil fraction.

In Fig. 4.23d, the spectrum of a cemented pisolite ore sample is included for comparison. Note the similarity of this spectrum to Fig. 4.21.

These results are not as definitive (particularly for the VNIR) as the geochemical trends. A more comprehensive survey (preferably of in situ material) is needed to evaluate fully the utility of SWIR remote sensing at the test site. Nevertheless, the results do show that the SWIR can give an indication of the presence of ore minerals at the surface.

4.9.8 Bauxite drilling geochemistry trends

In order to quantify the general statement of Evans (1975, p.962) on trends in the bauxite grade, and to make a comparison with results from the surface geochemistry study, the Commonwealth Aluminium Corporation Pty Ltd (Comalco) drilling data from Weipa Peninsula were obtained and examined. The drilling was done to establish regional grade trends, and was therefore sited on centres spaced at 2000 feet.

Figures 4.24 and 4.25 show respective plots of total average percentage SiO₂ and total average percentage Al₂O₃ (for individual drill holes) versus grid position. Data were taken from the most complete

drilling line available - the 20,000N line. Silica shows a rough increase from west to east, while alumina shows the opposite trend. Note that the Al_2O_3 values vary in the same manner as the soil geochemistry but are, on average, 20% lower in the soil samples than in the ore-grade material. On the other hand, SiO_2 values are 10 to 40% greater in the surface soil samples.

Because the trends viewed with Landsat are regional, and in order to include all of the available data, both sets of data were plotted again, this time reducing each of the north-south grid lines to an average value and plotting that value against east-west grid position (Figs 4.26 and 4.27). The results show stronger, more regular trends along the peninsula.

4.9.9 Image display of bauxite geochemistry

For displaying the available data in its entirety, geochemical values were entered into an image file. An example of the resulting 2-D pictorial representation appears in Fig. 4.28. With the application of a linear stretch to spread the observed geochemical values over the grey-level range 0-255, followed by density slicing, essentially the same trends emerge. Hotter colours, representing high geochemical values, appear in the west, with cooler colours appearing progressively towards the east.

The geochemical images were then resampled to bring them into registration and enable comparison with Landsat data. Figure 4.29 shows the resampled Al_2O_3 values with, of course, the same trends as Fig. 4.28. Figure 4.30 is the resampled total SiO_2 image, with an inverse

relationship to Al_2O_3 . Cooler colours are due to low values near the coast, with warmer colours indicative of higher percentages further inland.

Figure 4.31 displays values of ore thickness. A poorly defined pattern is apparent, with the thickest ore located to the south and to a lesser extent, the north of the peninsula, and with the thinnest zone running approximately west to east along the centre of the area. The structure therefore appears to be gently warped about an east-west axis.

4.9.10 Landsat/bauxite geochemistry correlation

Once the Landsat and geochemical images were spatially registered it became possible to undertake a statistical analysis of the data. The method used involved training areas chosen for relative homogeneity with respect to either Landsat image character (i.e. uniformity in colour and tone), or else geochemical values. Figure 4.32 shows the resultant training areas superimposed on the geochemistry grid (blue) and Landsat values from band 5 (green) and 7 (red).

Statistics (means, shown in Table 4.2, standard deviations and correlation coefficients for all Landsat and geochemical parameters) were then calculated for individual training areas. Some areas were rejected at this stage for a number of reasons. For instance, areas 1 and 11 fall directly over the road, which has high radiance values in all bands, and are therefore anomalous. Of areas that largely overlap, only one was included in the final analysis. Thus, training area 5 was rejected in favour of training area 15, and so on. An area was also rejected if composed of less than 100 Landsat pixels. It should also be noted that statistics were calculated only for areas where both Landsat

Table 4.2 Mean values of various Landsat MSS values and Al₂O₃, and their correlation coefficients, for Weipa training areas.

Training Area	5/6 Ratio x100	Band 6	Band 7	Al ₂ O ₃ (%)
1	126	112	62	54
5	129	100	57	50
6	113	172	71	50
7	121	102	58	52
8	114	122	74	51
12	75	144	100	48
14	128	124	71	51
15	123	102	57	49
17	75	144	100	48
18	81	139	93	48
A	0.74	-0.59	-0.68	1
B	0.69	-0.46	-0.55	1

A = correlation coefficients with Al₂O₃ for all training areas.

B = correlation coefficients with Al₂O₃ for areas 6, 7, 8, 14, 15 and 18 only.

and geochemistry data were available. Thus only a portion of training area 8 was treated.

Six training areas (Table 4.2) were ultimately selected and the mean values of the relevant variables estimated for each area. The most important variables used were Landsat bands 6 and 7, Landsat 5/6 band ratio (as a rough vegetation-index similar to TVI7), and the Al_2O_3 concentration. Correlation coefficients were then calculated using these mean values.

Table 4.2 also shows the Al_2O_3 concentration compared with the Landsat 5/6 band ratio. The relatively high correlation (0.69) using these limited data supports the qualitative observation (that a relationship exists between bauxite geochemistry and Landsat values) made as a result of interpretation of the histogram-normalised imagery.

4.10 Significance of Bushfires in Utilisation of Landsat Imagery

Bushfire scars are clearly evident even on unenhanced Weipa imagery. On Weipa Peninsula fires are generally started intentionally for a variety of reasons. If left for too long the undergrowth builds up to levels that become uncontrollable when they do ignite. Drilling crews also find progress much easier in recently burnt areas. Whatever their cause, fires are more likely near human activity. On the western end of Weipa Peninsula there is a considerably greater density of people compared to the eastern end. There has also been more drilling activity in this area, and, it may be assumed, more fire activity. The vegetation (Landsat MSS 5/6 ratio) correlation with geochemistry could thus result from the short term or cumulative effects of burning.

Several factors make this possibility less likely. Firstly, local Comalco staff assure the author that almost the entire peninsula is burnt every year, including the eastern end. Secondly, fires burn with different intensities at different times of the day. In most cases the undergrowth is almost completely destroyed, but only in the middle of the day does a fire burn with sufficient intensity to affect the upper portions of the (generally) tall trees. In this case the leaves on such a tree might wither and fall off within days. However, if fire were causing the documented effects, one would expect on this basis that the dominant patterns noted would be much more restricted in area - reflecting local intensity variations rather than regular regional trends.

Thirdly, it was noted in Section 4.7 that broad variations in the nature of the bauxite, in areas other than Weipa Peninsula, seem to match the observed Landsat tonal character. It seems unlikely that these trends could be caused by bushfires alone.

Needless to say, bushfires, which can become very extensive by the end of the dry season, reduce the effectiveness of Landsat spectral studies. From some multirate images studied it was observed that, during June, July and early August, fires are not very extensive. By late August and early September most parts of the plateau have become totally burnt. Image acquisition in this area, and other tropical study areas, would need to take these factors into account.

4.11 Detection of High-Grade Bauxite Areas

On the basis of the analysis completed thus far it may seem reasonable to assume that we could detect higher-grade bauxite areas

using optimally enhanced Landsat imagery. For instance, it may be that 'greenness' indicates higher Al_2O_3 grades at Weipa. At Andoom, however, the entire block seems 'greener' than Weipa, though this may be due to factors other than Al_2O_3 concentration (see Section 5.7). Add to this the Weipa Peninsula's uniqueness in this region, as the only block where a shallow aquifer is known. Presumably the aquifer's groundwater affects both the vegetation, and perhaps the bauxitisation process to some extent. As a result the application of results from Weipa, even to neighbouring areas, would depend on a thorough knowledge of the mechanisms involved in the formation of ore.

Nevertheless the image enhancement techniques described here do add an increment of information to that available from other sources (e.g. aerial photos) and, at the very least, are useful in the identification of patterns that can be followed up on the ground.

More quantitative application of the numerical techniques to areas outside Weipa Peninsula would have to wait on the more complete formulation of a reasonable model.

4.12 Regeneration Studies Using Landsat MSS Data

Comalco are committed to regeneration of the terrain following the mining procedure. A brief look at recent wet-season imagery over the Weipa and Andoom mines shows that healthy vegetation is currently growing over mined-out areas (Figure 4.33). Bare soil shows up white with high reflectance in all bands, and land covered with felled but uncleared trees shows as a blue-grey colour. Healthy vegetation is, of course, red in colour. Various shades of pink reflect varying maturities and types of regenerated forest.

Thus, multirate Landsat imagery should easily be able to monitor progress in the revegetation program where such large areas are involved. It will become particularly relevant with the advent of 30 m, Landsat D, TM imagery in Australia, which should also provide a better discrimination of vegetation and vegetation state.

4.13 Summary

The CSIRO/MXY produced a histogram normalised Landsat MSS image (bands 4, 5 and 7 colour composite) covering Weipa, the largest bauxite deposit in the world. This image discriminates the bauxite and aluminous laterite, developed on the western edge of Cape York Peninsula, from other geological units.

Detailed examination of the imagery by the author shows that there are variations in the colours exhibited by bauxite/laterite. On a regional scale, these variations correlate well with generalised observations on changes in the nature of the bauxite/laterite. Poorly developed laterite, for instance, appears pale (resembling underlying Cretaceous sediments) in comparison to well developed laterite.

There are also significant colour variations within areas of well developed laterite, particularly in the amount of red (band 7 contribution) in the image. This is therefore likely to be a result of variations in the vegetative cover.

Over Weipa Peninsula, where bauxite grades are highest and ore is currently being mined, there is a progression from greenest (dominance by band 5) to reddest tones from west to east on the imagery. Existing vegetation maps show no corresponding species variation. Field

observations and examination of aerial photography failed to reveal any obvious changes in tree density, crown size, or maturity along the peninsula. Although bushfires are common in the area, they are not likely to cause the regular changes seen on the imagery. The cause of the variations is therefore most likely to be related to changes in the vigour of the vegetation dominating the peninsula. However, the exact nature of the link between Landsat and bauxite geochemistry has not been established, nor has it been determined whether it is a direct, or an indirect relationship.

The colour variations are present only on dry-season imagery. Wet-season imagery appears to be dominated by effects related to the height of the water table.

The soil geochemistry shows variations in alumina, silica, titanium and iron that establish a quantitative basis for the previous qualitative observations on geochemical variation in the bauxite. There is a decrease in alumina, titanium and iron, and an increase in silica from west to east along Weipa Peninsula. The presence of these trends in the soil overlying bauxitic soil suggests that variations in the Landsat imagery could be related to the soil itself (i.e. varying iron content affecting band 5), or to the understorey, rather than due solely to trees that root in the ore zone (bands 6 and 7).

However, laboratory measurements of the VNIR spectra of soils show almost no absorption features attributable to iron, making a direct contribution to the Landsat response extremely unlikely on Weipa Peninsula. There are insufficient data to draw the same conclusion about the Andoom area.

Measurements of the SWIR spectra of the soil samples show the presence of features likely to be caused by kaolin and bauxite minerals. This finding is significant from an exploration viewpoint, because one would not necessarily expect to see signatures from these minerals in what amounts to ore overburden.

Variations in the ore geochemistry (from drilling data) also confirm the qualitative observations on variation of ore quality, and show similar trends to the soil geochemistry. Integration of the ore geochemical and Landsat data allowed correlation coefficients to be calculated. Values as high as .69 (between Al_2O_3 and MSS band ratio 5/6) have been established.

Although the relationships outlined above do not allow formulation of a definitive model, it is clear that the Landsat MSS imagery provides a useful increment of knowledge. Both Landsat imagery and high-resolution spectral measurements are therefore likely to be of some assistance in exploration for further deposits, or the rapid evaluation of known reserves. Landsat MSS imagery would also be of use in monitoring the regeneration of mined-out areas.

CHAPTER 5 MT TURNER PORPHYRY COPPER SYSTEM, GEORGETOWN INLIER, QUEENSLAND

5.1 Introduction

To date, the majority of remote sensing research has been undertaken in the U.S. A good deal of this research has concentrated on the porphyry copper deposits of the southwestern U.S., because of their size and the nature of the associated alteration products providing outstanding targets for both VNIR (iron oxide) and SWIR (clay mineral) remote sensing techniques.

The Mt Turner porphyry copper system has many characteristics similar to equivalent systems in the U.S. In particular, its size and alteration mineralogy are comparable to those of the U.S. counterparts, although the copper grades are very much lower. Mt Turner was therefore chosen as a test site to enable a comparison between its spectral properties and the published descriptions of a U.S. equivalent, the Silver Bell porphyry copper system.

Previous remote sensing investigation (Huntington, pers. comm., 1983) has shown that the Mt Turner system is detectable on Landsat MSS imagery because of anomalous iron (relative to the immediate environs) and vegetation, over the main alteration zone. However, several other, more distal, areas on the Landsat image have similar signatures, yet are not related to a porphyry copper system.

Therefore, the specific aim of the study is to identify the mineral assemblages due to alteration, and to discriminate them from assemblages due to weathering (which are widespread in the Australian environment).

The investigation includes processing and interpretation of airborne data, a field investigation, and laboratory spectral measurement of samples collected in the field. Some XRD and microprobe analyses were also obtained to aid the interpretation of the spectral data.

5.2 Regional Geological Setting

Immediately to the west of the Palaeozoic to early Mesozoic Tasman Orogenic Zone lies the Georgetown Inlier, comprising Proterozoic metamorphics and granites, and Palaeozoic volcanics and intrusives. In the north-western part of the Georgetown Inlier lies the Mt Turner porphyry copper prospect.

5.2.1 Host geology

The middle Proterozoic basement has been subdivided into Robertson River Formation, Delaney Granite, Aurora Granite and Forsayth Granite (Withnall, et al., 1980). The Robertson River Formation comprises mica schists and micaceous quartzites intimately associated with meta-dolerite, metagabbro, and amphibolites (mapped as dolerite). It has undergone multiple phases of deformation and metamorphism that have been radiometrically dated at 1570my, 1470my and 970my (Black, 1973). This work establishes a minimum age of 1570my for the Robertson River Formation. Outcrop is poor, vegetation moderately abundant, and iron-oxide staining widespread and severe. Minerals that produce absorption features in the SWIR are muscovite from the schists and quartzites, chlorite from the schists (and some basic rocks), and amphiboles from the basic rocks. Kaolin is sometimes present as a weathering product of feldspars, and is found both in schists and basic rocks.

The predominant basement rock in the survey area is the Delaney Granite - a medium-grained, porphyritic, muscovite-biotite granite. The Aurora Granite is a coarse to medium-grained, equigranular, leucocratic, muscovite-biotite granite-granodiorite, while the Forsayth Granite is a medium to coarse-grained, generally strongly porphyritic, biotite granite, that has been radiometrically dated at 1040my (Richards et al., 1966). The unaltered granitic terrain is topographically very subdued, outcrop generally being found only in creeks, or as groups of large, rounded boulders. Vegetation is sparse, with only scattered trees and light grass. By far the greatest contribution to the spectral response of these areas is from the ground surface, which is covered by a 'lag' of sand-sized grains derived from weathering of the granites. The major components of this lag are quartz, feldspar, and muscovite, quite a range of soil colours being produced by variable amounts of iron oxide staining (almost white in some areas, to very red in extreme cases). The feldspar grains often have a cloudy appearance due to breakdown to clay minerals during weathering. Muscovite flakes tend to lie flat on the surface, hence contribute a much larger portion of the total surface area than their true volume would suggest. Clays from the breakdown of feldspar and muscovite are the only components of the lag that will produce spectral features in the SWIR, while iron oxide staining will produce absorption at longer wavelengths in the VNIR.

Post-Proterozoic igneous activity is represented by the Mt Darcy Microgranodiorite - a strongly porphyritic biotite microgranodiorite containing ellipsoidal quartz phenocrysts. Associated with the microgranodiorite is a series of rhyolite plugs and dykes, mostly porphyritic, with feldspar and ellipsoidal quartz phenocrysts. The rhyolite often exhibits flow banding. Mapping by Bureau of Mineral

Resources (BMR) and Geological Survey of Queensland (GSQ) geologists has shown that the Post-Proterozoic intrusive history is complex at both Mt Turner and Mt Darcy. Several phases of intrusion have been recognised, with rhyolite stocks, associated breccia bodies, and north-south trending dyke swarms being interpreted as an early event. Several pulses of microgranodiorite, with associated breccias, followed. Detailed descriptions of these rocks, along with an interpretation of the sequence of events in the intrusive history, appear in Publication 379 of the Queensland Department of Mines (Baker and Horton, 1982). Where unaltered (only in the Mt Darcy area), these rocks occur in terrain very similar to the Proterozoic granites, and produce similar mineral assemblages from weathering.

Also occurring in the survey area are the remnants of Mesozoic sediments. They are commonly conglomeratic, and lie unconformably on older rocks. In some places they are associated with an underlying pallid zone, that largely comprises kaolin.

A simplified version of the geology at Mt Turner, derived from BMR 1:25,000 compilation sheets, appears as Fig. 5.1.

5.2.2. Alteration and mineralisation

Accompanying the Mt Darcy microgranodiorite and rhyolite igneous events was an extensive system of alteration and weak mineralisation. Two separate phases have been interpreted (Baker and Horton, 1982), the first and most extensive consisting of three concentric alteration zones centred on the main microgranodiorite stock.

The arrangement of these alteration zones is shown in overlay (A) to Fig. 5.2. The central area consists of biotite alteration, which

grades outwards onto a silicified and sericitised zone with disseminated and vein-controlled pyrite. Although fissure-controlled, for remote sensing purposes this zone can be considered as pervasively altered. The silicification has resulted in a series of low hills rising steeply more than 100m above the surrounding, fairly subdued, Proterozoic terrain.

A large percentage of these hills is covered by outcrop, float, or weathering products from the altered rocks. Every sample examined within this zone appeared to have been affected by the alteration processes to some extent. In addition, the presence of sulphides in the original rock has resulted in widespread iron staining, and the vegetation over this area is considerably thicker than over the low-lying areas. The rhyolite dykes, in particular, have a dense coverage of small, dark trees, making their presence obvious on aerial photography (Fig. 5.2).

The peripheral zone is arbitrarily defined as being outside the low hills of the silicified zone, and comprises a less dense distribution of quartz-filled fissures controlling sericite-chlorite-kaolinite-calcite, and epidote-chlorite-sericite alteration. The alteration is generally restricted to an envelope a few metres each side of the vertical fissures.

The second phase of alteration recognised by Baker and Horton (1982) is sericite-chlorite-kaolinite similar to the silicified-zone alteration. It is mainly recognised where it overprints the earlier biotite alteration (see overlay A to Fig. 5.2).

Late-stage sulphide veins up to 1m wide occur in the silicified and its peripheral zones. In the peripheral alteration zone the veins contain predominantly galena and sphalerite. Several of them have been mined for silver and lead, and Table 5.1 (after Baker and Horton, 1982) shows the recorded mine production.

Table 5.1 Recorded production from mines in the vicinity of Mt Turner (after Baker and Horton, 1982)

Mine	Ore (tonnes)	Gold (kg)	Silver (kg)	Lead (tonnes)	Copper (tonnes)
Aspasia 1916-29, 1936-37, 1947-52	716.0	1.168	457.064	285.4	0.8
Cobar Line of Reef 1911-29, 1937, 1947-50	879.5	0.862	447.795	332.2	0.2
Three Musketeers 1925-65	0.003	29.540	25.1	-	-
Morning Light 1904-10	498.4	21.219	-	-	-
Drummer Hill	No recorded production				

The overall sulphide content of the Mt Turner porphyry deposit has been estimated at less than 0.5%, with copper and molybdenum content estimated to be .01% (Baker and Horton, 1982). Present indications are therefore that the deposit is uneconomic.

Table 5.2 summarises the geological characteristics of Mt Turner and compares them to the Silver Bell porphyry copper deposit in Arizona, in the southwestern U.S. Silver Bell has been the subject of considerable remote sensing research, in particular as a test site in the Joint NASA/Geosat Test Case Study (Abrams et al., 1984).

5.3 Previous Remote Sensing Investigation

Previous work by the CSIRO/MXY Remote Sensing Group (J. Huntington, pers. comm., 1983) on Landsat imagery of the Mt Turner scene shows that the silicified alteration zone can be detected on a standard colour composite (Fig. 5.3). The topographic high, and presence of vegetation denser than the surrounding area, make this possible. A colour density-sliced ratio image (Fig. 5.4), depicting denser vegetation in blue tones, enhances the alteration zone quite effectively. In addition, a technique, similar to that of Segal (1983), for enhancement of limonitic zones in vegetated areas, was used to produce the colour ratio composite in Fig. 5.5. It depicts limonitic areas in shades of green, and vegetated areas in shades of red. This presentation discriminates Mt Turner from its immediate surrounds, but not significantly from some other iron-rich areas, such as mafic intrusives in the Robertson River Formation.

Table 5.2 Comparison of Mt Turner with the Silver Bell porphyry copper deposit (using data from Baker and Horton, 1982 and Abrams and Brown, 1984)

Feature	Silver Bell, USA	Mt Turner, Queensland
<u>1. Igneous Host Rock:</u>		
Shape	Elongate, irregular	Elongate multiple plugs, circular with radiating dykes
Controlling structures	Faults	None (?)
Sequence of intrusion	Qtz monzonite-rhyodacite	Rhyolite-granodiorite
Rock types mineralised	Pre-ore and host rock	Pre-ore and host rock
<u>2. Orebody</u>		
Shape	Oval, pipelike	Oval, pipelike
Dimensions	2500 x 2000m	2400 x 4000 m (to edge silicification)
Hypogene grade	0.4% Cu	0.01% Cu and Mo
<u>3. Peripheral Zone:</u>		
Alteration	Epidote, chlorite, calcite, sericite	Sericite, chlorite, epidote, kaolin
Mineralisation	pyrite (veins)	Galena, sphalerite, Ag (veins)
<u>4. Intermediate Zone:</u>		
Alteration	Quartz, sericite, clays	Quartz, sericite, kaolin, chlorite
Mineralisation	Pyrite, chalcopyrite (veinlet disseminated)	Pyrite, chalcopyrite, sphalerite (veinlet disseminated)
<u>5. Innermost Zone:</u>		
Alteration	Quartz, K-feldspar, biotite, anhydrite, sericite	Quartz, sericite, K feldspar, biotite, andalusite
Mineralisation	Pyrite, chalcopyrite, molybdenite, (veinlet disseminated)	Pyrite, chalcopyrite, molybdenite, bornite (veinlet disseminated)
<u>6. Breccia Pipes:</u>		
	Present and mineralised	Present and mineralised
<u>7. Supergene sulphide:</u>		
	Chalcocite	None

However, in the case of the Phyllis Mae prospect (arrowed in Fig. 5.5, to the west of Mt Turner) the distinct topographic and vegetation anomalies do not exist. The limited spectral capability of Landsat MSS is therefore unable to provide any indication of a mineralised environment in this area.

In addition to the CSIRO's work, and at the same time that the author was interpreting the high-resolution airborne data from Mt Turner, the survey contractor (GER Inc of New York) undertook a preliminary interpretation of the same data set. This was done without the benefit of ground-truth information. In their report (GER, 1983), they make some general observations that are duplicated in this thesis, but which bear repetition. Firstly, GER observed that all Australian mineral absorption features are weak in comparison to those detected in US surveys. This can be attributed to differences in the weathering histories of the two continents, with Australia's more severe weathering masking many of the spectral variations which would be seen in fresh rocks (see chapter 2, this thesis). Secondly, the presence of an ubiquitous phyllosilicate assemblage at Mt Turner was noted by GER, and illustrated in a "stacked profile" (GER, 1983, Fig. 3-8). They ascribed this to kaolin, whereas field checking, laboratory measurement of samples, and XRD analyses show that a mixture of muscovite/sericite and kaolin is responsible.

GER also utilised a waveform analysis technique (Tchebychev Analysis) for treatment of the Mt Turner data. Section 5.5.5.1 details the author's results using the same procedure. GER's results closely match the author's interpretation of the 'second-order effects' present in log residual images (see section 5.5.3). The major conclusion of

GER's report was that the area of greatest spectral absorption, attributed largely to muscovite, occurs outside the boundary of the main alteration zone (the author has pointed out that this is due to the increased vegetation density over the alteration zone, see section 5.5.3). GER made no distinction between the mineralogy over, and outside, the main alteration zone.

5.4 Laboratory Spectral Measurements

A fairly detailed field sampling program was completed, most sampling points being predetermined by examination of the airborne data (section 5.5.4). This was an attempt to explain some of the more subtle spectral variations present in the data. Samples of all major rock types and soils were collected, and more than 450 spectra were measured from the resulting collection. For many hand specimens, multiple spectra were recorded from weathered and 'fresh' (broken) surfaces. The spectral collection produced is too voluminous to reproduce here in its entirety, so only a few representatives of the major spectral types will be presented in the text. Spectra of those samples that have accompanying XRD analyses are presented in Appendix IV.

5.4.1 Weathering effects

One significant feature of the spectral collection is the relationship between weathered and 'fresh' surfaces. (For most samples from Mt Turner, fresh is a relative term, since samples in hand-specimens are usually pervasively altered or affected to some extent by weathering.) Almost without exception, absorption features present for fresh surfaces can also be seen from weathered surfaces, albeit as more

subdued effects. This rule holds even when a significant surface rind is present (Figs. 5.6a&b). The only cases from Mt Turner where it does not apply seem to be samples influenced by lichen on their outer surfaces (Figs. 5.7a&b). Lichen tends to flatten the spectrum, especially noticeable between 1.9 μ m and 2.2 μ m. In addition, the slope from 1.9 μ m to shorter wavelengths can be increased quite dramatically. At Mt Turner, though, the lichen is not likely to affect airborne survey results drastically, because it tends to gather most densely directly under heavy vegetation-cover - for instance on rhyolite dykes. In such cases the vegetation will probably provide the strongest response from its particular pixel.

5.4.2 Vegetation effects

Figure 5.9 shows the respective spectra of healthy, green vegetation, and of dry grass. Healthy vegetation will affect the log-residual spectra in two ways. Firstly, its presence means that less of the geology in a given pixel will be 'seen', thereby reducing the influence of mineralogical absorption-features. Secondly, absorption by moisture in the plant will cause a fall-off towards the water bands at 1.9 and 2.5 μ m. Healthy vegetation (although not as healthy as the sample shown in Fig. 5.9) is most common within the silicified alteration zone, and so has its greatest influence there.

The dry grass measured shows strong, broad absorption features at 2.1 and 2.3 μ m, due to cellulose. The loss of moisture in the foliage lessens the absorption by water, and the spectral features of cellulose can subsequently be seen. This leads to difficulties in differentiating

the effects due to vegetation from those of mafic minerals with absorption features in the same (2.3 μ m) region (see Section 5.5.6).

5.4.3 Laboratory spectral types

The 450 rock and soil samples measured can be divided into four main classes, although there are many cases where absorption features are intermediate between these 'end-members'. These four classes, which have been called Kaolin-, Sericite-, Muscovite- and Mafic-type spectra, are shown in Figures 5.9a-d.

5.4.3.1 Kaolin-type spectra

The Kaolin-type spectra (Fig. 5.9a) have the familiar characteristics of kaolin, with a major absorption feature near 2.2 μ m, and a doublet (seen here as a subtle shoulder) near 2.17 μ m. XRD analysis shows that, in most cases, the kaolin is present in proportions ranging from less than 5% and up to 20%. Quartz and feldspar are generally the dominant minerals (but have no SWIR spectral properties), and muscovite is almost invariably present, albeit in amounts similar to, or smaller than, kaolin. Exceptions are the samples from Cretaceous conglomerates and their associated pallid zones from MT5 and MTPM. Here the proportion of kaolin in the samples is greater than 20%. The Kaolin-type samples are almost invariably from outside the silicified zone, and represent the surface residuum from weathered (but unaltered) granites, or the granites themselves.

5.4.3.2 Muscovite-type spectra

Muscovite-type spectra (Fig. 5.9b) exhibit a single, strong absorption feature near $2.2\mu\text{m}$, and can be produced by the same surface residuum as the Kaolin-type spectra where its muscovite content is higher, or from the weathering products of the Robertson River Formation. This type of spectrum has been produced by less-altered samples and soils from within the alteration zone, but is much more common outside it.

5.4.3.3 Sericite-type spectra

Sericite-type spectra (Fig. 5.9c) are always derived from altered rocks. XRD analysis shows quartz and 'muscovite' only in the most-altered rocks, and various other minerals in less-altered samples. XRD has been unable to differentiate between the 'muscovite' (actually sericite) of the altered rocks, and that of the unaltered suite. The major difference between the Sericite-type and Muscovite-type spectra is the presence of secondary absorption features near 2.35 and $2.45\mu\text{m}$. An examination of the CSIRO/MXY collection of spectra yields several of muscovite. The secondary wings are present in them, but vary quite widely in strength. Because sericite (from within the alteration zone) and muscovite (outside it) have formed by different processes, it is not unreasonable to expect that their trace-element composition might be different. This hypothesis was checked by ion-microprobe analysis, but the results showed that there was no significant difference in composition between the samples examined (D. Cousens, pers. comm., 1984).

To investigate the phenomenon further, all altered-rock (sericitic) laboratory spectra were isolated from the background (muscovitic) spectra in a computer file. The two sets of spectra were then averaged to produce Figs. 5.10a&b. The background slope was removed from the averaged spectra using the "hull quotient" technique (Green and Craig, 1985), which has the effect of isolating the absorption features, enabling determination of their true shape. This process showed that the two groups of samples in fact have almost identical absorption features (Figs. 5.11a&b). The untreated reflectance spectra look different only because the Sericite-type spectra have much stronger absorption in all bands.

This process was carried further by sub dividing the spectra into smaller groups based on their nature (rock versus soil), and the rock type from which the sample was derived (Robertson River Formation, granite, etc.). Again, the results show that most spectra have a similar structure (see Appendix V).

5.4.3.4 Mafic-type spectra

Mafic-type spectra (Fig. 5.9d) contain absorption features in the 2.3 μ m, and longer, region due to the presence of amphibole, chlorite, clinozoisite or epidote. These minerals are present in two different environments. Amphibole and minor chlorite can occur as components of the mafic intrusives associated with the Robertson River Formation, or in the schists themselves. Chlorite, clinozoisite, and epidote can also occur as propylitic alteration-products in both the Mt Turner and Phyllis Mae regions.

5.5 Airborne Spectrometer Data

5.5.1 Acquisition

Overlay (B) to Figure 5.3 shows the location of the nine flight-lines flown over Mt Turner. In addition, a single line, MT5, was flown to the northwest, largely covering Robertson River Formation schists and dolerite. The data were acquired on the 27th September, 1982. Unfortunately the inverter supplying power to the spectrometer system overheated and failed several times during data acquisition. There was thus a significant time-difference between coverage of some flight lines. Lines MT4, MT7 and MT6 were flown between 12:26 pm and 12:45 pm, MT2 at 1:43 pm, and the remaining lines between 2:05 pm and 4:18 pm. The resultant variations in sun angle and shadowing, combined with shadowing caused by low-level cloud late in the afternoon, make the data set somewhat less than optimal. Some attempts to correct for these effects were made during data-analysis, as discussed below.

5.5.2 Analysis of radiance data - 'first-order' effects

The shape of the Mt Turner SWIR radiance curves is dominated by atmospheric features (compare Figs. 5.12a-k to Fig. 5.13). Figure 5.13 depicts the radiance of a 100% reflector at sea level, calculated using the LOWTRAN model (Kneizy et al., 1980). The overall bell-shape of the curve is produced by water absorption in the 1.9 and 2.5 μ m regions, while the sharp features at 2.01 and 2.035 μ m are due to absorption by atmospheric CO₂. Absorption features in the 2.2 μ m region due to water vapour are common to this spectrum and Figs. 5.12a-k. It is also in this wavelength region that dioctahedral phyllosilicates absorb energy. Close examination of Figs. 5.12a-k shows that the different

flight-line mean radiance curves exhibit variation in the depth of these absorption features. The relative intensity of absorption in the 2.17 and 2.2 μm regions also varies. This variation is indicative of the presence of dioctahedral phyllosilicate mineral(s), although the effects are too weak to allow an identification of the species. This can be considered a 'first-order' effect, but due to lithospheric influences.

Another notable point comes from the comparison of the Mt Turner radiance data with that from previous U.S. surveys documented by Collins et al. (1981, see Figs. 5.14a&b, this thesis). It can be seen from this comparison that the strength of the lithospheric first-order absorption features from Mt Turner is considerably less than in the published American data. Examination of radiance data from other Australian test sites flown in the same survey establishes that this is not a local phenomenon, but a widespread trend. Chapter 2 and previous studies by CSIRO/MXY workers (Gabell and Green, 1982, 1983) have examined the weathering histories of Australia and the U.S., and their relative effects on remote sensing.

These studies have shown that the spectral response of a target is likely to be affected to a large extent by the weathering history of the area. Australia's much longer weathering cycles, and the widespread occurrence of Tertiary lateritic weathering, mean that the contribution to reflectance by weathering products (including 'skins' on individual rocks) is likely to be marked. The muted nature of the absorption features that occur at Mt Turner is consistent with this expectation. It is further supported by the many laboratory measurements of field samples (section 5.4). For many of these samples, reflectances of both weathered and 'fresh' (broken) surfaces have been measured. In general,

spectral features prove to be the same, or similar, but are more subdued on weathered surfaces.

5.5.3 Analysis of log residual images - 'second-order' effects

The log residual technique is described in Chapter 3. It is designed to eliminate the unknown influences of albedo and incident illumination. However, it also removes the average mineralogical response of the whole flight line. In the case of data from Mt Turner it follows that the average spectral feature at $2.2\mu\text{m}$, due to the ubiquitous phyllosilicate minerals, is removed. This fact must be considered when interpreting the log residual spectra. However, there is the advantage that the more subtle spectral variations (which prove to be important at Mt Turner) are emphasised. Because there is no absolute reflectance standard in the airborne data, it is impossible to calculate true reflectance values. As a result, we cannot come to any definite conclusion about the 'average mineralogy' of the flight-line.


As previously stated, the implication of different relative depths of absorption features at 2.17 and $2.2\mu\text{m}$ is that there is a contribution by one or several minerals at one or both of these wavelengths. Knowledge of the geology of the area suggests that muscovite/sericite (with a major absorption feature at $2.2\mu\text{m}$) and kaolin are the most probable candidates. Therefore, the average flight-line reflectance is likely to be determined by the relative proportions of these two minerals. Their relative importance can really be established with confidence only by the examination of field-sample spectra (see section 5.4), which give true reflectance values.

A second problem arises because the log residuals were calculated separately for each flight-line. Log residuals derived from two different flight lines (with different illumination conditions and different atmospheric effects - see chapter 3) will not be directly comparable, although at Mt Turner in most cases this problem is not too severe.

Nevertheless, an attempt was made to rectify the problem by using a correction technique based on radiance data from points where flight lines intersect. Multiplicative correction factors (Gabell et al., 1983, see Appendix VI) were derived for each flight-line using MT9 as a 'base' line. Radiance data for all lines were then corrected, and log residuals for each line produced using all data from intersecting lines. Unfortunately, to date it has not been possible to correct for more than 60-70% of the radiance differences (due to sun angle, etc.) between flight lines. This shortcoming has introduced atmospheric noise in the log residuals, which in turn means that the data from different flight lines can not be directly compared. For this reason, the interpretation presented here has been derived from log residual data calculated from individual flight-line means.

When log residuals are displayed in image format it is possible to view portions of a flight-line, or even an entire line, of spectral data on an image processing system or as hard copy. Figure 5.15 depicts all flight-line data from the Mt Turner area as log residuals calculated using individual flight-line means. It shows that the data exhibit some obvious trends, or 'second-order' effects.

These can be subdivided into three categories. Type A is represented by an absorption feature (different shades of blue) at $2.2\mu\text{m}$



in the SWIR data, and absorption at wavelengths longer than about $0.7\mu\text{m}$ in the VNIR data. In this type, albedos are generally high, and the vegetation index low. Type B SWIR spectra generally show a minimal absorption (yellows and reds) at $2.2\mu\text{m}$, but more significant absorption features at longer wavelengths. The VNIR spectra show a reflectance maximum at wavelengths longer than $0.7\mu\text{m}$, and exhibit some of the features of a vegetation spectrum. Not surprisingly, then, the vegetation index tends to be high, and albedos low. Type C spectra do not occur as extensively as the others. They exhibit absorption minima both at $2.2\mu\text{m}$ and at longer wavelengths in the SWIR. The VNIR spectrum is generally not as clearly defined, and the albedo and vegetation indices tend to have intermediate values. A fourth type of spectrum, which we can refer to as 'background', can also be defined. It is seen in Figure 5.15 as greens and yellows in both VNIR and SWIR data. These areas differ little from their flight-line means. The overlay to Fig. 5.15 shows typical examples of these 'type' spectra for line MT9.

The classification of spectral data into these main types has been plotted and overlain on a geology map (Fig. 5.16). Although there are variations, type A spectra are most often found outside the major part of the alteration zone, on weathered but unaltered granites. Photo interpretation and field checking have shown that these are generally areas of barer soil, with only sparse vegetation. Type B spectra fall mainly in, or close to, the alteration zone. The silicified portion of the alteration zone consists of rocky hills rising steeply from the surrounding plains, with a cover of moderately dense vegetation. In addition, there are quite extensive areas of type B spectra outside the alteration zone. Many of them are found over areas mapped as Robertson River Formation and/or dolerite, where there is little outcrop, but

often a moderate vegetation cover. Field traverses showed that, in areas mapped as granite where type B spectra occur, similar surface conditions are present.

Type C spectra occur in, or near, the northern portion of the silification zone, where the topography is not so rugged, and vegetation less dense than in the central zone.

Thus the nature of the surface (e.g. bare soil, heavy vegetation, rocky slopes, etc.) tends to determine the log residual spectra and, to a large extent, these 'second-order' effects are due to this type of geomorphological variation. These effects are outlined in Table 5.3.

To summarise so far, then, lithospheric 'first-order' effects can be seen in the radiance data, which is dominated by absorption features due to the minerals muscovite or sericite, and kaolin, over much of the survey area. 'Second-order' effects are obvious in the log residual data, and represent variations in the nature of the surface targeted.

There is, however, also a third level of information available in the log residual data. Subtle variations in the shape of the spectra are not immediately obvious in Fig. 5.15, but can be seen in individual spectral plots. These 'third-order' effects are discussed in the following section, along with various methods attempted to characterise them.

5.5.4 Classification of log residual data - 'third-order' effects

Detailed study of one of the flight lines (MT4) was undertaken to determine the number of different SWIR spectral types present in the data. Boundaries were drawn on the log residual image, thirty-four

Table 5.3 Second-order effects interpreted from images of Mt Turner airborne log residual data

	Type A	Type B	Type C	Background
VNIR features	Abs. max. beyond 0.7 μ m (less vegetation)	Abs. min. beyond 0.7 μ m (vegetation)	Average or lower values	Average values
SWIR features	2.2 μ m abs. max.	2.2 μ m abs. min., abs. max. beyond 2.2 μ m	abs. at and beyond 2.2 μ m	Average values
Albedo	High	Low	Intermediate	Intermediate
Vegetation index	Low	High	Intermediate	Intermediate
Rock type	Unaltered rocks	Altered rocks, plus Robertson River Formation plus some granite	Altered granite and rhyolite dykes	Varies
Geomorphology	Subdued topography bare soils, sparse vegetation, only scattered outcrop	Steep, heavily vegetated slopes, rocky in alteration zone. Moderate to heavy vegetation, weathered soils outside	Moderately vegetated, gentler hills, rocky	Varies

coherent blocks being outlined along the flight line. These blocks were then averaged, and the log residual spectra plotted and examined. Very close matches were discarded, and a group of thirteen 'standard' spectra were retained. These spectra appear in Figs. 5.17a-n, which show that there are still fundamental similarities between some standards. For instance standards 9, 10 and 12 all show an absorption feature near $2.35\mu\text{m}$. In some cases, variation between spectral types (for instance, standards 2, 3 and 14) seems to be due mainly to the relative depth of features present. However, at this stage of the analysis all thirteen standards were retained because it was not known which spectra would prove to be typical of a particular rock-type or mineralogy.

Each flight-line was then processed by comparing all of its log residual spectra to each of the standard spectra in turn, using a least-squares method (Craig et al., 1984). The best match was recorded in an output file, along with a measure of the similarity. Thus every flight-line was classified, sample by sample, into one of thirteen groups. Comparison of the results with log residual images (Fig. 5.15) showed that major boundaries in the log residuals match perfectly with the major changes in the classification.

Figure 5.18 depicts the classification output from pixels 524 to 587 on line MT8. The solid lines indicate major changes that are also easily seen on the image log residual presentation. Broken lines represent boundaries that still exist, but are more subtle on the image, and were drawn on the basis of the classification. alone. Pixels 539 to 545 contain 3 pixels most similar to standard #11, 3 pixels most similar to standard #4, and one other. Pixels 555 to 578 contain 7 pixels most similar to standard #4, 11 pixels most similar to standard #11, and 6

other pixels. It is obviously difficult to classify either of these regions into a single existing category (although there are easier areas - pixel 529 to 535 are mainly classified as similar to standard #7). There are many areas in the outputs where a portion of a flight line is classified consistently into 2 or 3 categories. An attempt was therefore made to simplify the groupings to allow a coherent presentation of the classification results. This task was performed by examining the classification outputs and Figs. 5.17a-n. It was found that, in general, where the classification within one of the coherent blocks on the log residual image varied significantly, the spectral standards showed some similarities. For instance, standards #4 and #11 both have a 'ramp' shape, with negative log residual values at shorter wavelengths and positive values at longer wavelengths. Both curves also have a local minimum near 2.2 μ m. The standards were therefore grouped to minimise the number of classes, as follows:

'Standards'	Grouped into	'Type' spectra
2, 3, 14	→	Type 1 spectra
4, 11	→	Type 2 spectra
6, 8	→	Type 3 spectra
9, 10, 12	→	Type 4 spectra
5	→	Type 5 spectra
13	→	Type 6 spectra

Each 'type' spectrum according to the classification was then colour-coded, and the result overlain on the geology map to produce Fig. 5.19. Where the classification was too variable to allow a reasonable grouping into a 'type' spectrum, a blank area was left, although this

was not a common occurrence. The characteristics and distribution of the type spectra are outlined in the following sections.

5.5.4.1 Types 1 and 2 spectra

Type 1 spectra contain a single absorption feature of varying strength near $2.2\mu\text{m}$, and appear to be indicative of the presence of muscovite. Type 2 spectra are not as easily interpreted by examination of the standard spectra in Figs. 5.19d&k, but areas classified as type 2 tend to exhibit a weak-to-moderate absorption feature near $2.2\mu\text{m}$, and a shoulder near $2.17\mu\text{m}$, suggesting kaolin. Field-checking showed that both spectral types tend to occur together over poorly vegetated areas, where the soil is well exposed, and generally reflect the presence of a surface lag of sand-sized quartz, feldspar and muscovite fragments. This lag is mostly the result of weathering of fresh granites, but weathered muscovite schists and quartzites from the Robertson River Formation can also contribute to, or even dominate, the resultant spectra. Although any quantitative measurement has not been undertaken, it would be fair to observe that, firstly, the classification into type 1 or type 2 is dependent on the relative muscovite content of the soil, and secondly, that the classification is a more accurate representation of these mineral assemblages than is the geological mapping - which is, after all, an interpretation of the bedrock geology.

5.5.4.2 Type 3 spectra

These spectra, with a log residual maximum near $2.2\mu\text{m}$ and minima to either side, are more difficult to explain. Field work has shown that muscovite/sericite is almost ubiquitous in the Mt Turner region. The

log residual calculation removes not only albedo and illumination factors, but also the average mineralogical signature over a flight line. The maximum at $2.2\mu\text{m}$ must therefore be interpreted as a relative absence of muscovite/sericite, which is quite often indicative of the presence of vegetation, reducing any mineralogical signal. The absorption features at either side of the maximum are related to a combination of vegetation and mineral effects. The minerals amphibole, clinozoisite, epidote, talc and chlorite all have absorption features in the $2.3\mu\text{m}$ region, and all occur to some extent at Mt Turner. As the occurrence of more mafic mineral assemblages tends to coincide with a denser vegetation cover, the task of satisfactorily separating their spectral effects is made more difficult.

In general, though, occurrences of type 3 spectra over areas consisting of Robertson River Formation and dolerite (specifically much of the northern portion of MT5 and the end of MT9) are probably a result of the combination of mafic mineral, and vegetation, spectral features.

The large area of type 3 classifications to the south of the silicification zone is also interesting in this respect. The alteration overlay to Fig. 5.2 shows that this area contains a large number of altered, quartz-filled fissures, but is outside the influence of the silicification. The spectral classification indicates that alteration here is slightly different to that within the silicified zone. This finding is supported to some degree by the laboratory spectra of samples taken from the area, where there are indications of propylitic alteration minerals (see Figs. 5.20a&b). This alteration produces spectral effects similar to those of the mafic minerals of the Robertson River Formation.

5.5.4.3 Type 4 spectra

Type 4 spectra show weak absorption minima at $2.35\mu\text{m}$, and most also have a minimum at $2.2\mu\text{m}$. These features are interpreted as resulting from the combination of the effects of vegetation and strongly absorbing sericitic alteration (discussed further in Section 5.6). With the exception of a portion of flight-line MT2, and some other small areas, the silicified alteration-zone spectra have been classified as type 4. Outside this central zone are several smaller areas that have been given the same classification. Many of them (for instance the area one-fourth the way along MT8) are misclassifications in areas affected by cloud shadow. However, at some others there is evidence of alteration. Near the start (western end) of MT8, a significant concentration of sericitised, quartz-filled fissures corresponds with the type 4 spectra. Also of particular significance are the small zones near sample 80 on line MT9, and between samples 170 and 180 on line MT7. In both cases these areas consist of outcrops of sericitised (and propylitically altered ?) veins peripheral to the porphyry system. The area on line MT7 lies just to the north of the Three Musketeers line of lode and, in fact, the flight line passes between two costeans. The small area on MT9 passes directly over some minor workings, where no more than a few tonnes of rock have been removed from a shallow pit. These workings have not been incorporated in any geology map.

There are also five small areas on flight line MT5 to the northwest of Mt Turner that have been misclassified as type 4. The three areas at the southern end of the line are over kaolinitic Cretaceous conglomerate and its weathering products. Figs. 5.21a&b respectively show an average

spectrum from MT5, and a kaolin spectrum measured in the laboratory. It is not entirely clear why the misclassification should occur in this case, although the significantly different geology along line MT5 would almost certainly result in an anomalous flight-line mean.

The two areas in the northern portion of MT5 occur over unusually large and well exposed outcrops of metagabbro. The mafic minerals present produce weak, noisy absorption features at 2.26, 2.3 and 2.4 μ m (Fig. 5.22). The spectra indicate a mineralogy of chlorite and amphibole, so these spectra should have been classified as type 5.

The least-squares comparison, as well as being influenced by mineral absorption features, is also affected by the overall shape of the log-residual curve. The shape of the curve will, in turn, be influenced by a number of factors. This may be another reason for the consistent misclassifications on line MT5. Further work would be required to refine the classification procedure and overcome these problems.

The other notable aspect of the classification is the areas within the silicified zone that have not been classified as type 4. As yet, there is no explanation for the portion of flight line MT2 that appears as type 3. The other main area, though, where parts of flight lines MT1, MT6 and MT10 are classified as type 1, is consistent with the mineralogy on the ground. This area is over a creek, where the alluvium is derived from a much wider area than just the alteration zone.

5.5.4.4. Type 5 spectra

Type 5 spectra show a maximum at 2.2 μ m, and weak minima at 2.3 and

2.4 μ m. As previously discussed, the 2.2 μ m maximum is interpreted as an absence of muscovite/sericite relative to the rest of the flight line. The features at 2.3 and 2.4 μ m, though, closely match those of amphibole (compare Fig. 5.17e to Fig. 2.6). However, the distribution of type 5 spectra is extremely limited, with small areas on flight lines MT3, MT5 and MT10 being placed in this class.

5.5.4.5 Type 6 spectra

Type 6 spectra have an unusual shape that is difficult to interpret. The minimum near 2.1 μ m is similar to that of dry grass, but at 2.3 μ m there is only a local minimum rather than a deeper absorption feature (compare Fig. 5.17m to Fig. 5.8). Field checking in the few areas classified as type 6 showed patchy areas of dry grass, in amounts greater than usual for Mt Turner.

The third-order effects are summarised in Table 5.4.

5.5.4.6 Assessment of significance of classification scheme

The results of this scheme are obviously not perfect. Misclassifications are evident in a number of areas, but are particularly prevalent in line MT5. This is most likely to be due to the significantly different geology in this area, which results in an anomalous flight-line mean. In addition, the spectral effects of vegetation and propylitic alteration proved impossible to separate.

Nevertheless, there are a number of points that, in the author's opinion, make the overall result a qualified success. Firstly, the main alteration zone is better defined using this technique. Secondly, a

Table 5.4. Third-order effects interpreted from Mt Turner airborne log residual data

	Type 1	Type 2	Type 3	Type 4	Type 5	Type 6
SWIR 'standard' spectra	2, 3, 14	4, 11	6, 7, 8	9, 10, 12	5	13
Major spectral characteristics	Single 2.2 μ m absorption	2.2 μ m absorption, shoulder near 2.17 μ m	2.2 μ m abs. min. 2.1 μ m and/or 2.3 μ m abs. max.	Weak 2.2 μ m absorption. 2.35 μ m and sometimes 2.45 μ m abs.	Absorption near 2.3 μ m and 2.4 μ m	Strong 2.1 μ m absorption
Terrain type & vegetation	Mainly granitic terrain, little vegetation	Mainly granitic terrain, little vegetation	Almost any terrain. Moderate vegetation - dry vegetation a major factor	Altered zone, heavily vegetated	Altered terrain, or over basic rocks	Mainly dry vegetation?
Dominant minerals contributing to spectral effects	Muscovite (kaolin)	Kaolin (muscovite)	Amphibole, chlorite, epidote, clinozoisite (combined with vegetation effect)	Sericite	Mainly amphibole?	?

number of smaller areas of sericitic alteration, peripheral to the main alteration zone, were correctly identified. Thirdly, examination of the spectral plots points to a greater mineralogical input to the discrimination of alteration than any other technique. Thus, a significant increment of knowledge was gained by use of the scheme. Further development of the techniques, or related procedures, may result in the solution of some of the remaining problems.

5.5.5 Other analysis-techniques

Several other techniques to analyse the spectrometer data have been applied. Tchebychev analysis (see below) was attempted on both corrected radiance data and log residual spectra. The technique proved to be too unstable, in the form used, for the analysis of log residual data, but it was from this approach that the classification technique described in section 5.5.4 was developed.

In addition, several different band-ratio techniques have been tried, as discussed below.

5.5.5.1 Tchebychev analysis

Figure 5.23a depicts the Tchebychev coefficient ratio C_4/C_5 along flight line MT9. The silicified alteration zone lies between samples 280 and 450. Comparison with the classification (whose boundaries are marked on the plot) shows that there is some agreement between the two techniques. Type 1 and type 2 spectra have the highest C_4/C_5 values, with type 3 lower, and type 4 (alteration) tending to have the lowest values. However, there is some difficulty in separating some type 3 and 4 spectra, and it would be very difficult to interpret the subtle

changes present without considerable prior knowledge of the types of spectra present in the data.

5.5.5.2 Band ratios

Examination of the flight-line log residual images (Fig. 5.15) shows that the data fall naturally into a number of reasonably well-defined spectral bands. Table 5.5 summarises the boundaries used to create a series of narrow bands.

Radiance data were averaged over these intervals and stored in an output file. Figure 5.23b is a plot of the ratio of the 2.2 μ m to 2.3 μ m bands. Where muscovite/kaolin absorption is strongest (as over granitic terrain), the ratios are low. Conversely, where the 2.3 μ m absorption features are strongest (over alteration and more vegetated areas), the ratios are high. Comparison to the Tchebychev-coefficient plot shows that the two are inversely related, and that there is a similar information content in both. As with the Tchebychev plots, not all of the classification types consistently exhibit the same ratio values, but the important boundaries are reflected as noticeable changes in the data.

5.6 Correlation between Airborne and Laboratory Data

Precise comparison of airborne and laboratory spectra is, of course, impossible. The different units (radiance for airborne data, reflectance in the laboratory), and the vastly different fields of view, preclude such comparison. However, some interesting general observations are still possible, particularly if the laboratory data are

Table 5.5 Bands simulated after examination of Mt Turner airborne log residual data in image format.

		Wavelength (μm)	Channels	
	1	0.35-0.45	26- 90	R
V	2	0.45-0.52	91-141	E
N	3	0.52-0.60	142-199	T
I	4	0.63-0.69	222-265	I
R	5	0.76-0.90	317-419	C
	6	0.90-1.02	420-510	O
				N
	7	1.987-2.039	5-10	
S	8	2.073-2.142	15-22	P
W	9	2.159-2.237	25-33	B
I	10	2.254-2.314	36-42	S
R	11	2.314-2.374	43-49	
	12	2.392-2.452	52-58	

converted to a form of log residuals. This was done, using two different approaches.

Firstly, all of the laboratory spectra from Mt Turner were transferred into an XPUT file, and their log residuals calculated. It should be noted that these data are dominated by altered specimens, as the largest number of samples was collected from within the silicified zone. The airborne data, on the other hand, cover more unaltered (mainly granitic) terrain. Figure 5.24 is the mean of the laboratory spectra (in log form, and over the wavelengths covered by the GER instrument), and shows the absorption features of muscovite. The influence of kaolin is not apparent, although some subtle effects beyond the resolution capabilities of the instrument may be present. Figures 5.25a-c are the respective reflectance spectra (over the same wavelength interval), of dry grass, a Sericite-type spectrum, and a Mafic-type spectrum. Figures 5.25d-f are their log residuals.

The Sericite-type log residual shows the characteristic secondary absorption wings at 2.35 and 2.45 μ m, although the major absorption feature is much stronger than in the corresponding airborne data. This is due partly to the presence of healthy vegetation over the silicified zone, where the 2.2 μ m peak of vegetation tends to reduce the strength of the corresponding mineral absorption (see below).

Figures 5.25d&f are similar log residuals produced from very different materials. The similarity of both spectra to standards 5 and 6, in particular (Figs. 5.17e&f), is quite marked. It underlines the problem of differentiating spectral effects due to dry vegetation from those caused by minerals with 2.3 μ m absorption features.

The second approach involved modelling a 'typical' Mt Turner flight line. This was achieved by adding laboratory reflectance spectra in different proportions, then storing the results in a single XPUT file. The contents of the file were as follows;

Vegetation (moderately healthy)
Average Sericite
Average unaltered granite soil (Muscovite)
Average unaltered granite soil (Muscovite)
Vegetation + Sericite (2:1)
Vegetation + Sericite (1:1)
Vegetation + Sericite (1:1.5)
Vegetation + Sericite (1:2)
Vegetation + Muscovite (1:1)
Vegetation + Muscovite (1:1.5)

Mean of the above spectra

Note that the higher proportions of vegetation were not added to the Muscovite spectrum because the unaltered granite terrain is rarely heavily vegetated. The average unaltered granite spectrum was included twice because, on most lines, unaltered material forms a larger proportion of the line than altered material.

Once the data were in this format, the equivalent of log residuals were calculated. All plots of the input reflectance spectra, and their 'log residuals', appear in Appendix VII.

Two notable points arose from this exercise. Firstly, many of the shapes of airborne log residuals (Figs. 5.17a-n) are similar to the

shapes of the laboratory 'log residuals'. Secondly, laboratory 'log residuals' of Muscovite, or Vegetation + Muscovite, only produce a local minimum at 2.35 and 2.45 μ m, whilst Vegetation + Sericite mixtures tend to retain more of the spectral shape of sericite, resulting in much stronger features at these wavelengths (see Figs. 5.26a-d). This property is also seen in the airborne log residuals, and is a major factor in the identification of alteration using the classification scheme.

5.7 Significant Individual Spectra

One of the interesting developments from this study has been the identification, on the basis of their spectral properties, of two minerals whose presence in the survey area has not previously been documented. Figures 5.27a&b are, respectively, the airborne and laboratory spectra of an unusual mineral assemblage. The spectra are dominated by the absorption features of talc, and XRD analysis confirms that talc comprises greater than 20% of the sample. The soil sample was collected from a zone some tens of metres wide on flight-line MT8, and is thought to represent the weathering products of a mafic intrusive that has reacted with its granitic host-rock.

The second, and perhaps more significant mineral, is topaz. Within the silicified alteration-zone, a few pixels on flight line MT10 were classified as having type 6 spectra. The average airborne signal from this area is noisy, and difficult to interpret (see Fig. 5.28 and compare to Fig. 5.17m). As most of the surrounding pixels were classified as type 4, the area was visited and a number of samples collected. One of these samples produced the laboratory spectra shown

in Figs. 5.29a&b, with the unusual, sharp absorption feature at 2.1 μ m, as well as the more common 2.2 μ m (sericitic) feature. The 2.1 μ m absorption feature is characteristic of topaz (Hunt et al., 1973a), which XRD analysis has shown comprises between 5% and 20% of the rock. Examination of the airborne spectra over the area shows that the sharp topaz feature is not recognisable (Fig. 5.28). Field checking of this, and other, type 6 areas depicted in Fig. 5.19 indicates that they are generally related to dry vegetation rather than to a specific mineral assemblage.

5.8 Comparison with Silver Bell Porphyry Copper Deposit, Arizona, U.S.

The Silver Bell porphyry copper deposit in Arizona has been the subject of considerable remote sensing research, most recently as a test site in the Joint NASA/Geosat Test Case Study (Abrams et al., 1984).

At this test site the rocks range from Precambrian to Tertiary in age, with the great majority of exposures being Mesozoic and younger. Volcanic and plutonic rocks dominate with compositions ranging from basaltic to granodioritic. Mt Turner, on the other hand, is dominated by Precambrian granite and (to a lesser extent) metamorphic terrain, with some Carboniferous, granodioritic intrusives.

At Silver Bell the amount of outcrop exposure averages 30 to 40 percent, but a large amount of the remaining area is colluvium and talus on ridges and hill slopes. The composition of this material closely reflects the adjacent and subjacent geology, since the fragments are derived by essentially in-place weathering (Abrams and Brown, 1984). Because weathering is mechanical rather than chemical, soil profiles are poor or absent. However, at Mt Turner the silicified zone is the only

area where outcrop is substantial, with well-developed soil profiles predominating elsewhere. In these areas, indications of the underlying geology are given by surface lag deposits and soil colour.

The vegetation cover at Silver Bell is sparse, varying from 10 to 15% in lower elevations to as much as 20 to 25% in higher elevations. This range is in contrast to Mt Turner, where vegetation is variable and sparse only over unaltered granitic terrain. Over the silicified zone and areas of Robertson River Formation, vegetation generally ranges from 30% up to a maximum of about 60%.

The most extensive areas of alteration at Silver Bell are phyllic/argillic in nature - dominated by quartz-sericite-limonite assemblages. Other alteration products identified in thin section are kaolinite, montmorillonite, illite, chlorite, alunite and jarosite. Peripheral propylitic alteration comprises chlorite, epidote and minor vein calcite. These assemblages are remarkably similar to those found at Mt Turner, although propylitic alteration is more evident, and widespread, at Silver Bell. Both deposits have central zones of potassic alteration, comprising K-feldspar and biotite alteration that are difficult to recognise on the surface and have largely have been documented from examination of drill core.

In summary, the major differences between the two areas are 1) the more varied host rocks at Silver Bell, 2) the sparser and more even vegetation cover at Silver Bell, 3) the younger age of the Silver Bell region, leading to more prominent topography and hence better exposure and 4) the vastly different weathering regimes.

Figure 5.30 reproduces some of the field spectra of Abrams and Brown (1984). In direct contrast to Mt Turner, where unaltered but

weathered material has been shown to have essentially the same SWIR signatures as altered rocks (differing only in the strength of absorption), the unaltered material at Silver Bell is essentially spectrally flat. Only the altered material (except carbonate, with features at $2.35\mu\text{m}$) has strong SWIR absorption features. The same generally applies to the VNIR, because of iron-oxide signatures, thus enabling the accurate detection of alteration zones using enhanced imagery from a broad-band (NS001) scanner. However, at Mt Turner the increased vegetation cover over the alteration zone means that the strongest hydroxyl absorption features actually appear outside the main alteration zone. Therefore, only extensive analysis of high-resolution data is able to differentiate alteration based on mineralogical features.

5.9 Summary

The aim of the study at Mt Turner was to identify the mineral assemblages related to, firstly, alteration and, secondly, weathering, and to discriminate between these assemblages.

An earlier Landsat MSS study discriminates Mt Turner from the iron and vegetation poor, unaltered granite terrain immediately surrounding it, but not from the areas underlain by Robertson River Formation. The soil in these areas contains significant amounts of iron, and vegetation is denser than over unaltered granite terrain.

SWIR spectra measured in the laboratory fall into four groups - Sericite-type, Muscovite-type, Kaolin-type, and Mafic-type. Detailed analysis shows that the differences between Sericite-type and Muscovite-type spectra are due solely to variations in the strength of absorption

features. There is no detectable compositional difference, but Sericite-type spectra tend to occur within the main alteration zone, and Muscovite-type spectra, more randomly, outside it. Kaolin-type spectra are characteristic of weathering products. Mafic-type spectra are obtained from doleritic material associated with the Robertson River Formation, or from propylitically altered rocks. Dry vegetation produces absorption features in the same wavelength region as the Mafic-type spectra (2.3 μ m).

Variations in the airborne radiance-data produce lithospheric first-order effects that could delineate the alteration zones around most U.S. porphyry copper systems. However, this is not the case at Mt Turner, where the spectral response of weathering products from unaltered terrain (dominated by muscovite) and the alteration minerals (dominated by sericite) are similar.

A logarithmic procedure has been used to correct the radiance data for albedo and atmospheric variations, leaving reflectance information in the residual data (log residuals). These data are presented in an image format, where obvious variations represent second-order effects. The second-order effects are influenced mainly by geomorphological factors, and can be used to differentiate the limits of the alteration zone around Mt Turner. Such differentiation results from the presence of topographic and vegetation anomalies, and is approximately the same level of discrimination as available from the interpretation of Landsat MSS data.

Third-order effects are subtle variations within the log residual data that are most easily seen in detailed spectral plots. Six major spectral types have been interpreted from third-order variations,

reflecting a combination of mineralogical and vegetation influences. Classification of the data into one of the six third-order spectral groups is imperfect, but has resulted in differentiation between sericite (due to alteration) and muscovite (from the background areas). The major sericitic alteration zone has been more successfully outlined by this technique than any other, and a number of altered veins peripheral to the porphyry system have been correctly classified.

However, a more propylitic style of alteration is difficult to discriminate, with this classification procedure, from dry vegetation.

Analysis of the airborne data, and follow-up laboratory spectral measurements, have also resulted in the detection of two minerals previously unreported in the Mt Turner area. Talc was found outside the alteration zone, topaz near Mt Turner itself.

Broad-band scanner systems will not differentiate alteration at Mt Turner, as at Silver Bell, on the basis of increased absorption over the alteration zone. In fact, because of the vegetation anomaly over Mt Turner, the absorption features are stronger outside the alteration zone. Even in the absence of such a vegetation anomaly, the markedly weaker absorption features found in the Australian environment, and the presence of similar absorption by weathering products, makes success with these systems much less likely.

The study does confirm the ability of high resolution spectrometer data to map successfully significant alteration mineralogies. However, high signal-to-noise ratios and very careful processing and interpretation techniques are required to elucidate these effects in the Australian weathering environment.

CHAPTER 6 KAMBALDA NICKEL PROVINCE, EASTERN GOLDFIELDS, WESTERN AUSTRALIA

6.1 Introduction

This thesis deals with the analysis of remote sensing data from test sites affected by weathering to various degrees. Kambalda is an extreme case characterised by poor outcrop and deep weathering.

The specific aim of this study is the use of high-resolution spectral data to differentiate spectral effects due to weathering from those due to the primary mineralogical features of the Archaean rocks. Where residual mineralogy is detectable, it is also important to extract the maximum mineralogical information. Sub-division of residual material is vital, because nickel mineralisation is spatially related to contacts between mafic and ultramafic rocks. Any technique that assists in making distinctions between the two rock types will provide a useful exploration tool.

The study includes processing and interpretation of airborne and laboratory spectra, and field investigation. Some XRD analyses were also obtained to assist interpretation of the spectral data.

6.2 Regional Geological Setting

Western Australia is the world's third largest producer of sulphide nickel, after Canada and the USSR (Ross and Travis, 1981). The Archaean Yilgarn Block contains the bulk of this resource, hosted in volcanic and intrusive olivine-rich ultramafics. The linear, NNW-trending Norseman-Wiluna belt in the Eastern Goldfields contains all of the important

volcanic peridotite-associated deposits. The Kambalda deposits are easily the most significant of these, 70% of Western Australia's pre-mining nickel resource of grades greater than 1% concentrated in the Kambalda-St Ives region (Marston et al., 1981).

Apart from the mafic-ultramafic volcanic successions that host the nickel orebodies, the Norseman-Wiluna belt also contains other major components including a felsic volcanic-volcaniclastic suite, typically comprising dacitic to rhyodacitic lavas and fragmentals, bedded tuffs, conglomerate and chert. The volcanogenic rocks are also intruded by a suite of plutonic rocks consisting of quartz diorite, tonalite, granodiorite, adamellite, granite and syenite (Gemuts and Theron, 1975).

The Norseman-Wiluna belt is broken into a number of blocks by NNW-trending faults. Within each block, continuity of lithological sequences can be recognised over distances of greater than 100 km, but between blocks it is often difficult, or impossible, to correlate lithologies (Gresham and Loftus-Hills, 1981).

6.3 Detailed Geology

The Kambalda nickel field comprises two sequences of ultramafic, mafic and felsic volcanics, and sedimentary rocks, with the lower (Kambalda) sequence containing the bulk of the nickel ore. Figure 6.1 depicts the interpreted geology, and the location of the survey lines.

The Kambalda sequence consists of the footwall basalt, the ultramafic suite, the hangingwall basalts and associated sedimentary and intrusive rock-types (Gresham and Loftus-Hills, 1981). The footwall basalt is tholeiitic, and a generally fine-to medium-grained, dark

green, massive basalt. The hangingwall basalt formation consists of upper and lower members separated by a thin zone of sediments. The mineralogy of the basalts is variable, but is dominated by amphibole and chlorite.

The ultramafic suite has been sub-divided into three types, based on the rock's volatile-free MgO content, as follows:

picrites	15-28% MgO
peridotites	28-36% MgO
olivine peridotites	>36% MgO

These rocks originally comprised varying proportions of cumulate olivines and magnesium-rich liquid (Gresham and Loftus-Hills, 1981), but have undergone varying degrees of hydration, carbonatisation, and late-stage potassium metasomatism.

Where the rocks are hydrated, glass and pyroxenes are altered to tremolite and chlorite, while olivines are altered to serpentine (mainly var. antigorite). Carbonatisation resulted in the breakdown of tremolite and antigorite to talc-dolomite and talc-magnesite assemblages. It is also likely that both serpentinisation and carbonatisation upgraded pre-existing nickel sulphide accumulations (Donaldson, 1981).

The occurrence of biotite, replacing chlorite in mafic and ultramafic rocks, reflects a potassium metasomatic event. In areas of more intense alteration, vermiculite and montmorillonite are considered to have replaced biotite (Gresham and Loftus-Hills, 1981).

Sediments associated with the Kambalda ultramafic rocks are generally thin and discontinuous. Pale (cherty) and dark (carbonaceous) varieties are both common with chloritic or amphibole-rich varieties occurring less commonly. Argillaceous sediments also occur frequently.

Archaean granitoids, felsic and intermediate porphyries, and Proterozoic, diopside-rich dolerite dykes intrude the Kambalda sequence.

Figure 6.1 shows a sequence of felsic volcanic and sedimentary rocks overlying the Kambalda Sequence. These rocks do not crop out in the study area, being covered either by the remnants of lateritic duricrust, or by aeolian sands.

Eighty percent of the ore at Kambalda occurs at the base of the lowest ultramafic flow unit in the Kambalda Sequence - generally occupying elongate troughs in the footwall basalt/ultramafic contact (Gresham and Loftus-Hills, 1981). The remainder is hanging wall ore that usually occurs directly above contact ore at the base of the second or third ultramafic flow units.

6.4 Factors Affecting Remote Sensing at Kambalda

6.4.1 Weathering Effects on Primary Mineralogy

The Kambalda region has been subjected to two widely differing weathering regimes. Deep lateritic weathering processes were operative during the generally humid conditions that persisted until the early-middle Tertiary. The resultant weathered mantle has subsequently been altered and/or dissected during succeeding arid and semi-arid periods. The most obvious effects of the more recent arid conditions are the development of salt lakes and clay pans, calcrete, and large

accumulations of aeolian sands. Thus, in mapping the region, the first distinction one must make is between (a) residual material, represented by primary (Archaean) mineralogical components and their largely in situ weathering products, and (b) transported material (resulting mainly from processes operating during the arid periods).

Once this distinction has been made, the residual materials need further differentiation, based on their position in the profile. Division will generally be into one of two groups: (1) lateritic duricrust (either intact or as float), and (2) weathered rocks and soils that retain a part of their original mineralogical character. Obviously it is the latter group that is the most important for nickel exploration.

Where relief is at a maximum (i.e. Kambalda Dome), outcrop of relatively fresh material is at its best, with the least residual and lateritic material present. As one moves to the south, outcrop of Kambalda sequence rocks becomes progressively rarer. Basalts form low hills in the St. Ives region, but commonly produce only accumulations of float in the Tramways area. Outcrop of Bluebush-sequence rocks in the Democrat area is variable, but often good.

There are several factors that might be expected to affect the remote sensing of areas of outcrop in the Kambalda region. Basalts, for instance, commonly form rounded cobbles, and often have a weathered skin, that varies in thickness at different locations. These skins appear to be composed mainly of iron oxides, but their precise mineralogy has yet to be established. Lichens are also commonly developed on basalt cobbles, and it has previously been shown that they can have a profound effect on the spectrum of a sample (see chapter 5).

Ultramafic rocks (or, more precisely, their altered products) can be affected by case-hardening, with some surface iron oxide staining. Serpentinities have similar surface-weathering characteristics as basalts, but when carbonatised, the effect is generally not as obvious or well developed. The carbonatised ultramafics are softer than the other rocks, hence less resistant to weathering. As a result, true outcrop is rare, and only subcrop or heavy accumulations of float are present in the best-exposed areas.

XRD analyses of weathered, carbonatised ultramafic rocks show that the most common assemblage is talc, iron oxides and chlorite. Montmorillonite (after biotitised chlorite?) and kaolin sometimes occur as well, but carbonates (magnesite and dolomite) are rare. Where carbonates are found in the weathered rocks, they occur (except for a single sample) in minor quantities. The most diagnostic mineral for weathered, carbonatised ultramafics is therefore talc. It is resistant enough to occur in residual soils as well as in float, and has an very strong $2.32\mu\text{m}$ absorption band, making it extremely amenable to detection by remote sensing.

Argillaceous sediments do not generally crop out over large areas. These sediments, and felsic intrusives, may both contain kaolin from the weathering of feldspars.

Table 6.1 summarises the results of all XRD analyses of Kambalda samples, including data from fresh core, as well as weathered samples collected in the field. The data have been subdivided into a number of groups. Minerals in the left-hand column have VNIR or SWIR spectral signatures, and are theoretically capable of detection by remote-sensing techniques. The minerals in the right-hand column have no such

Table 6.1 Minerals identified by XRD analysis of samples from Kambalda.

	(VNIR or) SWIR signatures	No VNIR, SWIR signature
Common, often major components.	Talc*	Plagioclase*
	Chlorites*	Quartz*
	Amphibole (var. Tremolite)*	
	Serpentine (var. Antigorite)*	
	Kaolinite	
	Haematite ^x	
	Goethite ^x	
	Magnesite*	
	Dolomite*	
Rare, but can be major components where present.	Calcite*	
	Epidote*	
	Diopside	
	Natrojarosite	
	Montmorillonite	
Rare, only trace components where present	Muscovite	
	Gypsum	Magnetite*
	Vermiculite	Maghemite
	Chlorite-vermiculite	Pyrite ⁺
	Chlorite-montmorillonite	Pyrrhotite ⁺
	Tourmaline	Pentlandite ⁺
	Jarosite	

KEY

x = strong VNIR only

* = found in both weathered and core samples

+ = found in core samples only

signatures. The list of minerals has also been divided vertically. Commonly occurring, major components (such as one might expect to detect from the air) occur in the top row. Those minerals that occur less frequently, but can comprise a major proportion of the rock in which they are present, are listed next. One might expect to detect these minerals when measuring individual samples in the laboratory, or perhaps occasionally from the air. The last group comprises minerals that occur in quantities likely to be too small for detection, even under laboratory conditions.

6.4.2 Cultural and Vegetation Effects

As remote-sensing techniques integrate the reflected radiation from all objects within a pixel, the effects due to cultural features and vegetation must be considered, in addition to those of the target mineralogies.

As one might expect, the amount of disturbance produced by mining and related activity is at a maximum around Kambalda Dome. For this reason, only a single flight line is located in this area. Further to the south the amount of cultural disturbance decreases, although the operating Jan, Foster and Victory mines mean that there is still significant disturbance in the St Ives area. At Tramways and Democrat, cultural features are mostly limited to drilling tracks and pads.

The small pixel size of the airborne instrument (20 m square) means that a cultural feature (for instance a road) will generally dominate the spectral response of the pixel in which it occurs. The result is

usually an albedo higher than normal. Pixels affected in this way can, for the most part, easily be recognised, and ignored.

Vegetation in the Kambalda area tends to be moderately dense, averaging perhaps 25 to 30% cover and relatively uniform. The exceptions are over clay pans and salt lakes (zero vegetation) and isolated clumps of trees (up to about 60% cover in some small areas). It is dominated by eucalyptus, acacias, saltbush and bluebush. Its distribution is not uniform, but the heterogeneity seems to be related to geomorphology (e.g. no vegetation in clay pans) rather than the Archaean geology. This characteristic is in contrast to Mt Turner, where vegetation density is generally directly related to the underlying geology. It also means that some of the vegetation's spectral effects are removed in the data processing (see Section 8.3). Those remaining are generally weaker than effects produced by spectral absorption of minerals, hence are noticeable only outside the areas of significant residual mineral accumulations. In addition, at Mt Turner the absorption features of dry vegetation caused major problems. In particular, extensive areas that have a sparse tree cover, but are heavily covered by dry grasses, produce the most extreme spectral features at Mt Turner. There are no similar areas on the flight lines in the Kambalda area. For these reasons, vegetation at Kambalda poses fewer problems.

6.5 Previous Remote Sensing Investigation

As was the case with the data set from Mt Turner, the Kambalda airborne data was also analysed by GER, and a preliminary interpretation submitted to CSIRO (GER, 1983). Like the Mt Turner data, the Kambalda

data were interpreted without the benefit of any supporting ground-truth information. The same techniques were used for the analysis of both data sets, including the calculation of "residual" spectral information using a technique similar to that of Marsh and McKeon (1981). The absorption features evident in this residual data were assigned by GER to "chlorite, Mg-carbonate or talc" (for 2.3 μ m features) and "kaolin" (for 2.2 μ m features). Tchebychev Analysis was used to outline the zones of significant mineralogical absorption, but no attempt was made to subdivide the zones of 2.3 μ m absorption other than by the depth of the spectral features.

6.6 Laboratory Spectral Measurements

The data analysed in this section are derived from the field samples collected during October, 1983, sampling points being largely predetermined by interpretation of the airborne spectral data set. Rock and soil samples from all major spectral regions and soil types were collected. Most samples subsequently had their spectra measured in the laboratory, and some of them had XRD analyses provided by Western Mining Corporation (WMC). The minerals detected by XRD fall into two groups - those capable of being semi-quantitatively analysed, and those capable only of qualitative analysis. The results of these analyses are presented, wherever possible, with the spectra. Where minerals are present in non-quantifiable amounts, they are listed last, with a stroke separating them from the other minerals. Minerals for which semi-quantitative values are available are listed as percentages of the remaining portion of the rock.

The spectral collection produced is too voluminous to reproduce

here in its entirety, so only a few representatives of the major spectral types will be presented with the text. Spectra of all samples that have accompanying XRD analyses are presented in Appendix VIII.

One significant feature of the spectral collection is the relationship between weathered and 'fresh' surfaces. As for Mt Turner, fresh is a relative term, since all samples have undergone some degree of weathering. Again like Mt Turner samples (see p. 92, chapter 5), absorption features that are present on fresh surfaces are almost invariably seen on corresponding weathered surfaces, albeit as more subdued effects. This trend persists even in the case of basaltic and serpentine-rich rocks, which have commonly developed the significant surface-weathering rind (Fig. 6.2a,b&c).

The only cases where this rule does not seem to apply are for samples with a significant amount of lichen covering their weathered surfaces. This effect was also documented in the previous chapter on Mt Turner. At Kambalda, however, there is commonly also a lichen crust developed on the soil (Fig. 6.3a). The spectral effects of this type of lichen are similar to the 'rock lichens', with absorption features in the 2.1 and 2.3 μm regions. But, there is often an associated mineralogical signature (Fig. 6.3b), in contrast to the rock lichens, which tend to suppress all mineral effects when they cover the entire rock surface.

6.6.1 Laboratory spectral types

The laboratory data can be divided into a number of spectral types, based on the positions and shapes of the mineral absorption bands

present. Not unexpectedly, there is some overlap between these groups, due to the different mixtures of components.

Comparison between these data and airborne data is not directly possible for reasons outlined in the previous chapter. To repeat, the major difference is that laboratory spectra are 'true' reflectance spectra, whereas log residuals do not retain any specific spectral component present in the flight line mean. Ubiquitous minerals (for instance, resulting from weathering processes) will therefore not affect the log residual data, but will produce features in many of the laboratory spectra.

The laboratory reflectance spectra are categorised in the following sections.

6.6.1.1 Flat spectra

The first spectral group contains samples that show no absorption features in their reflectance measurements. Dark, cherty sediments (with XRD analyses of up to 100% quartz) are the most common rock type in this group (Fig. 6.4).

6.6.1.2 Variable absorption by water

The depth of the 1.9 μ m water absorption feature varies in this class of spectra (Figs. 6.5a-c). Strong 1.9 μ m absorption is invariably associated with high quartz-content of the soil, fluid inclusions in the quartz being the probable cause of these features.

6.6.1.3 2.2 μ m absorption features

The strength of absorption features in the 2.2 μ m region is highly variable. Where strong, these features usually show the diagnostic structure of kaolin, with a major absorption minimum at 2.208 μ m, and a shoulder near 2.17 μ m (Fig. 6.6a). Weaker absorption features are more difficult to assign (Fig. 6.6b), but are also likely to be caused by kaolin. An interesting phenomenon from the Kambalda area is the occurrence of kaolin-type absorption features associated with calcrete, but, at the same time, the absence of characteristic 2.34 μ m calcite absorption features. This is best illustrated by a single example, K14/31/S, a sample collected from an area with moderate absorption in the 2.2 μ m region of the airborne spectrum. The laboratory spectrum of the soils shows an asymmetric 2.2 μ m absorption feature, but nothing in the 2.3 μ m region (Fig. 6.7a). However, XRD analysis shows a composition of 75% calcite, 20% quartz and 5% talc, while acid applied to a hand specimen causes effervescence. Moreover, spectral measurement of the XRD powder shows the presence of both the 2.2 μ m feature and a broad 2.34 μ m (calcite) absorption feature (Fig.6.7b). It therefore seems that the 2.34 μ m calcite absorption feature is being suppressed in the unground hand specimen. The most likely explanation for this phenomenon is that fine-grained (crypto-crystalline?) kaolin is coating individual calcrete nodules. Phillips (1984) has reported such a phenomenon from an electronmicroprobe study of calcareous earths near Adelaide. Balasubramanian and Gopinath (1979), while studying bauxite minerals (including kaolin-group minerals), noted that the characteristic vibrations of these minerals in the IR (4000 to 625 cm^{-1} , or 2.5 to 16 μ m) can be detected in the early stages of crystallisation, even though the short range order is not detected by X-ray diffraction techniques.

Detailed mineralogical work would be required to confirm this effect at Kambalda.

6.6.1.4 2.3 μ m absorption features

There are several 2.3 μ m absorption features generated in samples from Kambalda, as one might expect from examination of Table 6.1. In the laboratory data, some of these features are obviously the result of dominance of the spectrum by a single mineral, but others are generated as a result of mixtures of spectral properties of two or more minerals. The 2.3 μ m region is the most important spectral region contributing to knowledge of the mineralogy at Kambalda. Individual 2.3 μ m absorption features are discussed in the following sections.

6.6.1.4.1 Talc

The spectrum of pure talc has a high reflectance, and relatively flat background slope, with an extremely strong, deep absorption feature at 2.32 μ m associated with weaker features centred on 2.39 and 2.47 μ m (Fig. 2.6). There is also a small shoulder on the 2.32 μ m absorption feature near 2.30 μ m, but the laboratory instrument used for measurement of the Kambalda samples lacks the resolution to detect it.

A number of spectra, with absorption features of quite variable strength, can be ascribed to the presence of talc. As the strength of talc absorption diminishes, the first noticeable effect on the shape of the absorption features is the disappearance of the 2.47 μ m minimum. However, the characteristic shapes at other wavelengths are retained over a much wider range of talc concentrations. Figures 6.8a,b&c depict the laboratory spectra of samples K10/304/F2/W (96% talc, 3% chlorite,

/1% magnetite, < 5% haematite), K11/W/67/S (65% quartz, 19% talc, 10% albite, 6% chlorite), and K3/88/S (78% quartz, 8% talc, 6% albite, 4% amphibole, 3% chlorite, <5% kaolinite, <5% haematite), respectively. Even at the low concentrations exhibited by K3/88/S, talc features can sometimes be seen. A further point of interest is that talc seems to have the strongest SWIR signal of all the minerals encountered at Kambalda. The strength of talc absorption features often dominate the spectra of samples that contain higher proportions of other minerals.

6.6.1.4.2 Chlorite

The spectrum of pure chlorite shows a lower reflectance than talc, and its background slope is curved, with lower values towards 1.4 and 2.5 μ m (Fig. 2.6). It has a major absorption feature near 2.34 μ m that is shallower and broader than for talc, and a weaker, but diagnostic, absorption feature at 2.0 μ m. This feature, combined with the 1.9 μ m water absorption band, results in a characteristic asymmetric feature in many samples. Chlorite also has a very sharp absorption near 2.26 μ m that can also be diagnostic ; talc and epidote have similar, but much weaker, absorption at this wavelength, so a prominent feature here indicates chlorite. The spectrum of sample K4/123/F/W (42% chlorite, 34% quartz, 23% plagioclase) is typical of chlorite (Fig. 6.9a). For many of the samples measured, chlorite shows the second strongest influence on the spectrum (after talc). Even where chlorite forms only a minor portion of the sample, its presence is often indicated by the 2.0 μ m absorption feature, because no other mineral found at Kambalda absorbs at this wavelength.

6.6.1.4.3 Amphibole

Like chlorite, amphibole has lower reflectance than talc, giving a curved background slope. Its dominant absorption feature lies at $2.32\mu\text{m}$, is narrower and deeper than chlorite's, but broader and shallower than talc's. It also has a secondary $2.4\mu\text{m}$ absorption that can appear either as a shoulder, or as a distinct minimum. In most cases the amphibole spectrum is affected to some extent by the spectral shape of other minerals, even when the percentage of those minerals is relatively low. Note that the spectrum in Fig. 6.9b (of K1/74/F1/W) contains only 7% chlorite, yet the $2.0\mu\text{m}$ absorption feature is still recognisable.

6.6.1.4.4 Mixtures

As noted above, in most cases where amphibole features are present, the amphibole spectrum is modified to some degree. Often this effect takes the form of a change in the shape or position of the amphibole absorption feature, but the proportions of different minerals required to effect those changes, and the severity of the effects, are quite variable. The nature of the surface (W or F) undergoing measurement may sometimes also influence the spectrum. Carbonate minerals, for instance, are conspicuously absent from weathered, surface samples (also confirmed by XRD analysis).

Figures 6.10a&b depict, respectively, spectra of K7/266/F/W (44% amphibole, 32% chlorite, 23% talc) and K7/180/F/W (61% talc and 33% chlorite), and show that talc need not be the most abundant mineral in order to dominate the spectrum. Hence there are relatively few cases where amphibole (confirmed by XRD analysis) dominates the laboratory

spectrum, and no examples yet are found among the airborne data. In most cases, therefore, the presence of a $2.32\mu\text{m}$ minimum has been attributed to talc unless other features of the spectrum are also consistent with amphibole. In all cases the mineralogy interpreted from airborne data needs to be checked against ground truth for unambiguous results.

Sample K1/31/F/P contains 50% amphibole and 43% chlorite, and spectral measurements of rock samples suggest that chlorite should dominate the spectrum. However, Fig. 6.10c is a spectrum of the XRD powder showing that it does not. Amphibole features are clearly dominant and only the $2.0\mu\text{m}$ absorption feature indicates the presence of chlorite.

Sample K6/448/F2/W2 comprises 42% amphibole, 25% chlorite and 5-10% epidote (only qualitative). This sample has a spectrum that superficially resembles amphibole, but has several important differences (Fig. 6.10d). The major absorption feature has migrated to a slightly longer wavelength ($2.34\mu\text{m}$), a shoulder has appeared at $2.26\mu\text{m}$, and the $2.4\mu\text{m}$ absorption has disappeared. Chlorite and epidote have features that could explain these modifications. The presence of chlorite is indicated by the $2.0\mu\text{m}$ absorption, but the shift of the major absorption to $2.34\mu\text{m}$ is more likely to result from the influence of epidote, which has a spectral shape similar to amphibole.

Several samples (particularly soils) comprise small amounts of a number of minerals. Sample K10/376/S, for instance, has minor quantities of calcite, amphibole, talc, kaolinite and montmorillonite recorded from XRD analysis. Its resultant spectrum (Fig. 6.11a) is difficult to interpret because of the shallow nature of the absorption

features. However, because one of the minima occurs at $2.32\mu\text{m}$, it can be inferred that talc (or talc and amphibole) is responsible.

Another sample that produces a shallow, broad absorption feature in the $2.35\mu\text{m}$ region is K10/273/F/W (Fig. 6.11b). Its XRD analysis has shown 40-50% diopside (non-quantitative). This spectrum is obviously difficult to differentiate from others with weak features produced by mixtures. However, as diopside is derived from Proterozoic dykes rather than Archaean rocks, failure to recognise its spectrum could prove significant. The sample was collected from an area mapped as basalt, and the airborne spectra in this region show only chlorite absorption features. It is therefore possible that the sample collected is not representative of the whole area.

6.7 Spectral Variation of Chlorites

During analysis of airborne SWIR spectra some variation was noted in the position of the sharp $2.26\mu\text{m}$ absorption feature of chlorite (Fig. 6.12). Variation in the position of the $2.34\mu\text{m}$ absorption minimum also occurs, but is easily accounted for by the influence of other minerals with spectral features in the same region.

As the CSIRO/MXY spectral reference collection includes chlorites of varying composition (mainly Fe and Mg contents), they were examined for any systematic trends in the wavelengths of their absorption features. No obvious trends were evident.

Hayashi and Oinuma (1967) reported results from a study of chlorites using absorption spectroscopy in the $3\mu\text{m}$ region. Their data show up to a $0.015\mu\text{m}$ (15nm) shift of Fe-chlorite absorption features to

shorter wavelengths with increasing Mg-content. This finding is consistent with theoretical considerations of bond lengths (and therefore vibration frequencies), relative to atomic weights of the elements involved. It is not unreasonable to expect a similar trend in the 2.0 to 2.5 μ m region with reflectance spectroscopy. Indeed, similar effects are seen in this region with, for instance, the carbonates.

So far there has not been a systematic study of the positions of absorption features of chlorites from Kambalda, or any other region, relative to their magnesium contents. Such a study could provide some extremely subtle mineralogical information from remotely sensed data.*

6.8 Airborne Spectrometer Data

6.8.1 Acquisition

A total of eighteen lines was flown on 30 September, 1982 in the Kambalda region. Of these lines, two were located on Lake Lefroy, and could be used in the future for modelling of reflectance. Two more flight lines, including one in the Bluebush area, did not pass over their respective target zones, and will not be considered here. Of the remaining fourteen lines, one (K1) is located over the southern portion of Kambalda Dome, seven (K2-K7 and K14) were flown over the St Ives region, five (K8-K10, K11West and K11East) are located over the Tramways region, and one (K13) was flown over the Democrat area (see Fig. 6.1). All lines were flown between 1:20 pm and 3:00 pm, with zero cloud cover giving near perfect conditions.

* Recent work by the author in collaboration with Dr. R. McLeod of the Darling Downs College of Advanced Education has confirmed that there is a systematic migration to shorter wavelengths of chlorite absorption features in the 2.26 and 2.33 micrometre regions with increasing magnesium content.

6.8.2 Analysis of radiance data - 'first-order' effects

Each flight line mean radiance spectrum is depicted in Figs. 6.13a-n. Like the Mt Turner airborne radiance spectra, they are dominated by atmospheric features. Unlike Mt Turner, however, there are no noticeable differences in the depth of the absorption in the 2.2 μ m region.

Examination of radiance data for effects due to absorption by minerals in the 2.3 μ m region (important at Kambalda, with talc, chlorite, amphibole, epidote, diopside and antigorite falling into this category) shows that the effects are very subtle. Figure 6.14a depicts an averaged radiance spectrum from an area with no significant mineralogy to produce absorption features, while a similarly derived radiance spectrum from a talc-rich zone is plotted below it (Fig. 6.14b). The absorption effects due to talc are subtle, and certainly much weaker than many examples of 2.3 μ m absorption reported in the literature (Collins et al., 1981). It is only when the log residual technique (chapter 3) is applied that talc features become apparent (Fig. 6.14d).

6.8.3 Analysis of log residual images - 'second-' and 'third-order' effects

Log residuals remove ubiquitous spectral features from the data. Hence, extensive mineralogical features and some of the effects due to widespread vegetation cover are effectively excluded.

Figures 6.15a-d depict the log residuals, in image format, from flight line K2. As with Mt Turner, there are some obvious trends, or

second-order effects present in the data. Interpretation at this stage involved the delineation, along a flight line, of boundaries between blocks, which appeared to be coherent. The data between these boundaries were averaged, and the block averages plotted. Visual examination of these plots aided the interpretation, which proceeded by allocating the blocks into one of a number of types, based on their spectral properties. Third-order effects are determined by interpreting a plot of the average spectrum for each block.

6.8.3.1. Type 1 spectra

The spectrally most distinct areas are those over salt lakes, clay pans, and highly disturbed areas (such as mullock heaps). During the survey there was considerable moisture in the salt lakes, with inches of water standing in some areas. The combination of very bright halite with water produces some unusual spectral effects. In the visible region (up to $0.7\mu\text{m}$) the halite produces extremely high radiance values, which at times saturated the instrument's detectors. The resultant large log residual values appear as bright red patches in the image presentation. In contrast, the near-infrared wavelengths (0.7 to $1.1\mu\text{m}$) are almost totally absorbed by the water, producing extremely low log residual values, and dark blue patches in the image presentation (Fig. 6.15d, blocks 20, 22 and 26). Very wet areas affect the SWIR similarly, extremely low radiance values, caused by broadening of the 1.9 and $2.5\mu\text{m}$ water absorption bands, lowering the radiance over the entire portion of the SWIR spectrum recorded. However, in some places, where the moisture content is lower, there is sufficient energy available between the two major water absorption minima to generate moderate to high log residual values in the $2.2\mu\text{m}$ region. Figure 6.16b depicts the laboratory

reflectance spectrum of a halite sample collected from Lake Lefroy. The moisture content is low, resulting in significant reflectance in the 2.2 μ m region. Over some sections of salt lake, a shallow absorption feature at 2.25 μ m was detected in airborne data Fig. 6.16a). An identical structure has been noted by Hunt et al. (1972), and is attributed to water absorption by fluid inclusions within the halite. At Kambalda, similar features are present in the airborne data acquired over mullock heaps at mine workings, and in some areas where transported dune sands predominate. Of five XRD analyses of dune sands, one showed an appreciable halite content. WMC personnel (D. Quick, pers. comm., 1983) have noted that extremely saline groundwater in the mines often results in a coating of salts on excavated rocks dumped on mullock heaps. It therefore seems reasonable that halite is responsible for many of these shallow 2.25 μ m absorption features. Type 1 spectra make an insignificant contribution to knowledge of the residual geology.

6.8.3.2 Type 2 spectra

The most obvious characteristic of type 2 spectra is the absence of strong absorption features in the SWIR data. Subsequent field checking has established that this characteristic generally reflects one of the fundamental sub-divisions discussed in Section 6.4. Most of the transported material in the area comprises aeolian sands, whose XRD analyses have shown quartz to be the overwhelming component. Minor albite, calcite, haematite, halite and kaolin are the other minerals that may be present. However, of these components, only calcite and kaolin are capable of producing strong absorption features in the SWIR region (calcite, as calcrete, produces unusual absorption features at Kambalda - see Sections 6.7.2 and 6.9.3.4). Thus, transported material

generally lacks strong absorption features in the SWIR, and this is mirrored in the airborne data.

6.8.3.3 Type 3 spectra

In contrast to Type 2 spectra, areas exhibiting significant absorption features in the SWIR are generally related to residual material. Remnants of lateritic duricrusts, for instance, tend to exhibit strong doublet absorption features in the 2.17 and 2.22 μm regions, the shapes of which indicate the presence of kaolin (Fig. 6.17). The residual weathered material derived from mafic and ultramafic rocks tends to produce absorption features in the region from 2.3 μm to longer wavelengths. In the Kambalda area this is, therefore, by far the most important region of the spectrum. From the log residual images, spectra with these 2.3 μm features can be further sub divided into two groups.

The first group comprises spectra with a quite sharp, deep absorption feature at 2.32 μm , and a second, weaker feature at 2.39 μm . These features are also visible on the log residual images (Fig. 6.15b). Figure 6.18 is the plot of a block mean from run K2 (samples 455 to 496). The spectral structure closely matches that of talc (see Fig. 2.6).

The second group contains more variable spectra, which makes interpretation more difficult. Examination of all of the block means from this group indicates that the absorption features are often similar to those of chlorite (refer again to Fig. 2.6), but other minerals (certainly amphibole and talc, and probably epidote) are also contributing to the spectral response. However, at this level of

interpretation (examination of log residual images), these effects are not always separable. Hence, this group is treated as a single entity for the moment, and these effects are attributed to 'mafic' minerals. Separation into component minerals (by examination of individual spectra) can be regarded as utilisation of 'third-order' variations (see 6.9.3.4).

Apart from one major exception, areas with strong SWIR absorption features are therefore indicative of the presence of residual material in the Kambalda region.

6.8.3.4 Type 4 Spectra

The major exception to the categorisation described above is due to the pattern exhibited by calcrete. The calcretes encountered in the Kambalda area are often most prominent in borrow pits, and other disturbed areas. XRD analyses indicate calcite, and hand specimens readily effervesce when acid is applied. However, airborne data, like laboratory spectra of the hand specimens, usually show calcrete-rich areas as having a 2.17 and 2.2 μ m doublet, characteristic of kaolin, rather than the 2.34 μ m absorption feature of calcite.

Table 6.2 summarises second-order effects interpretable from log residual image data.

6.8.4 Interpretation of data from flight line K2

The interpretations of the different spectra generated by averaging coherent blocks of data from flight line K2 are presented in Appendix IX, enabling an evaluation of the amount of spectral information (and

Table 6.2 Second-order effects interpreted from images of Kambalda airborne log residual data.

	Type 1	Type 2	Type 3	Type 3 (Talc)	Type 3 (Mafic)	Type 3 (Kaolin)	Type 4 (Kaolin)
VNIR Response	Extremely high values to 0.7 μ m, extremely low values beyond 0.7 μ m (due to water)	Lower values in the 0.4 to 0.7 μ m range than the 0.7 to 1.1 μ m region	Generally lower values in the 0.7 to 1.1 μ m region than in the 0.4 to 0.7 μ m range				Generally higher values in the 0.7 to 1.1 μ m region than in 0.7 μ m range
SWIR Response	Generally low. May have subtle 2.25 μ m absorption	Absence of strong absorption features	Strong absorption features	2.32 μ m absorption, strong and narrow. 2.38 μ m secondary feature	Absorption in the region longer than 2.3 μ m	2.17 & 2.2 μ m absorption doublet	Strong 2.16 to 2.2 μ m absorption doublet
Albedo	VNIR high, SWIR low	Moderate	Moderate to low				Moderate to high
Veg. Index	Very low	Moderate to high	Moderate to low				Moderate to high
Cause of spectral effects	Salt lakes, generally wet halite. Halite in drier areas, and in dune sands, on mullock heaps	Generally transported material, dominated by quartz sands. Vegetation	Residual material, outcrop, float and residual soils derived from Archaean precursors	Talc, derived from weathering of altered ultramafics	Contributions by chlorite, amphibole talc, epidote (antigorite ? and diopside?). Derived from ultramafic and mafic precursors. Can be sub-divided.	Kaolin, associated with lateritic ironstone remnants	Kaolin (?), as finely crystalline coating on calcrete nodules?

variation) present within a typical flight line. It also gives an appreciation of some of the difficulties inherent in the interpretation of log residual spectra. What, for instance, does a 'ramp' spectrum (increasing log residual values from shorter to longer wavelengths) represent? The answer lies in identification of the spectral content of the flight line mean, a task beyond the capabilities of available software.

For many of the blocks discussed in Appendix IX there are three separate spectral graphs. The first graph plots the log residual data over a minimum range on the y-axis, allowing the most accurate determination of the shape of individual spectra, hence the best chance of assigning the correct mineralogy. The second set of plots presents the same information on a constant y-axis scale, thus facilitating assessment of the relative strength of absorption features along a flight line. Finally, laboratory spectra of samples collected from each block, and their XRD analyses, are also presented for comparison wherever they are available.

6.8.5 Significant airborne spectra

Some aspects of the more important spectral types are discussed in the following sections, with particular reference to their correlation with ground truth.

6.8.5.1. Talc spectra

With very few exceptions the ultramafic units are identified by the presence of talc spectra. It is especially notable that many of the talc-rich areas defined by the spectral data agree well with the

interpreted boundaries. These areas are generally much more extensive than the accumulations of float or outcrop that can be mapped, suggesting extensive areas of residual soils developed from ultramafics in the areas covered. XRD analyses, and laboratory reflectance spectra of soil samples (see Section 6.7) support this interpretation.

One example of such a talc-rich soil comes from flight line K9. Here the soil is partially covered by lichen (Fig. 6.19a), but XRD analysis of exposed portions of the soil (at pixel 202) gave the composition: 44% quartz, 25% talc, 15% albite, 14% chlorite, 2% dolomite, and 1% calcite. The averaged log residual spectrum of pixels 201 to 203 shows a strong talc signal (Fig. 6.19b).

6.8.5.2 'Mafic' Spectra

A good agreement between spectral properties and geology is also evident with mafic spectra. The footwall and hangingwall basalts, with an amphibole/chlorite mineralogy, comprise the majority of the rocks in this category.

In most instances mafic signatures occur over, or between, mapped outcrops, but, in contrast to talc signatures, they are generally not recorded over much of the other ground between interpreted boundaries. In many cases the presence of transported sands or lateritic material effectively obscures any residual mafic minerals that may be present. However, there are a few instances where this is not the case.

6.8.5.3 Kaolin Spectra

Kaolin spectra are difficult to separate from some type 2 spectra

(an absence of strong features) because the two groups tend to overlap. For this reason only the strongest kaolin spectra have been included in the interpretive figures.

The most common cause of this spectral response is laterite, with duricrust or significant accumulations of ironstone float both producing kaolin features (see again Fig. 6.17).

6.8.6 Distribution of mineralogy interpreted from 'second- and third-order' effects

Interpretation of second- and third-order effects from all flight lines being considered at Kambalda is presented as overlays to Figs. 6.20 & 6.21, and in Figs. 6.22a&b. The solid boundaries on Figs. 6.20 and 6.21, compiled from 1:7500 map sheets by WMC, represent areas with significant accumulations of float or outcrop. The low percentage of mappable material is evident on this presentation. The dashed lines are interpreted boundaries, determined by WMC using considerable drilling and geophysical data acquired over a period of 15 years, in addition to the outcrop maps.

6.8.6.1. St. Ives

Of the seven flight lines in the St Ives area, six intersect ultramafic units (Fig. 6.20).

At first sight there are two notable exceptions (on flight lines K5 and K6) to the extremely good definition of ultramafic units by the distribution of talc. Figure 6.20 shows that kaolin signals have been detected in the airborne data where the flight lines cross the

ultramafic horizon near Foster Mine. However, field checking revealed that the flight lines pass over lateritic float rather than talc-rich ultramafic rocks in this area. Laboratory reflectance measurements produce characteristic kaolin features, in agreement with the airborne measurements.

Of the remaining flight lines, all except line K3 show a better correlation with the interpreted ultramafic boundaries than with the mapped areas of outcrop/float. Thus, even in the St Ives area, where outcrop is reasonably good, there are still additional indications of talc in residual soils. Along line K3 the distribution of talc spectra matches the mapped outcrop fairly well.

The result is almost as impressive for the distribution of mafic spectra. These spectra are always obtained over mapped areas of outcrop, and, in a few areas, there are indications of mafic minerals elsewhere (around pixel 300 on line K2, pixels 150-190 on line K14, and several areas on lines K4, K7 and K5). In addition, there are indications of variations in the mineralogy of the basalts, with diagnostic spectral features for various combinations of the minerals chlorite, amphibole and epidote in evidence (Fig. 6.20).

There is one area where the intersection of flight lines K2 and K4 produces slightly different spectral features (chlorite-amphibole versus amphibole-epidote). This effect may be because the signature interpreted is the average of an entire block of spectra. It is conceivable that different minerals could dominate the spectra of each of the blocks.

6.8.6.2 Tramways

Outcrop at Tramways is minimal, and there are only minor basalt occurrences, and scattered accumulations of ultramafic float (Fig. 6.21). There are, not surprisingly, few indications of mafic mineralogy, those that do exist occurring over known outcrop, with the exception of a few pixels around 270 on line K9. However, the occurrence of talc in the soil is detected extremely well, with extensive areas mapped over lines K11W and K9, in particular. Minor occurrences are also evident on lines K8 and K10. The result is an indication of talc distribution dramatically better than given by mapping alone.

The other common mineral detected is kaolin, due to numerous accumulations of lateritic float in the area.

6.8.6.3 Kambalda Dome

The interpretation of results from the single line flown over Kambalda Dome is depicted in Fig. 6.22a. The mineralogy interpreted from airborne data appears on the top segment of both Figs. 6.22a&b. The geology as mapped by WMC appears in the middle, and the bottom segment indicates the percentage of outcrop or float present. The results from Kambalda Dome are good, despite significant cultural disturbance in the area. The spectra are, however, displaced relative to the geology. At the eastern end of the line this shift is primarily a function of the instrument to camera alignment, but at the western end it is a geomorphological effect, movement of the surface material downslope obscuring the outcrop below on, which the geological map is based. Note that the footwall basalt (90% outcrop) is sub-divided by

the spectral signatures into a chlorite zone and an amphibole/chlorite zone, separated by a small region of 'background' spectra. Strong talc and talc/chlorite signatures are in evidence on both sides of the 'Dome'.

6.8.6.4 Democrat

The single line over the Democrat region traverses ultramafics, acid intrusive, basalts, sediments, and the mafic intrusions. Surface expression is generally poor to very poor, with only mafic intrusives having appreciable outcrop. Nevertheless, talc signatures from residual soils are in evidence near the start of the line (Fig. 6.22b). Kaolin signatures are common over the weathered acid intrusive, and a small ultramafic unit between pixels 240 and 260 is also detected, again due to talc in residual soils. A variety of mineralogy is interpreted from the areas of mafic intrusive, including amphibole/chlorite, chlorite, and amphibole/epidote.

6.8.7 Other analysis techniques

Several other techniques have been applied to analyse the airborne spectrometer data. Tchebychev analysis is the technique favoured by Collins (Collins et al., 1981, GER, 1983) but it suffers from the disadvantage that the effects of a particular mineral assemblage on the Tchebychev coefficients are not easily determined. As a technique for separating areas with 2.2 μ m absorption features from 2.3 μ m absorption features it is relatively useful, but the same goal is achieved by examination of log residual images. For the separation of subtle spectral differences, classification techniques (as used for Mt Turner),

and a combination of carefully chosen narrow band data, are often more successful, and always easier to understand.

Figures 6.23a&b depict the results of ratioing a number of narrow bands and plotting their variation along flight line K2. The wavelength intervals for these data were chosen by examination of the log residual images (Fig. 6.15a-d), but the values themselves were calculated from radiance data. The various combinations of bands were designed to maximise the information in the 2.3 μ m region, the most important spectral interval at Kambalda.

Figure 6.23a is the ratio of the integrated interval from 2.3018 to 2.3276 μ m with a 2.2158 to 2.3018 μ m band. The first interval is centred on talc's major absorption feature, whilst the second lies in an area where few minerals absorb energy. Any mineral with absorption features in the 2.3 μ m region should therefore give low values for this ratio. Four such areas are evident on the plot. It should be noted that these areas agree very well with the boundaries superimposed on all figures. (These are the boundaries interpreted from the log residual image, and the plots of their mean spectral response appear in Appendix VIII.) As one might expect, the two areas known to contain talc have the lowest ratio values, while the values from the chlorite and amphibole-rich areas are closer to background.

The second plot (Fig. 6.23b) is a ratio of the same narrow 'talc' band with a third band immediately adjacent to it, on the long wavelength side. The purpose of this ratio is to differentiate the extremely narrow talc absorption feature from broader absorption features, or features that are centred on longer wavelengths due to other minerals. In this presentation, the area containing most talc

(pixels 456-495) differs most from background. The second area (pixels 366-398) containing talc, as part of a talc-chlorite mixture, is still outlined, but is closer to background values than the first area. This change is due to the greater breadth of its major absorption feature, and the fact that it is centred on $2.33\mu\text{m}$. A small part of a third block (near pixel 300 of the 278-328 region) also exhibits lower-than-background values, indicating that there may be some contribution from a mineral with narrow $2.32\mu\text{m}$ absorption features (amphibole?) in this area.

Figure 6.24a is a plot of the log residual values in the 2.3018 to $2.3276\mu\text{m}$ (talc) band. Because the log residual process has been applied to these data, the values in this band reflect the relative depths of absorption features along a flight line. Again, as one might expect, the talc-rich areas exhibit the deepest absorption features.

From the information contained in these plots, the value of narrow-band scanner imagery can be inferred. With carefully chosen bands there should be no problem differentiating talc from mafic minerals, and, to some extent, separating areas dominated by different mafic assemblages.

In contrast the information available from a broad-band scanner system (such as the thematic mapper) is much less definitive (Fig. 6.24b).

6.9 Comparison of Airborne and Laboratory Spectra

At this stage, precise comparison of airborne and laboratory spectra is impossible. The different units (radiance for airborne data,

reflectance in the laboratory) and the vastly different fields-of-view, preclude such comparison.

However the data have shown in the case of flight line K2, that many laboratory spectral features are duplicated in the airborne data (see Appendix IX), particularly where the airborne log residuals show strong spectral features over talc-rich ultramafic terrain. There are minor problems in matching some of the $2.2\mu\text{m}$ absorption features which are in the airborne data because they are sometimes displaced to either side relative to laboratory spectra. This effect is attributed to the presence of material (halite, vegetation, etc.) that has not been included in the samples for laboratory measurement. Field spectral measurement is required to pin-point the source of some of these variations.

There are also problems in comparing two data sets with very different noise levels. The laboratory data have high signal-to-noise ratios, while the log residuals (being residuals) are very noisy in many cases. However, it is notable that some very minor features (for instance the shoulder at $2.30\mu\text{m}$ on talc's major absorption feature) consistently appear in association with other diagnostic features - even though they often appear to be below the noise levels. Future instruments should, therefore, be as sensitive as possible in order to maximise the detection of subtle, but significant, residual features, and at the same time minimise channel-to-channel variations.

6.10 Summary

The aim of the project at Kambalda was to differentiate spectral effects due to weathering and soil transport from the primary mineralogical effects due to Archaean rocks, and to identify the latter.

Variations in corrected SWIR airborne radiance data produce first-order effects, but this form of the data is dominated by atmospheric absorption features. In a similar - but unweathered - geological environment, first-order variations may be sufficient to delineate much of the mineralogy. However, at Kambalda (as with Mt Turner), this is not the case, ubiquitous weathering products tending to suppress mineral absorption features. Laboratory measurement of individual weathered samples shows that characteristic spectral features are still present in many cases, but too weak to over-ride the atmospheric effects found in radiance data.

The logarithmic procedure was used to correct radiance data for albedo and atmospheric variations. The resultant 'log residuals' were presented in an image format. In this form coherent blocks of data (with a similar spectral response) can be easily delineated.

Transported material (mainly quartz as dune sand) generally has a subdued spectral response, vegetation often contributing much of the signal. It is therefore the absence of strong mineral absorption features that tends to characterise this material. In future studies MIR data should provide more direct information about the mineralogy of the transported material.

Various materials produce moderate to strong absorption features in the SWIR. In the 2.2 μ m region kaolin features are common at Kambalda,

but particularly strong over laterite and calcrete accumulations. Both laboratory and airborne data show that calcrete does not have the expected absorption features of calcite, and this is attributed to the presence of kaolin coating individual calcrete nodules, which suppresses the calcite spectral features.

Mafic and ultramafic rocks of the Kambalda sequence are easily differentiated from other material by the presence of strong log-residual absorption features in the 2.3 μ m region. Several techniques, including log residual images, band ratios and Tchebychev analysis, are capable of highlighting this distinction. However, discrimination of spectral effects due to individual minerals requires much closer scrutiny of the data. Detailed examination of log residual images, and plots of block means derived from them, allow sub-division of the data on the basis of spectral shape and the precise location of absorption minima.

Talc-carbonate altered ultramafics are dominated by talc, which has a very characteristic spectrum. Examination of spectral plots from airborne data allows the discrimination of talc-rich areas from assemblages of other 'mafic' minerals. Furthermore, the influence of a number of different mafic minerals can be seen in the block means. The detection of talc, in particular, is significant in the context of regional exploration. The distribution of talc as determined from airborne data is much more extensive than mapped outcrop, indicating a significant component of talc in residual soils. In general, the talc distribution matches interpreted lithologic boundaries better than outcrop distribution, with one area of talc-chlorite outlined beyond the

area of mapped ultramafics. Mineral assemblages more characteristic of mafic rocks are usually easily differentiated from talc, although there is some overlap. Variations in the mineralogy of basalts are also detectable in the airborne data, with amphibole, chlorite and epidote all producing noticeable spectral features.

The importance of ground-truth, in the form of spectral measurements in either the field or the laboratory, cannot be overemphasised - especially given the current paucity of knowledge of the spectral properties of Australian terrain. The interpretation of the Kambalda airborne data set would inevitably have been much less detailed without the laboratory spectra.

Laboratory spectra measured from samples collected along the flight lines agree closely with airborne data in most cases, although additional information is often available from these data. Laboratory spectra may also provide information on the composition of chlorites.

From the limited data presented, it seems that a reduction in spectral resolution (for instance as required for many scanners) will inevitably result in the loss of some subtle mineralogical information, even if the instrument has very narrow bands. However, careful selection of bands based on detailed spectral measurements should minimise this loss. The advantages of a two-dimensional coverage of spectral data at Kambalda may outweigh this disadvantage.

Of more concern is the level of information that could be extracted from Landsat D, TM imagery (or data from similar broad-band airborne instruments). The differentiation of kaolin-rich areas from Archaean

rocks would be difficult with the broad-band information available in the SWIR. The differentiation of more subtle mineralogical variations (such as ultramafic from mafic rocks) will be correspondingly more difficult. However, this assessment does not take into account the amount of information available from other portions of the spectrum, and the advantages of an imaging system. In many cases Landsat MSS data, for instance, have surpassed expectations based on known spectral properties of the area under study.

As with Mt Turner, the Kambalda study confirms the ability of high-resolution spectrometer data to map significant mineralogies in economically important terrain. The detection of talc-rich zones characteristic of talc-carbonate altered ultramafics would be particularly significant in the context of a regional exploration program. However, the effects of weathering mean that careful processing and interpretation techniques are necessary to maximise the utility of the data.

With careful positioning of bandpasses, and use of the correct processing techniques, the identification of ultramafic, mafic and felsic lithologies should also be possible using high quality narrow-band scanner imagery. Broad-band systems (such as the Thematic Mapper) will not achieve the same level of discrimination.

CHAPTER 7 FORTESCUE GROUP BASIC VOLCANICS, HAMERSLEY BASIN, WESTERN AUSTRALIA

7.1 Introduction

This chapter describes a pilot study evaluating the potential of high-resolution spectral data for discriminating and identifying mineralogical variation within a basic volcanic rock suite. The samples studied come from the Fortescue Group of the Hamersley Basin, which falls between latitudes 21° to $23^{\circ}30'S$, and longitudes $116^{\circ}30'$ to $120^{\circ}30'E$.

Previous Landsat MSS investigation has discriminated large areas of metasomatic, hydrothermal alteration in some areas of the basic volcanics (Smith et al., 1978). The present study has two specific aims. The first is to examine high-resolution VNIR spectra of rock samples from the area, allowing an assessment of the contribution by outcrop to the Landsat MSS response. Secondly, high-resolution SWIR and MIR reflectance spectra are interpreted to identify spectral responses in other wavelength regions. These responses may assist in discriminating and identifying metasomatic alteration minerals, and mineralogical variations due to varying grades of regional burial metamorphism.

The study includes laboratory measurement, and interpretation, of VNIR and SWIR reflectance spectra of samples whose mineralogy has been determined by thin section examination. MIR laser reflectance measurements were also obtained, and interpreted.

7.2 Regional Geological Setting

With an area exceeding 100,000 km², the Archaean* Hamersley Basin forms one of the major geological features of Western Australia. The stratigraphy is summarised by Trendall (1975, 1979). The Mount Bruce Supergroup is the major component of the basin, and comprises the Fortescue, Hamersley and Turee Creek Groups.

The Fortescue Group, the subject of this study, is the oldest of the three groups. The main constituents are basic to intermediate volcanics, with some quartz sandstone and arkose at the base, and shale, minor felsic volcanics and jaspilite near the top. It reaches a maximum thickness of 4500m in the southern portion of the basin, but is much thinner (360m) in the north, near Nullagine (de la Hunty, 1963).

The Hamersley Group, which succeeds the Fortescue Group, is dominated by chemical sediments (jaspilites and dolomites) accumulated under very stable conditions. There are three major Iron Formations (mainly jaspilite) which form a major reserve of iron ore.

The youngest conformable group in the Hamersley Basin is the Turee Creek Group. It is present only in the southern portion of the basin. Figure 7.1 shows the distribution of these major components of the Hamersley Basin.

The overall structure of the basin is that of an asymmetric syncline. Dips are gentle (5° to 10° southwards) in the north, becoming progressively steeper to the south. Dips of 45° to 60° (to the north)

*Once considered a typical Proterozoic basin, recent geochronological work has shown a preferred age for initiation of the basin of about 2750my, making it Archaean (Trendall, 1983).

are common near the basin axis, and on the southern margin of the basin, near vertical and locally overturned limbs are present (Smith et al., 1982).

7.2.1 The Fortescue Group

Deposition of the Fortescue Group was initiated around 2750 my ago (Trendall, 1983). There were four main eruptive phases, separated by periods of volcanic quiescence when sediments accumulated. The eight recognised formations are in Table 7.1 (after Hickman, 1983) below :

Table 7.1 Formations of the Fortescue Group

	Formation Name	Constitution
Top	Jerrinah Formation	sandstones, siltstones, shales, cherts
	Maddina Basalt	basalts and andesites
	Kuruna Siltstone	sandstones, siltstones, shale (local)
	Nymerina Basalt	basalts, minor pyroclastics, sediments
	Tumbiana Formation	tuffs and carbonates
	Kylena Basalt	basalts and andesites
	Hardey Sandstone	sandstones, conglomerates, minor shale
Bottom	Mount Roe Basalt	basalts and andesites

7.3 Metamorphic Setting

Smith et al. (1982) showed that the Hamersley Basin has been subjected to regional metamorphism due to subsidence and burial. This

metamorphism describes a process whereby water-laden sequences are buried and heated. An increase in burial depth leads to a progression in metamorphic grade from prehnite-pumpellyite, through pumpellyite-actinolite and to greenschist facies as a function of associated thermal effects. Because of the role of expelled water, metasomatic alteration can also result, particularly in permeable parts of the sequence. Smith et al. (1978) have shown that, during regional burial metamorphism, extensive metasomatism has affected the volcanic pile in the Hamersley Basin. This process is conspicuously expressed in mineralogical variations mainly within the volcanic rocks of the Fortescue Group.

Smith et al. (1982) have shown that individual, relatively homogeneous lava flows have subsequently become markedly heterogeneous due to changes in rock chemistry and concomittant metamorphic mineral associations. This heterogeneity is most marked in, and adjacent to, the scoriaceous flow tops and volcanic breccia horizons (Fig. 7.2). These rocks had sufficient permeability to allow the passage of metamorphogenic fluids. In contrast, the central, more massive, parts of individual flows are the least altered. Figure 7.3 (after Smith et al., 1982) illustrates the amount of variation in silica and iron for two typical flows. While the massive, central parts of flows are relatively uniform, flow tops show a scatter of rock composition, a marked loss of Fe, Mg, Na, K, Mn, Rb, Ba, Sr, Pb and Rare Earth Elements, and a gain in Si, Ca and, in some samples, Al.

Smith et al. (1982) have also shown that the depth of burial has varied significantly across the Hamersley Basin, leading to the formation of four reasonably well-defined metamorphic zones (Z-I to Z-IV). Zones Z-I and Z-II fall within the prehnite-pumpellyite facies, Z-

III within the pumpellyite-actinolite facies and Z-IV in the greenschist facies. The boundaries of these metamorphic zones are shown on Fig. 7.4, along with the location of samples used for this study.

The mineralogy of basic volcanic samples from the area will thus depend on both metasomatic effects and metamorphic effects, leading to some quite complex mineralogical variations. In an attempt to simplify description of these effects Smith et al. (1982) introduced a terminology that will also be used here. Relict domain is used for those massive parts of flows in which the original magmatic mineralogy dominates, and the effects of metamorphic/metasomatic alteration are smallest. Beyond about late Z-III, this is no longer an appropriate term because of metamorphic equilibration. Uniform metadomain (denoting a relatively uniform bulk mineralogy and, where tested, rock composition, and therefore minimal metasomatism) is then used instead. The heterogeneous metasomatically altered portions of flows are comprised of various types of metadomains that are named from the dominant metasomatic mineral species (e.g. pumpellyite-rich metadomain, epidote-rich metadomain, etc.).

The mineralogical variation found by Smith et al. (1982) in each of the metamorphic zones Z-I to Z-IV is described in sections 7.3.1 to 7.3.4 respectively, with emphasis on the mineralogy of the samples used for this study. Table 7.2 summarises the mineralogy and includes a key to the abbreviations of mineral names used below.

7.3.1 Zone I - prehnite-pumpellyite zone

In flow tops a complete range exists between pumpellyite-rich, albitised rocks and silicified metasomatically altered rocks. Prehnite

Table 7.2 Summary of mineralogic variation with metamorphic grade in Fortescue Goup rocks (based on data from Smith et al., 1982).

	Metadomain	Transition	Relict domain
Z-I	pu+qtz ab+qtz+chl ab+qtz+pu+chl+sph	pr+pu+chl±[cpx]	[ca plag+cpx]+chl+sph±cc ± trace pu [ca plag+qtz]+chl+sph
Z-II	As above, but with epi epi+qtz+trace pu+sph		As above
Z-III	As above, but with act. Epidote assemblages more common epi+qtz+trace sph		As above, but with act. <u>Becomes Uniform Metadomain</u> ab+epi+act+sph common
Z-IV	epi+act+chl+access cc common		<u>Uniform Metadomain</u> ab+[cpx]+qtz+chl+act+tr.epi+pr ab+chl+act±pr±epi±sph

Abbreviation	Mineral name	Formula	Unique Spectral Response		
			VNIR	SWIR	MIR
pu	pumpellyite	$\text{Ca}_4(\text{Mg}, \text{Fe}^{2+}, \text{Mn})(\text{Al}, \text{Fe}^{3+}, \text{Ti})_5\text{O}(\text{OH})_3$	x	/	?
qtz	quartz	$[\text{SiO}_2\text{O}_7]_2 [\text{SiO}_4]_2 \cdot 2\text{H}_2\text{O}$ SiO_2	x	x	/
pr	prehnite	$\text{Ca}_2\text{Al}_2(\text{Si}_2\text{O}_{10})(\text{OH})_2$	x	/	?
ab	albite	$\text{Na}(\text{AlSi}_3\text{O}_8)$	x	x	/
chl	chlorite	$\text{Mg}_3(\text{Si}_4\text{O}_{10})(\text{OH})_2$ $\text{Mg}_3(\text{OH})_6$	x	/	/
sph	sphene	$\text{CaTiO}(\text{SiO}_4)$	x	x	x
cpx	clinopyroxene	$\text{Ca}(\text{Mg}, \text{Fe}, \text{Al})(\text{Si}, \text{Al})_2 \text{O}_6$	x	x	/
ca plag	calcic plagioclase	$\text{CaAl}_2\text{Si}_2\text{O}_8$	x	x	/
cc	calcite	CaCO_3	x	/	/
epi	epidote	$\text{Ca}_2\text{Fe}^{3+}\text{Al}_2\text{O} \cdot \text{OH}[\text{Si}_2\text{O}_7][\text{SiO}_4]$	x	/	/
act	actinolite	$\text{Ca}_2(\text{Mg}, \text{Fe})_5(\text{Si}_8\text{O}_{22})(\text{OH})_2$	x	/	/

is widespread as a minor or trace phase, but epidote is entirely absent from Z-I. Assemblages present in the suite of rocks used for this study are pu + qtz, ab + qtz + pu + chl + sph, ab + qtz + chl (see Table 7.2). Rocks from the transition between the flow top and the massive central part of a flow contain the assemblage pr + pu + chl ± [cpx] (Relict phases are enclosed []). In the more massive, central parts of flows relict phases dominate, with the assemblages [ca plag + cpx] + chl + sph ± cc ± trace pu and [ca plag + qtz] + chl + sph.

7.3.2 Zone II - prehnite-pumpellyite-epidote zone

At the commencement of this zone, trace amounts of epidote occur either in the groundmass or in partly altered plagioclase grains. About half-way through the zone, epidote-rich metadomains become particularly conspicuous. The single Z-II sample used in this study is from one of these metadomains, and contains epi + qtz + trace pu + sph. However, the flow tops still contain similar assemblages to Z-I, and pumpellyite is abundant, being the most conspicuous phase in the Z-II flow top outcrops. The variety of assemblages is increased by the presence of epidote in varying proportions. Relict domain assemblages are similar to those of Z-I.

7.3.3 Zone III - prehnite-pumpellyite-epidote-actinolite zone

The first appearance of actinolite marks the start of Z-III. Where pumpellyite or epidote is abundant, actinolite occurs only in trace quantities, but it is more common in albitised rocks and relict domains. An epidote-rich metadomain sample was used in this study, with an epi + qtz + trace sph mineralogy.

Relict domains are replaced by uniform metadomains towards the end of Z-III. An $ab + epi + act + sph$ mineralogy is most common, but the Z-II sample used here contains some relict pyroxene.

7.3.4 Zone IV - actinolite zone (greenschist facies)

The beginning of Z-IV is marked by the disappearance of pumpellyite. As for lower grades, flow tops are heterogeneous and have abundant metamorphic phases, but epidote-rich metadomains are most common ($ep + act + chl + acces. cc$). Central parts of flows are almost completely adjusted by metamorphism and are now termed uniform metadomains. They have little relict material, as evidenced by the samples used for this study containing $ab + [cpx] + qtz + chl + act + trace\ epi + trace\ pr$, or $ab + chl + act \pm pr \pm epi \pm sph$.

In summary, diagnostic minerals indicating changes in regional metamorphic grade are pumpellyite, prehnite, epidote and actinolite. Essentially ubiquitous minerals are quartz, albite, chlorite and sphene. However, the presence of large amounts of albite and/or quartz is indicative of metasomatic alteration, as is the presence of pumpellyite, prehnite and epidote in quantity.

7.4 Previous Remote Sensing Investigation

Smith et al. (1978) reported a study based on the use of Landsat 1 imagery covering a large area in the Z-I facies of the Fortescue Group. In particular, the study covered part of the Maddina Basalt.

Metasomatic alteration in the Maddina Basalt shows some similarities to the hydrothermally altered Keweenaw flood lavas of

Michigan (U.S.). In this area stratabound native copper deposits, with ore shoots ranging from 20 million tons to greater than 100 million tons, occur intimately associated with hydrothermal alteration in the Keweenawan lavas. Smith et al were investigating parallels between the two sequences in an attempt to assess the potential for similar mineral deposits in the Fortescue Group. They used Landsat imagery in an attempt to detect the extent of alteration in the Maddina Basalt. The study was very successful, for it was through interpretation of the Landsat data that the true lateral extent of the flow units and their associated metasomatism were recognised. Collectively a stratigraphic unit of altered lava flows has been mapped over a strike length of 350 km (Smith et al., 1978), whilst individual altered flows have been mapped over strike lengths exceeding 100 km.

In areas of flat or gently undulating terrain hydrothermally altered lavas have a thin, light-coloured, dusty soil. There are abundant float and sub-crop which exhibit thin, brown, oxidation coatings. Approximately 20% to 40% of the ground is covered by clumps of spinifex grass.

In contrast, the soils in similar topography over unaltered basalts are brown cracking clays. They are also strewn with cobbles and boulders, but spinifex covers only about 10% of the ground surfaces. Annual grasses and small, brown, herbal plants are in evidence. These differences are inferred to be the result of the disparity in total iron content between altered and unaltered material (Smith et al., 1978).

In some parts of the original study area, headward stream erosion has resulted in a hilly terrain. Soil has largely been stripped, and vegetation comprises a uniform cover of spinifex grass. In these areas

there was no detectable difference on the Landsat imagery between altered and unaltered lavas.

In those areas where lava alteration could be discriminated, the spectral responses of the different soil types and vegetation were thus held responsible for the differentiation by MSS, rather than the outcropping rock itself.

Laboratory VNIR spectra of representative rock samples from the region might therefore be expected to check this interpretation. In addition, laboratory measurements in the SWIR and MIR should establish whether there are detectable spectral differences in the other wavelength regions of interest for remote sensing.

7.5 Laboratory Spectral Measurements

Table 7.3 summarises the interpretations made from the Fortescue Group rock spectra. The spectra appear individually in Appendices X (VNIR), XI (SWIR) and XII (MIR).

7.5.1 VNIR W (weathered) surface spectra

In general the VNIR spectra of weathered surfaces are interpreted as being influenced by the presence of haematite. The samples from the same metamorphic zone (Z-I) as the Landsat study of Smith et al. (1978) show no significant difference in the position of their major absorption features. The absorption due to crystal field effects has a mean position of $.866\mu\text{m}$ with a variance of $.00013$ (10 spectra) for rocks from metadomains. The mean value is $.858\mu\text{m}$ with a variance of $.0001$ (6 spectra) for rocks from the relict domain. With the exception of

Table 7.3 Summary of the interpretation of laboratory spectra of samples from the Fortescue Group.

Sample	Mineralogy	VNIR W		VNIR F		SWIR W		SWIR F		MIR W		MIR F	
		λ	Interp.	Interp.	Interp.	Interp.	Interp.	Ratio	Interp.	Ratio			
METADOMAIN - Z-I	8288	pu+qtz	.864	he	pu (Fe ³⁺)	pu	pu	qtz+he	3.5	qtz	5.2		
	10093	ab+qtz+cpx+chl+sph	.866	W1	Fe ²⁺	clay	chl	qtz+he	3.1	qtz+ab?	4.6		
	10093		.867	W2		pu+clay	W2						
	10110	pr+pu+chl	.864	he	Fe ²⁺	chl+pu?	chl+pu	he	3.3	pr?+qtz	3.5		
	10109	pr+pu+chl+cpx	.867	W1	Fe ²⁺	pu+chl?	W1	pu+chl	qtz?+he?	5.0	pr?+qtz	2.5	
	10109		.849	W2		pu+chl?	W2						
	10115	pu+qtz	.853	he	pu (Fe ³⁺)	clay	pu	he+qtz?	2.8	qtz	5.0		
	10112	pu+qtz	.868	he	pu (Fe ³⁺)	clay	pu	he	4.0	qtz+?	3.1		
	10112		.894	goeth		clay+pu?							
	10103	ab+qtz+chl	.869	he	Fe ²⁺	min clay,chl?	chl	he+?	2.6	ab+qtz	2.5		
RELICT DOMAIN - Z-I	10100	plag+cpx+chl+sph	.851	he	Fe ²⁺	clay	chl	he (str)	1.9	plag+cpx?	2.4		
	10102	plag+cpx+chl+sph	.850	he	Fe ²⁺	clay	chl	he	2.1	plag+cpx?	2.3		
	10090	plag+cpx+chl+sph	.854	he	Fe ²⁺	clay+chl?	chl	he	2.5	plag+cpx?	2.6		
	10105	plag+cpx+chl+sph	.879	he	Fe ²⁺	kao?+chl?	chl	he (str)	2.4	plag+cpx?	1.9		
	11158-A	plag+cpx+chl+sph	.858	he	Fe ²⁺	clay+chl?	chl	he	2.4	plag+cpx?	1.9		
	10118	plag+cpx+chl+sph+cc	.857	he	Fe ²⁺	kao	chl	he (str)	1.9	plag+cpx?	2.0		
METADOMAIN - Z-II	10045	epi+qtz+tr pu+sph	-	-	epi (Fe ³⁺)	epi	epi	qtz+he	3.0	epi+qtz	2.1		
METADOMAIN - Z-III	10863	epi+qtz+tr sph	.856	he	epi (Fe ³⁺)	epi	epi	qtz+he?	2.9	epi+qtz	2.3		
RELICT DOMAIN - Z-III	10864-B	plag+cpx+chl+sph+epi	.862	he	Fe ²⁺	kao	chl	he	1.6	mafic	1.8		
UNIFORMLY ALTERED DOMAIN - Z-IV	10843	ab+cpx+qtz+chl	-	-	Fe ²⁺	clay+chl?	chl+epi?	he (str)	2.0	flat	1.6		
		+act+tr epi,pr	-	-	Fe ²⁺	chl	chl+pr?	he	1.5	mafic	1.4		
	10848	ab+chl+act+pr	-	-	Fe ²⁺	act+chl?	chl+epi	he	1.5	mafic	0.8		
12958	ab+chl+act+epi+sph	.874	he	Fe ²⁺	+act?								

KEY

pu	pumpellyite	qtz	quartz	goeth	goethite
ab	albite	cpx	clinopyroxene	clay	undifferentiated clay
chl	chlorite	sph	sphene	tr	trace
pr	prehnite	plag	calcium plagioclase	?	uncertain
cc	calcite	epi	epidote	min	minor
act	actinolite	he	haematite	str	strong
		kao	kaolin	-	no absorption

spectrum 10112 W2 (probably goethitic), the rest of the spectra appear to be haematitic - including spectrum 10112 W1 (Figs. 7.5a-c).

It is therefore not surprising that the study by Smith et al. failed to separate altered and unaltered material in hilly terrain, where outcrop is at a maximum. These results show that there is essentially no difference between the VNIR reflectances of the natural surfaces in the two groups of samples. This finding also supports the conclusion that the differences on Landsat imagery are due to the differences in soil development and vegetative cover.

In the higher grade metamorphic zones, the W surface spectra show either similar results to the Z-I rocks (haematitic characteristics, with absorption in the .856 to .974 μ m range, see Fig. 7.6a), or else a lack of absorption Fig. 7.6b). For the samples falling into the latter category (10045, 10843 and 10848), the hand specimens have less weathered surfaces. This characteristic can scarcely be due to a lower whole-rock iron content, as the altered Z-I rocks are iron deficient, yet have VNIR properties identical with the unaltered samples.

7.5.2 VNIR F (fresh) surface spectra

The VNIR F surface spectra fall into two categories. Most spectra have a concave shape, with a major absorption feature at a wavelength between .899 and .923 μ m, and sometimes a secondary feature at shorter wavelengths (Figs. 7.7a&b). Both features are interpreted as absorption due to the Fe²⁺ in the fresh rocks. The overall shape of the spectrum is also consistent with Fe²⁺ (Fig. 7.7c, after Burns, 1970). These spectra allow no separation of altered and unaltered samples.

The second type of spectrum appears to be restricted to samples with a pumpellyite + quartz or an epidote + quartz composition. Every one of these samples has a similar spectrum, with a minimum near $.49\mu\text{m}$, a minimum or a shoulder near $.65\mu\text{m}$ and (with the exception of 10112F) a minimum between $.89$ and $.949\mu\text{m}$. These spectra (Figs. 7.8a&b) bear a marked resemblance to that of goethite. However, there is no indication of goethite in thin section.

Burns (1970) presents a polarised absorption spectrum of an epidote containing 0.864 Fe^{3+} ions per formula unit (Fig. 7.8c). There is a strong absorption doublet at $.445$ and $.474\mu\text{m}$, with weaker, broader features at $.606$ and $1.06\mu\text{m}$. An absorption spectrum of Fe^{3+} in ferric ammonium sulphate solution shows similar structure (Burns, 1970, p.66). It is likely that these features in the Fortescue Group spectra are due to the Fe^{3+} in epidote and pumpellyite (which have similar structure - see Table 7.2). The slight variations in wavelength compared to Burns' spectra are likely to be due to differences in composition, resulting in different crystal fields.

7.5.3 Some comments on SWIR spectra

For rocks from this test site the SWIR spectral region can be expected to contain more mineralogical information than the VNIR. The key metamorphic minerals pumpellyite, epidote and actinolite all have characteristic SWIR signatures, as does chlorite - one of the ubiquitous phases.

Traditional methods of metamorphic petrology place boundaries between metamorphic zones at the 'first appearance' of characteristic minerals (usually detected in thin section). It is obvious that a

boundary drawn in this manner will be undetectable by remote sensing techniques. Rather, the first appearance of a mineral's absorption features in a spectrum will be the first detectable effect. In some cases key metamorphic minerals will not be capable of detection at all, either because they have no SWIR absorption features, or because they occur only as a minor phase. Table 7.4 lists those minerals occurring in the different metamorphic zones of the Fortescue Group that are likely to produce noticeable spectral effects.

Table 7.4 Minerals likely to dominate the SWIR spectrum for different alteration and metamorphic zones

	Altered flow tops	Relict domain
Z-I	pumpellyite	chlorite
Z-II	1. pumpellyite or 2. epidote (transitional to Z-III)	chlorite
Z-III	1. pumpellyite or 2. epidote	chlorite chl + epi + act (transitional to Z-IV)
Z-IV	epidote	chl + epi + act

Altered flow tops have extensive areas of pumpellyite development in Z-I. The pumpellyite spectrum is shown in Fig. 7.9, and is compared to the radiance of a 100% reflector at sea-level. The overall shape of the pumpellyite's spectral curve is quite distinctive, with a steep

fall-off from 2.1 μ m to the major absorption feature at 2.34 μ m. There are also several diagnostic, but minor, absorption features in the spectrum, with the most useful of these being at the unusual wavelength of 1.47 μ m. Comparison to the atmospheric absorption features in Fig. 7.9 shows that this feature should be detectable in a remote sensing mode, provided that atmospheric absorption does not vary significantly along a flight line.

At the start of Z-II, pumpellyite zones still predominate but, further into Z-II, areas of epidote development become important. In Z-III, pumpellyite and epidote are still both important but, in Z-IV, epidote alone is the major indicator of altered flow tops.

In relict domain rocks chlorite is spectrally the most important mineral in Z-I, Z-II and part of Z-III. For the higher-grade rocks of Z-III and Z-IV, chlorite + epidote + actinolite combinations are likely to produce the dominant spectral features.

Therefore, although it will be impossible to duplicate the results of Smith et al. (1982), it may be possible to use SWIR remote sensing to produce offset metamorphic boundaries based on the 'spectral dominance' rather than the 'first appearance' of key minerals. It could also be possible to differentiate the altered flow top material from relict domains.

7.5.4. SWIR W surface spectra

Table 7.2 indicates those samples with diagnostic W surface spectral features in the SWIR. In Z-I altered rocks there are clear indications of the presence of pumpellyite in spectrum 8288W (see also

Fig. 7.10a). More subtle indications, as shown in Fig. 7.10b, appear in the spectra 1011W, 10109W1, 10109W2, 10112W2 and 10093W2 (where a pumpellyite-rich vesicle appears on the surface of the sample). The remainder of the spectra, represented in Fig. 7.10c, exhibit weak, unidentifiable features near $2.2\mu\text{m}$ (probably due to kaolin) and broad features near $2.3\mu\text{m}$ that could be due to either chlorite or pumpellyite (whose spectra are quite similar except for additional absorptions between 1.4 and $1.9\mu\text{m}$ in the pumpellyite spectrum - compare Fig. 7.9 and Fig. 7.12a).

The Z-II and Z-III metadomain rocks (10045 and 10863) exhibit strong absorption features characteristic of epidote (Fig. 7.10d).

The relict domain samples show some spectra almost certainly of kaolin (10118W in Z-I, 10864BW in Z-III, see Fig. 7.11a), and one that could be kaolin (10105W from Z-I). In most other samples, unidentifiable, weak features near $2.2\mu\text{m}$ are nevertheless likely to be kaolin, while unidentifiable, weak features near $2.3\mu\text{m}$ are probably caused by chlorite (based on the known mineralogy determined from thin section identification by R. Smith, written comm., 1983).

These spectra cannot be differentiated from several of the Z-I metadomain spectra, indicating that remote sensing will not be completely successful in separating altered from unaltered rocks, or in definition of metamorphic grade (compare Figs. 7.11b and 7.10c). Nevertheless, there are enough spectra containing diagnostic features to make feasible the mapping of at least some pumpellyite-rich areas in Z-I to Z-III. Epidote-rich areas in Z-II to Z-IV should be easily and accurately mapped by means of their spectral properties.

One Z-IV sample (10848W) has a strong chlorite spectrum (Fig. 7.12a). Where chlorite dominates the spectrum of an unknown, that sample is most likely to originate from a relict domain, particularly in Z-I to Z-III.

Another Z-IV sample (12958W) exhibits actinolite features in its spectrum (Fig. 7.12b). Where an unknown contains enough actinolite to dominate the spectrum it is likely to be from Z-IV, and from a uniformly altered metadomain.

In summary, the indications are that a significant proportion (almost half) of the weathered surface spectra have detectable features indicative of either metamorphic grade or the presence of metasomatic alteration, or both. Based on past experience, some of these features are likely to be detectable from the air. It is also suggested that regional metamorphic variations are more likely to become clear as their two dimensional distribution is mapped in a regional survey. For instance, a remote sensing equivalent of the Z-I/Z-II boundary might be delineated, based on the first detection of epidote metadomains. These regions would become commoner towards higher grade areas. In addition, the presence of distinguishing spectral features from a sample (10093W2, see Fig. 7.10b) with a single pumpellyite-rich vesicle (occupying perhaps 10% of the field-of-view) suggests that relatively little of this material, scattered throughout a pixel, could produce noticeable spectral effects. It was shown in the previous chapter that as little as 10% talc effectively exposed in a residual soil resulted in quite strong absorption features that were easily detected from the air. On the basis of these observations it can be concluded that an airborne survey utilising SWIR spectrometry stands a fair chance of success.

Furthermore, and in contrast to the Landsat data, this success will be greater in the hilly terrain where outcrop is at a maximum and soil development at a minimum.

7.5.5 SWIR F (fresh) surface spectra

The SWIR F surface spectra are remarkable for their consistency. In every case the SWIR spectrum records the mineralogy that one would expect from the list of contained minerals, given that not all of these minerals produce SWIR spectral features. All of the Z-I relict domain samples, for instance, have strong chlorite spectra (Fig. 7.13a). Chlorite and calcite (a minor mineral in 10118) are the only minerals in this domain that produce SWIR absorption features. In the altered Z-I rocks, silicified and albitised samples also contain chlorite, hence can exhibit its spectral features (Fig. 7.13b). In contrast, however, those samples containing a significant amount of pumpellyite are easily discernible (see Figs. 7.14a&b).

A similar story can be told for the higher grade zones, where the mineralogy can also be accurately interpreted from the SWIR spectrum (see Figs. 7.15a-c).

In conclusion, it is obvious that there is a wealth of information available in the F surface spectra. Although of limited use for remote sensing (because of the prevalence of weathering rinds on outcropping rock), this finding does mean that a proximal assessment could prove invaluable in this environment for the identification of component minerals. For instance, Smith et al. (1982) note that the heterogeneity of the Z-IV flows is "harder to see in outcrop because epidote, for example, in Z-IV is essentially colourless".

7.5.6 MIR W (weathered) surface spectra

At first sight the MIR weathered surface laser reflectance spectra look disappointing. Like their VNIR equivalents, all samples appear to have a similar spectrum - that of haematite (Figs. 7.16a&c). There are, however, several examples where an additional peak near $9.3\mu\text{m}$ is evident (Figs. 7.16b&d, and samples 8288W, 10093W, 10109W, 10045W and 10863W in Appendix XII). This is near the wavelength at which quartz reflects most strongly (see Fig. 2.10). The samples listed are the most highly altered and consequently have the highest free silica content. To investigate further, a ratio was calculated between the reflectances at 9.3 and $11.2\mu\text{m}$ (close to the maximum and minimum reflectance of quartz) for all W spectra (see Table 7.3). The results show that all highly-altered metadomain, and transition, samples have ratio values in the range 2.6 to 5 (with a mean of 3.36 and a variance of .49 for 9 spectra). In contrast, relict domain and uniformly altered metadomain samples have values in the range 1.5 to 2.5 (with a mean of 1.97 and a variance of .12 for 10 spectra). Ratios derived from the two groups of spectra do not even overlap. This is a clear indication that laser reflectance remote sensing could accurately identify those metadomains where quartz is a significant alteration product.

7.5.7 MIR F (fresh) surface spectra

Like the VNIR and SWIR spectra, in the MIR the fresh surface spectra show stronger and more varied structure than their weathered surface equivalents.

Samples from relict domains in Z-I tend to show similar spectral structure (Fig. 7.17a). The reflectance of these samples shows some

variation in the 9.1 to 10 μ m region, then a fall-off to longer wavelengths. The region of maximum reflectance seems to be at shorter wavelengths than one might expect for mafic rocks. However, some of the features can be explained by a mixture of the spectral effects of pyroxene (a maximum at 9.3 μ m, and a shoulder at 10.5 μ m), and plagioclase (a maximum at 9.6 μ m, see Farmer, 1974 for absorption spectra of these minerals). The percentage reflectance differences in this group of samples is quite variable (5% for Fig. 7.17a, and up to 50% for spectra in Appendix XII). This is because some of the surfaces measured had been sawn, resulting in a specular component to the reflectance.

Samples from Z-I metadomains have a more distinctive spectral structure. Pumpellyite-rich, silicified rocks tend to exhibit strong reflectance maxima, with the same characteristics as quartz. Note that these maxima tend to occur closer to 9.2 μ m, the wavelength expected for quartz, than those in the spectra of weathered surfaces (compare Fig. 7.17b to Figs. 7.16b&d). An albitised sample (see Appendix XII) exhibits an additional maximum at 9.7 μ m, which is consistent with its high feldspar content. Samples from the transition to the relict domain are prehnite-rich, and have strong reflectance maxima at 9.75 and 10.7 μ m, presumably attributable to the prehnite (see Appendix XII).

Relict domain and uniformly altered domain samples from Z-III and Z-IV tend to have a convex shape, with maximum reflectance in the 10 to 10.2 μ m region (only weakly developed in Fig. 7.17c). This structure is consistent with that expected from a basic rock. Its shape is similar to that of the intermediate rock spectrum displayed in Fig. 2.11, but the position of the reflectance maximum is at a slightly longer wavelength for the Fortescue Group sample.

Z-II and Z-III metadomain samples (represented by Fig. 7.17d) have epidote + quartz compositions, and MIR reflectance curves that indicate a mixture of the spectral features of these two minerals (see Farmer, 1974 for a MIR absorption spectrum of epidote). Note that, like the Z-I metadomain samples, Z-II and Z-III fresh surface spectra have quartz maxima at $9.2\mu\text{m}$.

Paradoxically, despite the prominence of the quartz reflectance maxima of fresh surface altered samples, the discrimination of altered and unaltered material by the $9.3\mu\text{m}/11.2\mu\text{m}$ ratio is not as good (see Table 7.3). This is due to the increased complexity of these spectra, which have a wider variety of reflectance features at all wavelengths.

7.6 Summary

Regional burial metamorphism and associated massive metasomatism have affected the basic volcanic rocks of the Hamersley Basin. The metamorphic grade varies systematically across the basin, four different zones (Z-I to Z-IV) having been identified. Key metamorphic assemblages in each metamorphic zone can be recognised using high-resolution spectral data. However, remote sensing will not detect the metamorphic zone boundaries as mapped, these boundaries having been determined by the 'first appearance', in thin section, of key minerals.

Previous remote sensing investigation has shown that metasomatically altered areas can be discriminated by Landsat MSS imagery in flat and gently undulating terrain. High-resolution, VNIR laboratory spectra show that altered and unaltered rocks produce essentially the same spectral patterns from weathered surfaces. This result confirms the conclusions of Smith et al (1978), who attribute

discrimination by Landsat to the influence of soil development and vegetation cover, rather than outcropping rock.

Laboratory SWIR spectra allow identification of key alteration minerals (pumpellyite and epidote), and background minerals (chlorite and actinolite), from nearly 50% of the weathered surfaces measured. Therefore, it may be possible to define 'remote sensing' metamorphic zones, and identify areas of alteration, in an airborne SWIR survey.

The spectral measurements from fresh surfaces have absorption features that correlate extremely well with the mineralogy of the samples, as determined in thin section. Thus, a field-portable SWIR spectrometer could provide extremely useful information on metamorphic grade and the presence of hydrothermal alteration. This is true, in particular, in those cases where the grain size is too fine for mesoscopic recognition, and where microscopy would otherwise be required for definitive identification. Examples of this from the Fortescue Group include epidote (colourless in Z-IV) and pumpellyite.

Laboratory MIR laser reflectance measurements of weathered surfaces are dominated by responses due to haematite and quartz. The calculation of ratios at different wavelengths, designed to indicate the presence of quartz, allows the samples to be separated into two distinct groups. Altered (quartz-rich) samples have high 9.3 μ m/11.2 μ m ratios, whilst unaltered (quartz-poor) samples have much lower ratio values. Thus a remote sensing survey, utilising similar data, is likely to allow accurate identification of altered areas.

MIR measurements of fresh surfaces contain considerable variation that can be linked to changes in mineralogy. However, at the present

time the author knows of no operational laser MIR instrument that could take advantage of this information in either a remote, or a proximal, mode.

CHAPTER 8 PEAK HILL EPITHERMAL GOLD PROSPECT, LACHLAN FOLD BELT, NEW SOUTH WALES

8.1. Introduction

Chapter 8 describes a pilot study evaluating the potential of high-resolution spectral data for identifying mineralogical variation in hydrothermally altered terrain. Peak Hill is included as a test site because it exhibits a wider range of alteration mineralogy, and is less weathered, than Mt Turner, thus allowing a more complete assessment of high-resolution spectral techniques in Australia.

The investigation proceeds in two stages. The first stage consists of an orientation study on the spectral properties of the alteration assemblage. For this purpose a suite of powdered drill core samples was supplied by Gold Fields Exploration Pty Ltd (Gold Fields). On completion of the first stage, the author visited the area and collected a suite of samples from surface outcrops.

Thus the study is mainly laboratory-based, largely consisting of interpretation of VNIR and SWIR reflectance data. To aid the spectral interpretation, XRD analyses of most samples were obtained. In addition, Gold Fields provided the results of an extensive earlier survey on XRD mineralogy of core samples.

8.2 Location and Regional Geology

Peak Hill lies immediately to the northeast of the township of the same name, approximately 43 km north of Parkes in central western NSW. Figure 8.1 is a photocopy of a colour aerial photograph of the area. It

shows that Peak Hill is a moderately to heavily vegetated hill isolated on a cultivated plain. The amount of vegetation evident on Fig. 8.1 is typical of the foothills and mountainous terrain forming the uplands of eastern Australia. The areas of disturbance evident on Fig. 8.1 have been caused by mining, and a car body dump on the northern slopes of the hill.

The mineralisation occurs within a quartz-sericite-pyrophyllite-pyrite alteration zone, and it is presumably the silicification that has made the hill more resistant to erosion than the surrounding rocks.

During the period 1889-1919, some 2.338 tons of gold and 25.5 tons of copper were produced from the Peak Hill mines (Bowman, 1974). The mines consist of several open cuts as well as underground workings. The area has been investigated by a number of companies for its copper and gold potential, and has recently been exploited as a pyrophyllite deposit.

The disseminated gold-copper orebody occurs in (?) Late Silurian to Early Devonian volcanics and sediments of the Forbes Anticlinorial Zone, which, in turn, forms part of the Lachlan Fold Belt.

8.3. Detailed Geology and Alteration

The host rocks are northerly striking, moderately to steeply east dipping (and facing) dacitic tuffs, lesser lavas and related intrusives. The underlying rocks are early Ordovician andesitic volcanics, while the dacite is overlain by (?) Early Devonian shales, siltstones and fine sandstones (Bowman and Richardson, 1978 - see Fig. 8.2). The areas of relatively undisturbed outcrop comprise only 5 to

10% of the hill, and are small and widely scattered. They vary in size from a few square metres, to tens of square metres.

There have been two separate studies on the alteration mineralogy of the area - one by the NSW Geological Survey using XRD on surface samples, the other by Gold Fields using XRD on core samples.

Both studies delineate a pyrophyllite-pyrite alteration zone centred on the main workings, with indications of peripheral sericite (muscovite) and kaolinite zones. An induced polarisation (IP) survey by Anaconda outlined an anomalous zone centred on the old workings. Anaconda drilling confirmed that high IP response coincides with high sulphide content.

In addition, jarosite has been reported (Slansky, 1978) from the region of the Bobby Burns workings on the southern slopes of Peak Hill, and topaz (M. Hutton, pers. comm., 1984) from an outcrop on the periphery of the Great Eastern workings on the eastern side of the hill. J. Angus (written comm., 1984) has also reported diaspore from drill core.

Table 8.1 summarises the alteration minerals reported at Peak Hill, and indicates (for remote sensing purposes) whether each has a detectable SWIR spectral response. The distribution of the alteration minerals is discussed in some detail in Section 8.6.

8.4. Laboratory Spectral Measurements - Core Samples

8.4.1 Introduction

Twenty-one pulped drill core samples, and four split core samples (from three different drill holes) were sent to the author for spectral

Table 8.1 Minerals identified by XRD analysis in different studies at Peak Hill

NSW Geol. Survey	Gold Fields	SWIR Response
Quartz	Quartz	No (MIR only)
Pyrophyllite	Pyrophyllite	Yes
Mica	Muscovite	Yes
Kaolinite	Kaolinite	Yes
Feldspar	Feldspar	No
	Alunite	Yes
	Barite	No
	Smectite	Yes
	Jarosite	Yes
	Chlorite	Yes
	Topaz	Yes
	Diaspore	Yes

measurement as an orientation study of Peak Hill. VNIR spectra and SWIR spectra were recorded. All of these spectral plots, along with any other available mineralogical data, are included in Appendices XIII and XIV. For simplicity, the text includes only a summary of these interpretations (see Table 8.2), and representative spectral plots.

8.4.2 VNIR spectra

The VNIR spectra show features, due to iron, that fall into three categories. The first group comprises samples with either no iron absorption features, or weak features that appear to be due to Fe^{2+} (Fig.8.3a). This finding is not unexpected, because these samples were invariably collected below the base of oxidation. Above this base, absorption features appear indicating haematite (generally moderate to strong). These are widespread, and form the second category (Fig.8.3b). The third type of spectrum observed shows some of the attributes of goethite (8.3c). These features are generally only weak to moderate in strength.

8.4.3 SWIR spectra

There are clear indications of pyrophyllite, alunite and, in one sample, jarosite features in the SWIR spectra (see Figs. 8.4a-c, and compare to spectra in Figs. 2.5 and 2.9). In addition, there are weak indications of an undifferentiated dioctahedral phyllosilicate - denoted U (this could be kaolin) - and sericite (Figs. 8.5a&b). Although quartz does not have hydroxyl absorption features in the SWIR, it often contains fluid inclusions that cause broad absorption features in the 1.4 and 1.9 μm regions (see Figs. 6.5a-c). If enough quartz is present,

Table 8.2 Summary of the interpretation of laboratory reflectance spectra of core samples from Peak Hill

Sample No.	Hole No.	VNIR	SWIR
N33916▲	PHD5	H (s)	? very flat
N33919▲	PHD5	H? (m)	? very flat
N33933▼	PHD5	Fe ²⁺ (+3+?) (vw)	Pyp? + S? (VW)
N33964▼	PHD5	Fe ²⁺ (+3+?) (vw)	Pyp?? + S? (vw)
PHD5/42 = N33916 *	PHD5	H (s)	Pyp? + Q? (vw)
PHD5/51.6 = N33919 *	PHD5	H (s)	J (s)
PHD5/76.78 = N33933 *	PHD5	Fe ²⁺ ? (vw)	Pyp? + Ser? (vw)
PHD5/138 = N33964 *	PHD5	Fe ²⁺ ? (vw)	Al (w)
N33972▲	PHD6	H (s)	Al + U? (m)
N33977▲	PHD6	H (s)	Al + Pyp + U? (s)
N33984▲	PHD6	H (s)	Al (vs)
N33995▲	PHD6	H (s)	U? + Al? (w)
N37803▲	PHD6	H (m)	? very flat
N37808▲	PHD6	H (s)	Pyp (w)
N37812▲	PHD6	G? (m)	Pyp (m)
N37818▲	PHD6	G? (m)	Pyp (s)
N37824▲	PHD6	-	Pyp (s)
N37831▼	PHD6	Fe ²⁺ (w)	Pyp?? (vw)
N46274▲	PHD17	H (w)	Q?
N46279▲	PHD17	G (m)	Pyp (m) + J? (w)
N46288▲	PHD17	G (w)	Pyp (s)
N46296▲	PHD17	G (w)	Pyp (s)
N46303▲	PHD17	-	Pyp (s)
N46309▼	PHD17	-	Pyp (w)

* = Split Core Samples from same intervals as PHD5 pulps. All other samples are pulps.

KEY

VNIR

H = Haematite
 J = Jarosite
 G = Goethite
 Fe²⁺ = Fe²⁺
 Fe³⁺ = minor, undiff. Fe³⁺
 - = No Fe features

SWIR

Al = Alunite
 Pyp = Pyrophyllite
 S = Sericite
 U = undiff. dioctahedral
 phyllosilicate
 ? = uncertain
 Q = Quartz (see text)
 J = Jarosite

(v) = very
 (s) = strong (>10% reflectance)
 (m) = medium (5-10% reflectance)
 (w) = weak (<5% reflectance)
 ▲ = above base of oxidation
 ▼ = below base of oxidation

and contains fluid inclusions, then this spectral shape may be present, as appears to be the case in samples PHD5/42, and N46274 (Figs 8.6a&b).

8.4.4 Conclusions on data from core samples

This work indicates that several important alteration minerals are detectable from VNIR and SWIR spectral measurements. Although there were a number of samples that did not produce strong absorption features as expected (see comments in Appendix XIV), the results were generally encouraging. In particular, it should be noted that there are probably more strong absorption features in samples from above the base of oxidation than below it. The results were promising enough to justify the additional work described below.

8.5. Laboratory Spectral Measurements - Surface Samples

8.5.1 Introduction

A field trip to Peak Hill was undertaken in November, 1984. Samples were collected only from relatively undisturbed outcrops, and had their VNIR and SWIR spectra measured in the same fashion as the core samples. The interpretations are summarised in Table 8.3.

8.5.2 VNIR spectra

The VNIR plots of weathered surface spectra are dominated by the spectral features of haematite (Fig. 8.7a). Features caused either by lichen (see chapters 5 and 6), or by goethite (or jarosite), occur less commonly (Figs 8.7b&c). The equivalent fresh surface spectra also tend to be dominated by haematitic features.

Table 8.3. Summary of the interpretation of laboratory reflectance spectra of surface samples from Peak Hill

Location	VNIR		SWIR	
	W	F	W	F
PH1	K	H	Mo,K	K
PH2	H	H	L,J,K?	M,Q?,U?
PH3	nm	G?,P	nm	P,U
PH4 OCA	G,P?	G,P	P,U	P
PH4 OCB	nm	H,?	nm	P
PH4 SZ	nm	P,H,?	nm	P,D?
PH5	H,L	H,G,P	K,L	P,M
PH6	L	P	P,L	P
PH7	L	H,P	P,U,L	P,U
PH8	H?,L?	H,P	P,U	P
PH9	H,L	H	L,U	K,P
PH10	L	H,P	P	P
PH11	H,L	H	L,P,M	P,M
NT1	L?	G	K,L	K
NT2	H	H	U	K,M
NT3	L?,H	G,H	T?,L,P	P,Q?,T?,G?
NT4	L,-	H	T?,U	T?,Q?,P
NT5	L	G	L,U	U,Q?,G?
NT6	H? (vw)	-	T?,P,U?	T?,K,Q?,U
NT7	L	H	P,U	P,U
BB1	L	H	L,M	M
BB2	H	G?	J	J
BB3	H	H	K?L?	U,Q?
BB4	H	H	M,U?,J	M,K
BB5	L	G?	U,L,J	M,J
BB6	G*	G*	J	J
BB7A	L	U	L	M
BB7B	L	H	L	Q?
BB8	L?	H	L,U,Q?	U,Q?
BB9	L	G?	U,J	J
BB10	L?	G?	U	M,J
BB11	L	H	L	M
BB12	H	-	nm	M
BB13	H (w)	H	K	K,M?

* N.B. Sample BB6 has exceptionally deep absorption, probably due to jarosite. Goethite and jarosite can not be unequivocally separated in the VNIR with this instrument, so all spectra have been shown as goethite.

KEY

- | | | |
|---------------|-----------------------------------|-------------------|
| T = Topaz | Mo = Montmorillonite | H = Haematite |
| K = Kaolinite | L = Lichen | - = no features |
| D = Diaspore | P = Pyrophyllite | ? = uncertain |
| G = Goethite | M = Muscovite (sericite) | nm = not measured |
| J = Jarosite | U = Undiff. dioct. phyllosilicate | - = no features |
| Q = Quartz | | vw = very weak |

One notable feature of a few of these spectra is the presence of $3\nu_{OH}$ absorption features due to kaolinite and pyrophyllite in the $0.95\mu\text{m}$ region (Figs. 8.8a&b). Only a few weathered-surface spectra show this effect, consistent with previous studies (Appendix I, Gabel et al., 1985). All VNIR spectra of surface samples appear in Appendix XV with their corresponding XRD data, where it is available.

8.5.3 SWIR spectra

The SWIR spectra of samples from Peak Hill are particularly informative. The spectral features of pyrophyllite and kaolinite (Figs. 8.9a&b), and muscovite and jarosite (Figs. 8.10a&b) occur most commonly. In addition, there are several samples which exhibit more unusual spectral characteristics. Figures 8.11a&b depict photographs of a representative sample, and spectra of its weathered and fresh surfaces. These spectra have absorption features centred on 2.08 and $2.17\mu\text{m}$. Because they occur in measurements of both weathered and fresh surfaces, and because of their sharp nature, they cannot be attributed to lichen. The $2.17\mu\text{m}$ minimum is very similar to pyrophyllite absorption features interpreted from samples elsewhere in the area, whilst the $2.08\mu\text{m}$ minimum occurs at the same wavelength as that of topaz (see Hunt et al., 1973a). It should also be pointed out that one of the samples was collected from an area known to contain topaz (M. Hutton, pers. comm., 1985), specifically to test the possibility of its detection. The other samples were collected from areas away from this single, known occurrence. However, routine XRD analysis of several of these samples showed only quartz. Examination of a thin section of one sample showed that quartz is indeed the major component, but that the rock contains a small amount (a few %) of a phyllosilicate, with small

inclusions of a second mineral. These minerals could not be confidently identified from thin section, so the tentative assignment of the spectral features was not confirmed. Nevertheless, this example does illustrate the capability of the high-resolution spectral technique to provide information not available from examination of hand specimens, and, in some cases, information which requires sophisticated mineralogical techniques for any further indication of a sample's composition.

As with other case studies documented in this thesis (chapters 5, 6 and 7), the presence of significant mineralogical information in spectra of samples with appreciable surface coatings of lichen or iron oxides is also particularly encouraging.

All SWIR spectra of surface samples measured and interpreted for this report appear in Appendix XVI. The interpretations have also been summarised in Table 8.3. Note that the interpretations are summarised for all spectra from each location rather than individually.

Spectral features due to pyrophyllite, sericite, kaolinite, jarosite, montmorillonite, lichen and an unidentifiable dioctahedral phyllosilicate were all detected from weathered surfaces. Topaz, diaspora and also some effects due to high quartz content were also tentatively interpreted.

Fresher, broken surfaces yielded spectral features interpreted as due to all of these materials except lichen and montmorillonite. As expected, absorption features are better defined, and stronger, than on weathered surfaces.

The only mineral with SWIR spectral properties reported from Peak Hill (see Table 8.1), yet not detected in spectra of surface samples, is alunite. This fact is somewhat surprising, particularly since alunite was recognised from its absorption features in the spectra of the pulped drill core samples. However, since alunite was not detected in the XRD analyses either, it is assumed that alunite-bearing rocks do not crop out at the surface.

8.6. The Distribution of Alteration Minerals

It was possible to compare the mineralogy interpreted from spectral data with existing information (from XRD studies) on the distribution of alteration minerals.

Fig. 8.12 shows the location of the XRD samples (circles) on Gold Fields' grid over the area. The distribution of the outcrop samples collected by the author for spectral measurement is shown on the same plot (crosses). Note that, in the case of surface samples, the mineralogy shown in the following figures is a summary of all of the spectral features interpreted from each location (including W and F surface measurements of multiple hand specimens and 'uncertain' interpretations, where they occur).

Figures 8.13 to 8.17 depict, respectively, the distribution of pyrophyllite, muscovite, kaolinite, pyrite and alunite as determined from the XRD analyses of core samples. As the XRD data are semi-quantitative, they have been divided arbitrarily into three classes, with less than 20%, 20% to 50% and greater than 50% indicated by the size of the circle used on all of the plots. In addition, boundaries drawn around the circles represent the two classes containing more than

20% of a particular mineral, and the enclosed area has been hatched.

Each of Figs. 8.13 to 8.15 has an accompanying overlay, showing the distribution of the same mineral interpreted from spectral measurements of surface samples. The overlay to Fig. 8.16 shows the distribution of jarosite (as interpreted from spectra) to enable a comparison of its distribution to that of pyrite in drill core. In the case of the interpretations from spectral data, no distinctions have been made on the basis of the strength of the absorption features present. However, the comparison of the hatched areas to the spectral data is probably valid, because a significant percentage of an alteration mineral would generally be required to cause interpretable absorption features.

Figure 8.13 and its overlay show a very good match between the outcrop samples interpreted as having pyrophyllite spectral features, and the >20% area defined by drill core analysis.

Figure 8.14 and its overlay show that sericite (muscovite) appears to be concentrated in a zone peripheral to the central pyrophyllite zone (also shown for comparison). The mismatch between the distribution of muscovite as determined from XRD and spectral analysis can be largely explained by the differences in the location of the sampling points in the two surveys (see Fig. 8.12).

Figure 8.15 shows that kaolinite in the subsurface tends to be concentrated in areas peripheral to the central pyrophyllite zone, and peripheral to, but overlapping, the muscovite zone. However, the surface samples show a much less well-defined zonation. This could be due to one of two factors. Firstly, kaolinite forms readily in the surface environment as a weathering product, so the distribution as

determined by SWIR spectroscopy may be largely influenced by weathering rather than hydrothermal alteration. The second possibility is that the spectra are accurately reflecting the distribution of hydrothermal kaolinite at concentrations below the 20% cut-off used to define the hatched area in Fig. 8.15.

The author considers the former possibility the more likely, especially when it is considered that the strongest kaolinite spectrum measured in the survey was collected from outside the known area of alteration (see Fig. 8.9b).

Figure 8.16 shows that pyrite in core samples is widespread, but it does occur at its highest concentrations in the central pyrophyllite and muscovite zones. In contrast, the overlay to Fig. 8.16 shows that jarosite appears to be preferentially developed in the southern (downslope) portion of Peak Hill, away from the sulphide-rich zone. This observation indicates that an additional geomorphological process, not the simple in situ weathering of pyrite, is controlling the jarosite distribution at the surface.

Figure 8.17 shows that alunite (from drill-core analysis) occurs in an area closely related to muscovite (also determined by analysis of core). However, no spectral features interpreted as being caused by alunite were found in the surface sample spectra.

Figure 8.18 is a summary diagram comparing the all samples with interpretable spectral features to the zones of >20% pyrophyllite, muscovite and kaolinite derived from XRD data. Although the interpretation of spectral features was based on W and F surfaces, if W surface spectra were to be considered alone a similar distribution would result.

Figure 8.18 shows the locations of a few samples with spectral features tentatively interpreted as being due to diaspore and topaz. The topaz? samples all lie on the northeastern margin of the pyrophyllite zone, while diaspore was found associated with pyrophyllite in a single sample on the northern margin of the pyrophyllite zone. The presence of spectral features attributable to those two minerals (in both W and F surface spectra), even if unconfirmed by other analysis techniques, is still seen as being significant. Both are important minerals that provide an insight into the style of alteration. Both are also particularly difficult minerals to recognise in the field. In addition, although topaz was known to exist in the vicinity of location NT6, it was not known from the other two locations where its presence has been indicated. Diaspore has not previously been reported from surface samples at Peak Hill.

Thus the spectral work has resulted in a moderately accurate reproduction of known zonation of hydrothermal alteration minerals, and, in addition, has indicated the existence of two previously undocumented mineral zones. Jarosite forms one of these zones on the southern slopes of Peak Hill, whilst topaz is interpreted to form a sub-zone in the northeastern portion of the pyrophyllite zone. In addition, diaspore has been interpreted from the spectrum of a single surface sample.

8.7 The Potential for use of Remote Sensing Techniques at Peak Hill

8.7.1 Proximal sensing

A field-portable spectrometer can be used in two different ways. Firstly, it can be used purely as an aid to mineral identification. In this mode, the field-of-view (FOV) would probably be quite small (of the

order of 10 cm^2), and broken rock surfaces would attract at least as much attention as undisturbed, weathered surfaces. The type of information from such usage should closely approximate the results reported here. Presuming that such an instrument is available, a relatively fast and cheap method of producing an alteration map would result.

Alternatively, the field instrument can be used as a tool in support of an airborne (or spaceborne) remote sensing effort. In this case, the ideal FOV would be of the order of several square metres, and ideally should be capable of taking measurements of tree crowns as well as the ground surface. In this case weathered rock surfaces, soils, grasses and leaf litter would all be measured in an attempt to characterise the whole environment spectrally.

The laboratory spectra presented here show that there is considerable potential at Peak Hill for the extraction of mineralogical information in both of these postulated modes of operation (but particularly in the first).

8.7.2 Remote sensing

The potential for a successful space-borne remote sensing investigation is not as good. Fig. 8.1 shows that Peak Hill is moderately- to well- vegetated, and it has also been noted that the percentage of outcrop is not large, and that the outcrops themselves are generally of a size the order of which is only a few square metres. In addition, outcrop is often lichen-covered.

There is no doubt that mineralogical signatures would be obtained by an airborne instrument, but they would inevitably be dominated by the areas disturbed by mining. If an area equivalent to an undisturbed Peak Hill were to be 'flown' as an airborne spectrometer target, a successful evaluation would require very accurate location, and a spatial resolution of better than 5 metres to allow assessment of individual outcrop signatures. AIS would fulfil these requirements.

8.8 Summary

Laboratory reflectance spectra of samples from Peak Hill exhibit features characteristic of a number of alteration minerals. Alunite, pyrophyllite, muscovite, haematite, goethite and jarosite were identified from the spectra of pulped and split core samples.

Pyrophyllite, muscovite, kaolinite, montmorillonite, jarosite, haematite and goethite have all been detected from the spectra of surface samples, and confirmed by XRD analysis. Topaz and diasporite have been interpreted from the spectra of surface samples, but were not confirmed by XRD analysis. The distributions of pyrophyllite, as determined by XRD analysis of drill core, and from interpretation of the spectra of surface samples, match closely. Both techniques also identify a peripheral muscovite zone, while XRD of fresh core shows a kaolinite alteration zone outside this. Kaolinite is more widespread at the surface, probably due to the effect of weathering. A peripheral jarosite zone at the southern end of the central pyrophyllite zone does not match the distribution of pyrite in core. The location of jarosite on the lower slopes of Peak Hill, and its absence in core samples from below the base of oxidation, suggest that a geomorphological process

controls its distribution. The spectra of surface samples also indicate that topaz may be present in a number of locations in the northeast of the pyrophyllite zone. Only one of these occurrences was previously known. Diaspore has also been interpreted from the spectrum of a single sample ; its presence at the surface has not previously been noted. Both of these significant minerals are very difficult to identify in hand specimens.

Peak Hill, like most of the eastern uplands of Australia, would be a difficult target for an airborne remote sensing survey because of the amount of vegetation cover.

PART III. : DISCUSSION OF RESULTS AND THEIR IMPLICATIONS
FOR FUTURE REMOTE SENSING APPLICATIONS IN AUSTRALIA

CHAPTER 9 DISCUSSION OF RESULTS AND THEIR IMPLICATIONS FOR FUTURE REMOTE SENSING APPLICATIONS IN AUSTRALIA

9.1 Introduction

When the research documented in this thesis began, remote sensing techniques were rapidly being developed to utilise wavelength regions longer than the visible and near infrared (VNIR). Preliminary laboratory, field and airborne data from the U.S. had already shown that considerable useful information was available from the wavelength region beyond that covered by the Landsat MSS (0.4 to 1.1 μ m). Diagnostic information on hydroxyl-bearing minerals and carbonates in the short wavelength infrared (SWIR) region (1.1 to 2.5 μ m) was particularly promising for geological applications.

Although considerable research had been undertaken in Australia on Landsat MSS data, there was a paucity of knowledge on the high-resolution VNIR spectral properties of Australian terrain, and a complete lack of data in the SWIR and middle infrared (MIR) spectral regions. It was also clear that Australia's extensive and deep weathering and subdued topography were likely to result in mineral assemblages different from those found over similar geology in the southwestern U.S., where the bulk of remote sensing research has been undertaken to date, and where aridity and juvenile topography combine to minimise chemical weathering. The work documented here shows that the degree of chemical weathering is indeed one of the keys to the usefulness and type of information available from remote sensing data.

To assess the utility of remote sensing in Australia, high-spectral-resolution data have been presented from five test sites

situated in diverse geological environments. VNIR and SWIR data have been included from all areas, but MIR data were presented for samples from a single test site. Analysis of the SWIR data was the most exhaustive, because it is in this region of the spectrum that the bulk of the new mineralogical information has been identified.

9.2 The VNIR

The Weipa study shows that Landsat MSS data, despite its coarse spatial and spectral resolution, can still provide useful geological information. Colour variations in enhanced MSS imagery can be related qualitatively to regional variations in the nature of bauxite/laterite. A more quantitative relationship has also been established, with a correlation coefficient of .69 calculated for ore geochemistry and Landsat 5/6 band ratio values.

The variations in the MSS data, although correlating with ore geochemistry, are likely to be caused by vegetation differences, variation in plant vigour being the most likely cause. There are no obvious changes in vegetation species distribution, tree density, crown size or tree maturity detectable on colour IR photography, or in the field. Bushfires are also unlikely to account for the observed variations.

High-spectral-resolution VNIR laboratory measurements of soils show that, on Weipa Peninsula, they are unlikely to directly contribute to the observed Landsat MSS trends. Soils from other areas (e.g. Andoom) may make a minor contribution to these trends.

Although not analysed in detail, airborne VNIR data from Mt Turner and Kambalda exhibit variations that often coincide with changes in the SWIR spectral data. Changes in vegetation cover and iron oxide content are the most likely cause of the observed effects. The high-resolution VNIR data from Mt Turner do not allow significant additional (mineralogical) discrimination over that provided by Landsat MSS imagery.

High-resolution VNIR laboratory spectra of samples from the Fortescue Group basic volcanics show that weathered surfaces have very similar VNIR (haematitic) characteristics, regardless of metasomatic alteration, or variations in metamorphic grade. This finding supports the conclusions of earlier workers (Smith et al., 1978), who suggested that metasomatically altered and unaltered rocks are discriminated on Landsat imagery because of differences in their soil and vegetation cover. Measurements of fresh surfaces of the same rocks are dominated by absorption due to Fe^{2+} , except for samples containing epidote and pumpellyite, which exhibit Fe^{3+} absorption characteristics.

VNIR spectra of weathered surfaces of samples from Peak Hill are also dominated by haematitic absorption features. Some samples also exhibit weak $3\nu_{\text{O-H}}$ absorption features due to pyrophyllite and kaolinite. It may be possible to utilise these features for the identification of clay mineralogy using low-cost (silicon detector array) field instruments.

In summary, the VNIR region has provided useful information from Weipa, but weathered samples from most other test sites primarily exhibit haematitic absorption features. It may be that an appreciation of the two-dimensional distribution of iron oxide mineralogy (already

provided by narrow-band imagery from instruments such as the Canadian MEIS II scanner, Fraser et al., 1984) will prove to be of greater economic significance.

9.3 The SWIR

Both airborne and laboratory SWIR measurements have provided a wealth of mineralogical information, all test sites yielding significant data. It has been shown that gibbsite/boehmite (ore minerals) are present, and detectable, in soil samples overlying the bauxite at Weipa. At Mt Turner, high-resolution airborne measurements discriminated the sericitic alteration (on mineralogical grounds) much better than simulated scanner data, and existing Landsat MSS imagery. Talc was identified from airborne data, and topaz from its laboratory spectrum, even though neither had previously been reported from the area.

At Kambalda the residual Archaean mineralogy was easily differentiated from widespread weathering products. Talc, a most important mineral characterising ultramafics, was readily identified from its airborne spectral response (sharp 2.32 μ m absorption), and its distribution accurately mapped. This work showed that talc is widespread outside mapped occurrences of outcrop and float, thereby establishing that it also forms a significant component of residual soils. Several other minerals are also identified from airborne data. The most extensive of these minerals are amphibole and chlorite (associated with basic volcanics, and absorbing in the 2.32 to 2.35 μ m region) and kaolin (associated with calcrete and lateritic weathering products, with 2.2 μ m absorption features). The existence of distinctive

spectral features associated with felsic, mafic and ultramafic lithologies therefore provides a means of separation of these major rock-types. It should be possible to utilise this knowledge for remote sensing surveys in other, geologically similar, areas.

The SWIR is also moderately successful in aiding the identification of the minerals pumpellyite, actinolite and chlorite, and very successful in the identification of epidote, from the weathered surfaces of samples from the Fortescue Group basic volcanics. This finding suggests that a SWIR airborne spectrometer survey would meet with some success in delineating areas of metasomatic alteration, and mapping variation in the grade of regional burial metamorphism. The information available from measurements of fresh surfaces of the same samples is even more comprehensive, giving another indication of the potential value of a field-portable instrument. Such an instrument can be expected to aid in the identification of the above-mentioned key metamorphic and alteration minerals in the field. Normally, only laboratory-based XRD and microscopy provide this sort of detailed information to the metamorphic petrologist.

At Peak Hill a number of hydrothermal alteration minerals have been readily identified from measurements on both weathered and fresh surfaces of samples. Pyrophyllite, sericite and kaolin distributions have been mapped on the basis of their spectral properties, the results being in good agreement with a previous survey based on XRD analysis of core samples. In addition, a jarosite zone has been recognised, and diaspore and topaz tentatively interpreted from spectra of surface samples. All of these minerals provide an important insight into the nature of the alteration, and all are extremely difficult (sometimes

impossible) to identify using only a hand lens. Peak Hill therefore provides another example of an environment where proximal sensing techniques could be employed to great advantage. Because of the amount of vegetation covering Peak Hill, it would be a difficult remote sensing target. An airborne instrument, such as the AIS, with high spectral-resolution, and capable of acquiring small ($\sim 5\text{m}$) pixels, may have some success at Peak Hill and in other, similarly vegetated areas in eastern Australia. The coarser resolution available from Landsat TM makes a successful result less likely in these environments.

9.4 The MIR

Although spectra have been measured for samples from only a single test site, this wavelength region looks particularly promising. The weathered-surface spectra from Fortescue Group samples were separated into two distinct groups on the basis of a $9.3\mu\text{m}/11.2\mu\text{m}$ ratio. One of these groups has high ratio values, indicative of increased quartz content (silicified samples), while the second group has lower ratio values (unaltered samples). An airborne survey utilising only the wavelengths used for the ratio could be expected to delineate areas of metasomatic alteration.

As with other wavelength regions, the MIR fresh surface measurements show a greater number of spectral features due to their mineralogical composition than do weathered surfaces. This will be an advantage where high-resolution measurements (such as the laser reflectance data presented in this thesis) can be made, but a disadvantage where an insufficient number of spectral bands are available to take advantage of this variation.

9.5 The Effects of Weathering

The amount of chemical weathering in an area is directly related to the amount of information available from remote sensing techniques. In general, because of convergence of mineralogies as weathering proceeds, the more complete the weathering process the less representative of the the underlying rocks is the surface, and the less diverse the information available from remote sensing. This remark applies both to a complete weathering profile, and to the development of surface 'rinds' on individual samples, where local surface depletion and enrichment occurs. The exceptions will obviously be in cases where secondary minerals, derived from weathering processes, are themselves indicators of economic interest (e.g. gibbsite/boehmite in soils overlying bauxite ore at Weipa, and where alunite/jarosite are formed as weathering products in acid, sulphide-rich, environments).

Mt Turner and Kambalda provide good examples of the effect of weathering in contrasting 'felsic' and 'ultramafic' environments. In both cases, only the most resistant primary minerals survive the weathering process, and are easily detected using SWIR techniques. In the felsic terrain, where muscovite from weathering and sericite from hydrothermal alteration predominate, major absorption features are all in the 2.2 μ m region, hence difficult to separate. In the ultramafic terrain, where talc (with a 2.32 μ m absorption feature) survives in residual soils, the differentiation from weathering products with 2.2 μ m absorption features is considerably easier.

At Kambalda it was also found that calcrete nodules exhibit the absorption characteristics of kaolin (probably due to a fine surface coating of the mineral), rather than those of calcite. Subsequently,

there is no confusion of the $2.34\mu\text{m}$ calcite absorption features with those of the residual Archaean minerals. In the (surface) Archaean samples examined, there was also a paucity of residual carbonate (from talc-carbonate alteration of the ultramafics) due to weathering.

As suggested in chapter 2, the spectral effects in Australia are unquestionably much weaker than those described in remote sensing studies from the U.S. Nevertheless, this work has shown that although of diminished amplitude in Australia, the signal is still detectable with appropriate instrumentation and data-processing techniques. Some of the diagnostic (airborne) features discussed in the thesis are as small as .01 on the log residual scale. For a rock with a reflectivity of 10%, this corresponds to a reflectivity change of 0.1%. In order to detect this magnitude of change reliably, a system is required that has a noise equivalent reflectance difference ($NE\Delta\rho$) in the range of 0.03 to 0.05%. At $2.2\mu\text{m}$ the $NE\Delta\rho$ for the Thematic Mapper is 2.5%. This discrepancy of several orders of magnitude becomes considerably worse when the widths of the spectral bands required to discriminate these minerals are considered. The $NE\Delta\rho$ is likely to reduce by a further order of magnitude. From these considerations, it is obvious that rotating mirror instruments will not provide solutions to many remote sensing problems in Australia.

9.6 The Effects of Vegetation

Healthy, green vegetation has distinctive spectral structure in the VNIR, and a lack of absorption features in the SWIR. However, once vegetation begins to lose moisture, the spectral characteristics of cellulose start to become apparent, resulting in absorption in the 2.1

and 2.3 μ m regions. Absorption in the 2.3 μ m region is particularly troublesome because many minerals display absorption features there. Spinifex grass, which is widespread in Australia, also shows the spectral structure of dry vegetation (Horsfall et al., 1984). However, if vegetation is evenly distributed along a flight line, much of its spectral contribution is removed by the log residual technique, leaving mineralogical effects as the major variation (Green and Craig, 1985).

9.7 Scanners or Spectrometers?

Simulated scanner data shows that there will inevitably be some loss of information compared to high-resolution spectrometer measurements, although it could be minimised using very narrow bands. A simulated broad-band (TM-type) ratio, using data from Kambalda, failed to discriminate the minerals identified using high-resolution data. However, this simulation did not take into account information available from other regions of the spectrum, and the advantages of an imaging system.

In fact, such systems offer several advantages. In particular, it has been shown that, in Australia, the position of a target within the weathering profile is important. For instance, little useful spectral information is available from a duricrust but, lower in the profile, where some original mineralogy persists, more diagnostic information can be obtained. A two-dimensional image allows an appreciation of the relative position in the weathering profile. A three-dimensional (stereoscopic) capability would be even more effective if it could be incorporated into a high spectral-resolution remote sensing system. However, the requirement for high spectral-resolution, and the

radiometric sensitivity required to detect some of the effects documented in this thesis, can not be achieved with the short dwell-times afforded by most rotating-mirror instruments. One short-term solution to this problem is the simultaneous acquisition of scanner imagery and high spectral-resolution spectrometer data.

The MIR spectral region also shows particular promise. More research is required, especially in Australia, to evaluate more fully the capabilities of different instruments operating in this region.

The author therefore believes that an ideal instrument for use in Australia should have the following characteristics :

1. High SWIR spectral resolution.

The existence of sharp, diagnostic absorption features just longer than the $1.4\mu\text{m}$ atmospheric absorption band (e.g. pumpellyite in Fortescue Group rocks), the occurrence of subtle shifts of absorption features related to mineral composition (e.g. chlorites at Kambalda) and the occurrence of spectral features at unexpected wavelengths (e.g. $2.1\mu\text{m}$ absorption due to topaz at Mt Turner) makes contiguous coverage from 1.44 to $2.5\mu\text{m}$, with a spectral resolution of better than $.0016\mu\text{m}$, a necessity for general geologic applications.

2. Some VNIR and MIR capability.

A few moderately narrow bands in the VNIR should suffice to provide some information on the distribution of vegetation and iron oxides. Bands centred on $.68$ and $.75\mu\text{m}$ for vegetation, and $.45$, $.75$, $.85$ and $.90\mu\text{m}$ for iron oxides should be regarded as a minimum requirement.

Insufficient data have been presented in this thesis to define requirements for MIR applications in Australia, but a multiband configuration is obviously desirable. The high sensitivity of the CO₂ laser instrument (from which data are presented in chapter 7) makes it an attractive possibility.

3. Imaging capability.

An imaging capability rather than (or as well as) a profiling capability will allow determination of the geomorphic context of a site, and will allow the distribution of critical minerals to be mapped.

4. High signal-to-noise ratios.

Noise equivalent reflectance differences (NE $\Delta\rho$'s) of .03 to .05% (see section 9.5) are required to confidently interpret some of the diagnostic log-residual features documented in this thesis.

5. Capability of spatial resolutions in the 5 to 10m range.

The moderate- to well-vegetated terrain in Eastern Australia (e.g. Peak Hill) requires a ground resolution of the order of 5m to discriminate small geologic targets. In addition, research by the CSIRO/MXY over a number of sites has shown that there is usually a useful increment of information in Aircraft Thematic Mapper imagery with an increase in resolution from 20m to 10m (J. Huntington, pers. comm., 1986).

The new technology of two-dimensional detector arrays (e.g. the AIS) have the required characteristics for the SWIR, if flown in an

aircraft. Unfortunately, this conclusion introduces the problem of acquisition of enormous volumes of data. However, with the continued development of sophisticated computer hardware, and software processing techniques, this problem will certainly become less formidable with time. Less sophisticated instrumentation will probably suffice for the VNIR, but the definition of requirements for the MIR must await considerably more research.

Finally, this thesis has shown that there is considerable potential for a field-portable instrument that could be used for 'proximal' sensing. The author believes that development of a relatively cheap, fast and easy-to-use instrument for the field geologist would provide immediate benefits to the mineral exploration industry.

- Abrams, M.J., Ashley, R.P., Rowan, L.C., Goetz, A.F. and Kahle, A.B., 1977. "Mapping of hydrothermal alteration in the Cuprite mining district, Nevada, using aircraft scanner images for the spectral region 0.46 to 2.36 micrometres", *Geology* v.5, p.713-718.
- Abrams, M.J. and Brown, D., 1984. "Silver Bell, Arizona, Porphyry Copper Test Site Report", in Abrams, M.J., Conel, J.E. and Lang, H. (eds), "The Joint NASA/Geosat Test Case Project", Final Report AAPG, Tulsa, Oklahoma.
- Abrams, M.J., Conel, J.E. and Lang, H.R., (eds), 1984. "The Joint NASA/Geosat Test Case Project", Final Report, AAPG, Tulsa, Oklahoma.
- Albert, N.R.D. and Chavez, P.S., 1977. "Computer-enhanced Landsat imagery as a tool for mineral exploration in Alaska", US Geological Survey Professional Paper 1015, p.198-200.
- ASP, 1975. "Manual of Remote Sensing", American Society of Photogrammetry, Falls Church, Virginia, 2123p.
- Andrews, J.T., 1970. "Geomorphological study of post-glacial uplift, with particular reference to Arctic Canada", Inst. of Brit. Geog., Sp. Pub. No. 2, London, 156p.
- Baker, G., 1958. "Heavy Minerals from the Weipa Bauxite and Associated Sands", unpub. CSIRO Mineragraphic Investigation Report 751.
- Balasubramanian, K.S. and Gopinath, H., 1979. "Infrared studies of bauxitic minerals from different profiles of Western India", in "Lateritisation Processes", Proc. of the International Seminar on Lateritisation Processes, Trivandrum, India, 11-14 Dec., 1979, p.109-113.
- Black, L.P., 1973. "Tables of isotopic ages from the Georgetown Inlier, North Queensland", Bur. Miner. Res. Geol. Geophys. Aust. Rec. 1973/50.

- Bowman, H.N., 1976. "Peak Hill Sericite", unpub. New South Wales Geological Survey Report GS 1976/128.
- Bowman, H.N. and Richardson, S.J., 1978. "A brief investigation of the Peak Hill disseminated copper-gold deposit", unpub. New South Wales Geological Survey Report GS 1977/278.
- Buckingham, W.F., 1981. "A mineralogical characterisation of rock surfaces formed by hydrothermal alteration and weathering - application to remote sensing", unpub. Ph.D. Thesis, Univ. of Maryland.
- Burns, R.G., 1970. "Mineralogical applications of crystal field theory", Cambridge University Press, Cambridge, 211p.
- Butt, C.R.M., 1981. "The nature and origin of the lateritic weathering profile, with particular reference to Western Australia", in Doyle, H.A., Glover, J.E., and Groves, E.D.I. (eds), "Geophysical Prospecting in Deeply Weathered Terrains", Pub. Geol. Dep. and Extension Service, Univ. West. Australia, No.6, p.11-29.
- Butt, C.R.M., 1983. "Weathering and the Australian Landscape", in Smith, R.E. (ed.), "Geochemical Exploration in Deeply Weathered Terrain", CSIRO Melbourne, ISBN 0-043-03557-5, p.41-50.
- Butt, C.R.M. and Smith, R.E., 1980. "Conceptual models in exploration geochemistry, No.4", The Association of Exploration Geochemistry sp. pub. 8, Elsevier, Amsterdam, 275p.
- Chiu, H.Y. and Collins, W.E., 1978. "A spectroradiometer for airborne remote sensing", *Photogram. Eng. Remote Sensing*, v.44, p.507-517.
- Churchill, J., Craig, M. and Green, A.A., 1983. "Software for the processing of airborne multichannel line-trace data", unpub. CSIRO Institute of Energy and Earth Resources Restricted Investigation Report 1390R.

- Coffey, D.D. and Hollingsworth, P.C., 1971. "Shallow Aquifer Investigations, Weipa, North Queensland", unpub. report for Comalco Aluminium Ltd.
- Coleman, F., 1972. "Frequencies, tracks and intensities of tropical cyclones in the Australian region 1909-1969", Comm. Aust. Bur. Met., Meteorological Summary.
- Collins, W., Chang, S.H. and Kuo, J.T., 1981. "Infrared airborne spectroradiometer survey results in the Western Nevada area", Columbia Univ., Aldridge Lab. Appl. Geophysics, Final Rept. to NASA, Contract JPL 955832.
- Craig, M., Churchill, J. and Green, A.A., 1984. "Software for the processing of airborne multichannel line-trace data", unpub. CSIRO Institute of Energy and Earth Resources Restricted Investigation Report 1508R.
- de la Hunty, L.E., 1963. "Balfour Downs, Western Australia", 1:250,000 Geological Series Sheet SF/51-9, Explanatory Notes, Geol. Survey West. Aust.
- Donaldson, M.J., 1981. "Redistribution of ore elements during serpentinization and talc-carbonate alteration of some Archaean dunites, Western Australia", *Economic Geology*, v.76(6), p.1698-1713.
- Doutch, H.F., Smart, J., Grimes, K.G., Gibson, D.L. and Pavell, B.S., 1973. "Program report on the geology of the southern Carpentaria Basin in Cape York Peninsula", unpub. Bur. Miner. Res. Aust. Rec. 1973/187.
- Eberhardt, J.E., Green, A.A., Haub, J.G., Lyon, R.G.P. and Pryor, A.W., 1984. "CO₂ laser reflectance of rocks for geologic remote sensing", in Proceedings, IUGS/UNESCO Seminar on Remote Sensing for Geological Mapping, Orleans, Feb. 1984, p.233-250.

- Edwards, A.B., 1957. "Quartz and Heavy Minerals in Weipa Bauxite", unpub. CSIRO Mineragraphic Investigation Report 749.
- Edwards, A.B., 1958. "Quartz and Heavy Minerals in Bauxite at Weipa N.10000/W15,000 Pit", unpub. CSIRO Mineragraphic Investigation Report 750.
- Engel, J.L. and Weinstein, O., 1981. "The Thematic Mapper - An overview", *in* Internat. Geoscience Remote Sensing Symposium, Munich. Digest, New York Inst. Electrical Electronics Engineers, v.1, p.wp1.1-1.7.
- Evans, H.J., 1959. "Aluminium in Australia", *Chemical Engineering and Mining Review*, v.51(11), p.1-8.
- Evans, H.J., 1971a. "Weipa Bauxite Deposits", Abstract in Bur. Miner. Res. Bulletin 141, p.222.
- Evans, H.J., 1971b. "Bauxite Deposits of Weipa", *in* McAndrew, J. (ed.). "Geology of Australian Ore Deposits".
- Evans, H.J., 1975. "Weipa Bauxite Deposits, Queensland", *in* Knight, R.L. (ed.) "Economic Geology of Australia and Papua New Guinea".
- Farmer, V.C., 1974. "The Infrared Spectra of Minerals", Monograph 4, Mineralogical Society, London, 539p.
- Fitzpatrick, E.A., 1980. "Soils, their formation, classification and distribution", Longman, London, 353p.
- Fraser, S.J, Green, A.A., Huntington, J.F., Cocks, T., Roberts, G., Stacey, M., Cook, R., Churchill, J., Craig, M. and Hornibrook, M. J., 1985. "The MEIS-II Project", unpub. CSIRO Institute of Energy and Earth Resources Restricted Investigation Report 1572R.
- Gabell, A.R. and Green, A.A., 1982. "Future Remote Sensing Techniques for Australian Mineral Exploration", Invited Presentation - Remote Sensing Session, ANZAAS Conference, Sydney, May, 1982.

- Gabell, A.R., Huntington, J.F., Green, A.A., Cocks, T.D. and Hornibrook, M.J., in press. "Clay mineral absorption features in the 0.9 to 1.1 micrometre region and their implication for proximal and remote sensing", *in* "Remote Sensing for Exploration Geology", Proc. of the 4th Thematic Conf. of the Int. Symp. on Remote Sensing of Environment, San Francisco, April 1985.
- Gabell, A.R. and Green, A.A., 1983. "Implications of Second Generation Remote Sensing Systems for Australian Geology". *in* Supplement to Geol. Soc. Australasia Workshop on Geochemistry of Deeply Weathered Terrain, p.77-84.
- Gabell, A.R., Huntington, J.F., Green, A.A. and Craig, M., 1983. "Interpretation of high resolution, airborne, visible and near infrared spectroradiometer data over the Mt Turner porphyry copper system, Georgetown, Queensland", unpub. CSIRO Institute of Energy and Earth Resources Restricted Investigation Report 1454R.
- Gabell, A.R., Huntington, J.F., Green, A.A. and Craig, M., 1984. "Interpretation of high resolution, airborne, visible and near infrared spectroradiometer data over Kambalda, Western Australia", unpub. CSIRO Institute of Energy and Earth Resources Restricted Investigation Report 1484R.
- Gemuts, I. and Theron, A., 1975. "The Archaean between Coolgardie and Norseman - stratigraphy and mineralization", *in* Knight, R.L. (ed.) "Economic Geology of Australia and Papua New Guinea, I : Metals", p.66-74.
- GER, 1983. "Airborne spectroradiometer surveys over Mt Turner and Kambalda", Report prepared for CSIRO and AMIRA, by Geophysical Environmental Research, Inc., New York.
- Goetz, A.F.H. 1984. "High spectral resolution remote sensing of the land", SPIE v.475, "Remote Sensing", p.56-68.

- Goetz, A.F.H. and Rowan, L.C., 1981. "Geologic remote sensing". *Science*, v.211, p.781-791.
- Goetz, A.F.H., Rowan, L.C. and Kingston, M.N.J., 1982. "Multispectral Orbital Radiometry for Mineral Identification", in "Remote Sensing for Exploration Geology", Proc. of the 2nd Thematic Conf. of the Int. Symp. on Remote Sensing of Environment, Fort Worth, 6-10 Dec., p.205-206.
- Green, A.A. and Craig, M.C., 1985. "Analysis of aircraft spectrometer data with logarithmic residuals", in Proc. of the Airborne Imaging Spectrometer Data Analysis Workshop, 8-10 April, Pasadena, p.111-119.
- Green, A.A., Huntington, J.F., Roberts, G.P. and Brandt, L., 1980. "Improving the value of Landsat Imagery for mineral exploration. Part A : Image Processing System", unpub. CSIRO Institute of Energy and Earth Resources, Restricted Investigation Report 1248R.
- Gresham, J.J. and Loftus-Hills, G.D., 1981. "The geology of the Kambalda nickel field, Western Australia", *Economic Geology* v.76(6), p.1373-1416.
- Grimes, K.G., 1974. "Mesozoic and Cainozoic geology of the Lawn Hill, Westmoreland, Mornington and Cape Van Diemen 1:250,000 sheet areas, Queensland", unpub. Bur. Miner. Res. Aust. Rec. 1974/106.
- Grubb, P.L.C., 1971. "Genesis of the Weipa Bauxite Deposits, N.E. Australia", *Mineral. Deposita*, v.6, p.265-274.
- Hayashi, H. and Oinuma, K., 1967. "SiO absorption band near 1000 cm⁻¹ and OH absorption bands of chlorite", *Am. Min.*, v.52, p.1206-1210.
- Hickman, A.H., 1983. "Geology of the Pilbara Block and its Environs", Geol. Survey West. Aust. Bulletin 127.

- Horsfall, C.L., Green, A.A., Huntington, J.F. and Craig, M., 1984. "A preliminary interpretation of high resolution airborne, visible, near and short wavelength infrared spectroradiometer data from Mt Isa, Queensland", unpub. CSIRO Institute of Energy and Earth Resources Restricted Investigation Report 1469R.
- Hunt, G.R., 1980. "Electromagnetic radiation : The Communication link in Remote Sensing", in Siegal, B.S. and Gillespie, A.R. (eds), "Remote Sensing in Geology", p.5-46.
- Hunt, G.R. and Ashley, R.P., 1979. "Spectra of Altered Rocks in the Visible and Near Infrared", *Economic Geology* v.74, p.1613-1629.
- Hunt, G.R. and Salisbury, J.W., 1970a. "Visible and near infrared spectra of minerals and rocks : I Silicate minerals", *Modern Geology*, v.1, p.283-300.
- Hunt, G.R. and Salisbury, J.W., 1970b. "Visible and near infrared spectra of minerals and rocks : II Carbonates", *Modern Geology*, v.2, p.23-30.
- Hunt, G.R., Salisbury, J.W. and Lenhoff, C.J., 1971a. "Visible and near infrared spectra of minerals and rocks : III Oxides and hydroxides", *Modern Geology*, v.2, p.195-205.
- Hunt, G.R., Salisbury, J.W. and Lenhoff, C.J., 1971b. "Visible and near infrared spectra of minerals and rocks : IV Sulphides and sulphates", *Modern Geology*, v.3, p.1-14.
- Hunt, G.R., Salisbury, J.W. and Lenhoff, C.J., 1972. "Visible and near infrared spectra of minerals and rocks : V Halides, phosphates, arsenates and vanadates", *Modern Geology*, v.3, p.121-132.
- Hunt, G.R., Salisbury, J.W. and Lenhoff, C.J., 1973a. "Visible and near infrared spectra of minerals and rocks : VI Additional silicates", *Modern Geology*, v.4, p.85-106.

- Hunt, G.R., Salisbury, J.W. and Lenhoff, C.J., 1973b. "Visible and near infrared spectra of minerals and rocks : VII Acidic igneous rocks", *Modern Geology*, v.4, p.217-224.
- Hunt, G.R., Salisbury, J.W. and Lenhoff, C.J., 1974a. "Visible and near infrared spectra of minerals and rocks : VII Intermediate igneous rocks", *Modern Geology*, v.4, p.237-244.
- Hunt, G.R., Salisbury, J.W. and Lenhoff, C.J., 1974b. "Visible and near infrared spectra of minerals and rocks : IX Basic and ultrabasic rocks", *Modern Geology*, v.5, p.15-22.
- Hunt, G.R., Salisbury, J.W. and Lenhoff, C.J., 1976a. "Visible and near infrared spectra of minerals and rocks : XI Sedimentary rocks", *Modern Geology*, v.5, p.211-217.
- Hunt, G.R., Salisbury, J.W. and Lenhoff, C.J., 1976b. "Visible and near infrared spectra of minerals and rocks : XII Metamorphic rocks", *Modern Geology*, v.5, p.221-228.
- Huntington, J.F., 1984. "Landsat 4 Thematic Mapper Preliminary Evaluation", unpub. CSIRO Institute of Energy and Earth Resources Restricted Investigation Report 1504R.
- Huntington, J.F., Gabell, A.R. and Green, A.A., 1982. "A Landsat Study of the Weipa Bauxite Province, North Queensland", unpub. CSIRO Institute of Energy and Earth Resources Restricted Investigation Report 1302R.
- Kahle, A.B. and Goetz, A.F., 1983. "Mineralogic information from a new airborne thermal infrared multispectral scanner", *Science*, v.222, p.24-27.
- Kneizy, F.X., Shettle, S.H., Gallery, W.O., Chetwynd, J.H., Abreu, L.W., Selby, J.E.A., Fenn, R.W. and McClatchey, R.A., 1980. "Atmospheric Transmittance/Radiance : Computer Code LOWTRAN 5", Air Force Systems Command, USAF, Environmental Research Paper No.697.

- Loughnan, F.C. and Bayliss, P., 1961. "The Mineralogy of the Bauxite Deposits Near Weipa, Queensland", *Am. Mineralogist*, v.46, p.209-217.
- Lyon, R.J.P., 1962. "Evaluation of infrared spectrophotometry for compositional analysis of lunar and planetary soils", Stanford Research Institute Report, California.
- Lyon, R.J.P., 1964. "Evaluation of infrared spectrophotometry for compositional analysis of lunar and planetary soils. Part II : Rough and powdered surfaces", Stanford Research Institute Final Report, NASA CR100.
- Lyon, R.J.P. and Patterson, J.W., 1966. "Infrared spectral signatures - a field geological tool", Proc. of the 4th Symposium on Remote Sensing of Environment, University of Michigan, p.215-230.
- Lyon, R.J.P., 1977. "Mineral exploration applications of digitally processed Landsat imagery", US Geological Survey Professional Paper 1015, 271-292.
- MacGeehan, P., 1972. "Vertical zonation within the Aurukun bauxite deposits, North Queensland, Australia", in Proc. of the 24th IGC, 1972 - Section 4.
- Marsh, S.E. and McKeon, J.B., 1983. "Integrated Analysis of High-Resolution Field and Airborne Spectroradiometer Data for Alteration Mapping", *Economic Geology*, v.78, p.618-632.
- Marston, R.J., Groves, D.I., Hudson, D.R. and Ross, J.R., 1981. "Nickel sulfide Deposits in Western Australia : A Review", *Economic Geology*, v.76, p.1330-1363.
- McAndrew, J. and Edwards, A.B., 1956. "Boehmite and Gibbsite in Weipa Bauxite, Queensland", unpub. CSIRO Mineragraphic Investigation Report 748.

- McFarlane, M. J., 1971 "Lateritization and Landscape development in Kyagwe, Uganda" *Quart. J. Geol. Soc. Lond.*, v.126, p.501-539.
- McFarlane, M.J., 1976 "Laterite and Landscape", Academic Press, London, 151p.
- NASA, 1972. "Earth Resources Technology Satellite-1 symposium proceedings". Goddard Space Flight Center, Maryland, 27 Sep. National Aeronautics and Space Administration Report X-650-73-10.
- NASA, 1973a. "Symposium on significant results obtained from the Earth Resources Technology Satellite-1". Goddard Space Flight Center, Maryland 5-9 Mar. National Aeronautics and Space Administration, SP-327, 1.
- NASA, 1973b. "Third Earth Resources Technology Satellite-1 Symposium". Goddard Space Flight Center, Maryland, 10-14 Dec. National Aeronautics and Space Administration, SP-351, 1.
- NASA, 1975. "Proceedings of the NASA earth resources survey symposium". L.B.J. Space Center, Houston, 9-12 Jun., National Aeronautics and Space Administration, TMX-58168.
- NASA, 1985. "Imaging Spectrometry : The Next Step in Remote Sensing", NASA Jet Propulsion Laboratory Publication, Los Angeles, 14p
- Ollier, C.D., 1978. "Early landform evolution", in Jeans, J.L. (ed.) "Australia, A Geography" Sydney Univ. Press, Sydney p.85-98.
- Petersen, U., 1971. "Laterite and Bauxite Formation", *Economic Geology*, v.66, p.1070-1071.
- Pedley, L. and Isbell, R.F., 1971. "Plant communities of Cape York Peninsula", *Proc. Roy. Soc. Qld.*, v.82, p.51-74.
- Phillips, S.E., 1984. "An Electron Microscope Study of Calcareous Fine Earths", abstracts from the 9th Biennial Conference of the Australian Clay Minerals Society, Canberra, 26-28 Nov., 1984.

- Plumb, K.A. and Gostin, V.A., 1973. "Origin of Australian bauxite deposits", unpub. Bur. Miner. Res. Aust. Rec. 1973/132.
- Reeves, R.G., Kover, A.N., Lyon, R.J.P. and Smith, H.T.U., 1975. "Terrain and Minerals : Assessment and Evaluation", in ASP "Manual of Remote Sensing", p.1107-1338.
- Richards, J.R., White, D.A., Webb, A.W. and Branch, C.D., 1966. "Isotopic ages of acidic igneous rocks in the Cairns hinterland, North Queensland", Bur. Miner. Res. Geol. Geophys. Aust. Bulletin 88.
- Roberts, G.P., 1982. "An on-line, raster-scan, colour-image display system using charge-coupled memories for refresh storage", unpub. M.Sc. Thesis, Univ. of NSW, 156p.
- Rose, A.W. and Burt, D.M., 1979. "Hydrothermal Alteration", in Barnes, H.L. (ed.), "Geochemistry of Hydrothermal ore Deposits", p.173-235.
- Ross, J.R. and Travis, G.A., 1981. "The Nickel Sulfide Deposits of Western Australia in Global Perspective", *Economic Geology*, v.76, p.1291-1329.
- Rouse, J.W., Haas, R.H., Schell, J.A., Deering, D.W. and Harlan, J.C., 1974. "Monitoring the vernal advancement and retrogradation (greenwave effect) of natural vegetation". NASA/GSFC Type III Final Report, Greenbelt, Maryland, 371p.
- Rowan, L.C. and Lathram, E.H., 1980. "Mineral Exploration", in Siegal, B.S. and Gillespie, A.R. (eds), "Remote Sensing in Geology", p.553-605.
- Rowan, L.C., Goetz, A.F. and Ashley, R.P., 1977. "Discrimination of hydrothermally altered and unaltered rocks in visible and near infrared multispectral images", *Geophysics*, v.42, p.522-535.

- Rowan, L.C., Wetlaufer, P.G., Goetz, A.F., Billingsley, F.C. and Stewart, J.H., 1974. "Discrimination of rock types and detection of hydrothermally altered areas in south-central Nevada by the use of computer-enhanced ERTS images", US Geological Survey Professional Paper 883.
- Schellmann, W., 1979. "Considerations on the definition and classification of laterites", in "Lateritisation Processes", Proc. of the International Seminar on Lateritisation Processes, Trivandrum, India, 11-14 Dec., 1979, p.1-10
- Schmidt, R.G. and Bernstein, R., 1977. "Evaluation of improved digital-processing techniques of Landsat data for sulfide mineral prospecting", US Geological Survey Professional Paper 1015, p.201-212.
- Segal, D.B., 1983. "Use of Landsat Multispectral Scanner Data for the definition of limonitic exposures in heavily vegetated areas", *Economic Geology*, v.78(4), p.711-722.
- Slansky, E., 1978. "Jarosite from Peak Hill", New South Wales Geological Survey Report Mineralogy 1978/23, GS/1978/195.
- Smart, J., 1977. "Aurukun, Qld. 1-250,000 Geological Series", Bur. Miner. Res. Aust. Explan. Notes SD/54.7.
- Smith, R.E., Green, A.A., Roberts, G. and Honey, F.R., 1978. "Use of Landsat-1 Imagery in Exploration for Keweenaw type Copper Deposits", *Remote Sensing of Environment*, v.7, p.129-144.
- Smith, R.E., Perdrix, J.L., and Parks, T.C., 1982. "Burial Metamorphism in the Hamersley Basin, Western Australia", *Jnl. of Petrology*, v.23(1), p.119-143.

- Specht, R.L., 1958a. "Botany and Plant Ecology", *in* Specht, R.L. and Meunford, C.P. (eds), "Climate, geology, soils and plant ecology of the northern portion of Arnhem Land", Melbourne University Press, Melbourne, v.3.
- Specht, R.L., 1958b. "Geographical relationships of the flora of Arnhem Land". *in* Specht, R.L. and Meunford, C.P. (eds), "Climate, geology, soils and plant ecology of the northern portion of Arnhem Land", v.3, p.415-478.
- Specht, R.L., Salt, R.B. and Reynolds, S.T., 1977. "Vegetation in the vicinity of Weipa, North Queensland". *Proc. Roy. Soc. Qld.*, v.88, p.17-38.
- Taranik, J.V., 1978. "Characteristics of the Landsat multispectral data system", US Geological Survey Open-File Report 78-187.
- Titley, S.R., (ed.), 1978 "Advances in Geology of the Porphyry Copper Deposits Southwestern North America", Univ. of Arizona Press, Tucson, 560p.
- Trendall, A.F., 1975. "Main areas of Proterozoic sedimentary rocks in the Hamersley Basin", *in* "The Geology of Western Australia". West. Aust. Geol. Survey Memoir 2, p.119-143.
- Trendall, A.F., 1979. "A revision of the Mount Bruce Supergroup", West. Aust. Geol. Survey Ann. Report, p.63-71.
- Trendall, A.F., 1983. "The Hamersley Basin", *in* Trendall, A.F. and Morris R.C., (eds), "Iron Formations : Facts and Problems", Elsevier, Amsterdam, p.69-129.
- Valentin, H., 1959. "Geomorphological reconnaissance of the northwest coast of Cape York Peninsula (northern Australia)", *in* Proc. of the 2nd Coastal Geogr. Conf., Louisiana, p.213-31.
- Valeton, I., 1972. "Bauxites". Elsevier, Amsterdam, 213p.

Weidner, V.R. and Haia, J.J., 1981. "Reflection properties of pressed polytetrafluoroethylene powder", *Jnl. Opt. Soc. Am.*, v.71, p.856-861.

Withnall, I.W., Bain, J.H.C. and Rubenach, M.J., 1980. "The Precambrian Geology of Northeastern Queensland", *in* Henderson, R.A. and Stephenson, P.J. (eds), "The Geology and Geophysics of Northeastern Australia", Geol. Soc. Aust., Queensland Division, Brisbane, p.109-127.

APPENDIX I Clay mineral absorption features in the 0.9 to 1.1 micro
metre region and their implications for proximal and
remote sensing (Gabell et al., 1985).

CLAY MINERAL ABSORPTION FEATURES IN THE 0.9 TO 1.1 MICROMETRE
REGION AND THEIR IMPLICATION FOR PROXIMAL AND REMOTE SENSING

A.R. Gabell, J.F. Huntington, A.A. Green, T.D. Cocks, and M.J. Hornibrook

CSIRO Division of Mineral Physics
Sydney, Australia

ABSTRACT

In infrared reflectance spectra of minerals, the second overtone of the fundamental O-H stretch occurs near $0.95\mu\text{m}$, but is much weaker than the first overtone (near $1.4\mu\text{m}$) or the stretch/band combinations (2.0 to $2.5\mu\text{m}$) which are used in remote sensing of clay minerals. The mode and frequency of occurrence of $3\nu_{\text{OH}}$ features warrant investigation because they can be detected using only silicon photodiodes. This offers significant advantages of cost, availability and sensitivity of detectors.

The $3\nu_{\text{OH}}$ features were found to occur in the spectra of all hydroxyl-bearing mineral standards measured. As might be expected, the features are less common in the spectra of fresh rocks, and least common and weakest in the spectra of weathered rock surfaces. Nevertheless, the laboratory data show examples in all of these categories which have useful and detectable $3\nu_{\text{OH}}$ features.

Successful application of the measurement technique outside the laboratory is shown to be possible using "typical" instruments under a variety of atmospheric conditions. This depends, however, on a constant water content in the atmosphere, or on successful monitoring of any changes. The technique is not yet fully evaluated.

INTRODUCTION

Routine VNIR (0.4 to $1.1\mu\text{m}$) laboratory spectral measurement of some hydrothermally altered rock samples has revealed the presence of clay mineral absorption features in the $0.95\mu\text{m}$ region. These features are generally consistent with those observed in the SWIR (1.1 to $2.5\mu\text{m}$). Similar VNIR features have been described in the past, and assigned as the second overtone of the fundamental O-H stretch (Hunt *et al.*, 1971). However, in these cases only the most intense features have been noted. We decided to investigate these absorption features in clay mineral and natural rock samples to determine their strength and frequency of occurrence.

If it proves possible to use them for proximal (ground-based) or remote sensing the presence of these features means that some clay mineralogical information might be obtained from the use of VNIR (Si photodiode) technology alone. This would offer significant advantages in cost, availability and sensitivity of detectors. The major disadvantages of working in this region are the proximity of an atmospheric water absorption feature, and the weakness of the second overtone features.

Background Theory

Hydroxyl-bearing minerals absorb energy in a number of regions in the electromagnetic spectrum. The strongest of these features is the fundamental O-H stretch (denoted ν_{OH}) which occurs near $2.8\mu\text{m}$ (see Fig. 1a). The fundamental O-H stretch is not utilised for remote sensing because it occurs in

a region of total atmospheric absorption. The fundamental cation-O-H bend (denoted δ_{OH}) occurs in the 8 to 15 μm region (Fig. 1b). The absorption features caused by O-H stretch and bend combinations ($\nu_{OH} + \delta_{OH}$) are utilised for remote sensing because, although weaker than the fundamentals, they occur in an atmospheric "window" between 2.0 and 2.5 μm . The example shown in Fig. 1d is of synthetic gibbsite, but many other examples are recorded in the literature (Hunt and Salisbury, 1970, Hunt et al., 1971, 1973).

The first overtone of the fundamental O-H stretch (denoted $2\nu_{OH}$) occurs at approximately twice the frequency of the fundamental, hence near 1.4 μm (see Fig. 1d). In most cases atmospheric absorption in this region obscures the spectral variation due to mineralogy. In exceptional cases (gibbsite is one of these) the mineral absorption feature may be shifted relative to the atmospheric absorption. In such cases, there is some potential for utilising these features in high spectral resolution remote sensing.

The second overtone of the fundamental O-H stretch (denoted $3\nu_{OH}$) occurs at approximately 0.95 μm (Fig. 1c), but is much weaker than even the first overtone. However, it does occur in a region of only partial atmospheric absorption. In exceptional cases (and once again gibbsite is such an example) the third overtone (denoted $4\nu_{OH}$) may be detectable (see Figs. 1c and 1e).

$3\nu_{OH}$ FEATURES OF SOME CLAY STANDARDS

Hunt et al., (1971) have reported the presence of $3\nu_{OH}$ absorption features from the laboratory spectra of several powdered samples. As these spectra were all plotted on a 0-100 percentage reflectance scale, only the strongest absorption features were noted. Fig. 1e shows the result of scaling the gibbsite VNIR spectrum to the full dynamic range of the data. The spectral features in the region of interest are obviously enhanced, thereby increasing the chance of detecting them, and allowing a more detailed interpretation.

We have recorded the VNIR spectra of a number of hydroxyl-bearing mineral standards. The spectra were recorded using a Reticon detector array interfaced to a Tracor Northern Multichannel analyser. The light source was a quartz-halogen lamp, while the reference standard used was halon (Venable et al., 1976). All of the spectra shown in Figs. 2a to f were recorded from powdered samples. The brucite and gibbsite samples are synthetic, whilst the other samples come from the A.P.I. clay mineral standards collection, as supplied by Wards.

These six samples show considerable variation in the shape and precise position of their absorption minima. The background spectra plotted between 0.9 μm and 1.0 μm with a fine line represent atmospheric transmission on an average mid-latitude summer's day (with a range of 45% to 98% transmission). These plots are included mainly to show the positions of the major atmospheric absorption features in relation to mineralogical features.

$3\nu_{OH}$ FEATURES OF SOME NATURAL ROCK SURFACES

In addition to the relatively pure mineral standards shown in Fig. 2, we have routinely measured natural, weathered rock surfaces in the laboratory. The spectra of hydrothermally altered (a to c) and weathered (d) rocks from two different locations in New South Wales, Australia, are depicted in Fig. 3. The $3\nu_{OH}$ absorption features closely resemble those of the standards in Fig. 2. The mineralogy interpreted from SWIR spectra (1.4 μm to 2.5 μm) and XRD analysis supports the interpretation of the $3\nu_{OH}$ features in each case.

Although each of the plots in Fig. 3 result from the measurement of a weathered surface, it should be noted that $3\nu_{OH}$ features have not been observed for every sample which exhibits hydroxyl absorption features in the SWIR. Furthermore, $3\nu_{OH}$ features are more common, and stronger, on fresher, broken surfaces. Nevertheless, Figs. 3 a-d demonstrate that it is possible to derive

some information on the clay mineralogy of a natural, weathered surface of a rock using VNIR spectral data alone.

THE EFFECT OF IRON OXIDES

The observation that $3\nu_{OH}$ features are, in the main, weaker in the spectra of weathered surfaces prompted an investigation into the effects of iron oxide on the spectral properties of different minerals. Thus, powdered brucite, gibbsite, pyrophyllite and kaolin were physically mixed with various quantities (expressed in weight percent) of hematite powder. The resultant spectra showed a fairly regular, but non-linear, decrease in overall reflectance, and in the depth of the $3\nu_{OH}$ features. The spectra of brucite plus 0%, 1%, 5% and 10% hematite are shown in Fig. 4.

The results for all of the hydroxyl-bearing minerals are shown in Fig. 5, with band depth plotted versus the log of the weight fraction of hematite (after the method of Clark (1983)). The results show that although there is often a steep decrease in the depth of the $3\nu_{OH}$ feature within the addition of hematite, for at least some minerals it can remain detectable at levels of at least 10% hematite by weight.

FIELD MEASUREMENT

The data presented so far indicate that significant information can result from laboratory measurement of the $3\nu_{OH}$ absorption feature. The question remains as to whether the feature can also be observed through the atmosphere outside the laboratory.

To assess the viability of detecting the $3\nu_{OH}$ absorption features with field-portable spectroradiometers or airborne remote sensors, we modelled the radiometric sensitivity of several representative instruments using the LOWTRAN atmospheric transmission model. The results, expressed in terms of noise equivalent reflectance ($NE\Delta\rho$), were obtained for instruments using Si photo-diodes with average D's ($1-5 \times 10^{12} \text{ cm-Hz}^{1/2} \text{ w}^{-1}$) and assuming reasonable engineering. Table I presents the conclusion of our calculations.

TABLE I SENSITIVITIES OF REPRESENTATIVE INSTRUMENTS

Instrument	Aperture	B/width	IFOV	$d^*_{\lambda\rho\kappa}$	$NE\Delta\rho$ Dry	$NE\Delta\rho$ Tropical
Field Portable Spectroradiometer	75mm	1nm	6mr		More than adequate (long integration)	More than adequate (long integration)
Airborne Spectroradiometer	75mm	1nm	6mr		<.00081	<.005
Multispectral Scanner	same as Daedalus DS-1260	5nm	5mr	$5 \times 10^{12} \text{ cm-Hz}^{1/2} \text{ w}^{-1}$	<.0015	<.008

N.B. 1 $NE\Delta\rho$'s expressed as reflectance to enable direct comparison to y-axis scales on figures.

- 2 Calculations completed for (a) dry atmosphere
 (b) mid-latitude summer (average)
 (c) tropical atmosphere

The results shown indicate that it is within instrument capabilities to detect the $3\nu_{OH}$ features illustrated (perhaps with the exception of the multispectral scanner operating in a tropical atmosphere).

However, these calculations have been made assuming that the atmospheric water vapour content is constant. Any temporal change (for field portable instruments) or spatial change (for airborne instruments) will therefore have a significant effect. For instance, a topographic variation of 100 metres from near sea level can result in a 15% difference in the depth of the atmospheric water absorption band. Successful measurements would require either hardware designed to overcome this problem (e.g. a dual-beam field portable instrument which focusses on target and standard simultaneously), or some technique to monitor atmospheric variations. In the case of an airborne survey over changing topography, monitoring changes in two different atmospheric absorption features may enable any variation due to topography to be detected. At this stage, however, the potential of the technique has not been fully tested.

CONCLUSIONS

The data presented here show that it is possible to derive useful information on the clay mineralogy of source samples using laboratory VNIR (.4 to 1.1 μm) spectral data alone. This offers significant advantages in cost, availability and sensitivity of detectors over those more commonly used in remote sensing in the SWIR (1.1 to 2.5 μm).

The $3\nu_{OH}$ features were found to occur in every laboratory spectrum of "pure" hydroxyl-bearing mineral standards measured. The absorption features can be diagnostic of mineralogy by their shapes and precise positions. Although $3\nu_{OH}$ features were found to be common in the spectra of fresh surfaces of hydrothermally altered and weathered rocks, they are not always present when a SWIR signature is apparent.

The features are least common and weakest on weathered surfaces of rock samples. Mixing of "pure" powdered standards with powdered hematite shows that the $3\nu_{OH}$ features rapidly weaken with increasing iron oxide content. Nevertheless, in some samples they were still detectable with up to 15% hematite by weight in the mixture.

Calculations have shown that "typical" instruments have the sensitivity to detect the $3\nu_{OH}$ features outside the laboratory under a variety of atmospheric conditions. However, a major constraint is that the water content of the atmosphere must remain constant, or be accurately monitored. If this condition is not met, then the variation due to atmospheric absorption will be greater than that due to mineralogical absorption in the critical wavelength region.

REFERENCES

- Clark, R.N., 1983, "Spectral Properties of Mixtures of Montmorillonite and Dark Carbon Grains: Implications for Remote Sensing Minerals Containing Chemically and Physically Adsorbed Water", *Jnl. Geophys. Res.* v. 88, No. B12, pp 10, 635-10,644.
- Hunt, G.R. and Salisbury, J.W., 1970. "Visible and Near Infrared Spectra of Minerals and Rocks: I Silicate Minerals", *Mod. Geology*, v1, pp 283-300.
- Hunt, G.R., Salisbury, J.W. and Lenhoff, C.J., 1971, "Visible and Near Infrared Spectra of Minerals and rocks: III Oxides and Hydroxides", *Mod. Geology*, v2, pp 195-205.
- Hunt, G.R., Salisbury, J.W. and Lenhoff, C.J., 1973, "Visible and Near Infrared Spectra of Minerals and Rocks. VI Additional Silicates", *Mod. Geology*, v4, pp 85-106.

Venable, W.H., Jr., Weidner, V.R. and Hsia, J.J., 1976. "Information sheet on optical properties of pressed Halon coatings", Natl. Bur. of Stand., Washington, D.C.

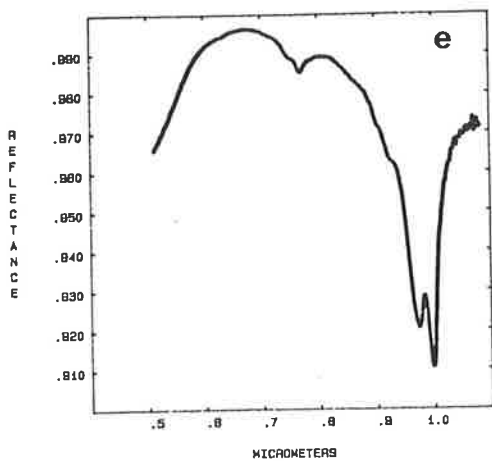
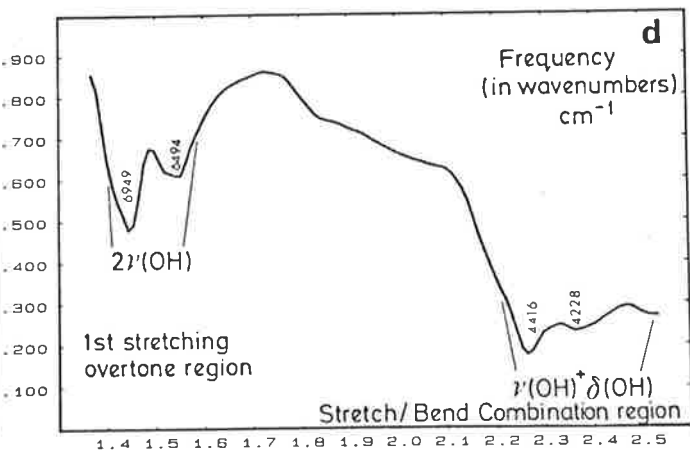
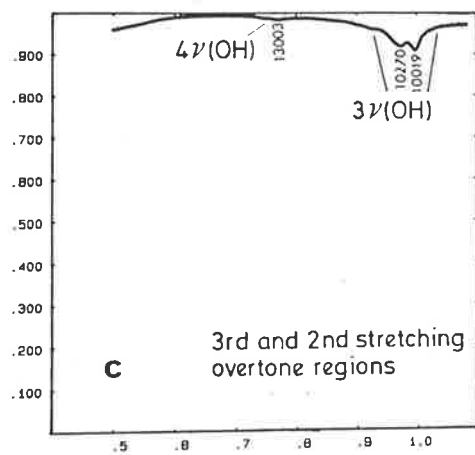
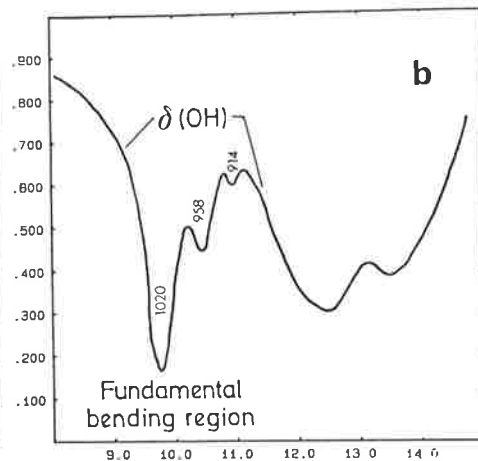
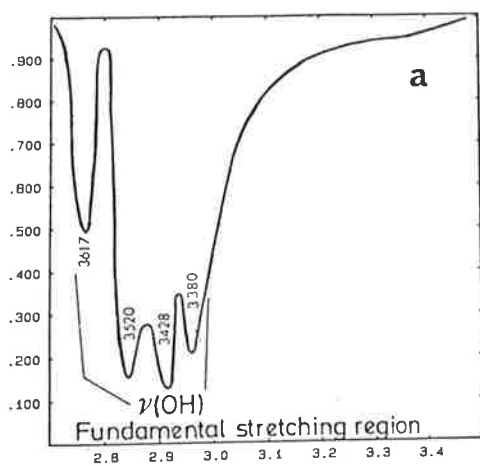


Figure 1. The spectrum of gibbsite

- a) The fundamental stretching region (2.7 μm) to 3.5 μm) - transmission spectrum
- b) The fundamental bending region (8.0 μm to 15.0 μm) - transmission spectrum
- c) VNIR (0.4 μm to 1.1 μm) - reflectance spectrum
- d) SWIR (1.1 μm to 2.6 μm) - reflectance spectrum
- e) VNIR (0.4 μm to 1.1 μm) - reflectance spectrum - as for plot c), but with plot scaled to the full dynamic range of the data.

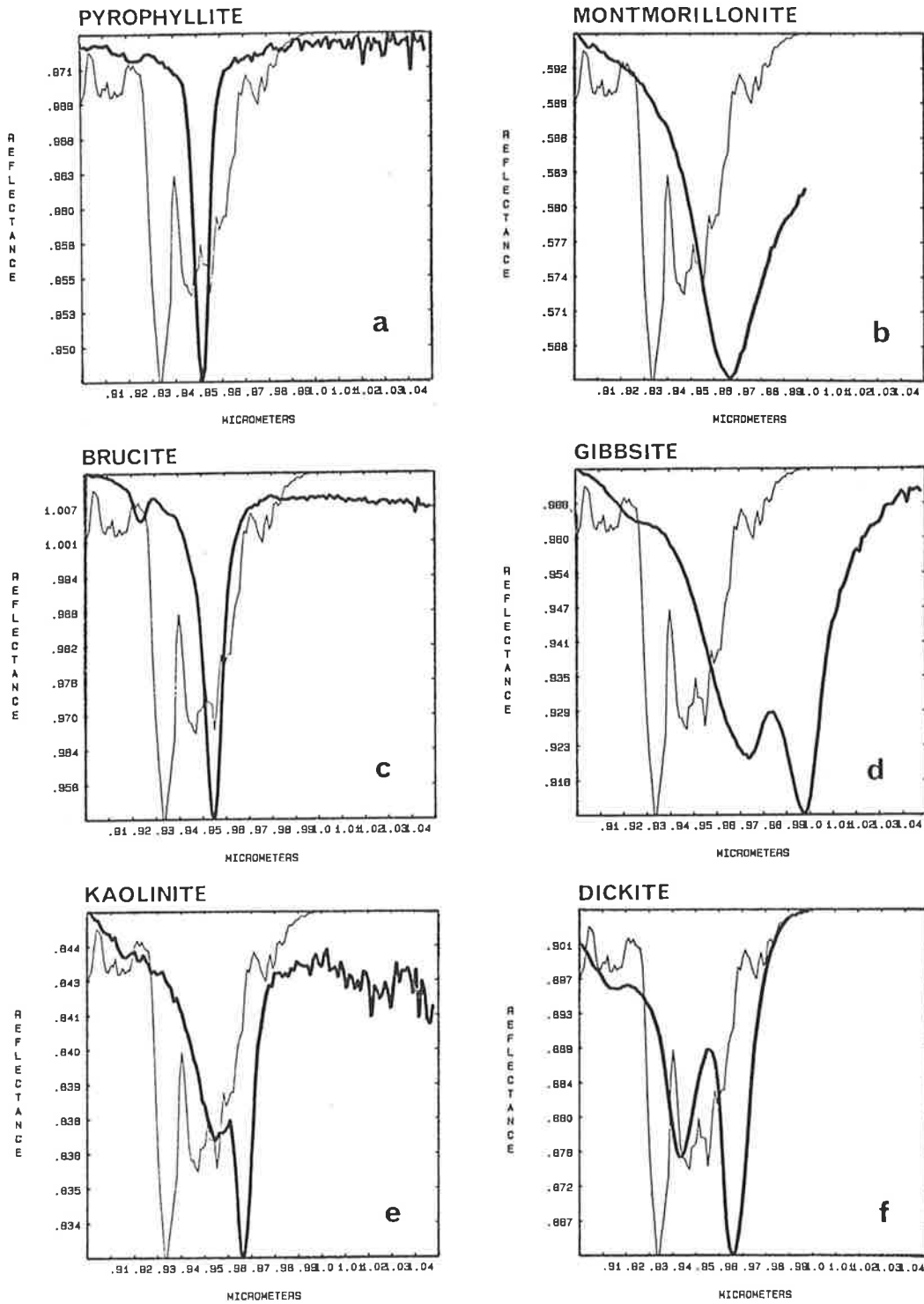


Figure 2. VNIR (0.9 μm to 1.05 μm) reflectance spectra of powdered samples. Atmospheric transmission is also shown on each plot.

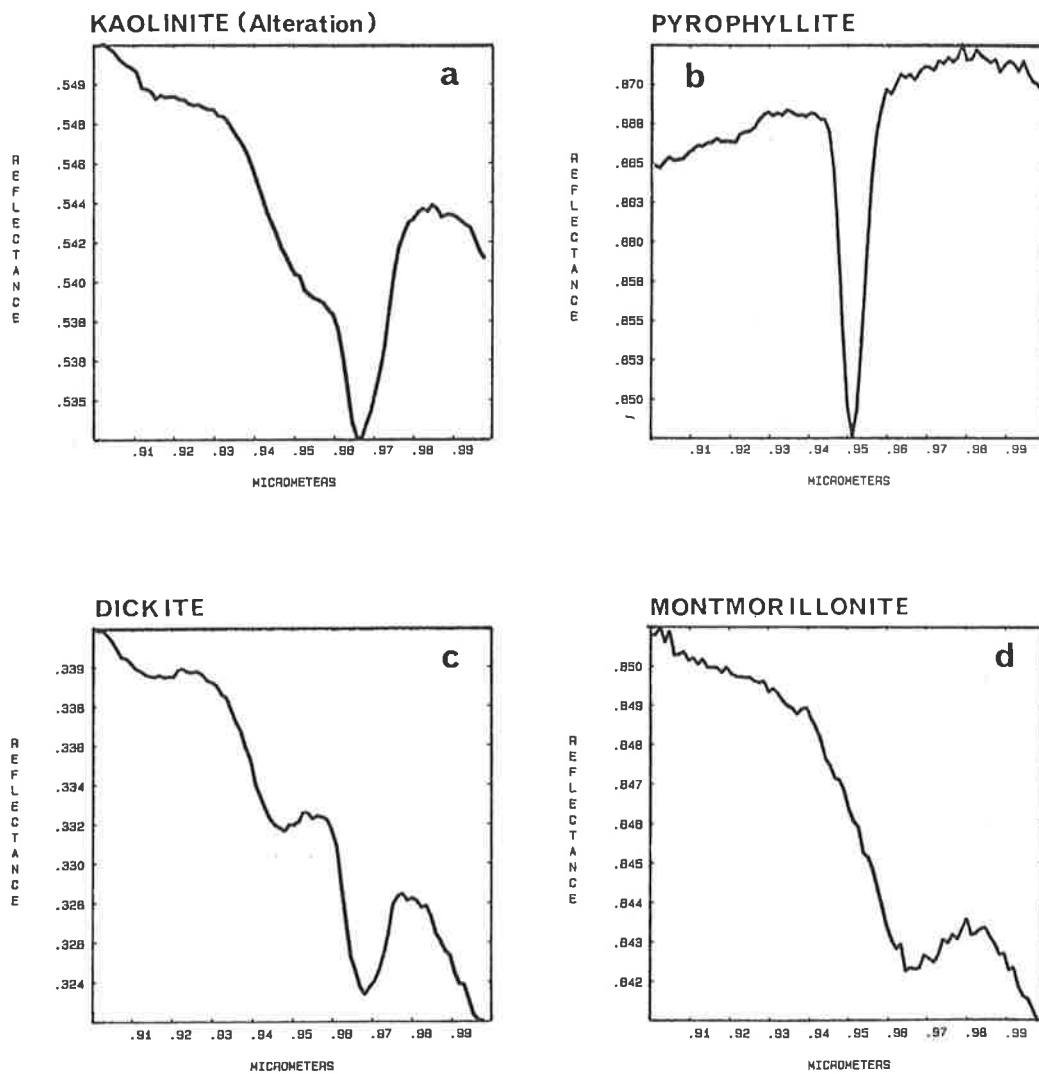


Figure 3. The VNIR (0.9 μ m to 1.0 μ m) reflectance spectra of some natural rock surfaces. Spectra a) to c) are of hydrothermally altered samples, while spectrum d) is only weathered.

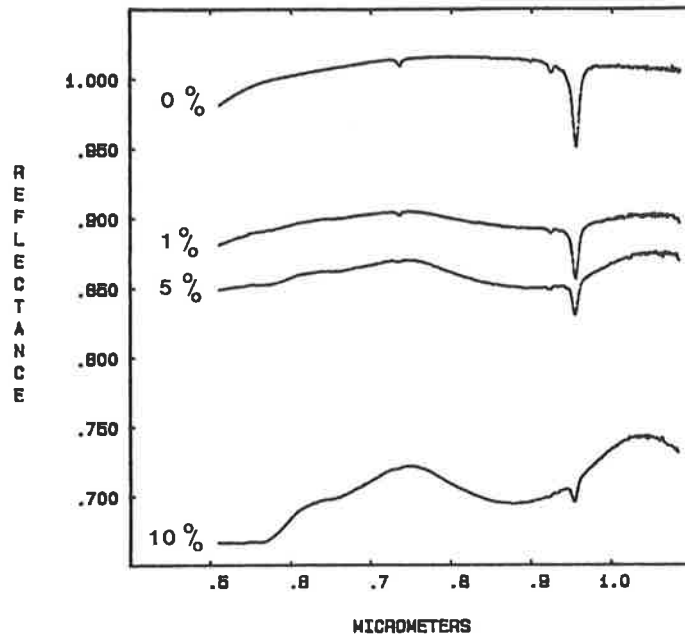


Figure 4. The VNIR (0.4 μm to 1.1 μm) reflectance spectra of brucite plus 0%, 1%, 5% and 10% hematite

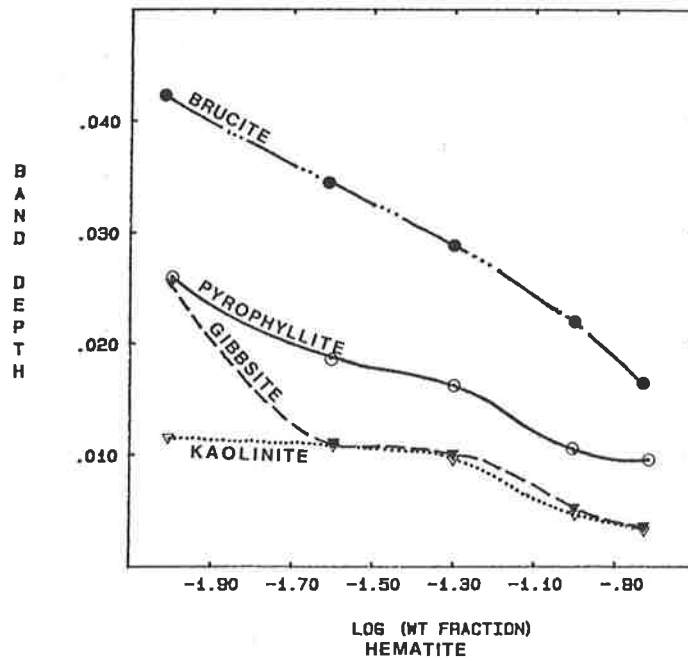


Figure 5. Plots of band depth versus log of five weight fractions of hematite for four different powdered minerals

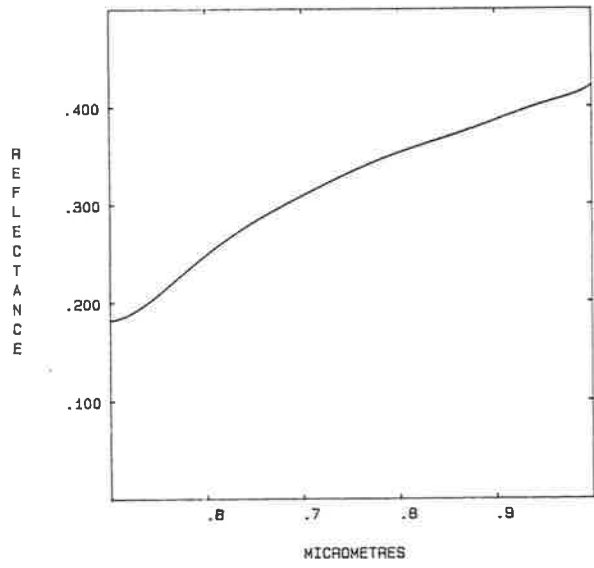
APPENDIX II VNIR laboratory reflectance spectra of soil samples from Weipa.

The VNIR spectra in this appendix have been smoothed by Tchebychev reconstruction (see text, section 3.3.2.3 - this process is also illustrated using one of the Weipa sample's spectra on the last page of this appendix).

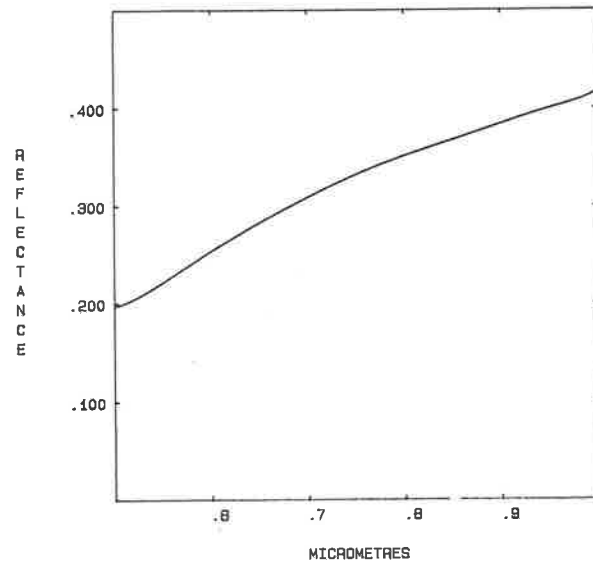
The plots, with a few exceptions, are presented in an order consistent with the relevant sample's position on the Weipa grid, progressing from west to east. For each sample the grid position and the iron content (determined by wet chemistry and expressed as Fe_2O_3) are shown at the top of each plot.

There is a marked lack of absorption features in these spectra, only a few samples (generally those with greater than 6% Fe_2O_3) exhibiting subtle absorption features due to iron. A single sample of cemented pisolite ore has strong iron oxide absorption features, and has been included for comparison.

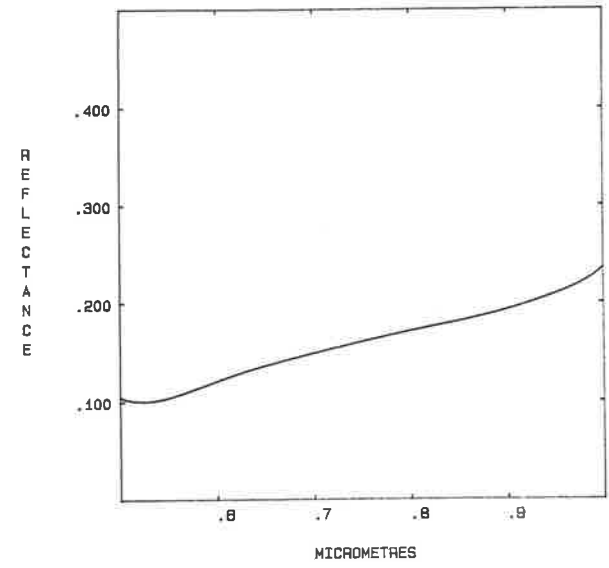
WEIPA N10 E12 FE2O3 8.5%



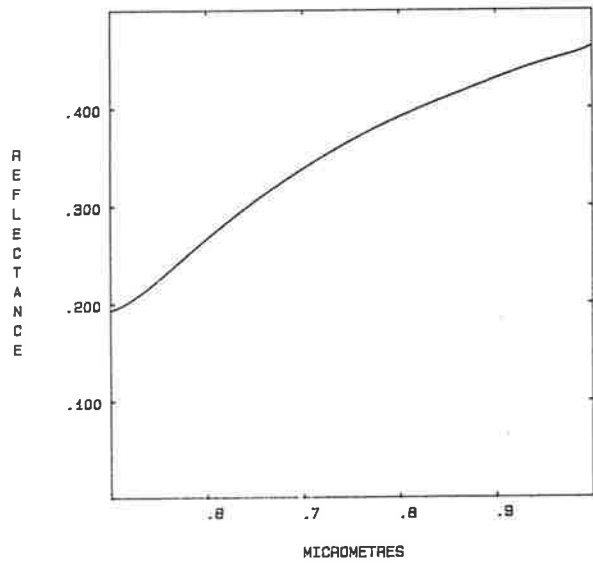
WEIPA N10 E18 FE2O3 4.88%



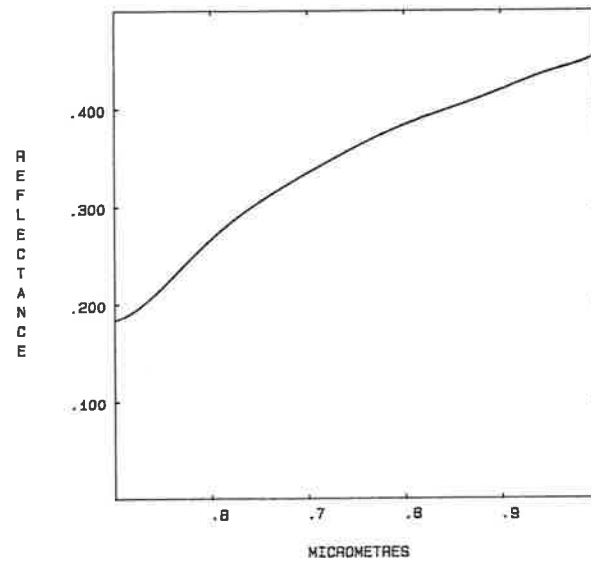
WEIPA N32 E21 FE2O3 7.05%



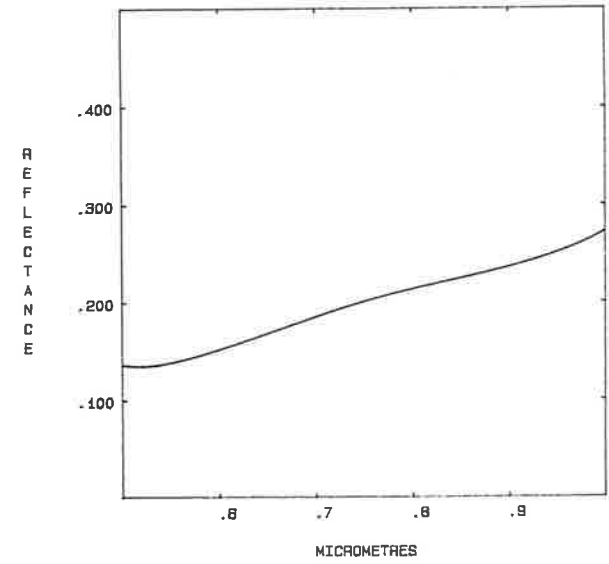
WEIPA N10 E24 FE2O3 5.65%



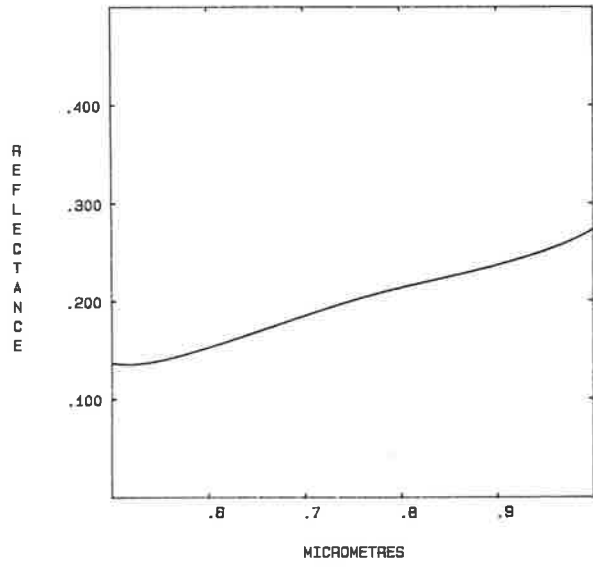
WEIPA N10 E28 FE2O3 4.58%



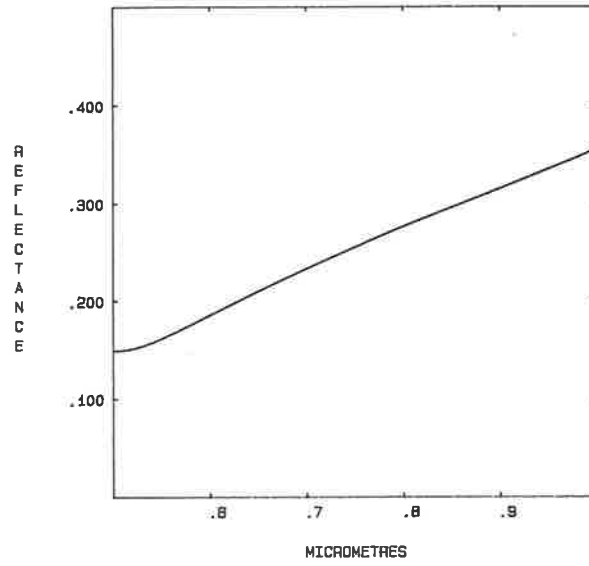
WEIPA N10 E32 FE2O3 8.3%



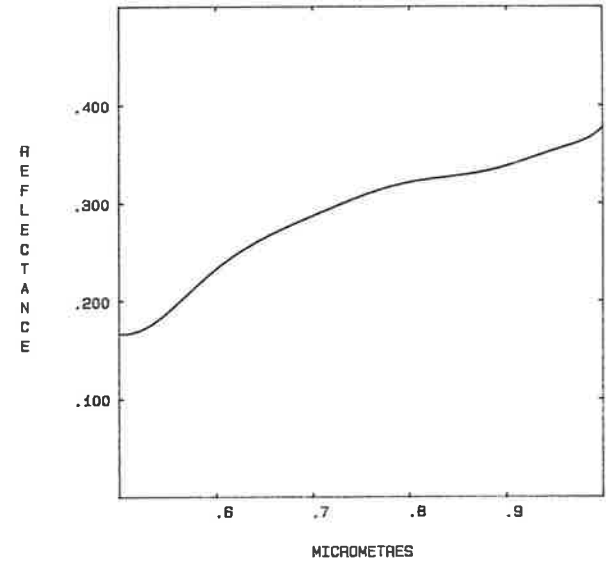
WEIPA N10 E32 FE2O3 8.3%



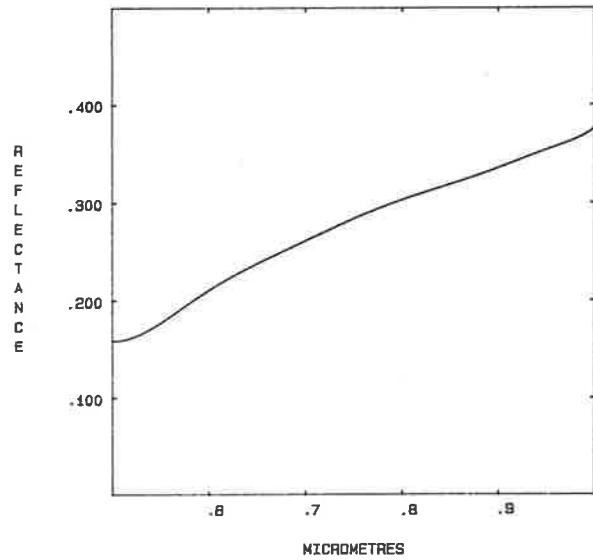
WEIPA N10 E38 FE2O3 3.6%



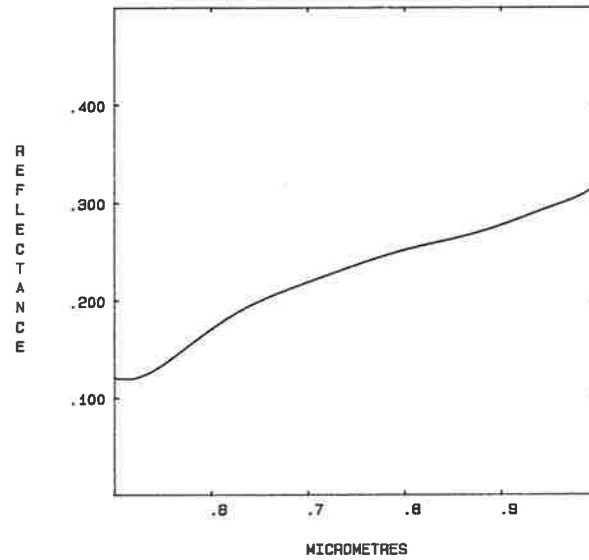
WEIPA N10 E40 FE2O3 8.85%



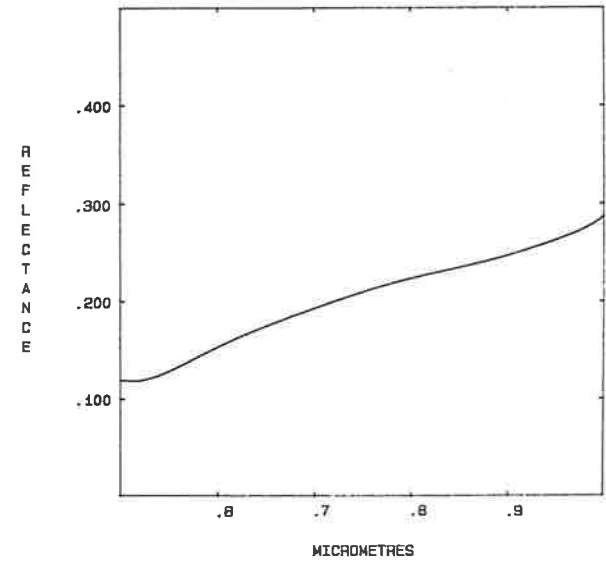
WEIPA N10 E48 FE2O3 4.0%



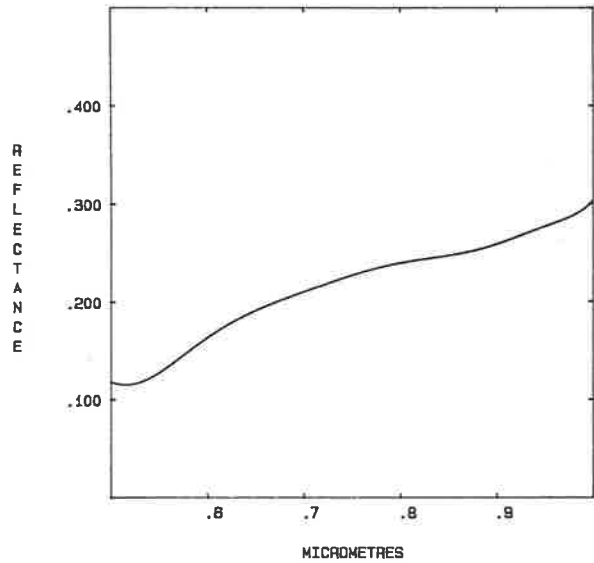
WEIPA N10 E50 FE2O3 4.4%



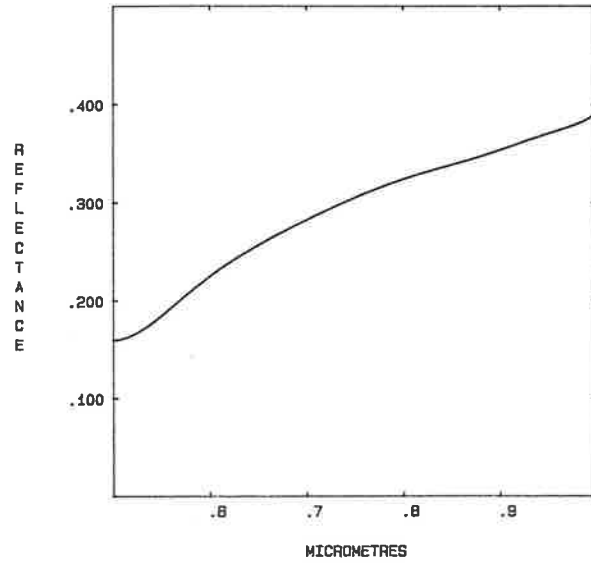
WEIPA N20 E50 FE2O3 2.72%



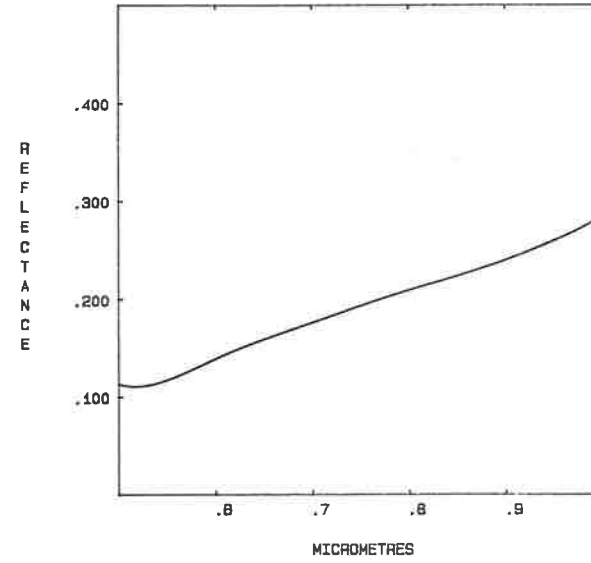
WEIPA N32 E21 FE203 7.05%



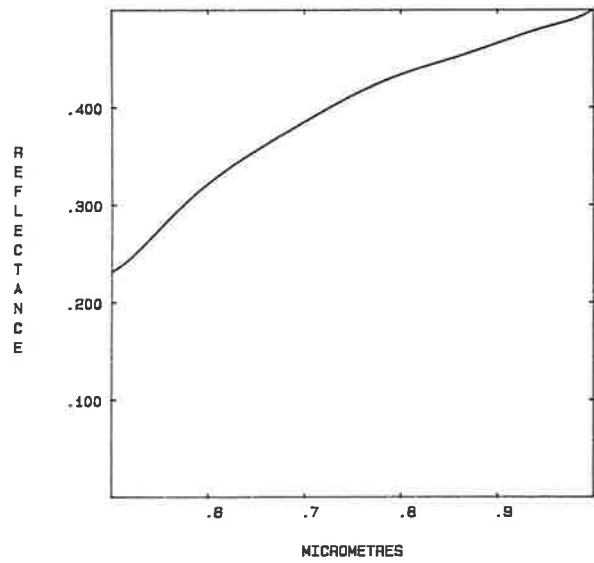
WEIPA N20 E64 FE203 2.85%



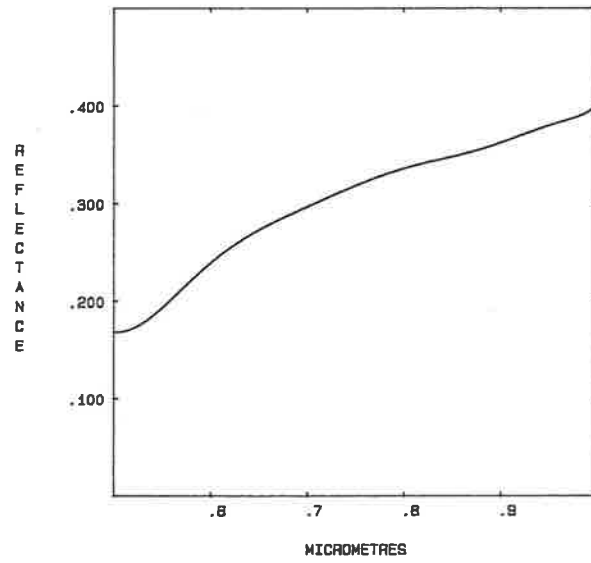
WEIPA N20 E68



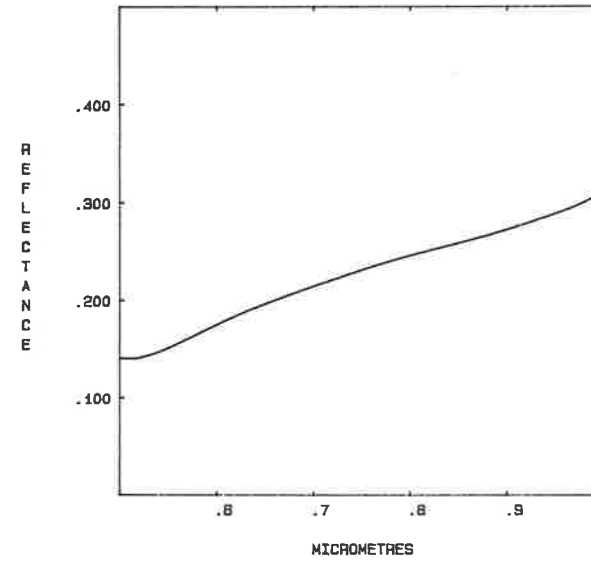
WEIPA N18 E64 FE203 2.34%



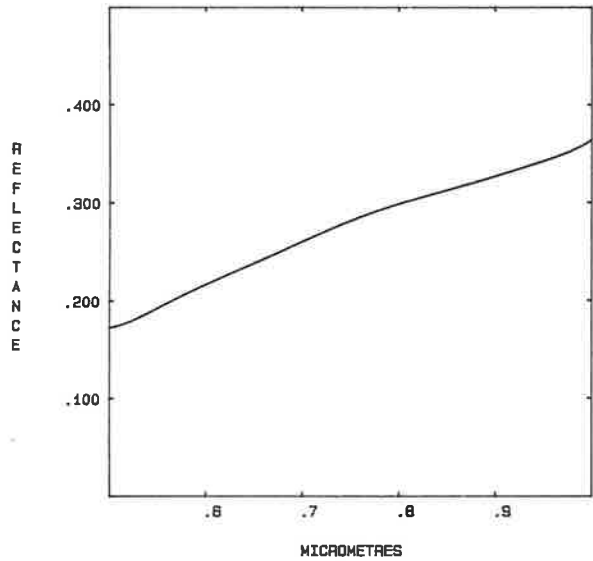
WEIPA N20 E64 FE203 4.88%



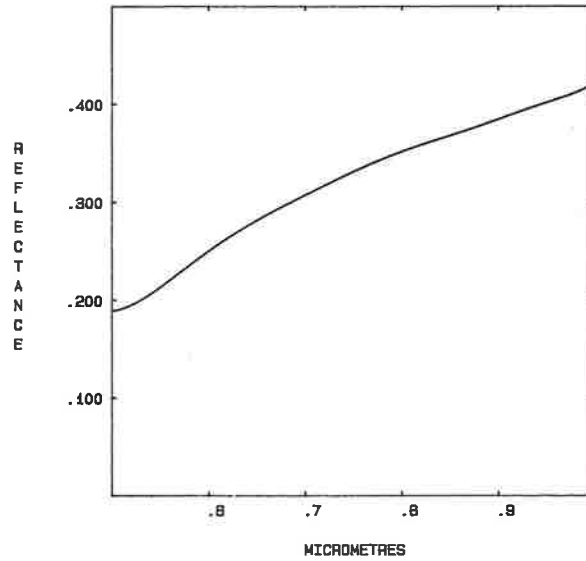
WEIPA N20 E68 FE203 3.96%



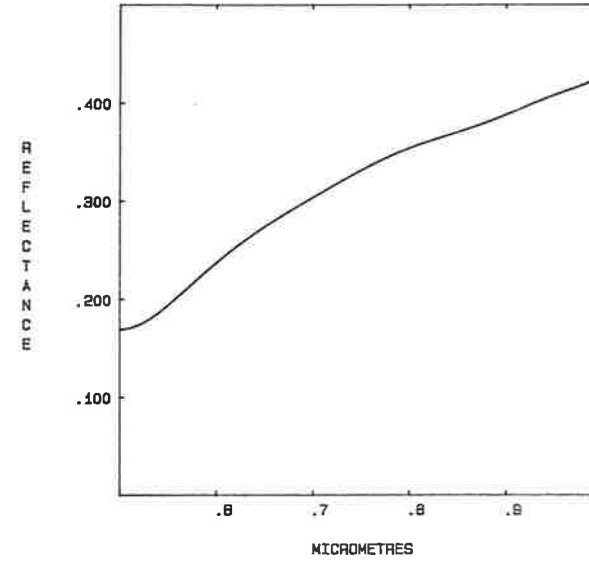
WEIPA N20 E70 FE203 8.35%



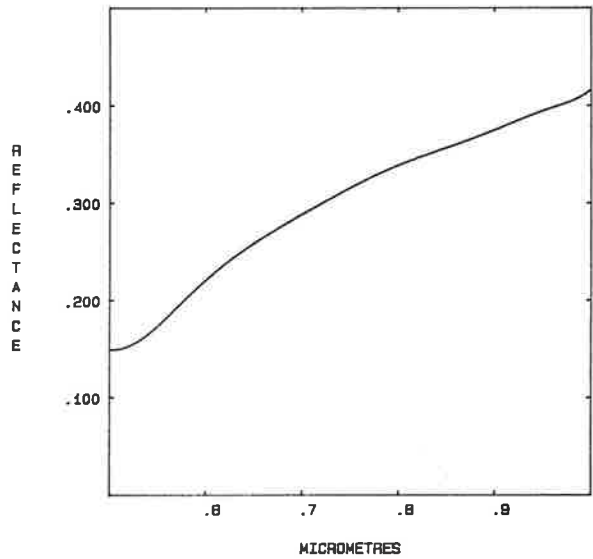
WEIPA N20 E74 FE203 4.94%



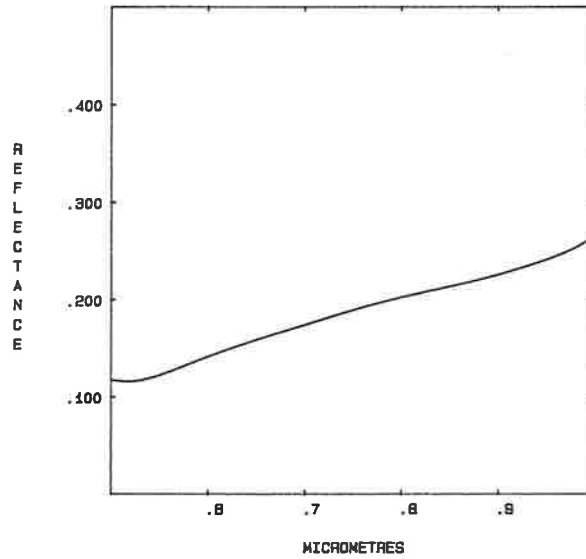
WEIPA N20 E78 FE203 3.88%



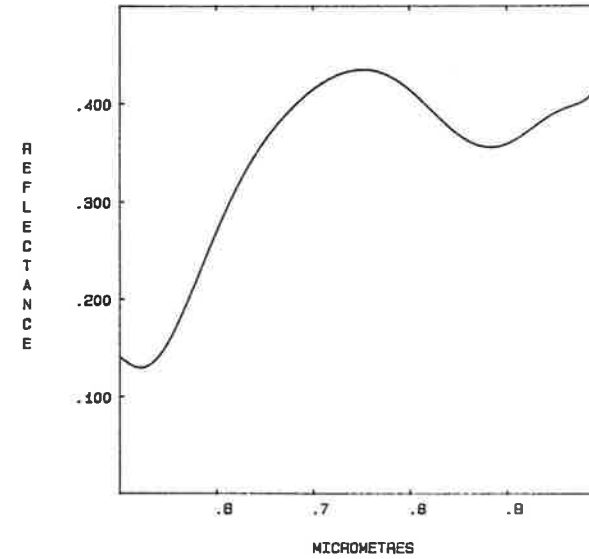
WEIPA N20 E82 FE203 1.33%



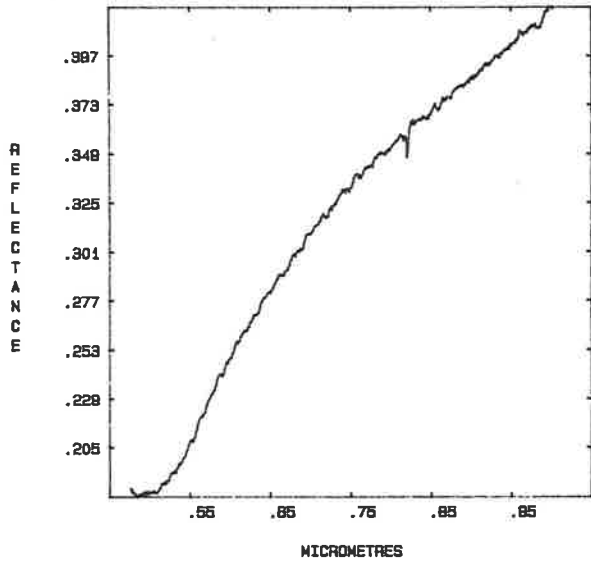
WEIPA N35 E80 FE203 4.88%



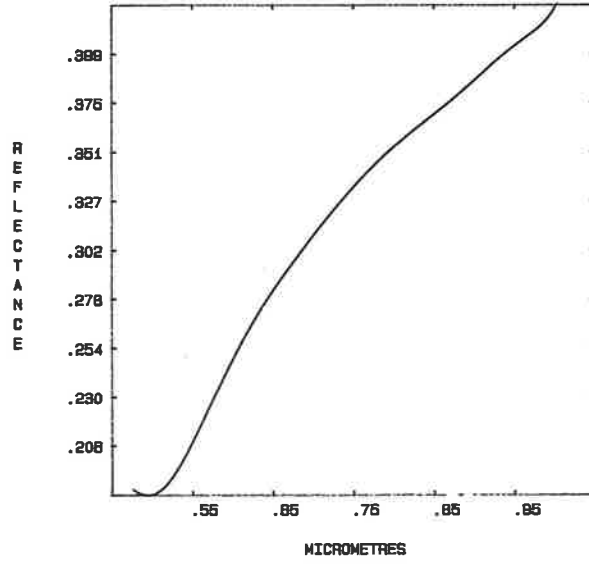
WEIPA - ANDOM CEMENTED PISOLITES



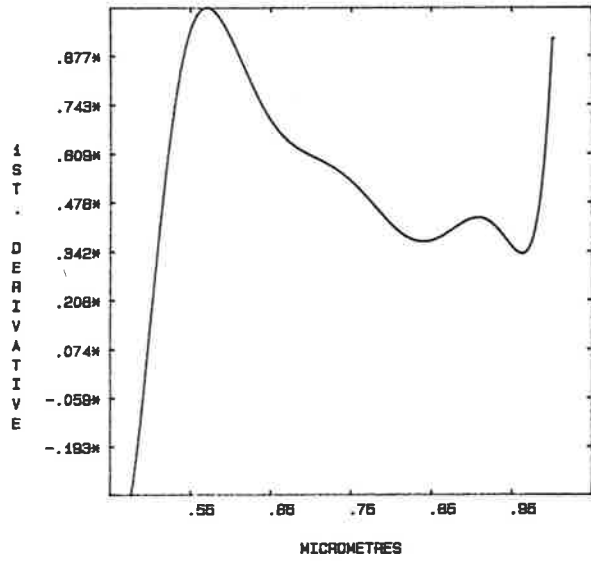
WEIPA N10 E12 FE203 8.5%



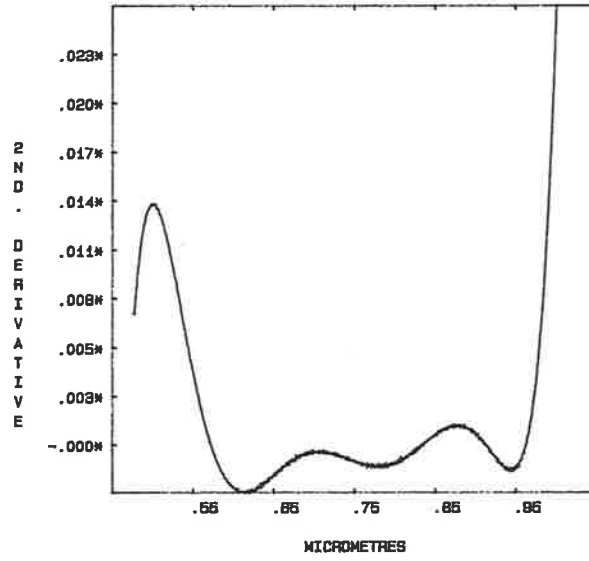
WEIPA N10 E12 FE203 8.5%



WEIPA N10 E12 FE203 8.5%



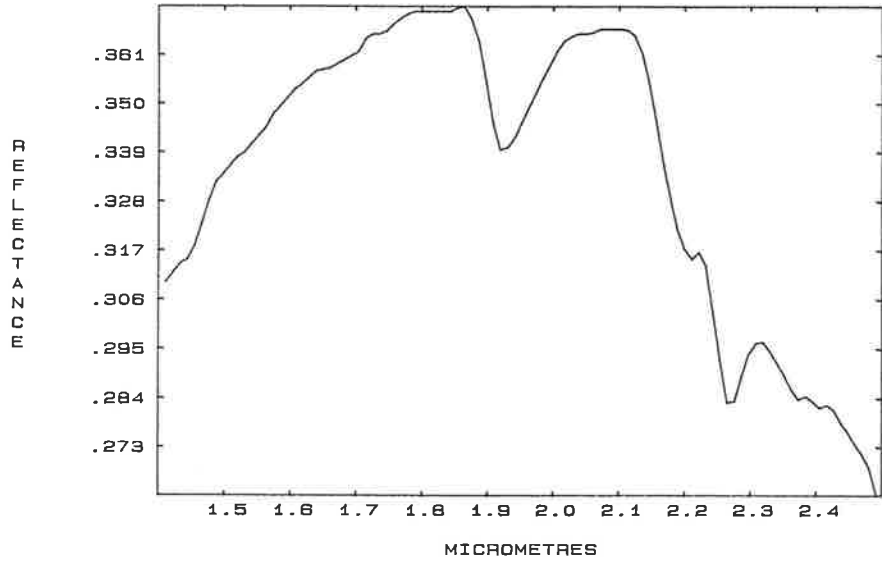
WEIPA N10 E12 FE203 8.5%



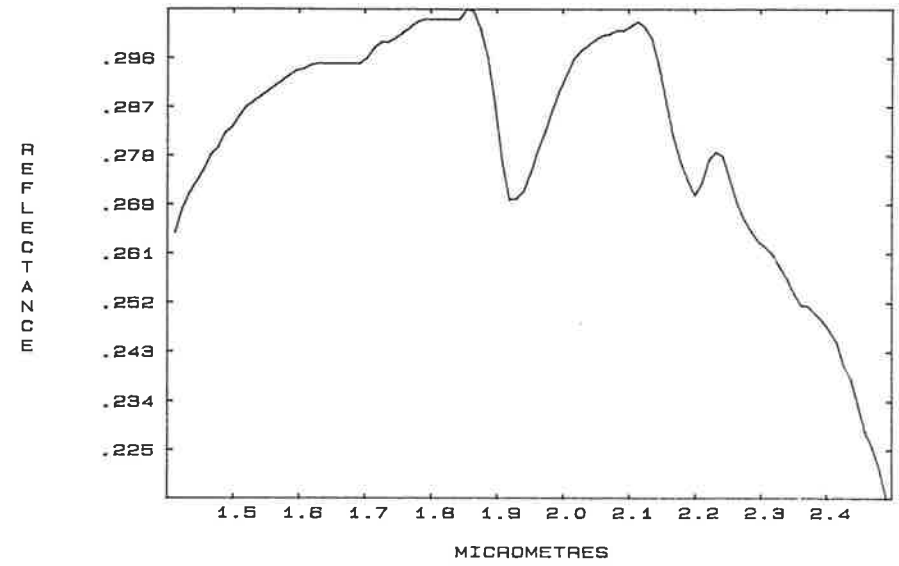
APPENDIX III SWIR laboratory reflectance spectra of soil samples from Weipa.

Like the VNIR data, the SWIR spectra are presented, with a few exceptions, in an order matching the relevant sample's position on the Weipa grid, progressing from west to east. The grid position is shown at the top of each plot. Most of the spectra exhibit absorption features of varying strength at 2.2 and 2.27 μ m that have been attributed respectively to kaolin and bauxite minerals (gibbsite and boehmite ?). There is no systematic variation in the strength of these absorption features along Weipa Peninsula.

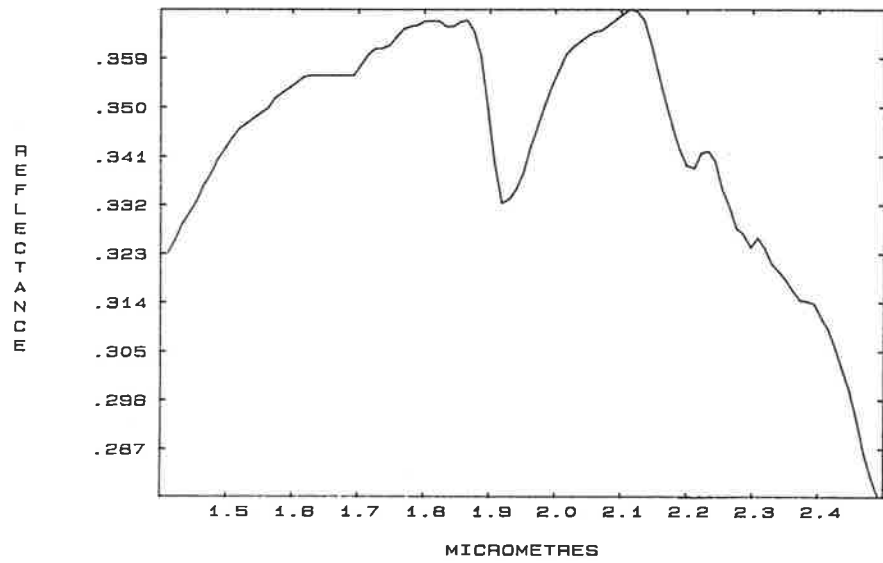
31/7/84 WEIPA N10 E12



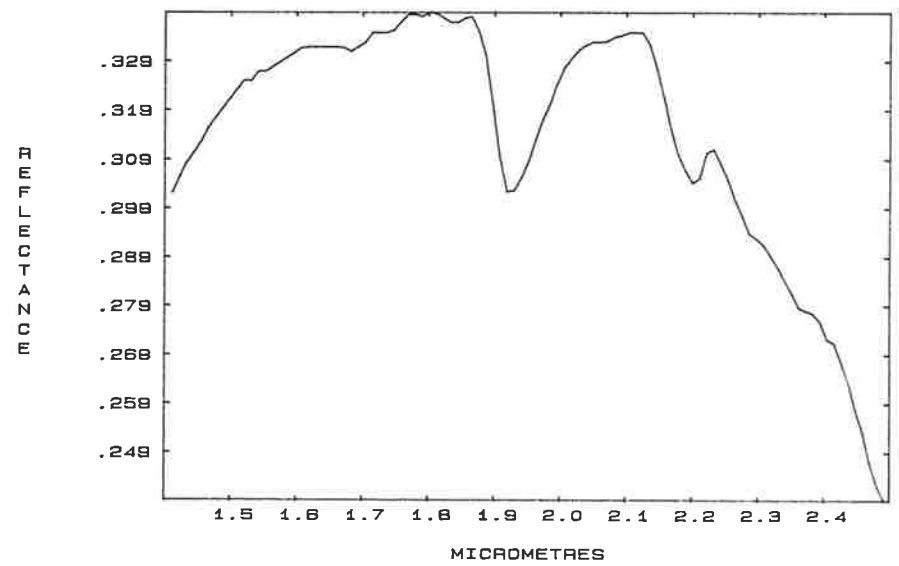
31/7/84 WEIPA N10 E18



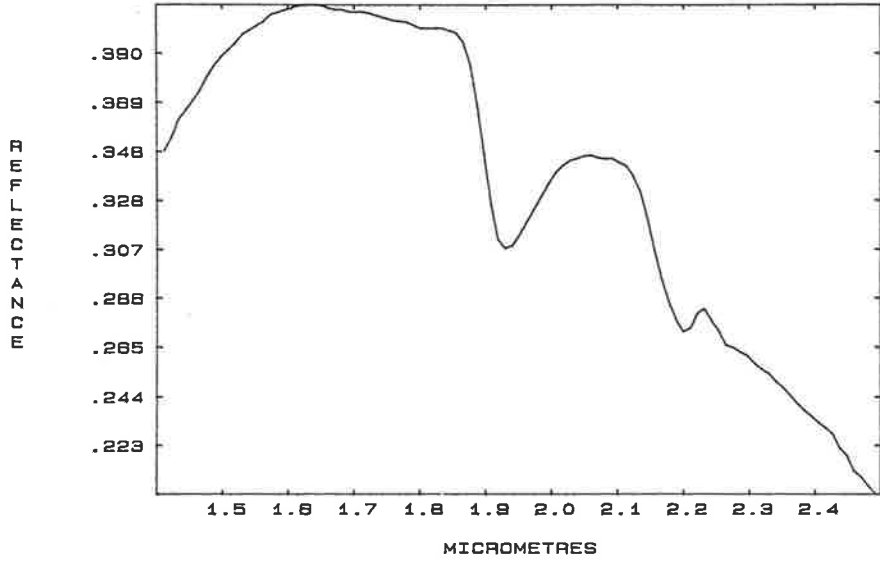
31/7/84 WEIPA N10 E24



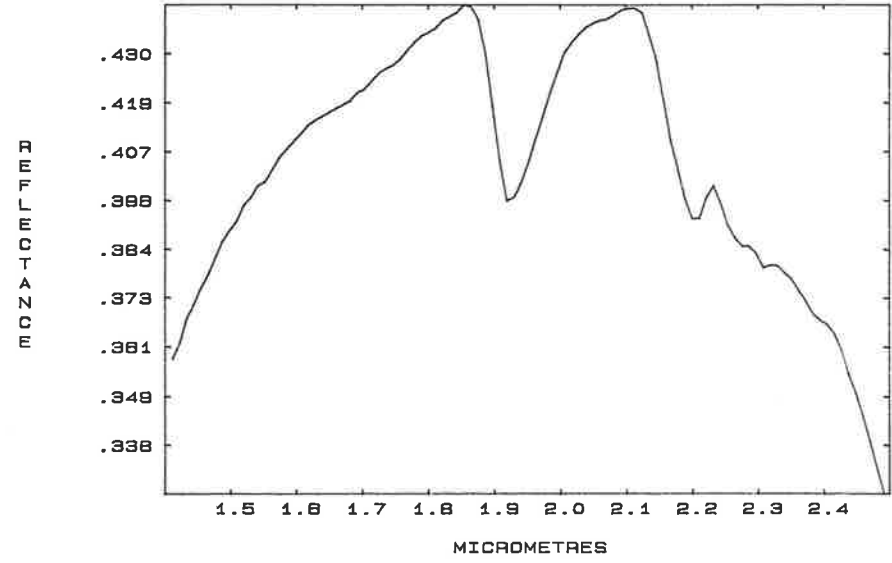
31/7/84 WEIPA N10 E28



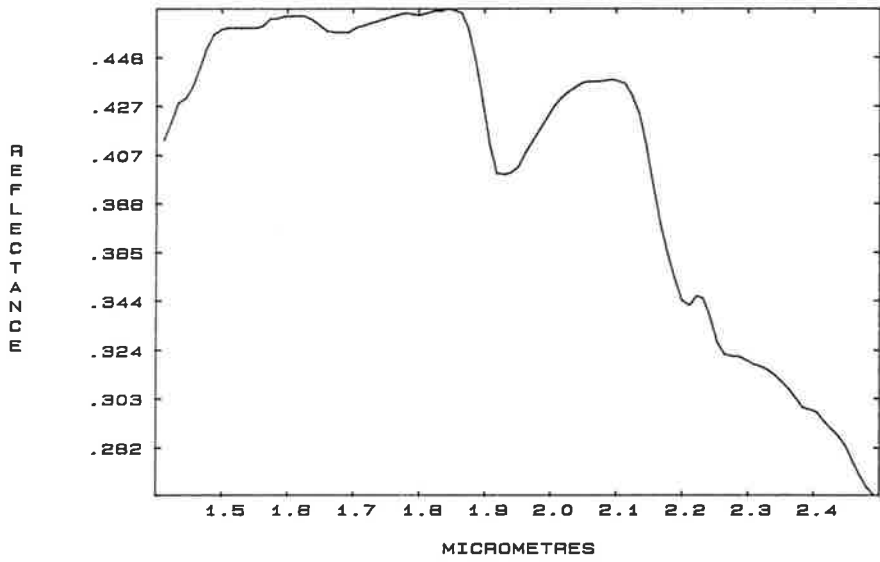
31/7/84 WEIPA N10 E32



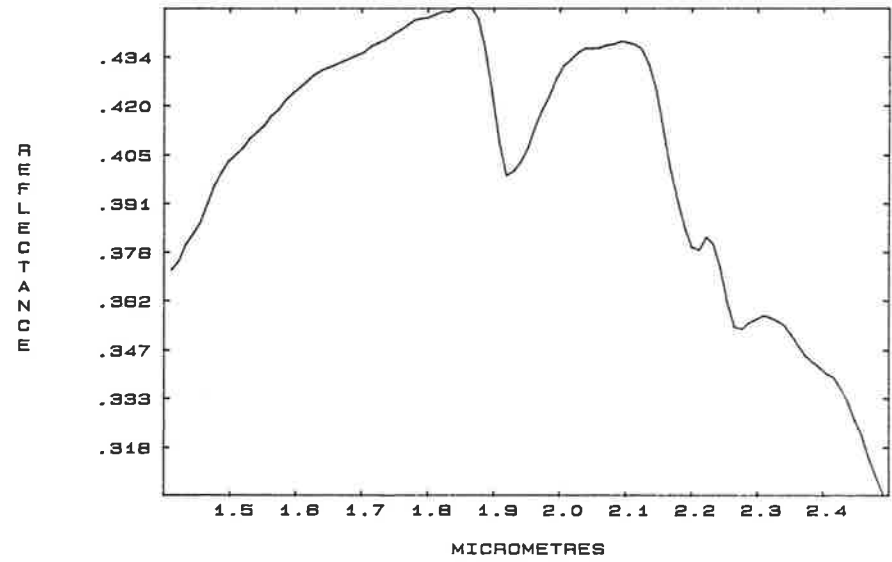
31/7/84 WEIPA N10 E36



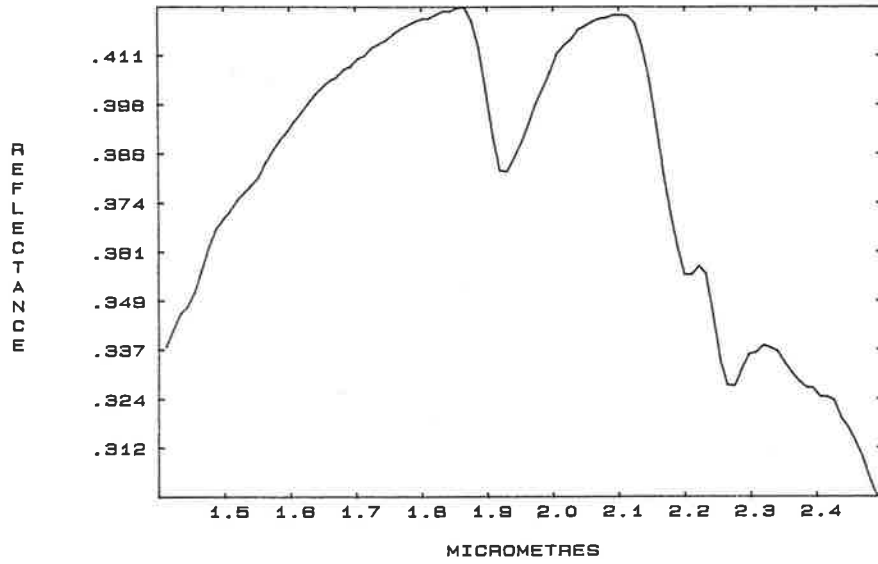
31/7/84 WEIPA N10 E40



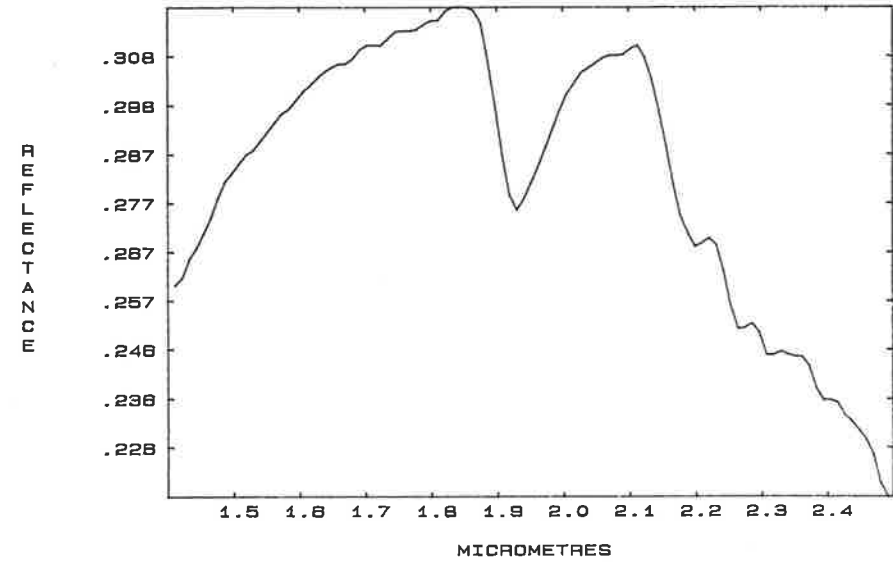
31/7/84 WEIPA N10 E48



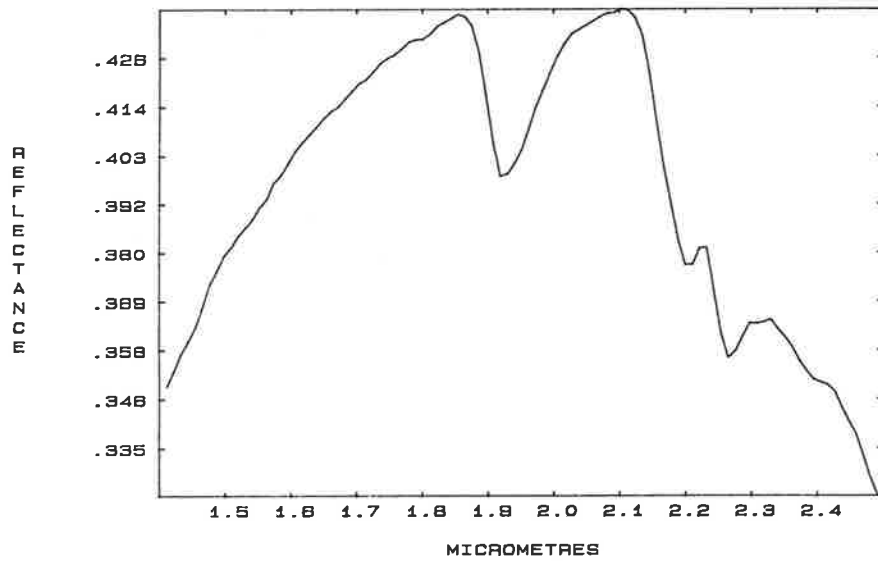
31/7/84 WEIPA N10 E50



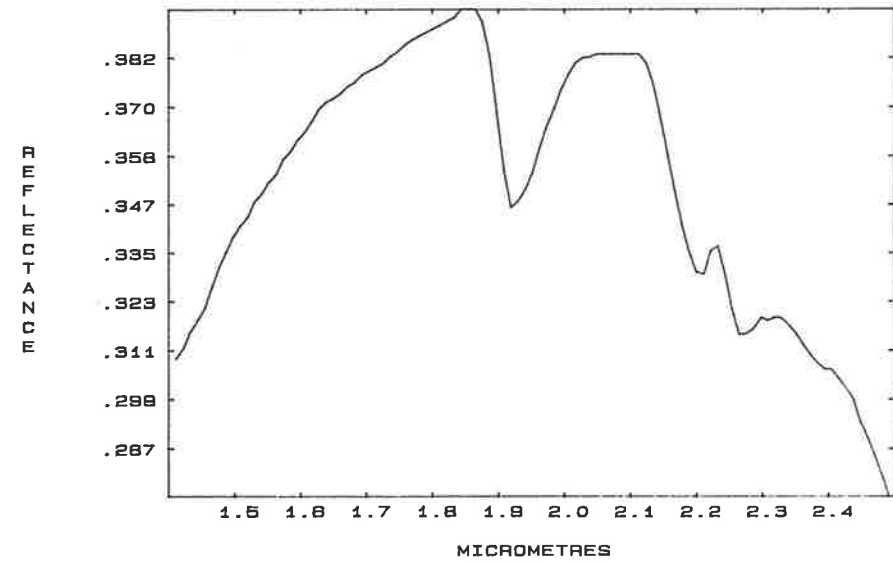
31/7/84 WEIPA N20 E50

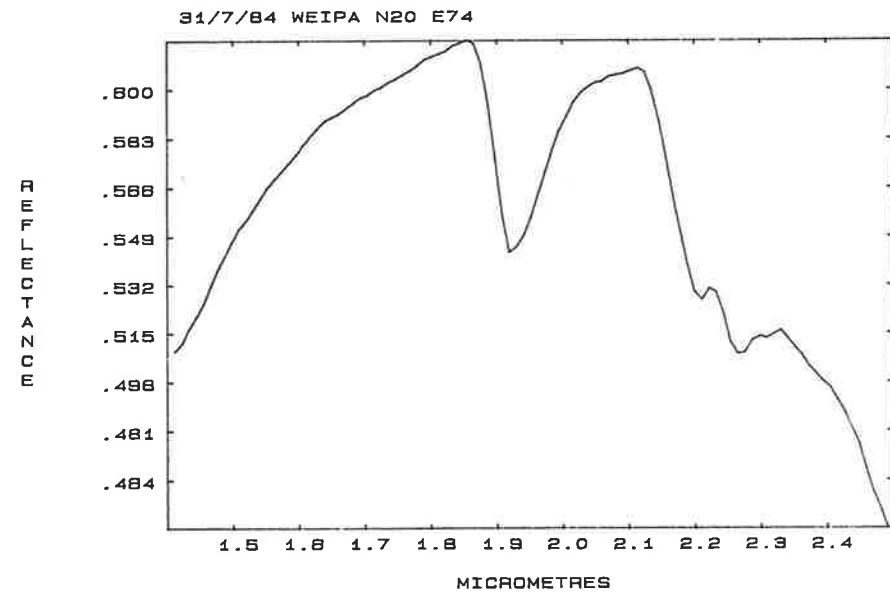
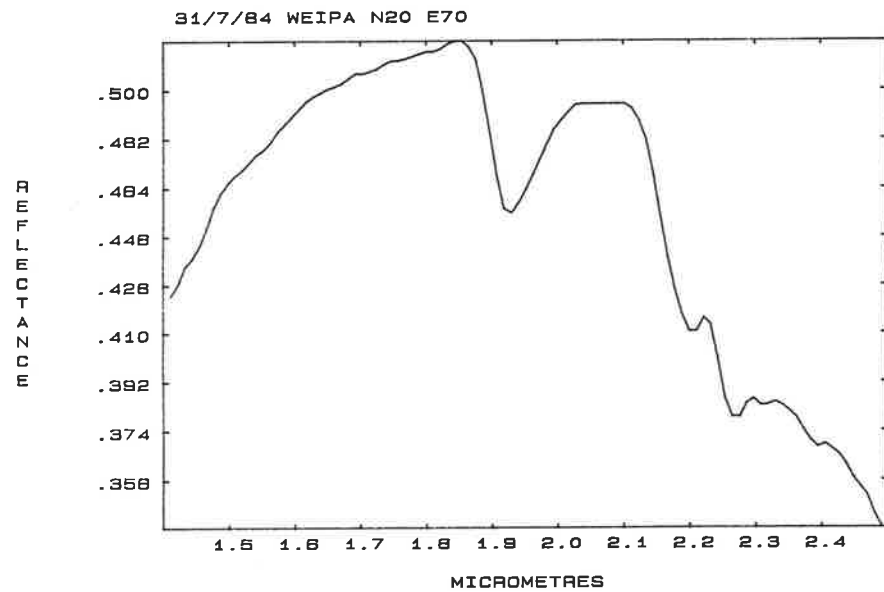
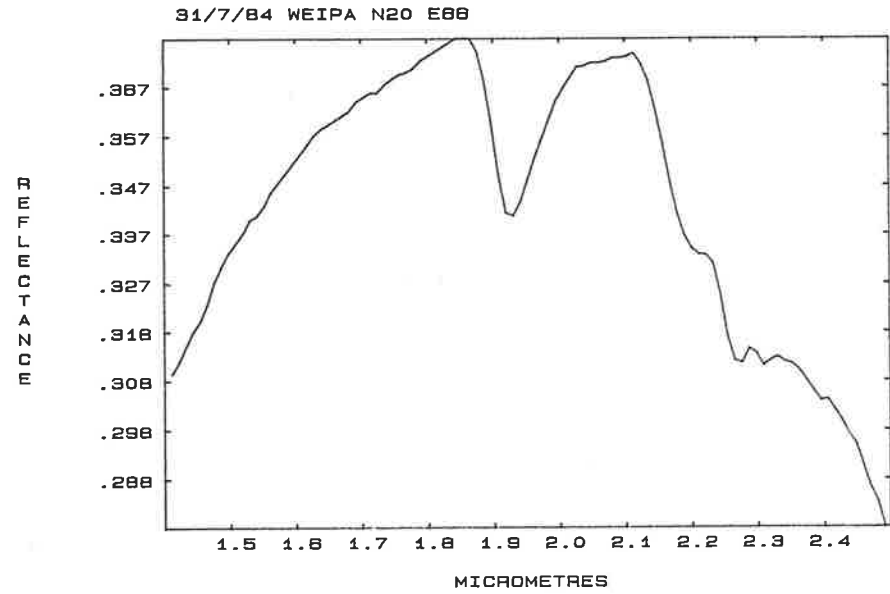
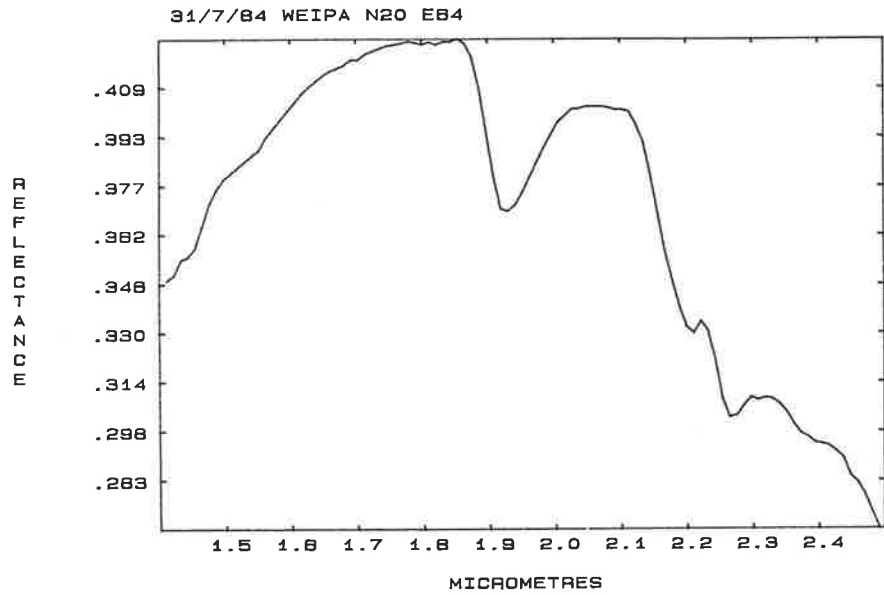


31/7/84 WEIPA N20 E54

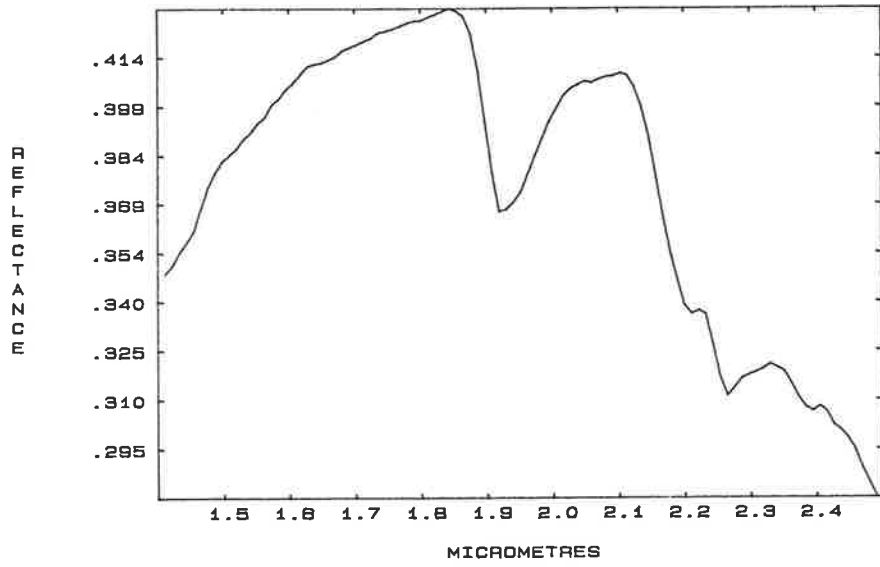


31/7/84 WEIPA N20 E58

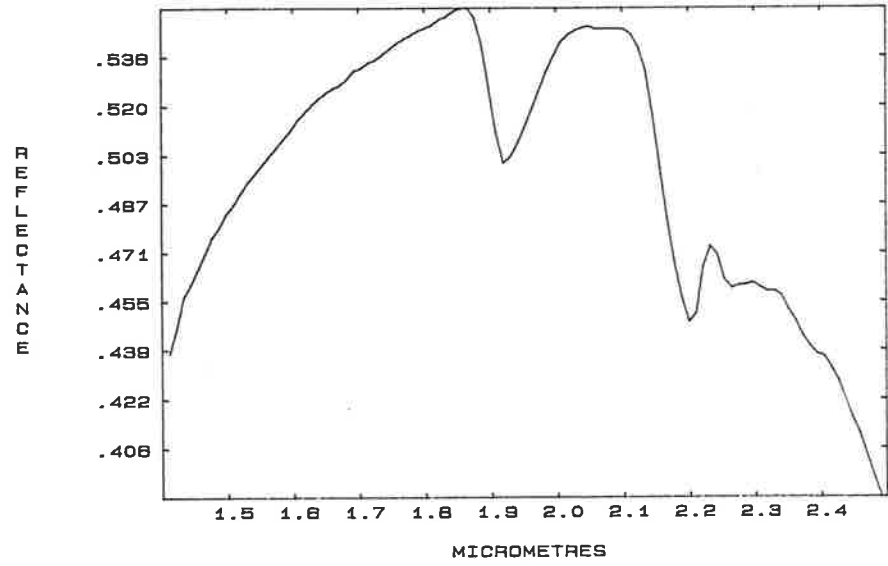




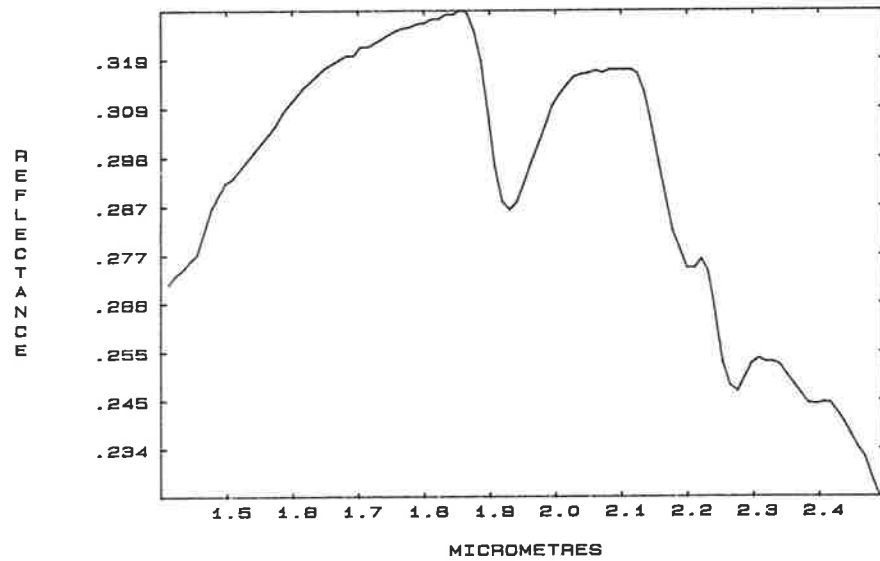
31/7/84 WEIPA N20 E78



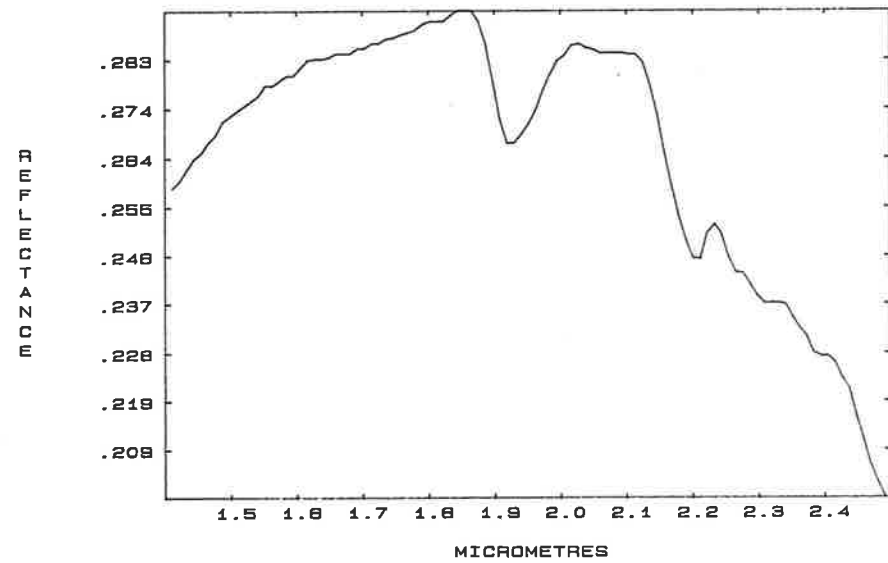
31/7/84 WEIPA N20 E82



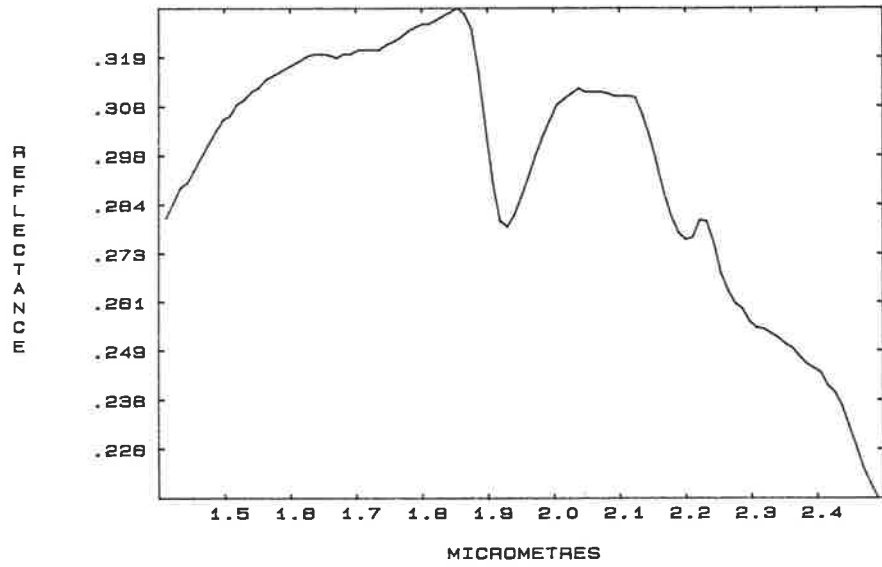
31/7/84 WEIPA N35 E80



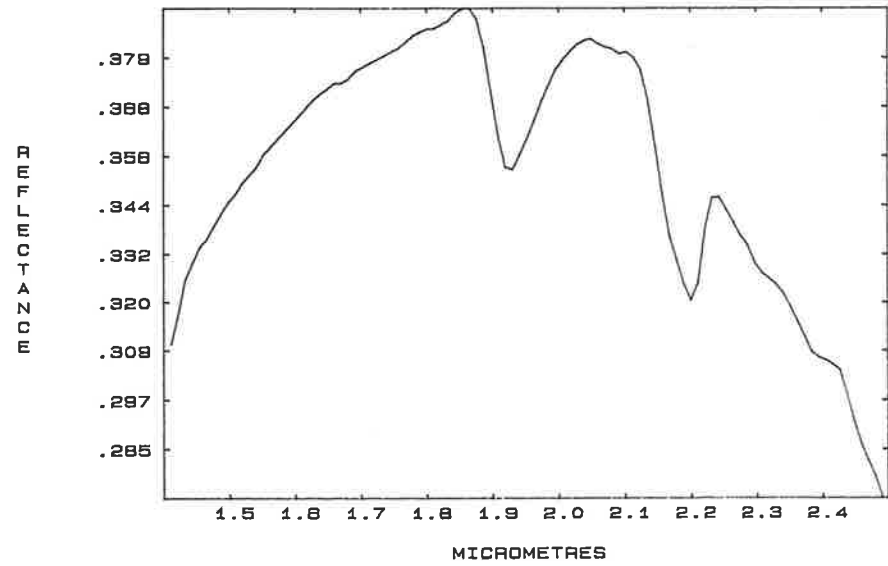
31/7/84 WEIPA N35 W25 PISOLITES ONLY



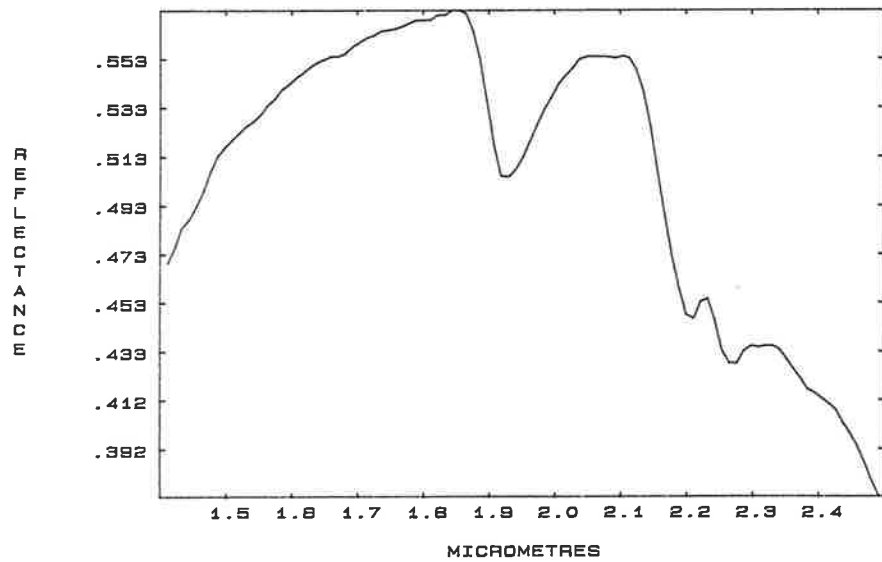
31/7/84 WEIPA N92 E21



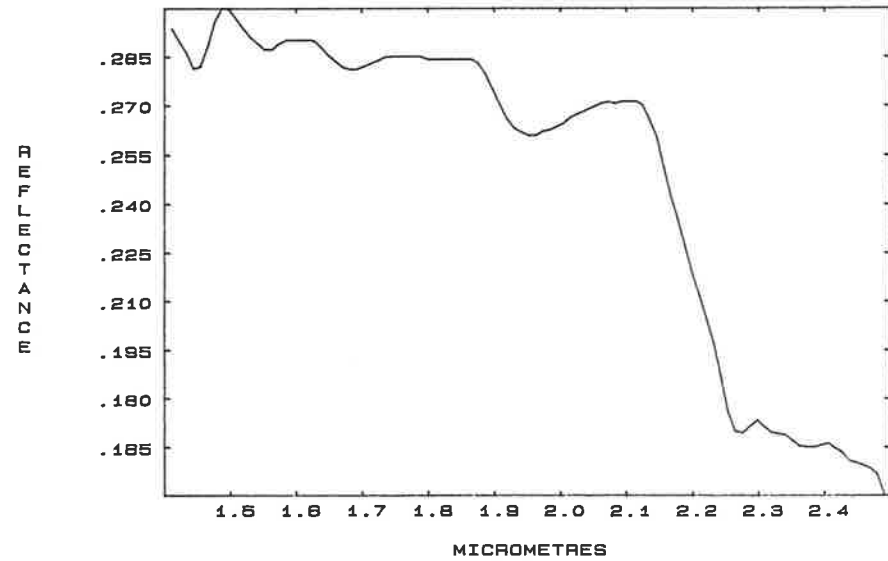
31/7/84 WEIPA N90 E50



31/7/84 WEIPA N18 E84



31/7/84 ANDOOM N21 W13 CEMENTED PISOLITE



APPENDIX IV SWIR laboratory reflectance spectra of samples with XRD
analyses from Mt Turner.

Appendix IV contains laboratory reflectance spectra of Mt Turner samples that have been analysed by XRD. The composition of each sample is shown at the top of each spectral plot, with minerals listed in descending order of abundance.

The spectra are presented in classes representative of the different types of sample found at Mt Turner (these classes are subdivisions of the laboratory 'type-spectra' discussed in the text). For instance, the first class comprises weathered-surface spectra of sericitic altered granite and rhyolite samples from the main silicified zone. The last spectrum in each class is the average spectrum of all samples in the class that have undergone spectral measurement.

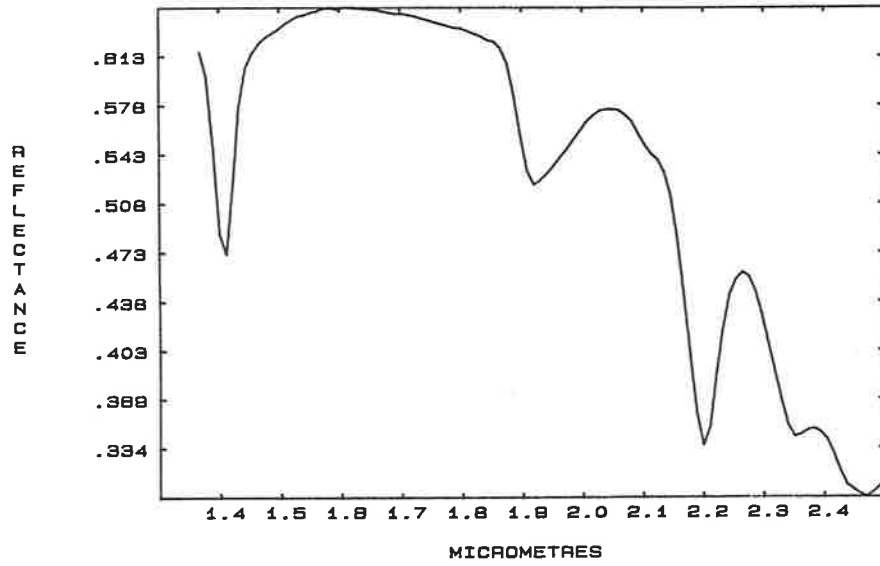
KEY TO XRD MINERAL IDENTIFICATION

QTZ	Quartz	GOETH	Goethite
KSP	K-Feldspar	HEM	Haematite
SM	Smectite	CHL	Chlorite
MUSC	Muscovite/Sericite	FSP	Plagioclase
KAOL	Kaolin	EPI	Epidote
AMP	Amphibole	TR	Trace

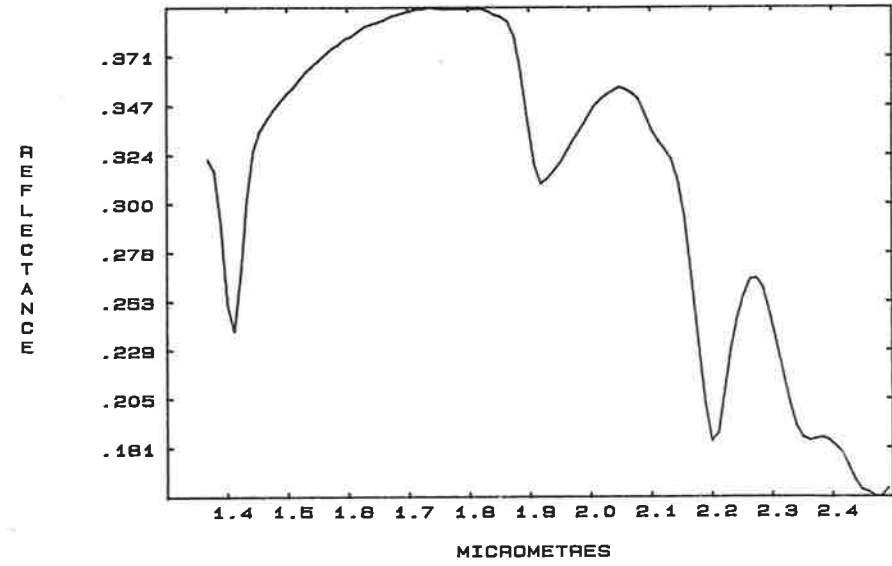
Note that XRD analysis does not discriminate muscovite and sericite.

W SPECTRA - SERICITIC GRANITE AND RHYOLITE FROM MAIN ALTERATION ZONE

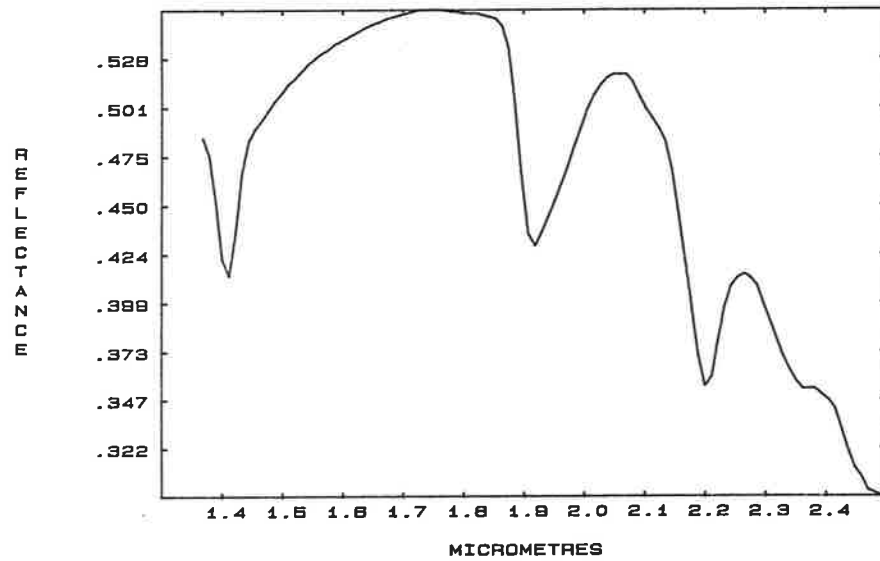
MT10/274/1/W QTZ, KSP, FSP, SM, MUSC, TR.KAOL



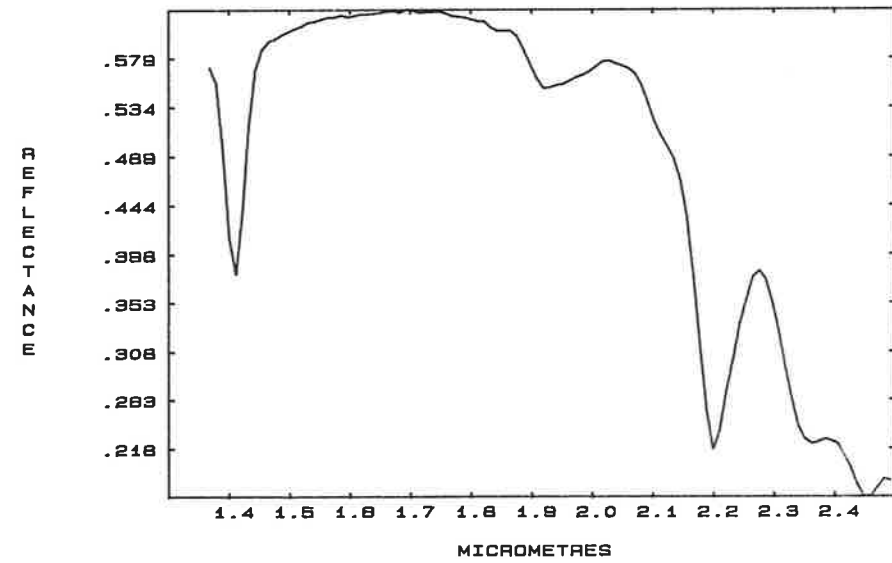
MT3/208/1/W QTZ, MUSC



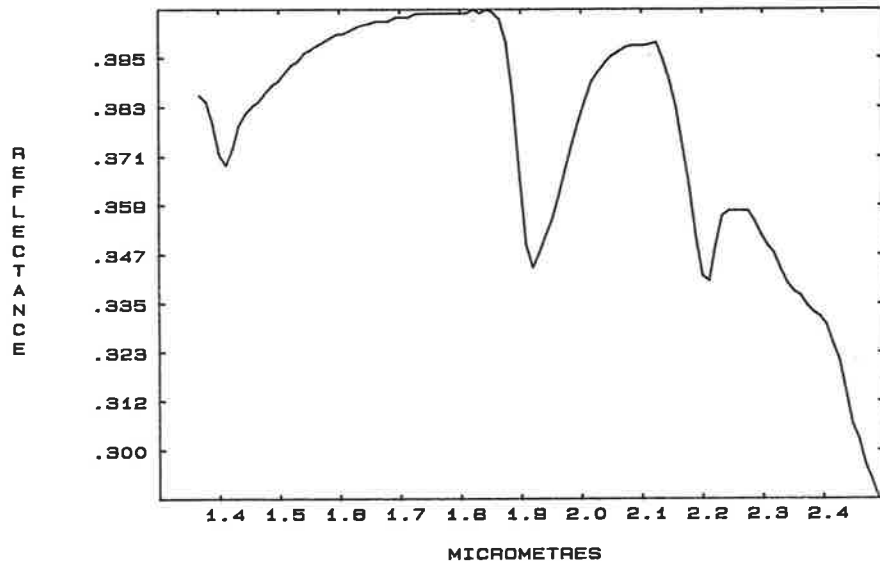
MT10/316/2/W QTZ, MUSC, TR.KAOL



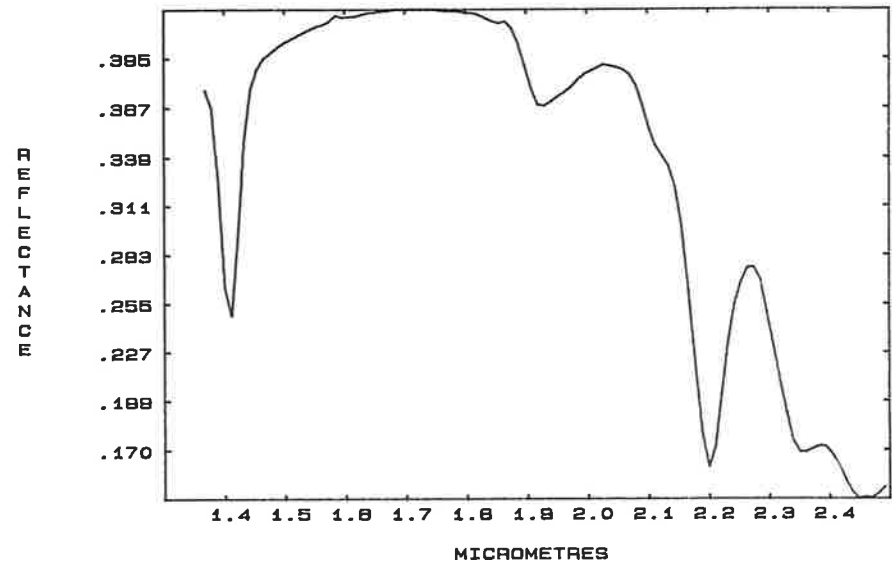
MT1/528/1B/W QTZ, MUSC



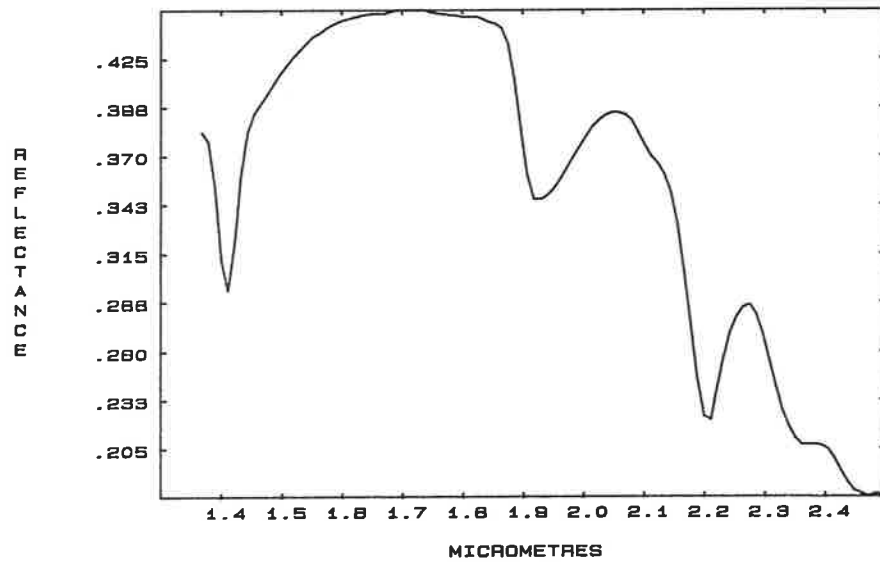
MT1/808/1/W QTZ, MUSC, KSP, KAOL



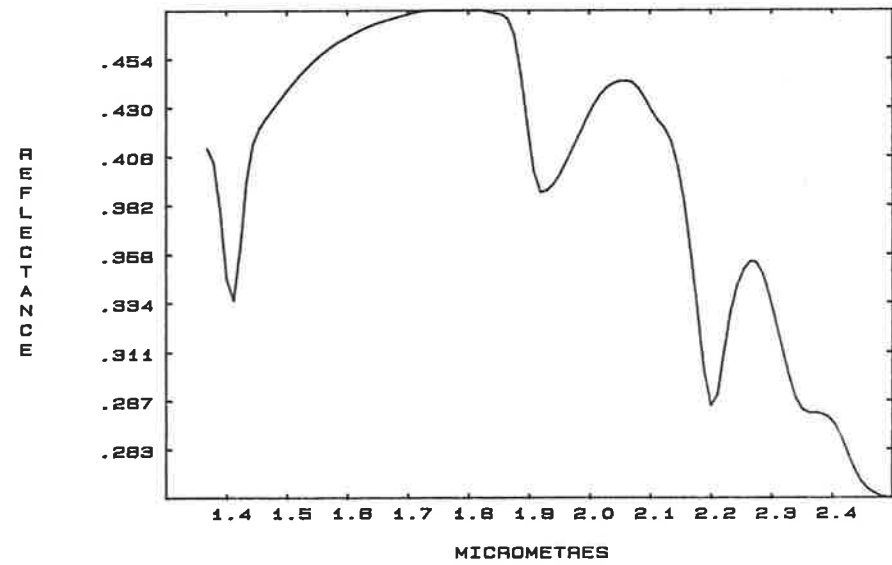
MT1/812/1/W QTZ, MUSC



MT4/174/1/W QTZ, MUSC, TR. KAOL, KSP

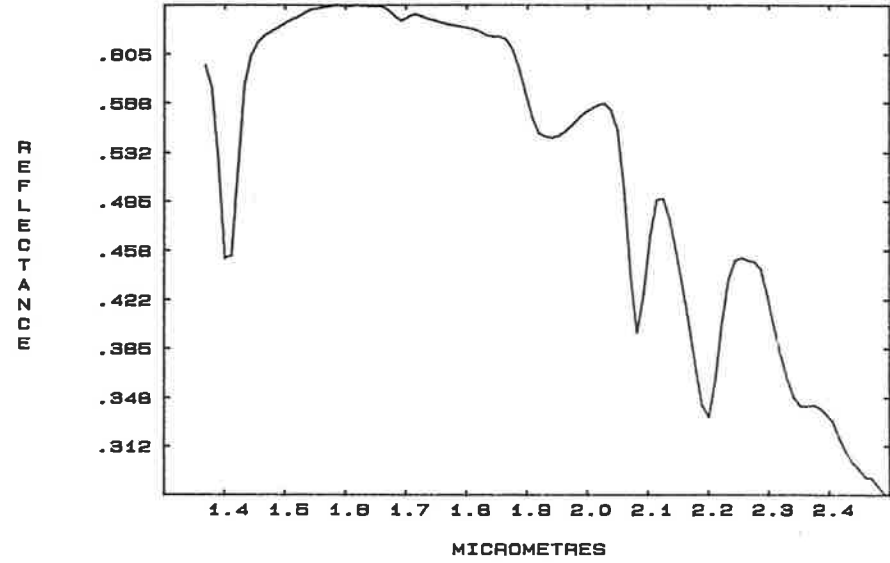


AV ALT GRAN. + RH FROM SILICIFIED ZONE W

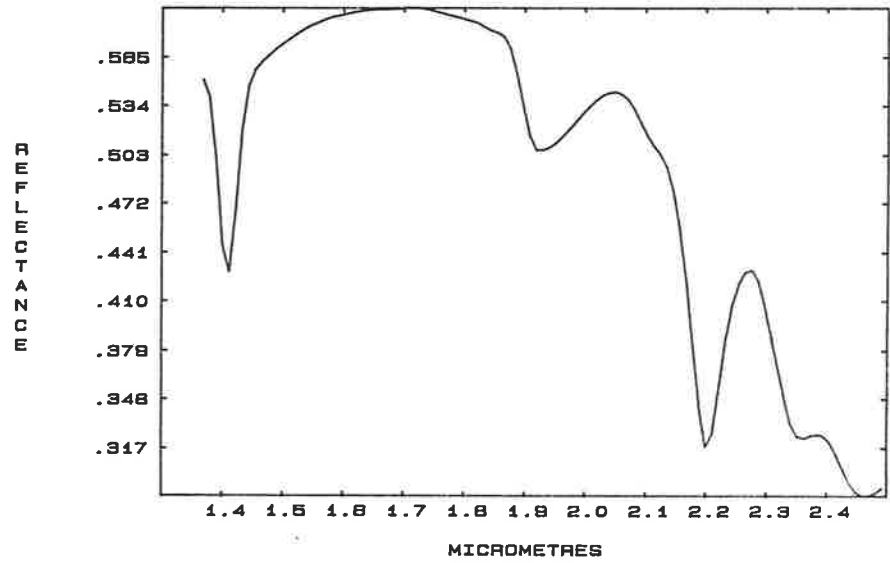


F SPECTRA - SERICITIC GRANITE AND RHYOLITE FROM MAIN ALTERATION ZONE

MT10/348/3/F QTZ, TOPAZ, MUSC, TR. KAOL

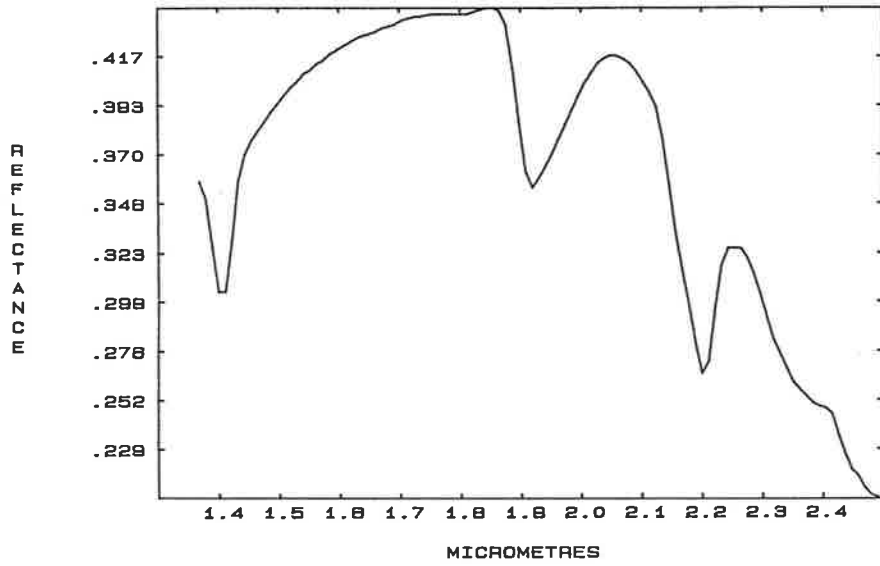


AV ALT GRAN. + RH FROM SILICIFIED ZONE F

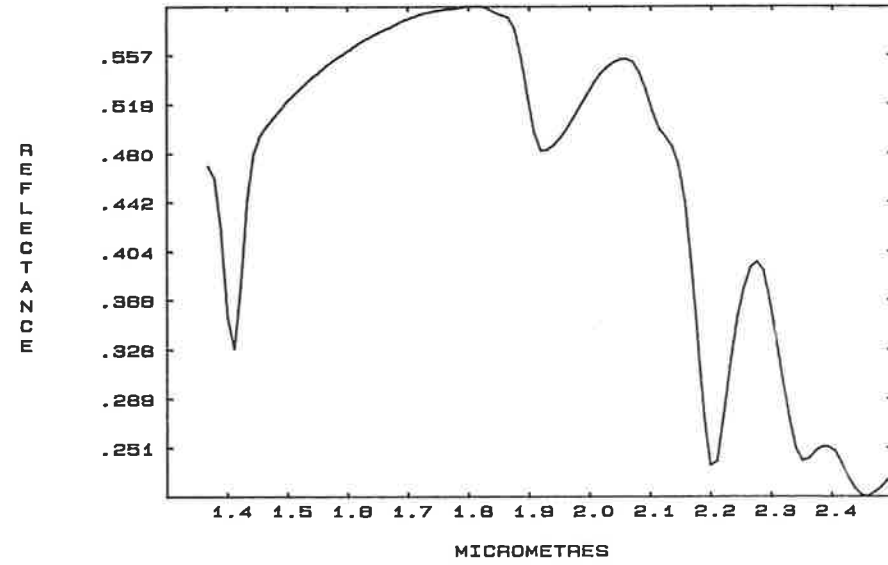


W SPECTRA - SERICITIC ROBERTSON RIVER FORMATION FROM MAIN ALTERATION ZONE

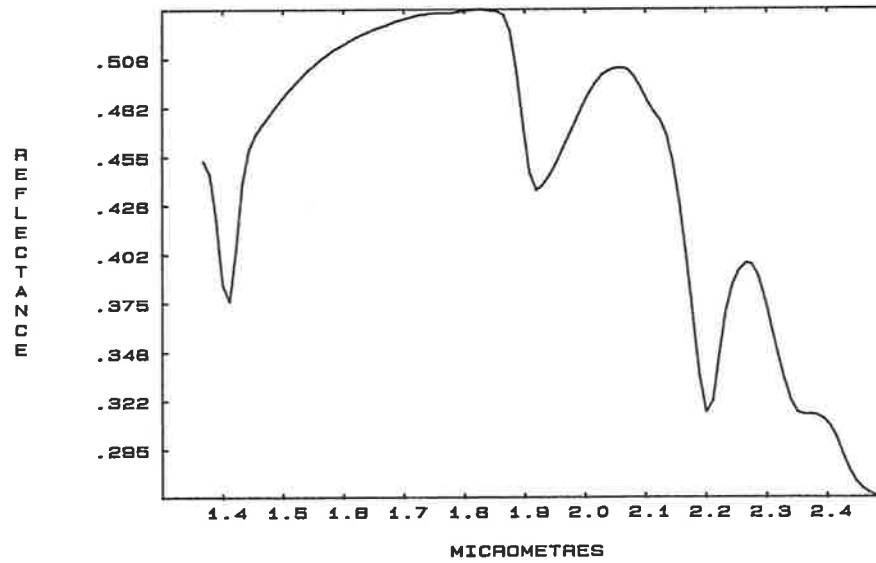
MT10/288/1/W QTZ, GOETH, KAOL, HEM, TR. MUSC



MT1/861/1/W QTZ, MUSC

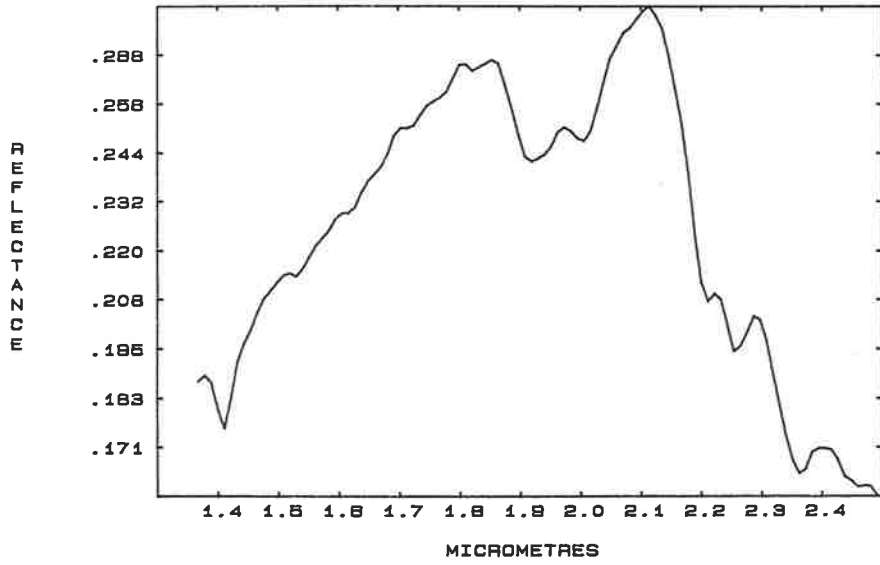


AVERAGE RRF FROM SIL ZONE W

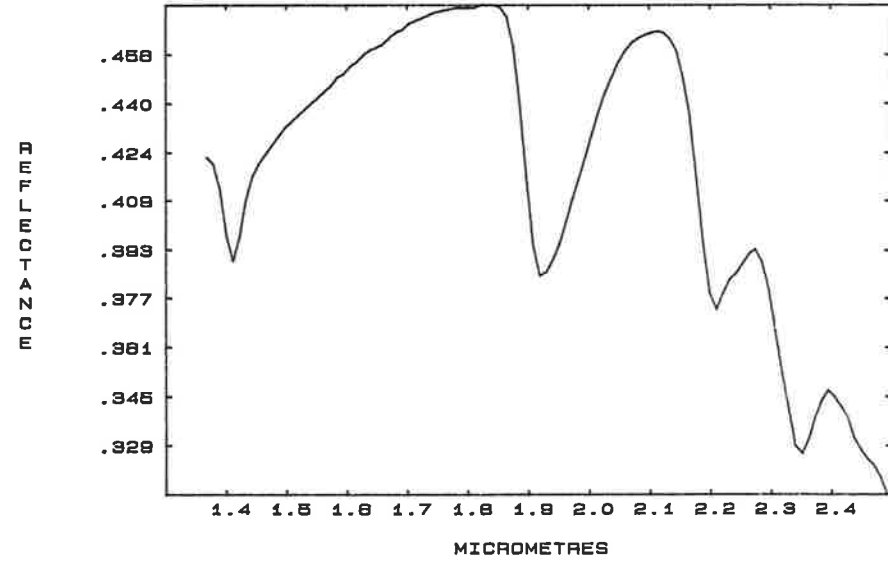


F SPECTRA - SERICITIC SAMPLES FROM OUTSIDE MAIN ALTERATION ZONE

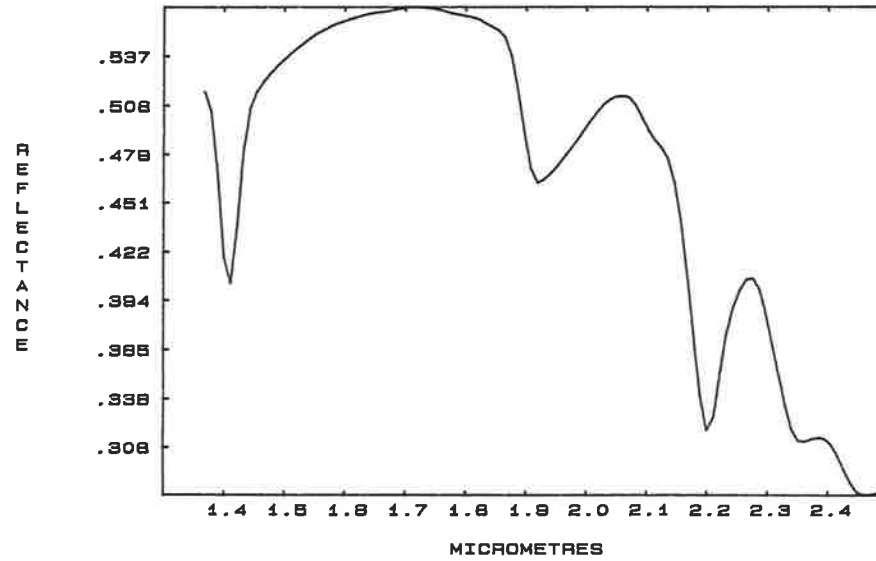
MTB/250/3/F QTZ, CHL, GOETH, TR.MUSC



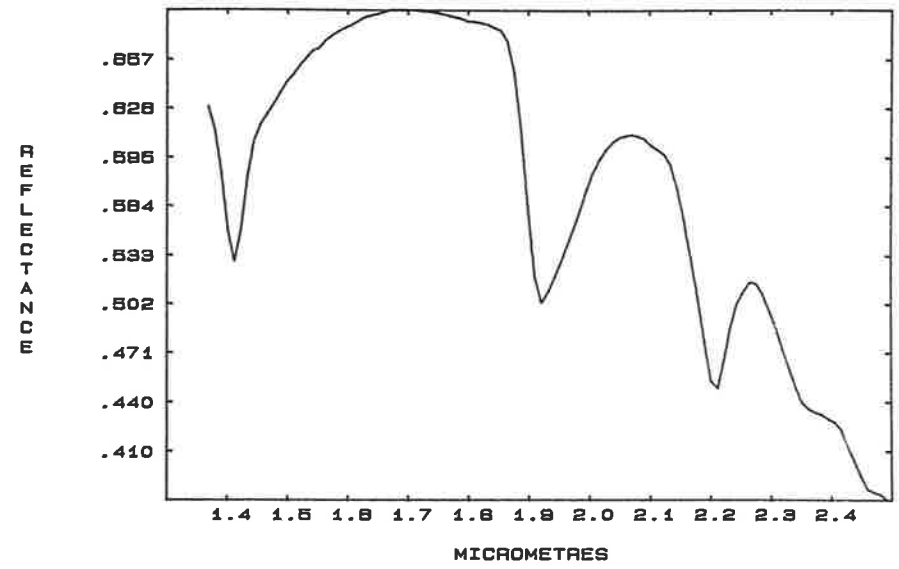
MTB/495/1/F KSP, QTZ, FSP, TR.MUSC, CHL, EPI



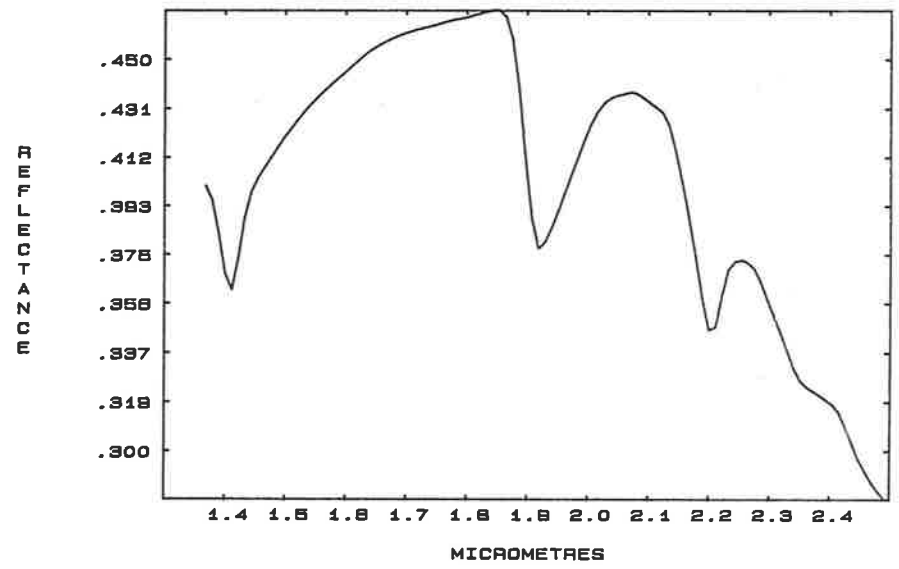
AVE ALT FELSICS OUTSIDE SIL. ZONE F



W SPECTRA - UNALTERED GRANITE
MT10/189/9/W QTZ, FSP, KSP, MUSC, TR.KAOL

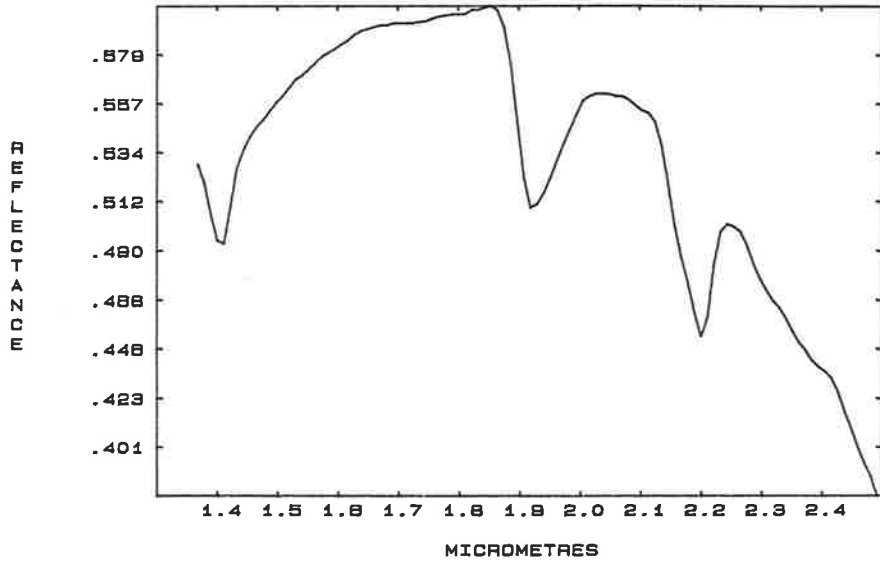


AVERAGE UNALTERED GRANITE W

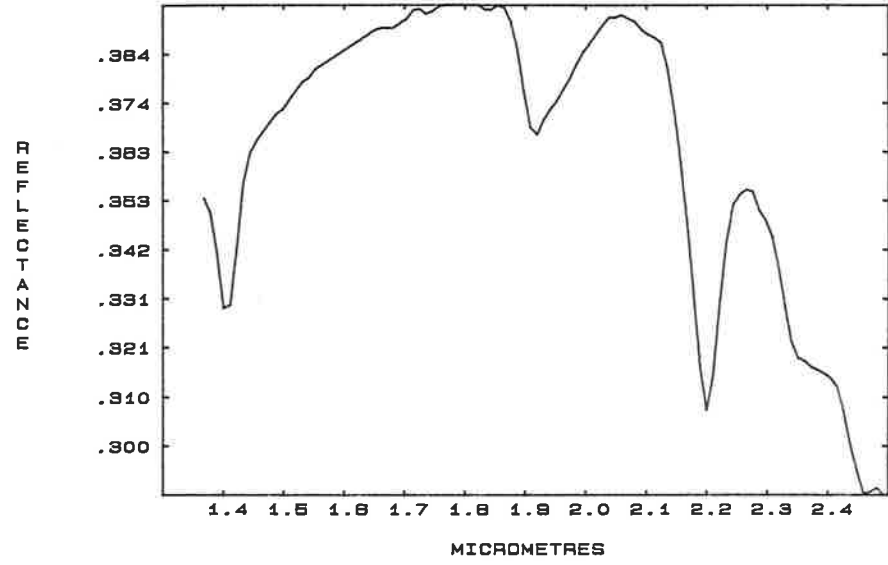


SOIL SPECTRA - UNALTERED, WEATHERED GRANITE

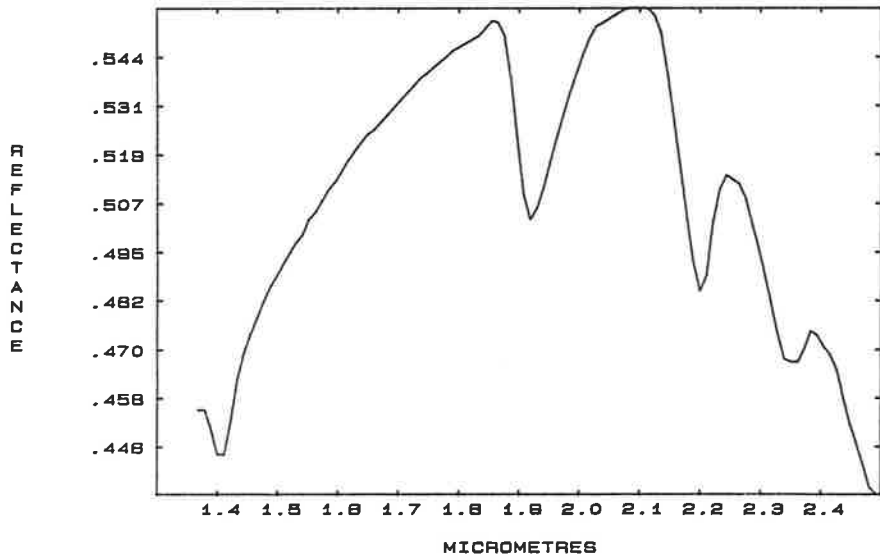
MT1/284/S QTZ, FSP, KSP, MUSC, TR.KAOL



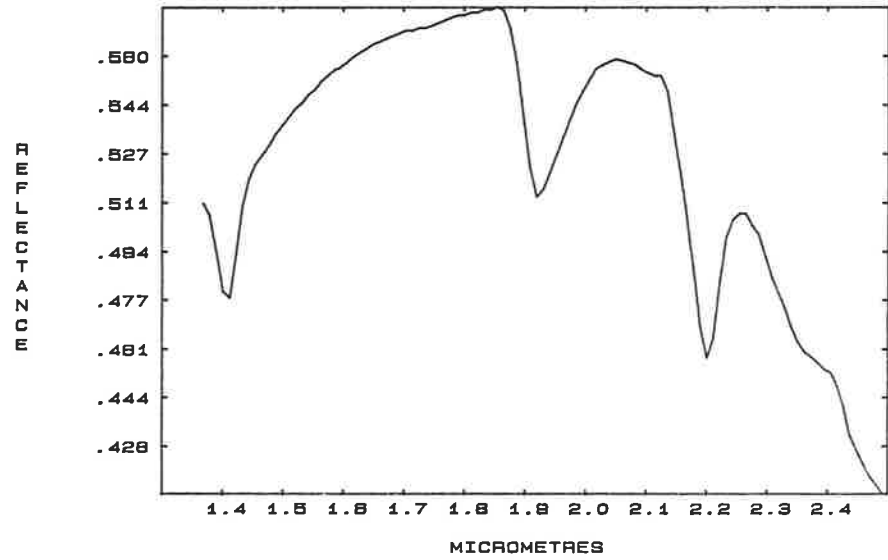
MT7/170/S QTZ, KSP, MUSC, TR.GOETH, KAOL, FSP



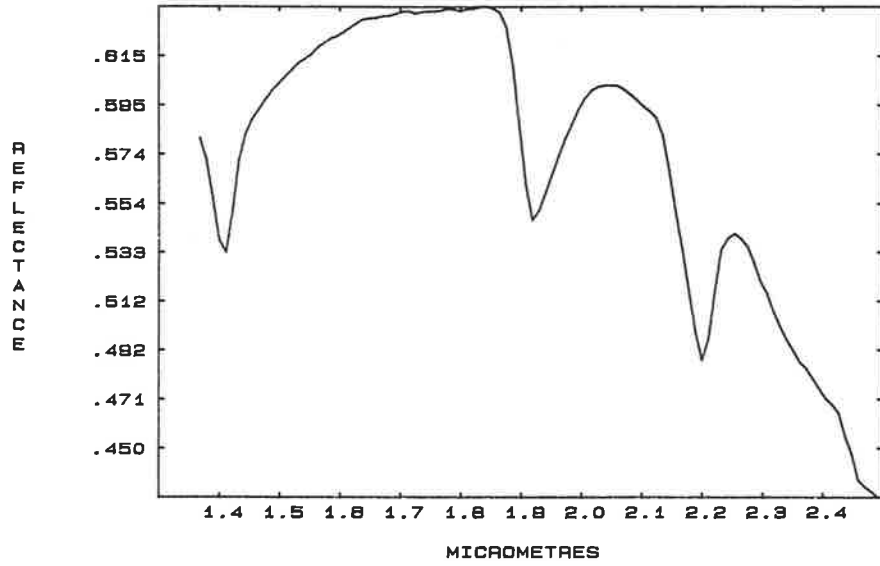
MT7/218/S QTZ, KSP, MUSC, TR.FSP



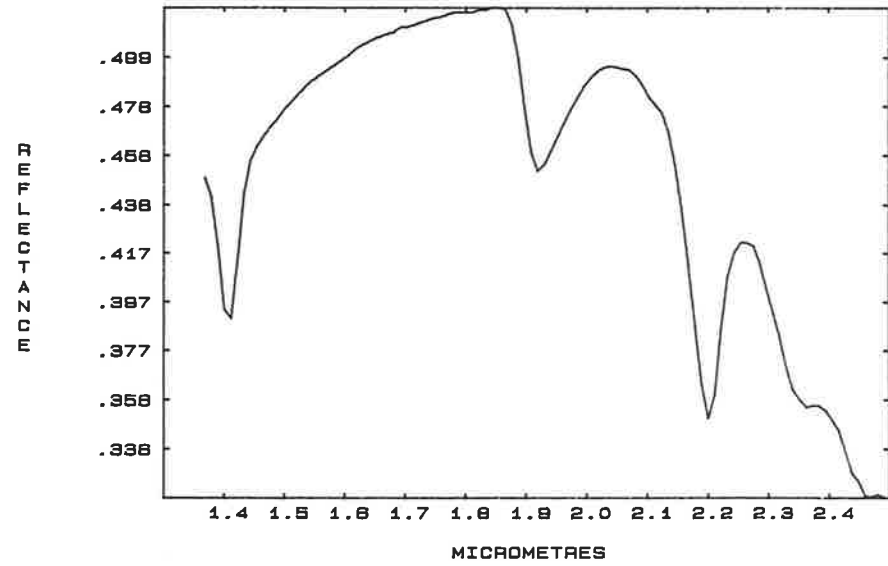
MT8/288/S QTZ, KSP, MUSC, TR.KAOL, FSP



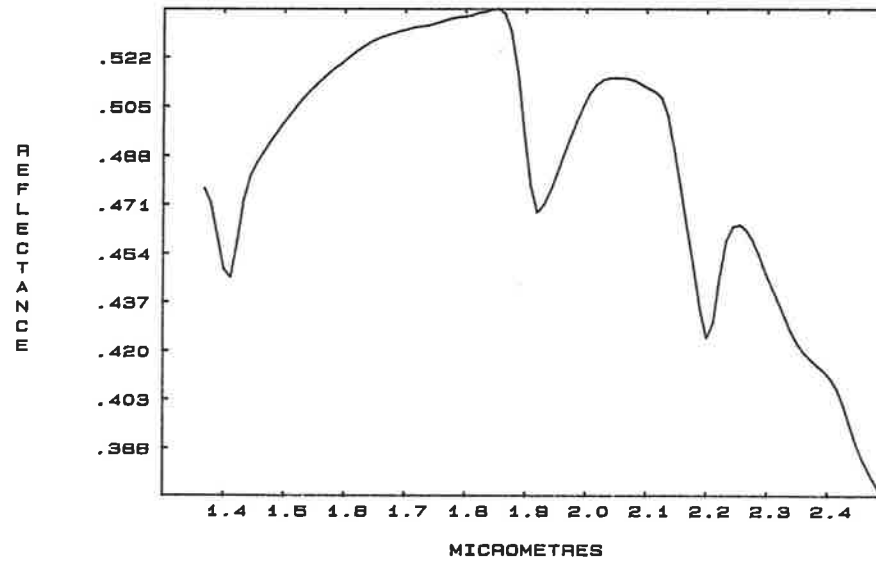
MTB/838/S KSP, QTZ, FSP, MUSC, TR.KAOL



MT4/33/S QTZ, MUSC, KSP, TR.KAOL, FSP

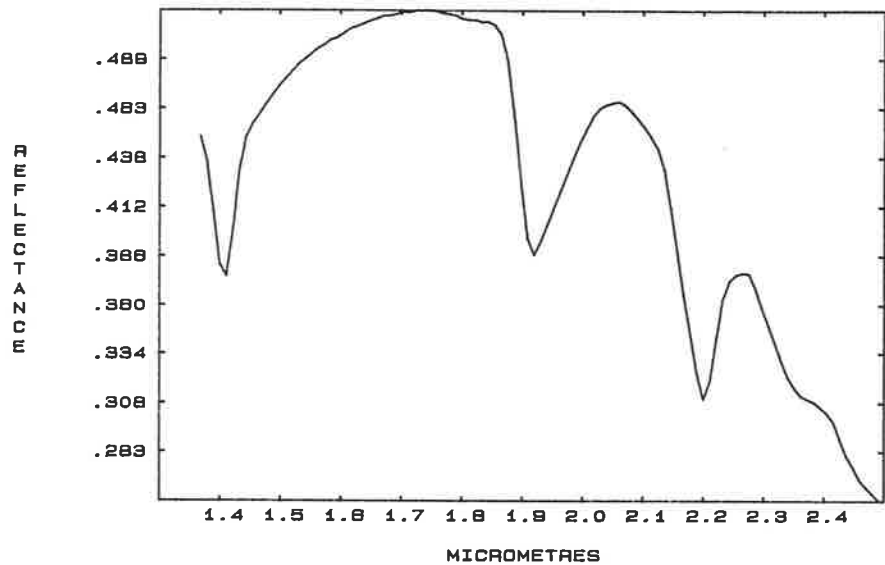


AVERAGE UNALTERED GRANITE SOIL

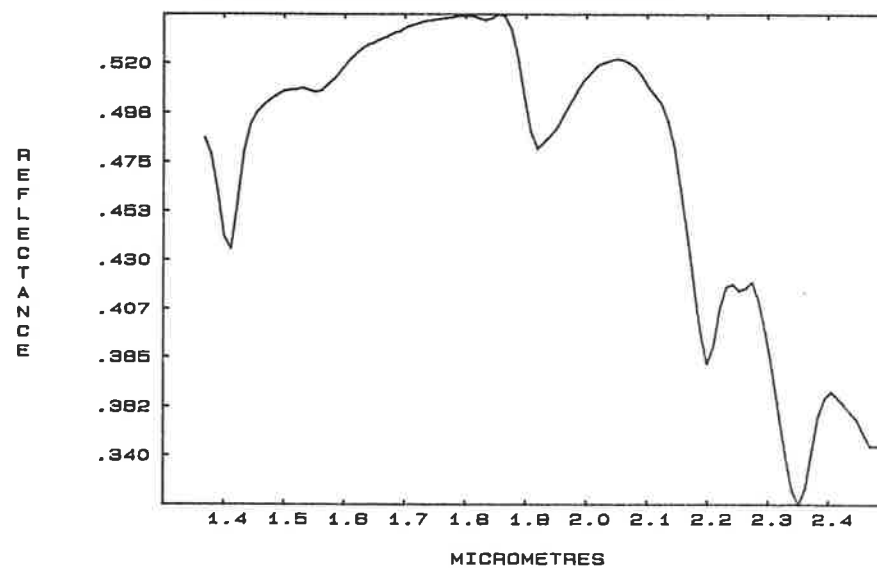


SOIL SPECTRA - UNALTERED, WEATHERED ROBERTSON RIVER FORMATION AND MIXTURES

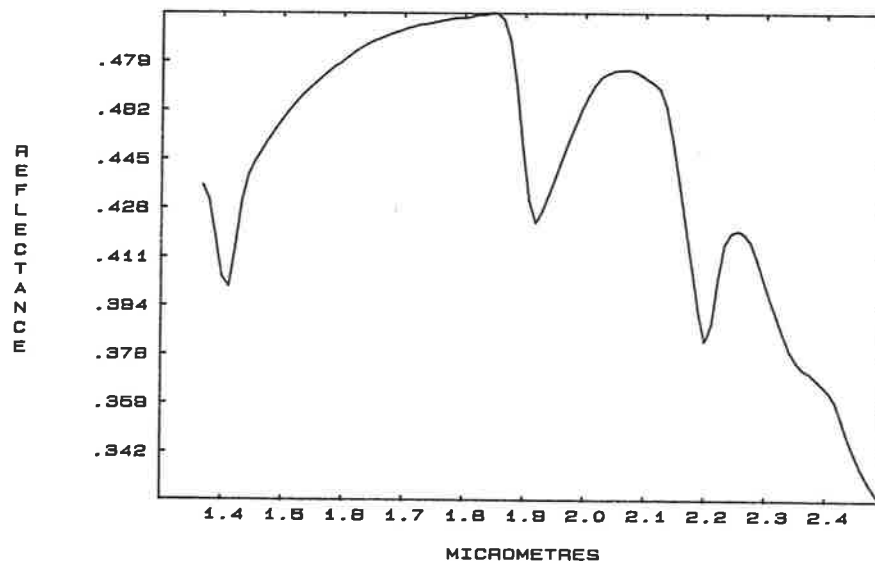
MT1/888/S QTZ, KSP, MUSC, TR.KAOL, FSP



MT2/82/S MUSC, QTZ, CZ, TR.KAOL, FSP, KSP

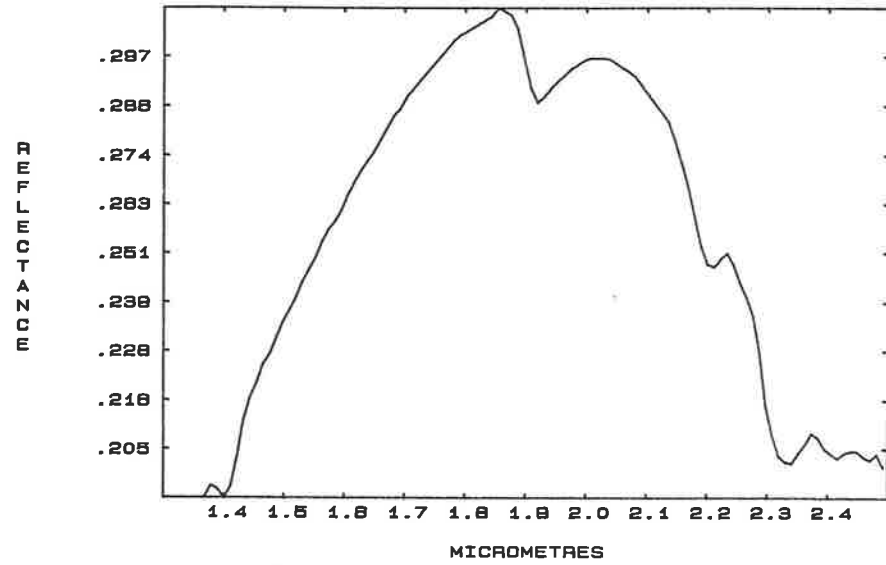


AVERAGE REF & MIXTURE SOILS

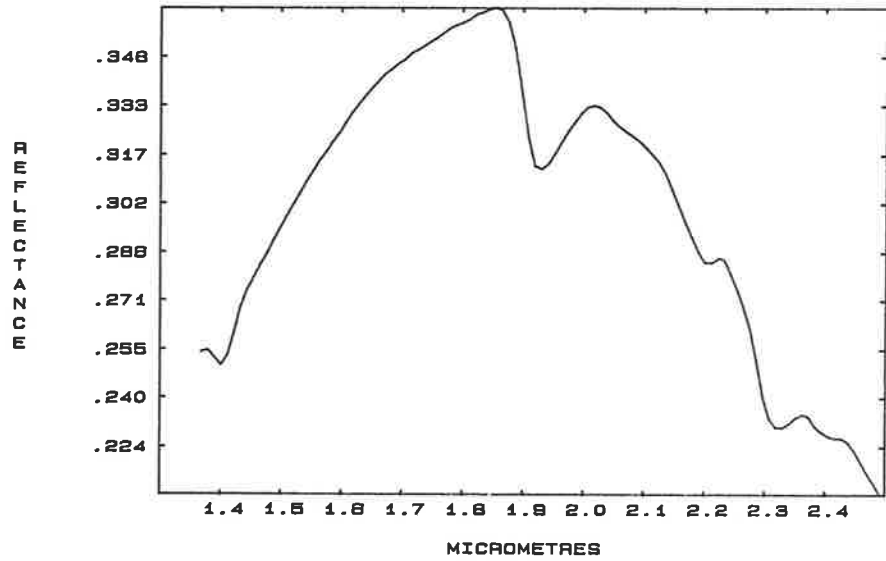


W SPECTRA - DOLERITES

MT8/880/3/W AMP, QTZ, AN, TR.MUSC, KAOL, FSP

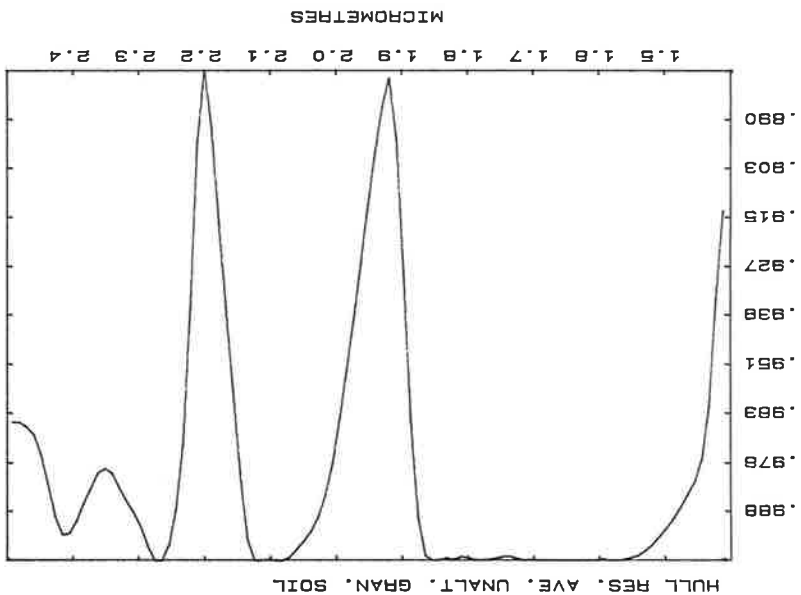
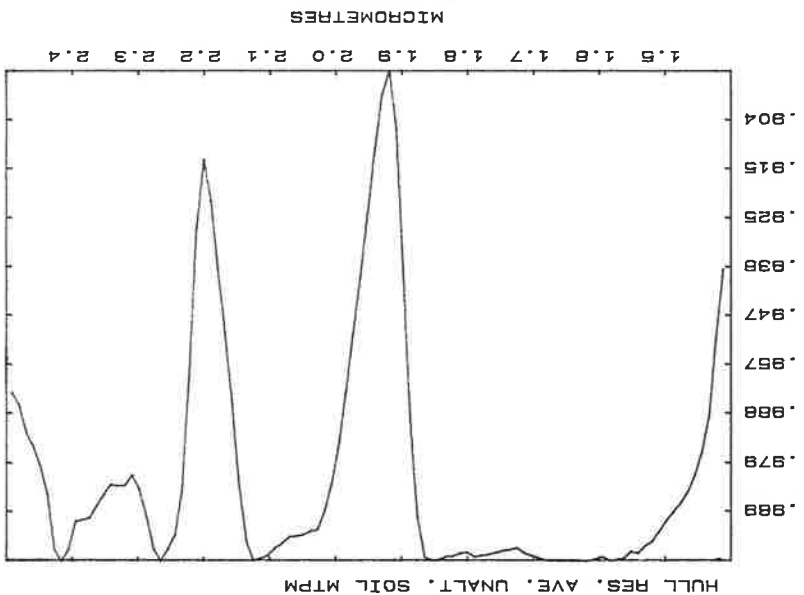
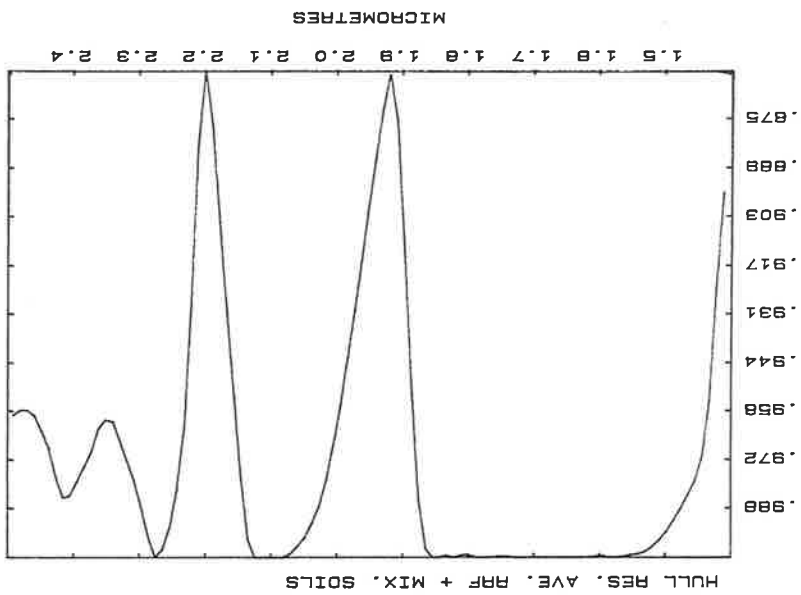
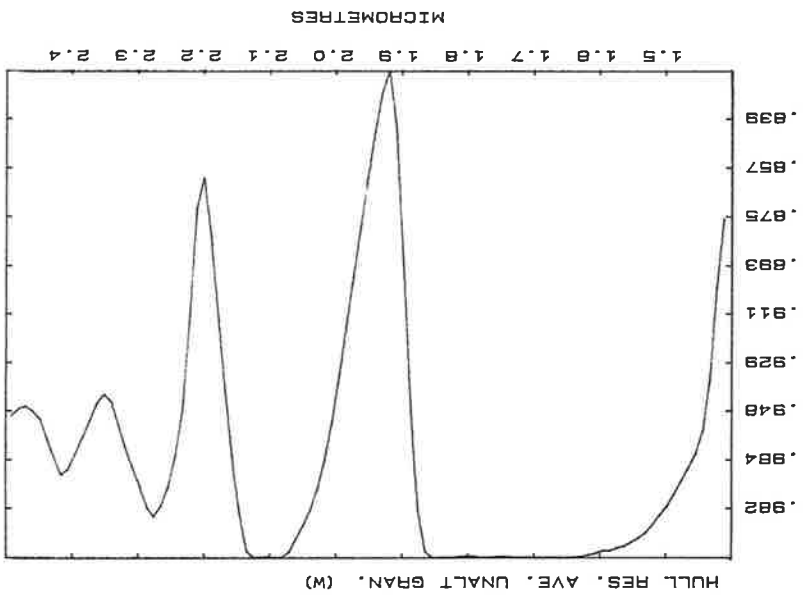


AVERAGE DOLERITE W



APPENDIX V Hull residuals of averaged SWIR laboratory reflectance
spectra from Mt Turner.

Hull residual plots (see Green and Craig, 1985) are presented for a number of (averaged) laboratory spectra of different groups of rock and soil from Mt Turner. At the top of each hull residual plot is a label denoting its origin. W represents weathered-surface spectra, F represents fresh-surface spectra. Data derived from samples collected within the main silicified sericitic alteration zone are marked SZ, while altered samples collected outside this zone are marked NON-SZ. Note the similarity of the absorption features of all (non-mafic) samples, regardless of their alteration state, type of material (rock or soil), type of surface measured (W or F) and lithology (Robertson River Formation (RRF) or felsics).



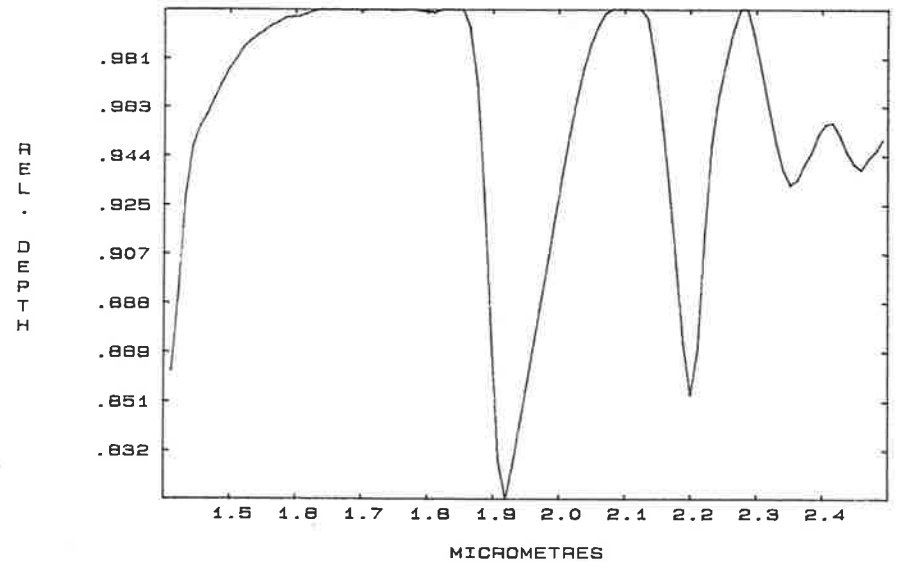
TRANSMITTANCE

TRANSMITTANCE

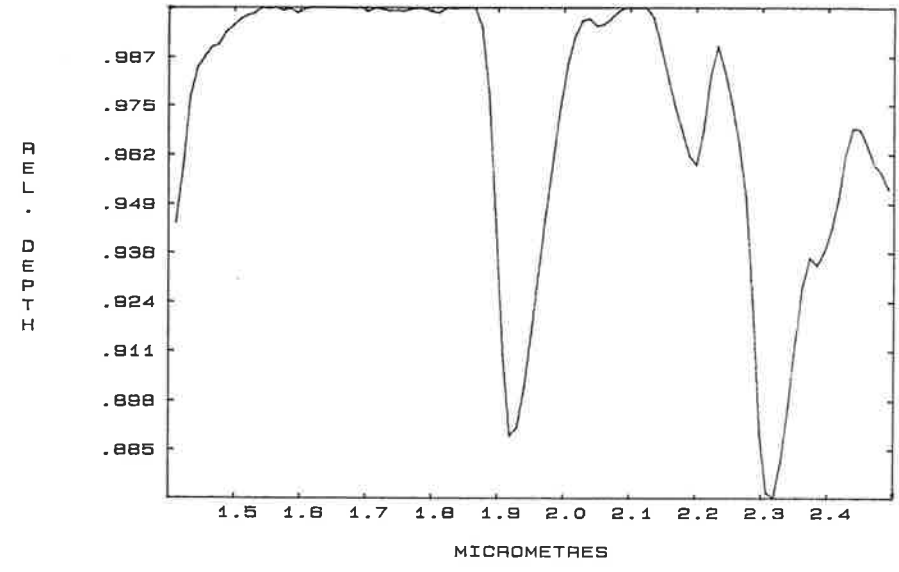
TRANSMITTANCE

TRANSMITTANCE

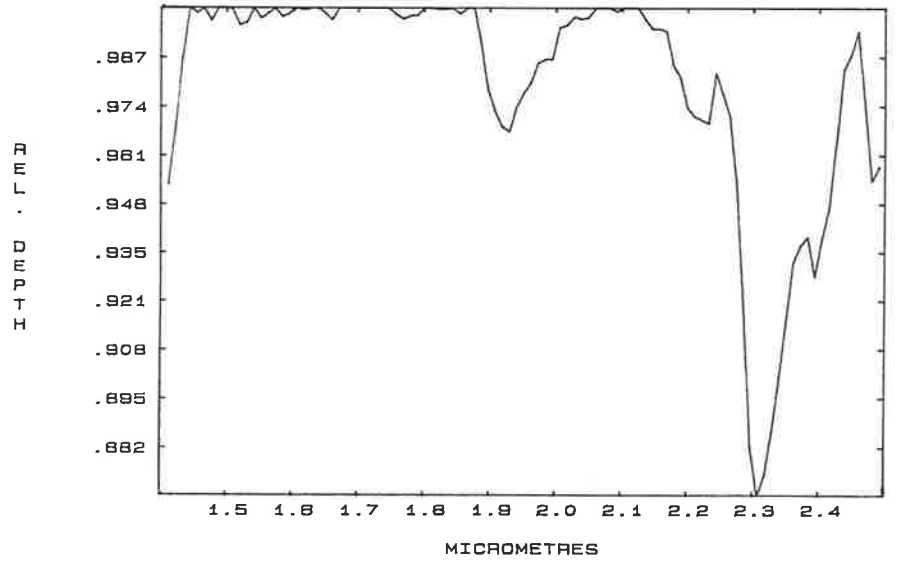
HULL RES. AVE. UNALT. GRAN. (F)



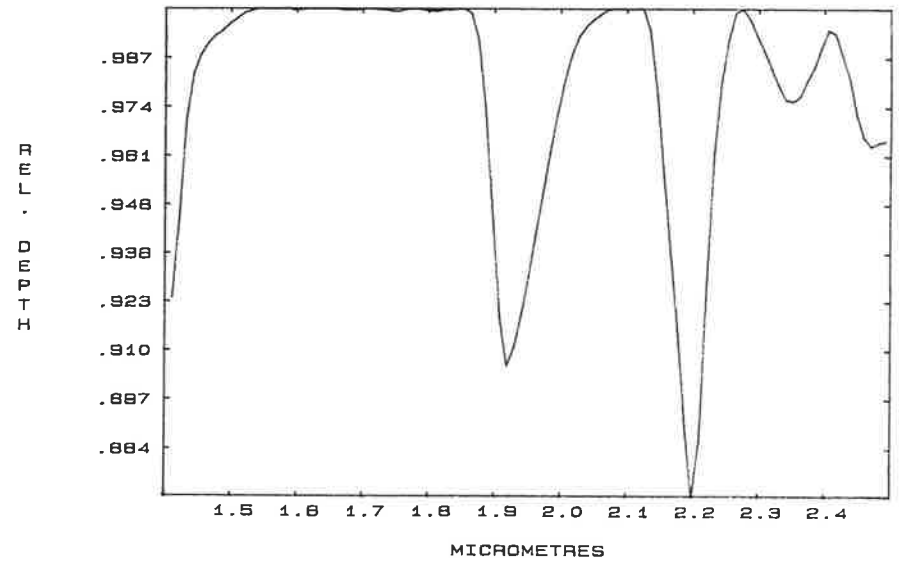
HULL RES. AVE. DOLERITE (W)

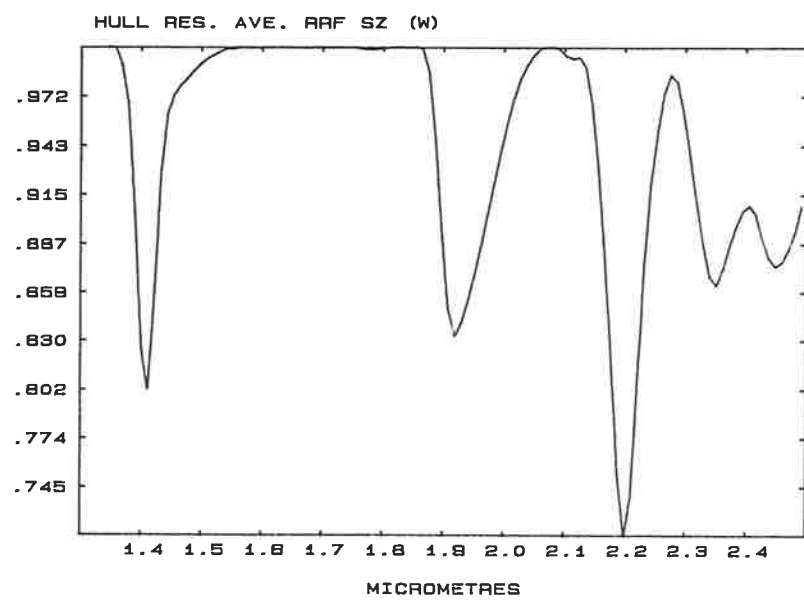
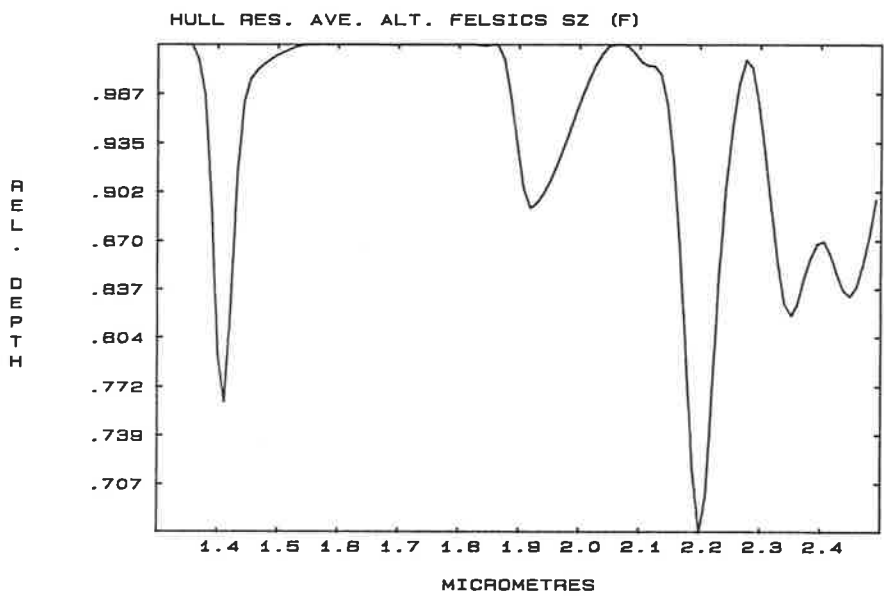
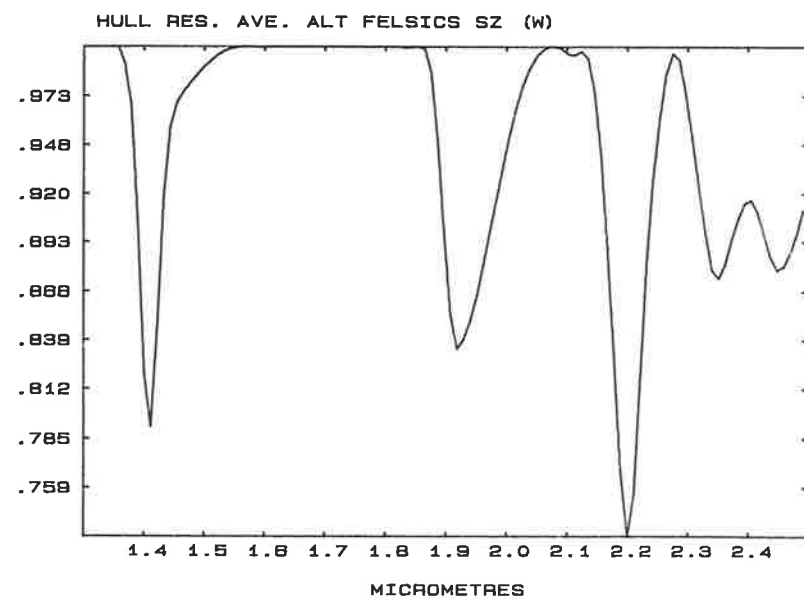
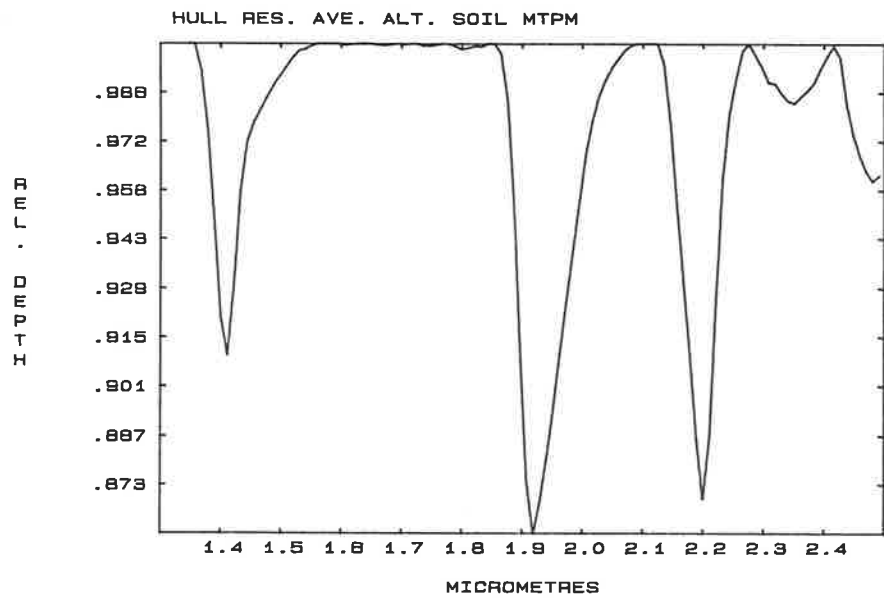


HULL RES. AVE. DOLERITE (F)



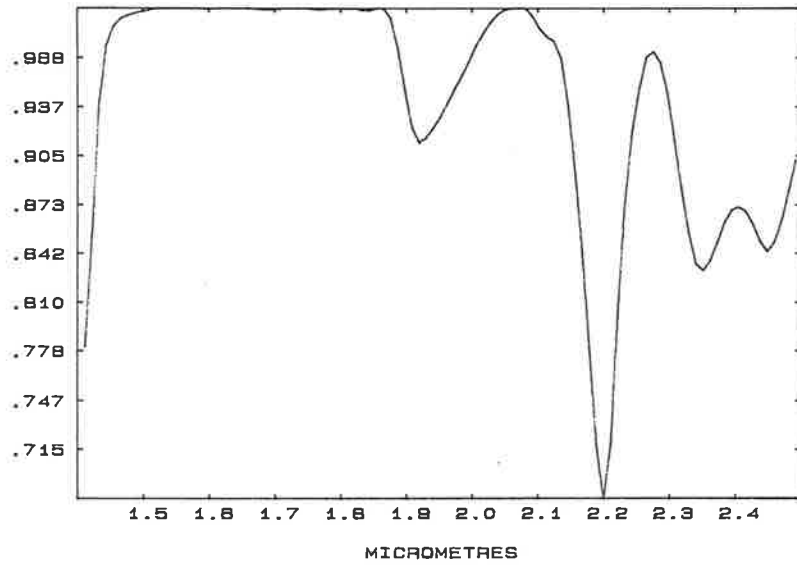
HULL RES. AVE. ALT. SOILS SZ





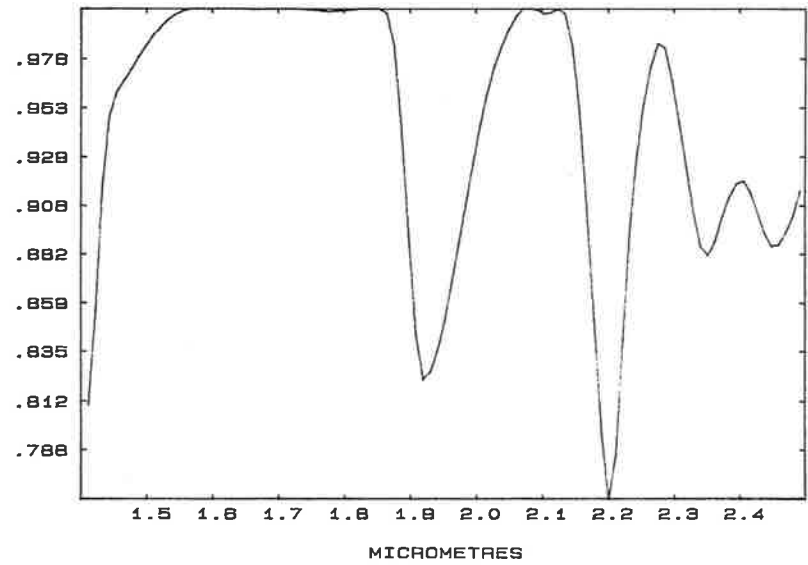
DEPTH

HULL RES. AVE. RRF SZ (F)



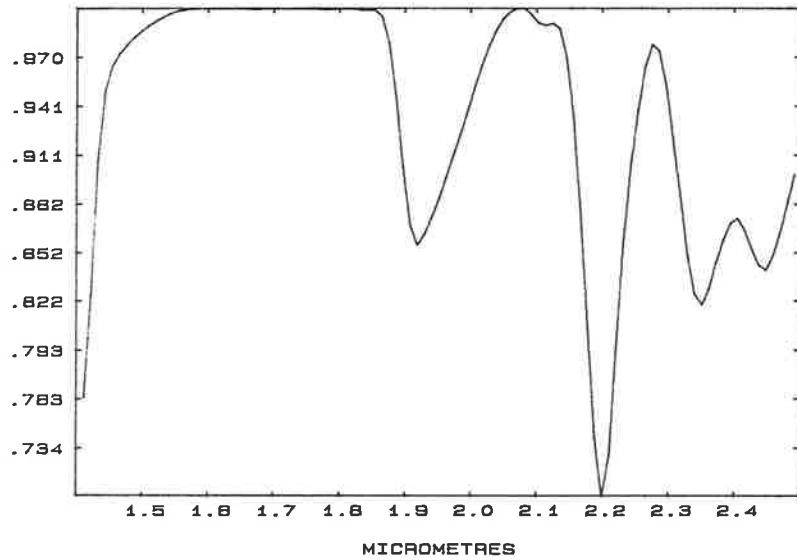
DEPTH

HULL RES. AVE. ALT FELSICS NON-SZ (W)



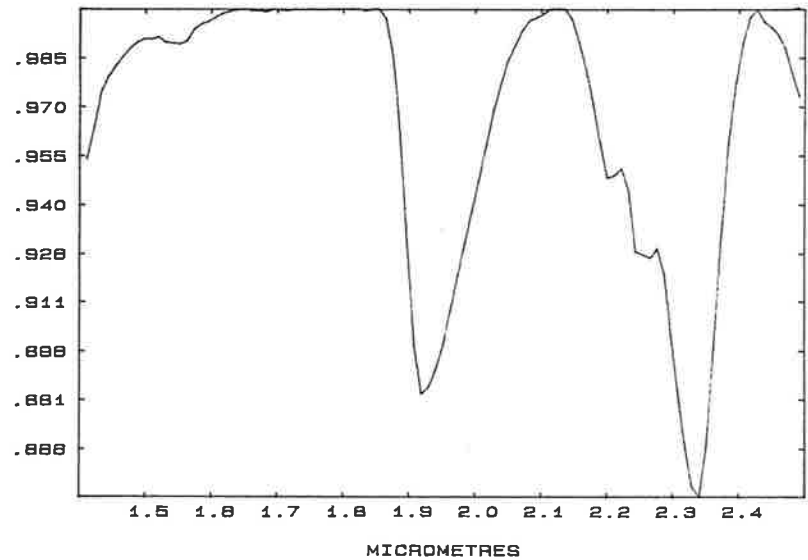
DEPTH

HULL RES. AVE. ALT FELSICS NON-SZ (F)



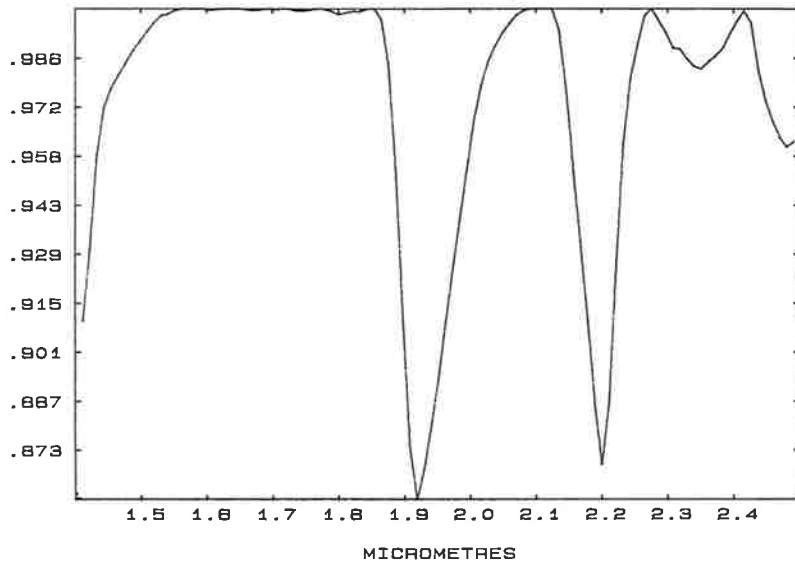
DEPTH

HULL RES. AVE. PROP. ALT. MTPM



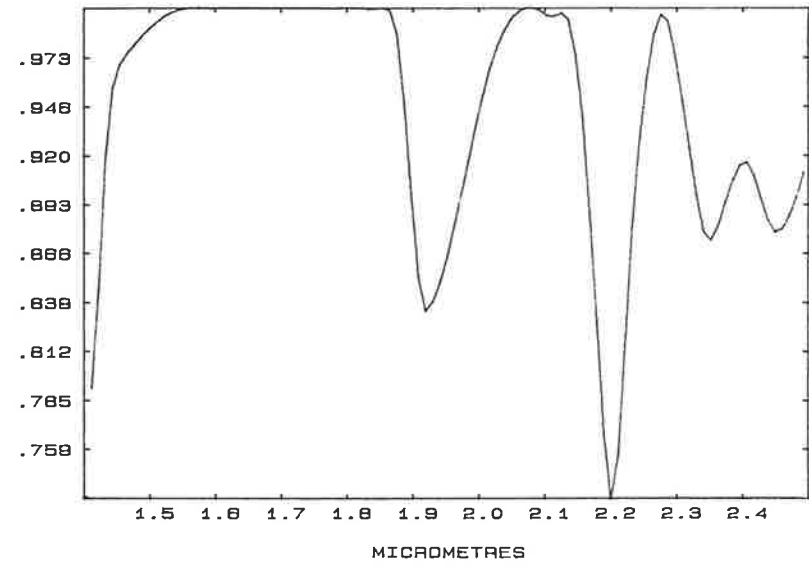
R
E
L
D
E
P
T
H

HULL RES. AVE. ALT. SOIL MTPM



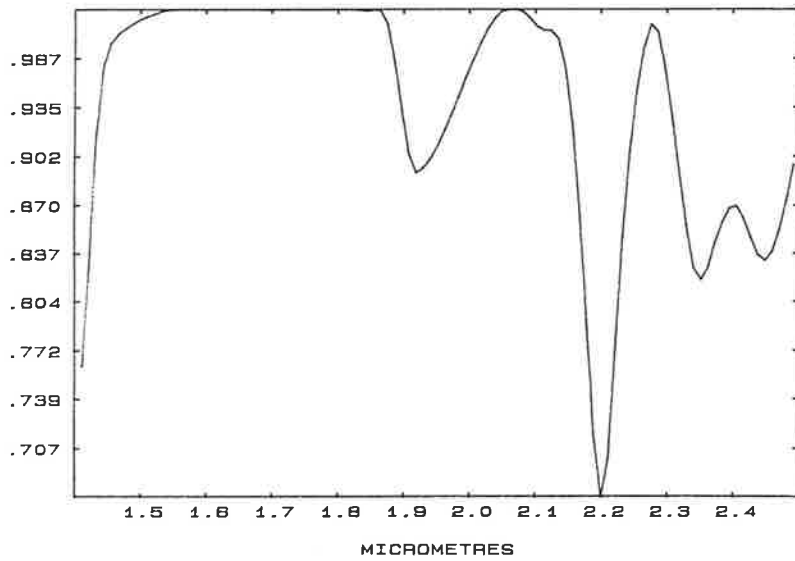
R
E
L
D
E
P
T
H

HULL RES. AVE. ALT. FELSICS SZ (W)



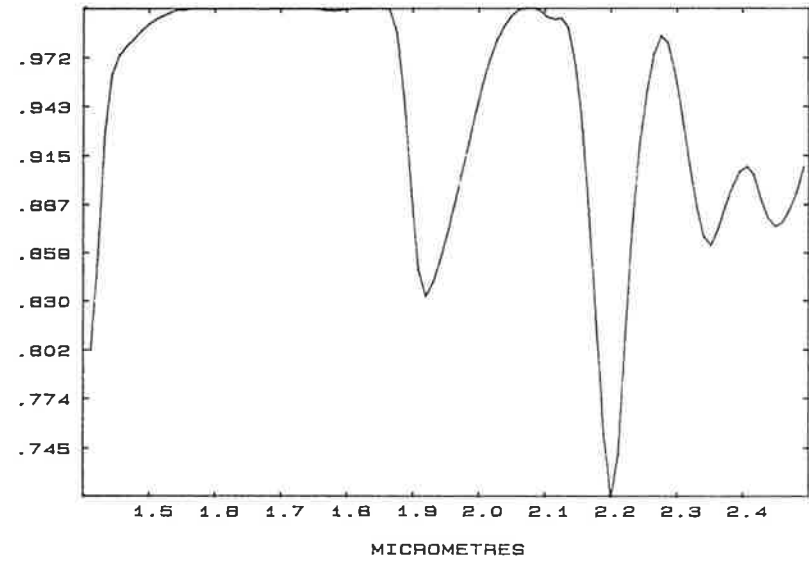
R
E
L
D
E
P
T
H

HULL RES. AVE. ALT. FELSICS SZ (F)



R
E
L
D
E
P
T
H

HULL RES. AVE. RRF SZ (W)

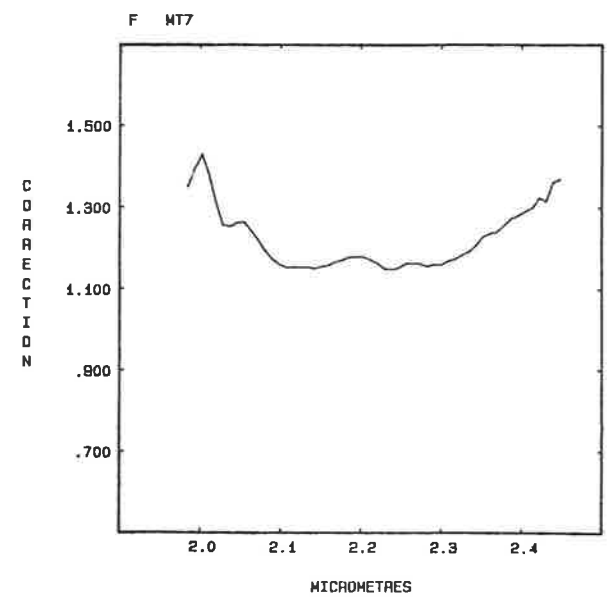
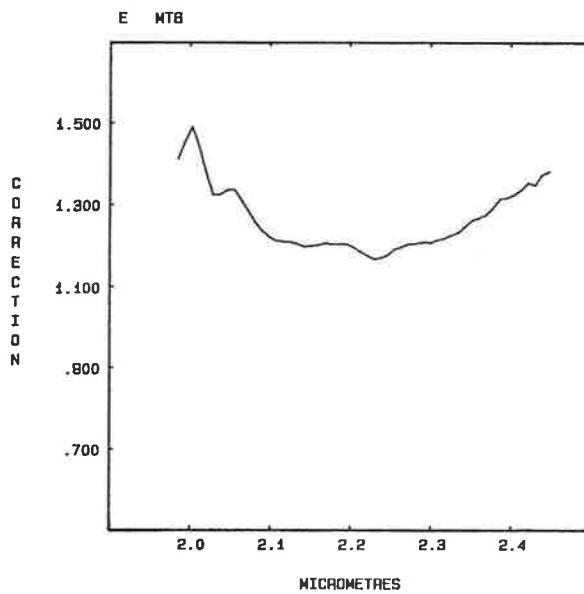
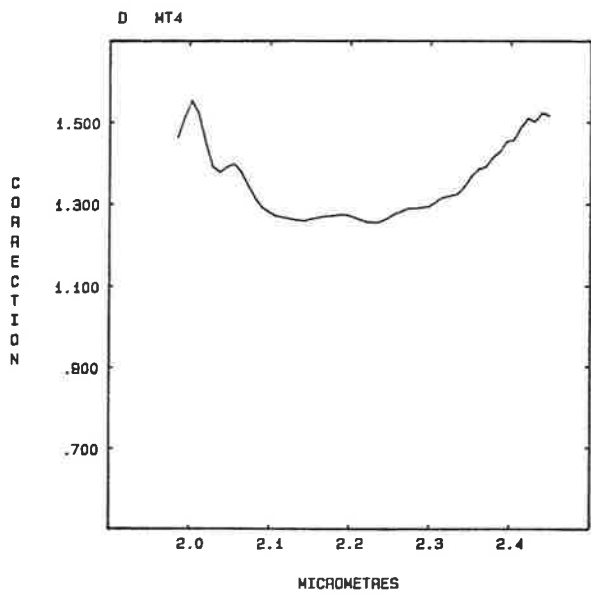
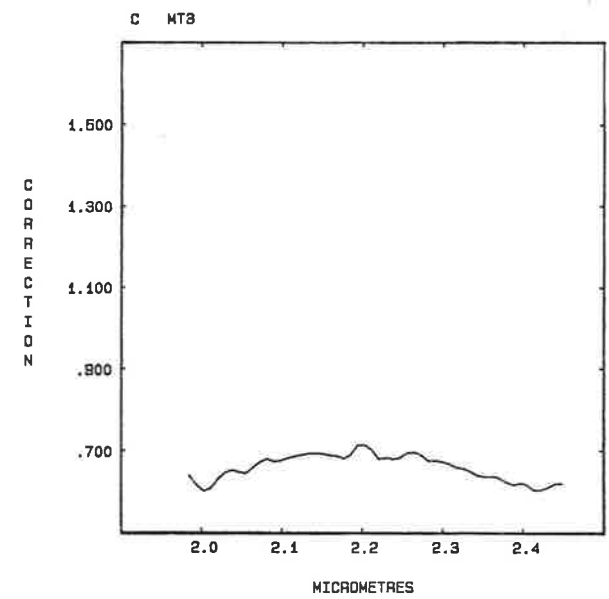
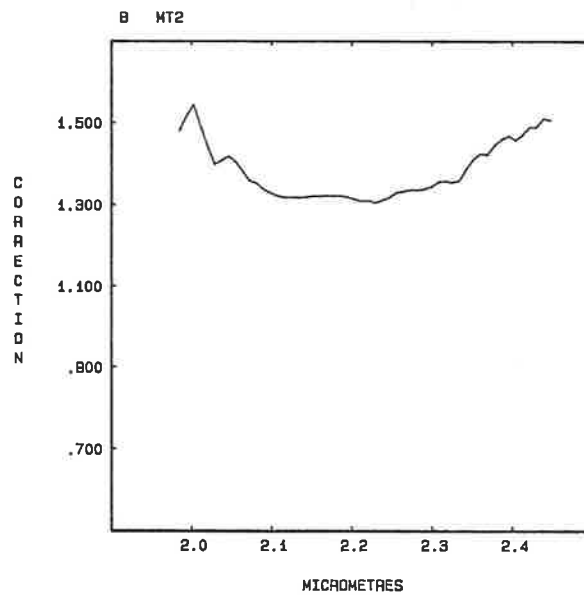
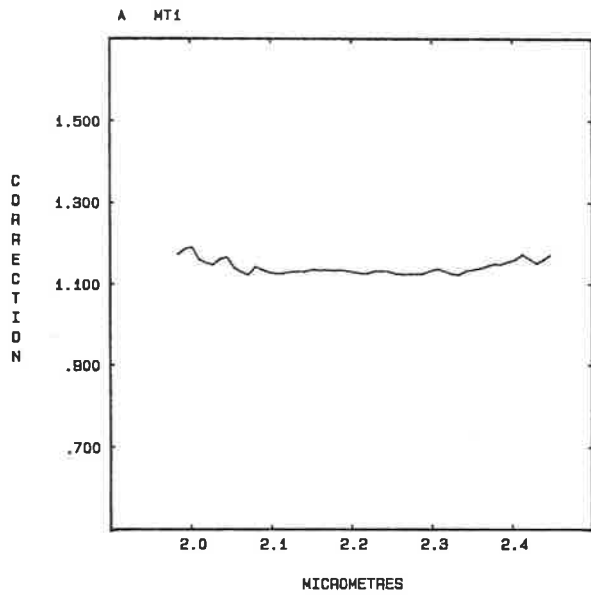


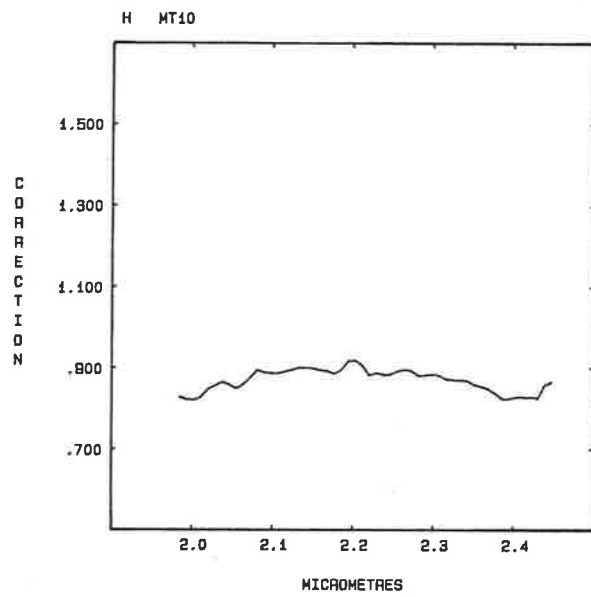
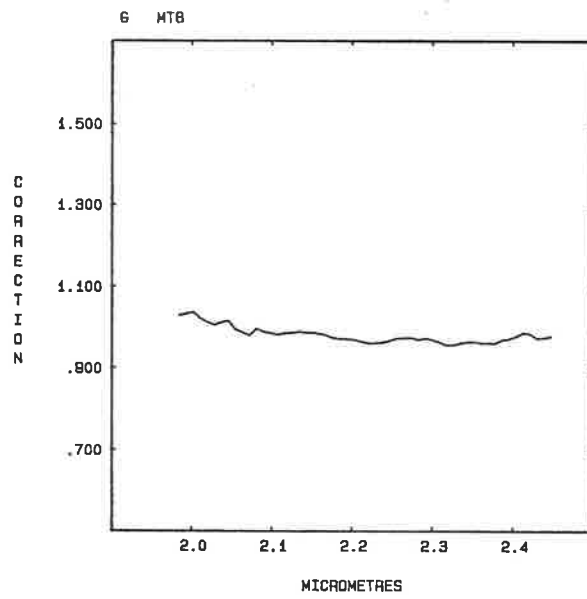
APPENDIX VI Correction factors for time differences between flight
lines at Mt Turner.

The accompanying figures (labelled A to H) represent the correction functions derived from spectra on intersection points of flight lines. All lines were corrected using MT9 as a reference. The software for this procedure was developed by Drs A. Green and M. Craig of the CSIRO/MXY. A correction function for MT9, if plotted, would appear as a horizontal straight line with unit height ($y = 1$).

The curves exhibit the gross features of a radiance spectrum. They also vary regularly with respect to the time each was flown relative to MT9. MT8, for instance, was flown immediately before MT9, and has a correction factor close to unity. MT1 was flown just before MT8 (at 2.05 pm, about 30 minutes before MT9), and needs a slightly larger correction. MT2 was flown about an hour before MT9 (at 1.43 pm), and MT6, MT7 and MT4 within 20 minutes of each other an hour before that. These correction functions are inverted relative to the normal radiance spectrum.

Lines flown after MT9 were, in order of flying, MT10 and MT3. MT10 is also close to a horizontal straight line at unity, but has a slight curvature in the same direction as a normal radiance curve. MT3 has a slightly larger correction of the same nature.



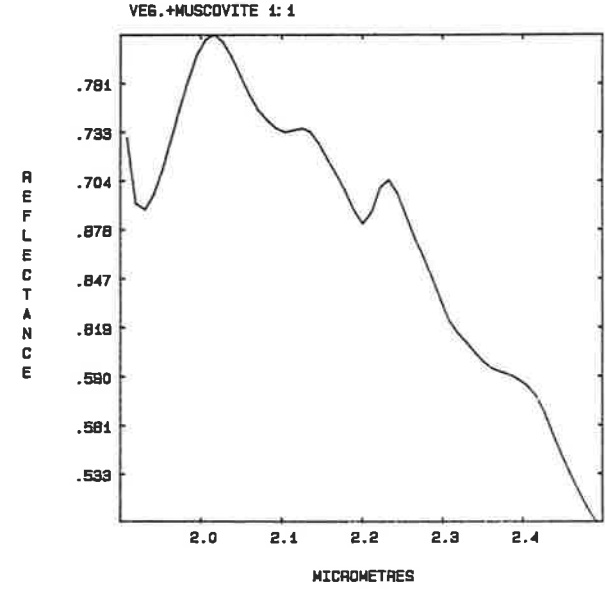
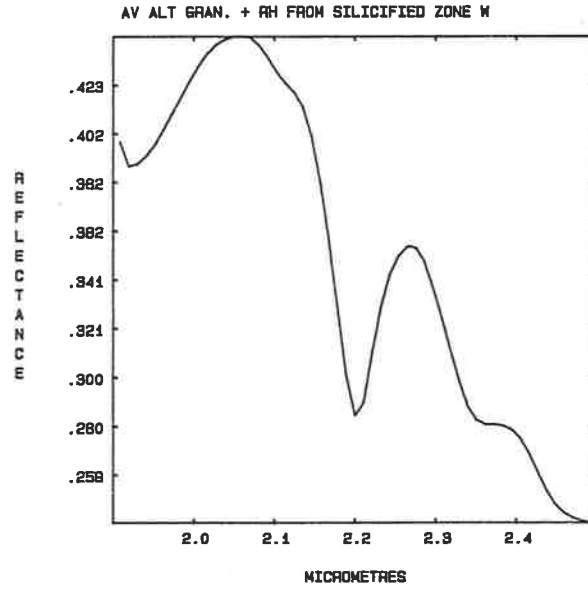
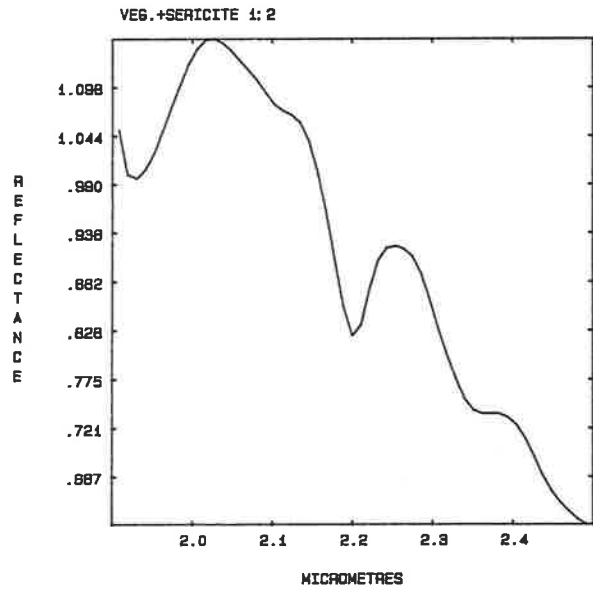
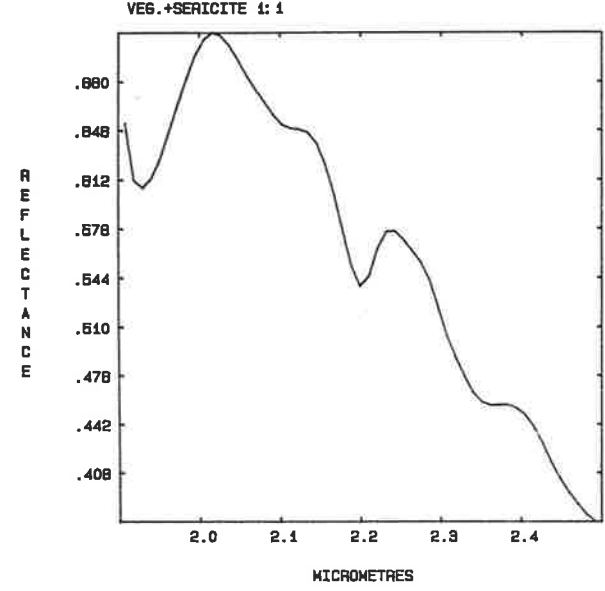
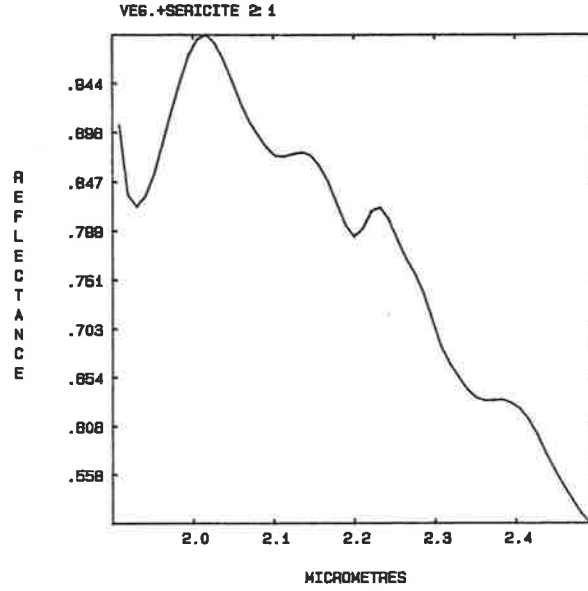
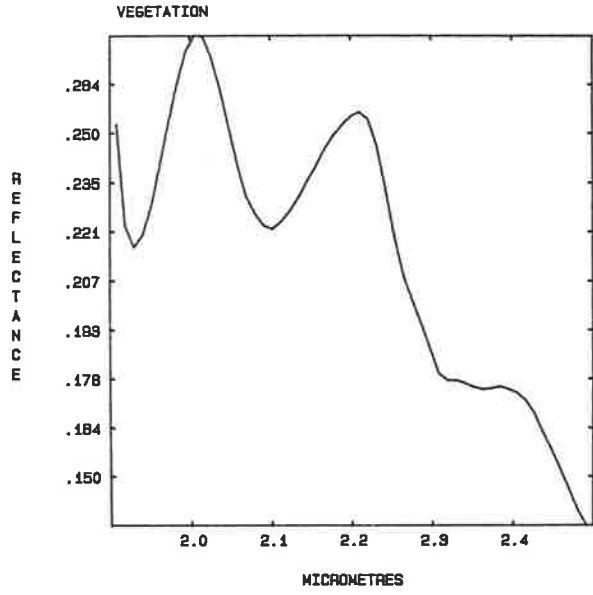


APPENDIX VII Log residual spectra derived from modelling of mixtures
of MT Turner SWIR laboratory reflectance spectra.

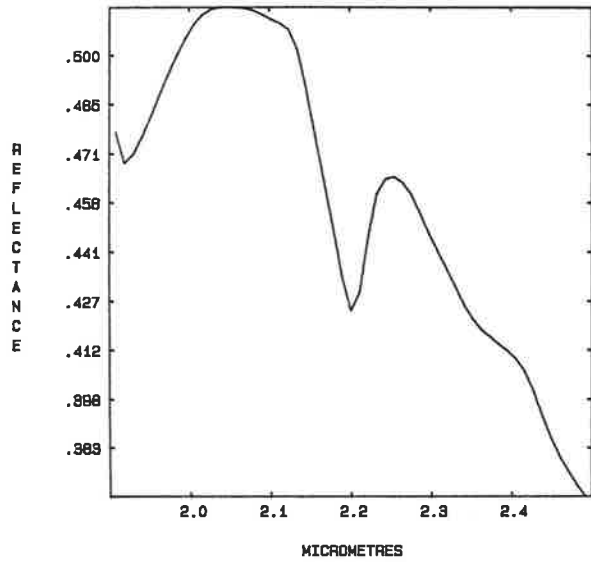
The first two pages of plots in this appendix are derived by the (weighted) addition of reflectance spectra of vegetation and geologic materials. The weightings used are based on field estimates of the different mixtures of these components found at Mt Turner. The resultant group of reflectance spectra has been treated in a similar fashion to the airborne data with, firstly, the mean (last plot on the second page) and, secondly, the 'log residuals' (last two pages) having been calculated.

The shapes of these 'log residual' plots, and the relative strength of many of their absorption features, bear a close resemblance to the airborne log residual type-spectra depicted in Figs. 5.17a-n.

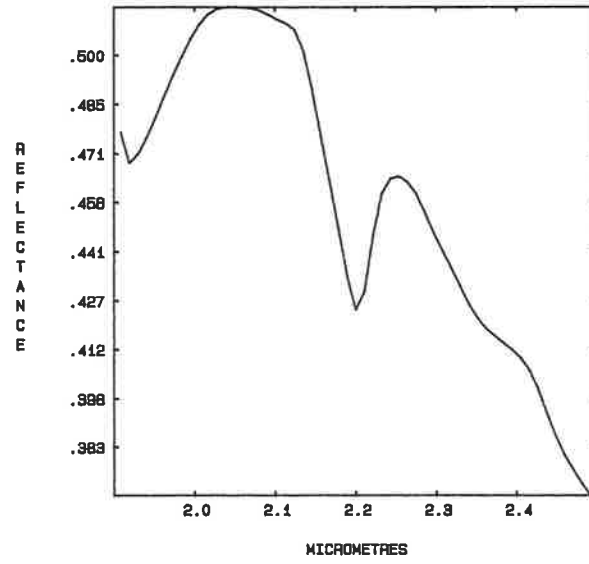
INPUT LABORATORY REFLECTANCE SPECTRA



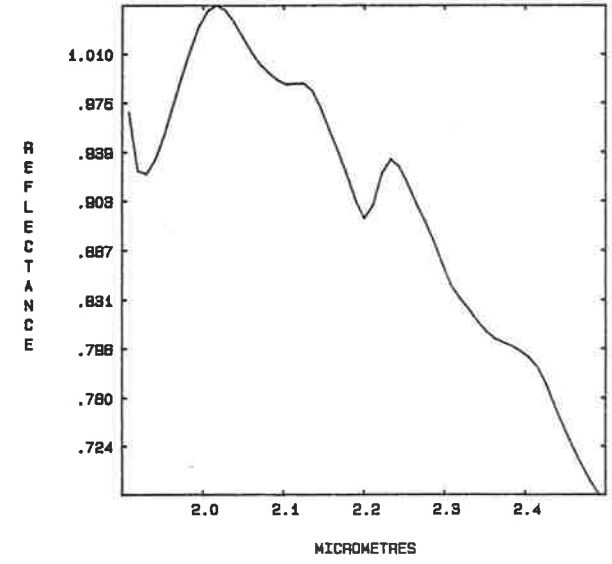
AVERAGE UNALTERED GRANITE SOIL



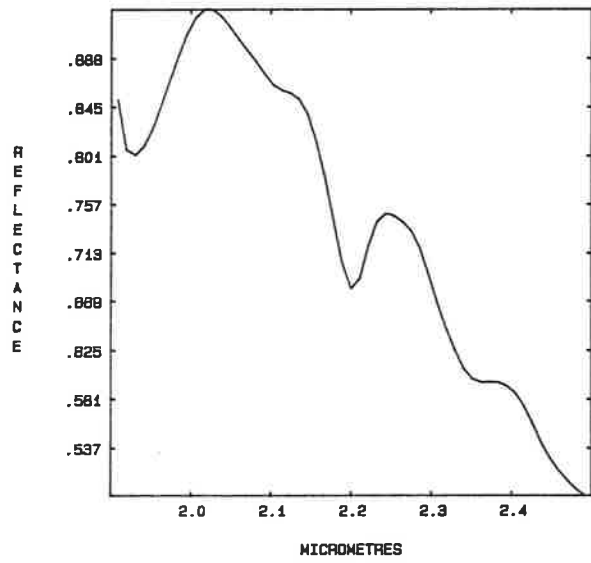
AVERAGE UNALTERED GRANITE SOIL



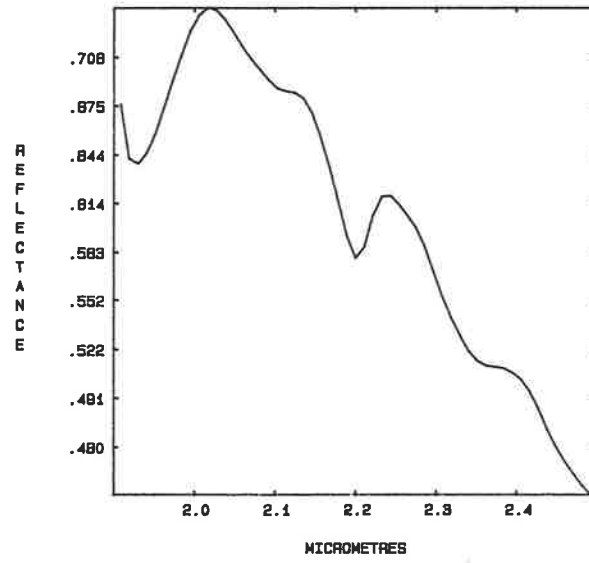
VEG.+MUSCOVITE 1:1.5



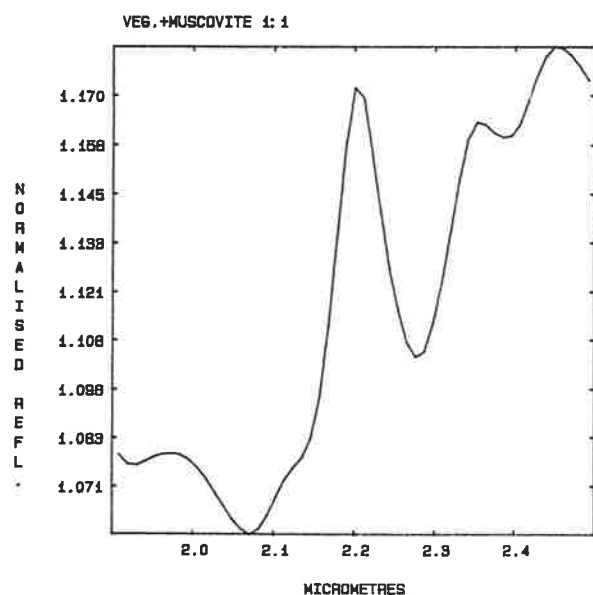
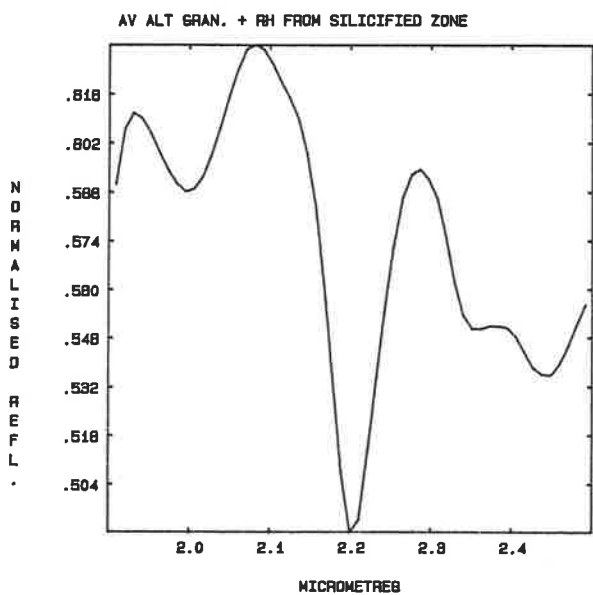
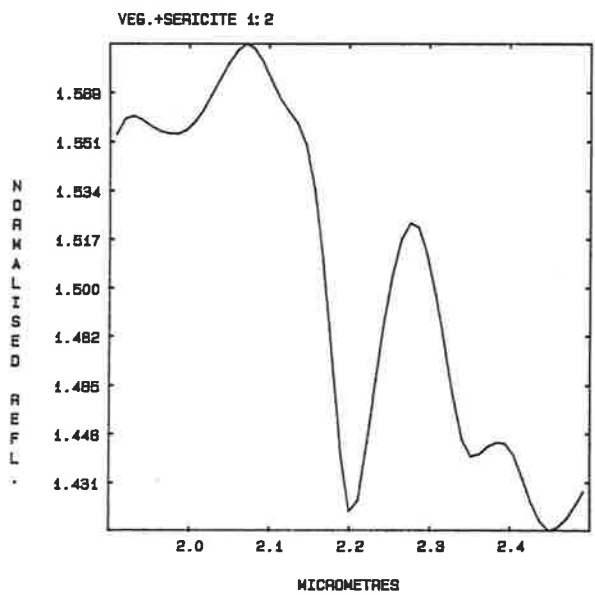
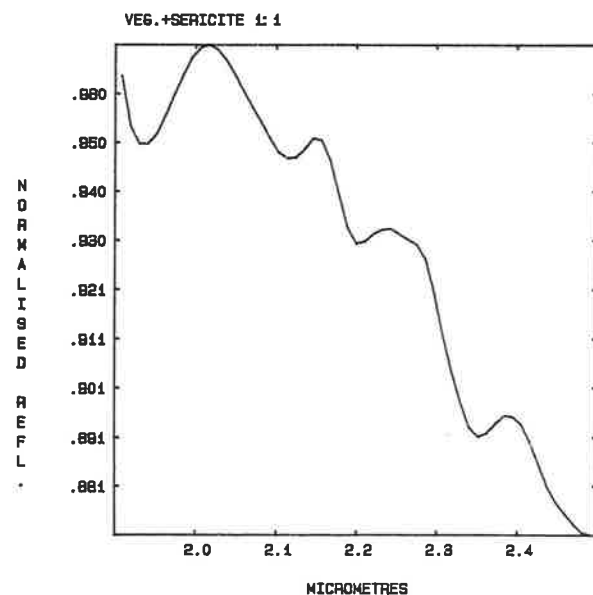
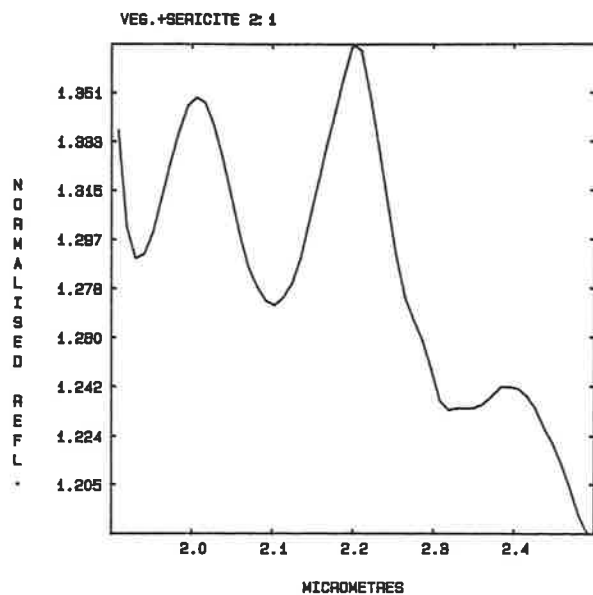
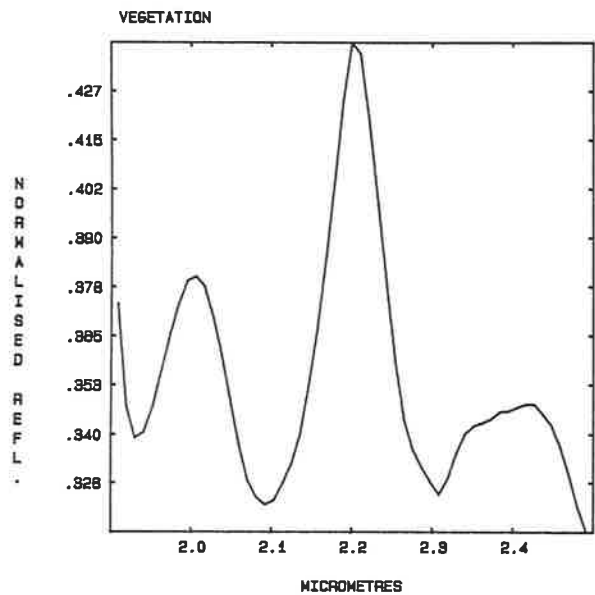
VEG.+SERICITE 1:1.5



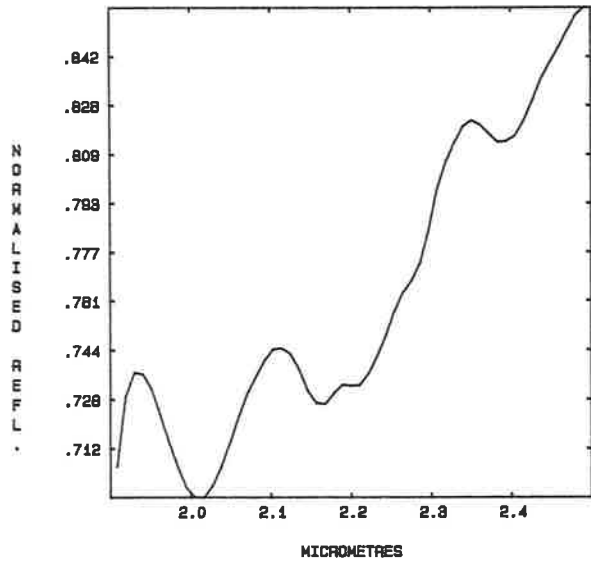
MEAN



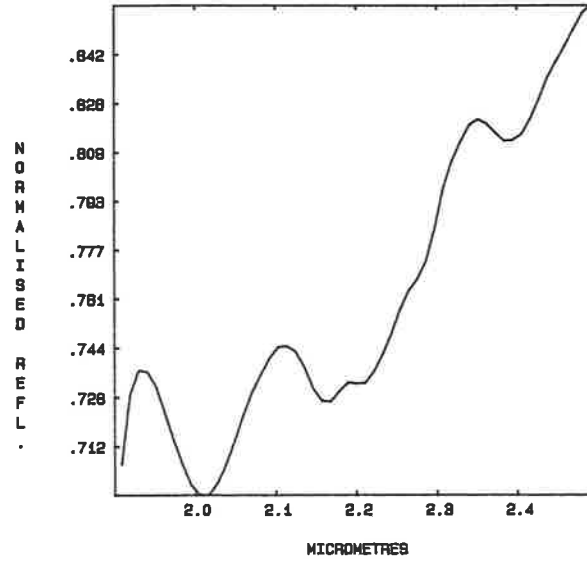
LOG RESIDUALS OF INPUT REFLECTANCE SPECTRA



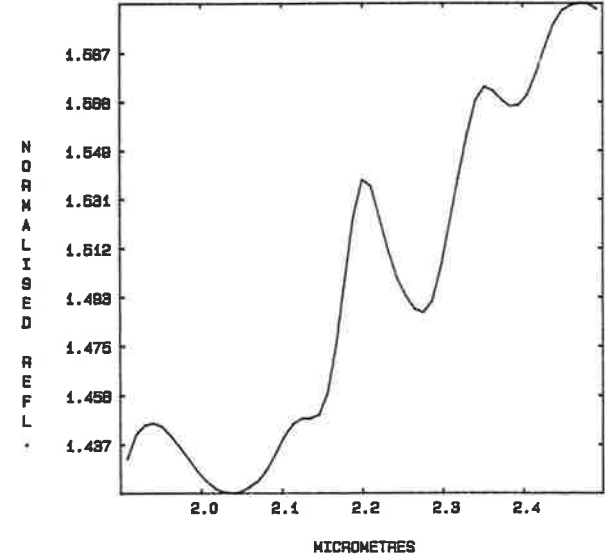
AVERAGE UNALTERED GRANITE SOIL



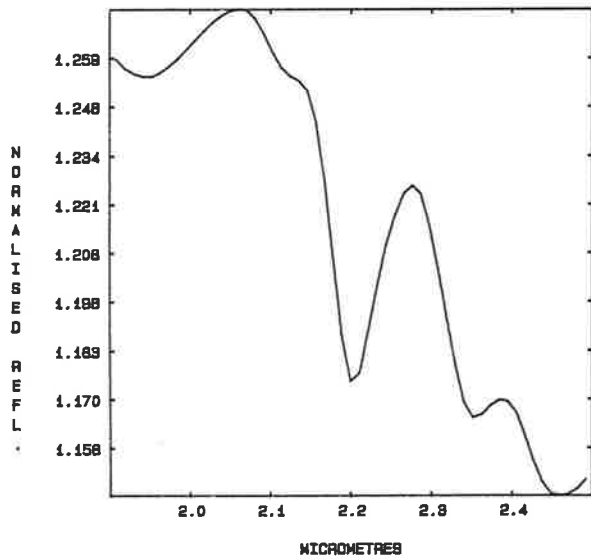
AVERAGE UNALTERED GRANITE SOIL



VEG.+MUSCOVITE 1: 1.5



VEG.+SERICITE 1: 1.5



APPENDIX VIII SWIR laboratory reflectance spectra of samples with XRD analyses from Kambalda.

The Kambalda spectral plots are grouped on the basis of their dominant spectral features. XRD analyses are shown at the top of each plot, with minerals listed in order of decreasing abundance.

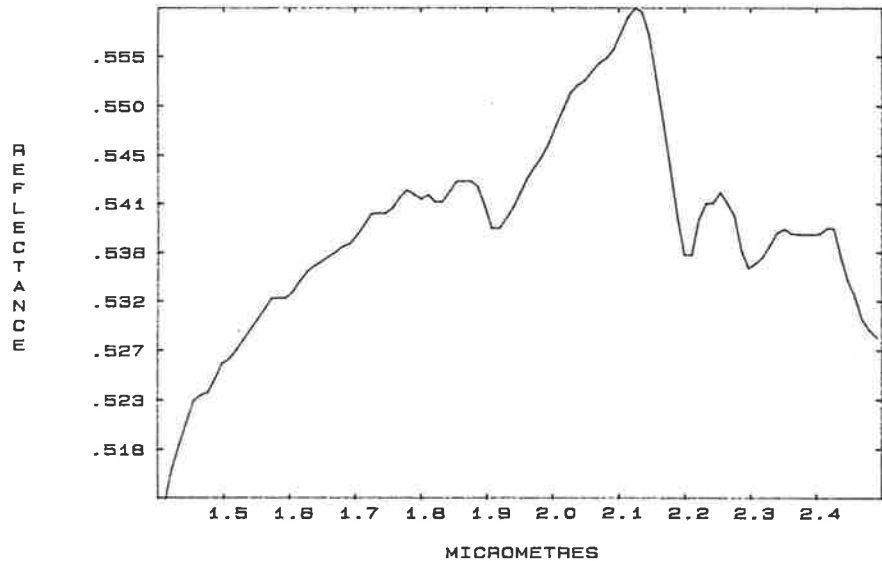
Flat spectra show some structure in these presentations because they have been plotted utilising the full scale on the y-axis. In such cases the noise level is clearly visible.

KEY TO XRD MINERAL IDENTIFICATION

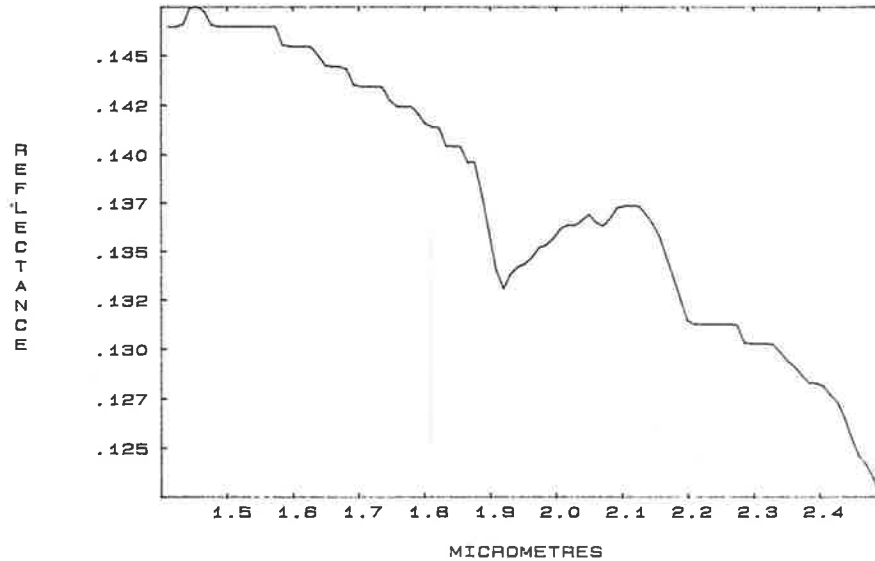
AMP	Amphibole	Q	Quartz
CHL	Chlorite	AB	Albite
TC	Talc	CAL	Calcite
HEM	Haematite	BI	Biotite
EP	Epidote	DOL	Dolomite
ANT	Antigorite	KAO	Kaolin
MO	Montmorillonite	DI	Diopside
MAG	Magnetite	HAL	Halite
PL	Plagioclase	GO	Goethite

FLAT SPECTRA

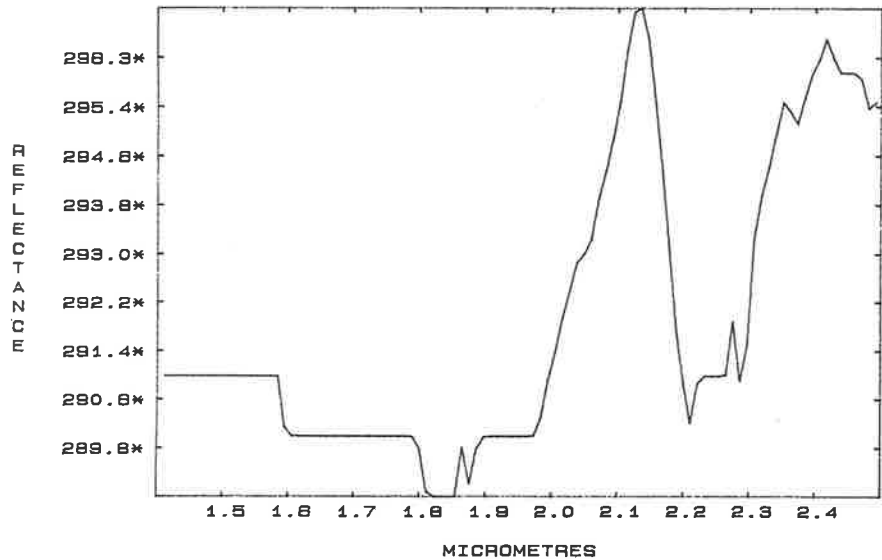
K1/30/S/P AB48Q38TC8CHL4AMP3BI1/HEM<5



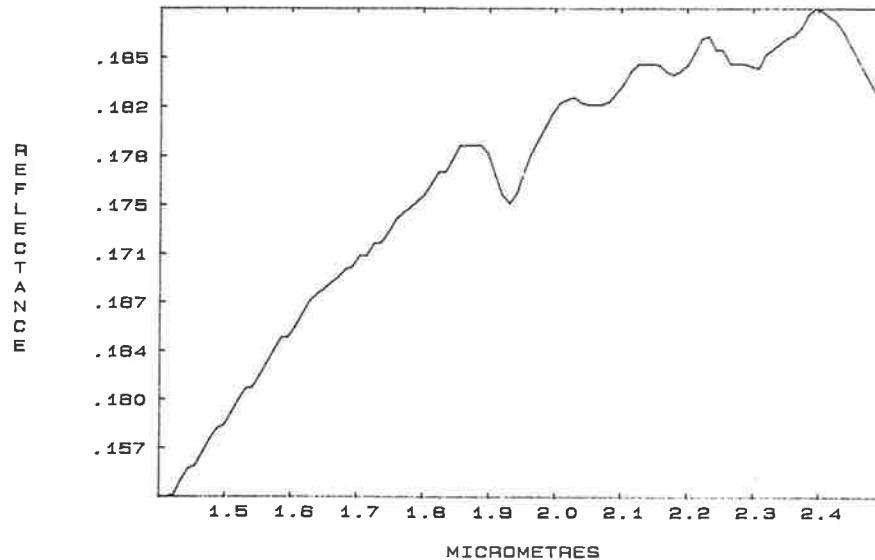
K2/290/F2 Q98 TC1 CAL1/HEM<5



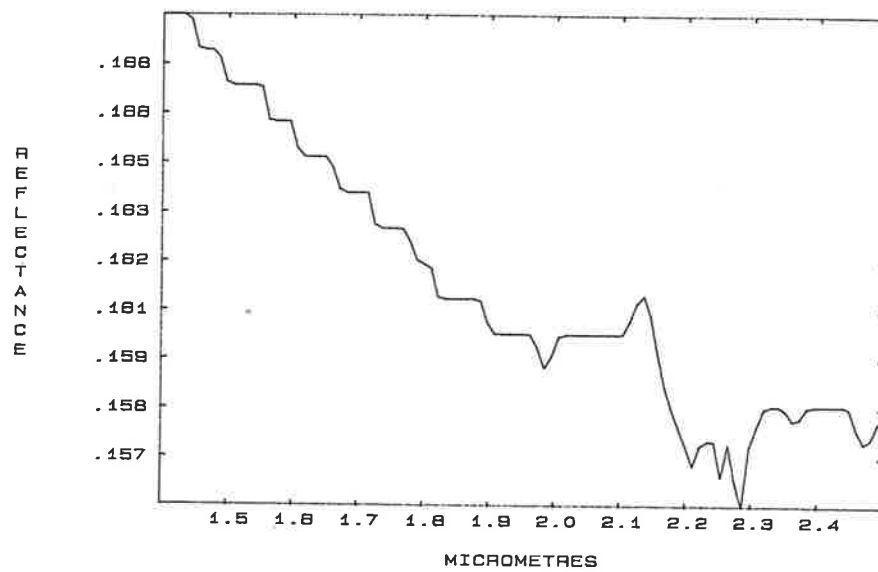
K2/290/F2/P Q91 CAL5 AB4/HEM<5



K2/440/F Q100 BLACK CHERT

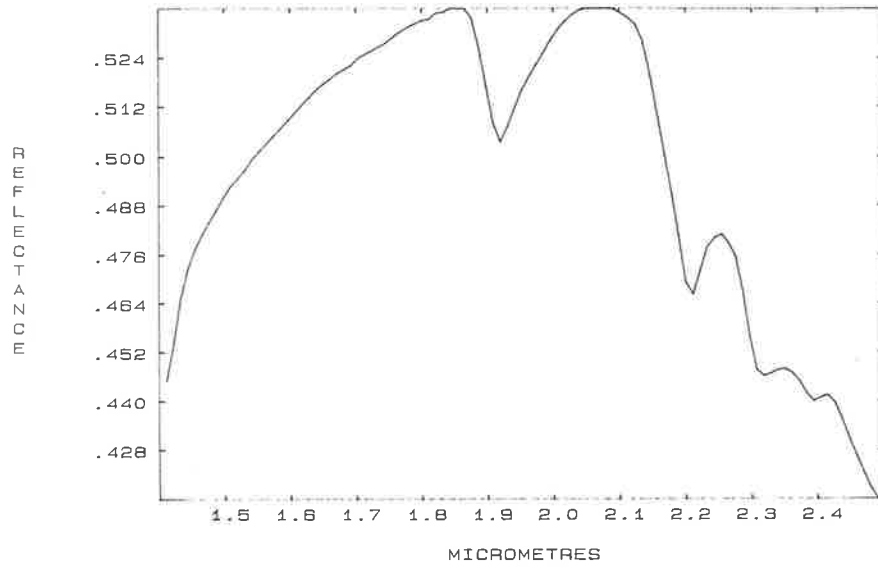


K2/440/F/P Q100

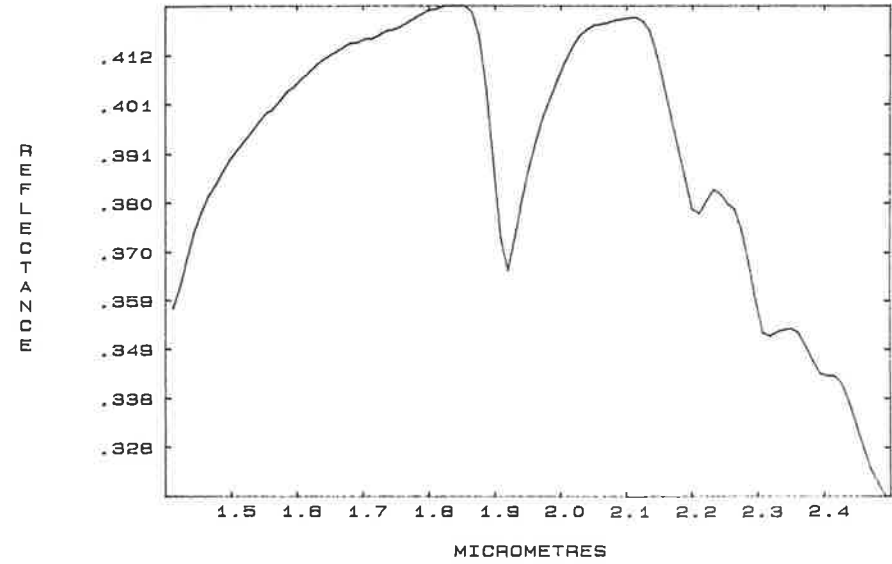


SPECTRA WITH 2.2 MICROMETRE ABSORPTION FEATURES

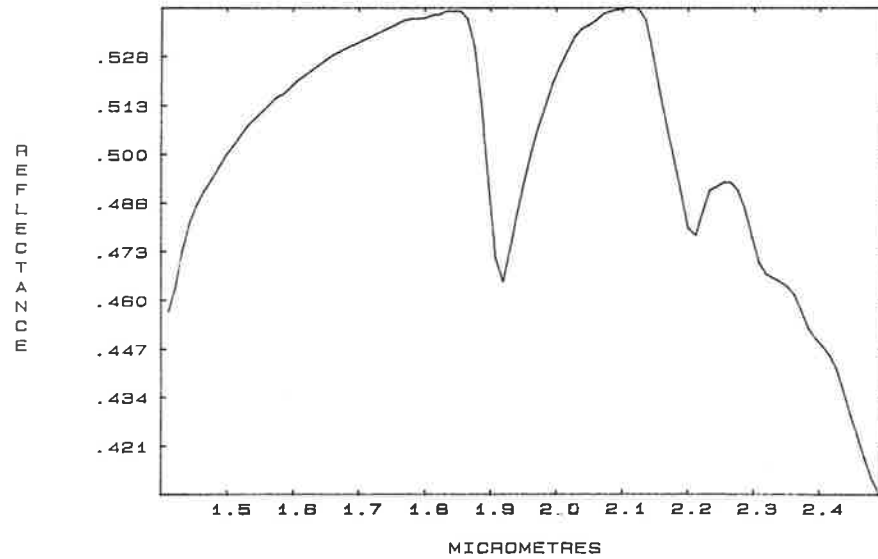
K1/30/S AB48 Q38 TC6 CHL4 AMP3 BI1/HEM<J



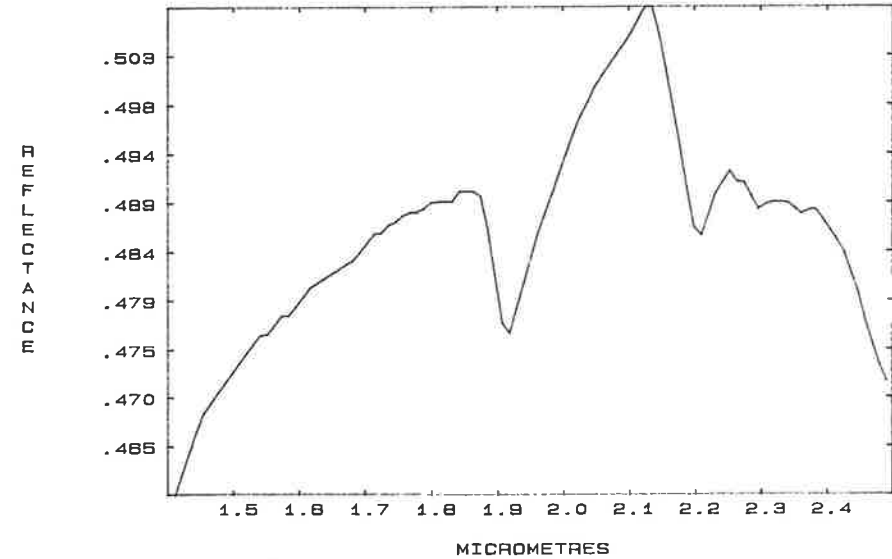
K1/131/S Q68 AB11 AMP8 TC7 CHL6 BI1/HE5



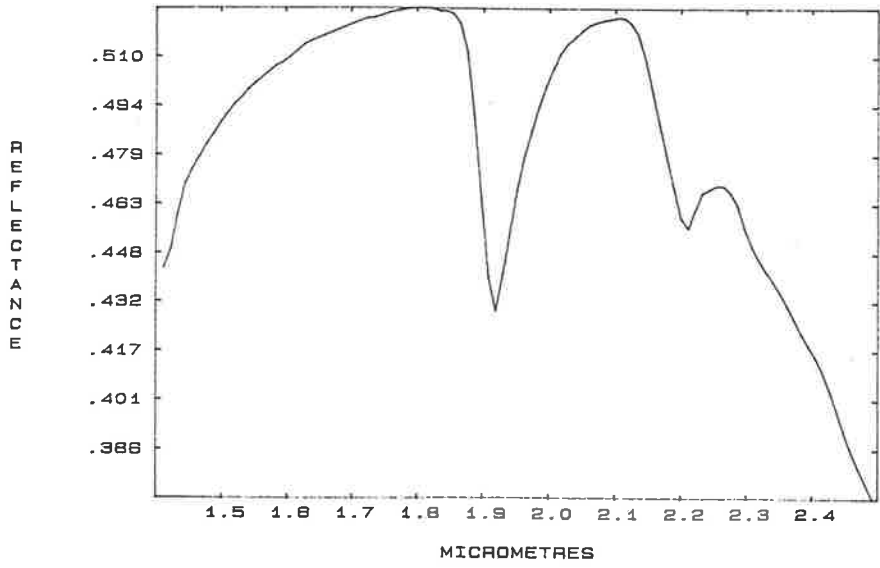
K2/290/S Q91 CAL5 AB4/HEM<5



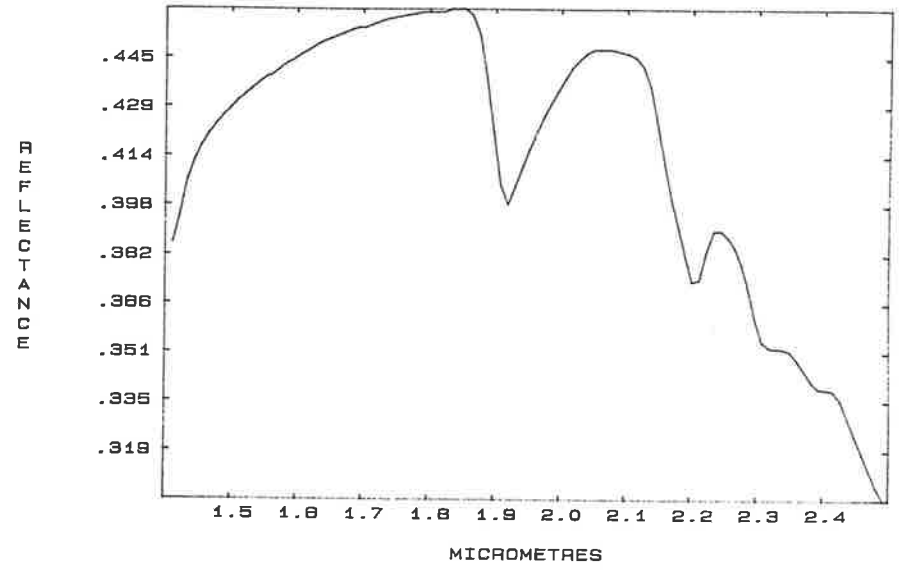
K2/290/S/P Q91 CAL5 AB4/HEM<5



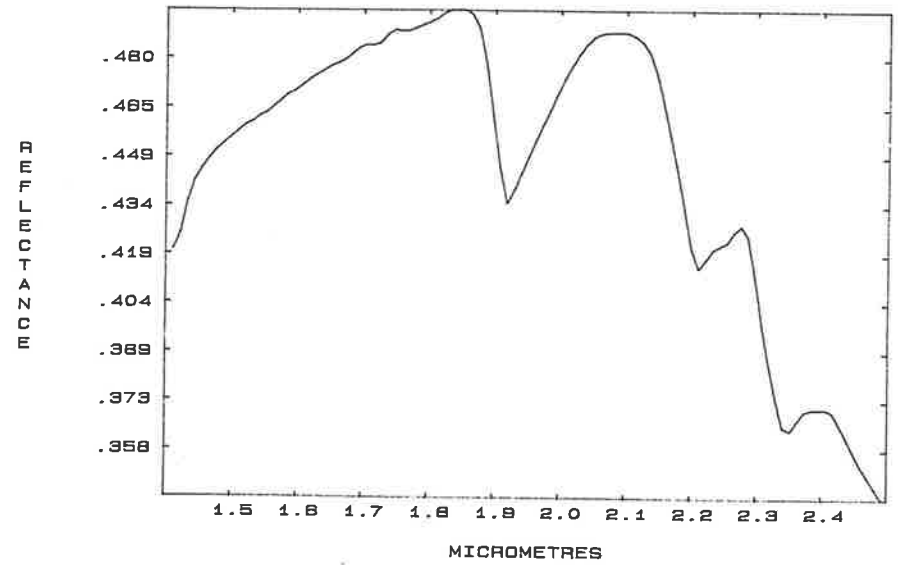
K3/70/S Q85 CAL5 AB5 AMP4 TC2/KA0<5, HE<5



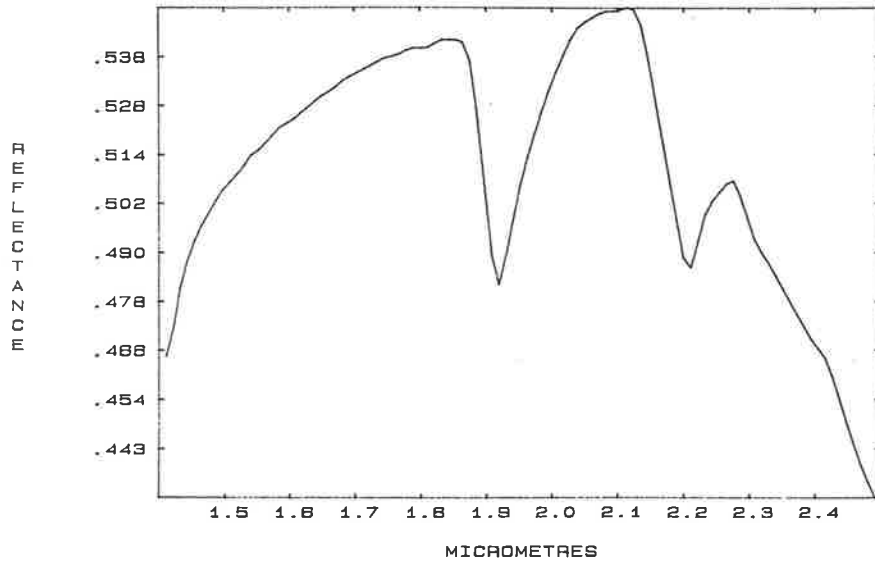
K4/134/F/W Q82 TC8 AB5 CHL4/KA0<5, HEM<5



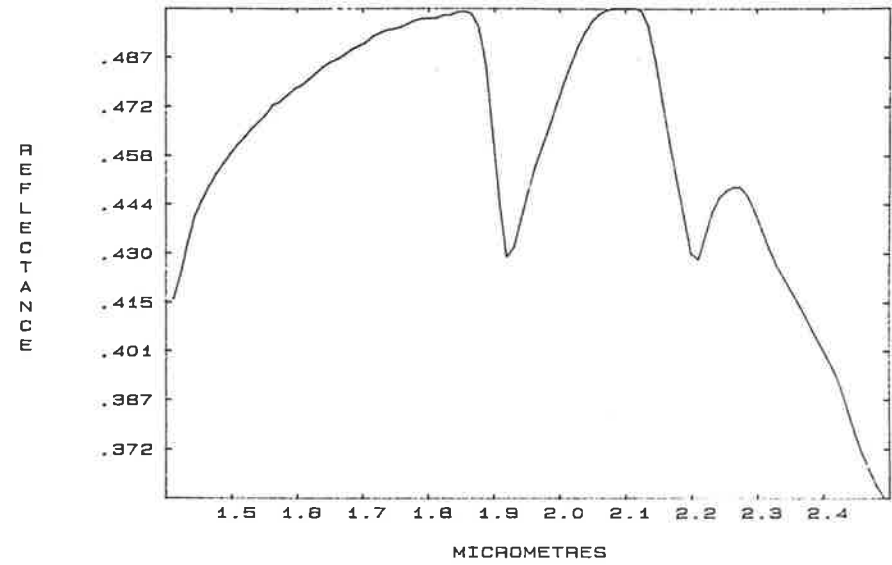
K4/332/F/W AMP54 CHL28 PL12 Q8/EP<5



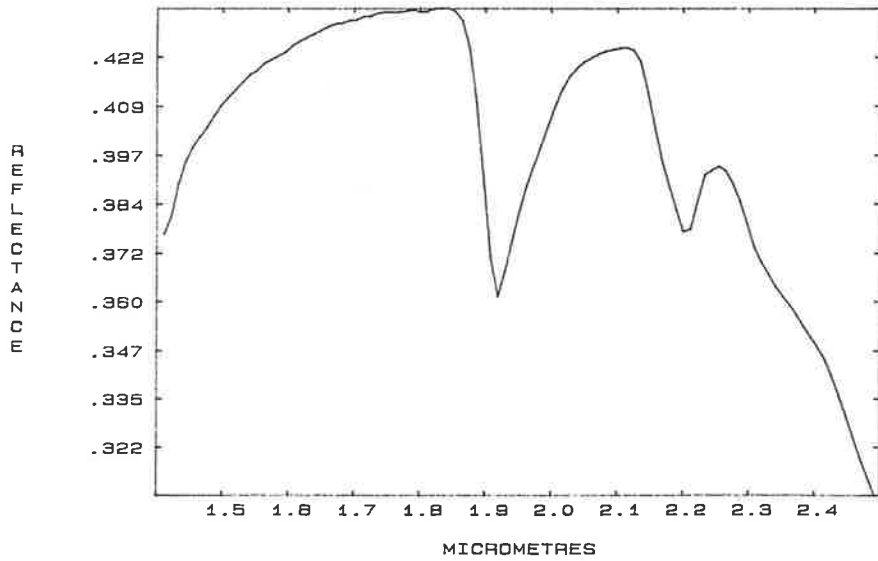
K7/194/S Q75 CAL23 AB2/HEM<5



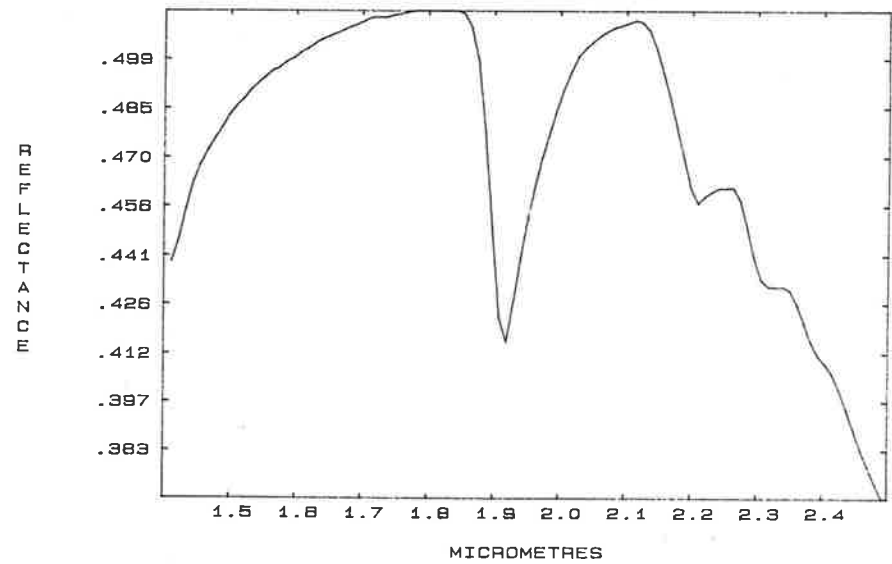
K7/221/S Q92 AB5 CAL4/KAO<5, HAL5-10, HE<5



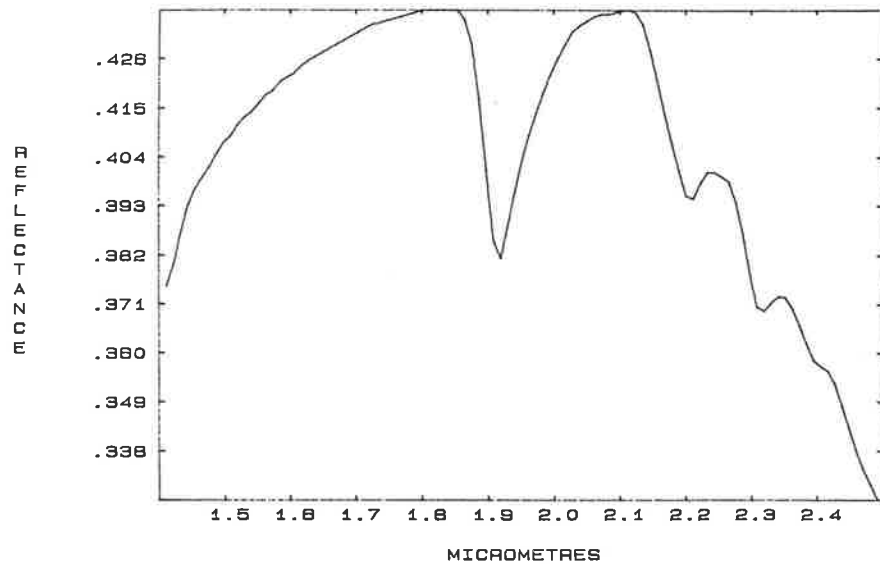
K7/310/S Q98 AB2/HEM<5



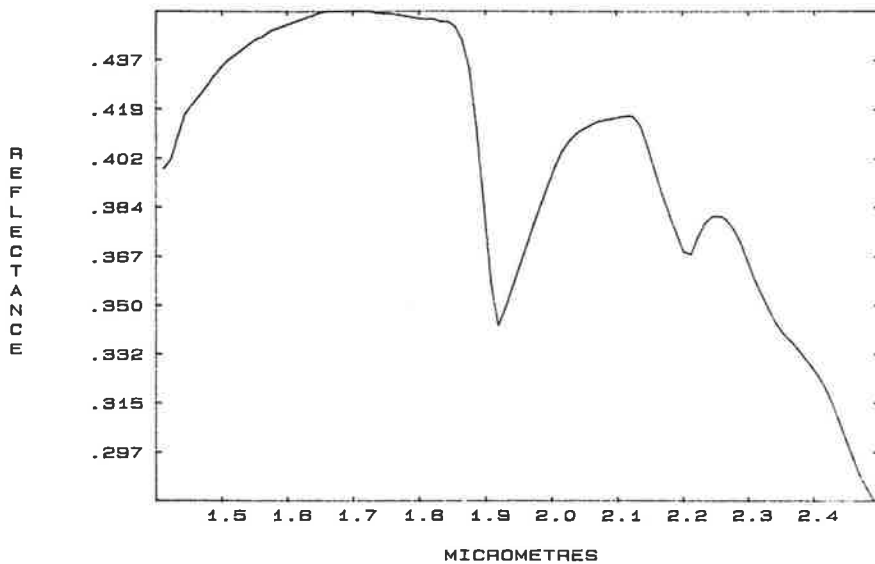
K10/376/S Q63AB11CAL9AMP8TC4/KA0, HEM, M05



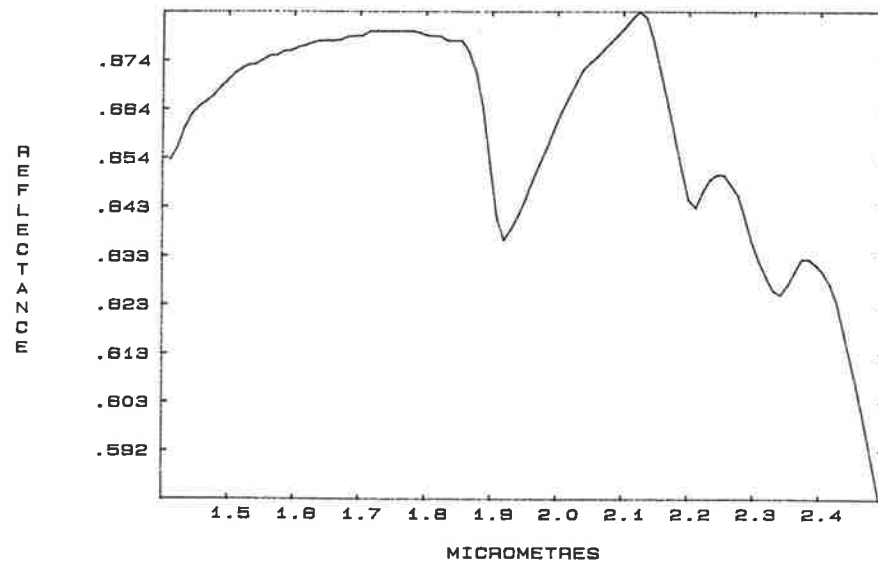
K11W/15/S Q62 TC13 AB10 CHL8 AMP8/HEM<5



K14/31/S CAL75 Q20 TC5

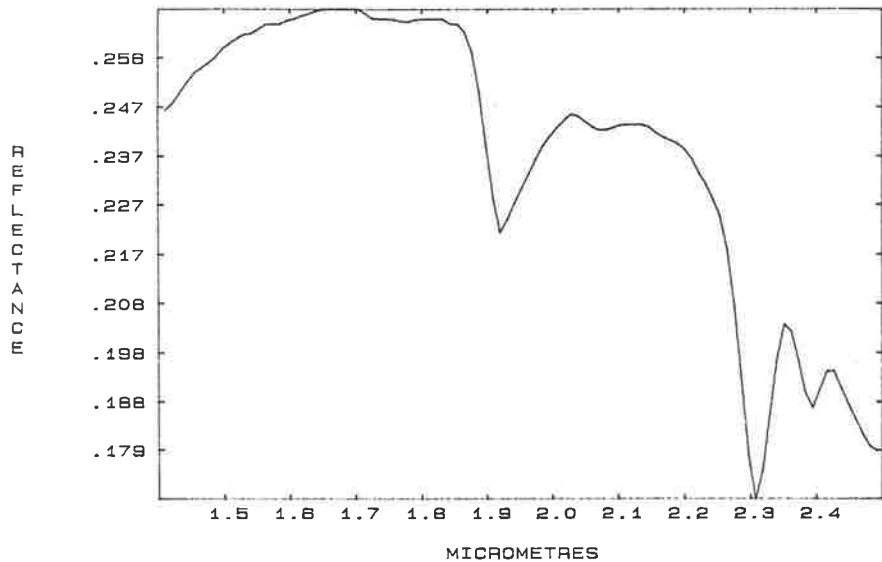


K14/31/S/P CAL75 Q20 TC5

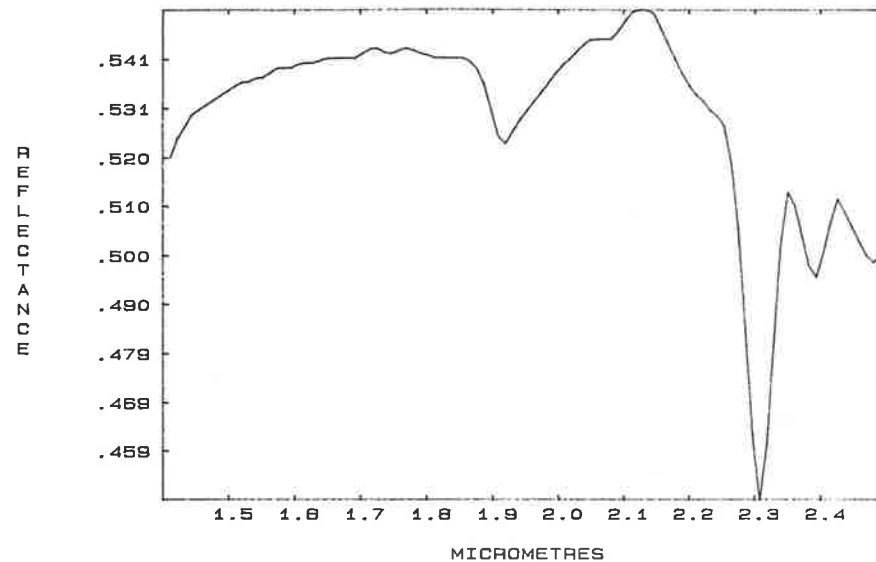


TALC SPECTRA

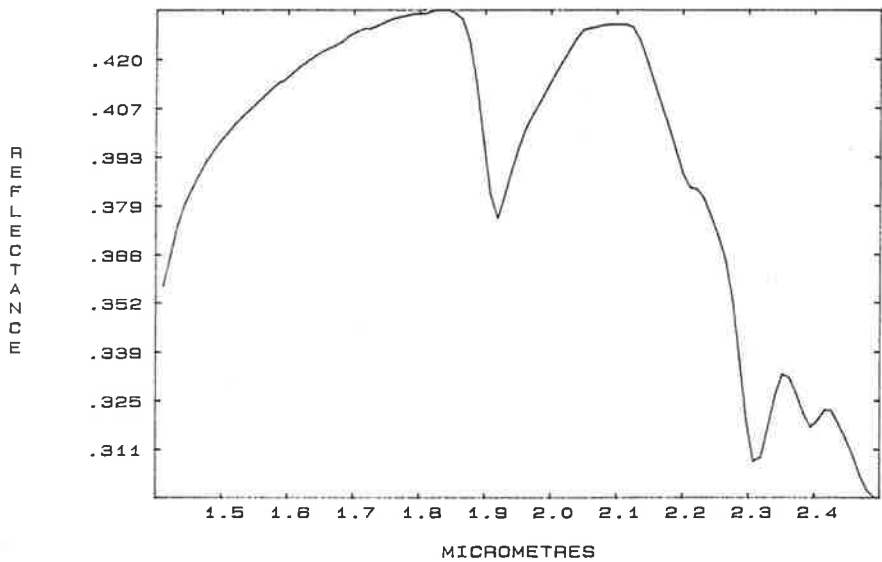
K1/103/F1/W TC77 AMP9 CHL8 PL3 Q1 BI1



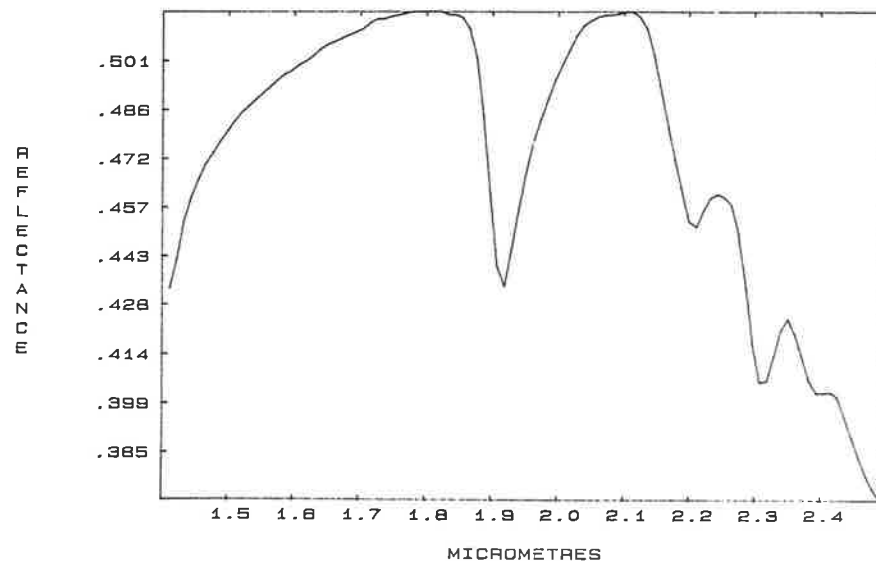
K1/103/F1/P TC77 AMP9 CHL8 PL3 Q1 BI1



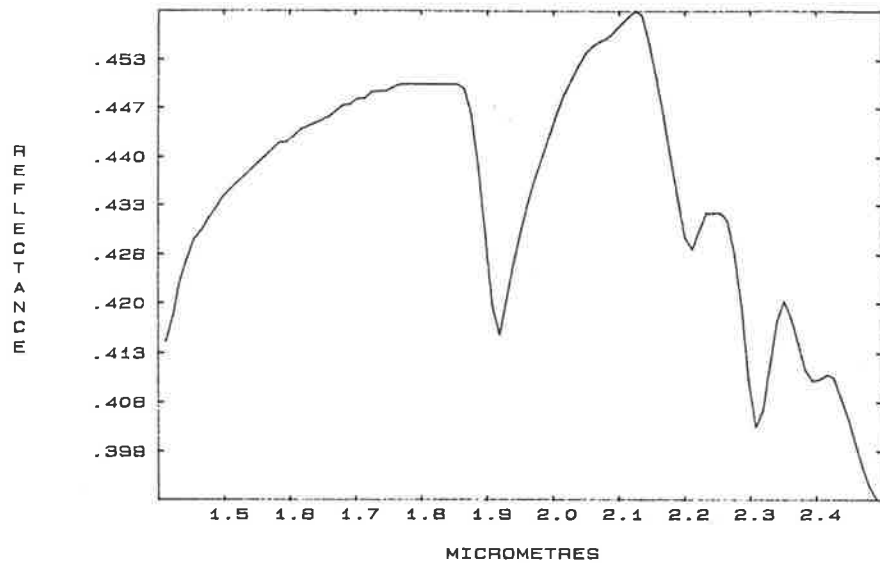
K2/370/S Q58 TC25 CHL7 AMP5 ANT3 CAL2 GO



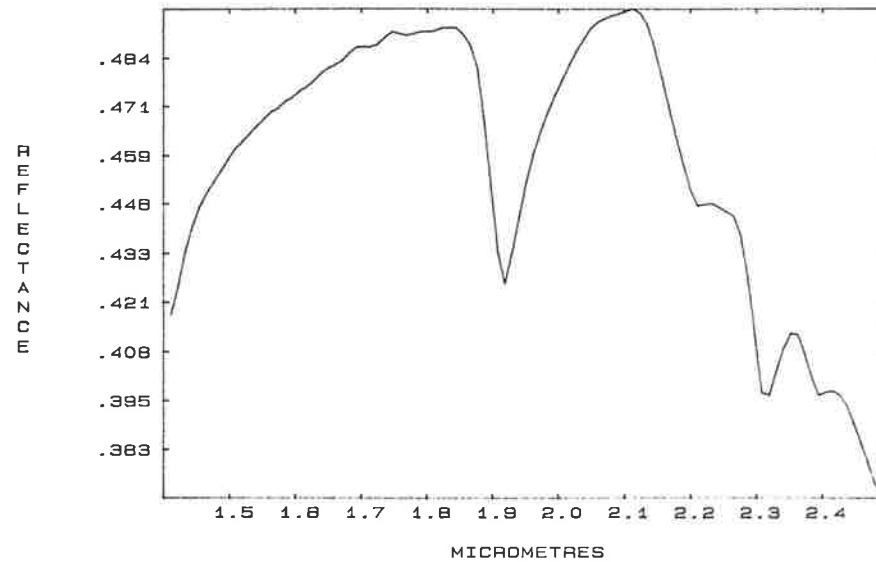
K2/470/S Q43 TC40 CHL12 AB4 BI1/HEM<5



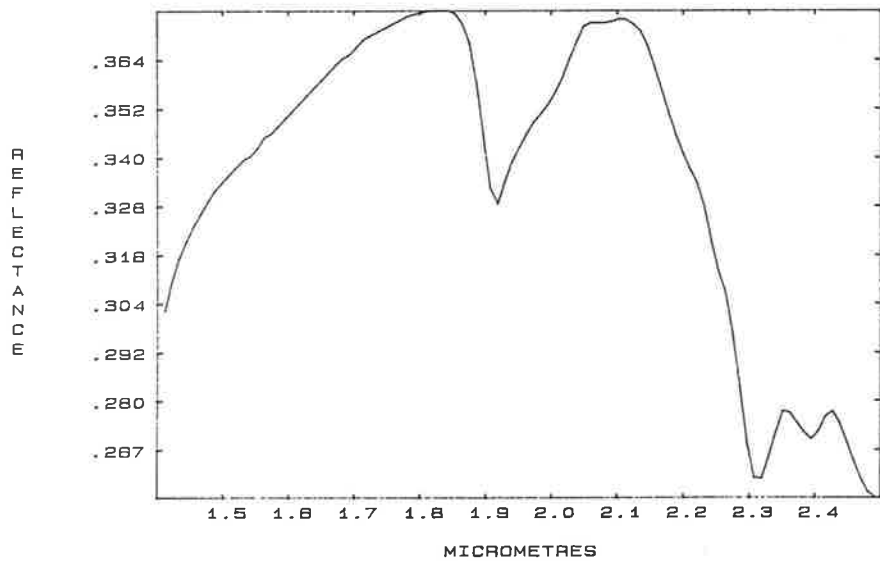
K2/470/S/P Q43 TC40 CHL12 AB4 BI1/HEM<5



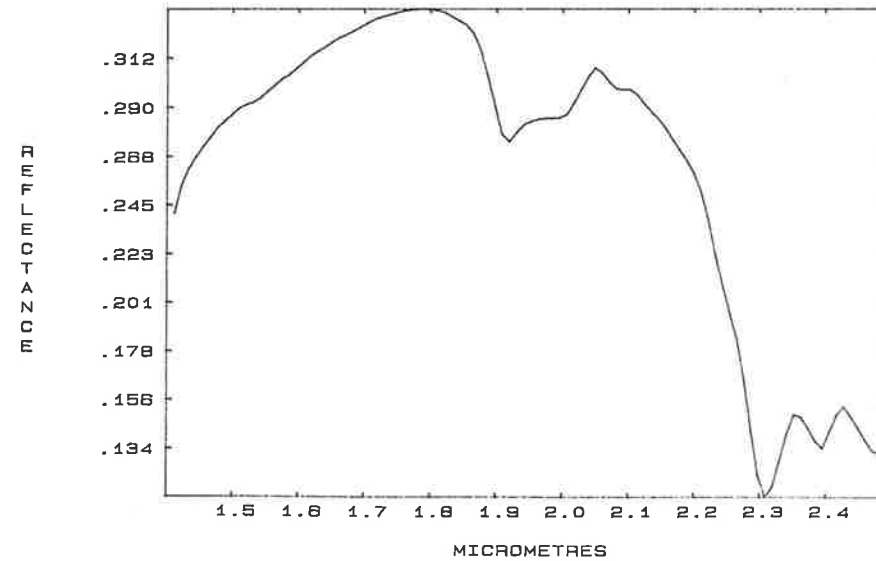
K3/88/S Q78 TC8 AB6 AMP4 CHL3/KA0<5, HE<5



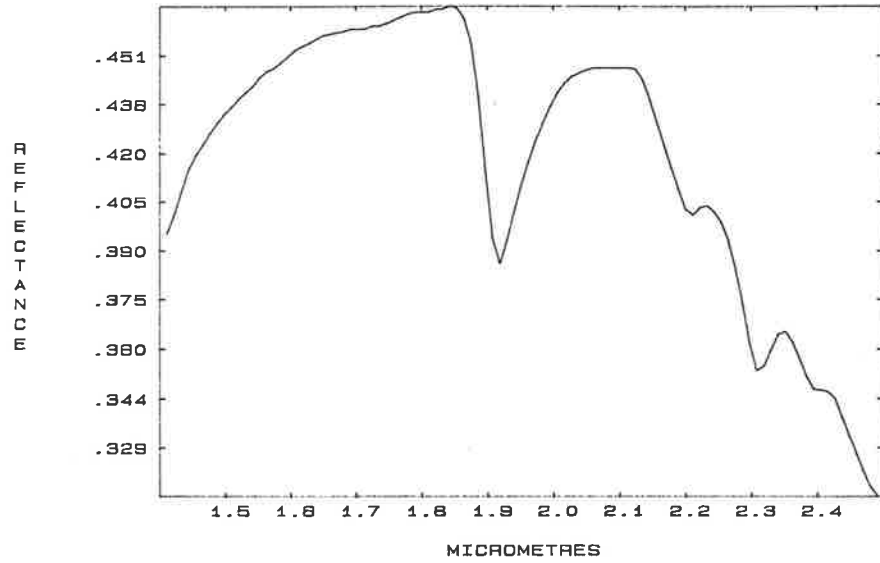
K3/120/F Q48 TC29 CHL16 AB4 AMP3/KA0<5



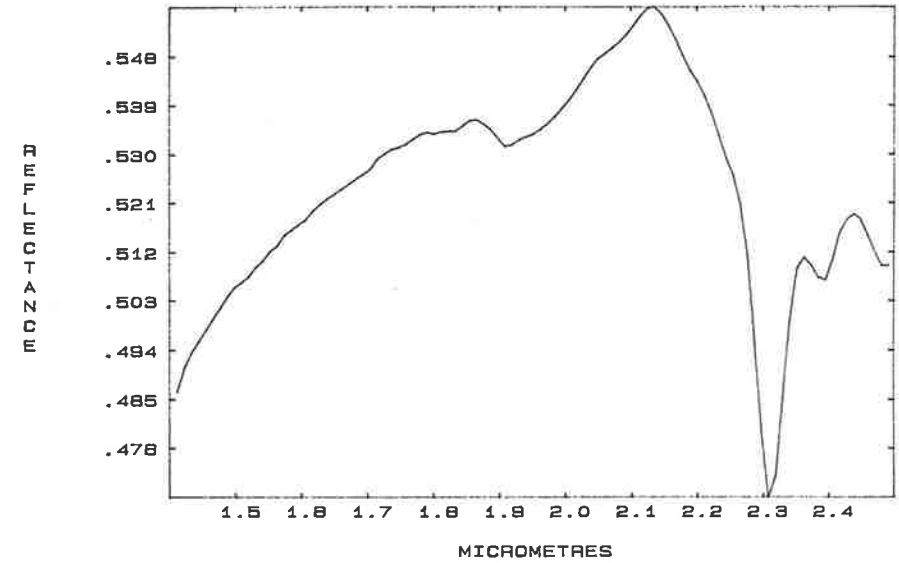
K4/143/F/W TC87 Q19 CHL15/KA0<5, HEM<5



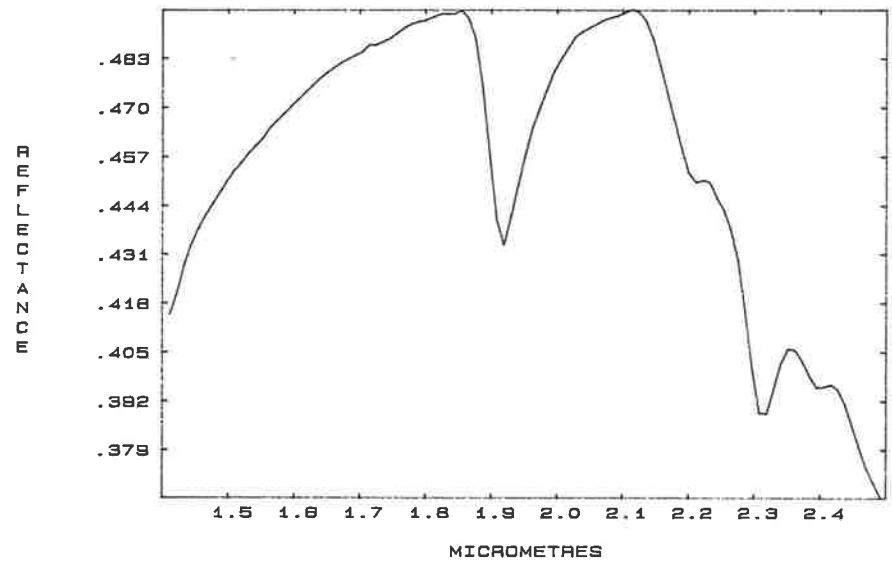
K4/144/S Q57 TC22 CHL12 AMP5 AB3



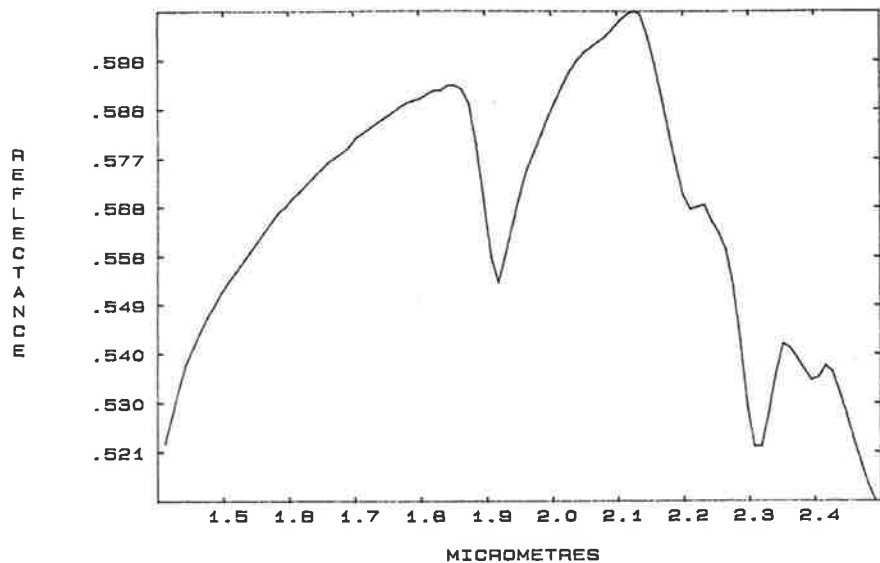
K8/277/F/P TC88 CHL30 AB3 Q2/HEM5-10



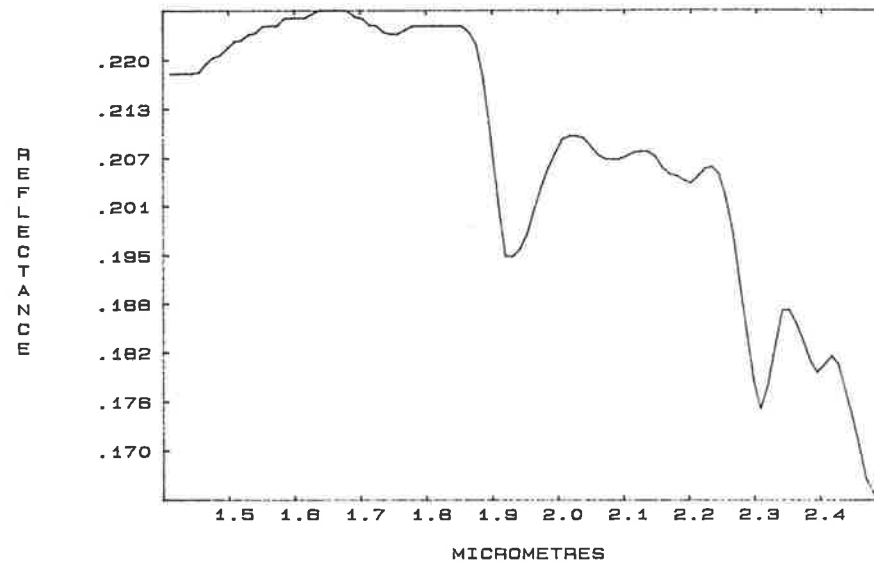
K9/202/S Q44 TC25 AB15 CHL14 DOL2 CAL1



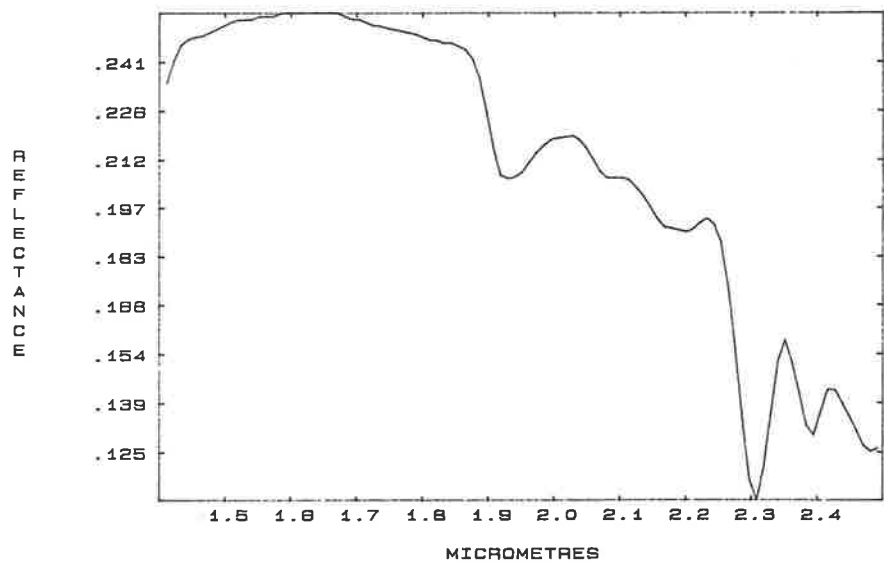
KB/202/S/P Q44 TC25 AB15 CHL14 DOL2 CAL1



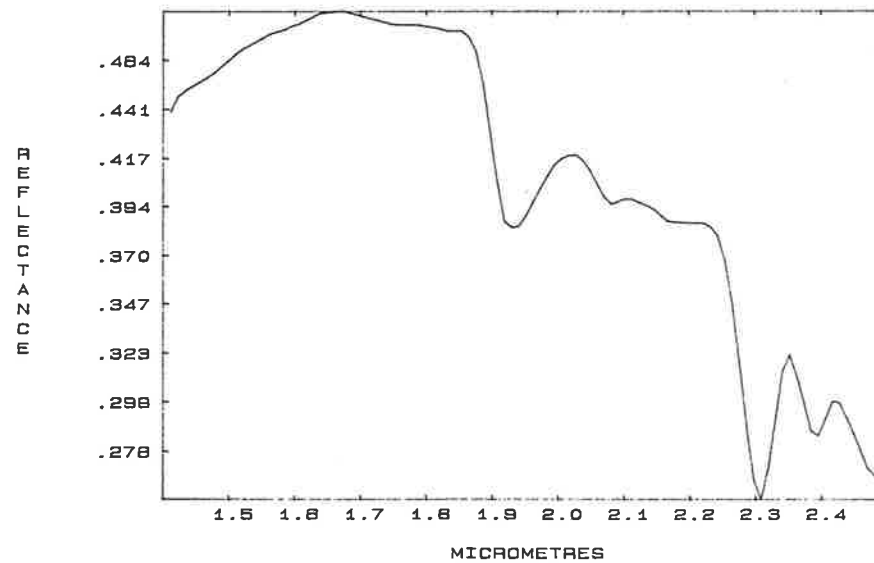
25-11-83 K10/304/F1/W



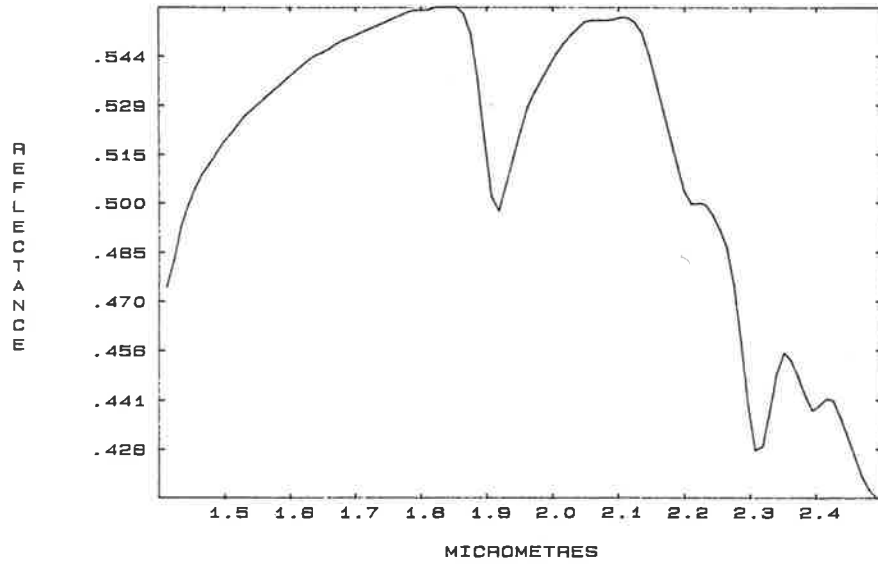
K10/304/F3/W TC98 CHL3 MAG1/HEM<5



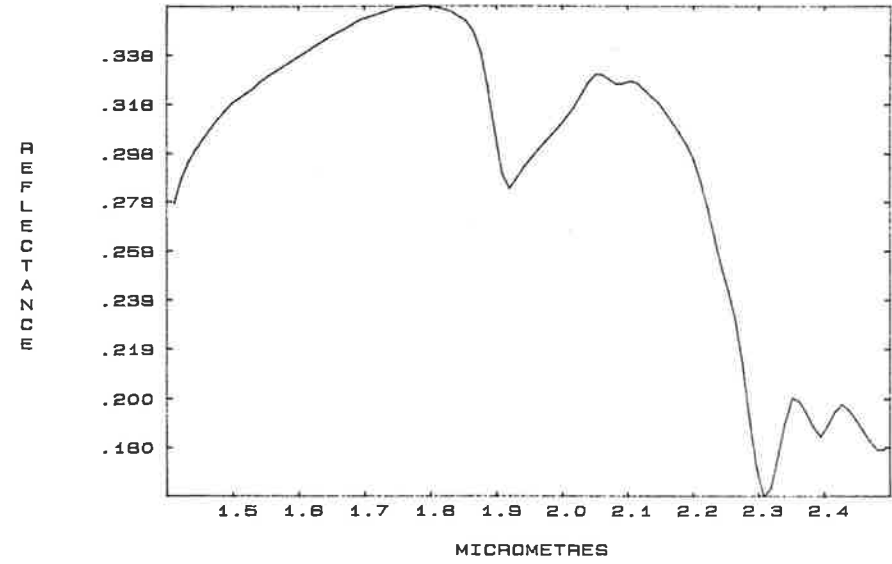
K10/304/F2/W TC98 CHL3 MAG1/HEM<5



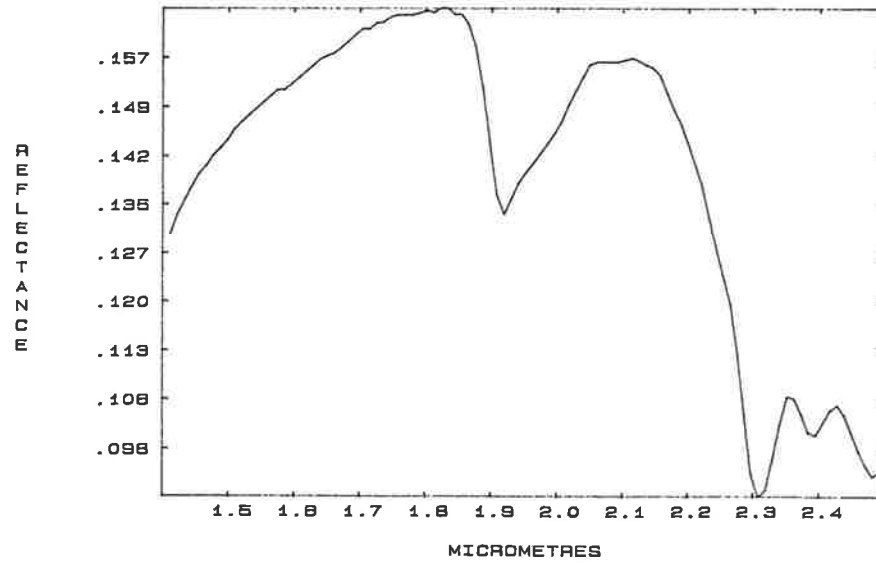
K11W/87/S Q85 TC19 AB10 CHL8



K11W/87/F/W TC70 CHL24 Q9 DOL3

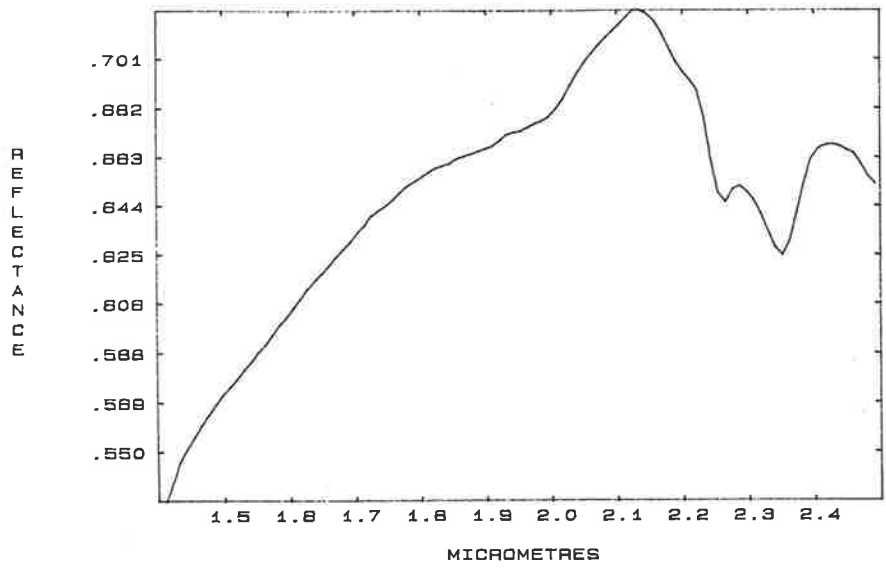


K13/20/F/W TC39Q24AB17CHL11ANT4AMP3/HE<5

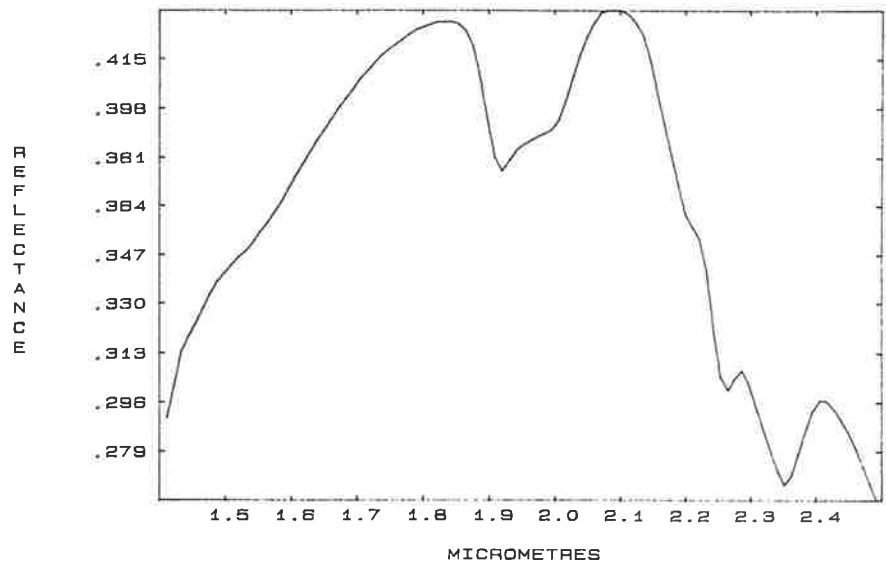


CHLORITE SPECTRA

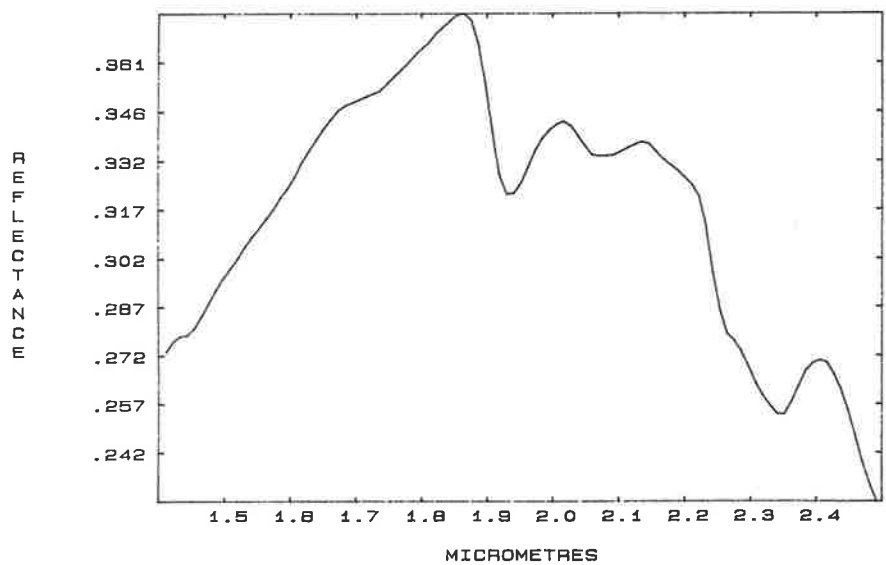
K1/41/F/P Q48 CHL45 PL5 AMP3 BI1



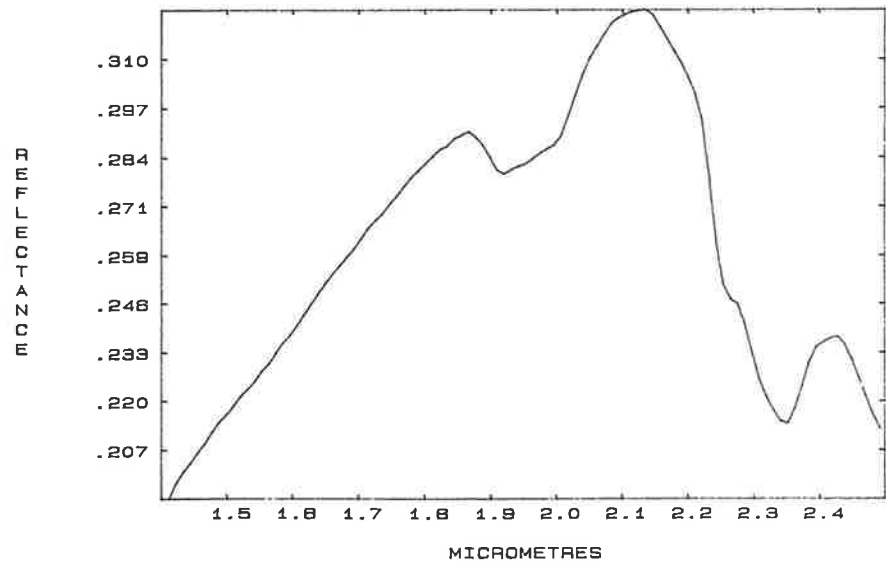
K4/123/F/W CHL42 Q34 PL23



K11W/72/F/W AB34 CHL25 DOL23 Q18

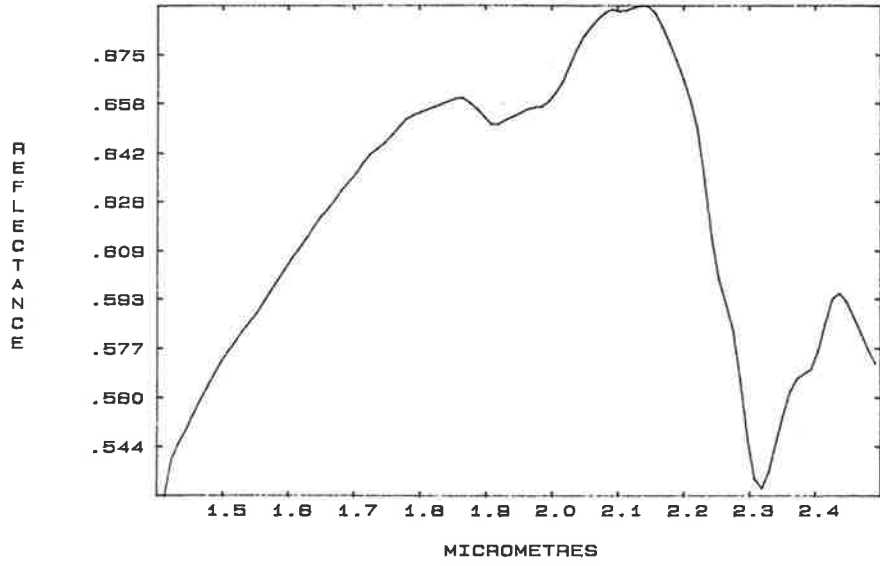


K11W/72/F2/W AB38 CHL25 DOL13 TC1/60<5

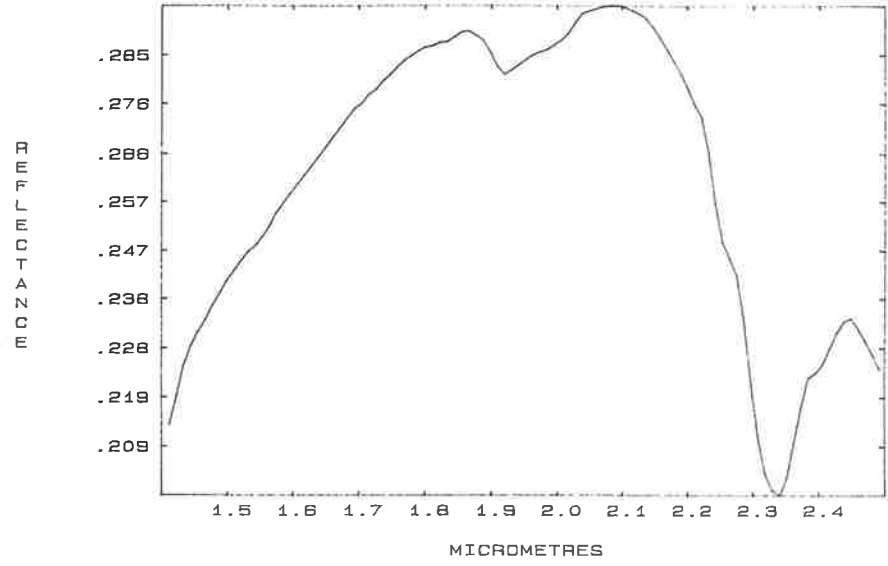


AMPHIBOLE SPECTRA

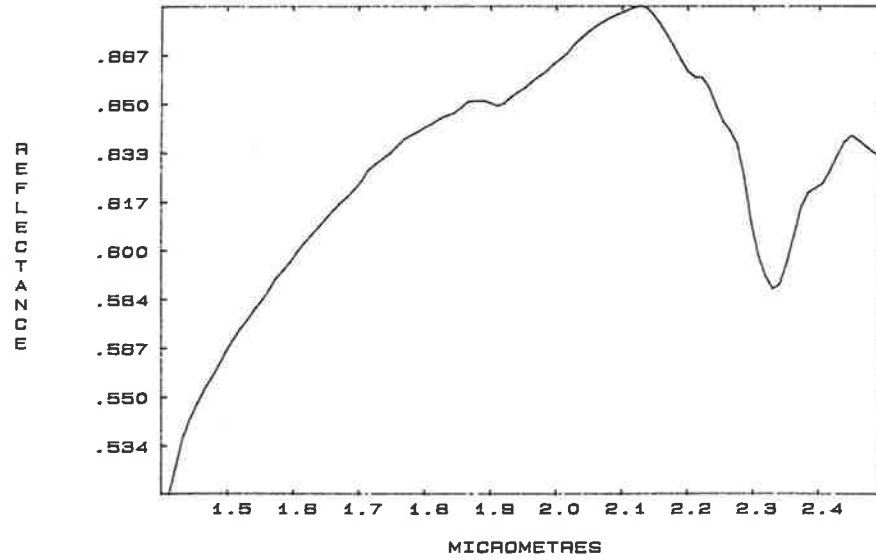
K1/31/F/P AMP50 CHL43 Q4 TCS



K1/74/F1/W AMP70 PL18 CHL7 Q5

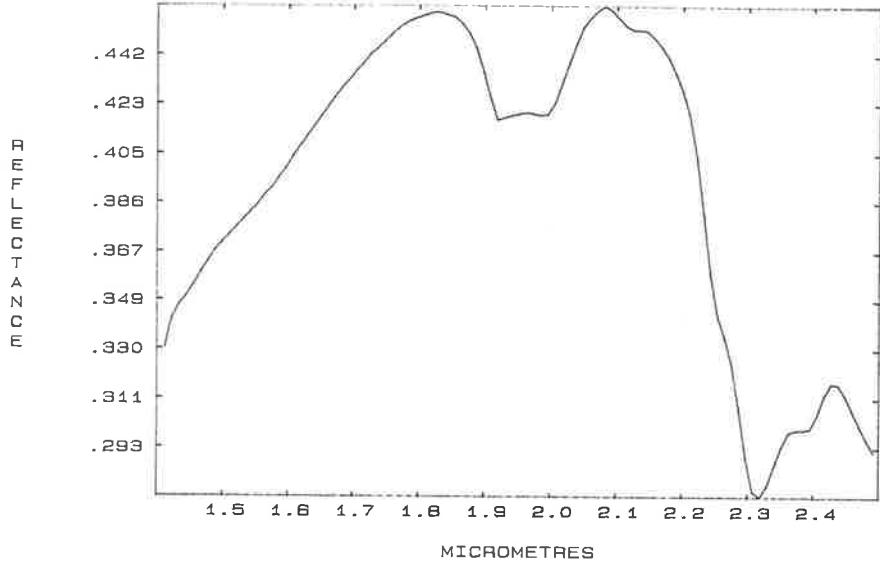


K1/74/F1/P AMP70 PL18 CHL7 Q5

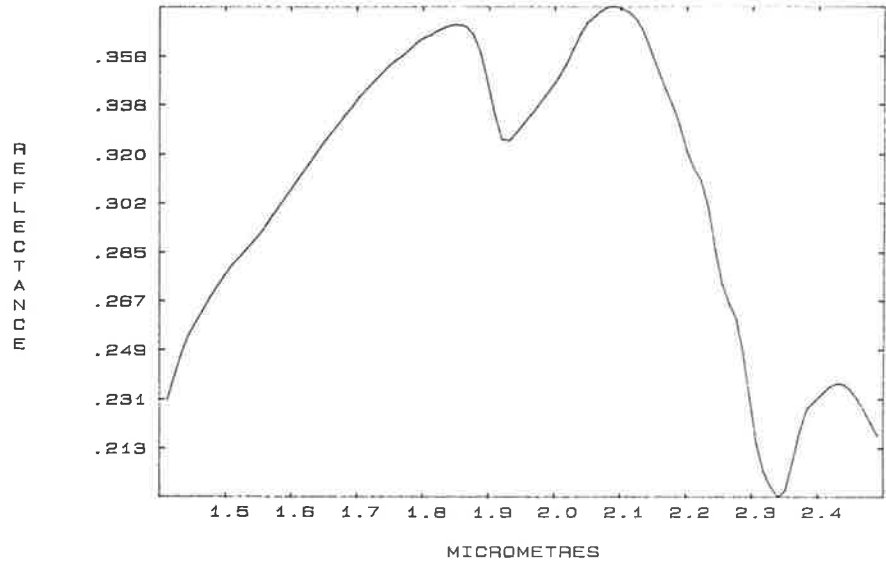


SPECTRA WITH 2.3 MICROMETRE FEATURES DUE TO MIXTURES, OTHERS

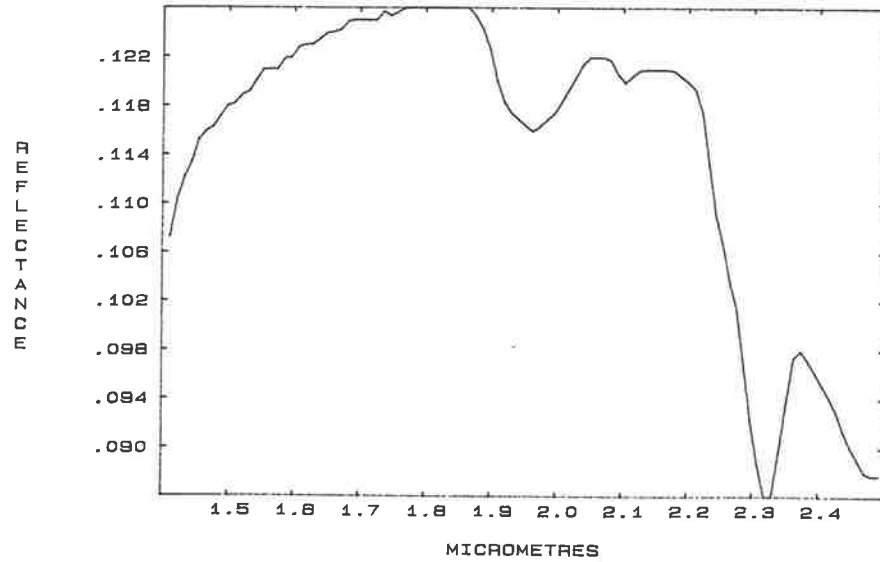
K1/31/F/W AMP50 CHL43 Q4 TC3



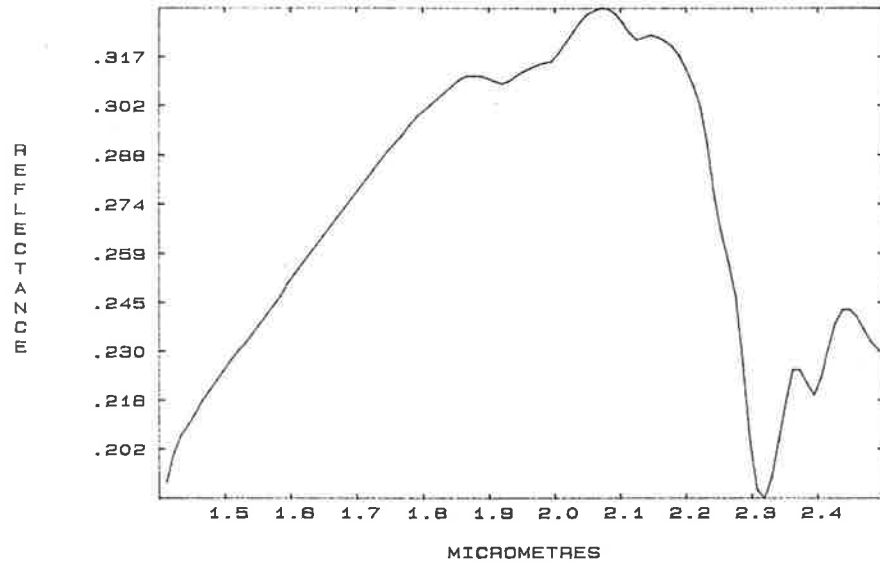
K1/41/F2/W Q46 CHL45 PL5 AMP3 BI1



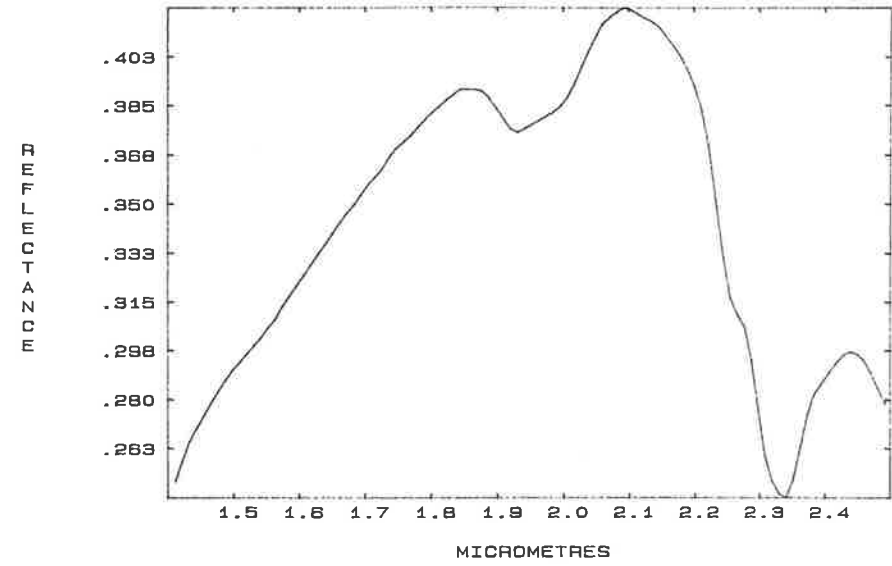
K3/111/F/W ANT100



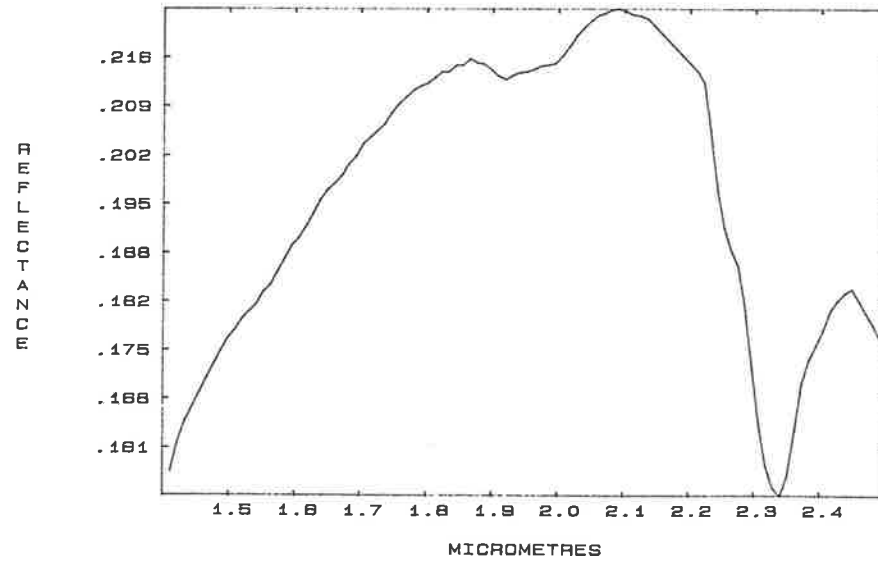
KB/440/F/W AMP38 AB25 Q21 CHL18/EP5-10



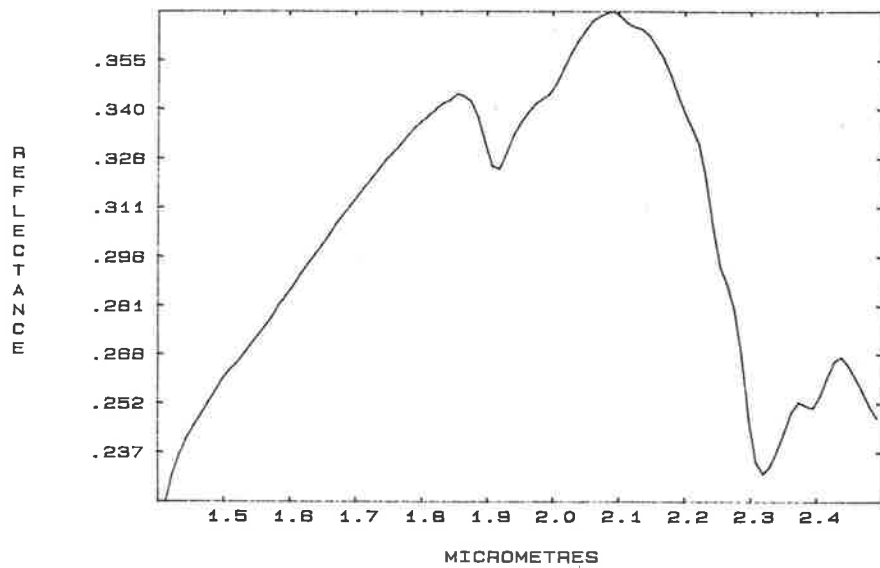
KB/448/F2/W2 AMP42 CHL25 Q20 AB14/EP10



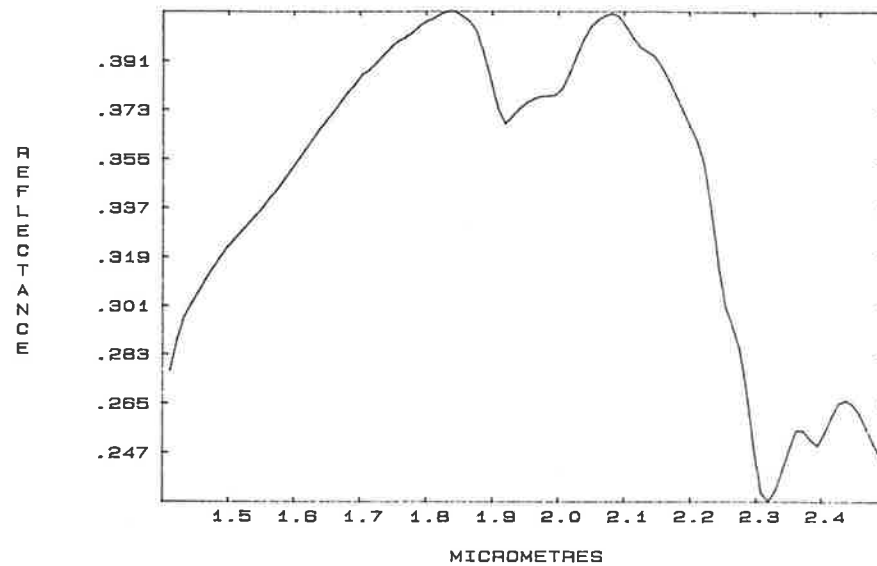
KB/448/F2/W1 AMP42 CHL25 Q20 AB14/EP10



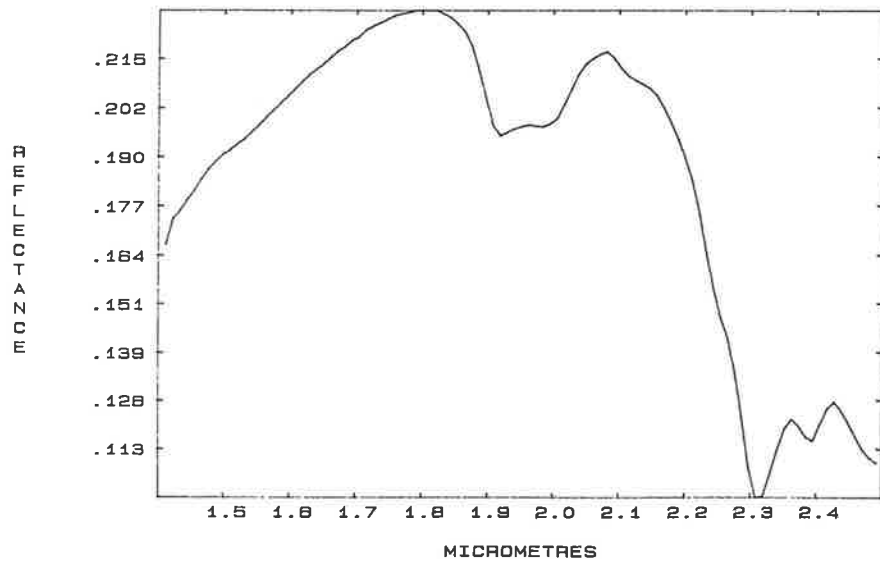
K7/155/F/W AMP48 AB25 CHL22 Q5



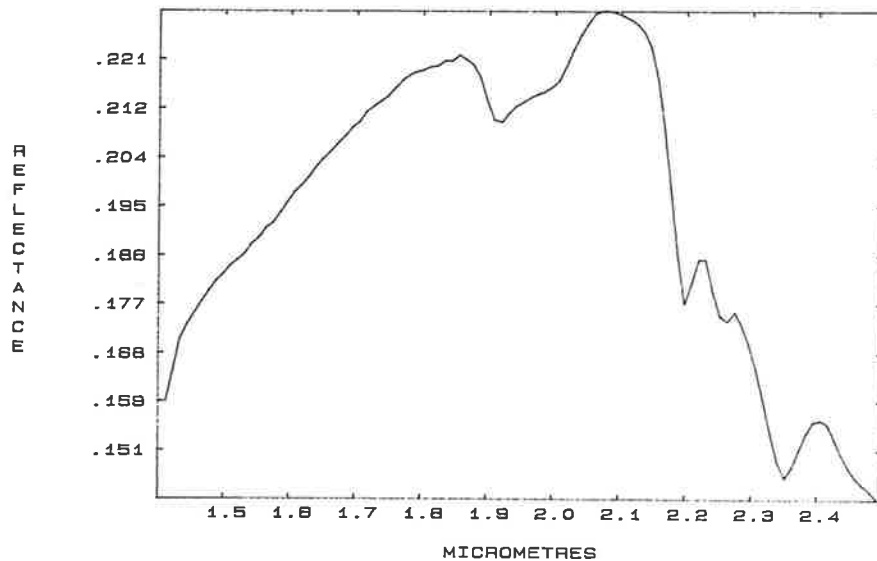
K7/180/F/W TC81 CHL33 PL4 AMP1



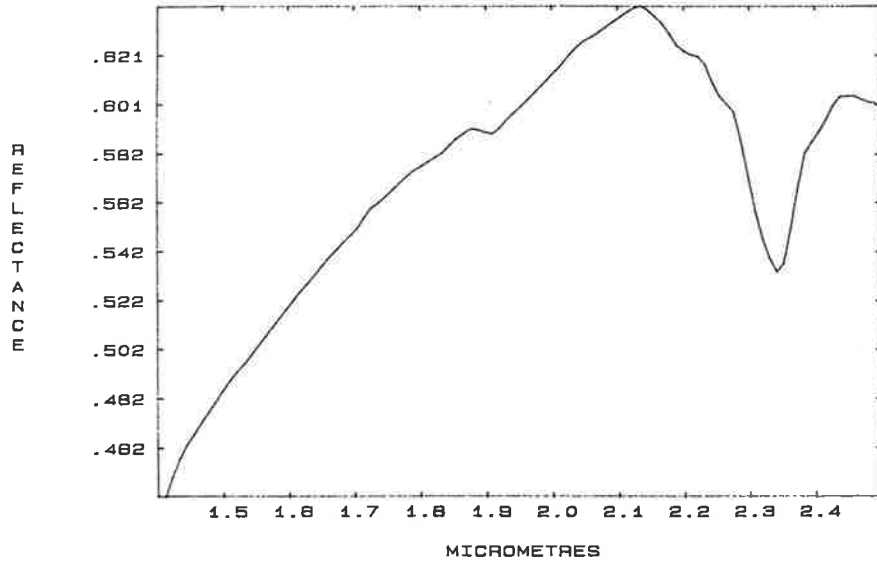
K7/268/F/W AMP44 CHL32 TC23



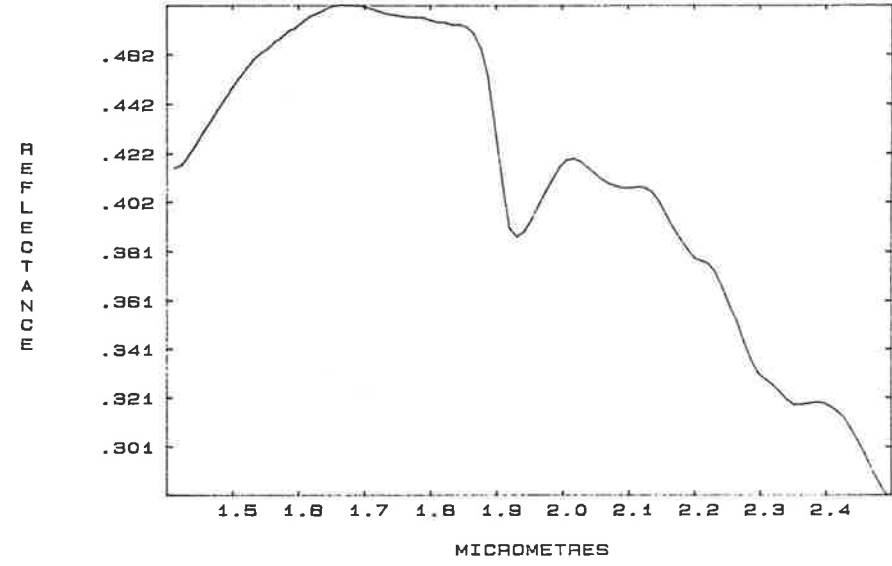
K8/141/F/W AMP74 AB15 Q8 CHL3/EP5-10



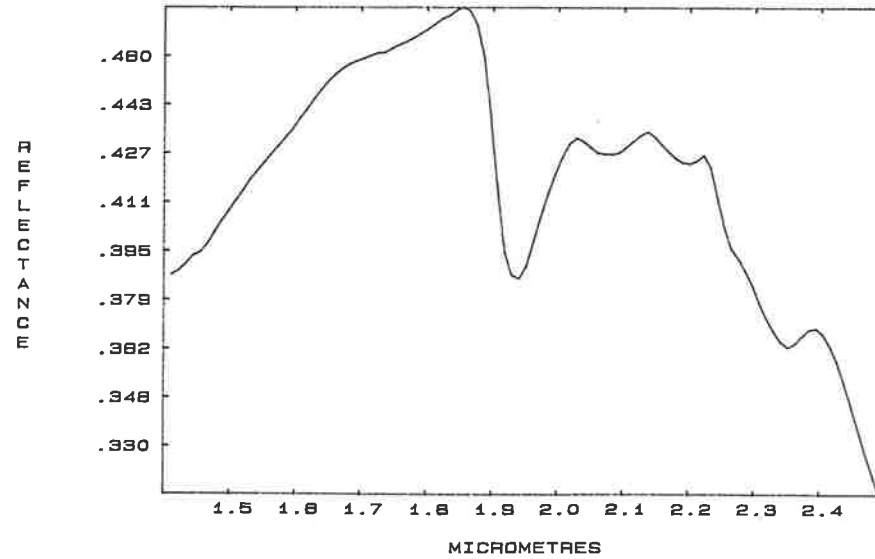
K9/141/F/P AMP74 AB15 Q8 CHL3/EP5-10



K10/273/F/W PL90 Q8 CHL2/DI40-50



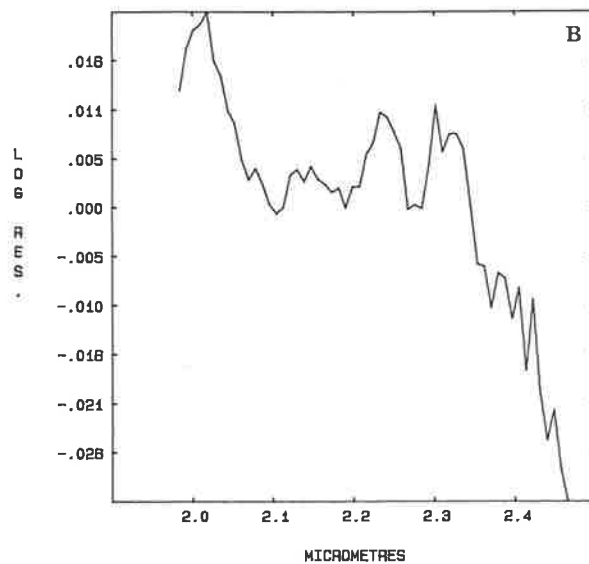
K13/35/F/W Q33 DDL25 AB18 CHL16 CAL4 AMP



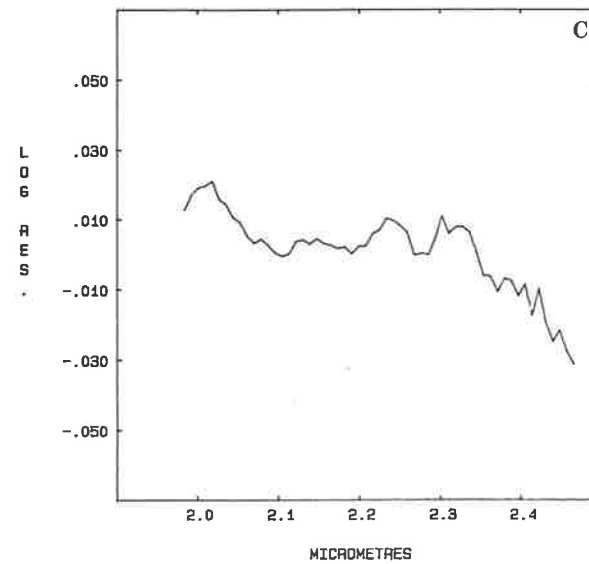
APPENDIX IX Interpretation of data from flight line K2 - SWIR laboratory reflectance and airborne log residual spectra.

The bulk of the spectral data (airborne and laboratory) from flight line K2 are presented here. Each row of plots has been derived from a single 'block' along the flight line (each block having been delineated from images of the log residual data - see Figs. 6.15a-d). Data from two 'blocks' appear on each page. Where the laboratory spectrum of one or more samples have been measured, a representative spectrum has been included in the first column (Plot A). The second column (Plot B) represents log residual airborne data plotted utilising the maximum range on the y-axis scale, which gives the best definition of spectral features. The last column of each row (Plot C) represents the same airborne log residual data plotted on a constant y-axis scale to allow an appreciation of the relative strength of absorption from different blocks.

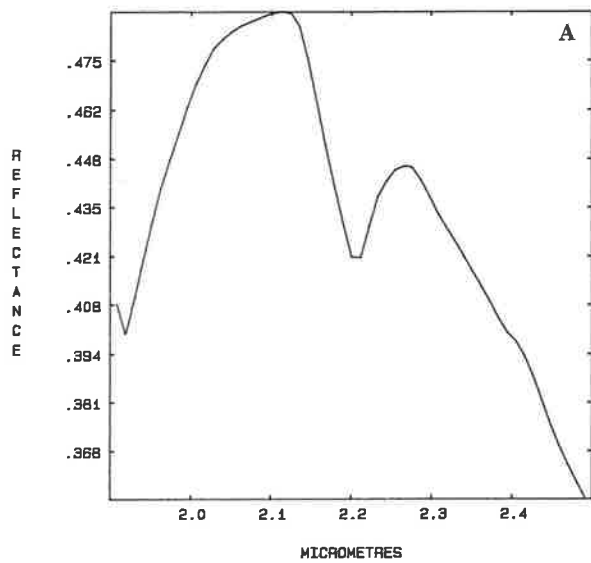
SA. 4-42



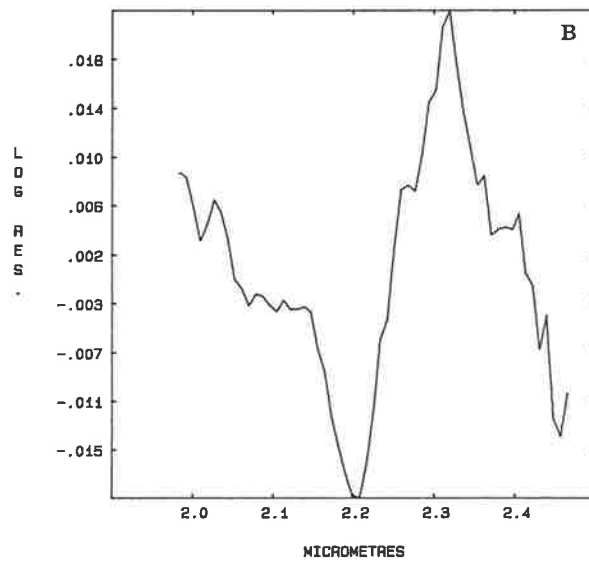
SA. 4-42



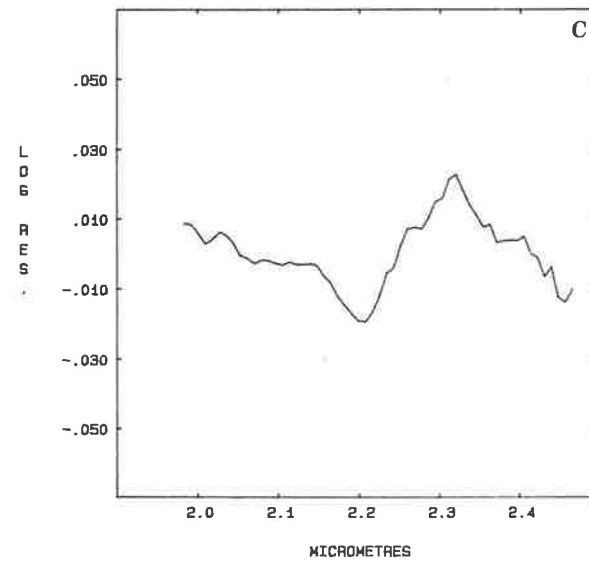
B-12-83 K2/50/S

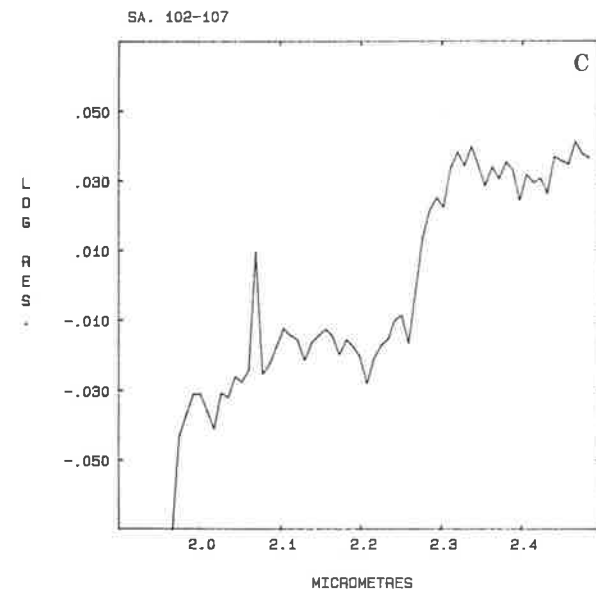
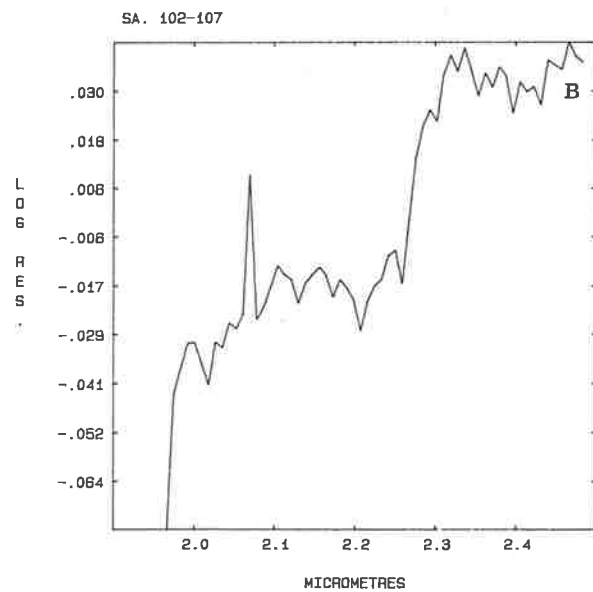
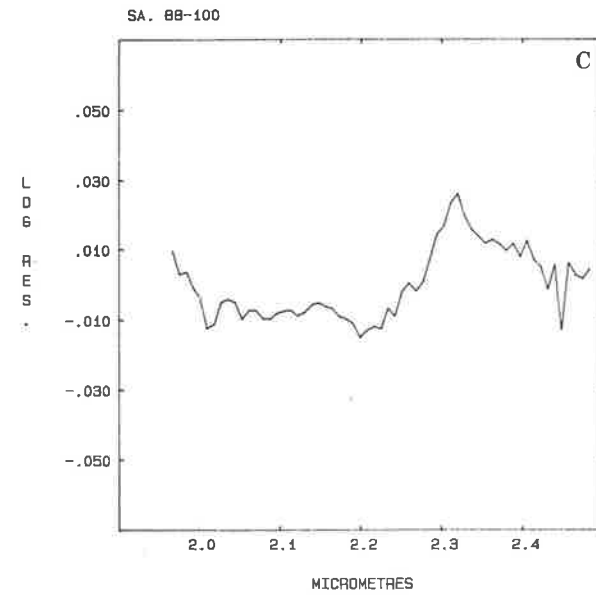
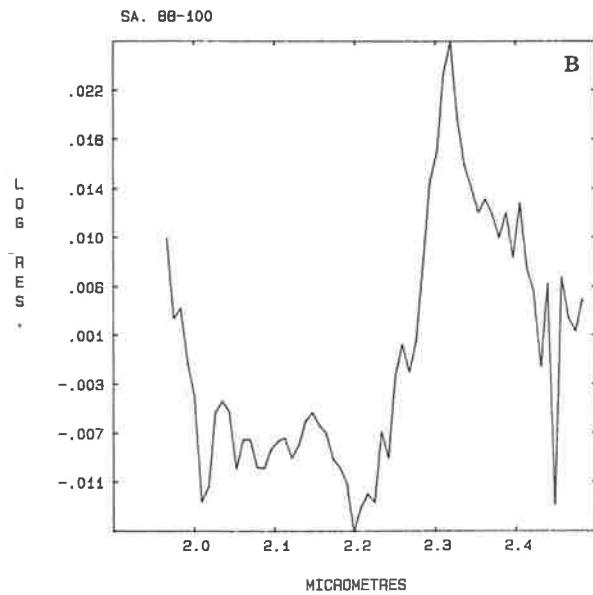
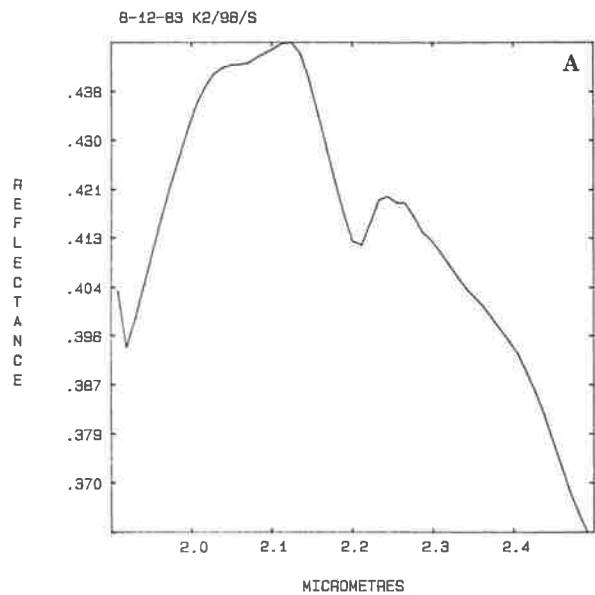


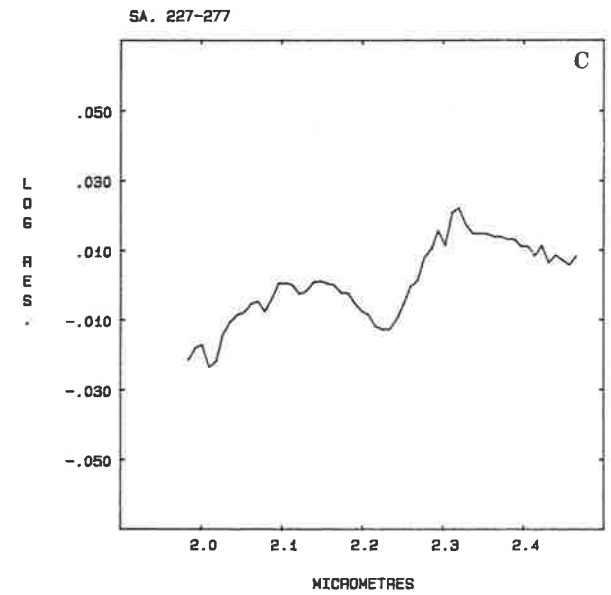
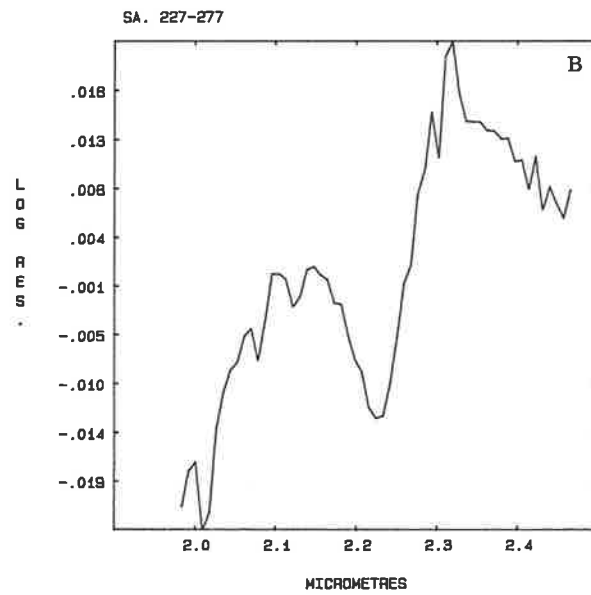
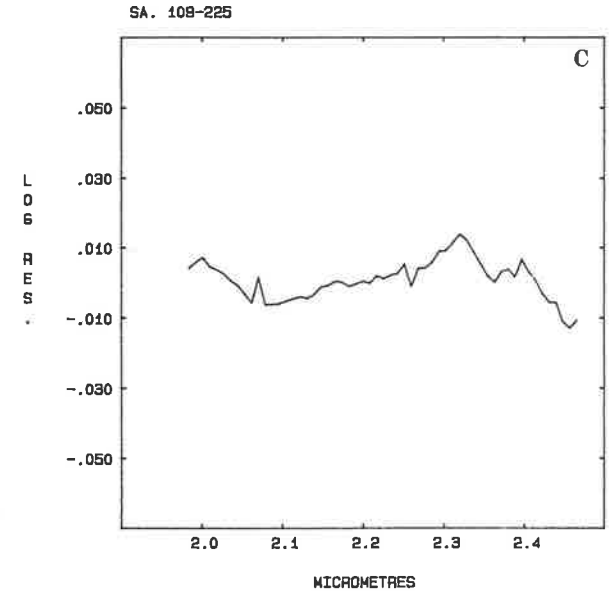
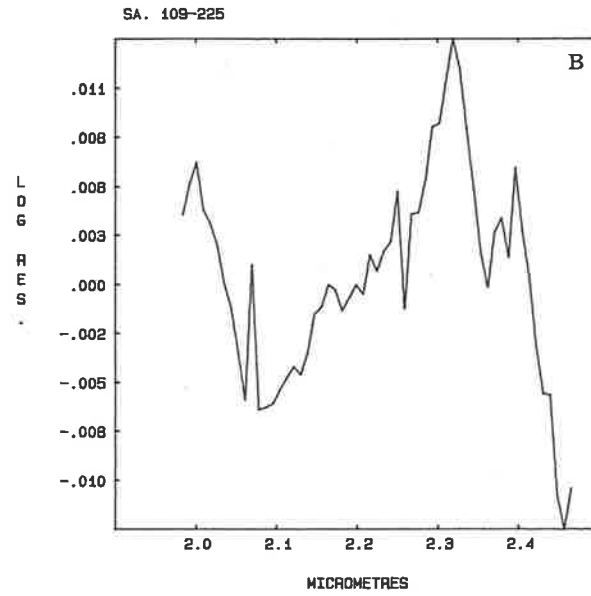
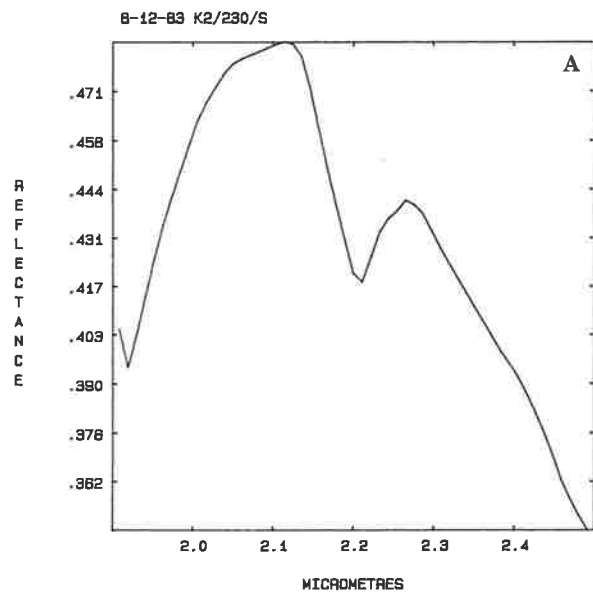
SA. 44-86

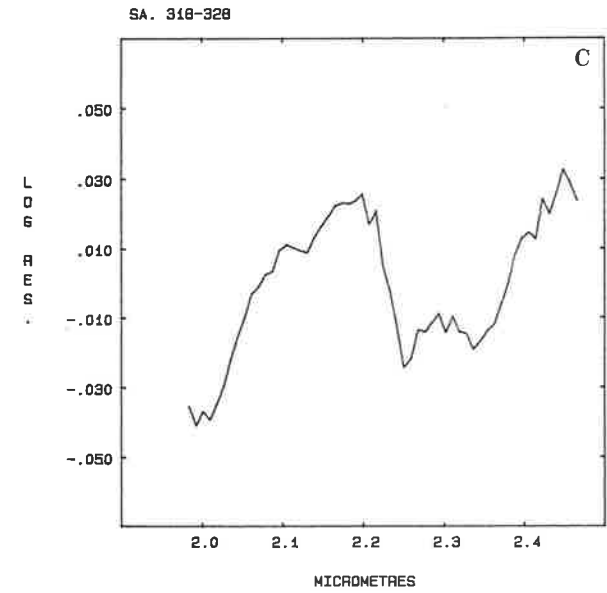
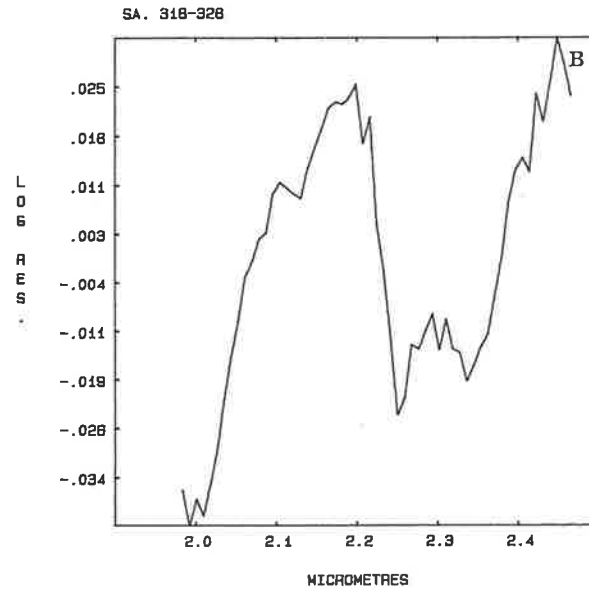
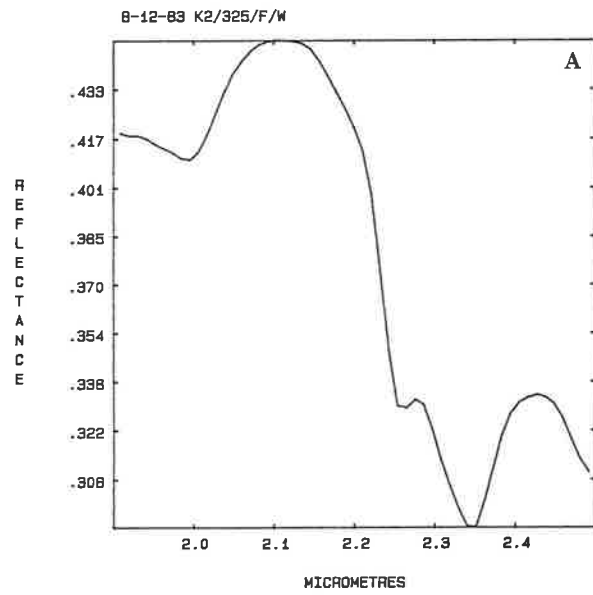
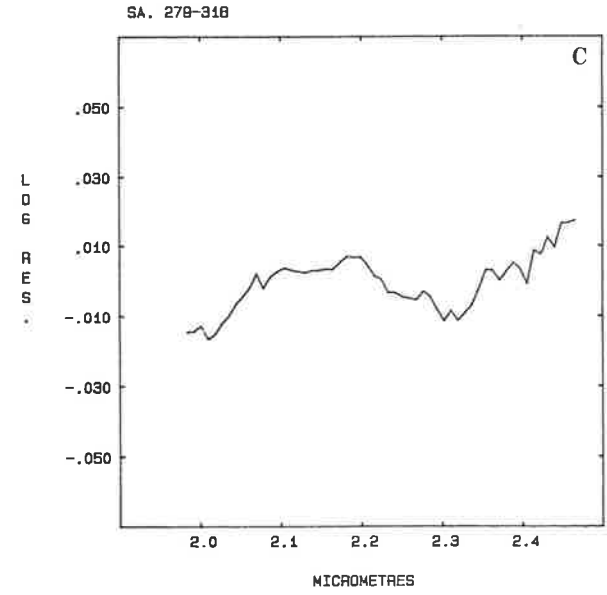
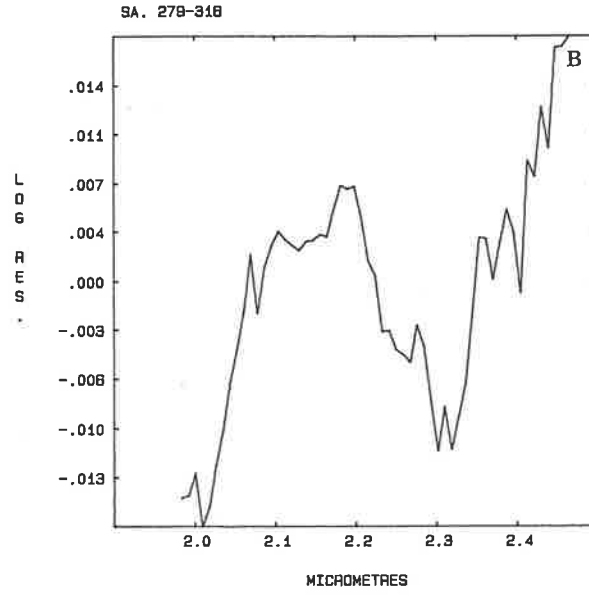
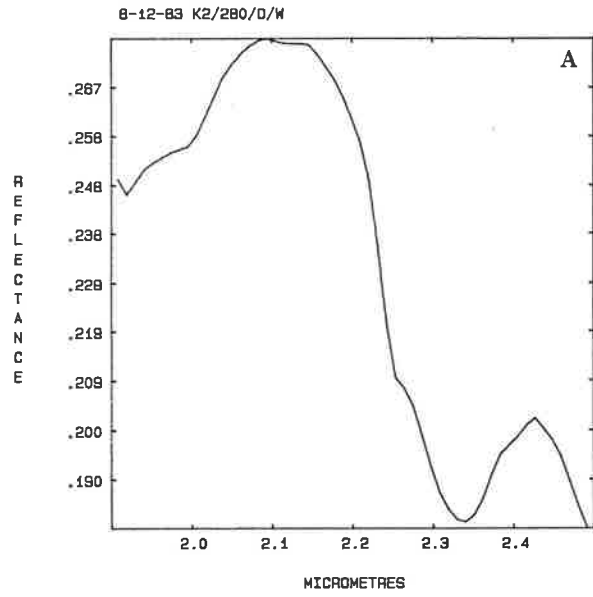


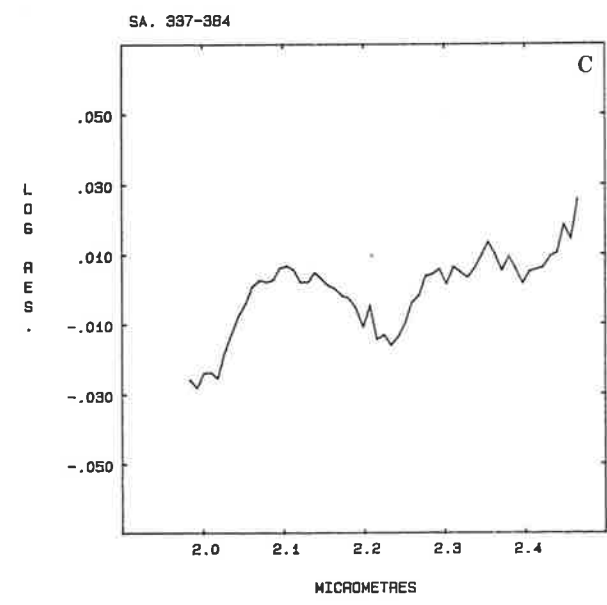
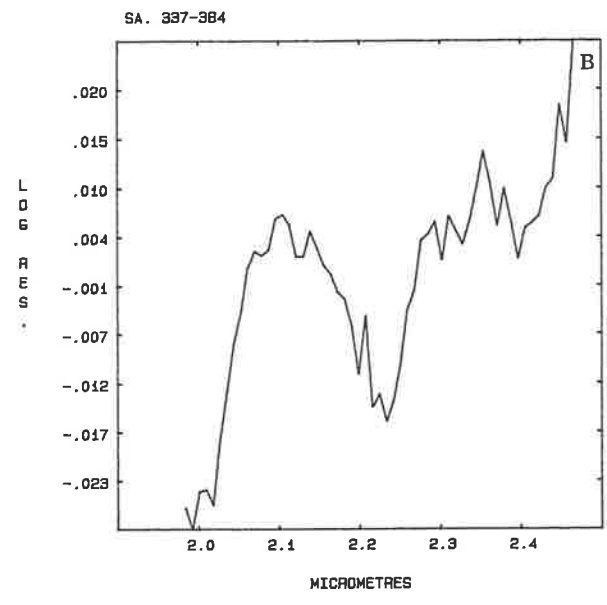
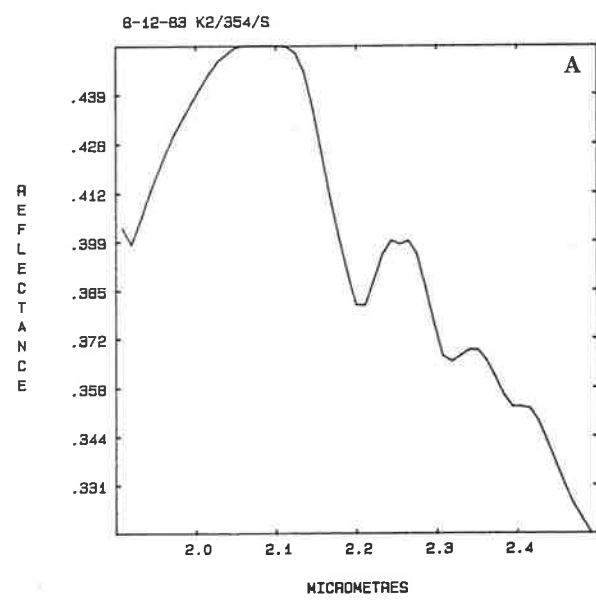
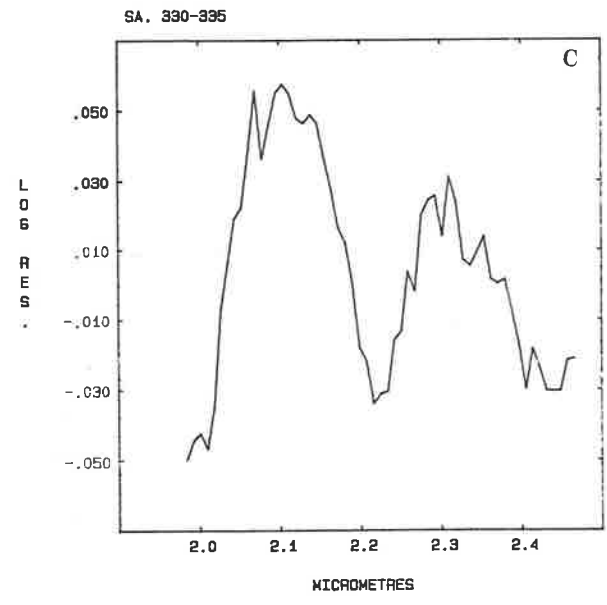
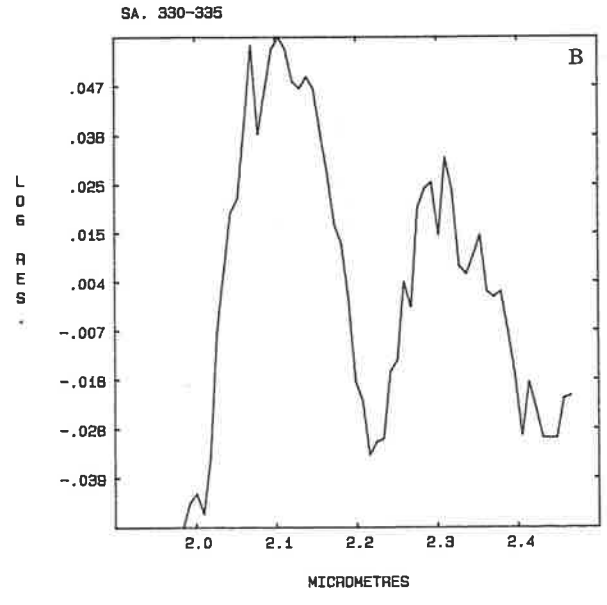
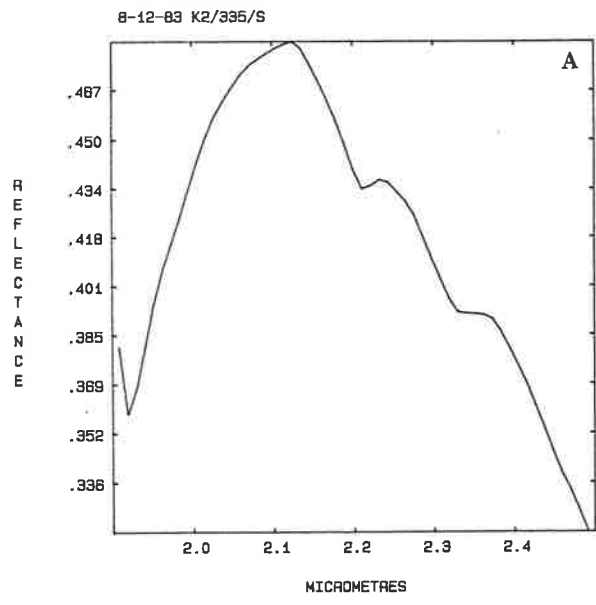
SA. 44-86



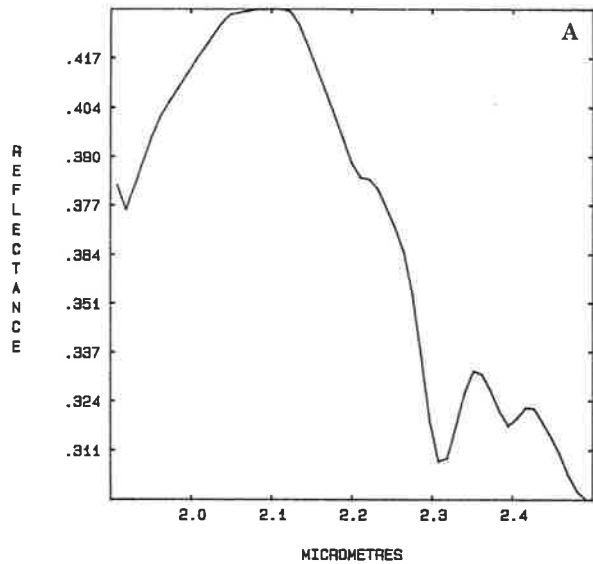




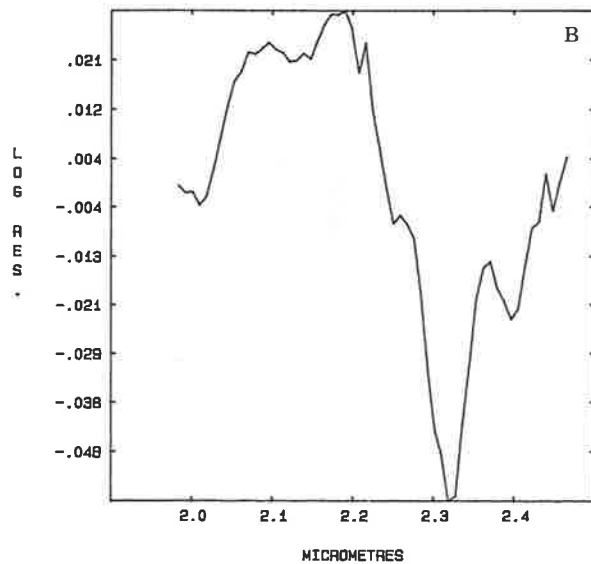




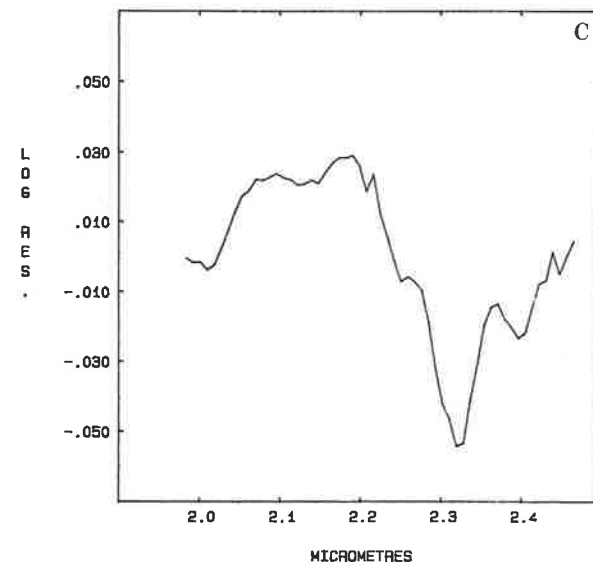
K2/370/S Q58 TC25 CHL7 AMP5 ANT3 CAL2 60



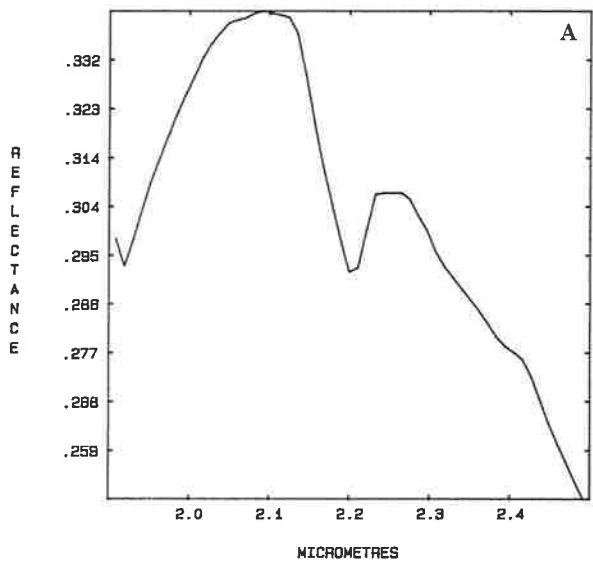
SA 388-398



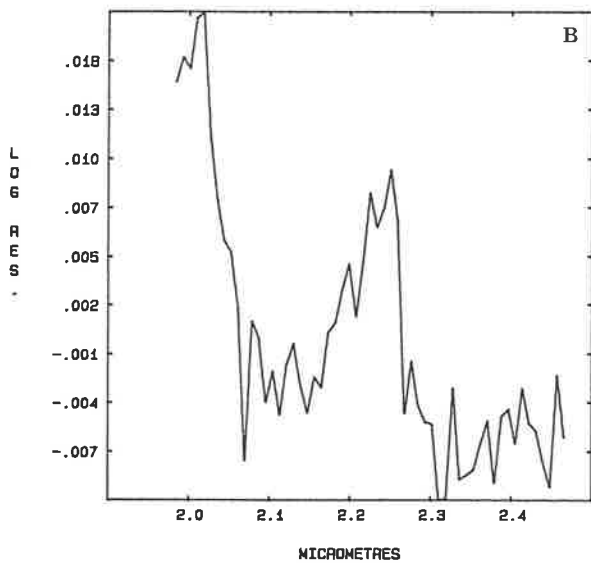
SA 388-398



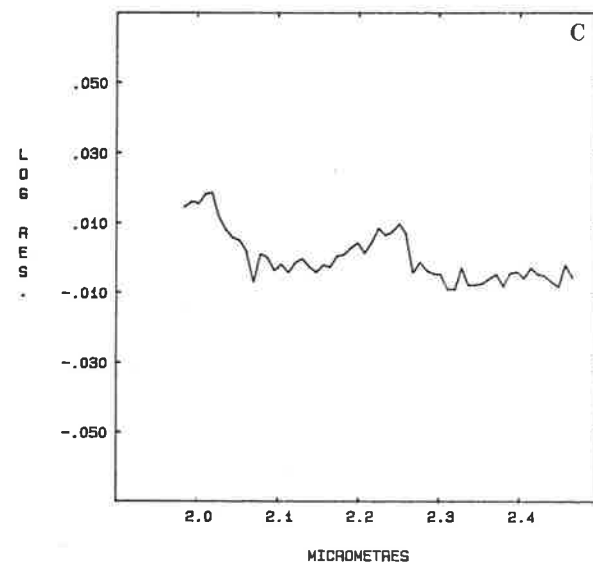
K2/415/S

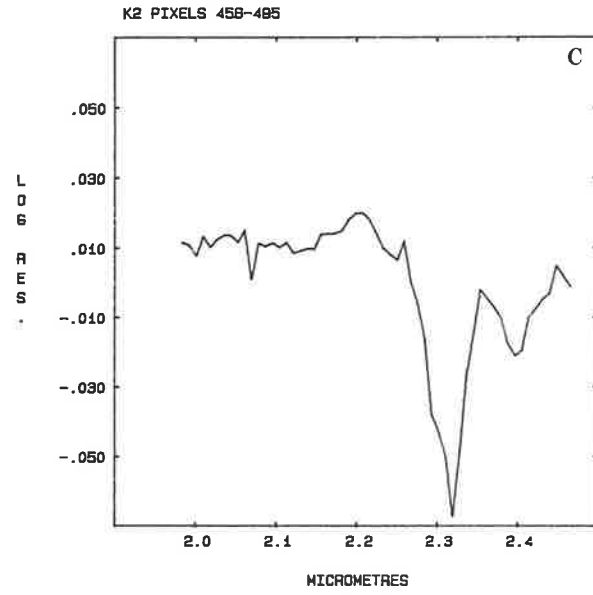
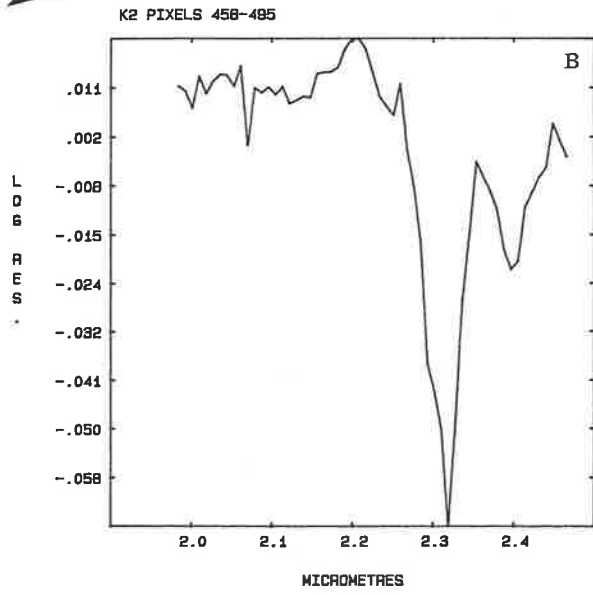
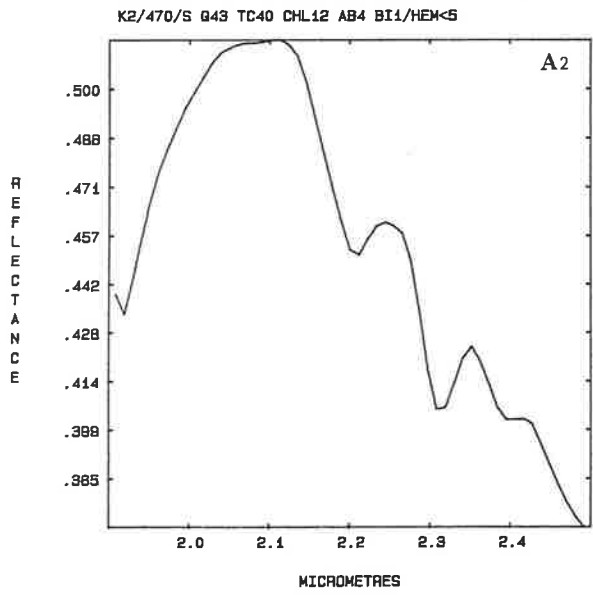
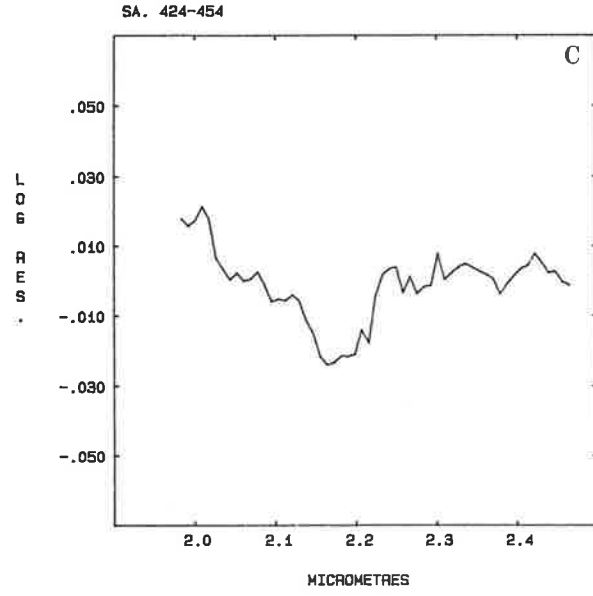
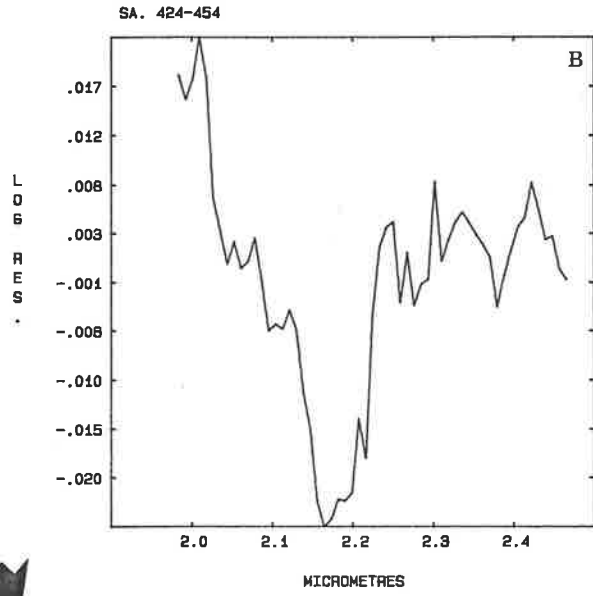
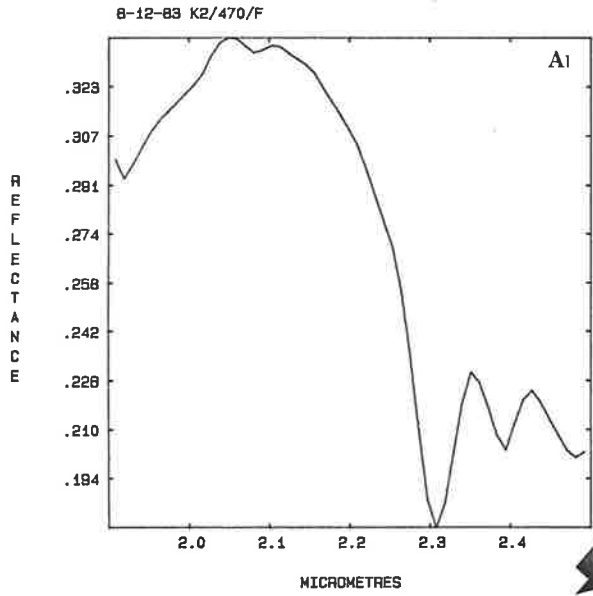


SA. 398-422

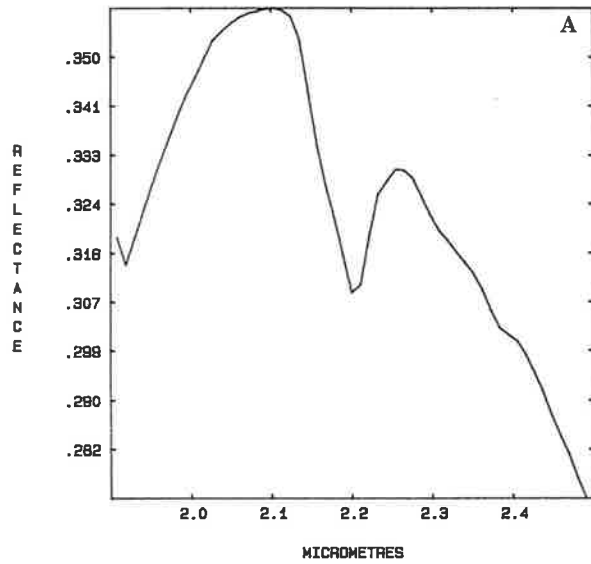


SA. 398-422

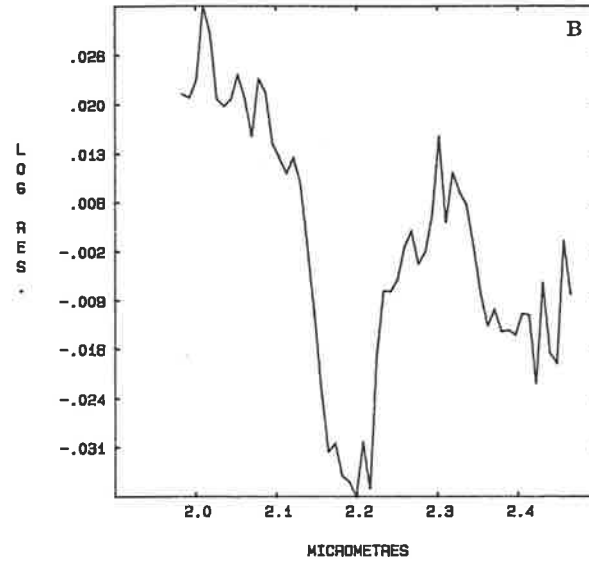




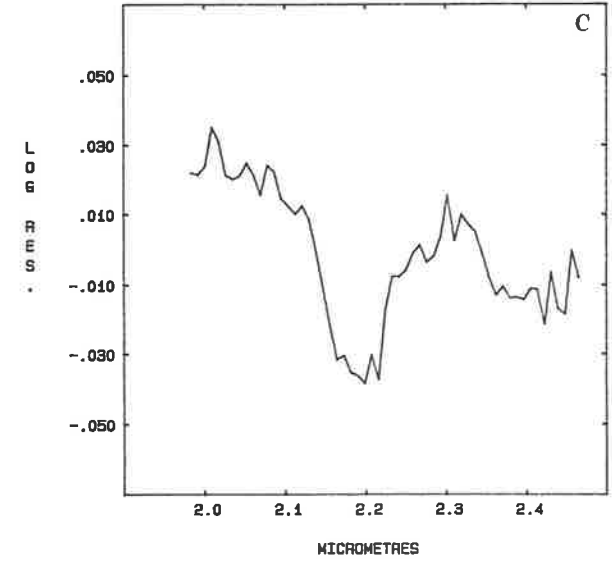
8-12-89 K2/498/SF



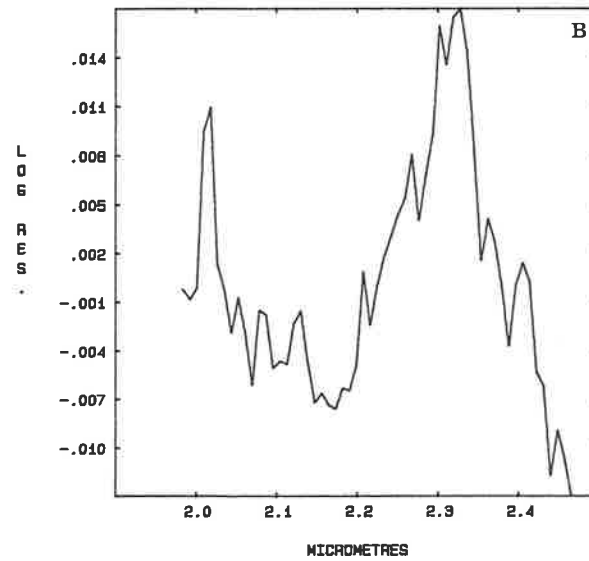
SA. 497-524



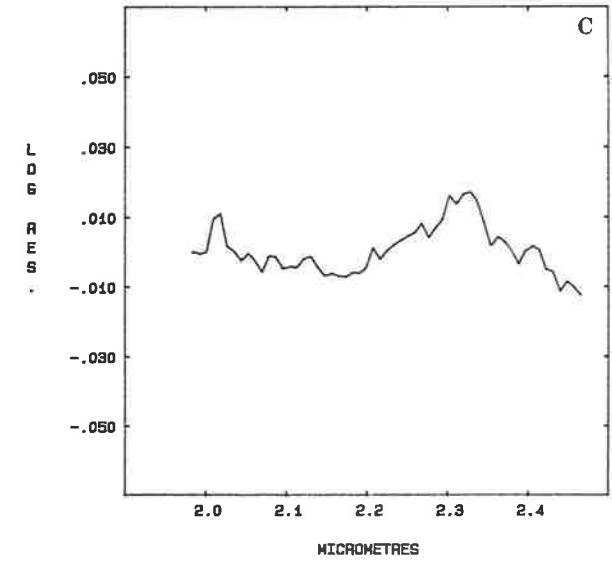
SA. 497-524



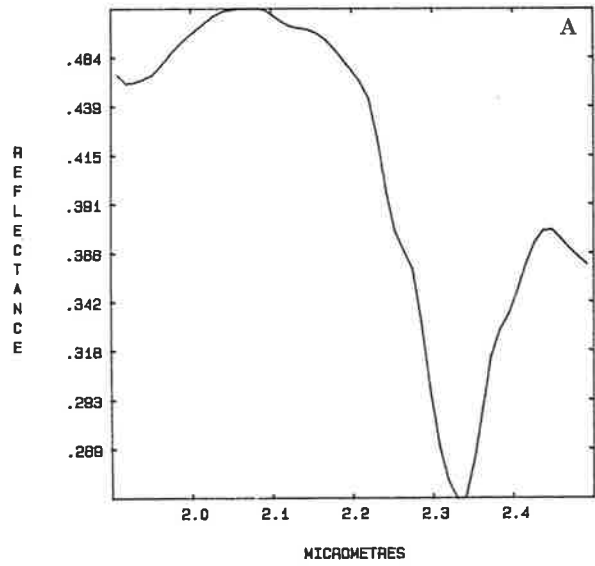
SA. 528-580



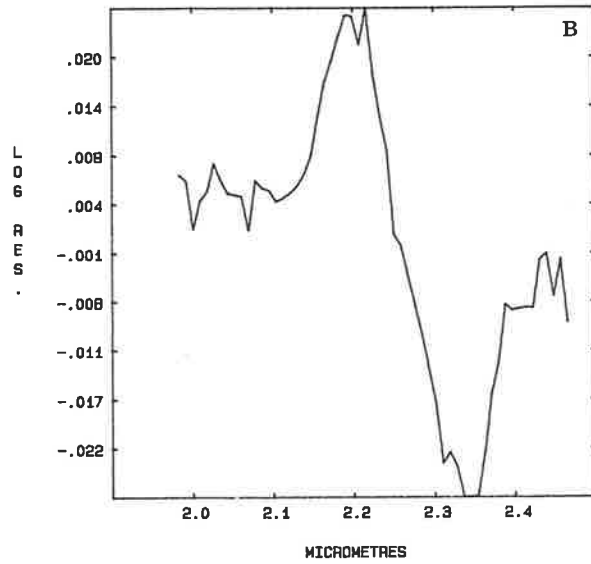
SA. 528-580



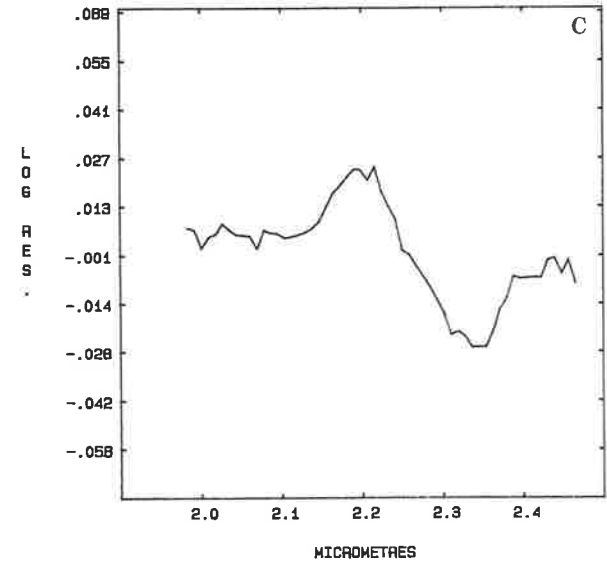
8-12-83 K2/B11/F1/W



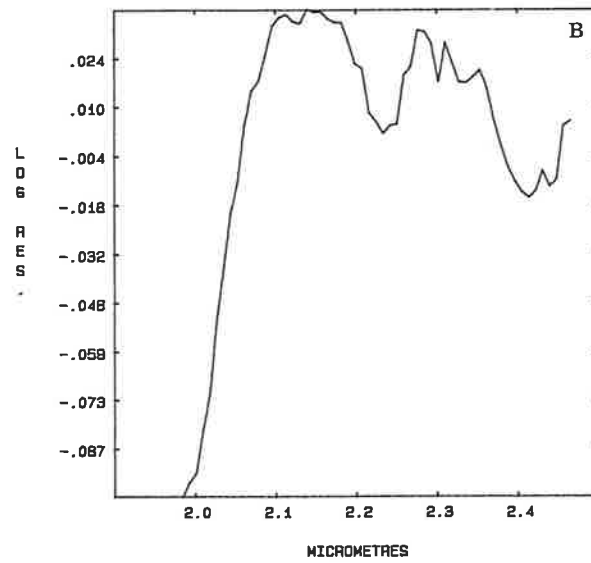
SA. 582-825



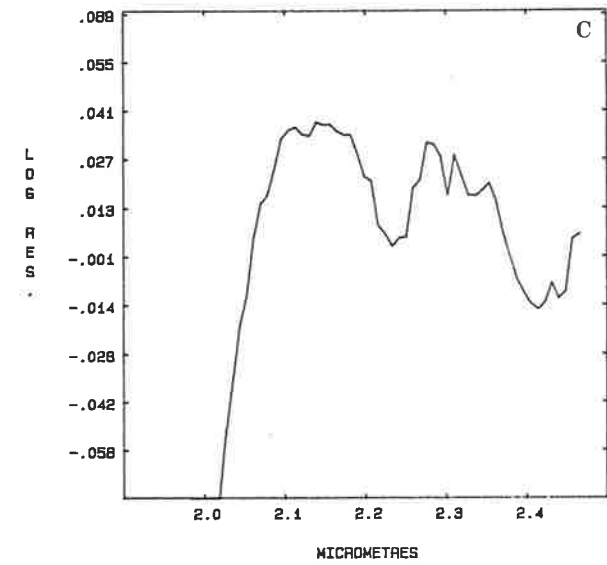
SA. 582-825

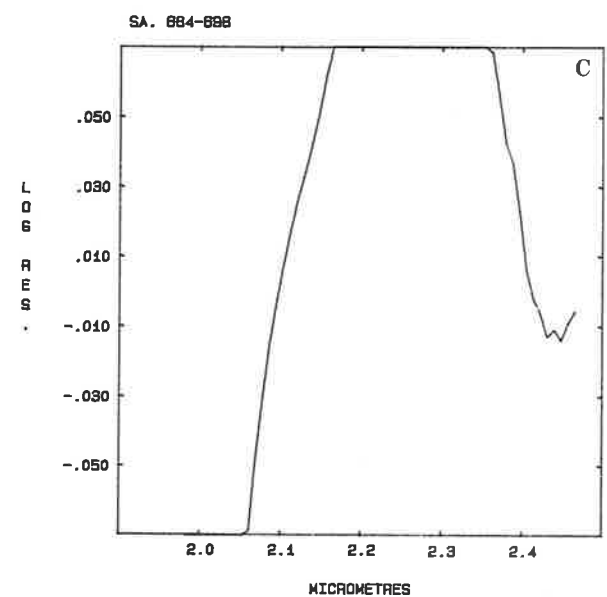
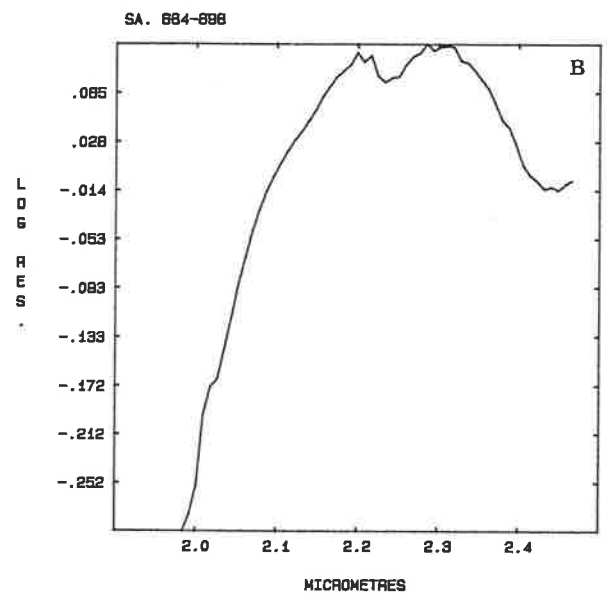
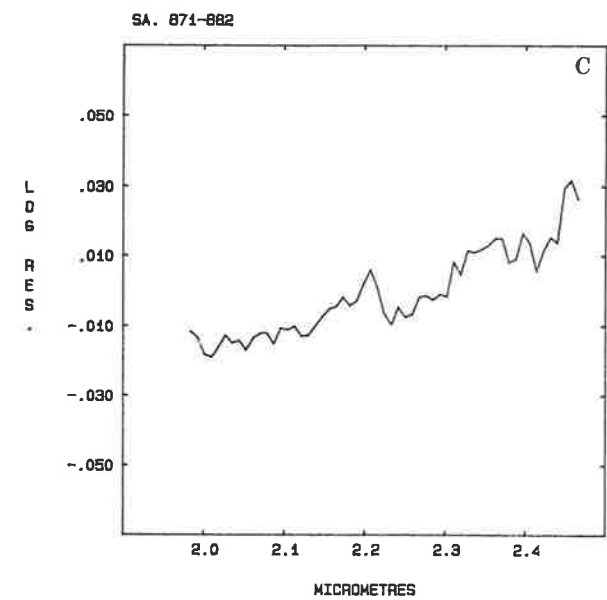
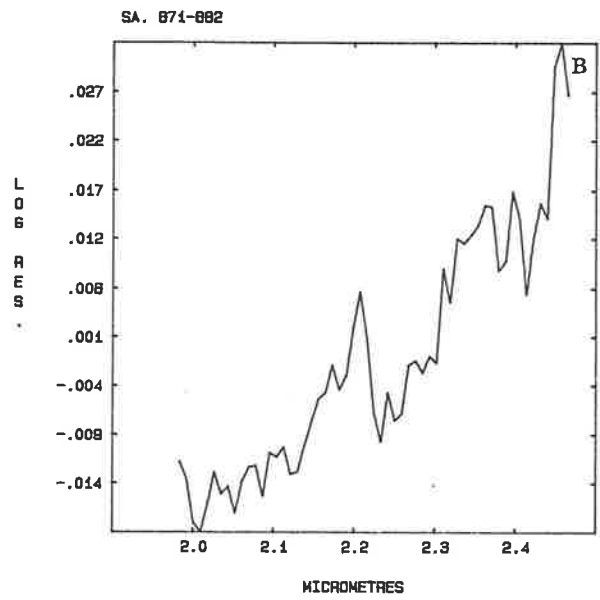


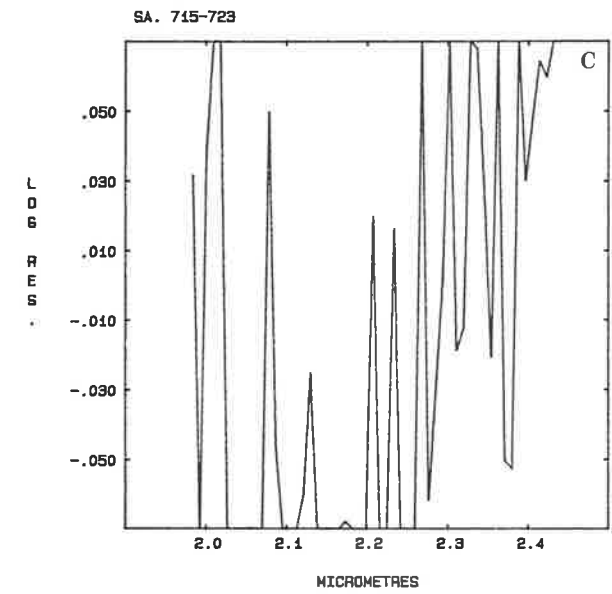
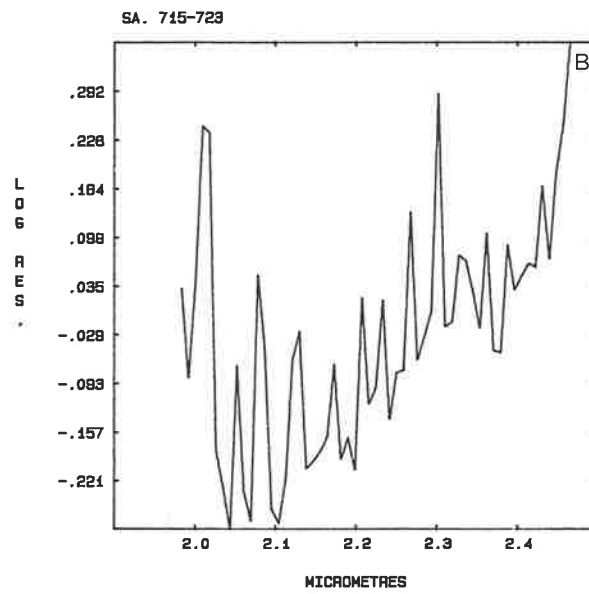
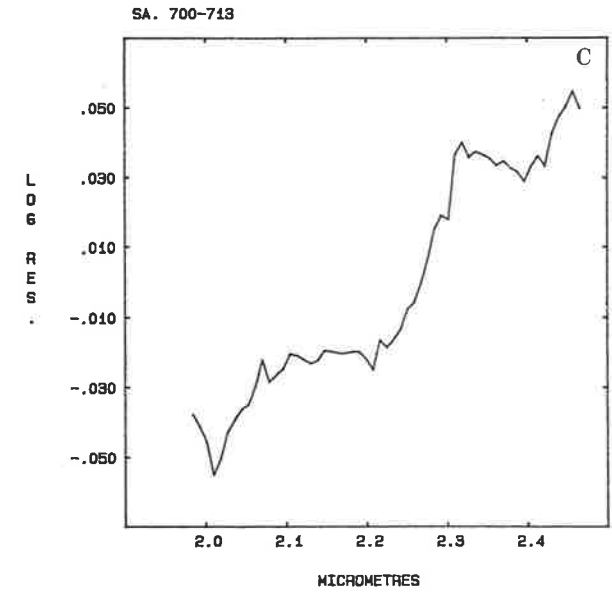
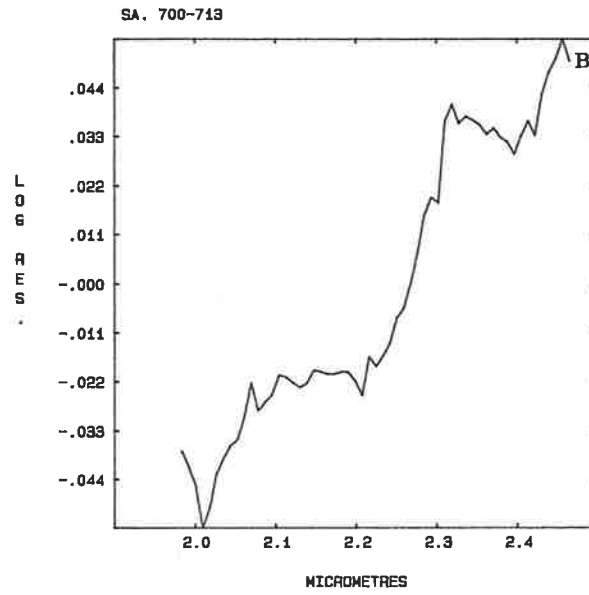
SA. 827-888

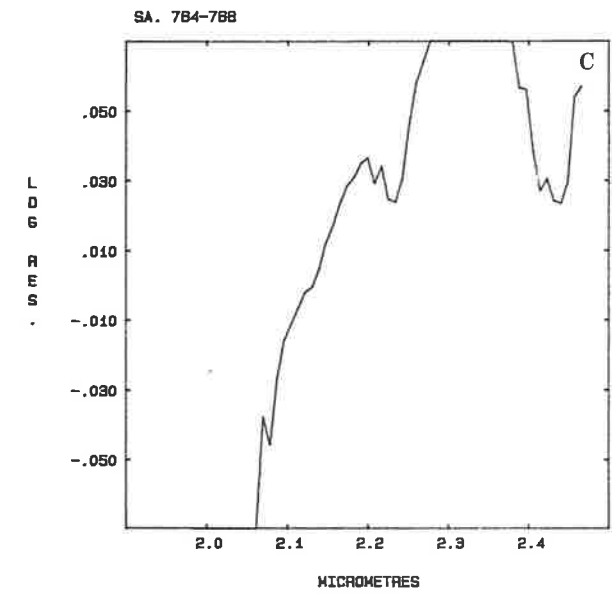
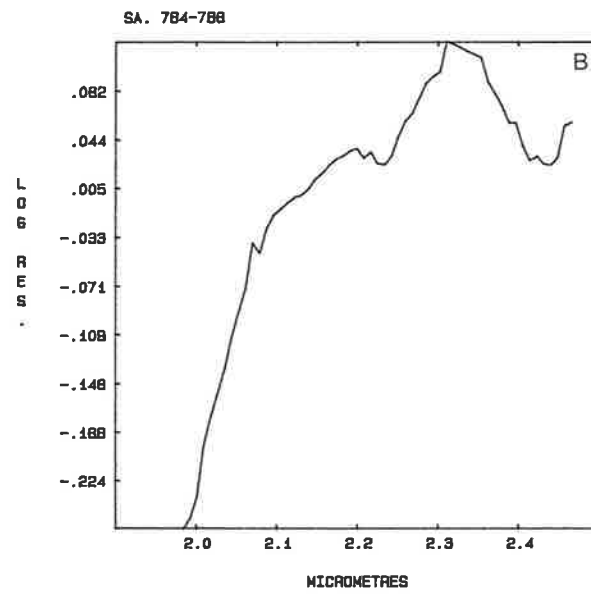
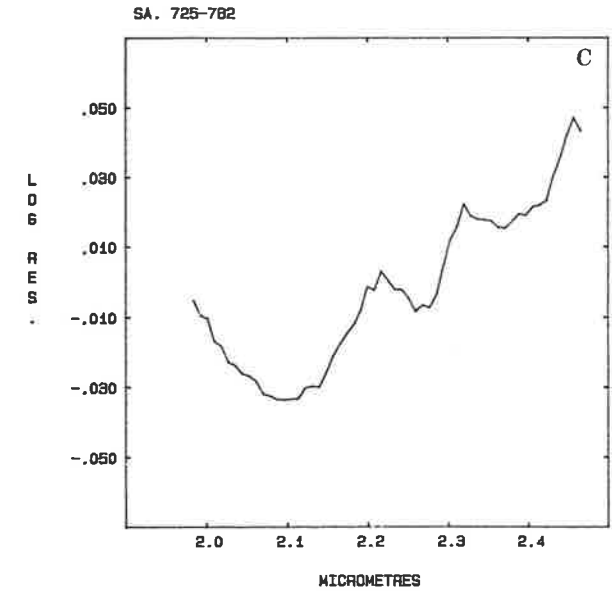
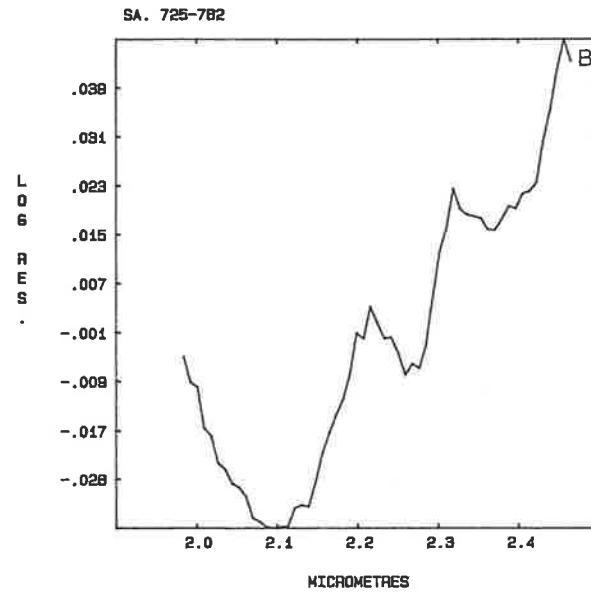


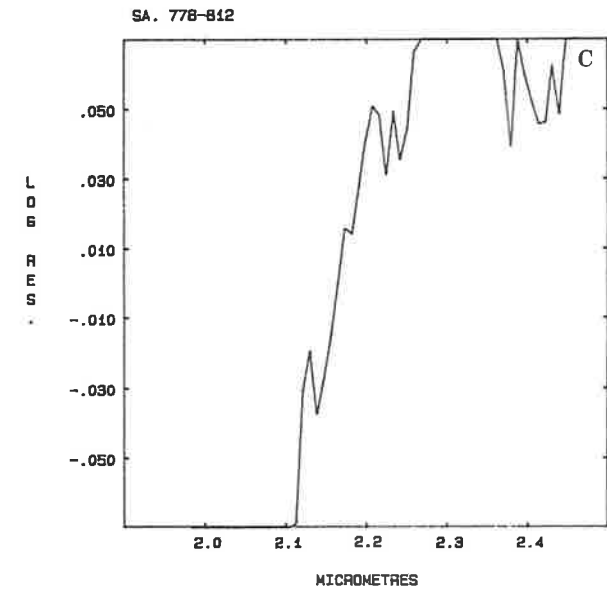
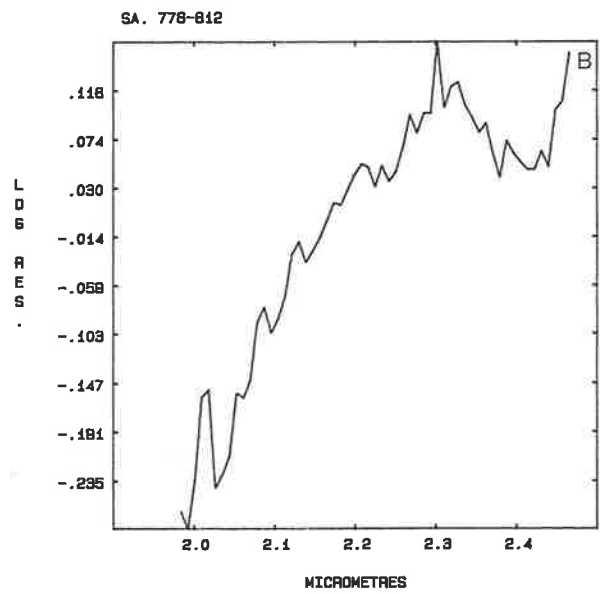
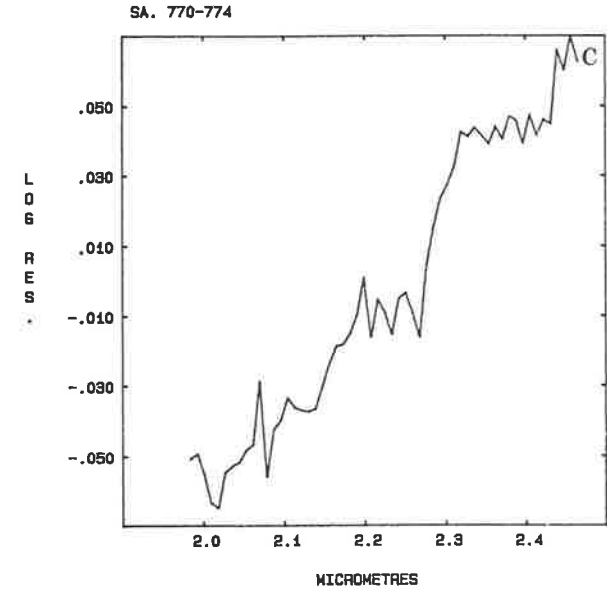
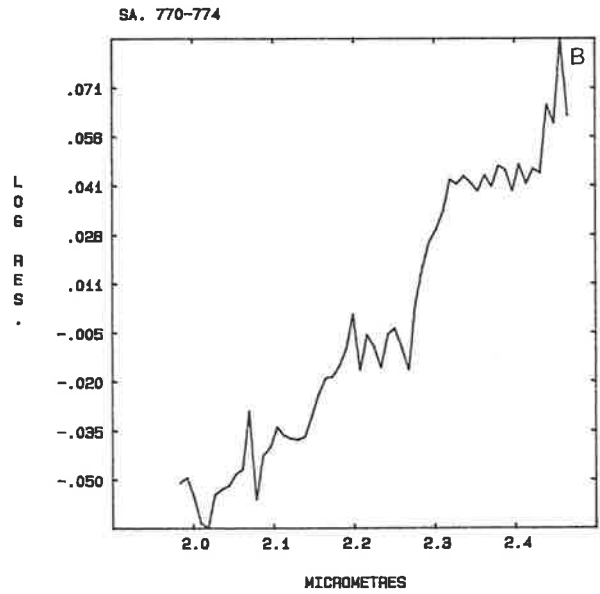
SA. 827-888









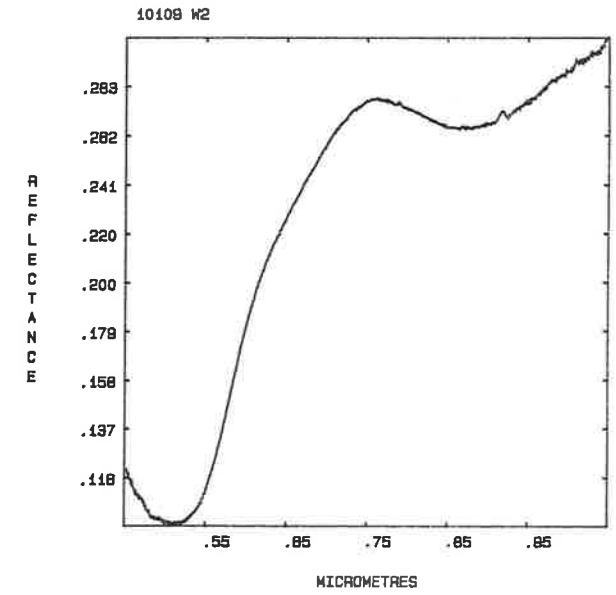
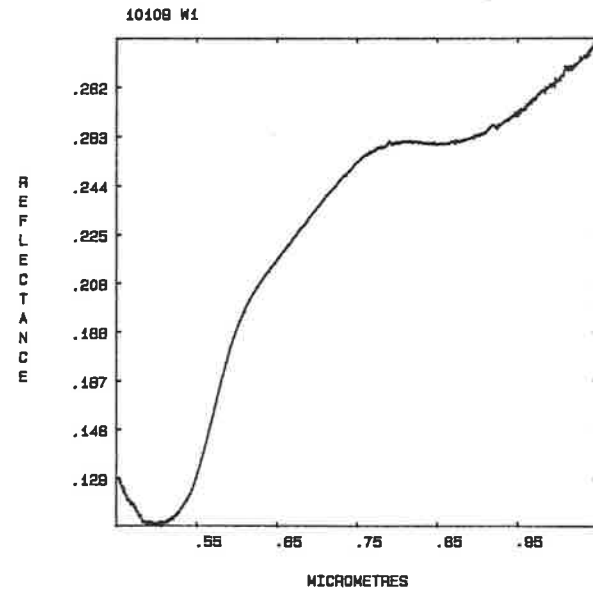
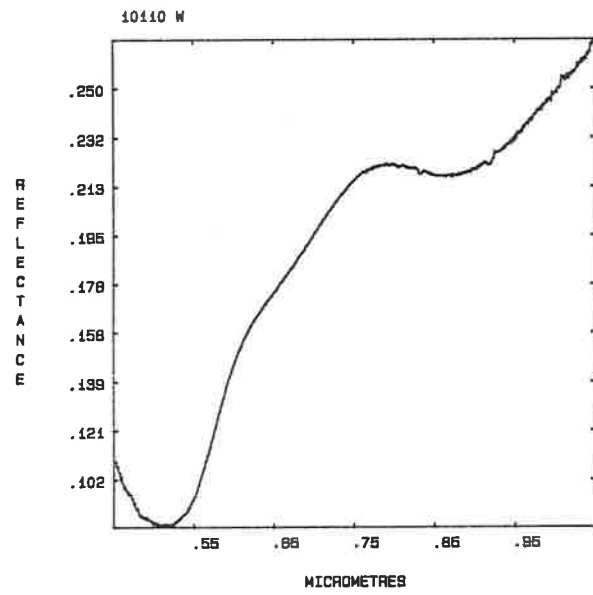
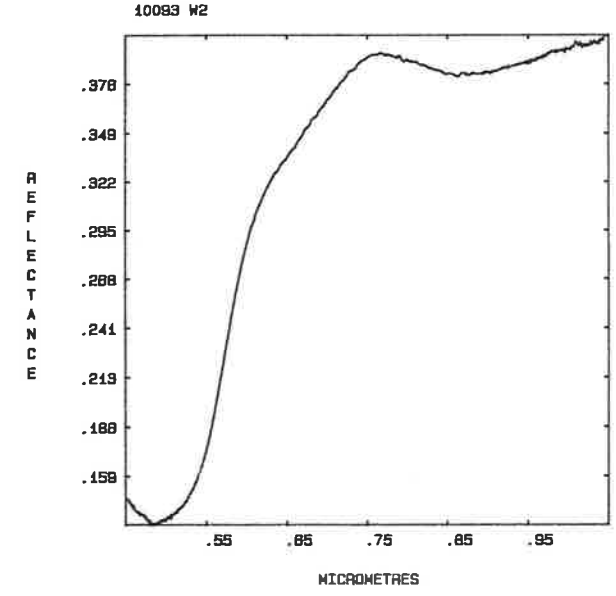
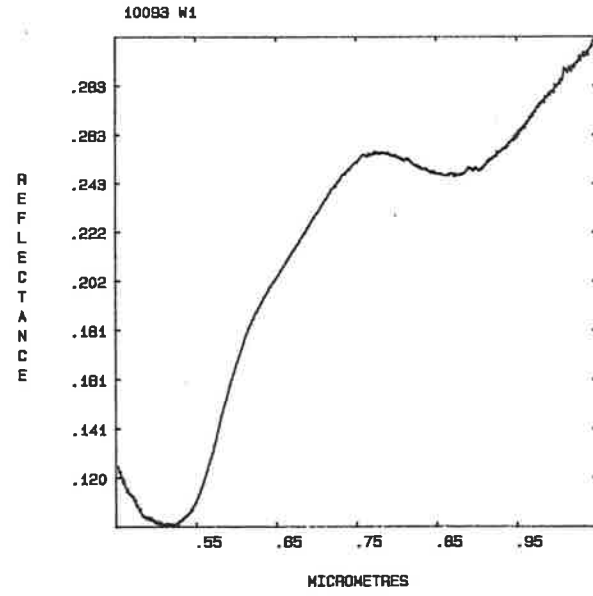
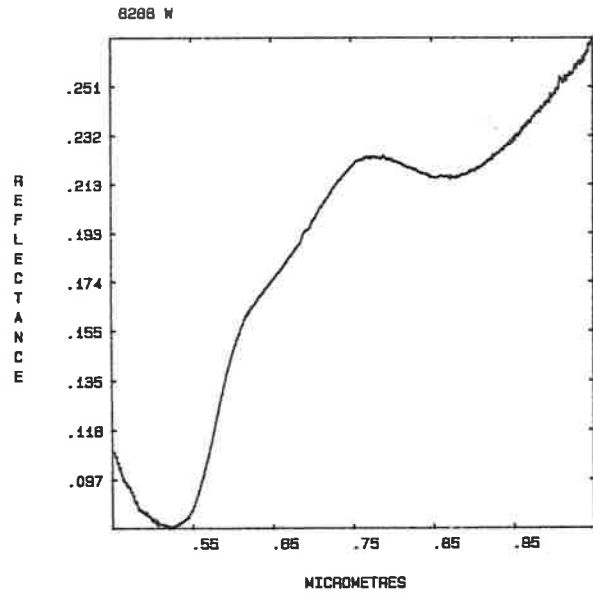


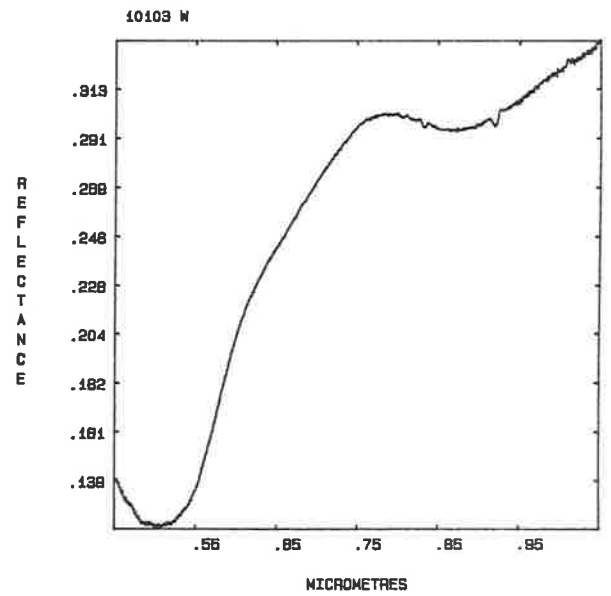
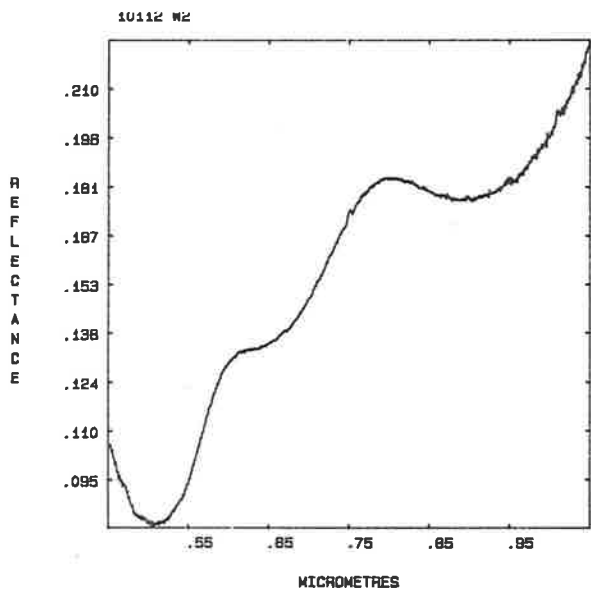
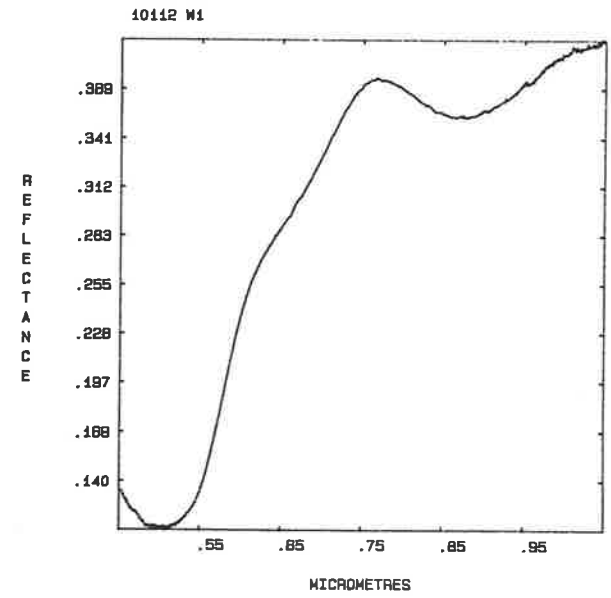
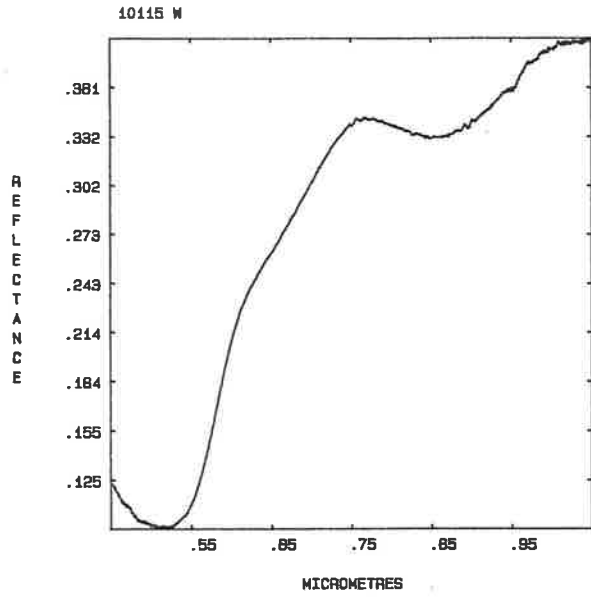
APPENDIX X VNIR laboratory reflectance spectra of samples from the Fortescue Group.

The VNIR spectra in this appendix have been subdivided into groups according to the nature of the surface measured (weathered or fresh) and the metamorphic/metasomatic character of the sample. For instance, the first group of plots are spectra of weathered surfaces of samples from the metadomain (altered rocks) of Z-I (the lowest metamorphic grade).

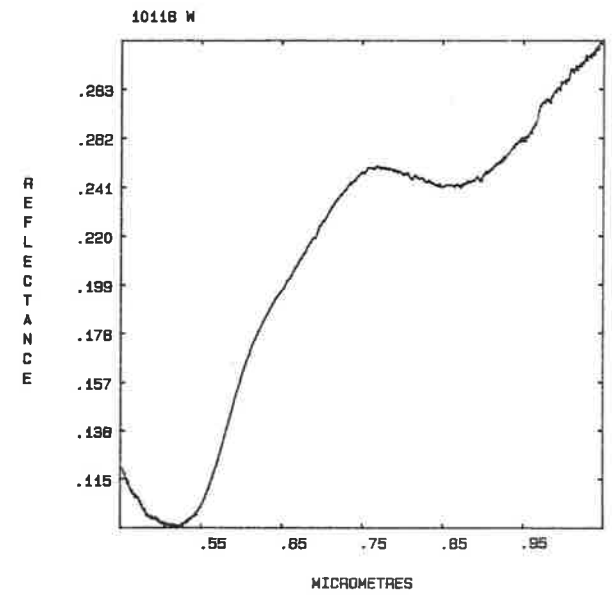
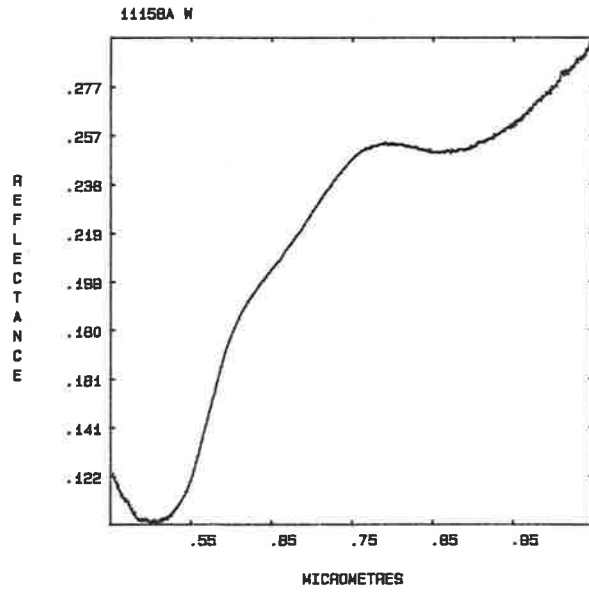
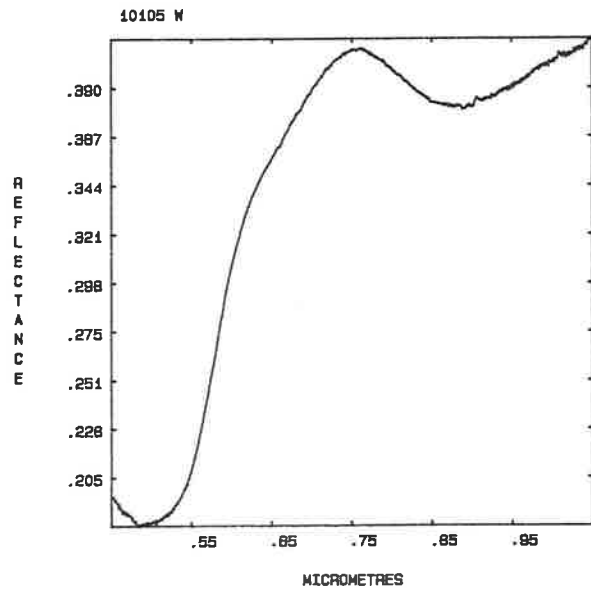
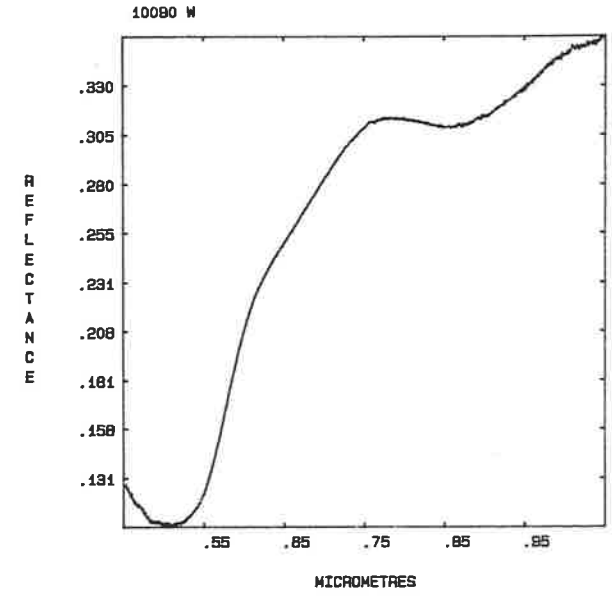
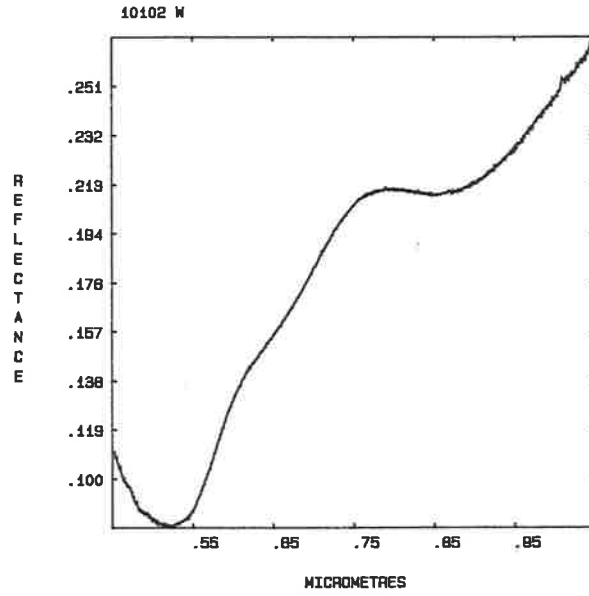
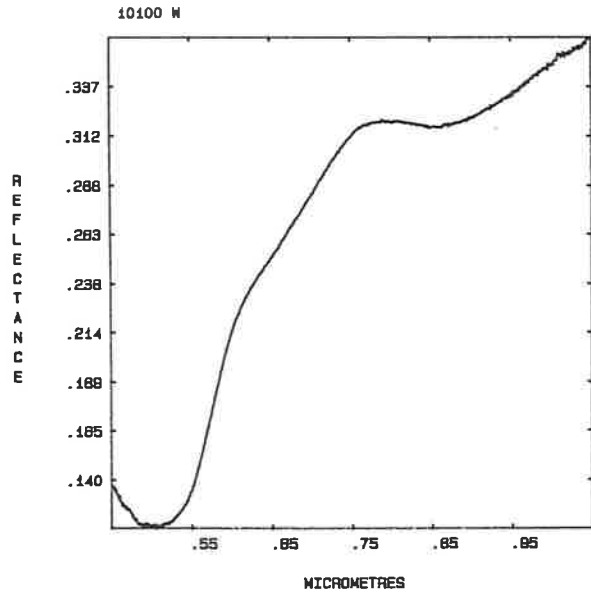
Note that altered versus unaltered rocks, and those from different metamorphic zones, are not separable on the basis of their VNIR W spectral characteristics. Refer to Table 7.3 for the interpretation of each spectrum.

VNIR W SPECTRA - Z-I METADOMAIN AND TRANSITION SAMPLES

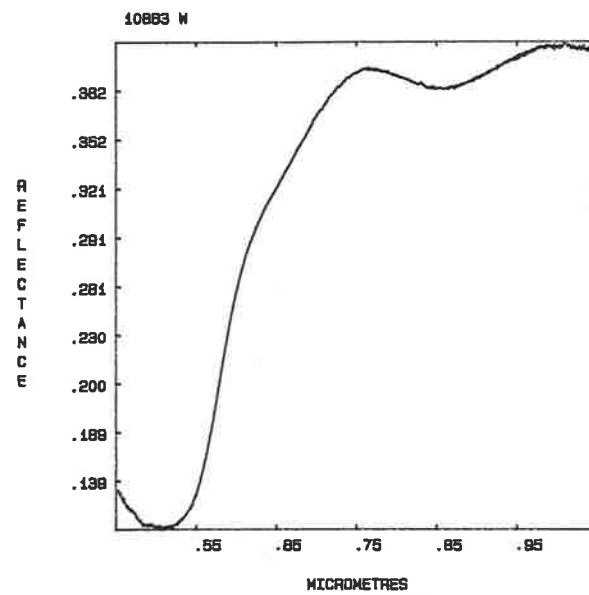
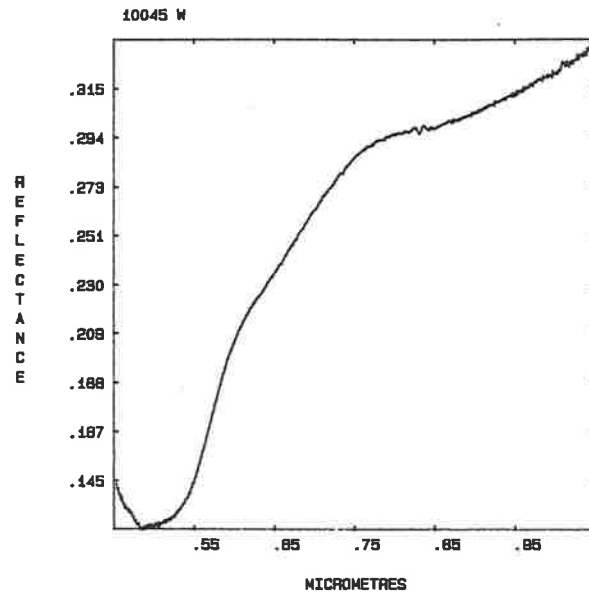




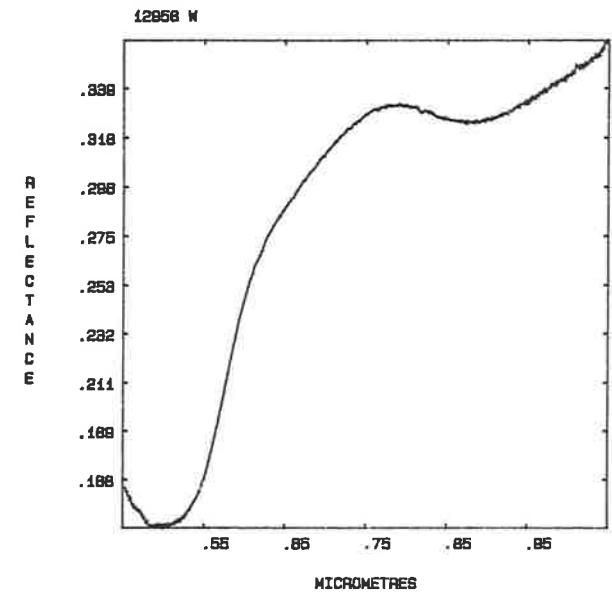
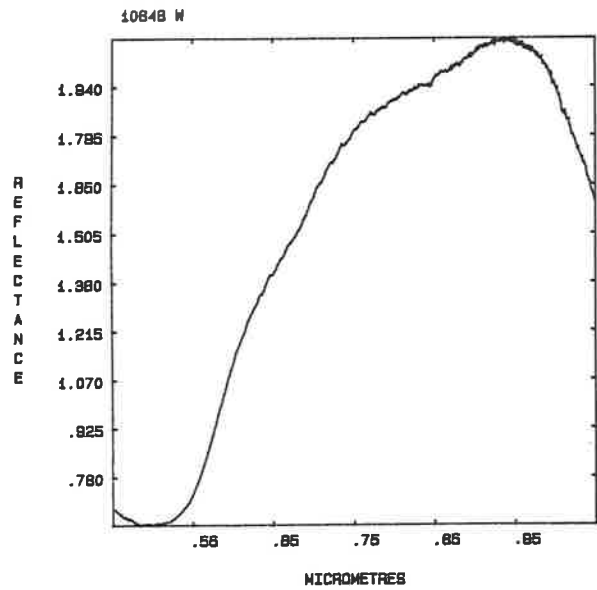
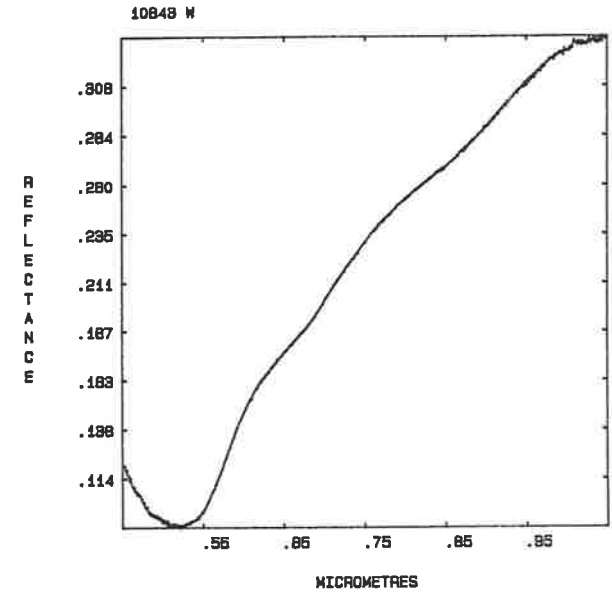
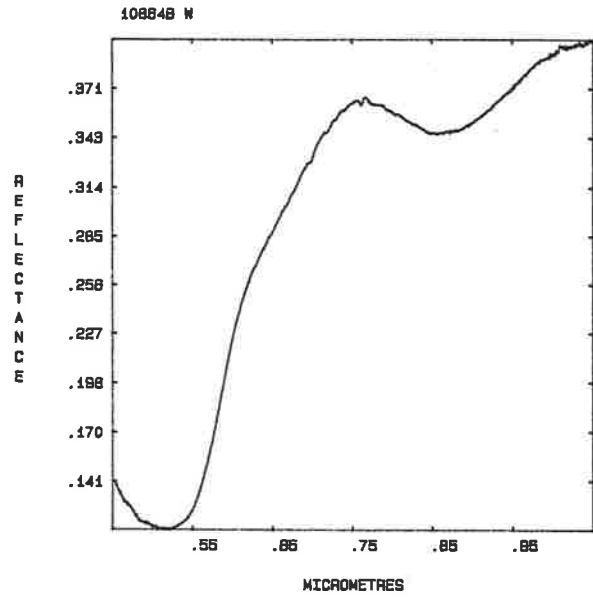
VNIR W SPECTRA - Z-I RELICT DOMAIN SAMPLES



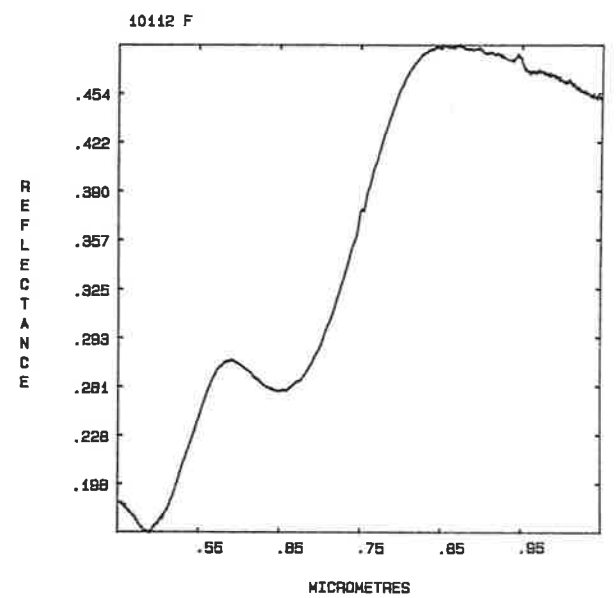
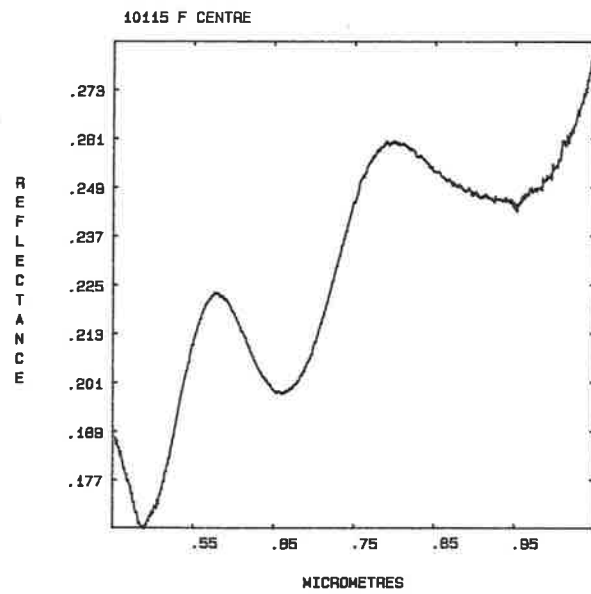
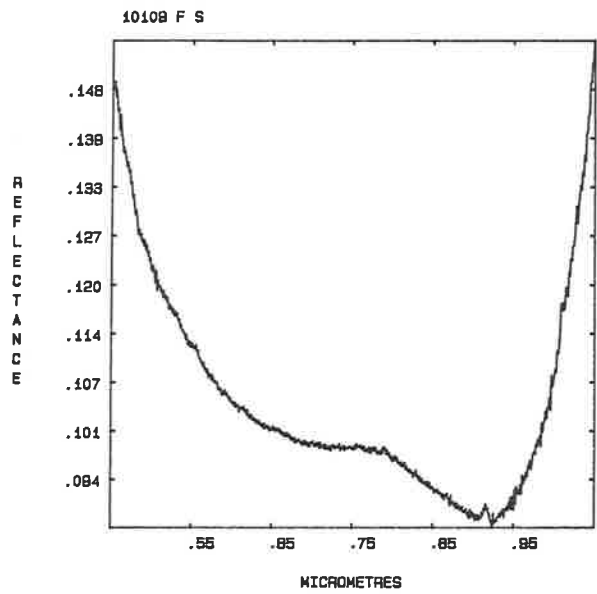
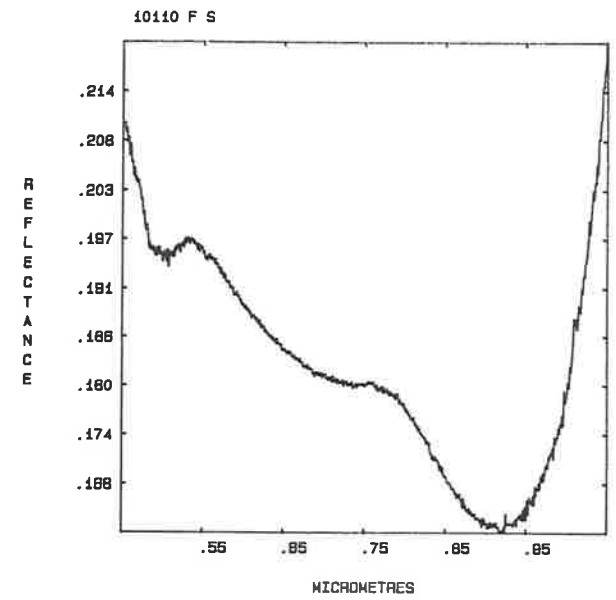
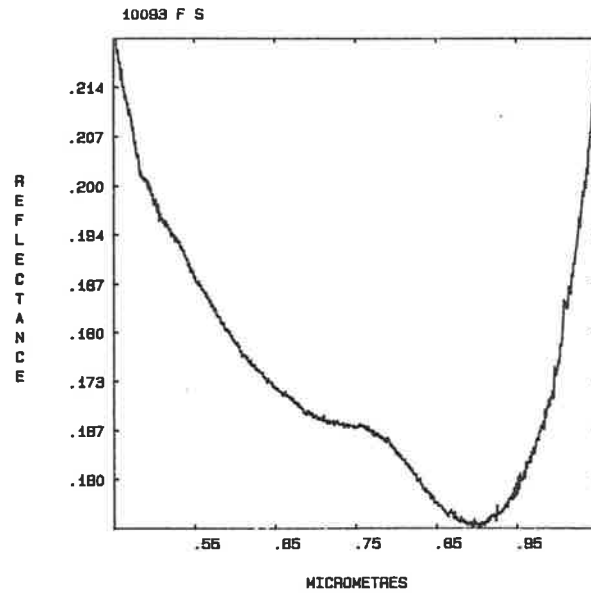
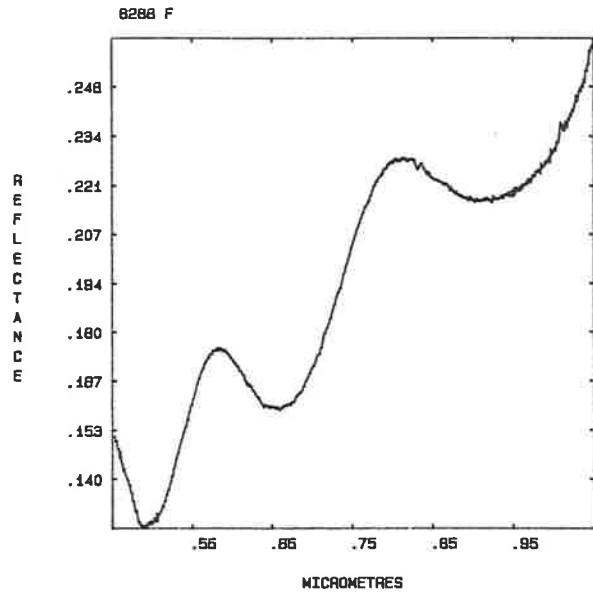
VNIR W SPECTRA - Z-II AND Z-III METADOMAIN SAMPLES



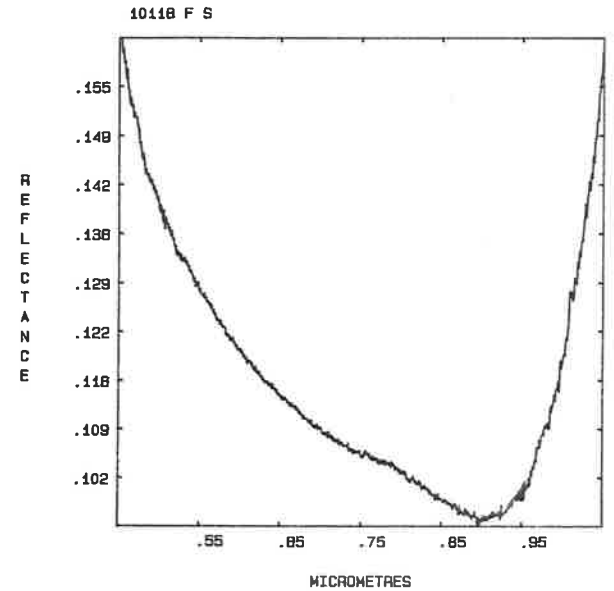
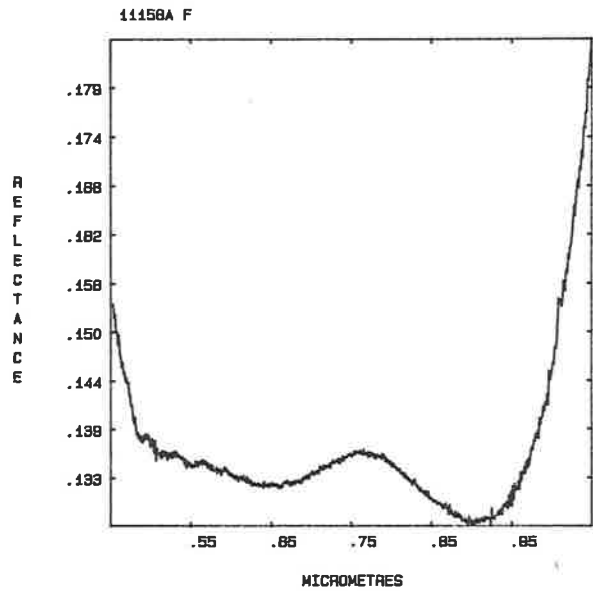
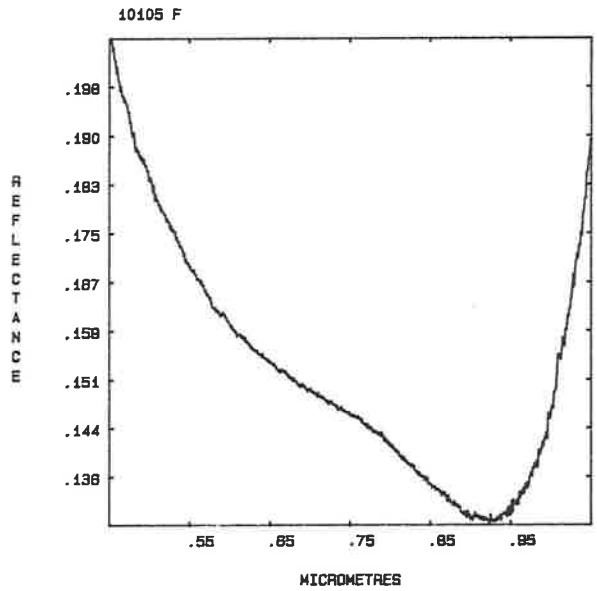
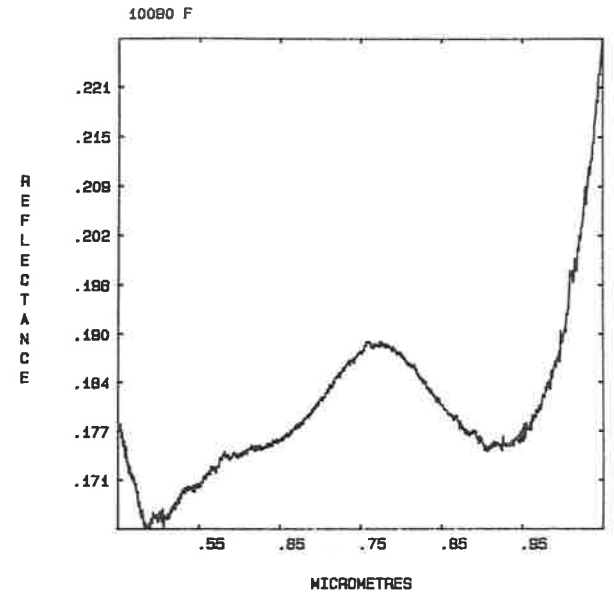
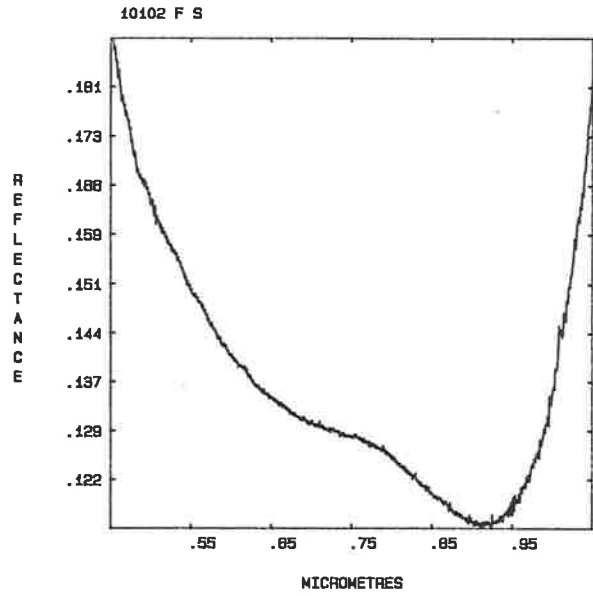
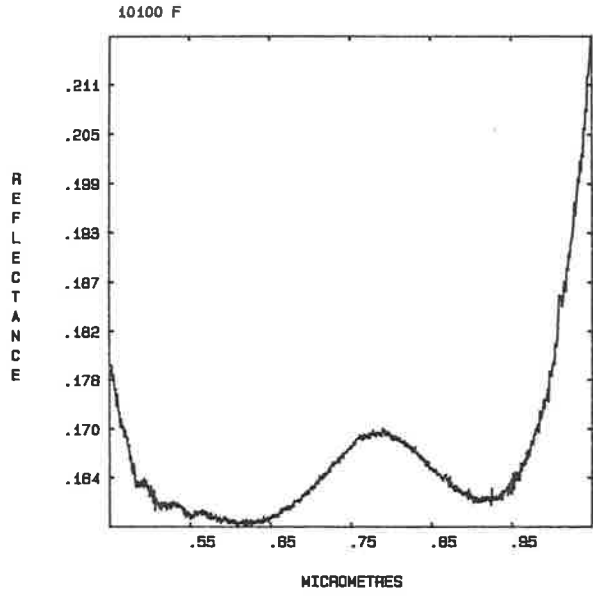
VNIR W SPECTRA - Z-III RELICT DOMAIN AND Z-IV UNIFORMLY ALTERED METADOMAIN



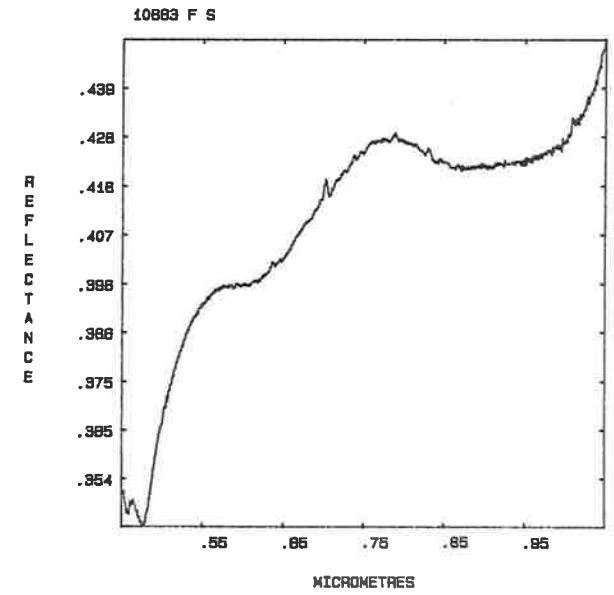
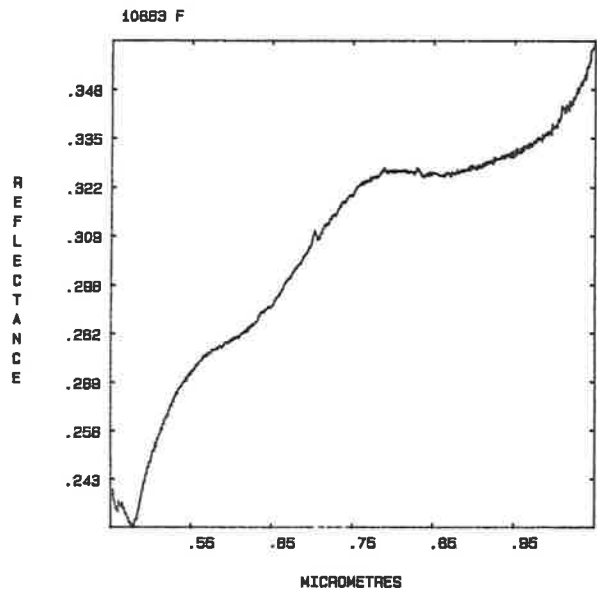
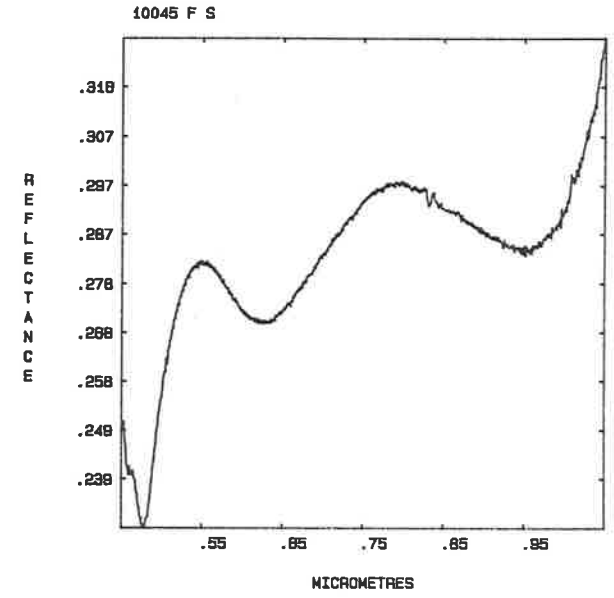
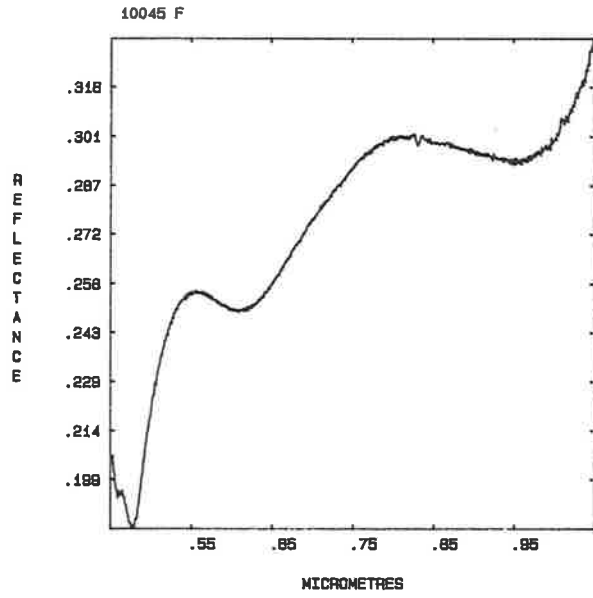
VNIR F SPECTRA - Z-I METADOMAIN AND TRANSITION SAMPLES



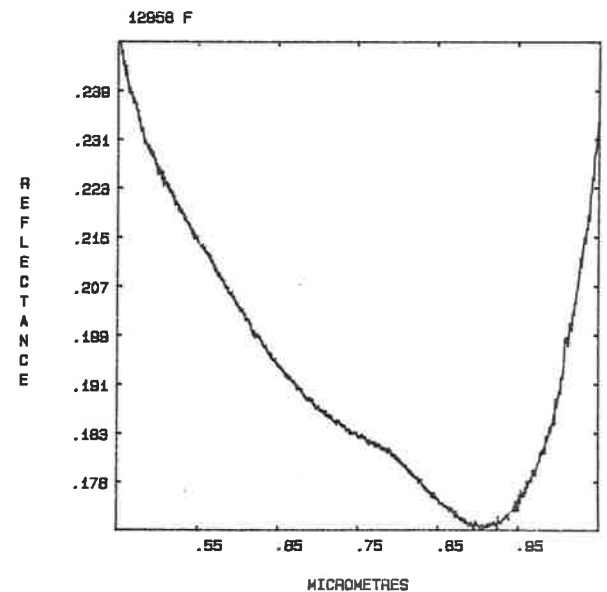
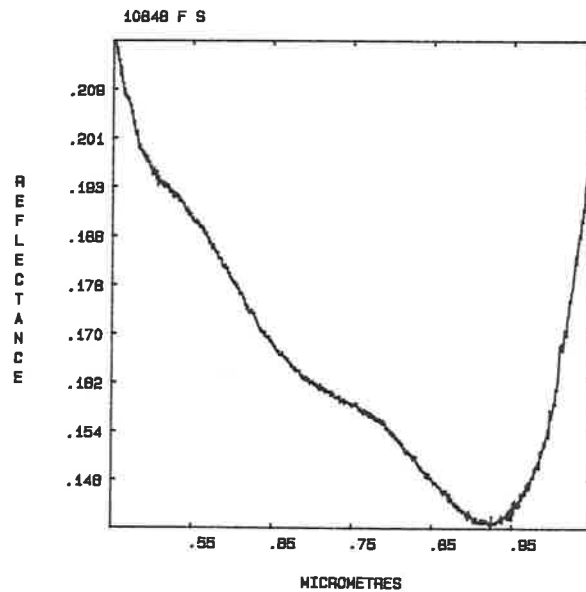
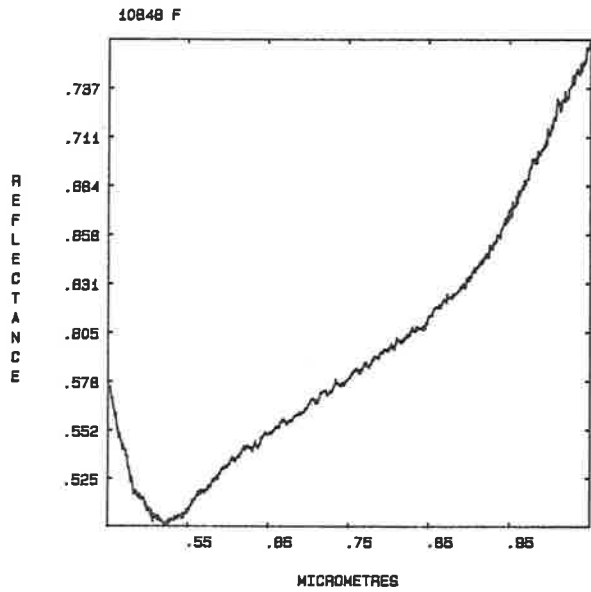
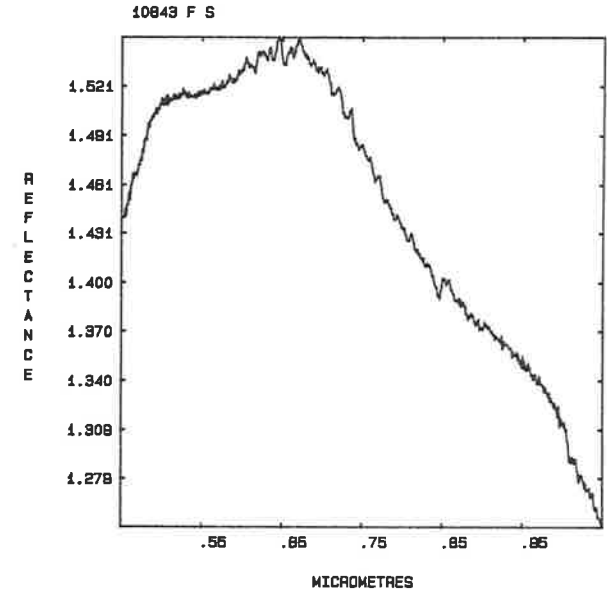
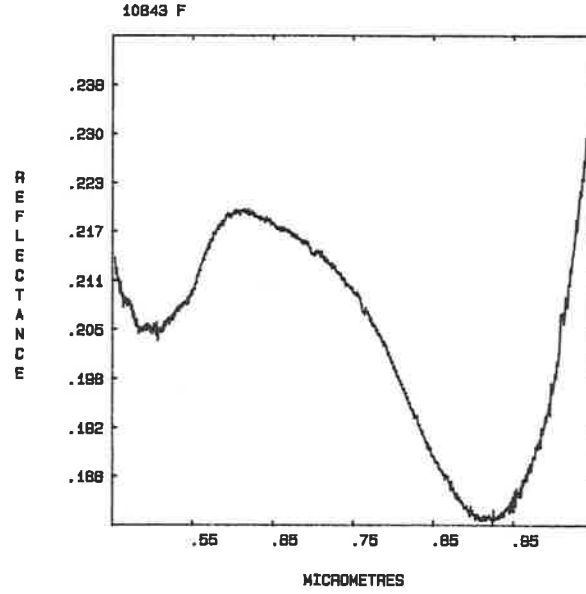
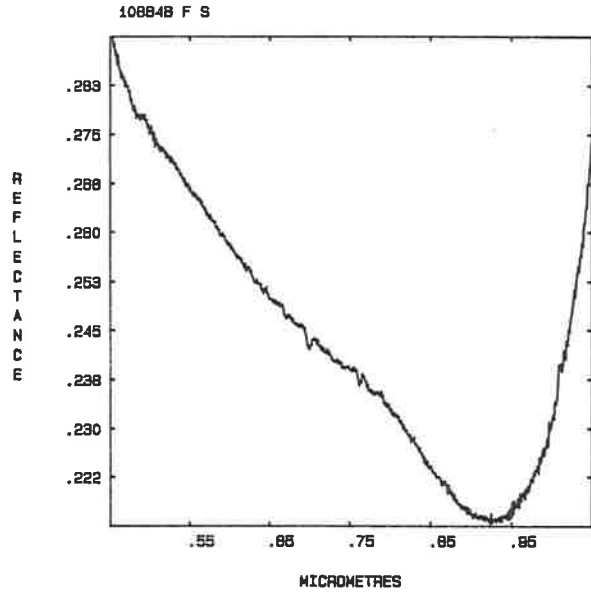
VNIR F SPECTRA - Z-I RELICT DOMAIN SAMPLES



VNIR F SPECTRA - Z-II AND Z-III METADOMAIN SAMPLES



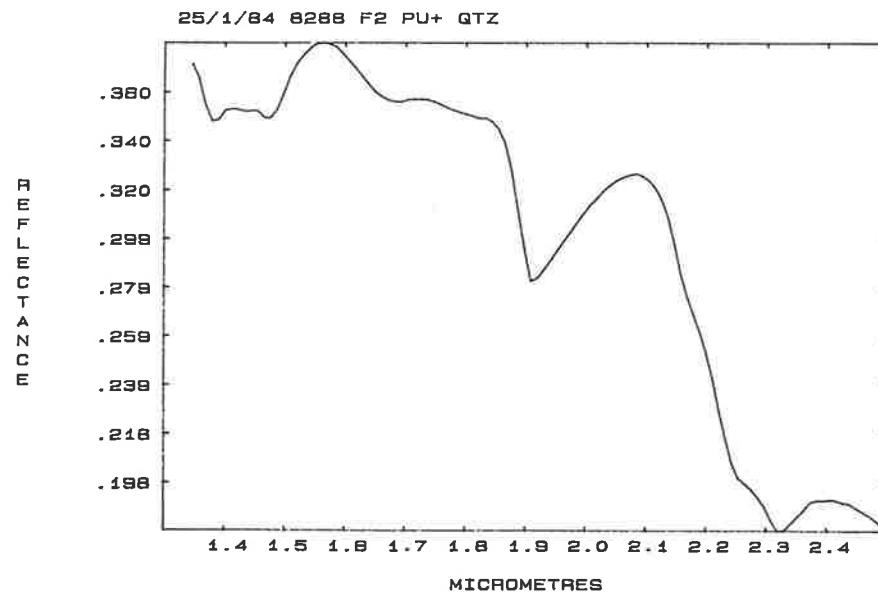
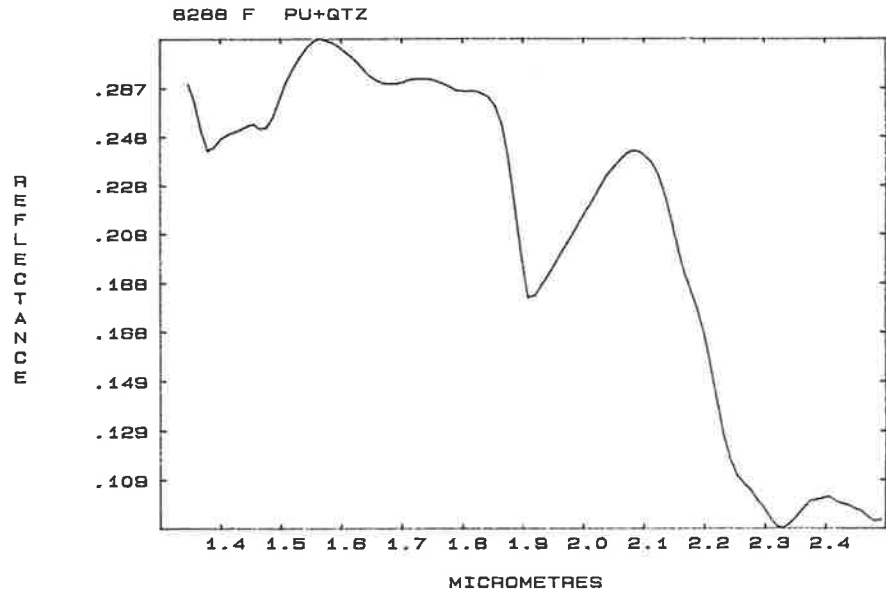
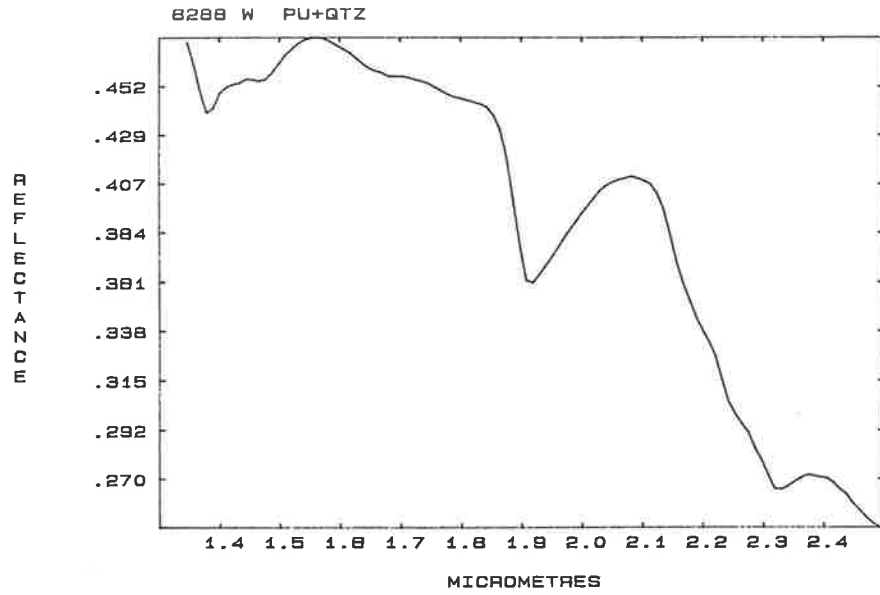
VNIR F SPECTRA - Z-III RELICT DOMAIN AND Z-IV UNIFORMLY ALTERED METADOMAIN

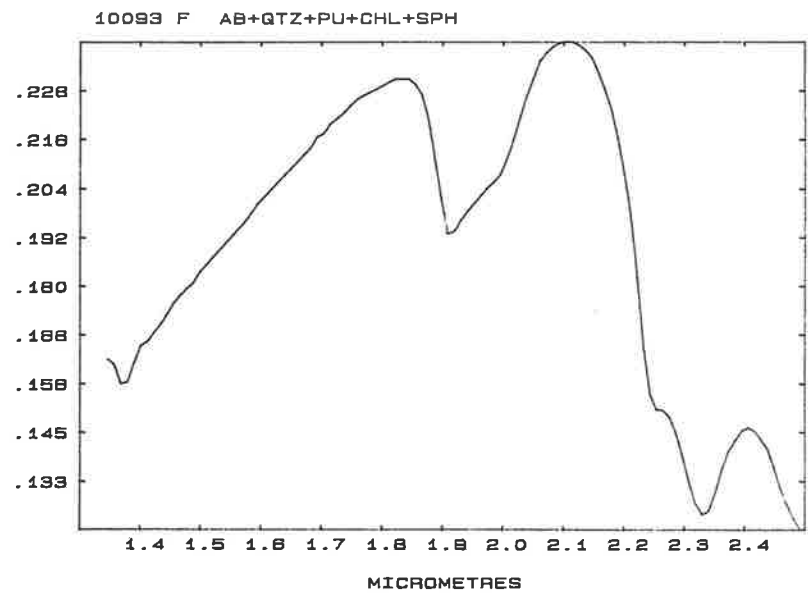
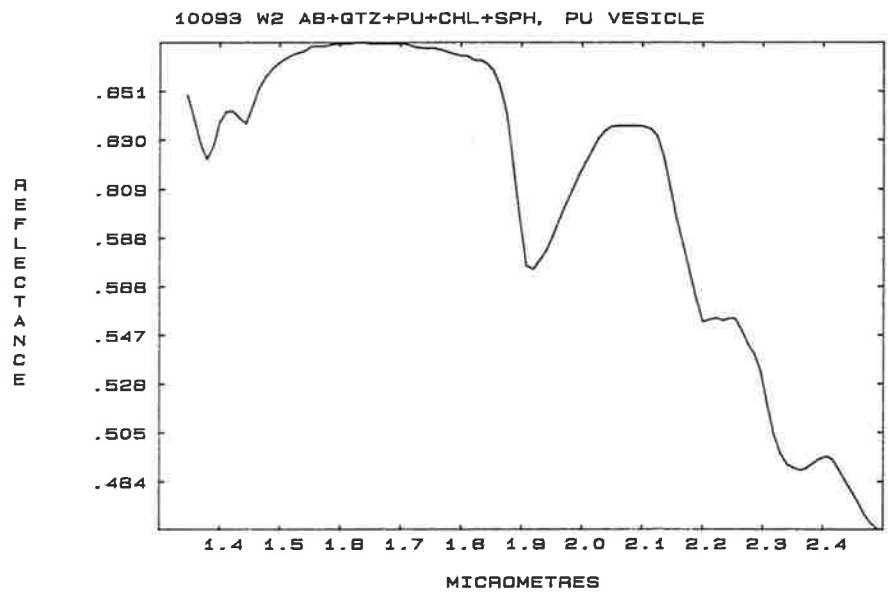
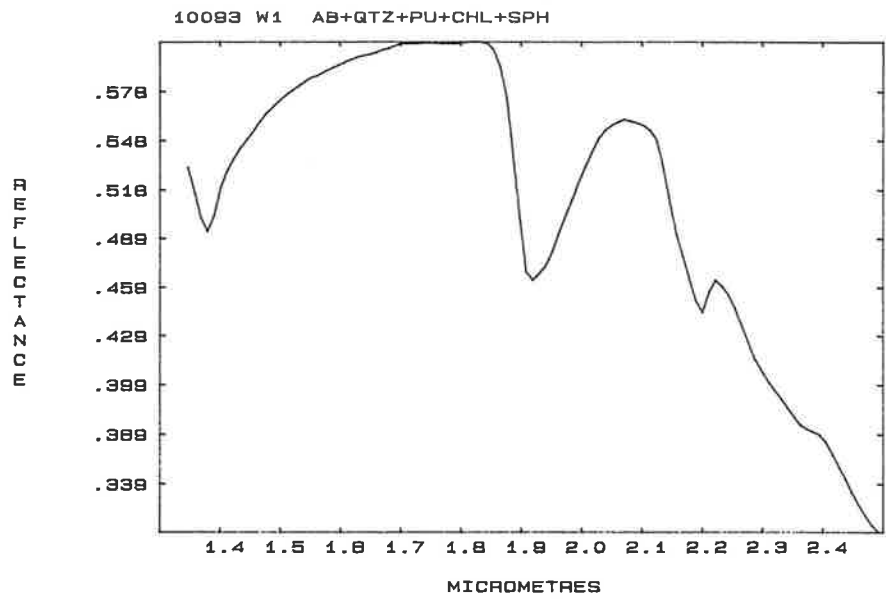


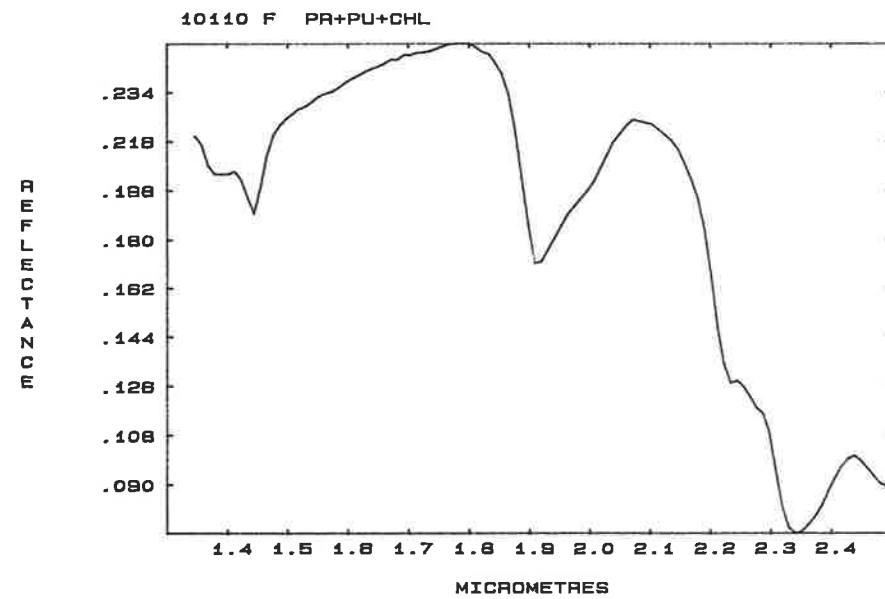
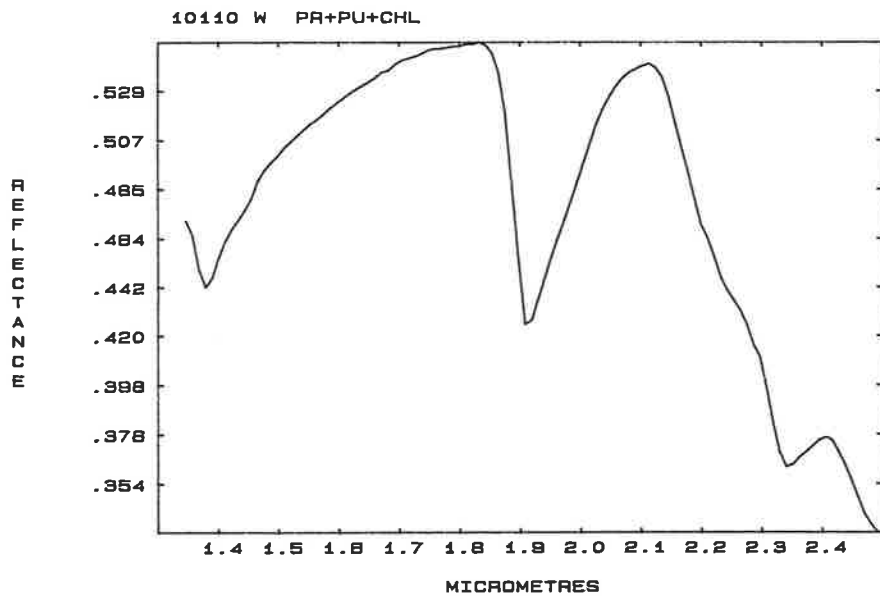
APPENDIX XI SWIR laboratory reflectance spectra of samples from the Fortescue Group.

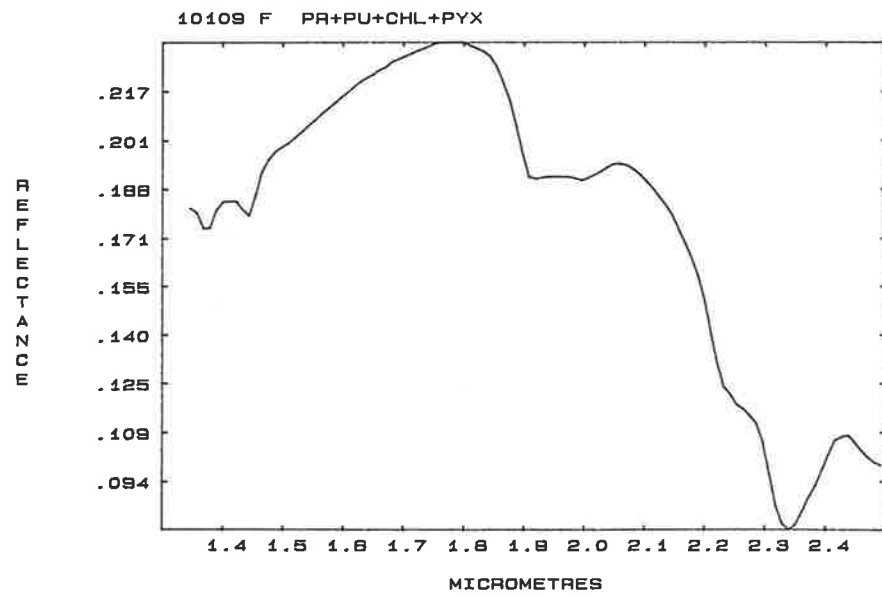
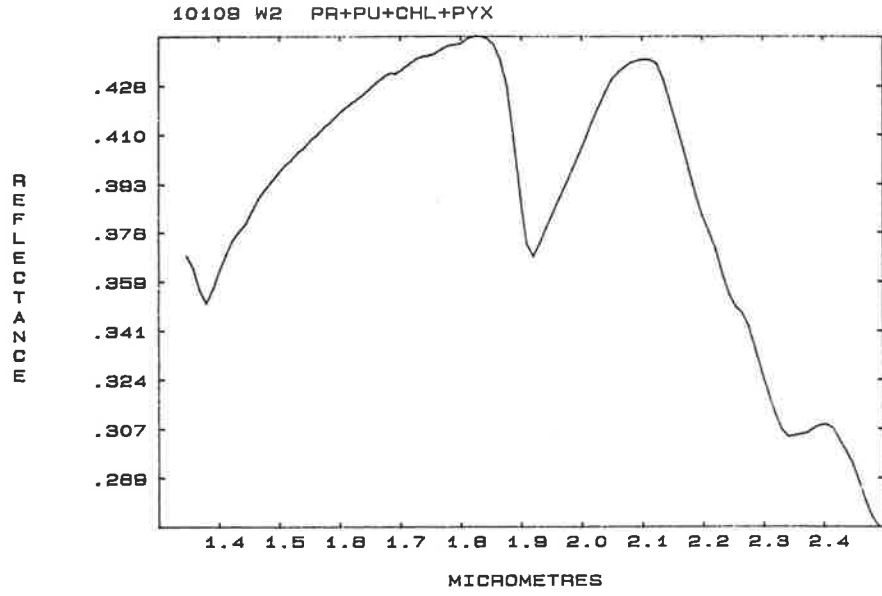
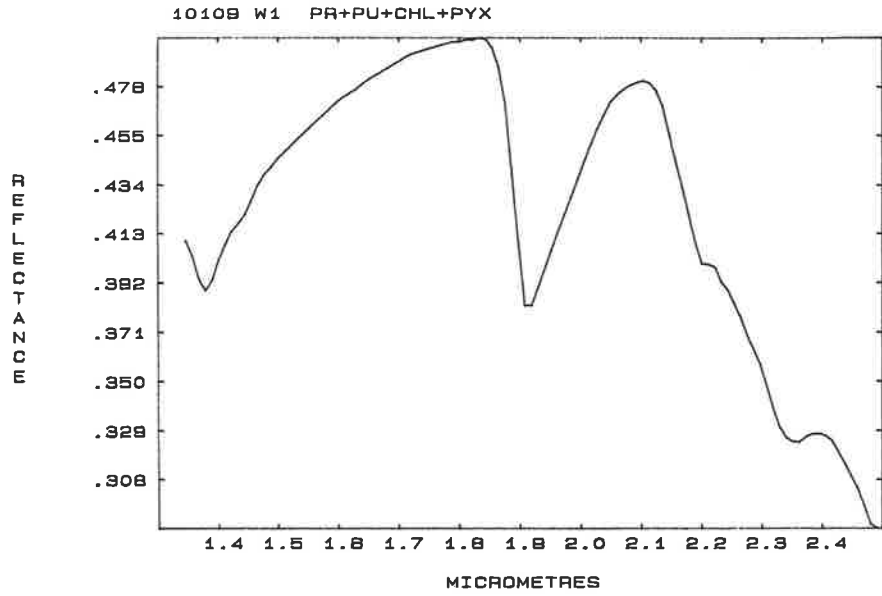
The SWIR spectra presented here have been divided into groups according to the metamorphic and metasomatic characteristics of each sample. For instance, the first group of plots are spectra of samples from the metadomain (altered rocks) of Z-I (the lowest metamorphic grade). All spectra for each sample appear on the same page. The data are in the same order as listed in Table 7.3, which should be consulted for the interpretation of each spectrum.

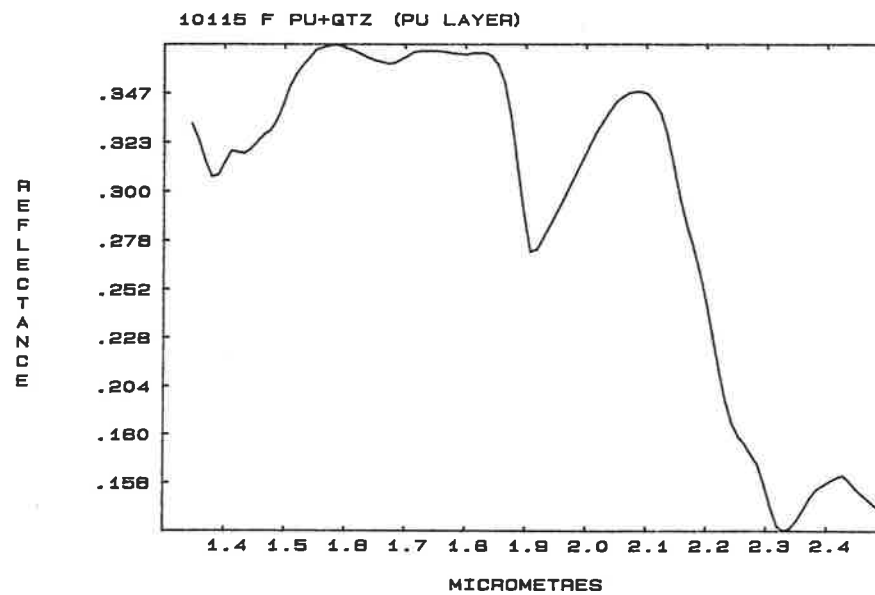
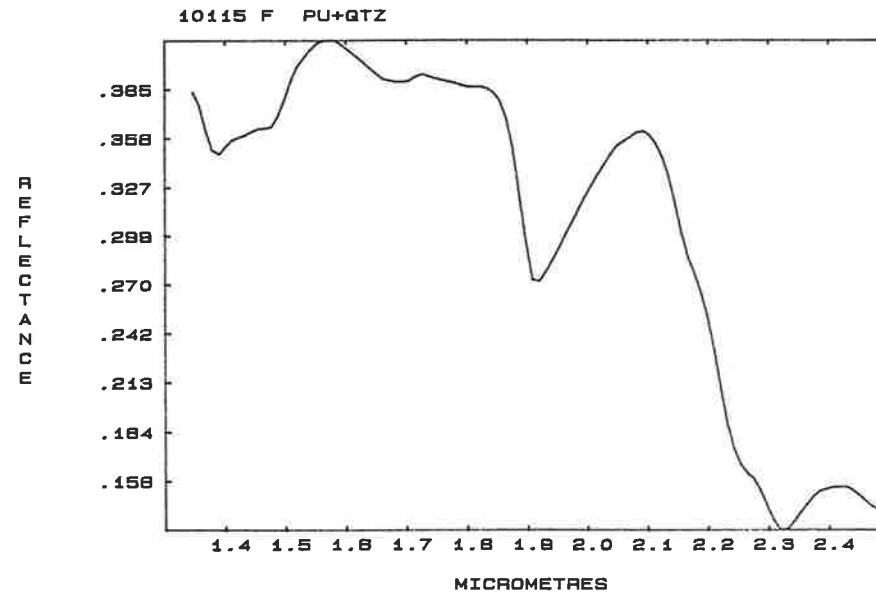
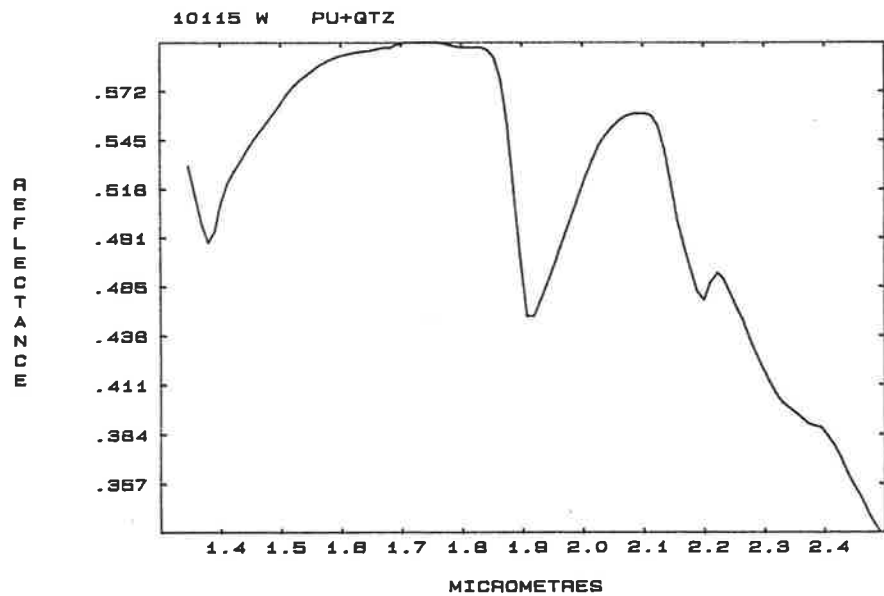
SWIR SPECTRA - Z-I METADOMAIN AND TRANSITION SAMPLES

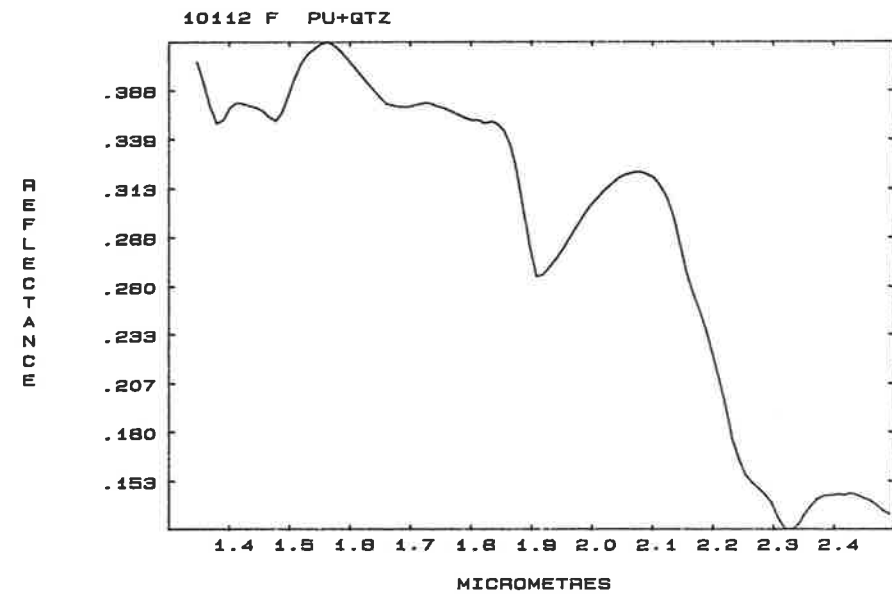
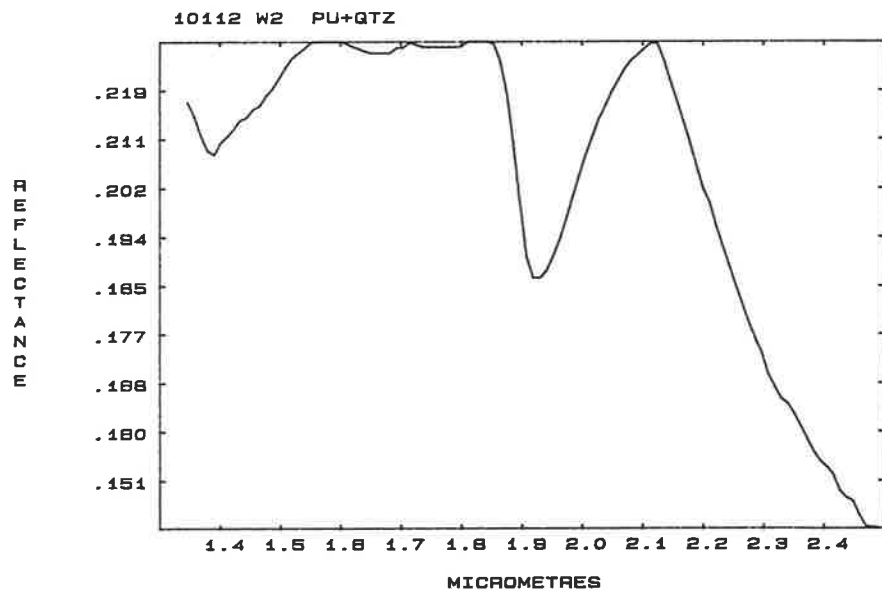
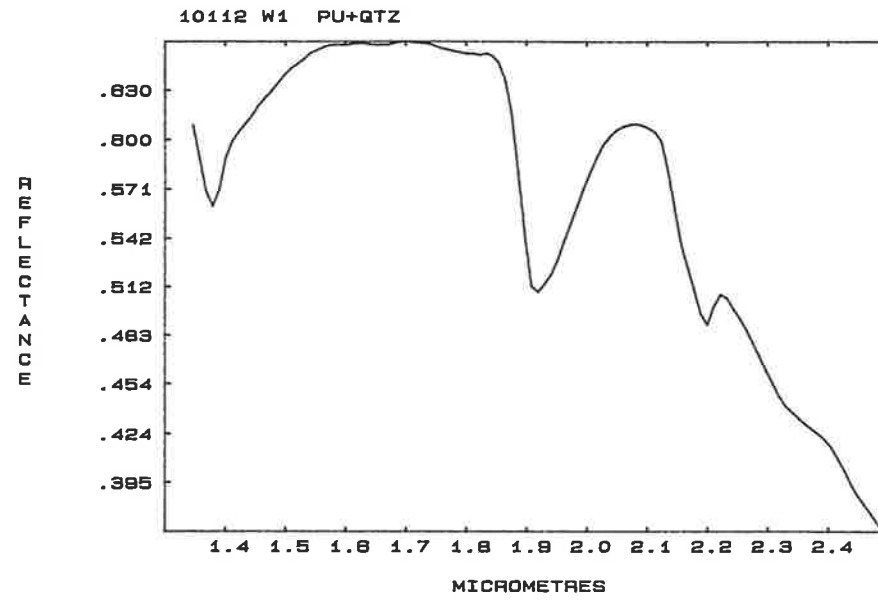


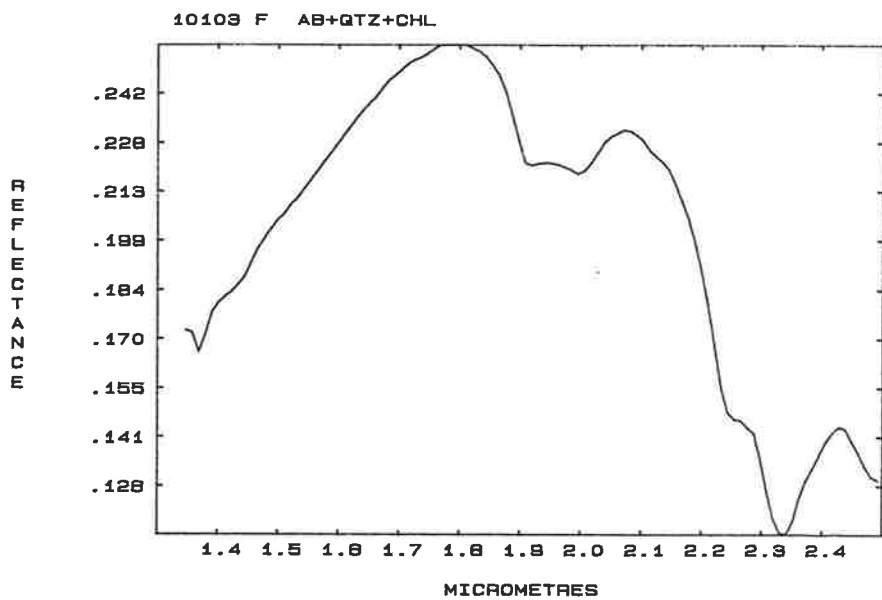
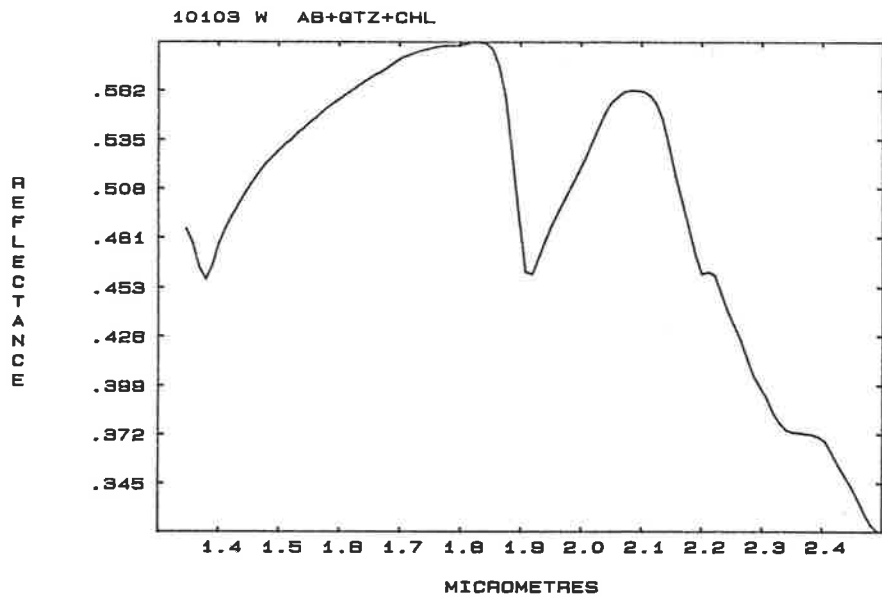






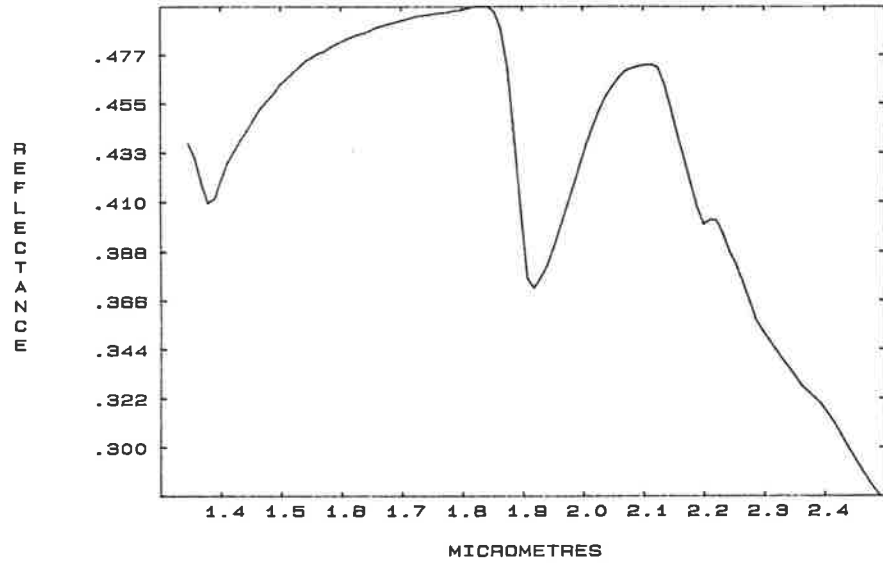




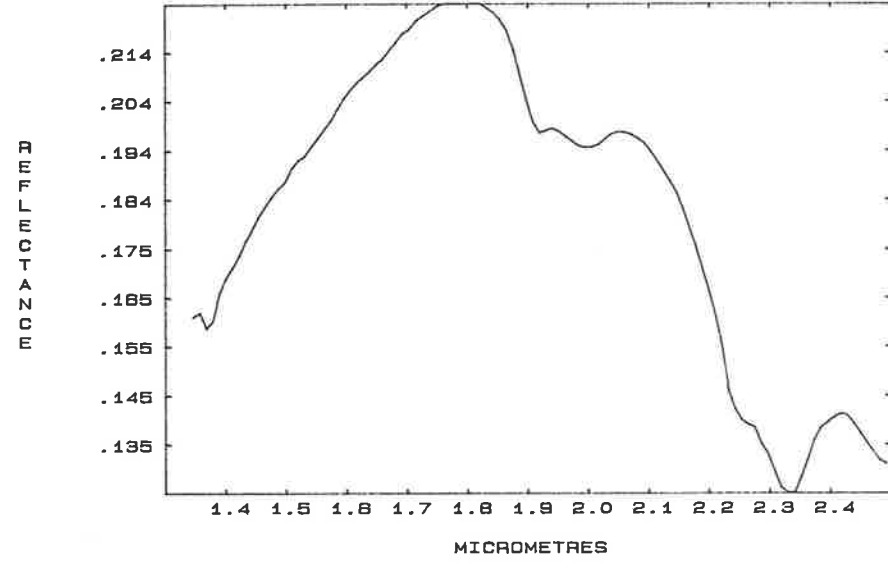


SWIR SPECTRA - Z-I RELICT DOMAIN SAMPLES

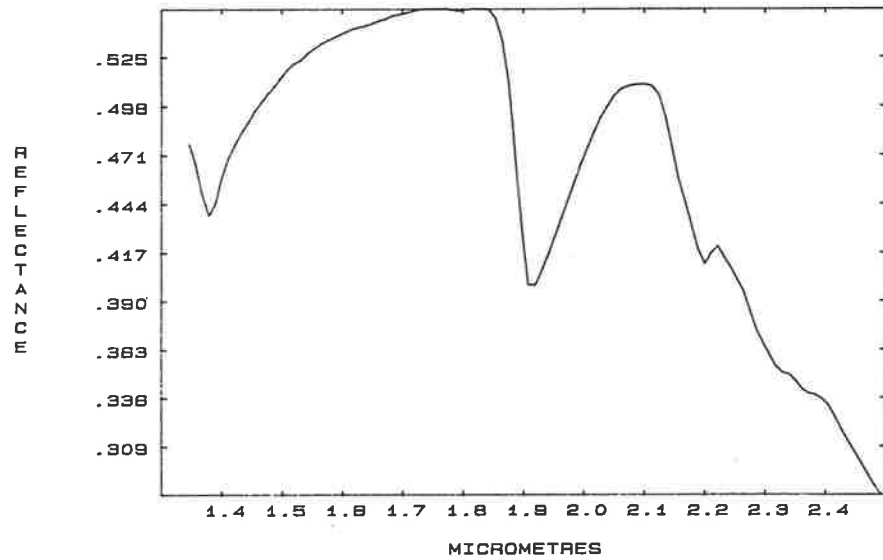
10100 W CA PLAG+PYX+CHL+SPH+TR.PU



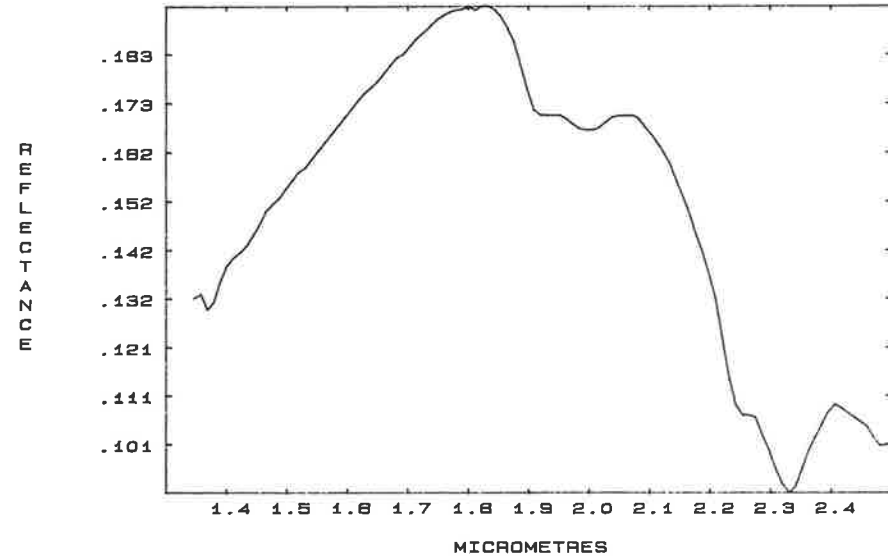
10100 F CA PLAG+PYX+CHL+SPH+TR.PU



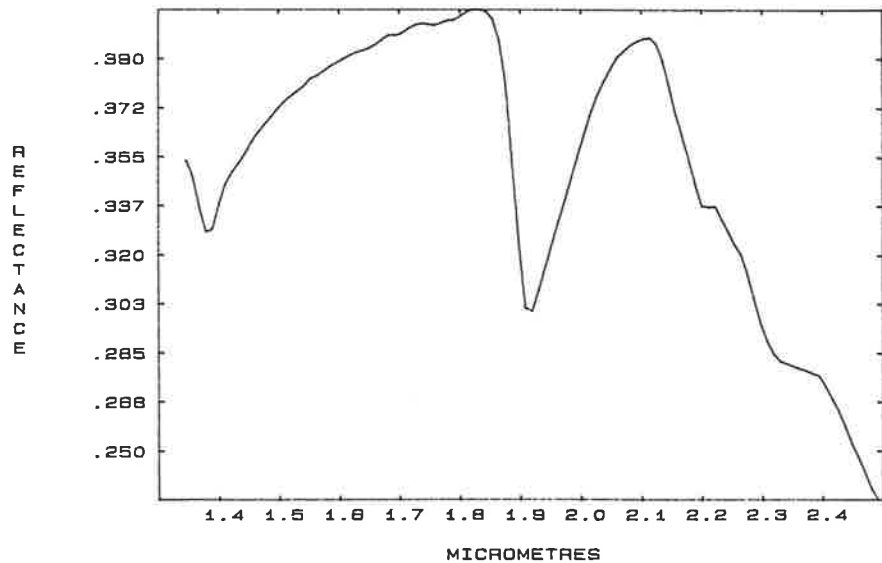
10102 W CA PLAG+PYX+CHL+SPH



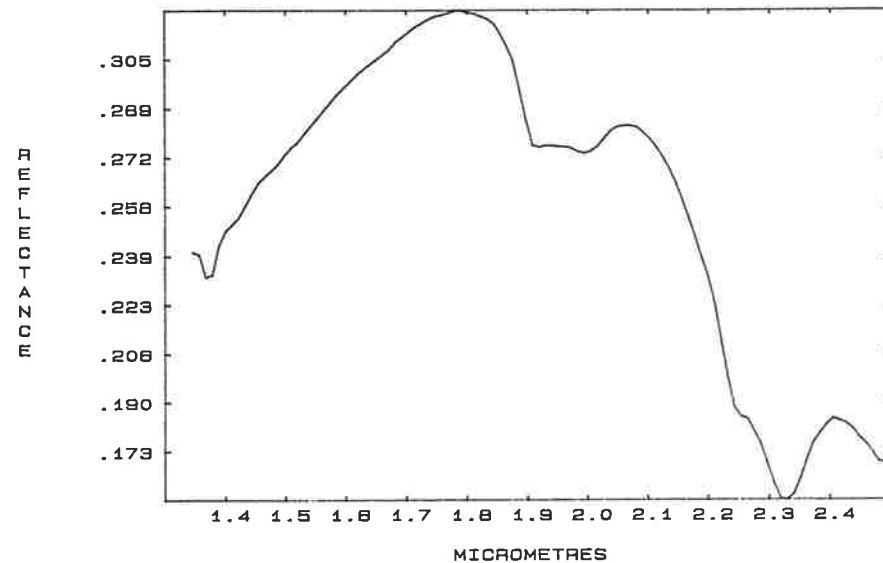
10102 F CA PLAG+PYX+CHL+SPH



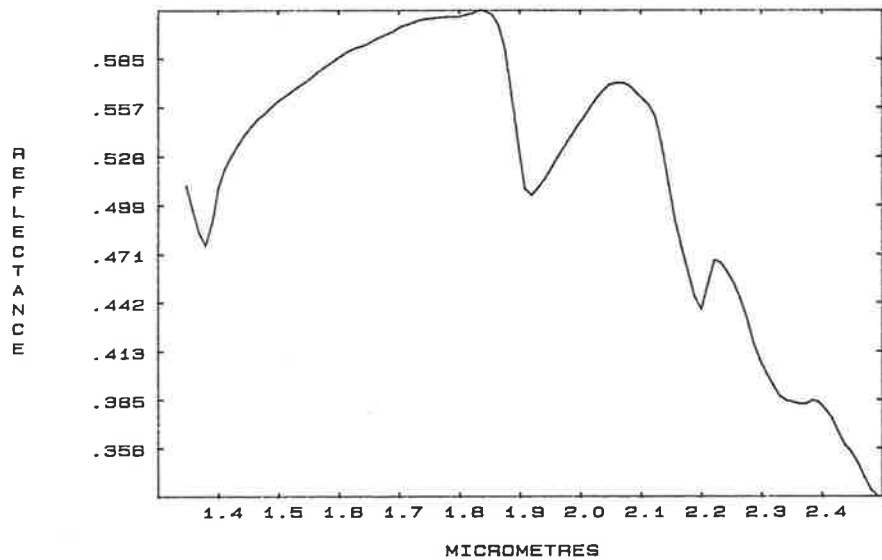
10090 W CA PLAG+PYX+CHL+SPH



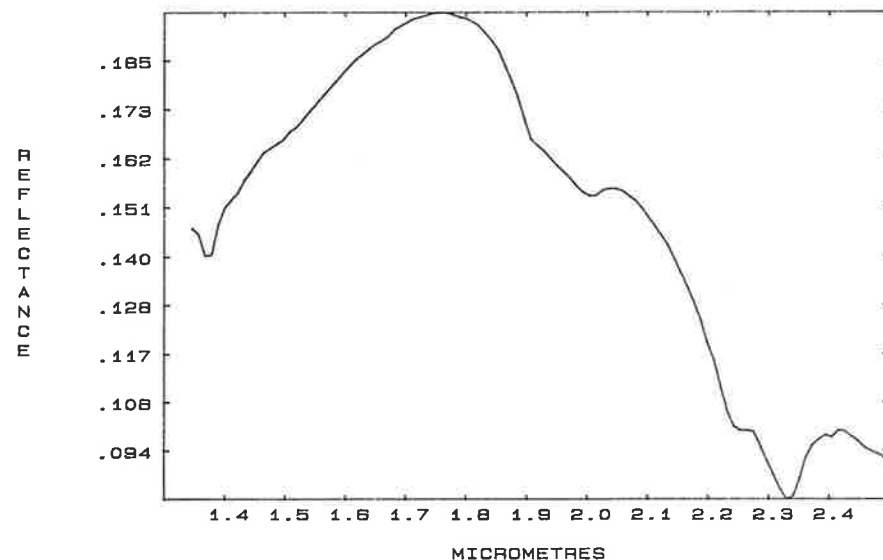
10090 F CA PLAG+PYX+CHL+SPH



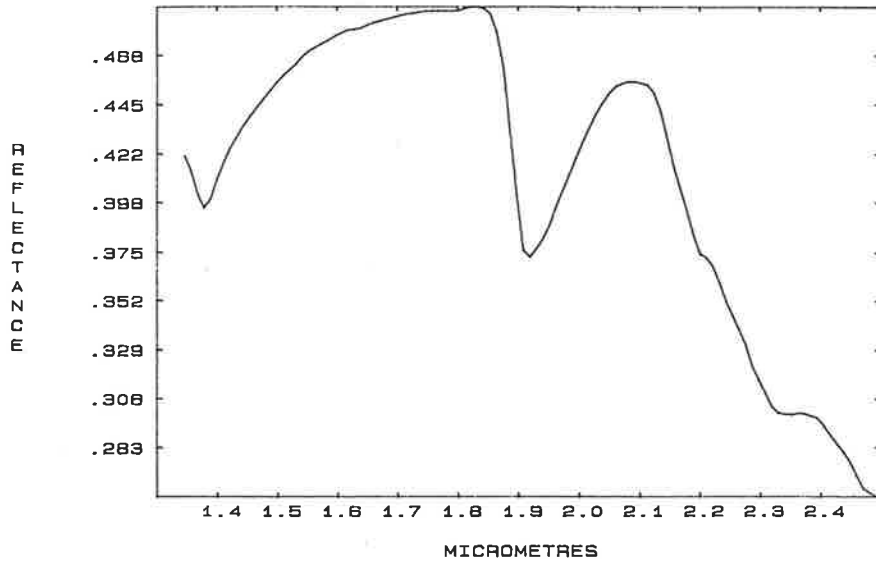
10105 W CA PLAG+PYX+CHL+SPH



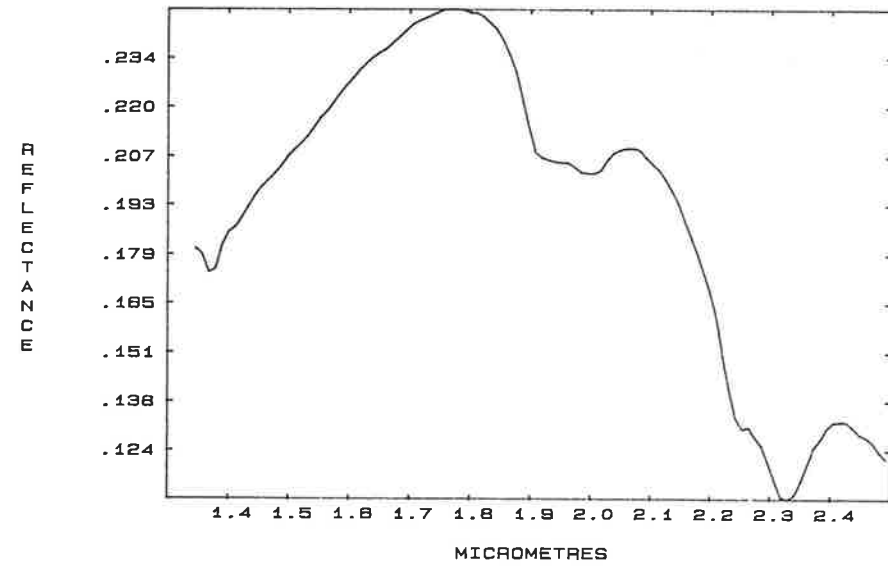
10105 F CA PLAG+PYX+CHL+SPH



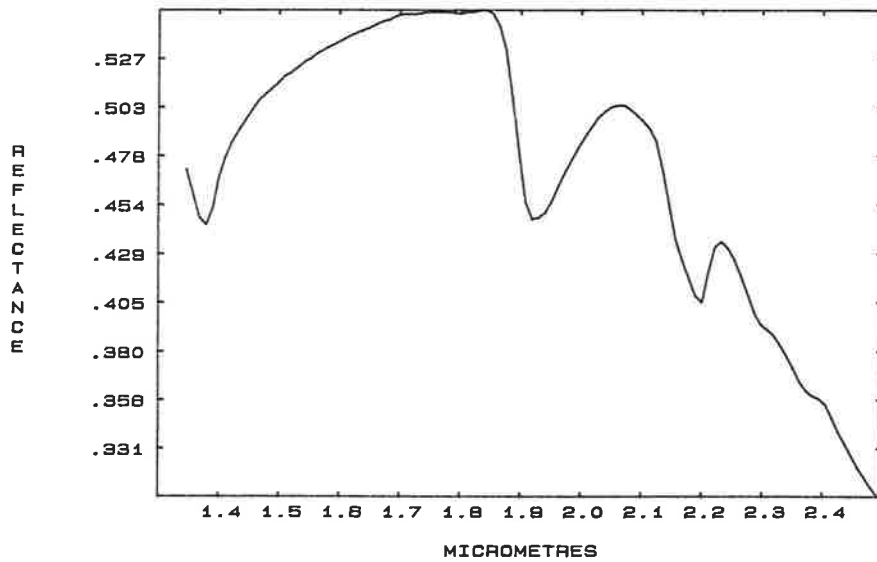
11158A W CA PLAG+PYX+CHL+SPH



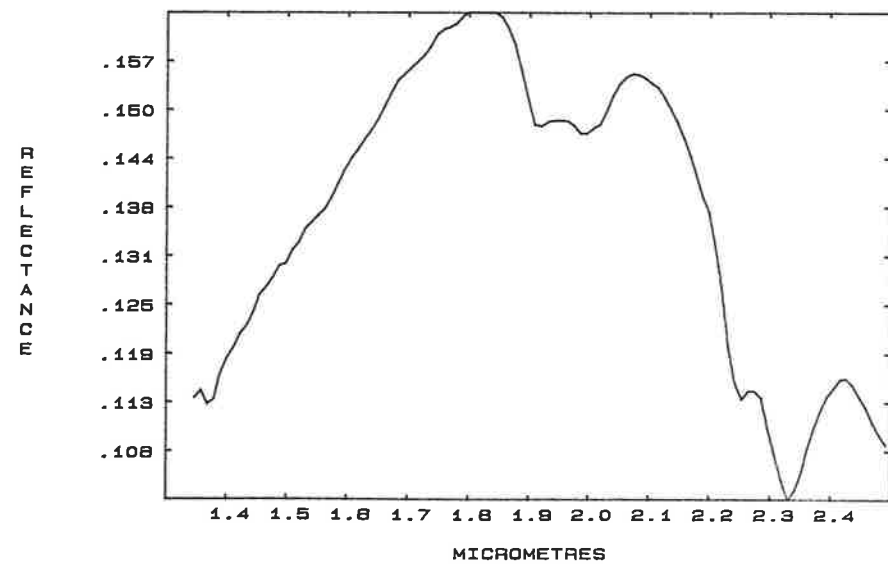
11158A F CA PLAG+PYX+CHL+SPH



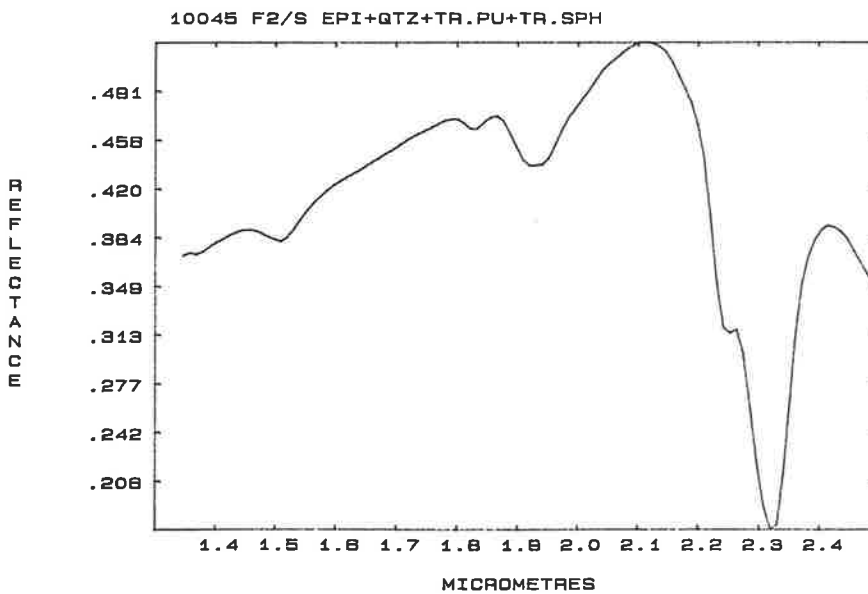
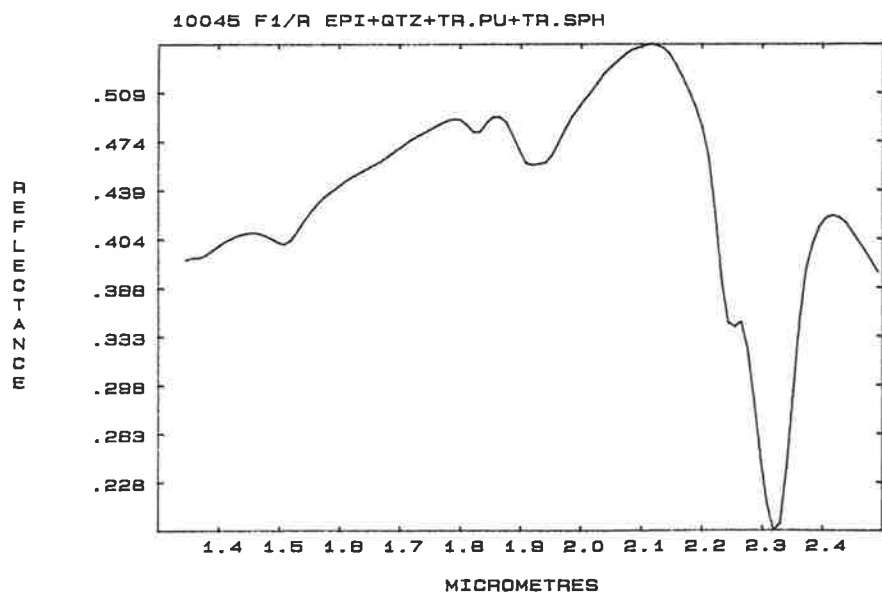
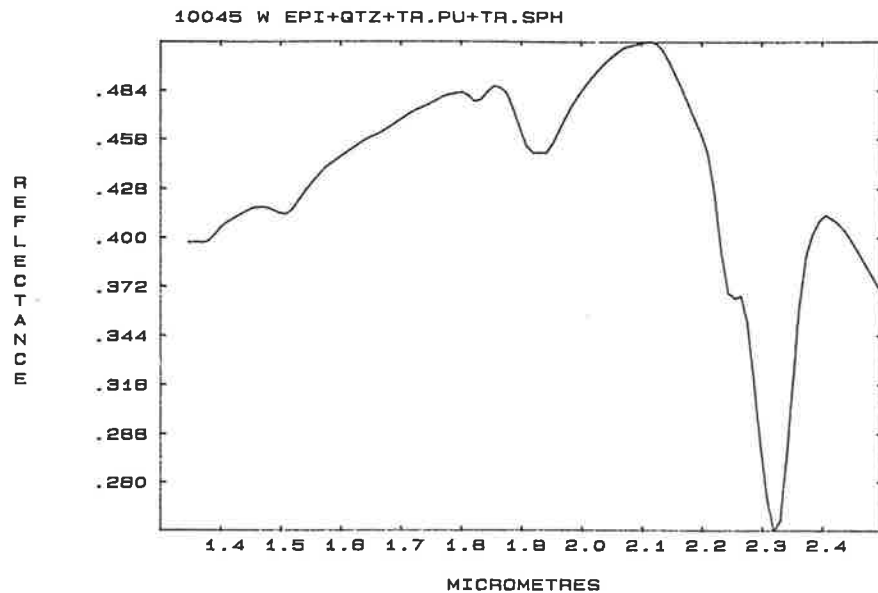
10118 W CA PLAG+PYX+CHL+SPH+CC

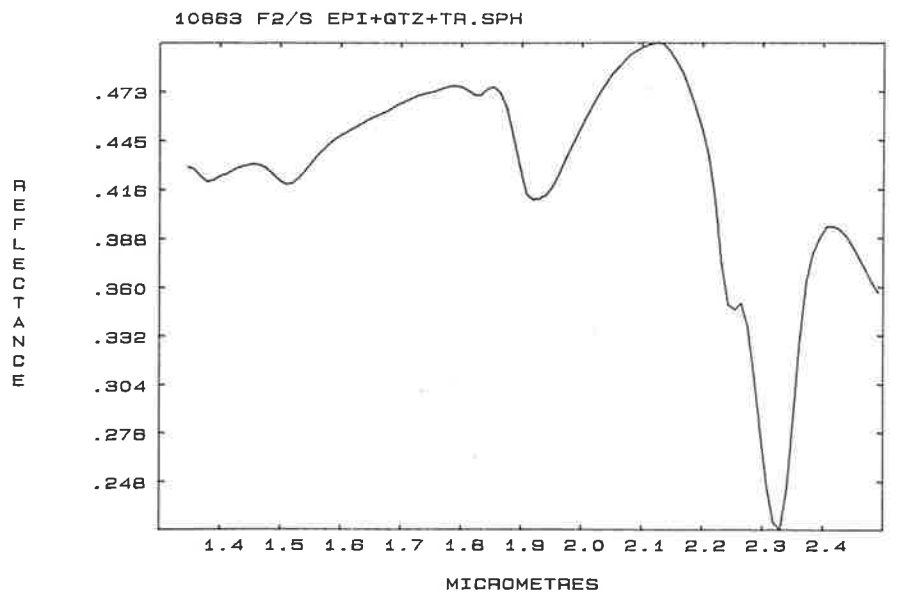
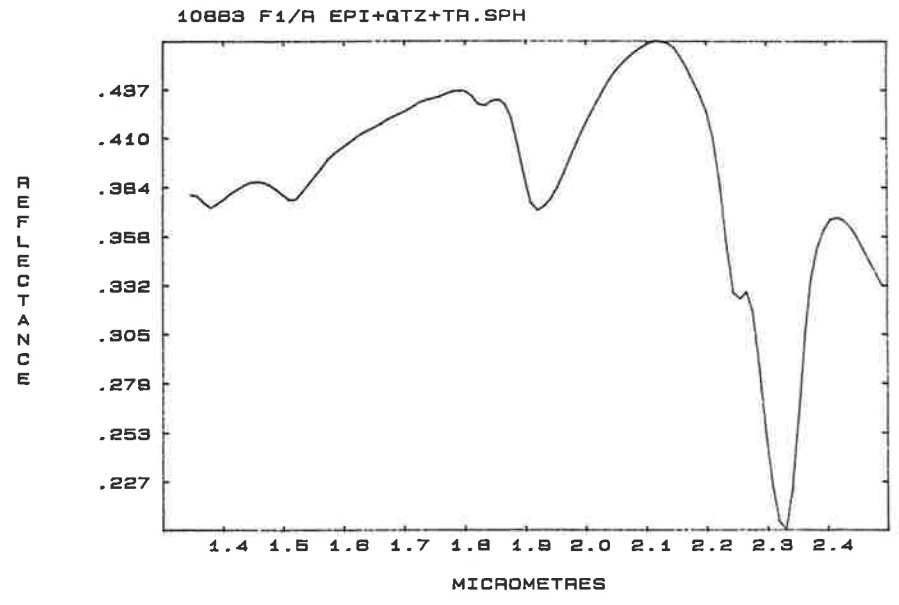
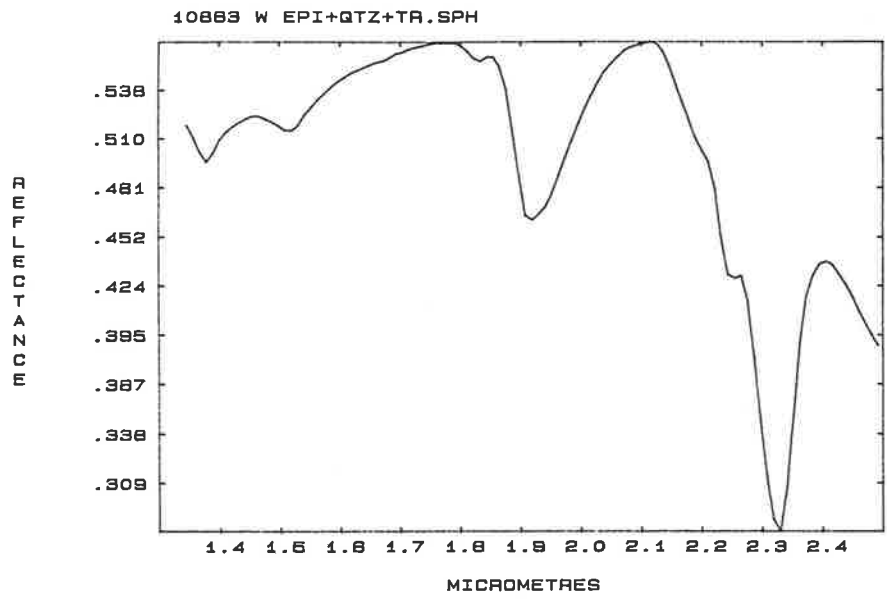


10118 F CA PLAG+PYX+CHL+SPH+CC

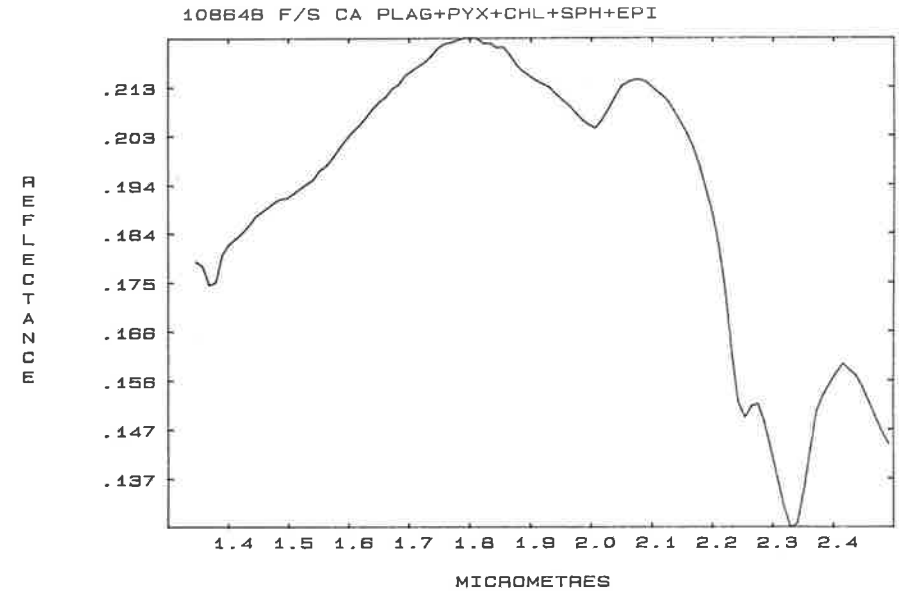
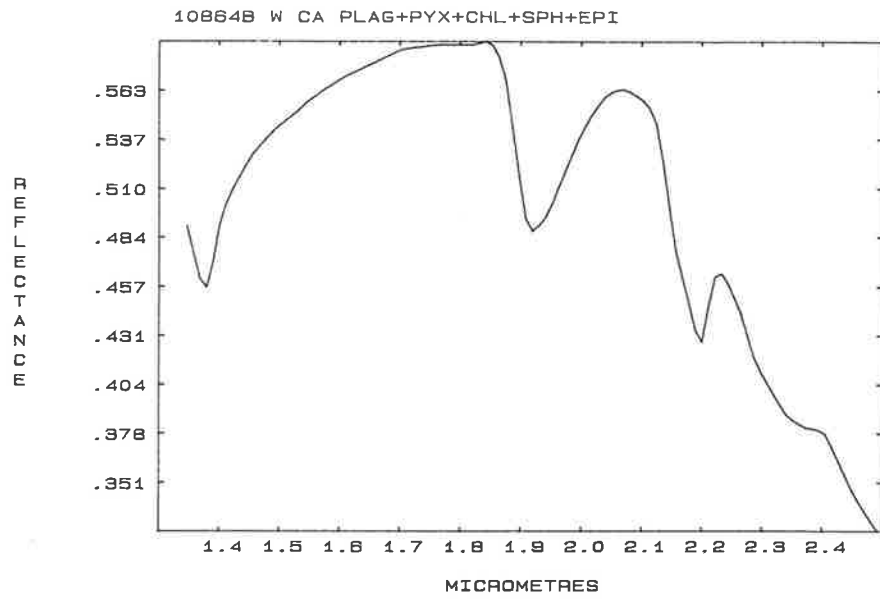


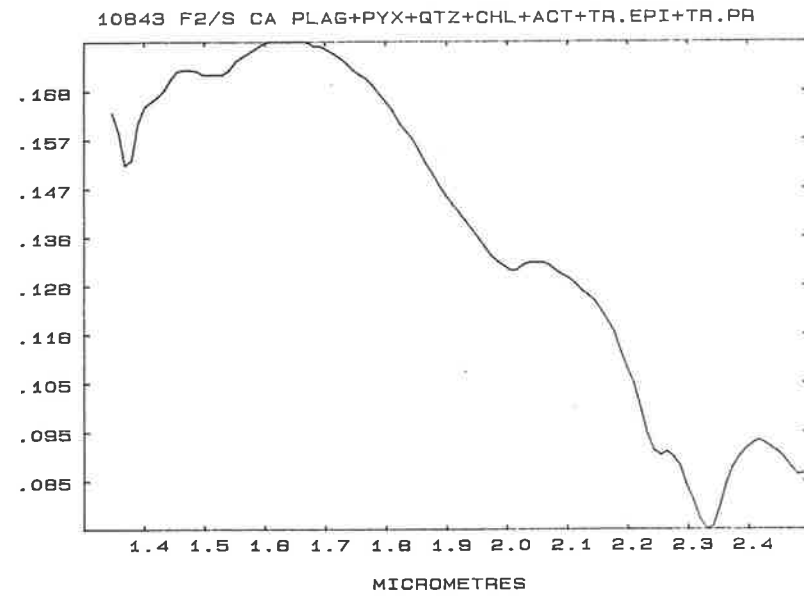
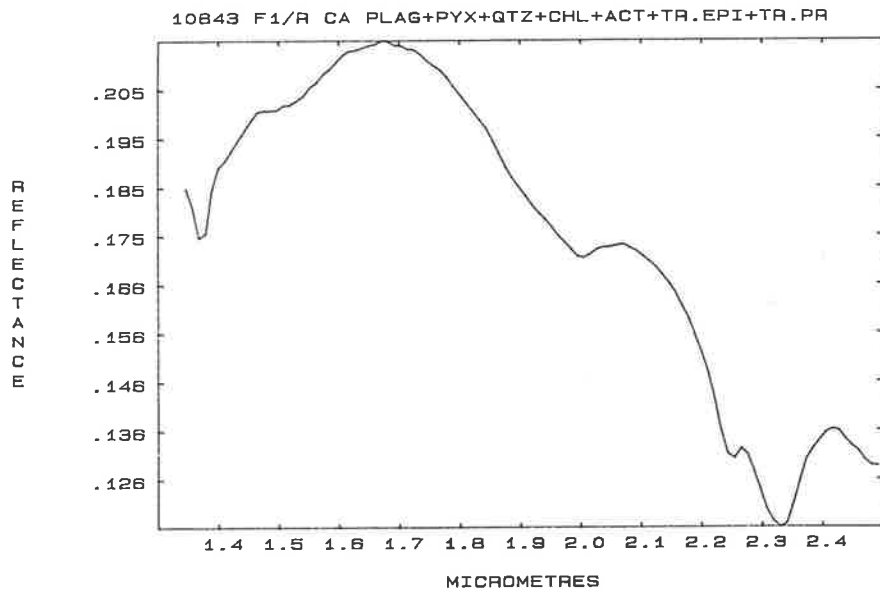
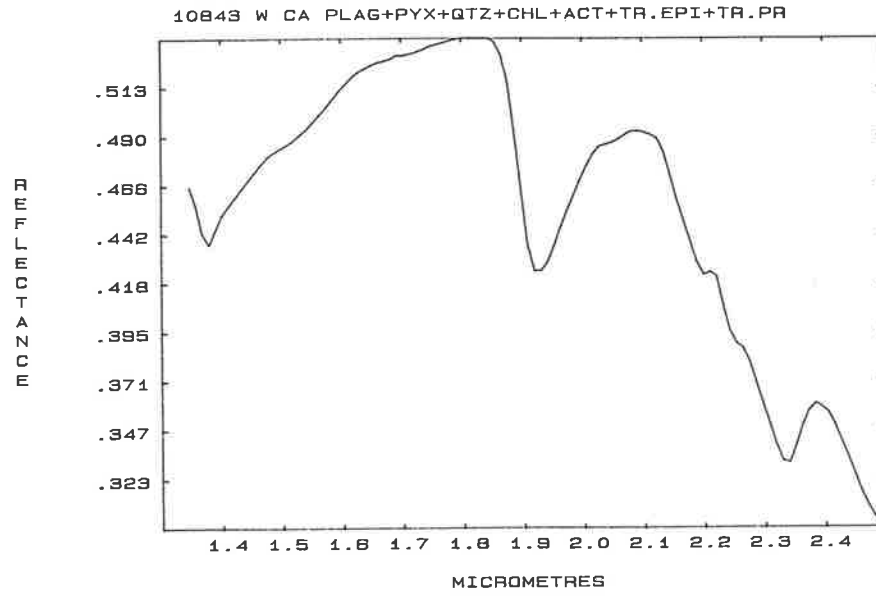
SWIR SPECTRA - Z-II AND Z-III METADOMAIN SAMPLES

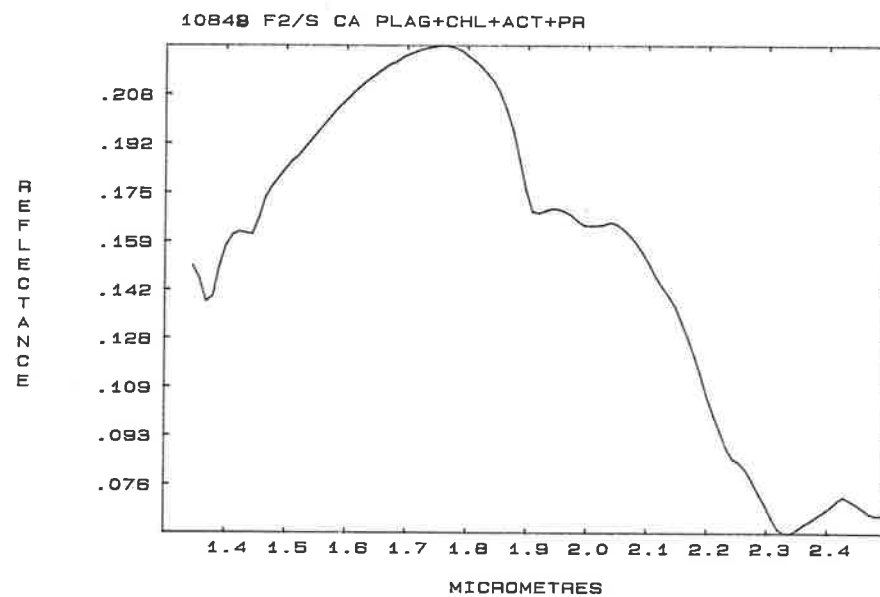
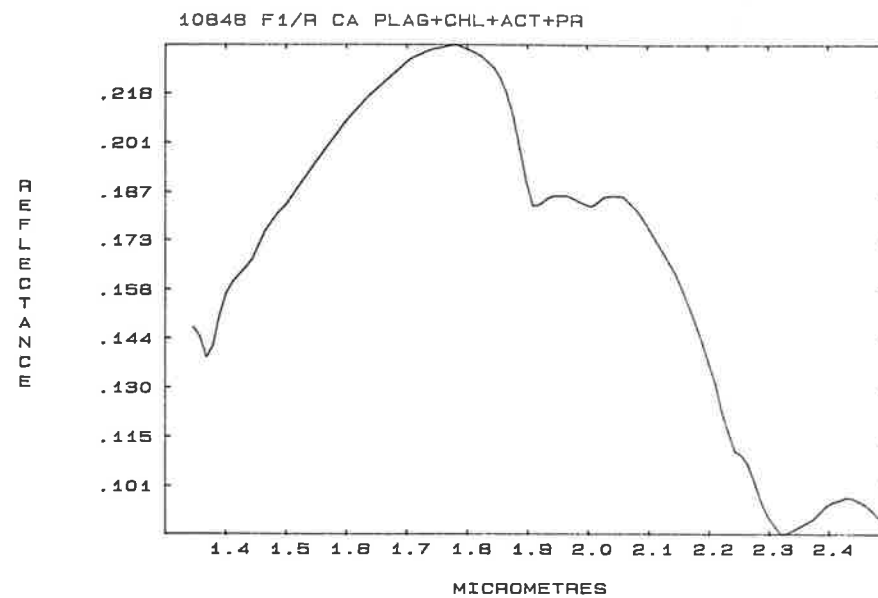
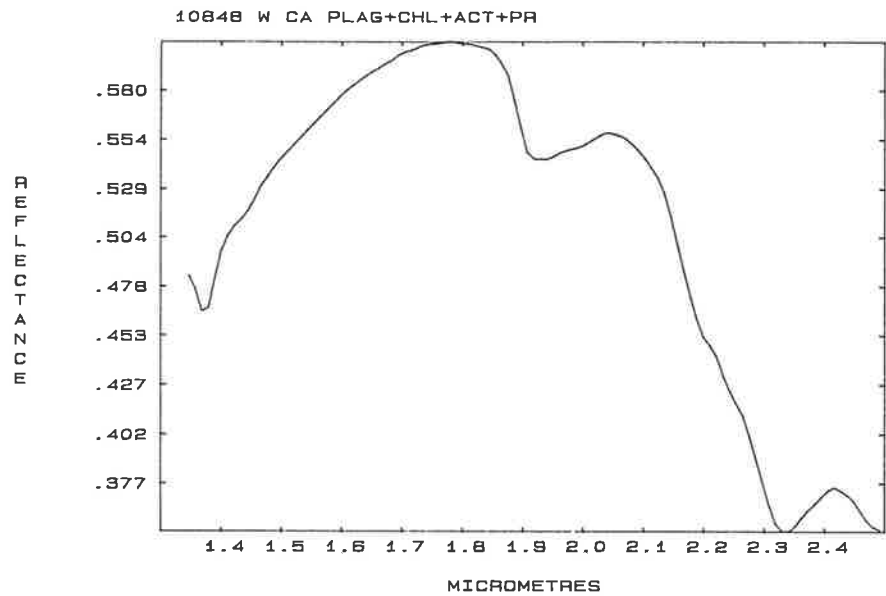


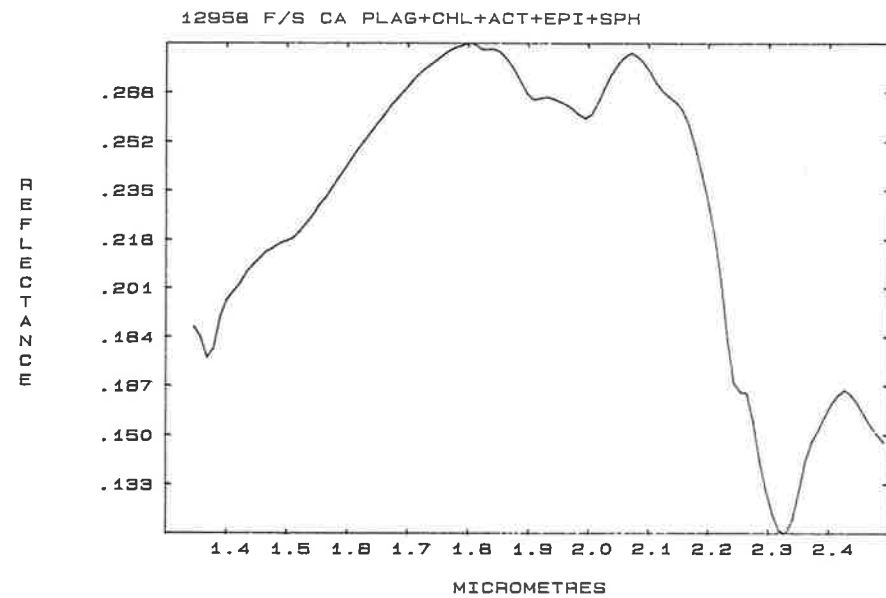
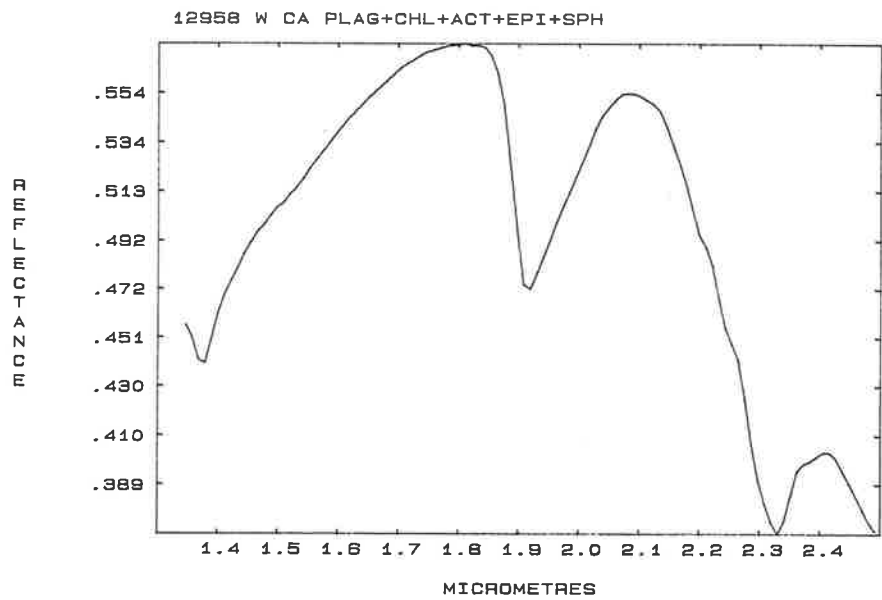


SWIR SPECTRA - Z-III RELICT DOMAIN AND Z-IV UNIFORMLY ALTERED METADOMAIN









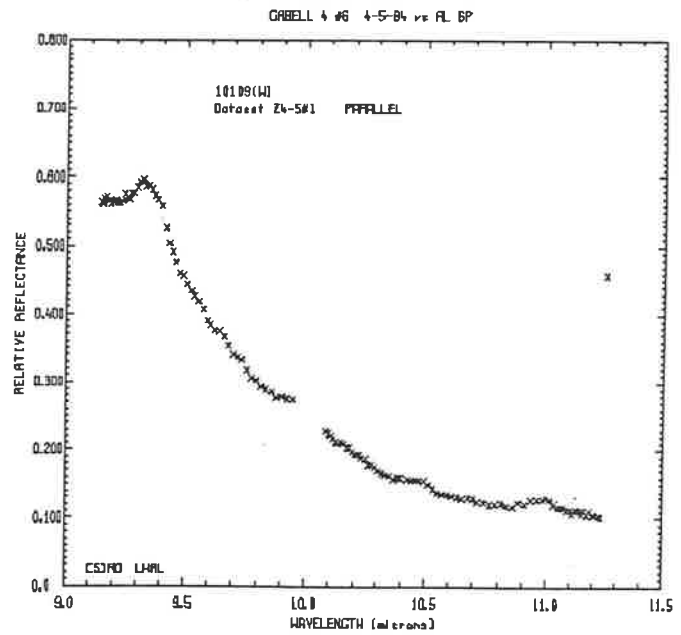
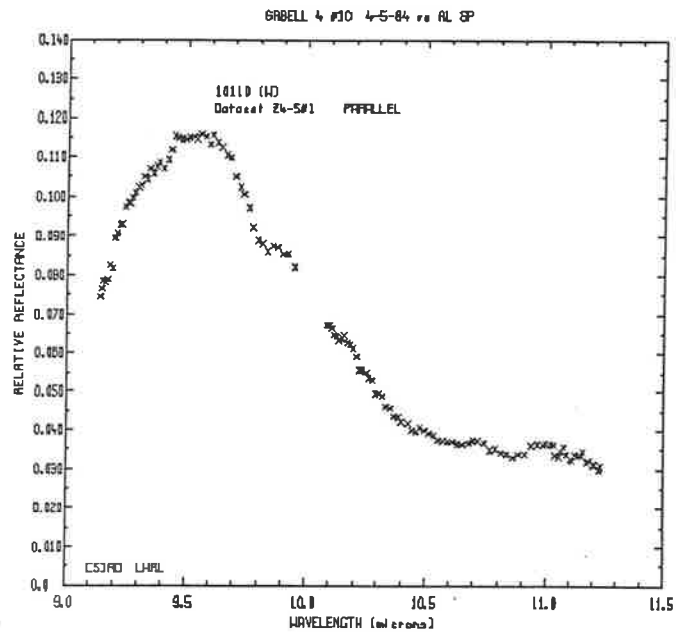
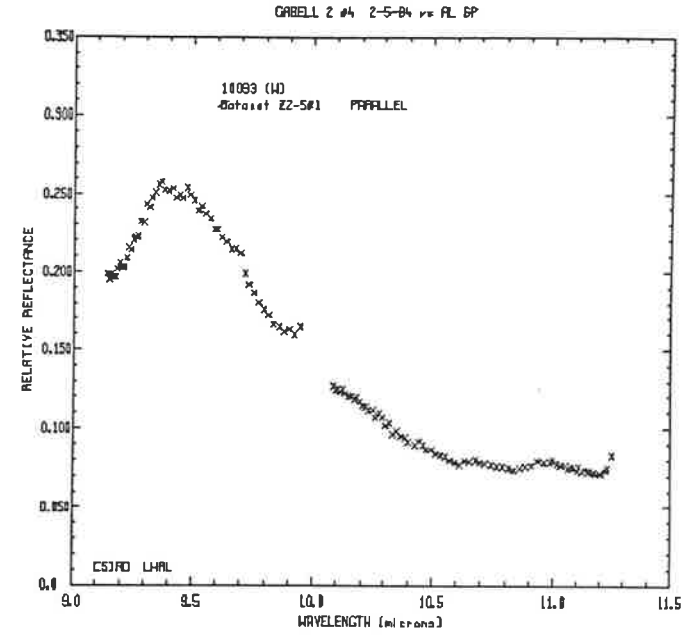
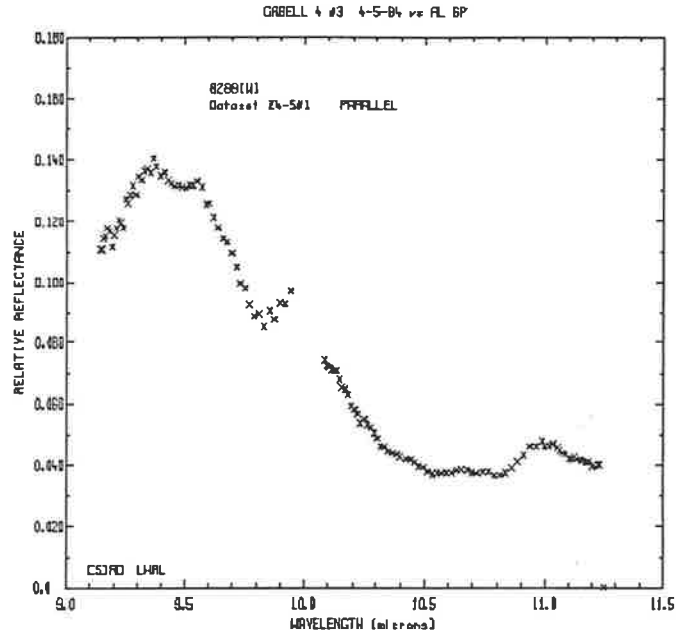
APPENDIX XII MIR laboratory (laser) reflectance spectra of samples
 from the Fortescue Group.

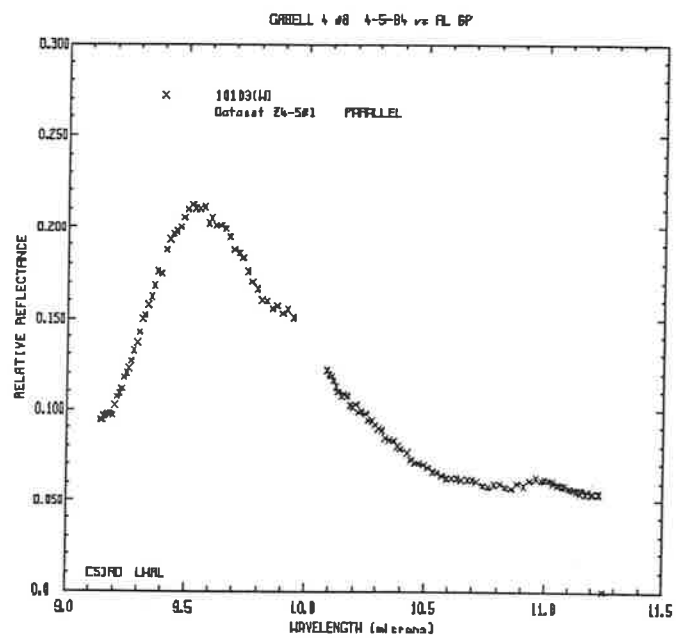
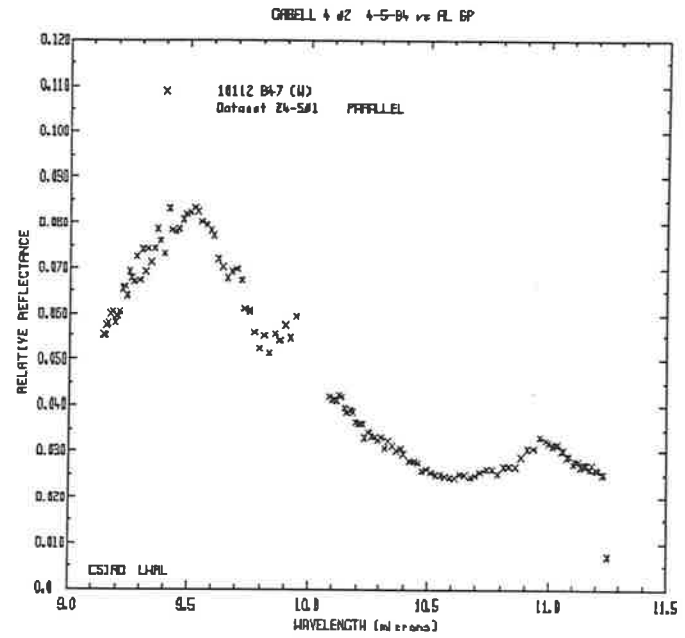
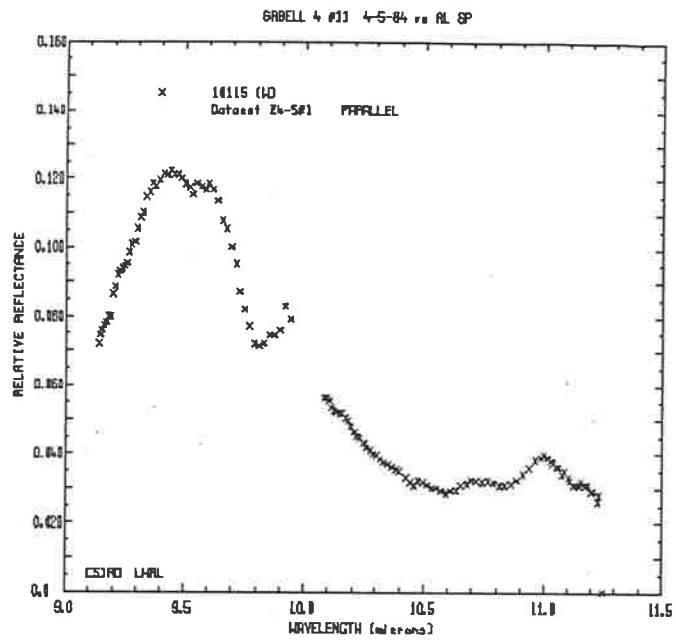
The MIR spectra are sorted on the basis of the nature of the surface measured (weathered or fresh) and the metamorphic/metasomatic character of the sample. The W spectra are presented first, having been subdivided into smaller groups on the basis of metamorphic zone, and the part of the flow (metadomain or relict domain), from which the sample was collected. Thus, spectra of weathered surfaces of samples from the metadomain (altered rocks) of Z-I (the lowest metamorphic grade) appear together, first.

The F spectra appear after the W spectra, and have been sorted in a similar fashion. The order in which the spectra appear is the same as that listed in Table 7.3, which should be consulted for the interpretation of spectral features.

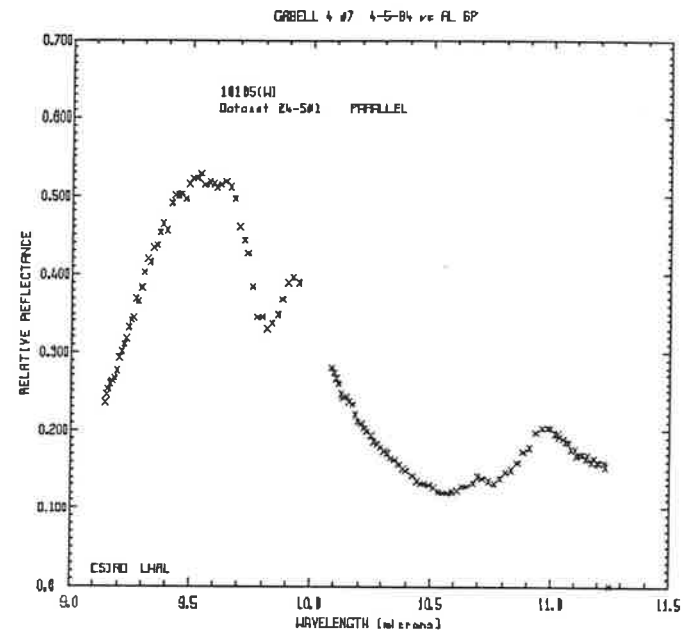
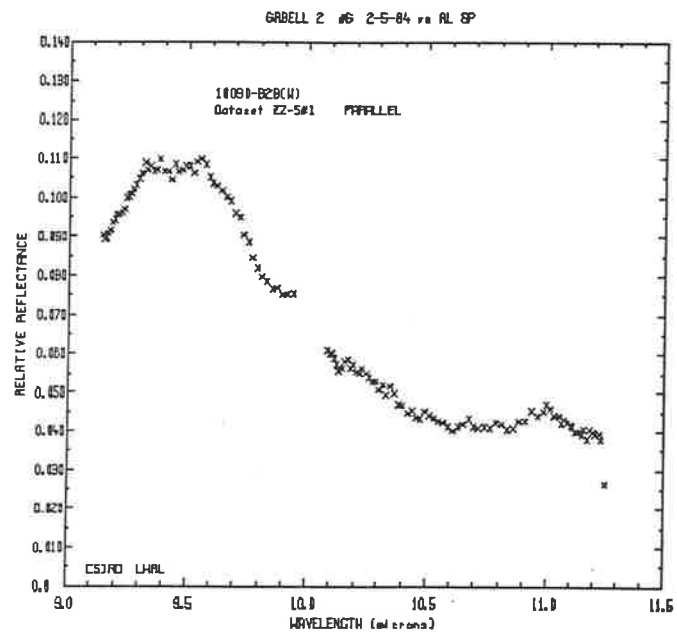
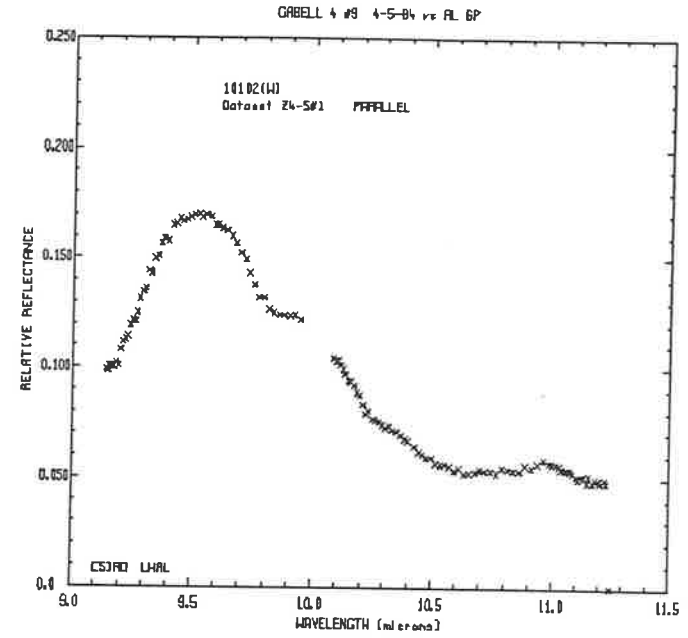
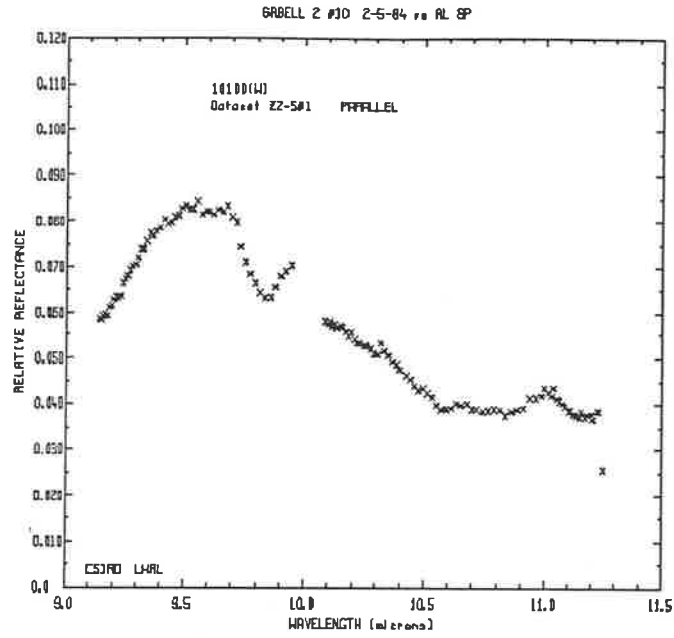
The F spectra of the prehnite-rich samples (10110 and 10109) and the albitised sample (10103) discussed in section 7.5.7 of the text, appear as the 3rd, 4th and last plots in the relevant group of spectra.

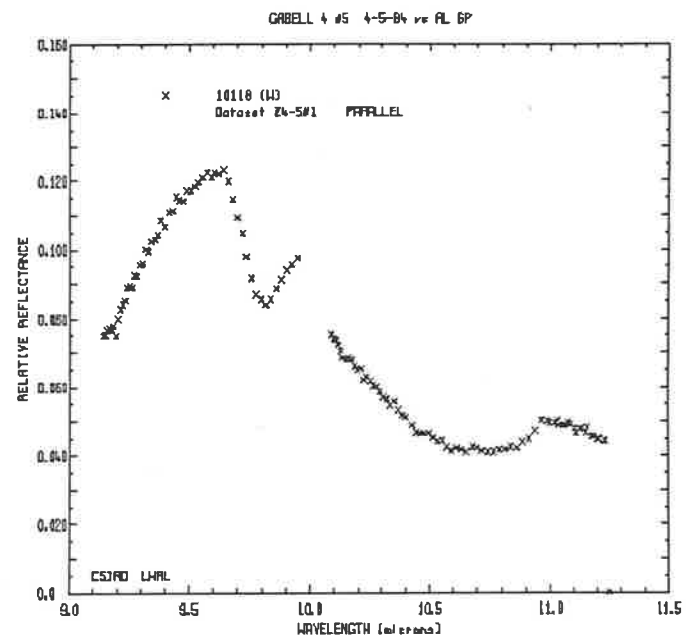
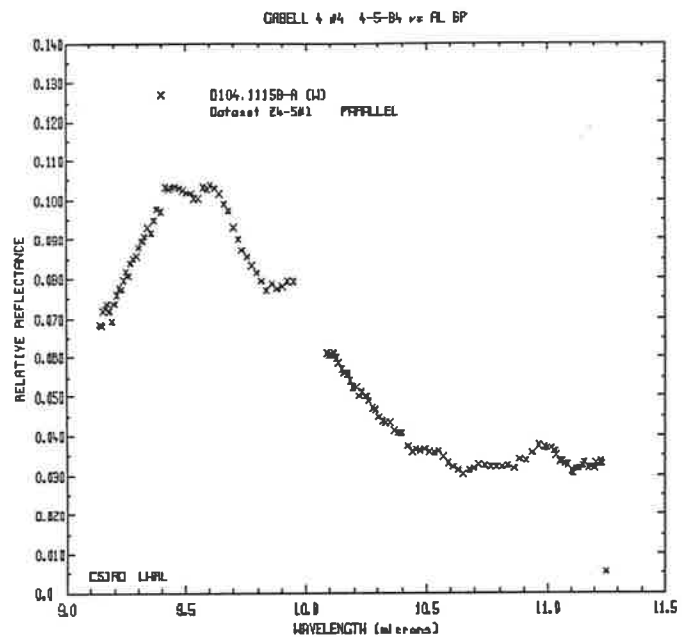
MIR W SPECTRA - Z-I METADOMAIN AND TRANSITION SAMPLES



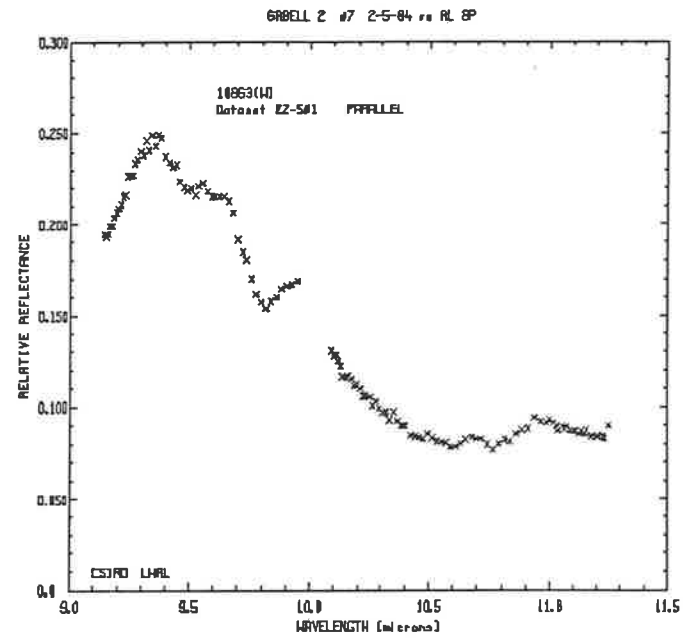
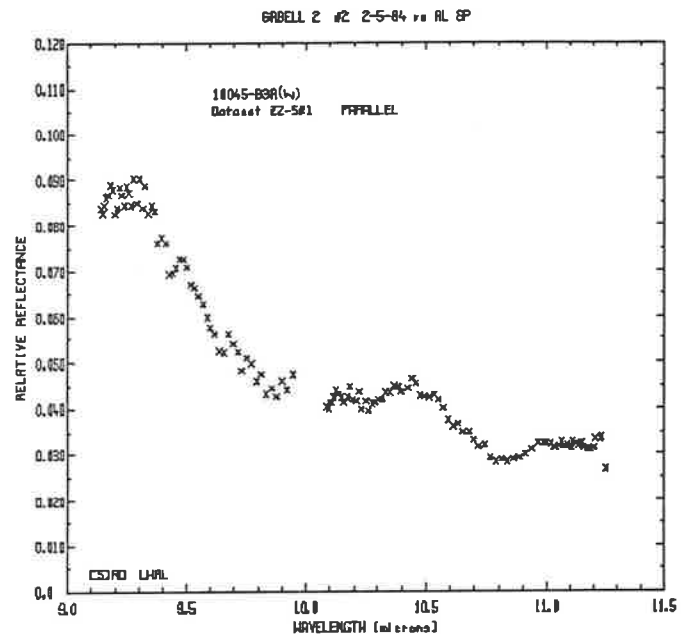


MIR W SPECTRA - Z-I RELICT DOMAIN SAMPLES

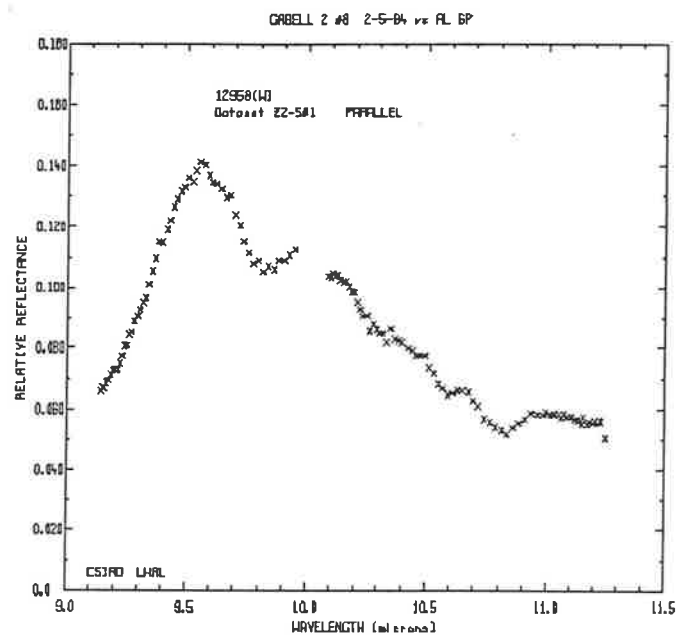
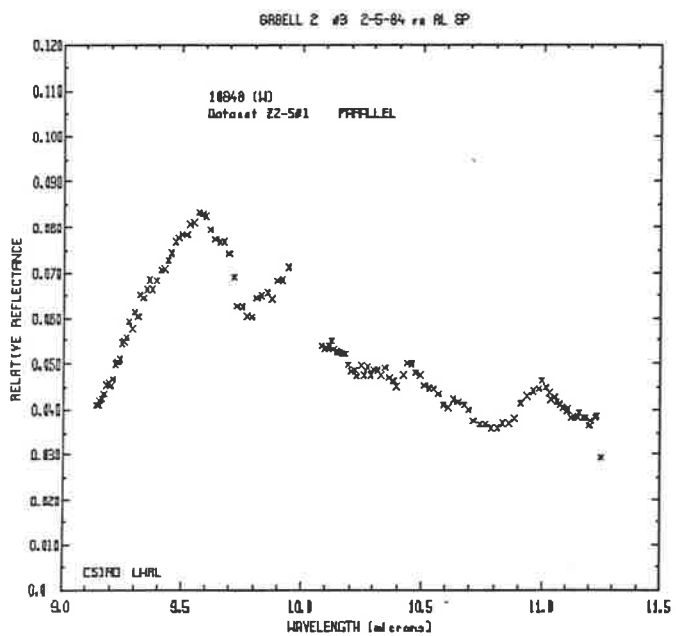
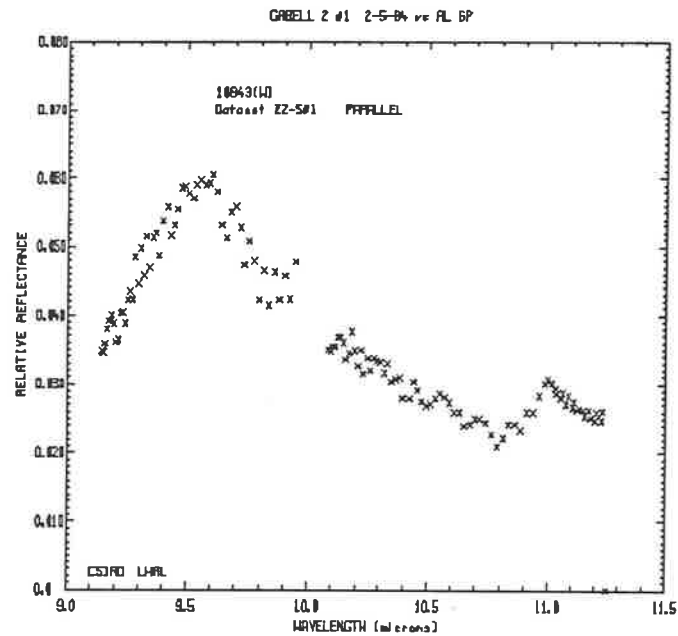
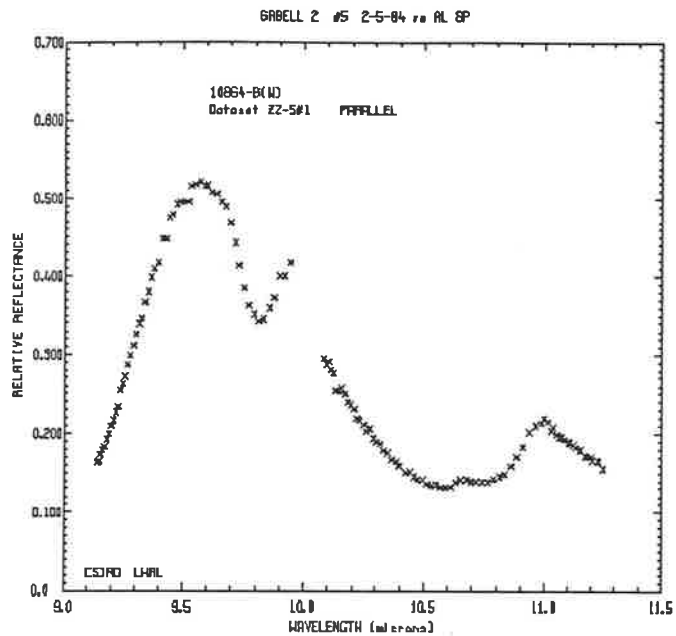




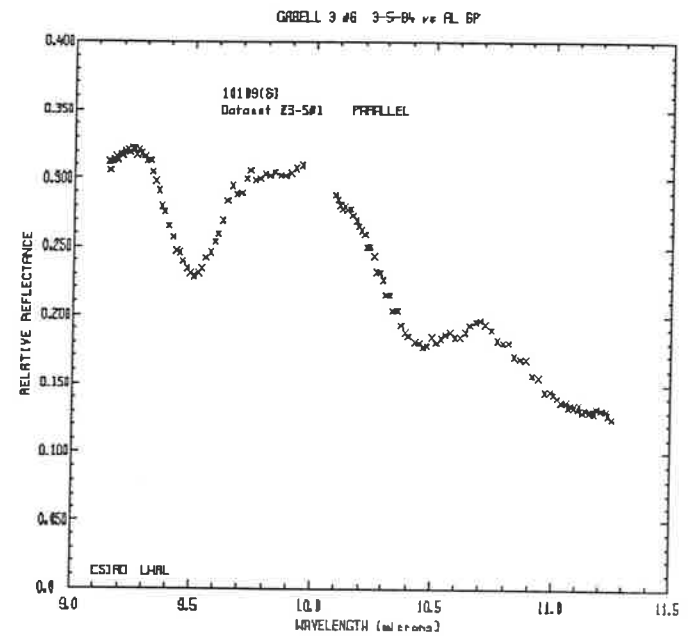
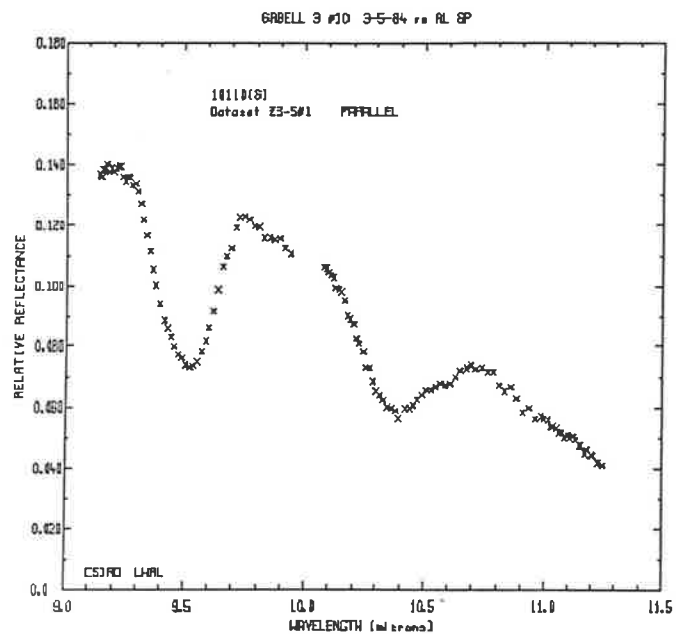
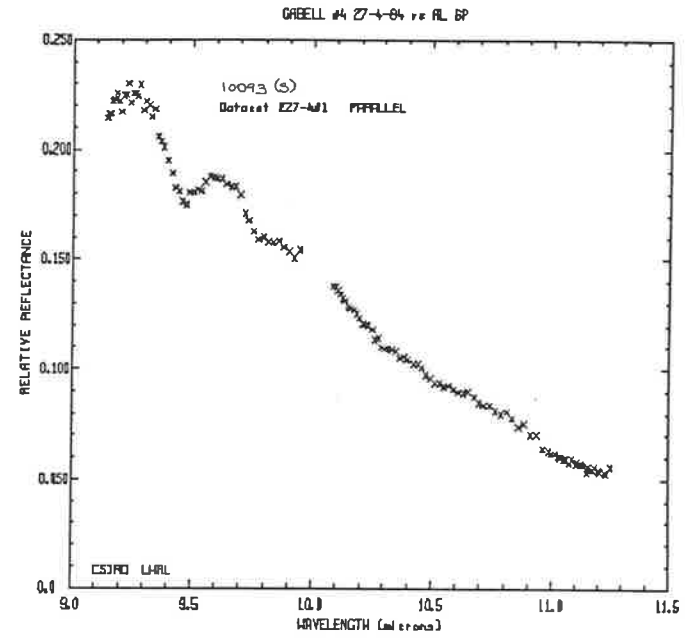
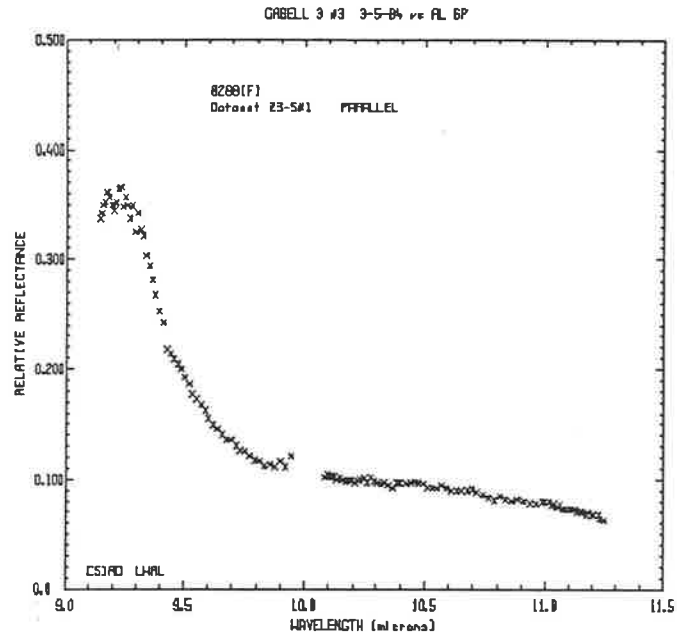
MIR W SPECTRA - Z-II AND Z-III METADOMAIN SAMPLES



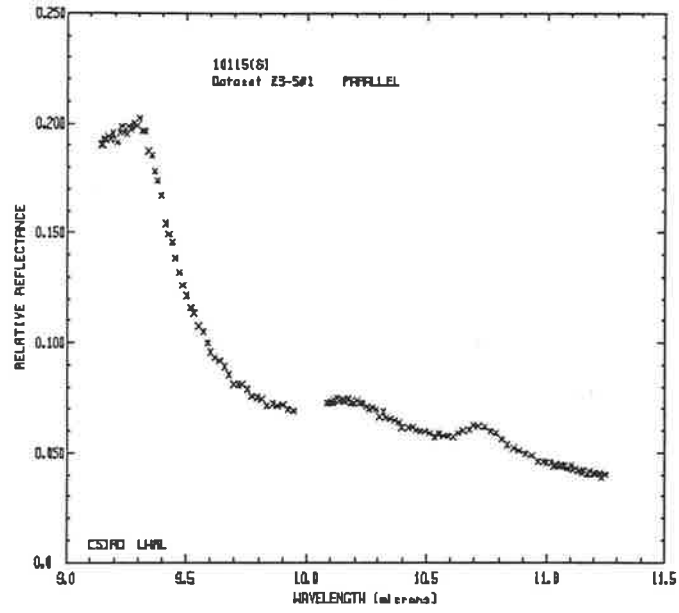
MIR W SPECTRA - Z-III RELICT DOMAIN AND Z-IV UNIFORMLY ALTERED METADOMAIN



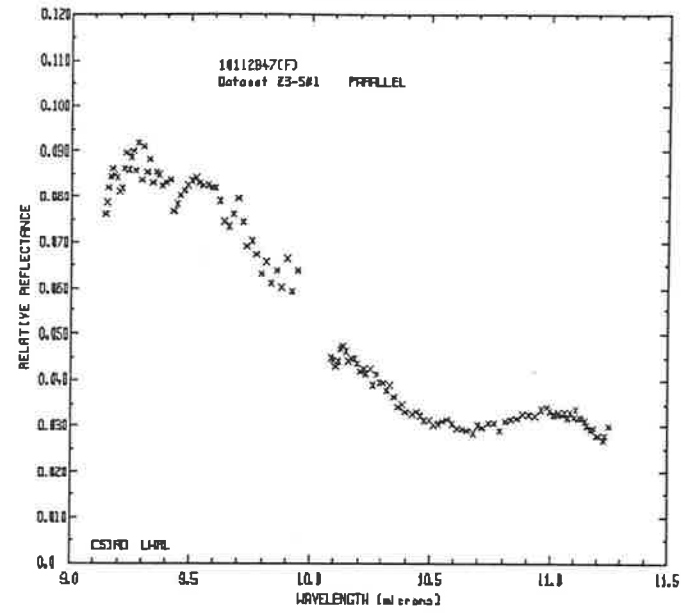
MIR F SPECTRA - Z-I METADOMAIN AND TRANSITION SAMPLES



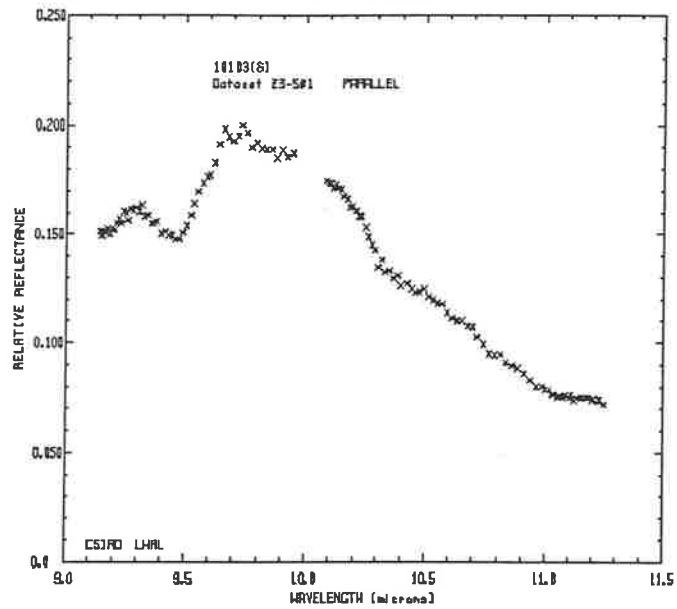
GABELL 3 #11 3-5-84 vs RL BP



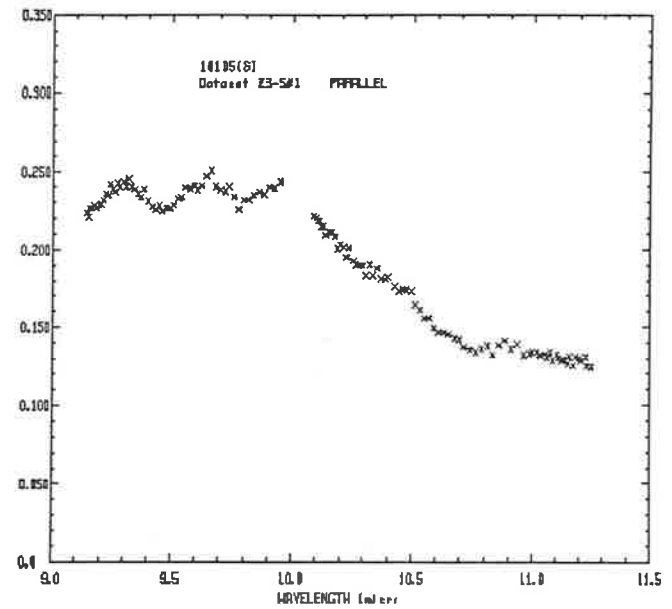
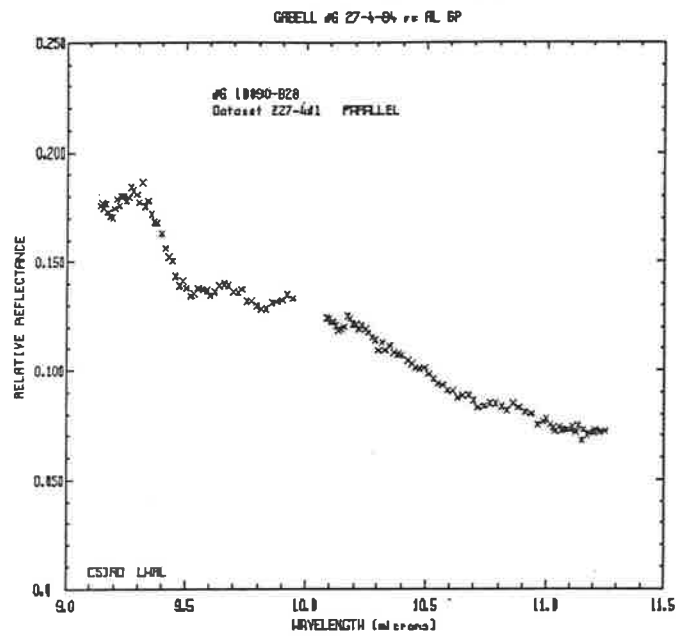
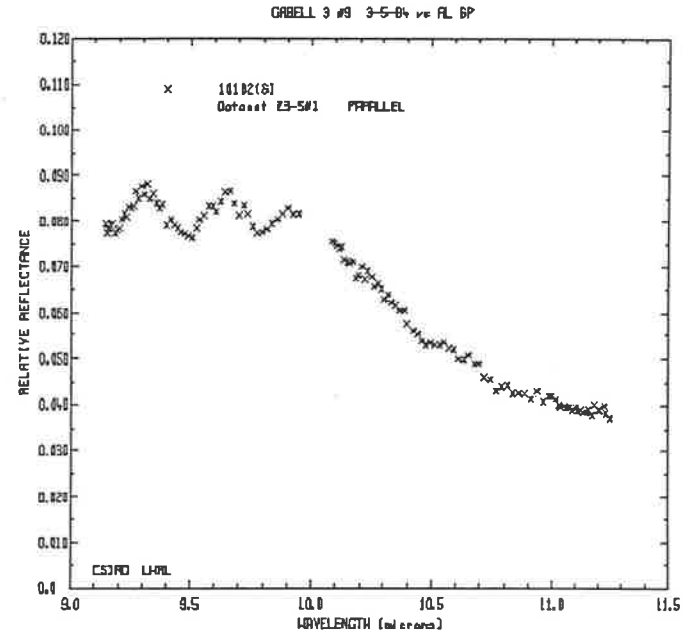
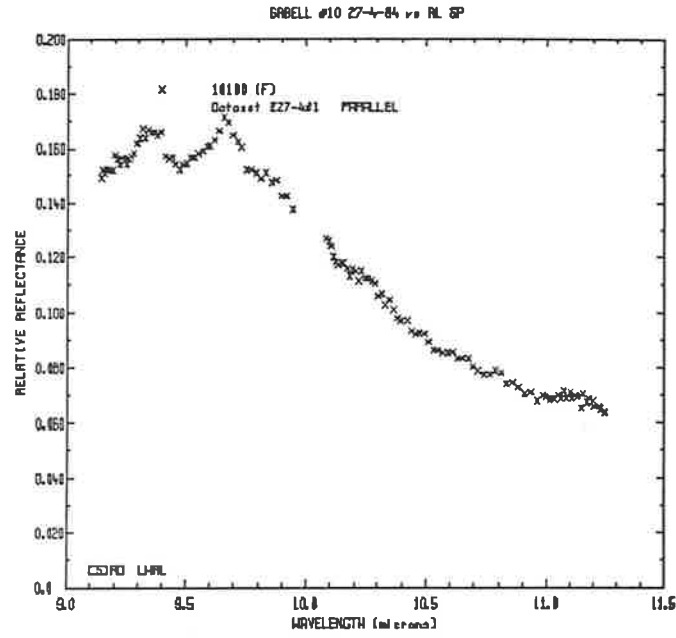
GABELL 3 #2 3-5-84 vs RL BP

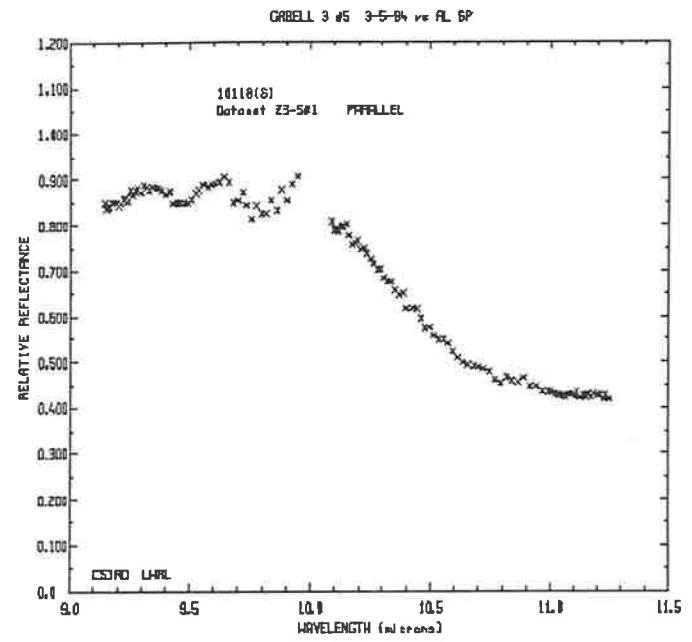
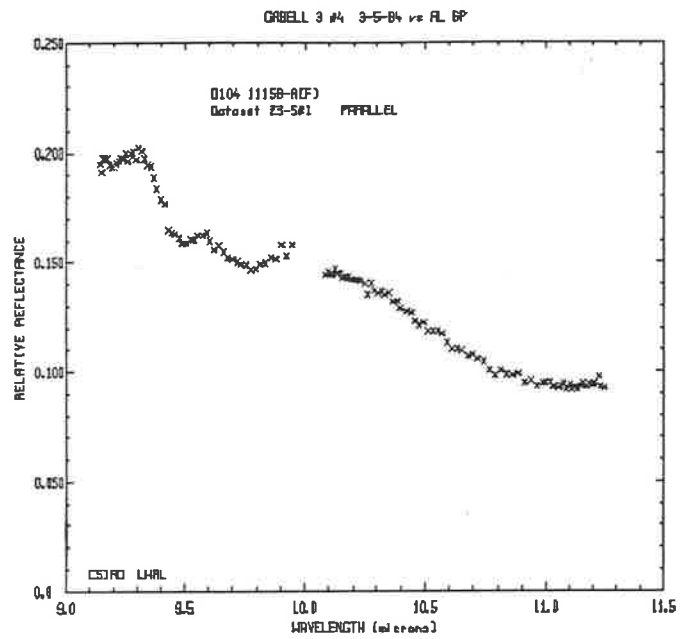


GABELL 3 #8 3-5-84 vs RL BP

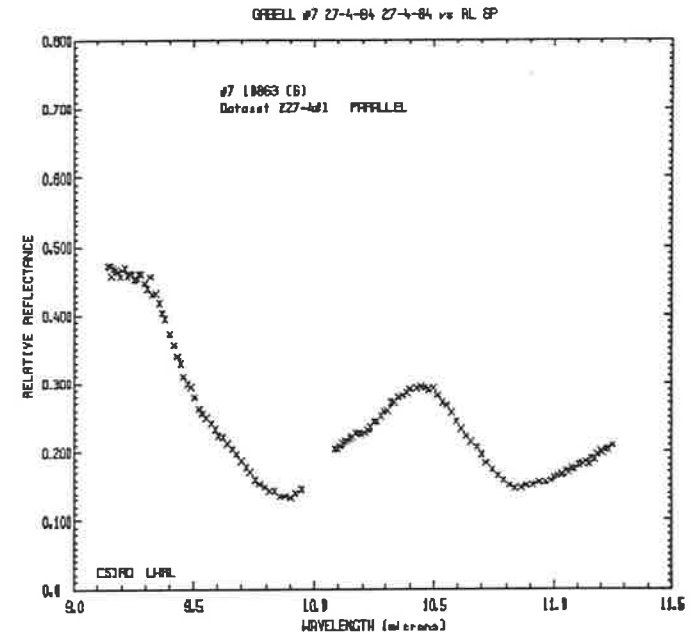
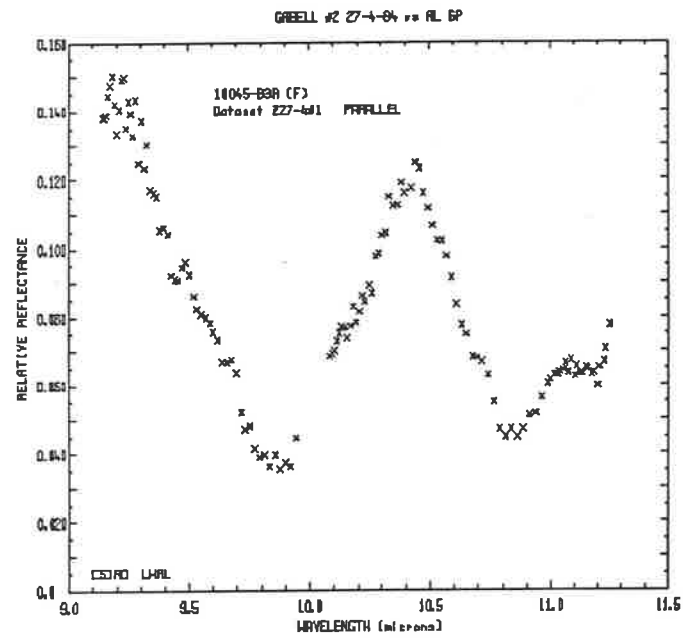


MIR F SPECTRA - Z-I RELICT DOMAIN SAMPLES

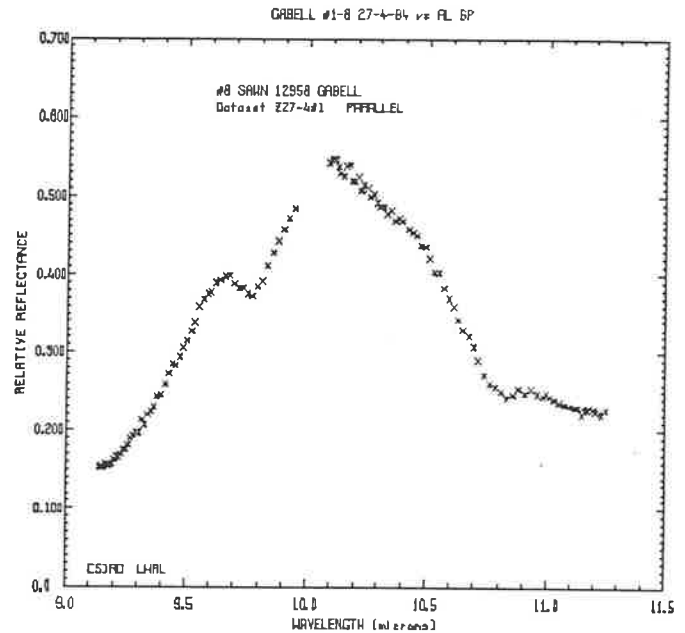
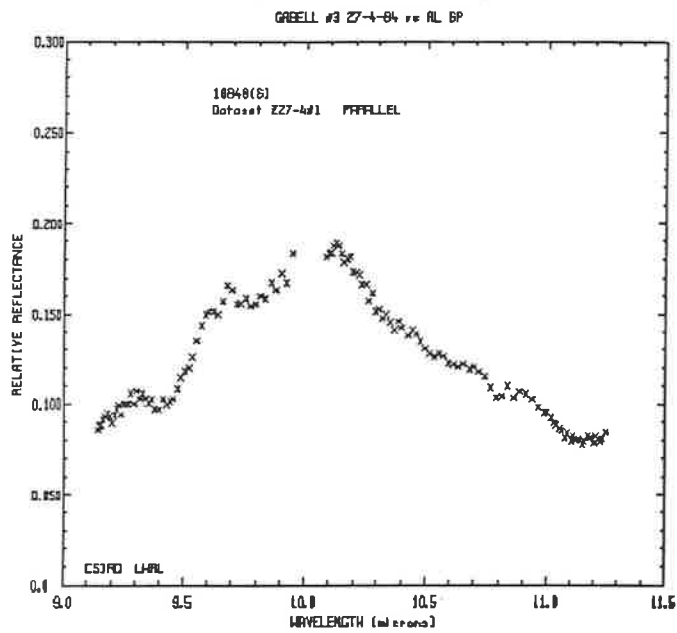
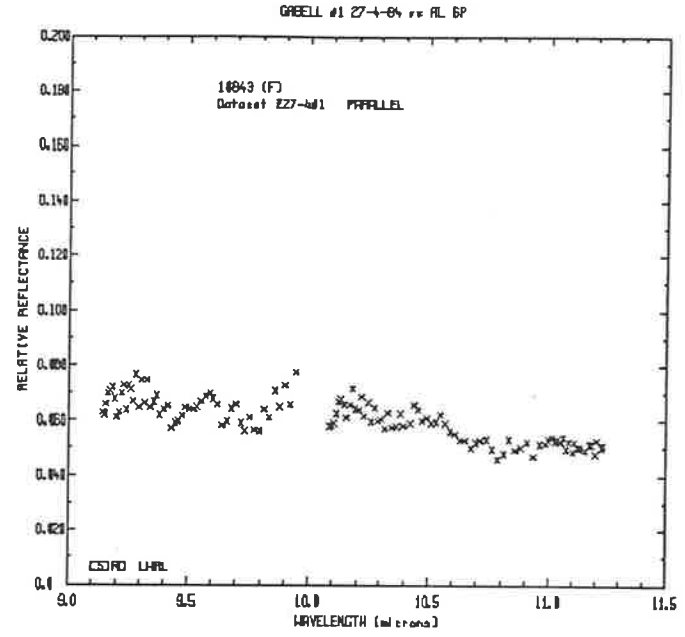
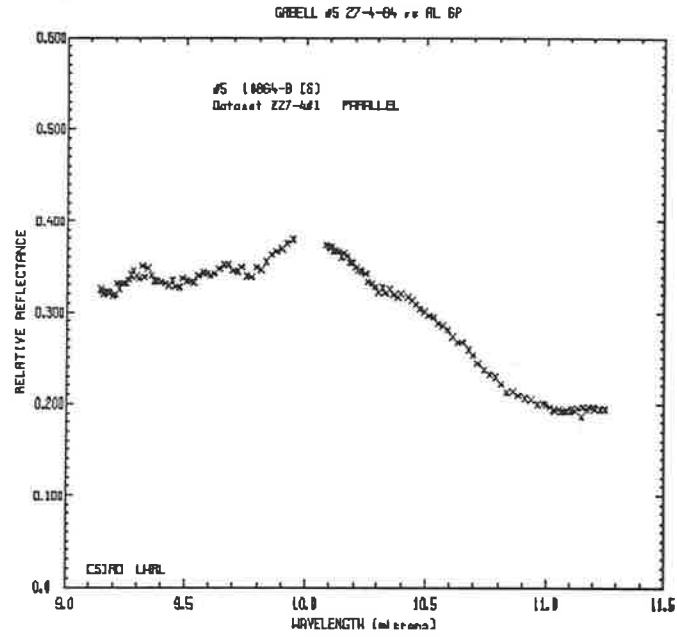




MIR F SPECTRA - Z-II AND Z-III METADOMAIN SAMPLES



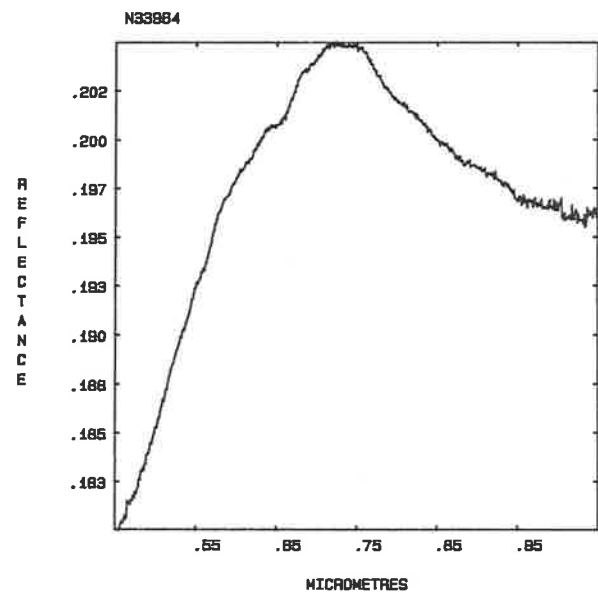
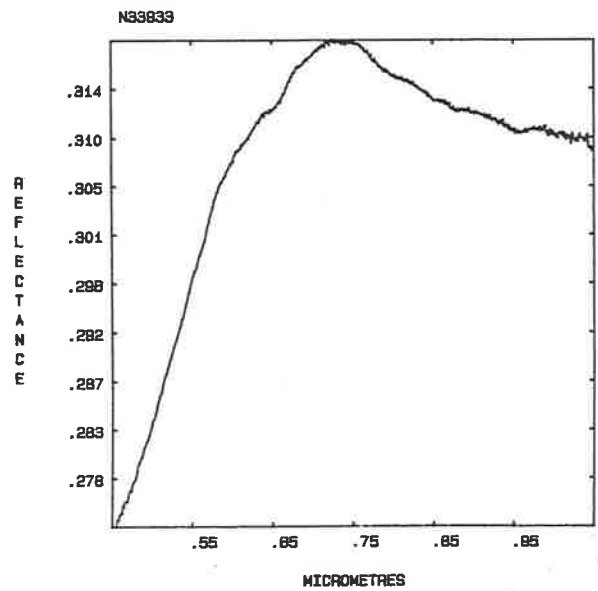
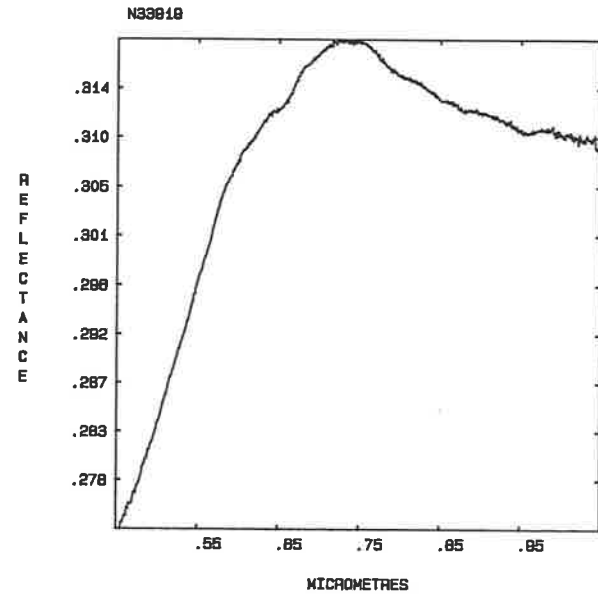
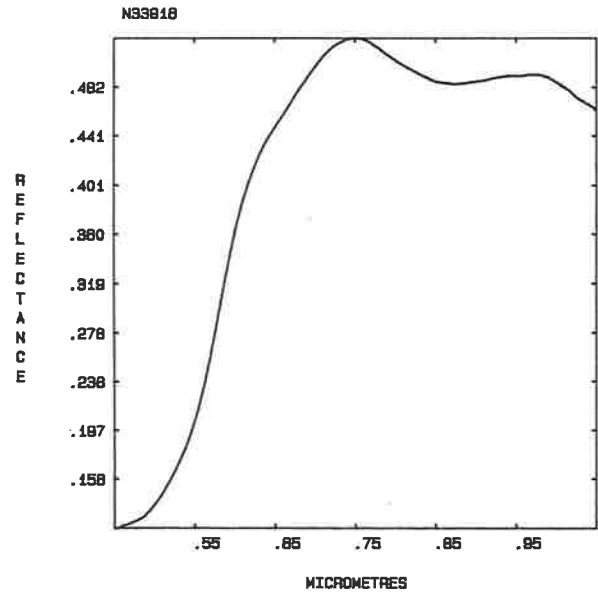
MIR F SPECTRA - Z-III RELICT DOMAIN AND Z-IV UNIFORMLY ALTERED METADOMAIN

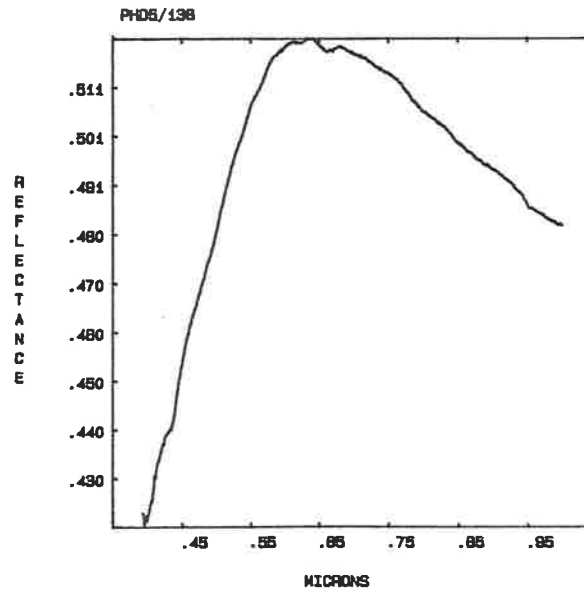
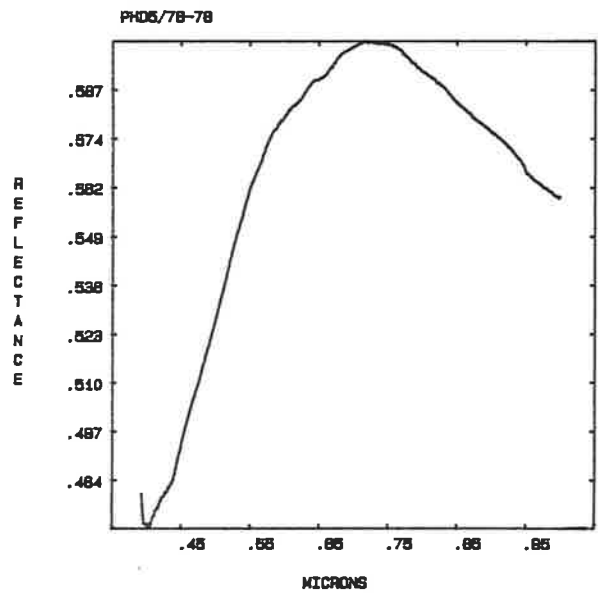
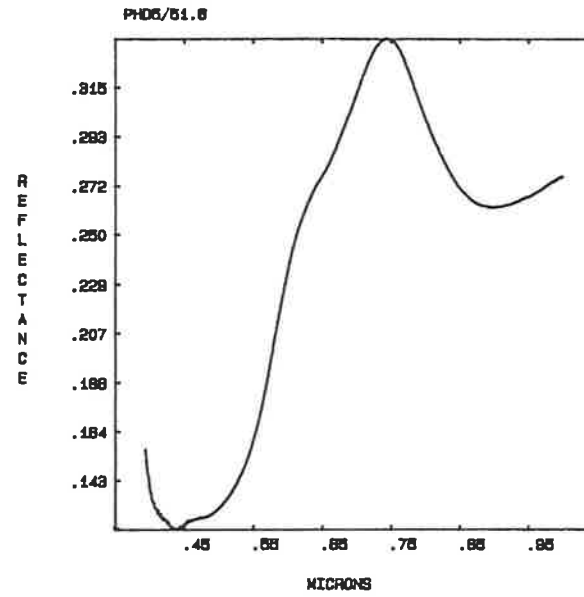
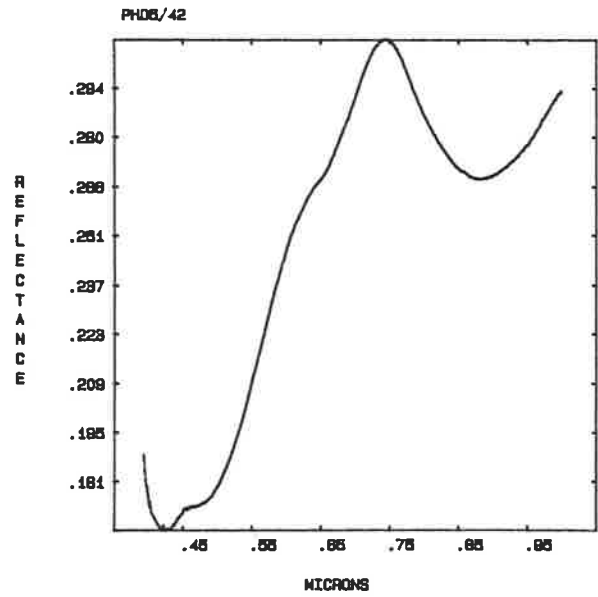


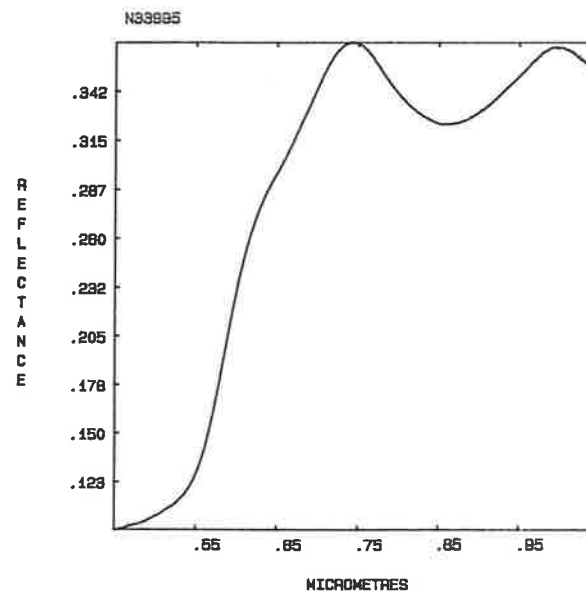
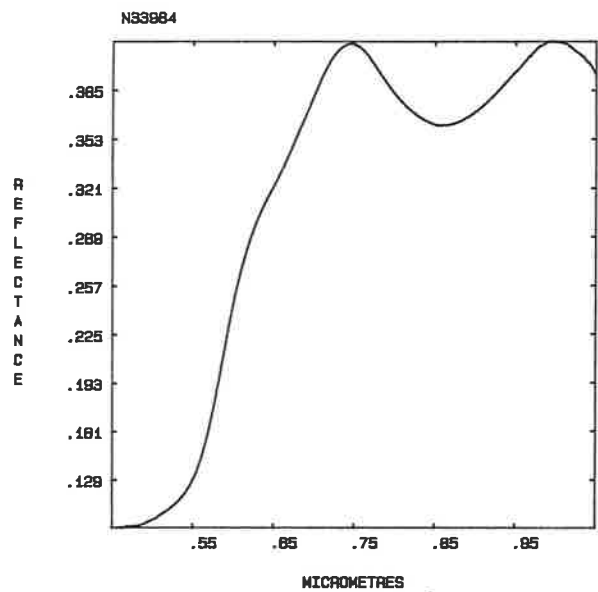
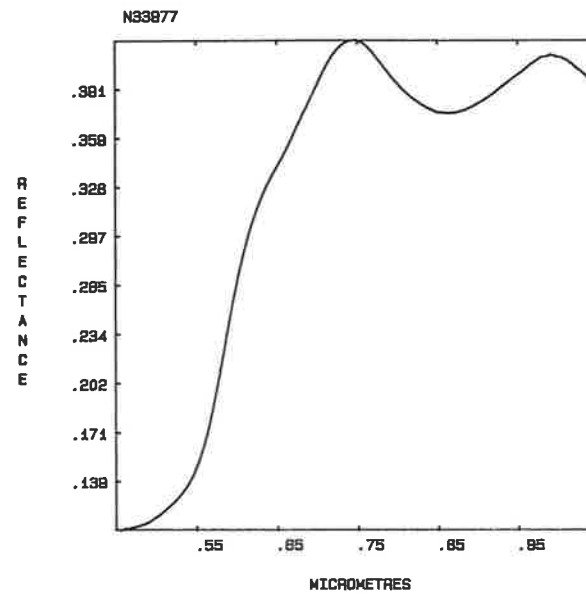
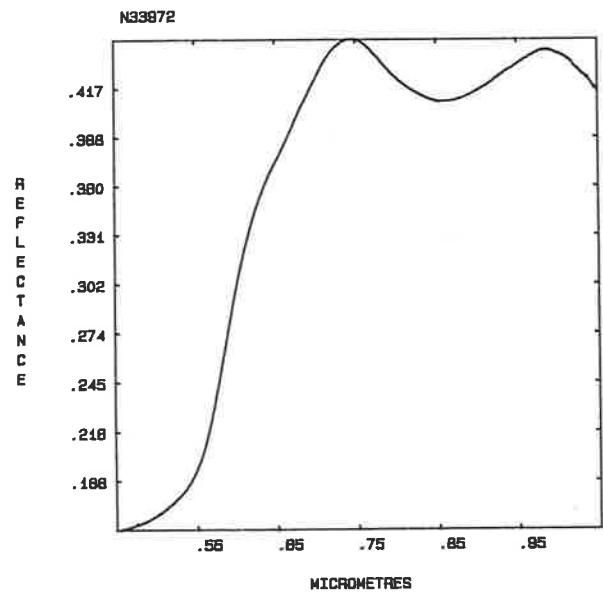
APPENDIX XIII VNIR laboratory reflectance spectra of core samples from
Peak Hill.

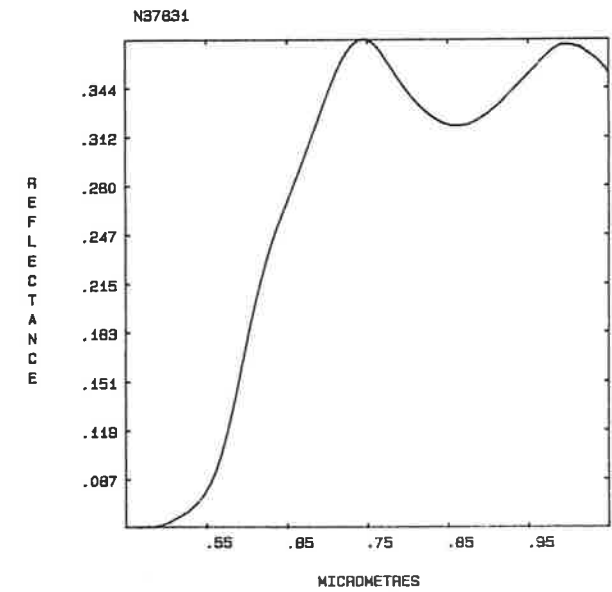
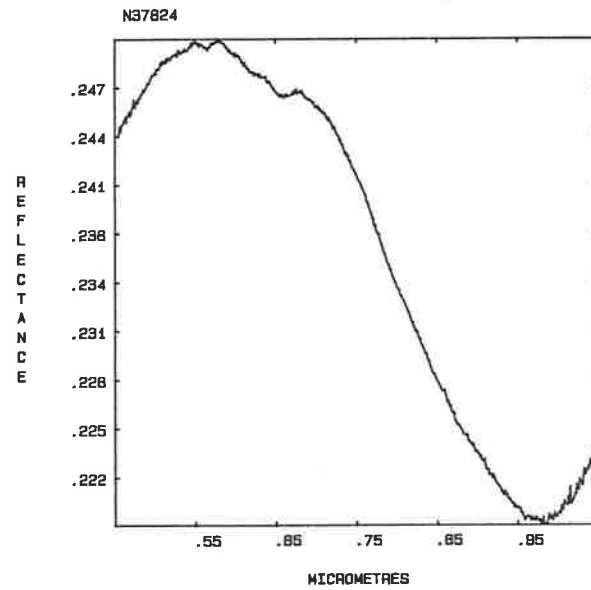
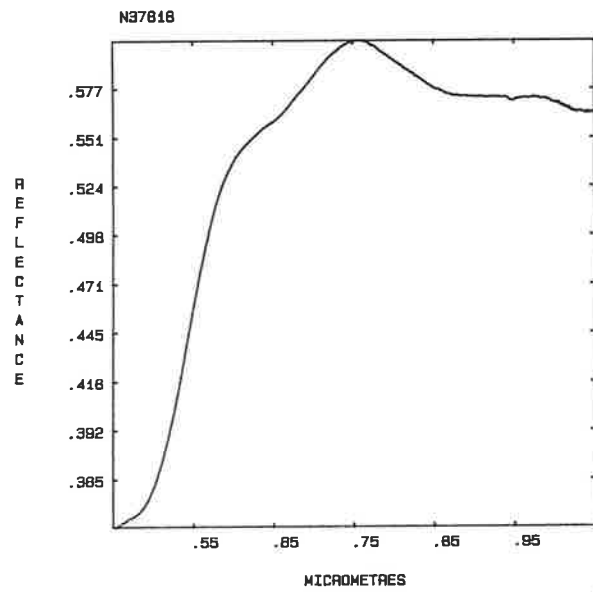
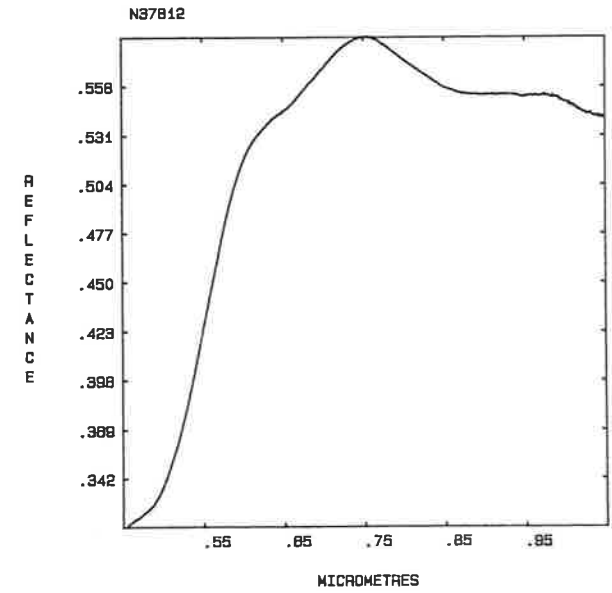
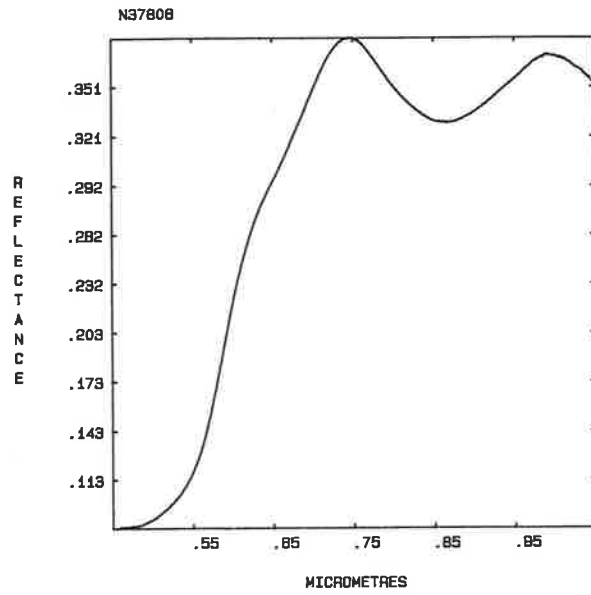
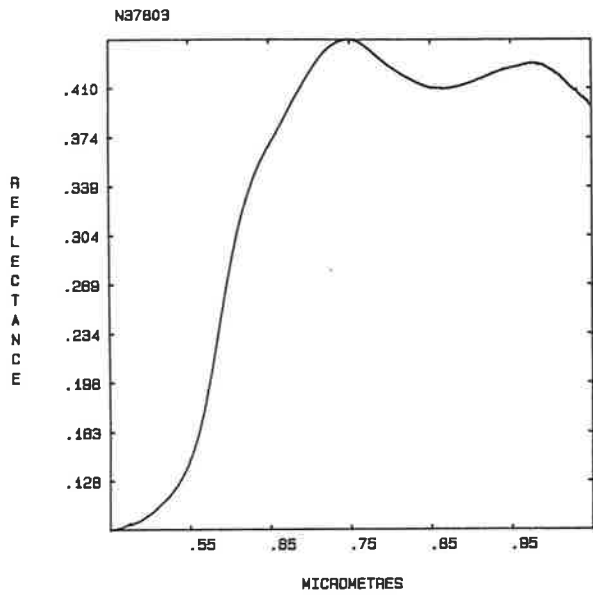
The VNIR spectra of Peak Hill core samples appear in this appendix in the same order as listed in Table 8.2, which should also be consulted for the interpretations.

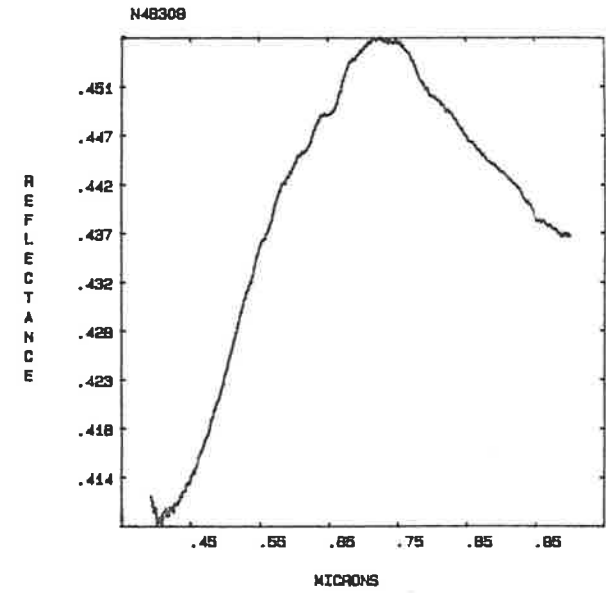
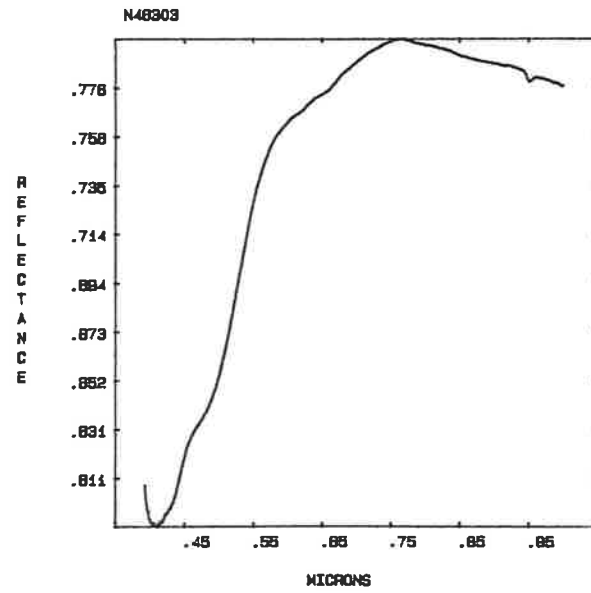
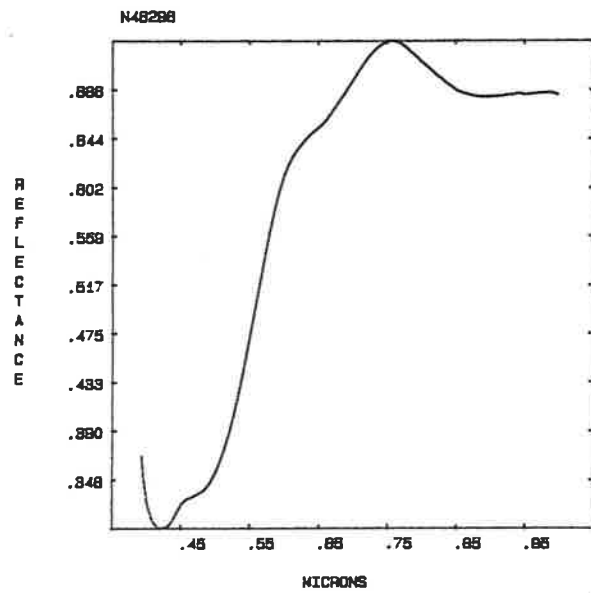
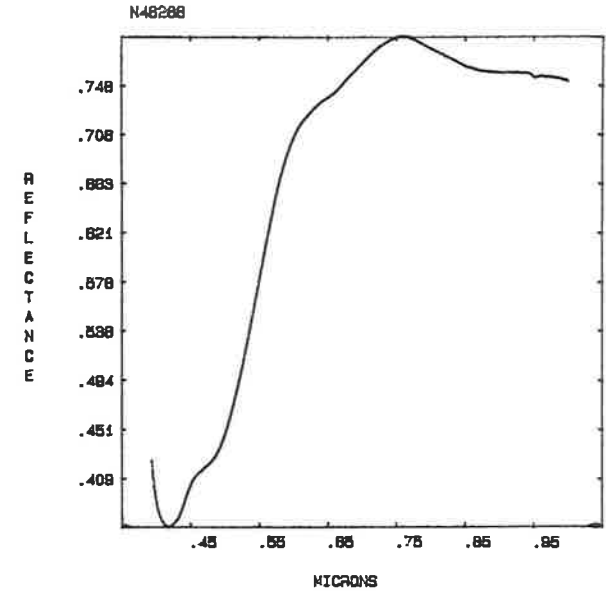
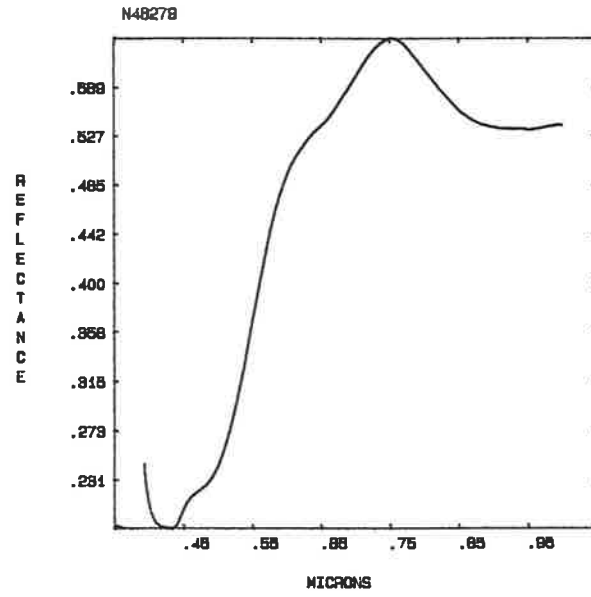
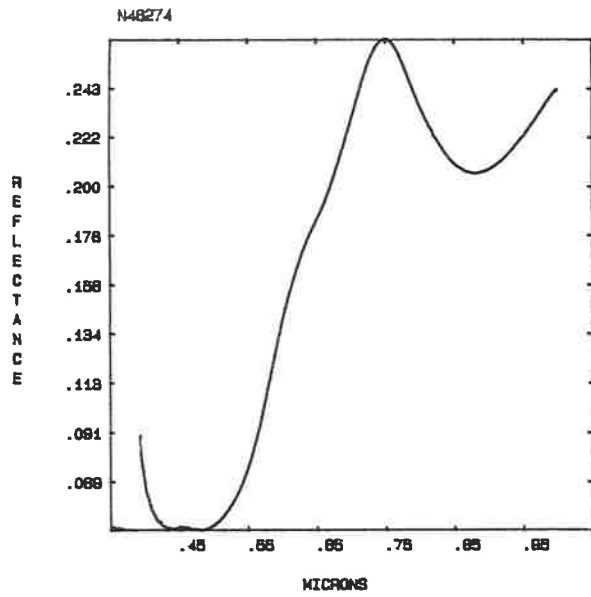
The only XRD data available for these samples are for N33933 (30% pyrophyllite, 20% sericite), N33964 (30% sericite, 10% alunite, 10% pyrophyllite), N37842 (30% pyrophyllite, 15% kaolinite) and N46309 (40% pyrophyllite, 5% alunite, 5% sericite).











APPENDIX XIV SWIR laboratory reflectance spectra of core samples from
Peak Hill.

The SWIR spectra of Peak Hill core samples appear in this appendix in the same order as listed in Table 8.2, which should also be consulted for the interpretations.

The only XRD data available for these samples are for N33933 (30% pyrophyllite, 20% sericite), N33964 (30% sericite, 10% alunite, 10% pyrophyllite), N37842 (30% pyrophyllite, 15% kaolinite) and N46309 (40% pyrophyllite, 5% alunite, 5% sericite).

Some of the more prominent spectral features are marked as follows:

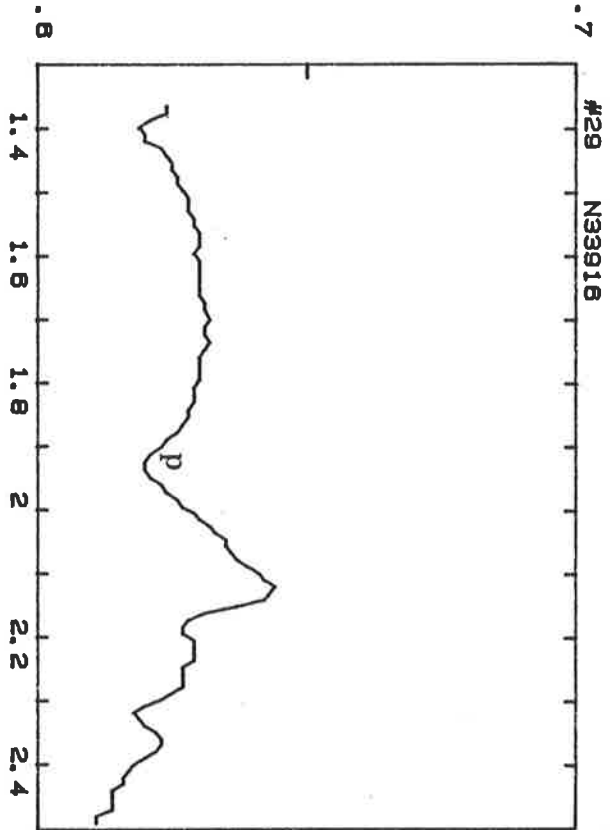
a - alunite

j - jarosite

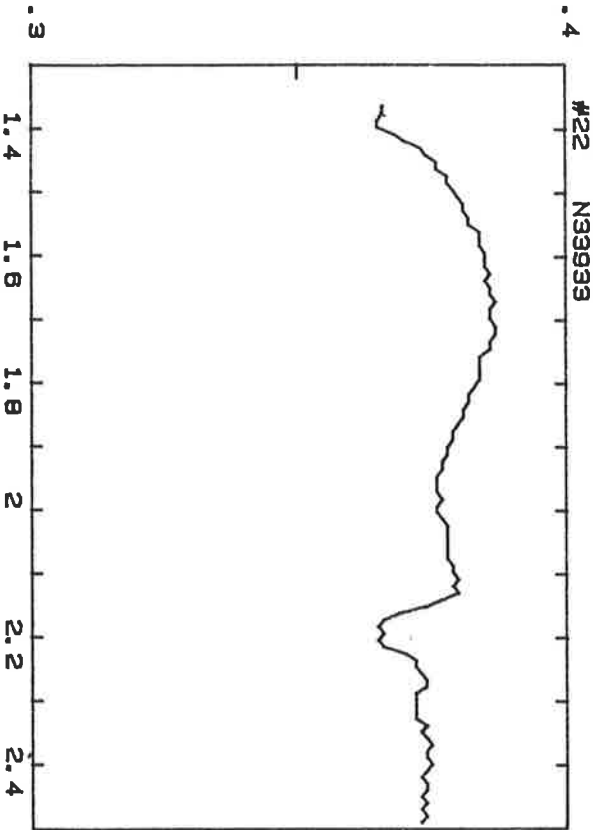
p - pyrophyllite

Some of the spectral features of pulped core are not as strong as might be expected from the XRD analyses, even though the samples are similar in appearance to those that do have well developed absorption features. Sample N33933 (30% pyrophyllite and 20% sericite) is one such example. The equivalent split core sample, however, exhibits stronger absorption features. The fine grain size of the pulped samples may be to blame, with 'pilling' and subsequent coating of some minerals with absorption features by aspectral mineral species (e.g. quartz).

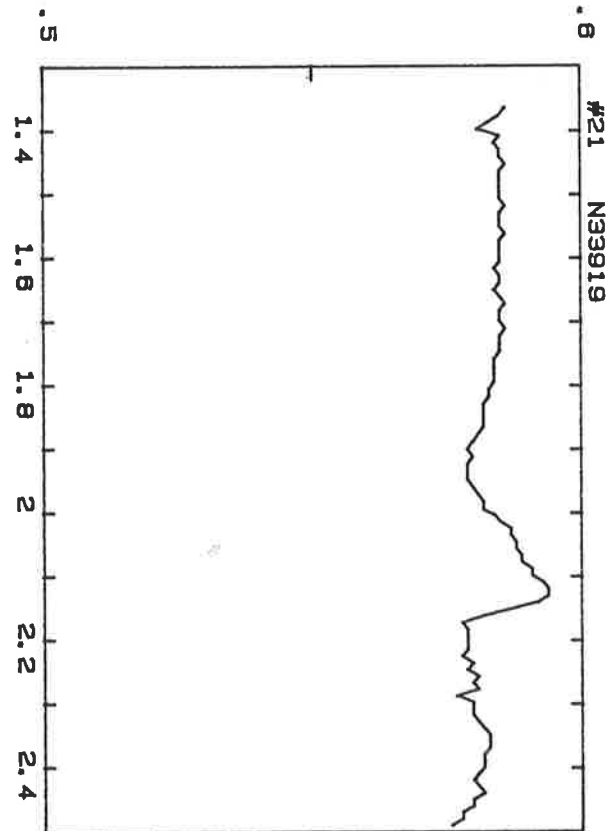
REFLECTANCE



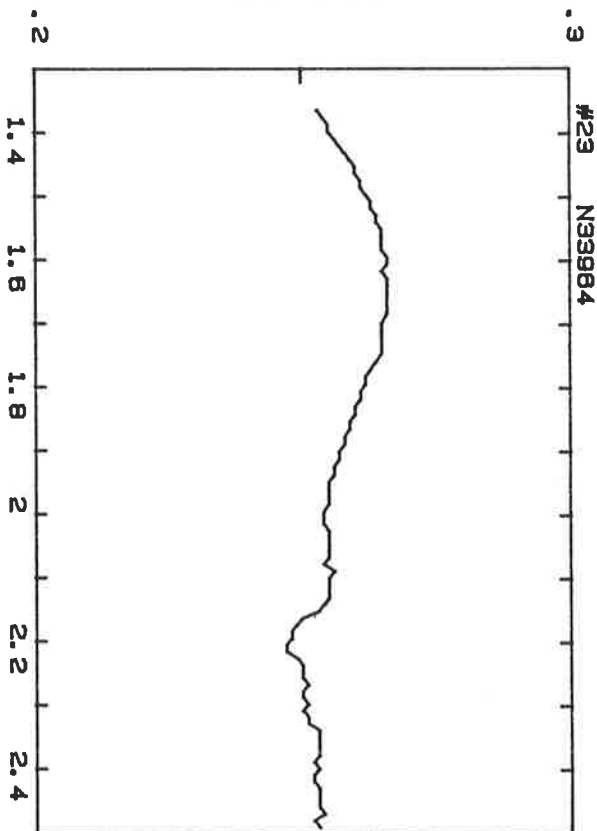
REFLECTANCE

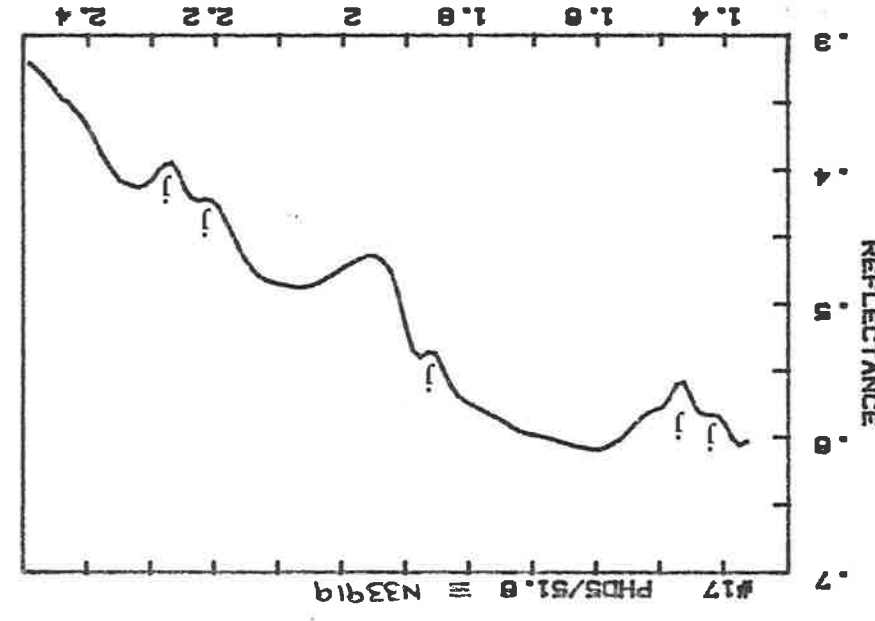
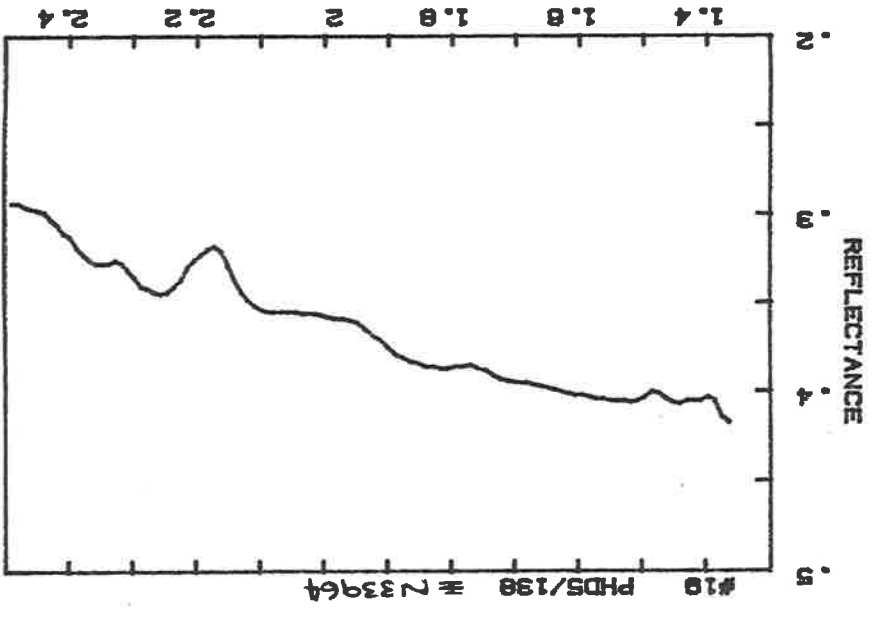
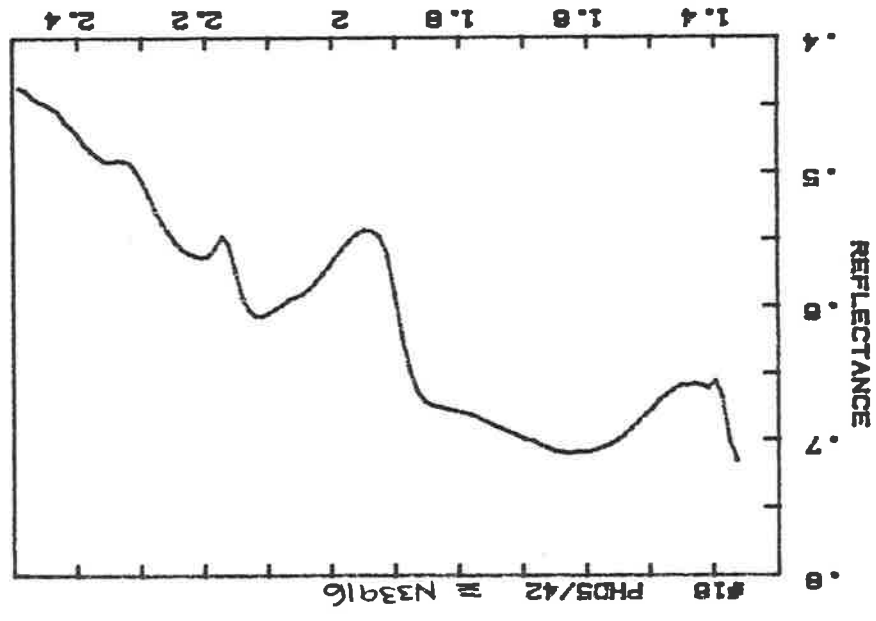
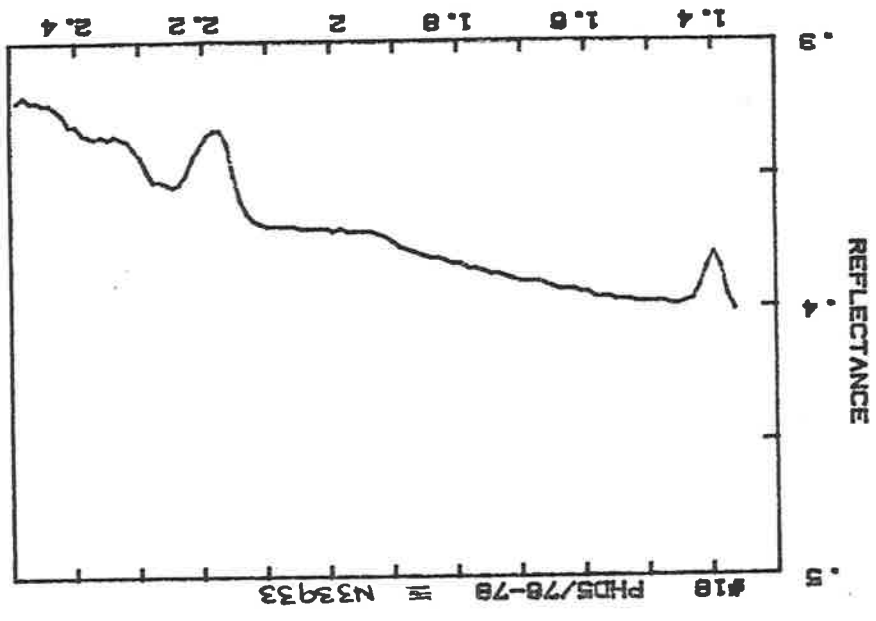


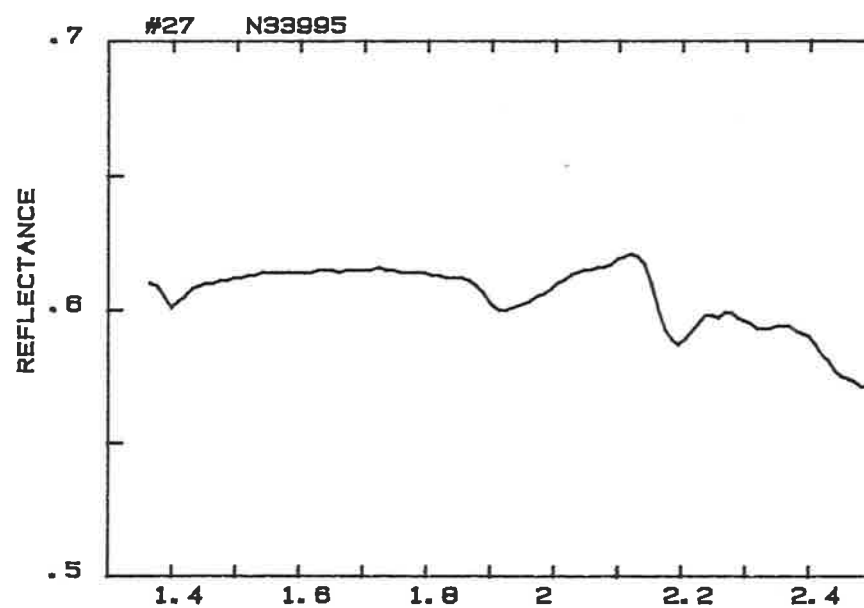
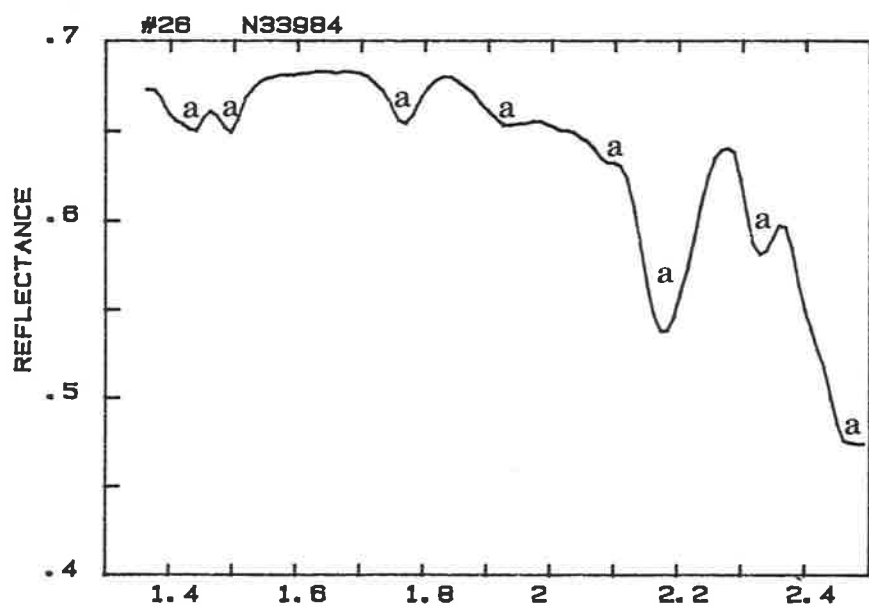
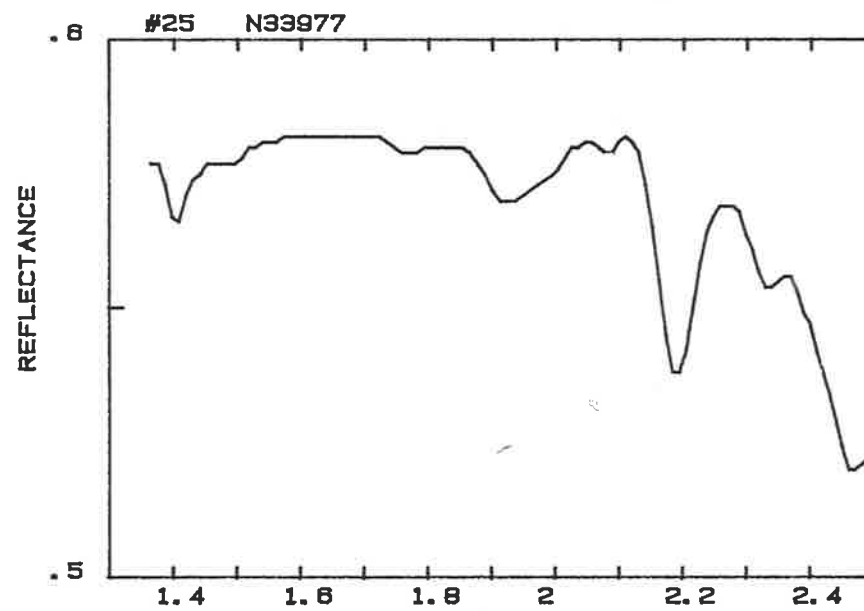
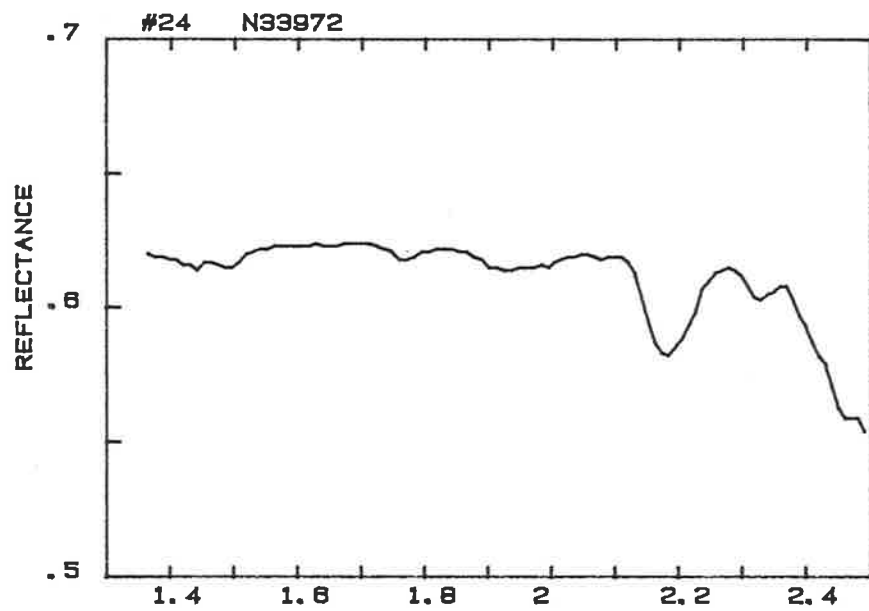
REFLECTANCE

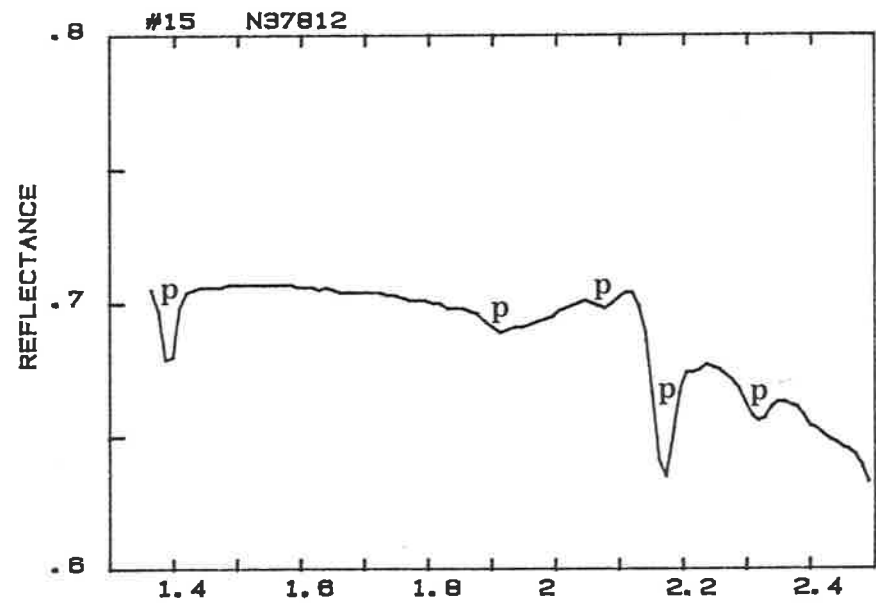
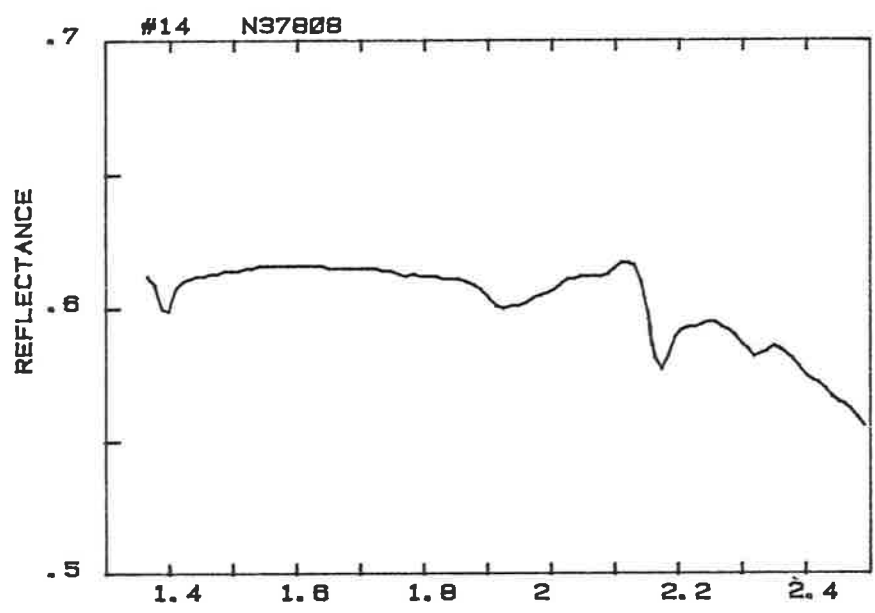
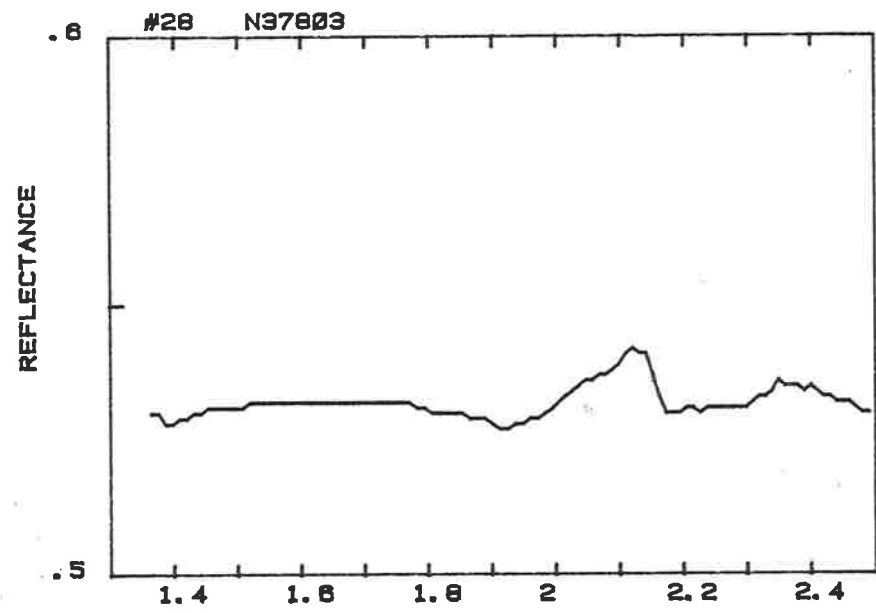
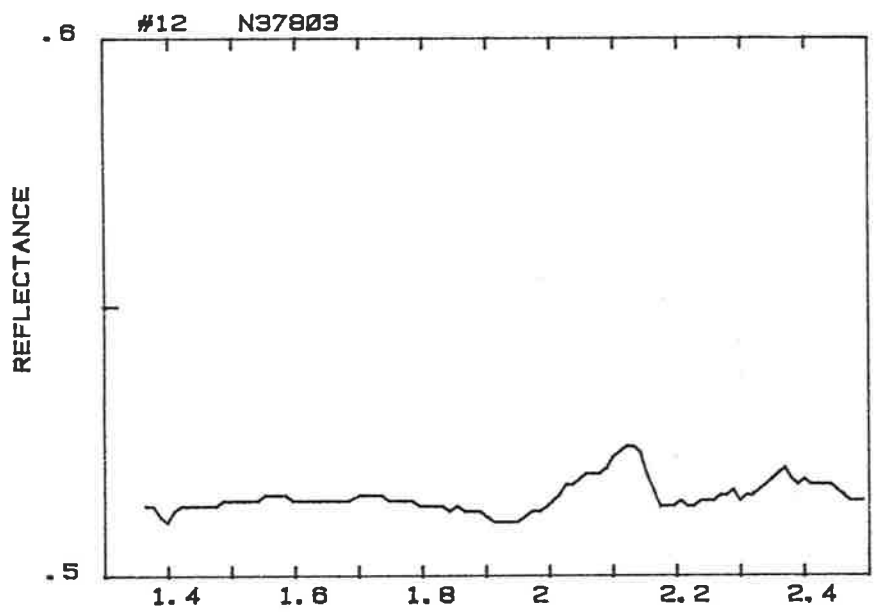


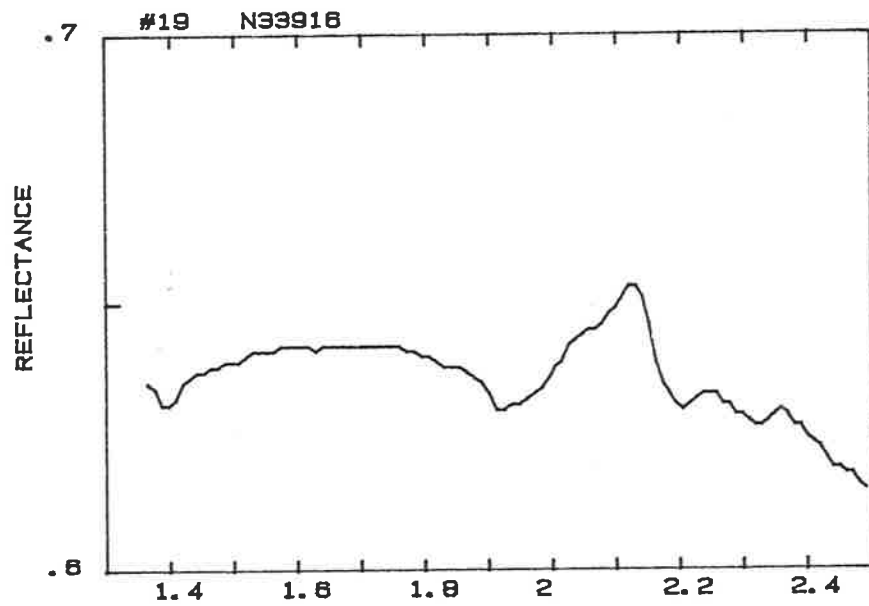
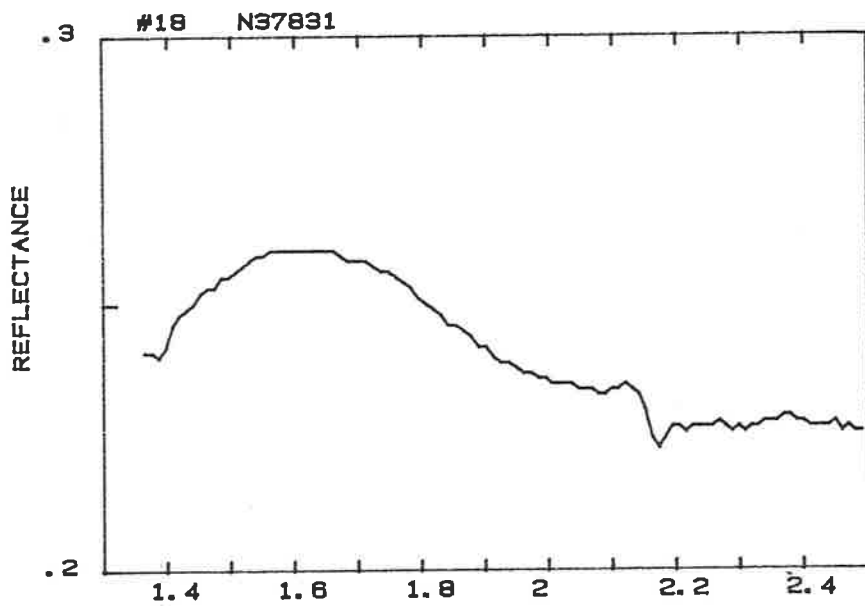
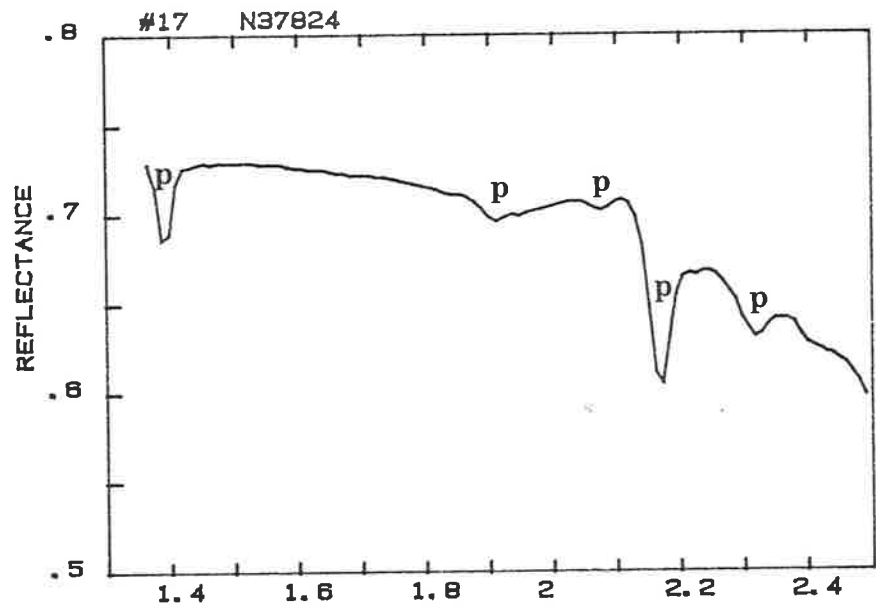
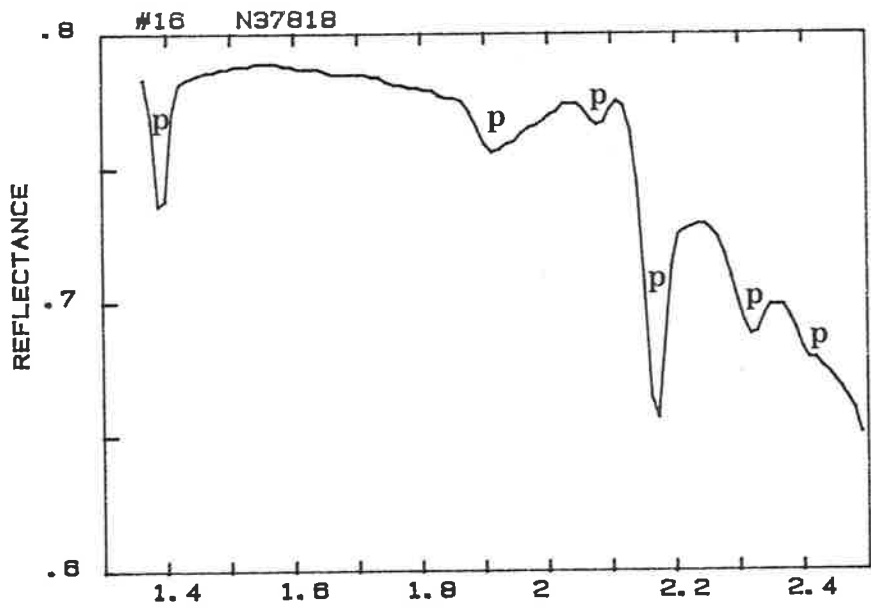
REFLECTANCE

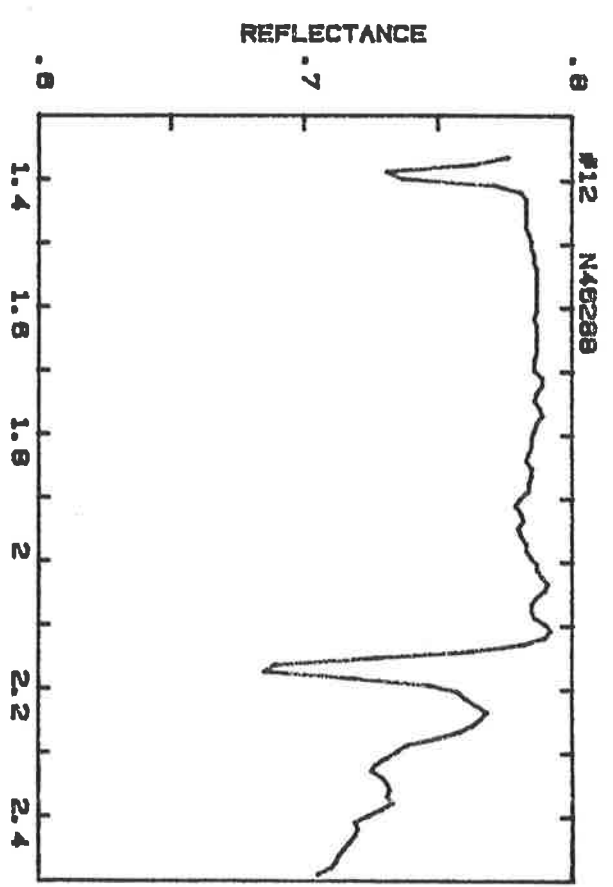
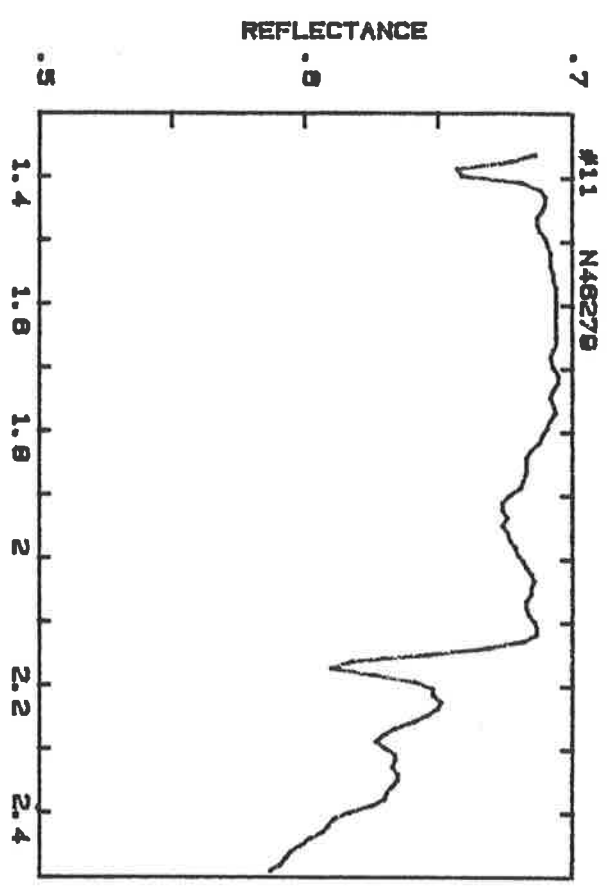
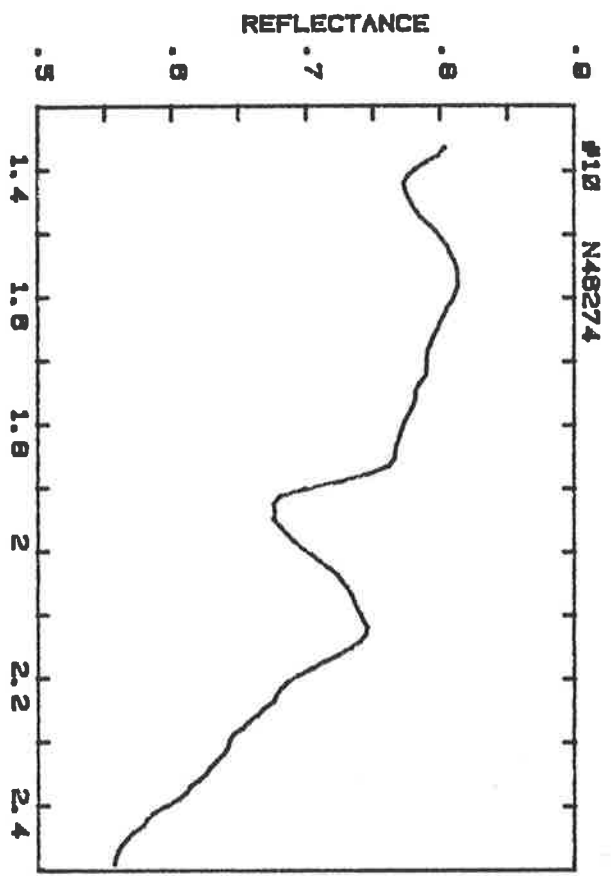


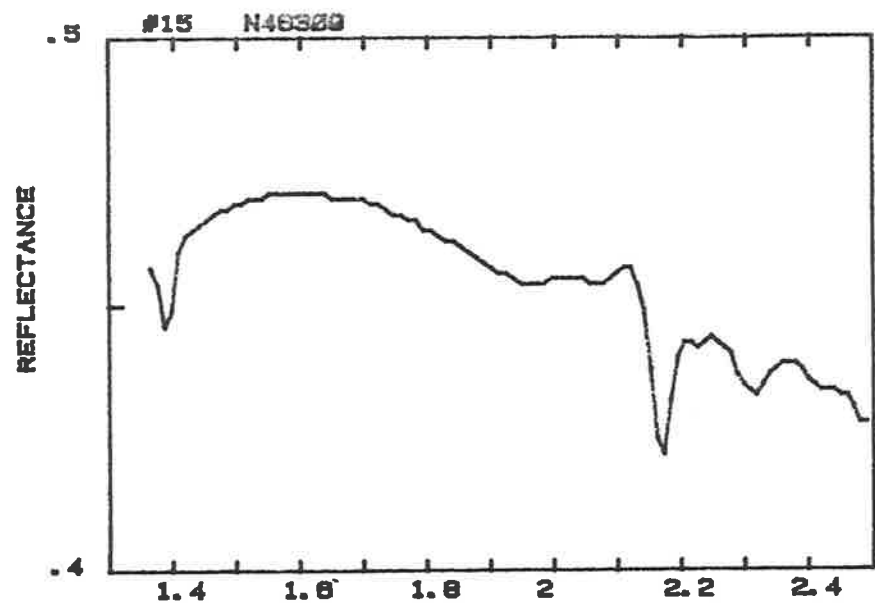
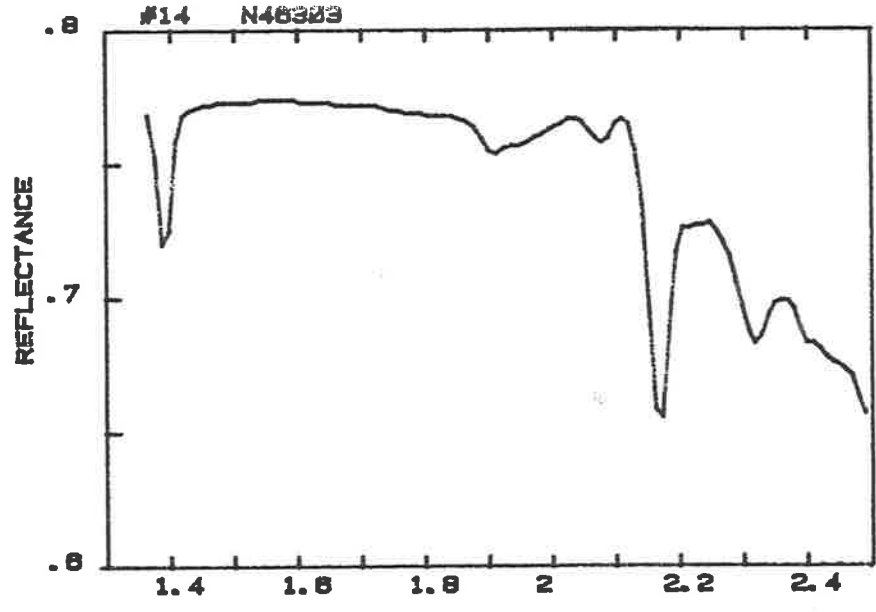
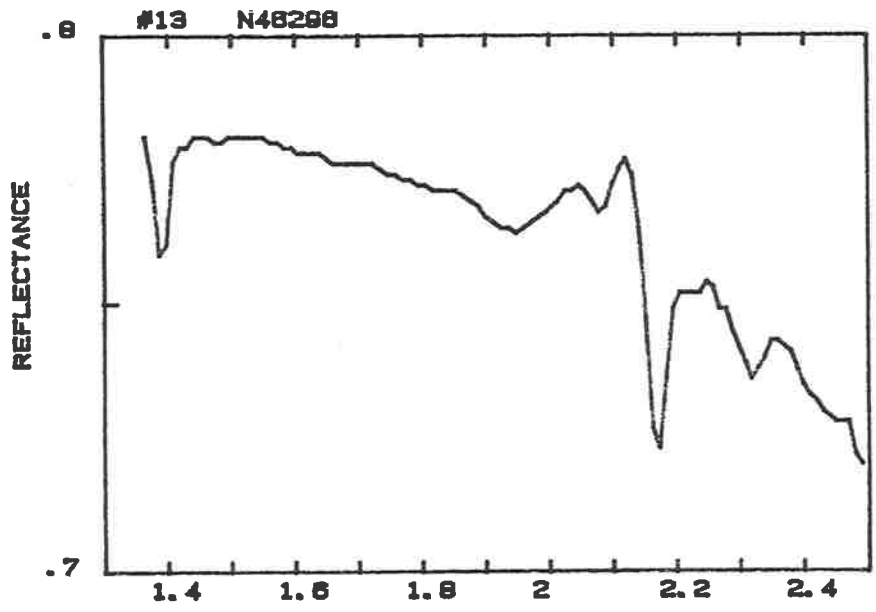










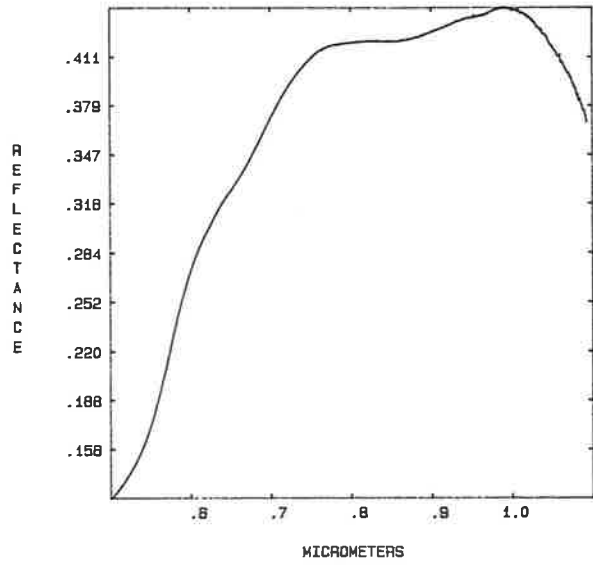


APPENDIX XV VNIR laboratory reflectance spectra of surface samples
from Peak Hill.

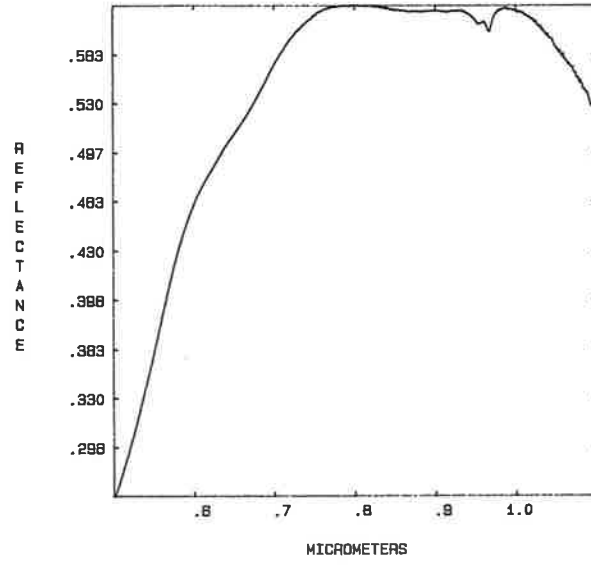
The VNIR spectra of Peak Hill surface samples appear in this appendix in the same order as listed in Table 8.3, which should also be consulted for the interpretations. XRD data, where available, appears at the top of each spectral plot. The key to abbreviations of mineral names is the same as used for Table 8.3. Minerals are listed approximately in descending order of abundance.

Note that the sharp $.42\mu\text{m}$ jarosite absorption feature could not be detected in the VNIR spectra. Because the jarosite spectrum is otherwise impossible to confidently discriminate from goethite, all spectra were interpreted as goethitic. Therefore, there may be some spectral features caused by jarosite, but assigned to goethite. This can be checked by looking at the SWIR spectrum, which has distinctive absorption features if jarosite forms a significant component of the sample.

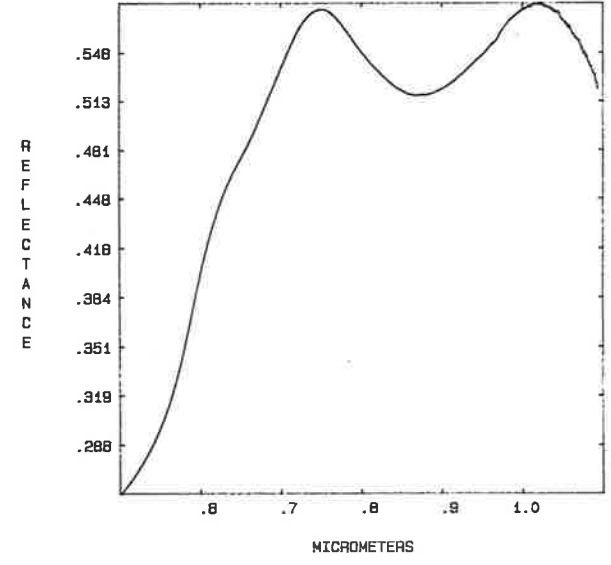
PH 1 W1 XRD Q,K,P, sulphate



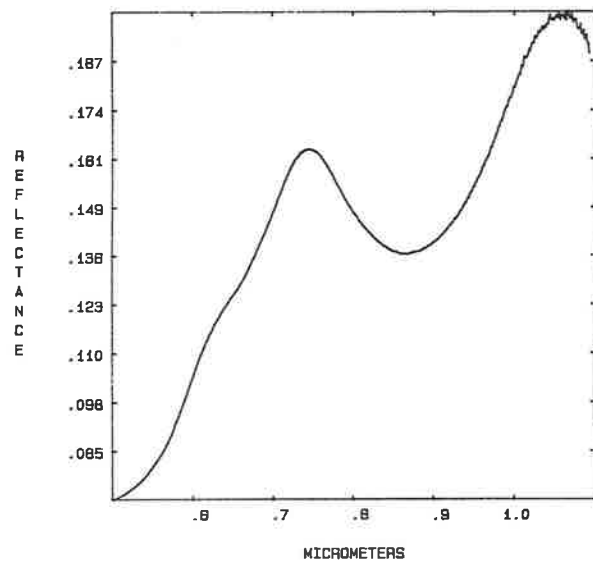
PH 1 W2



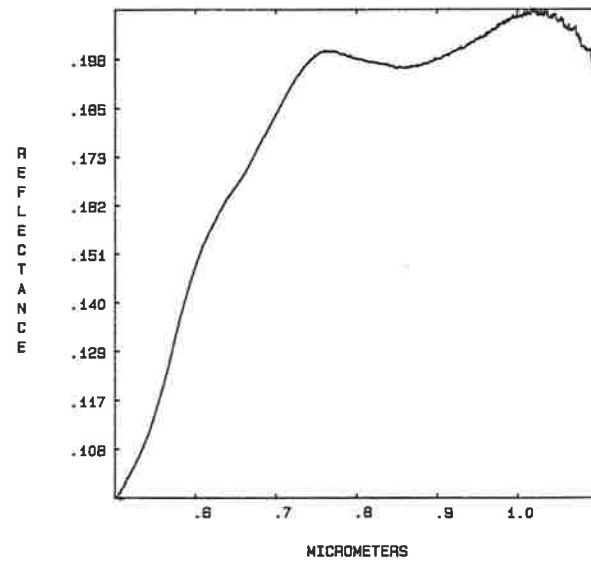
PH 1 F



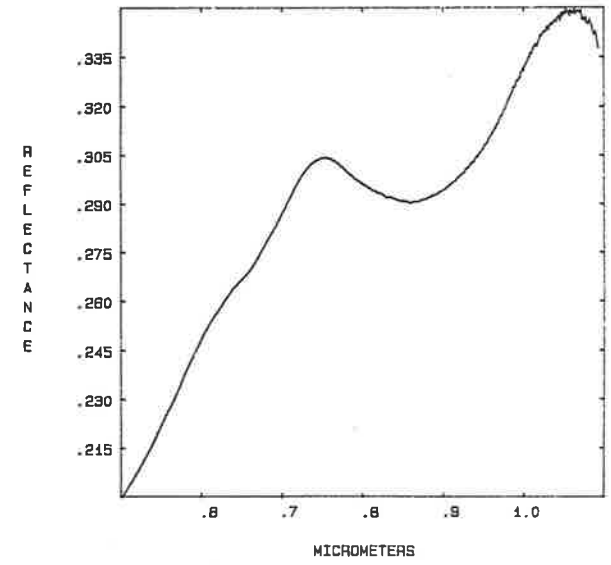
PH 2A F

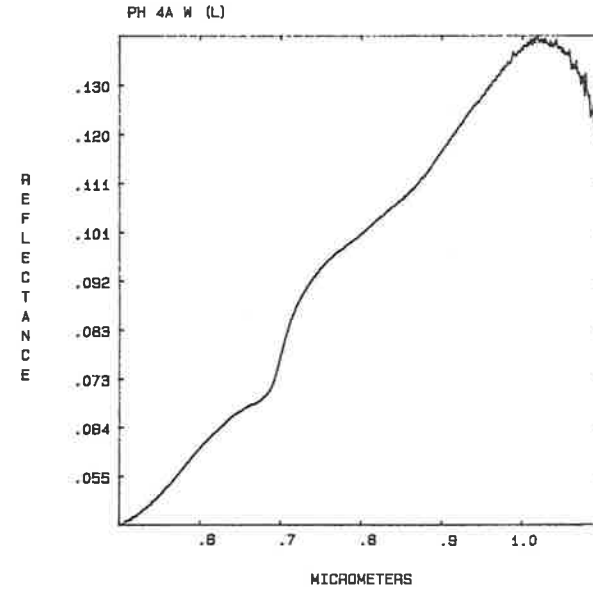
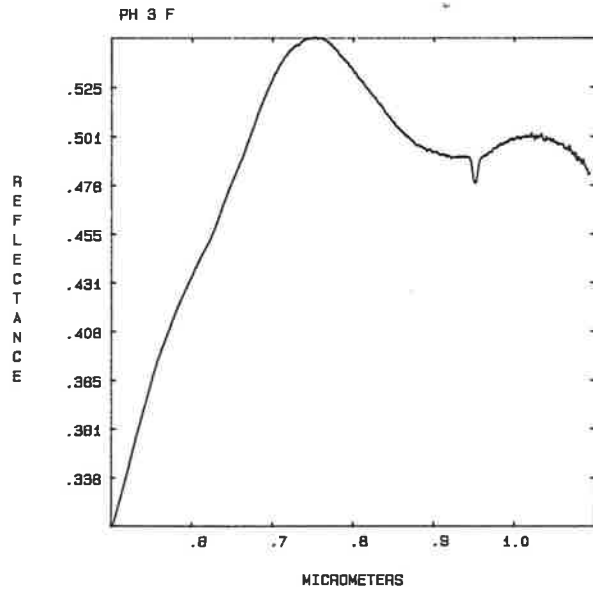
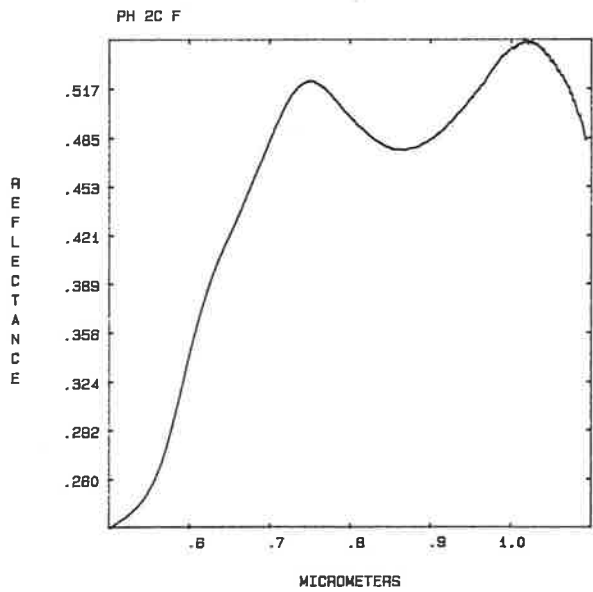
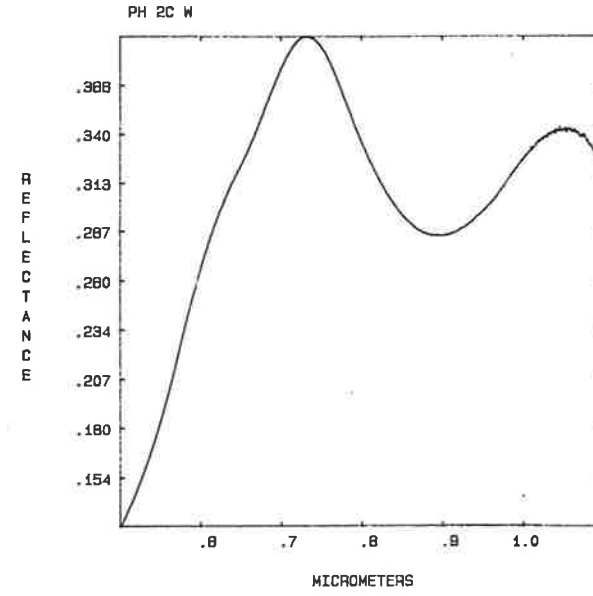
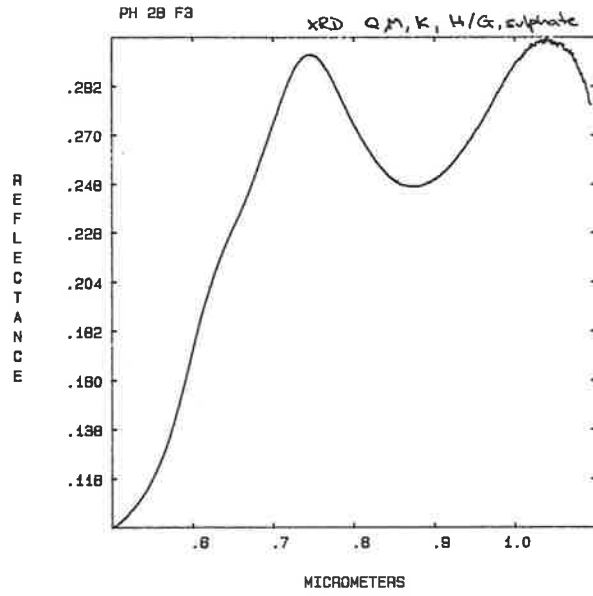
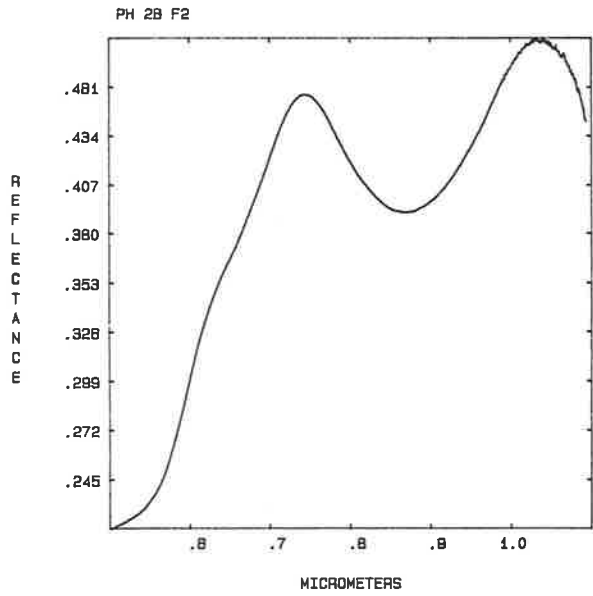


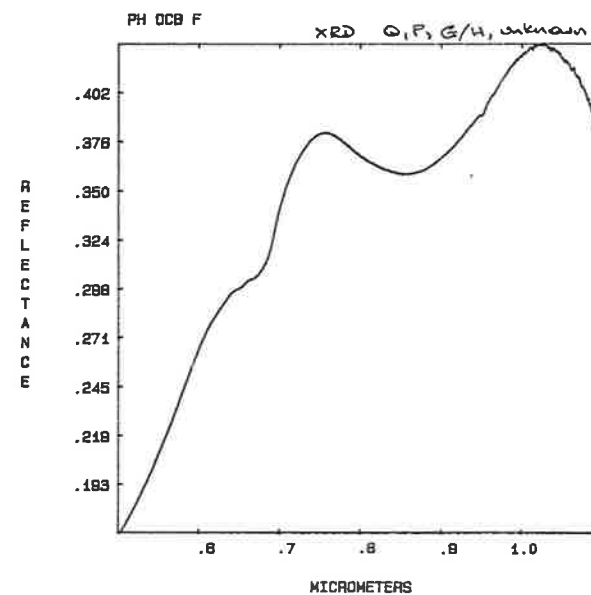
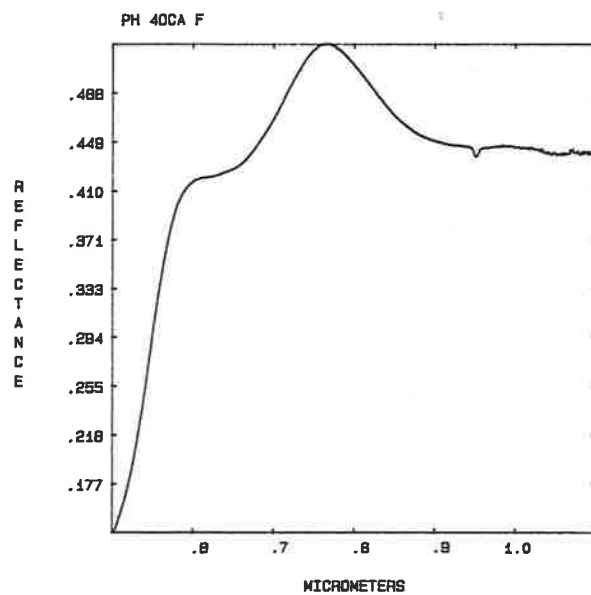
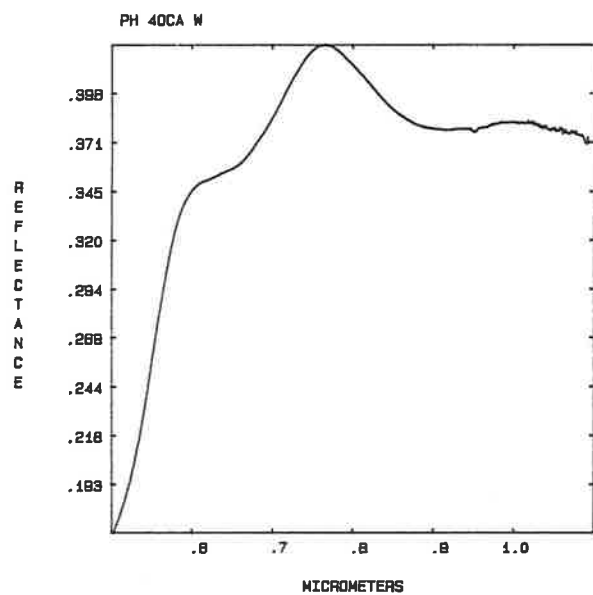
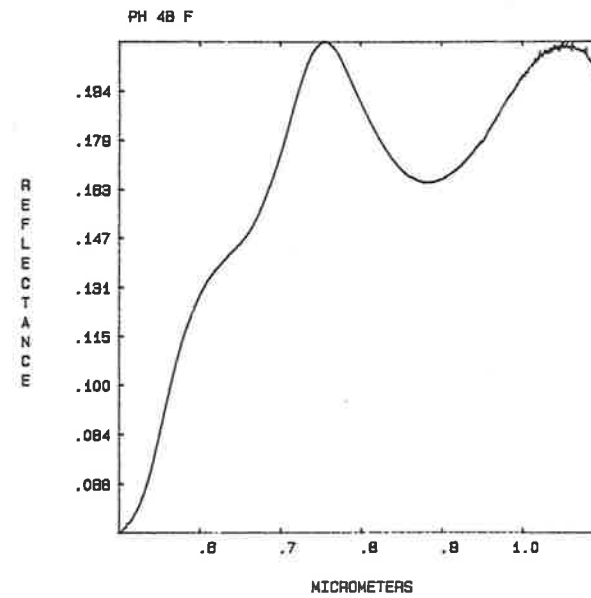
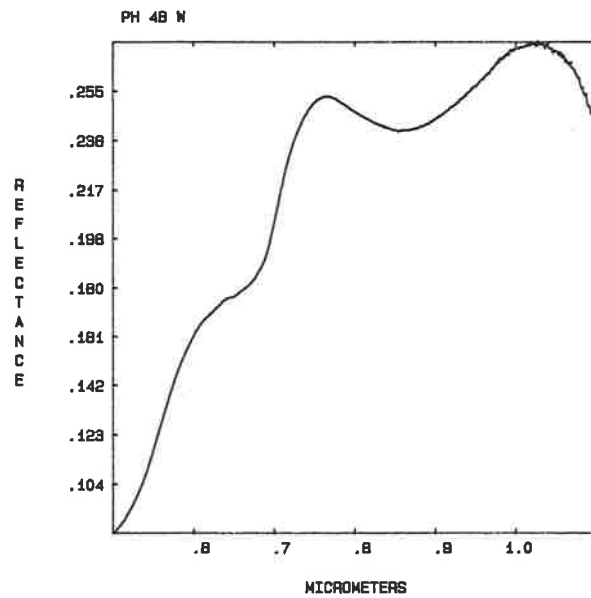
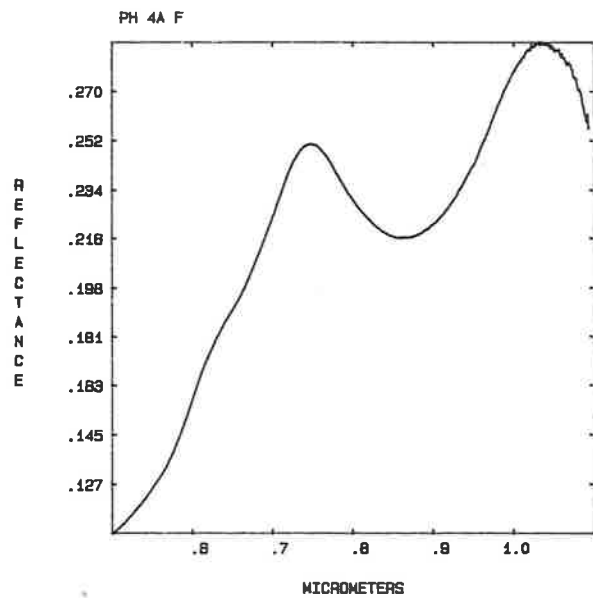
PH 2B W

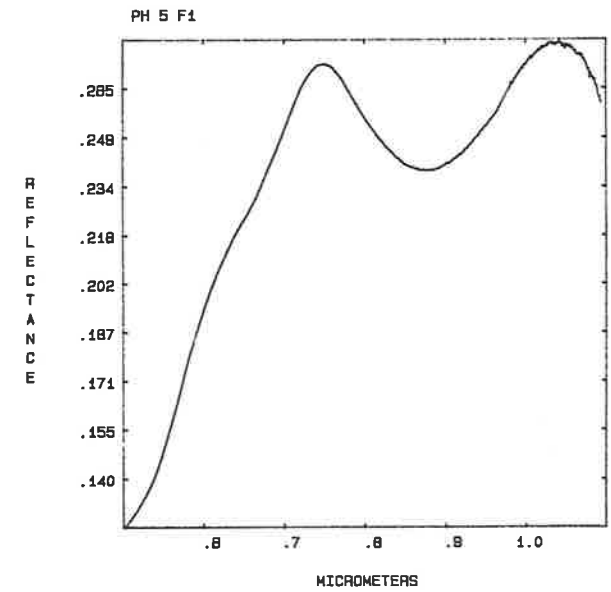
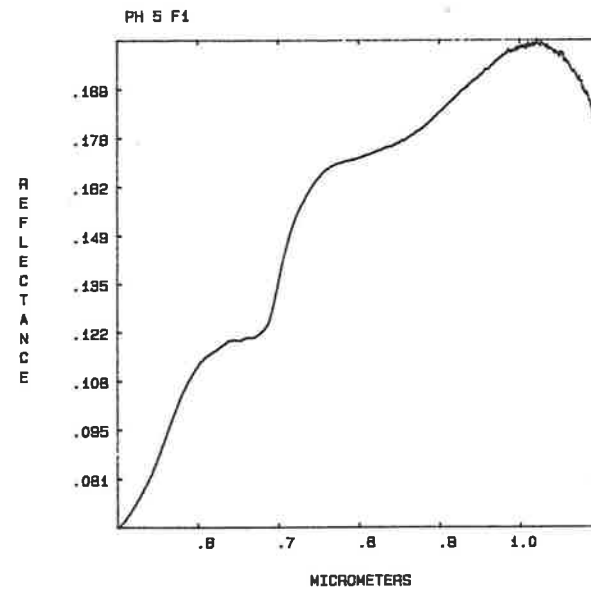
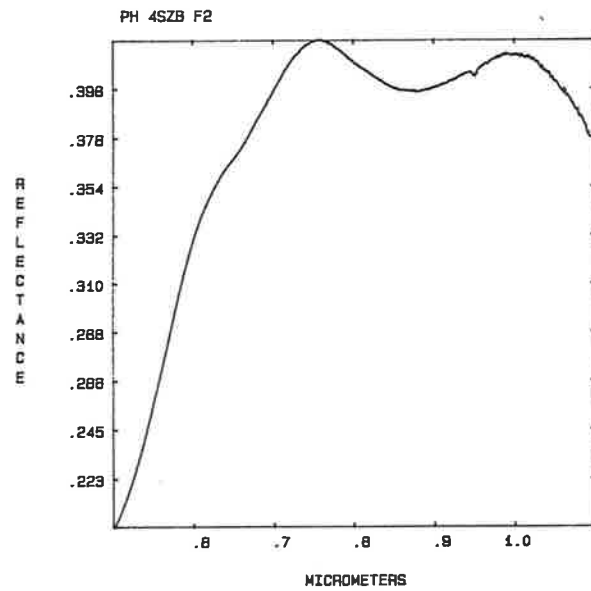
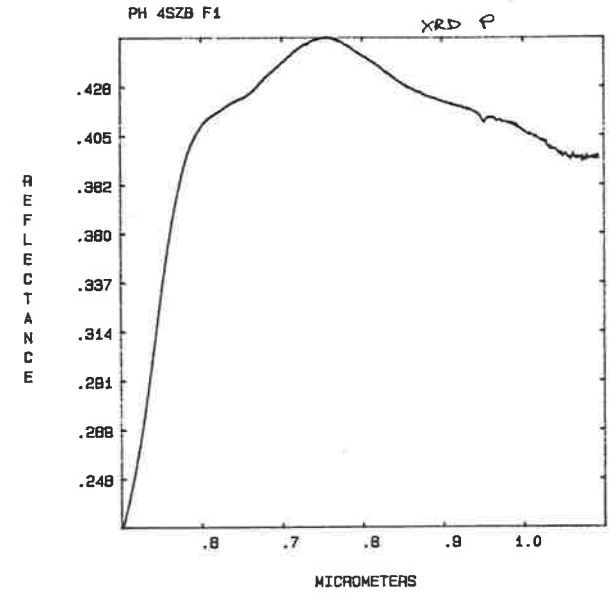
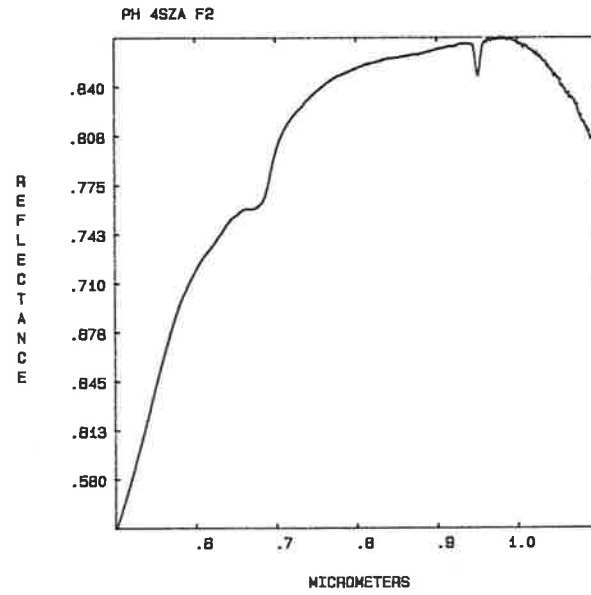
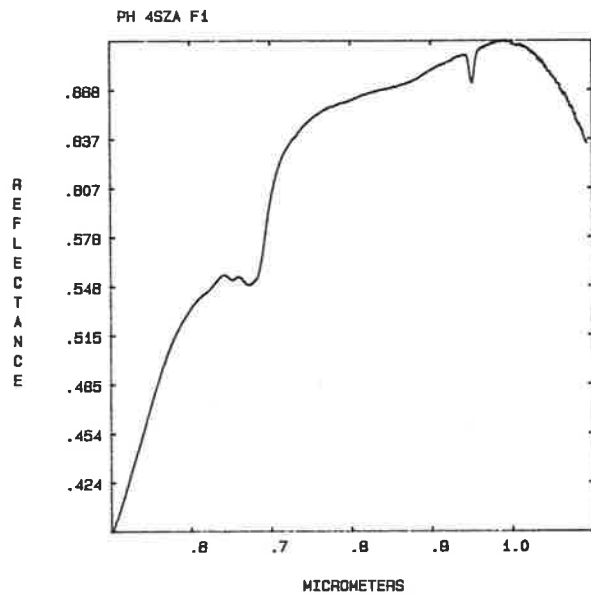


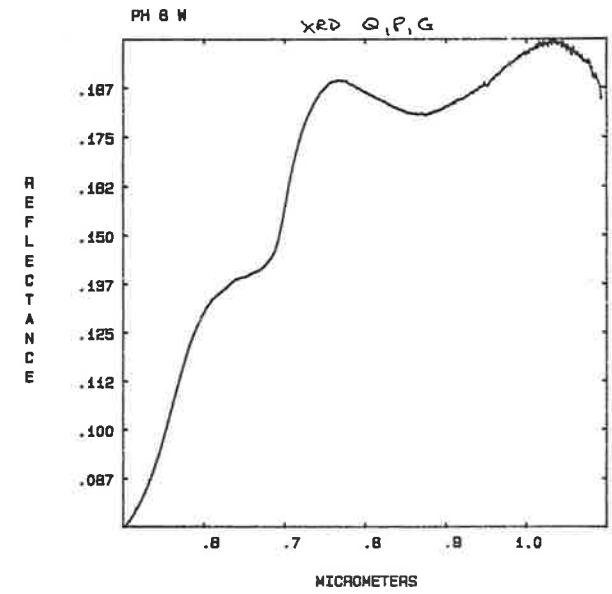
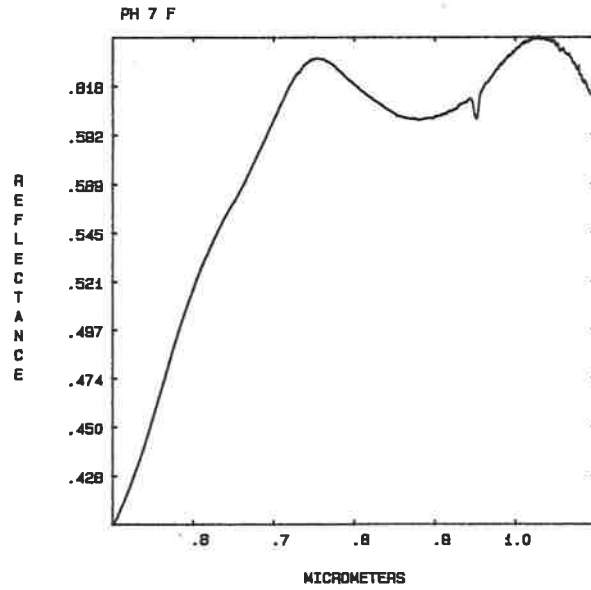
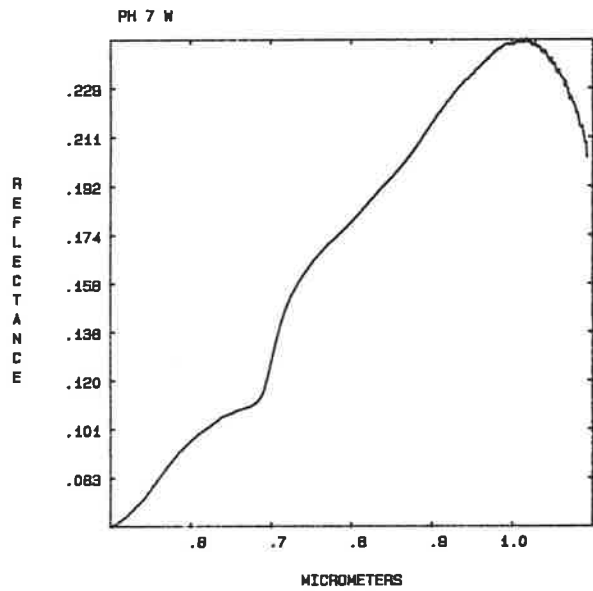
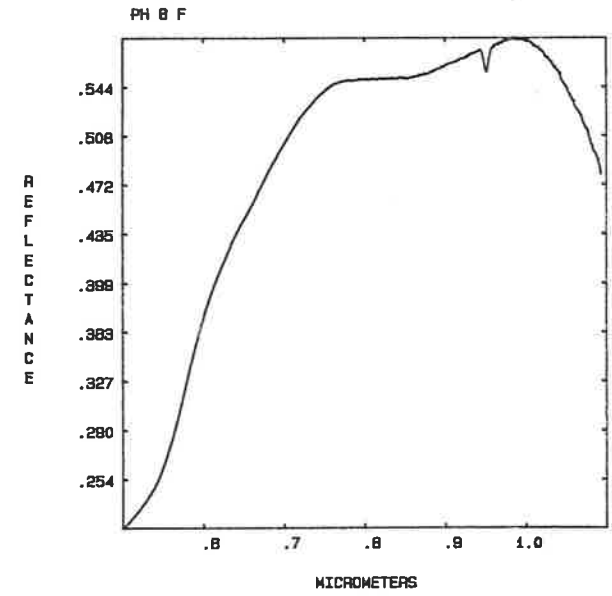
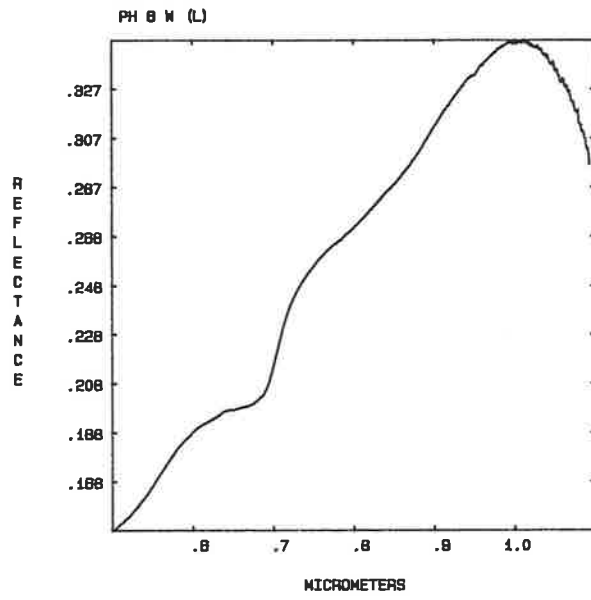
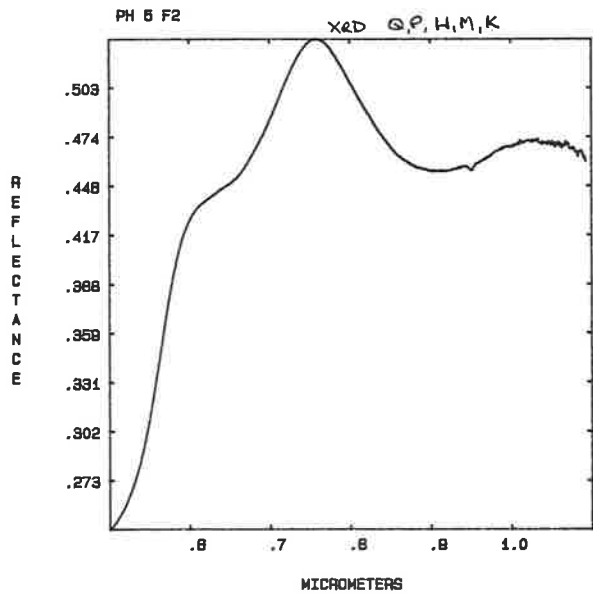
PH 2B F1

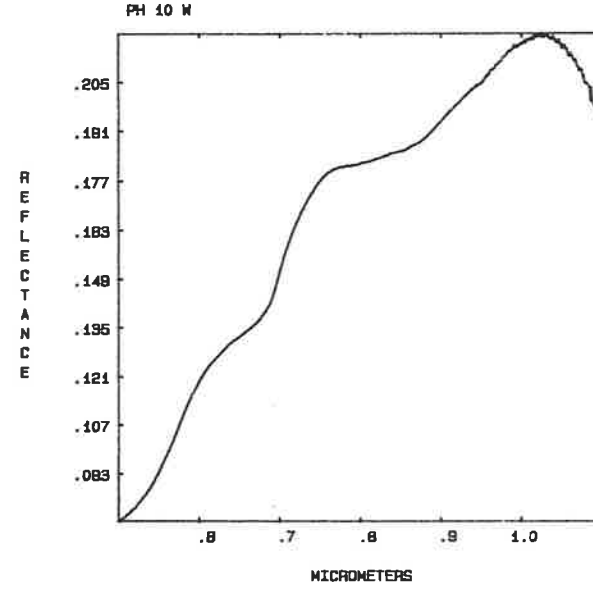
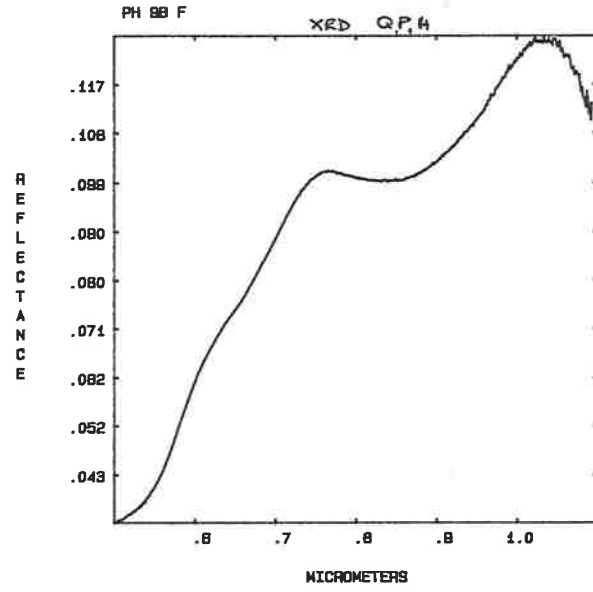
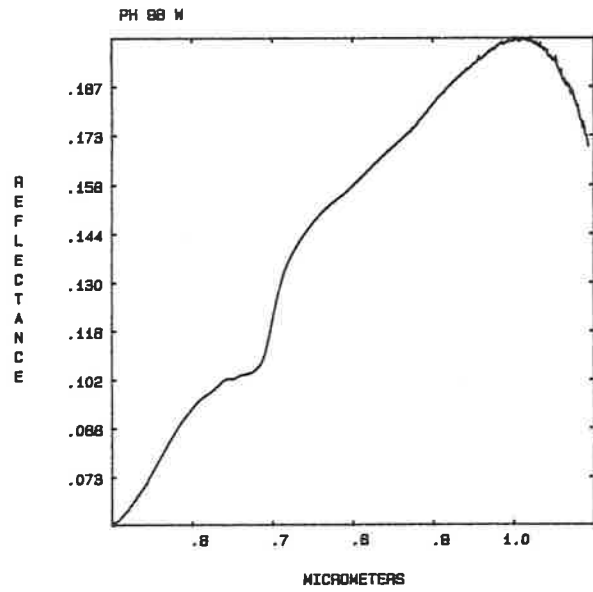
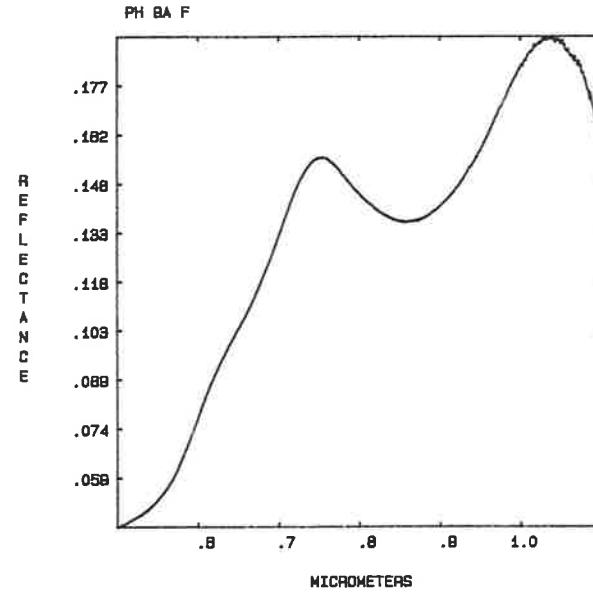
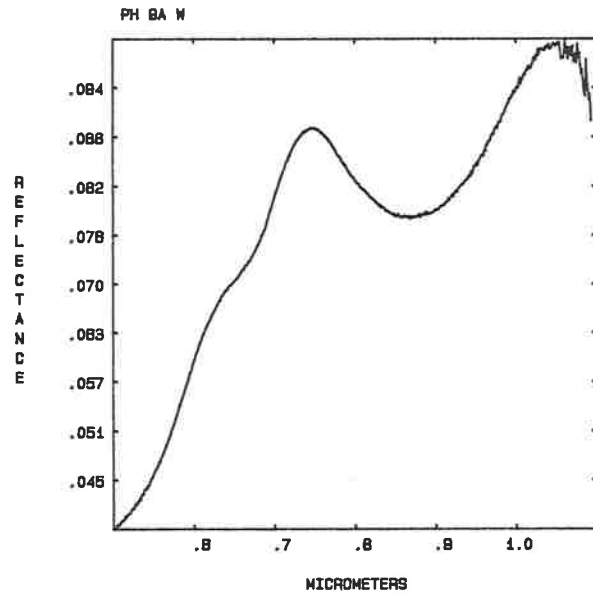
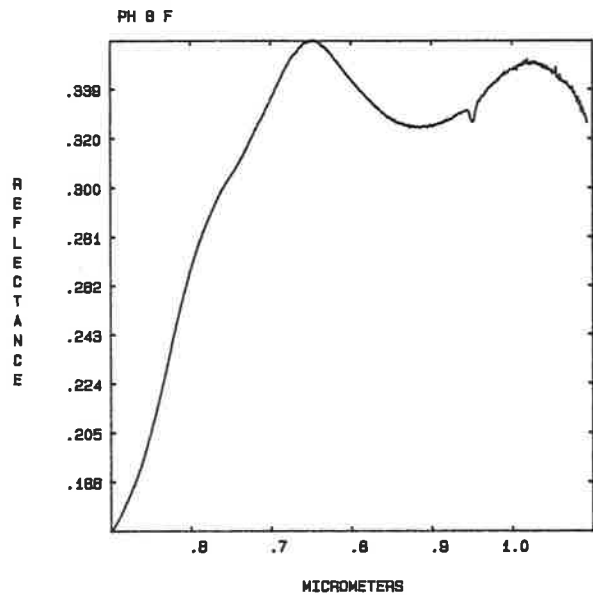


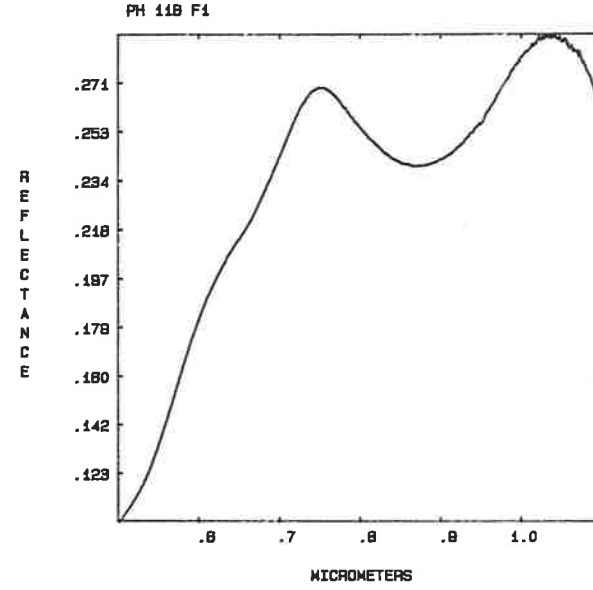
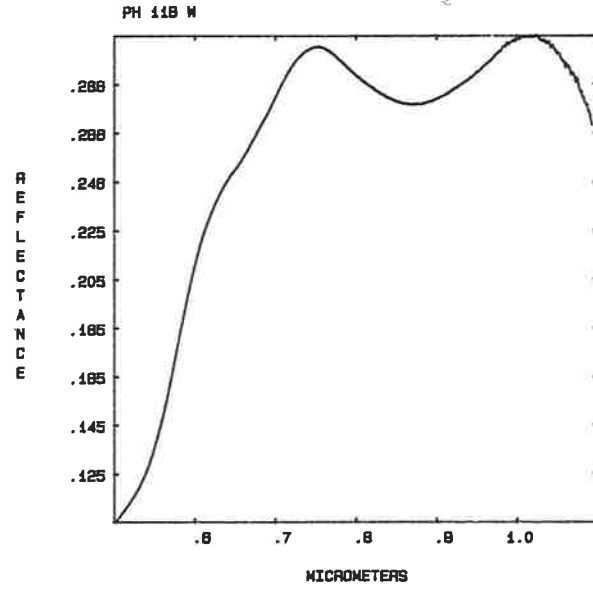
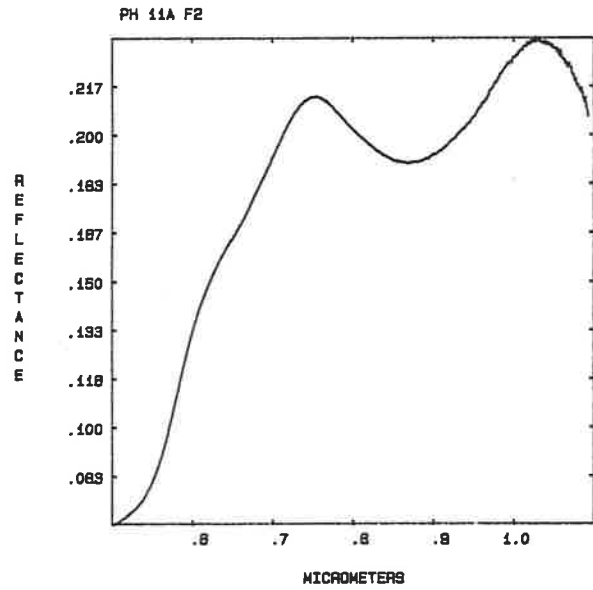
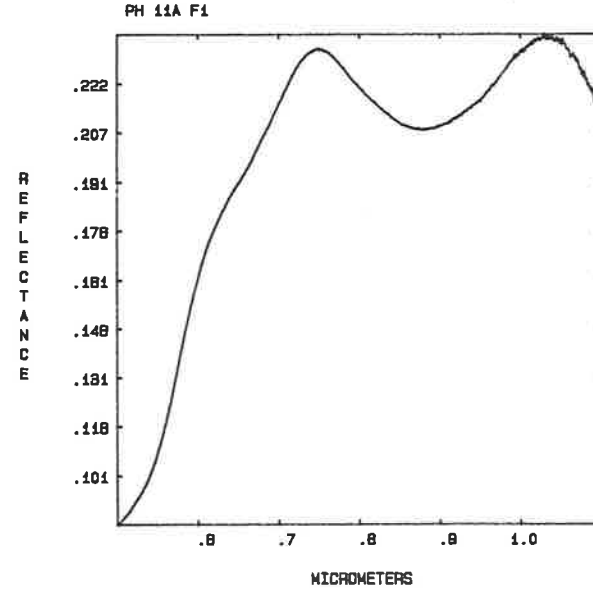
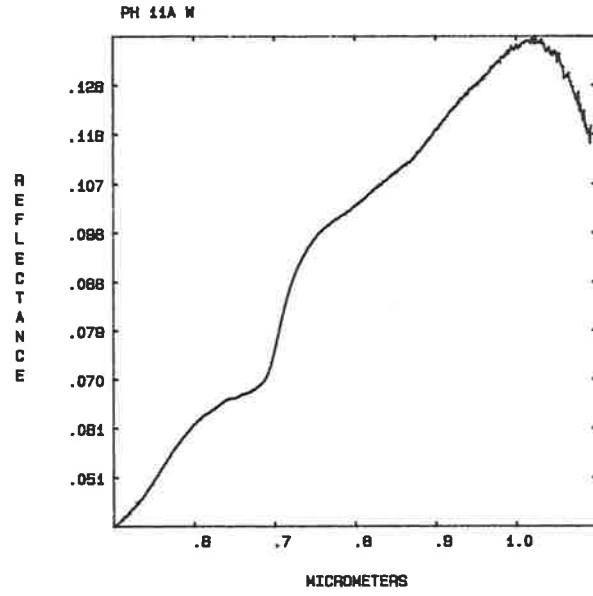
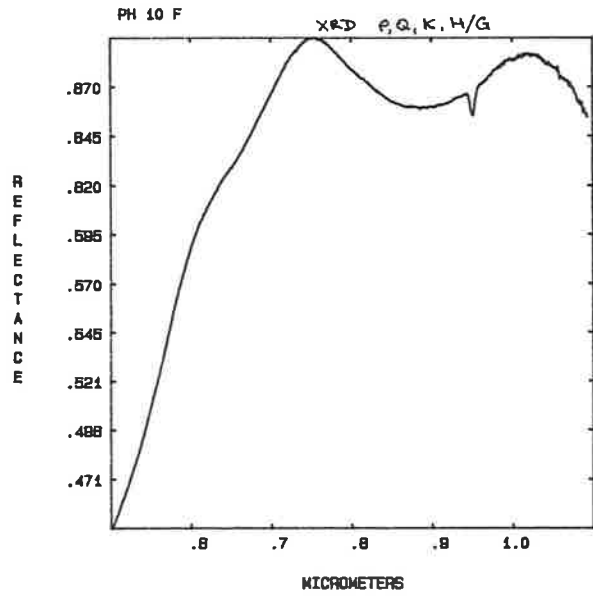




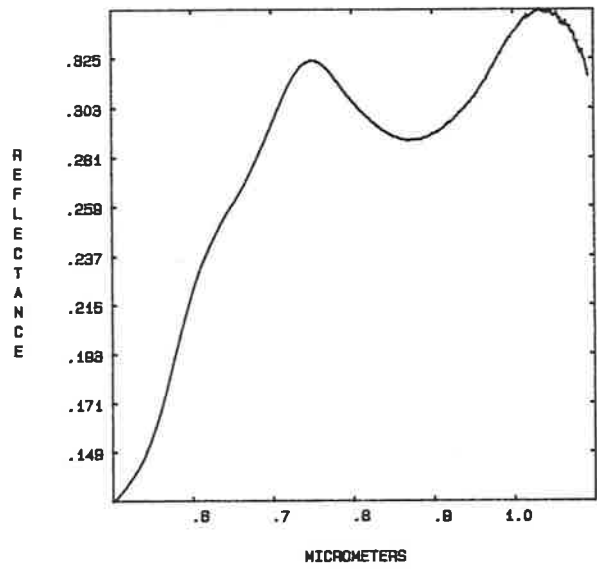


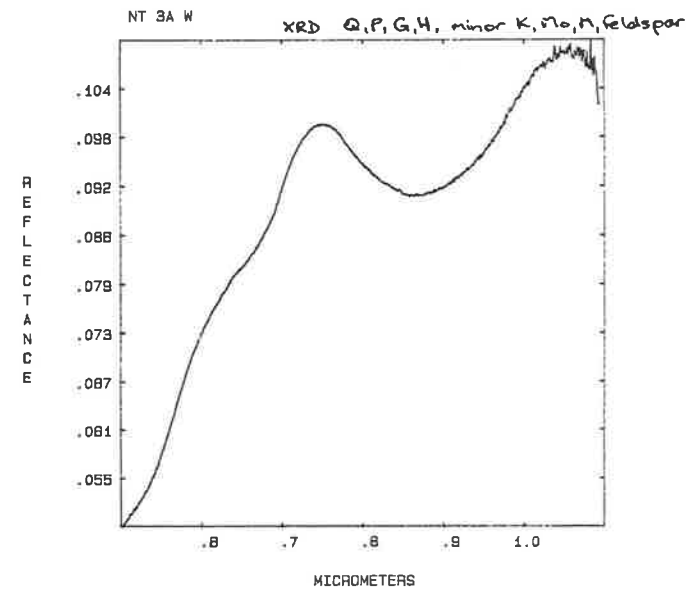
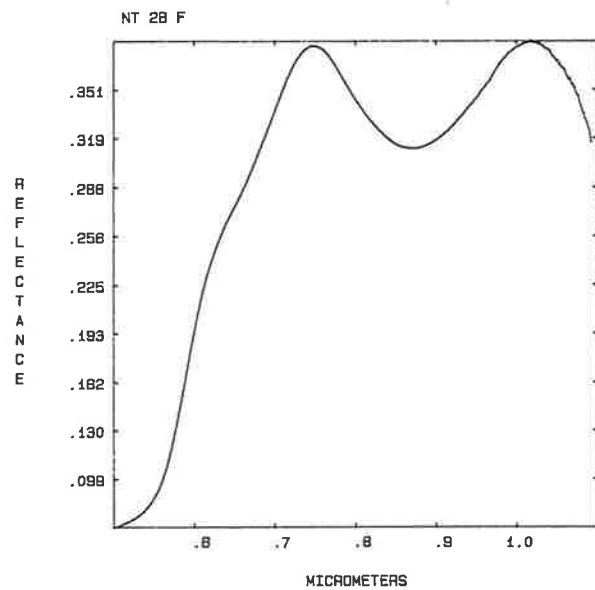
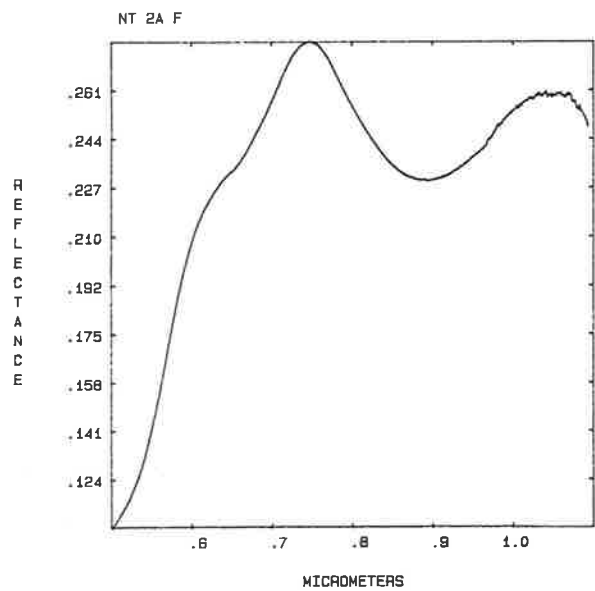
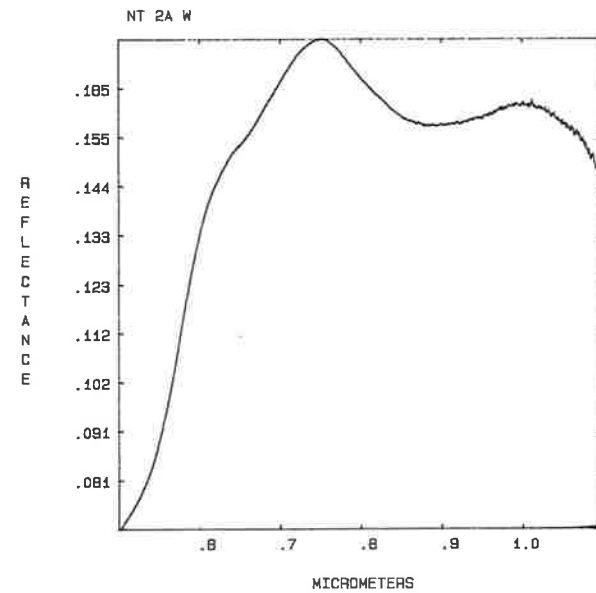
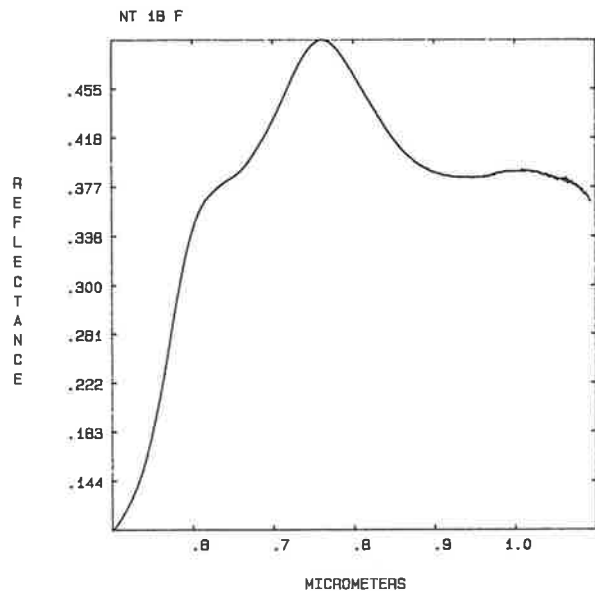
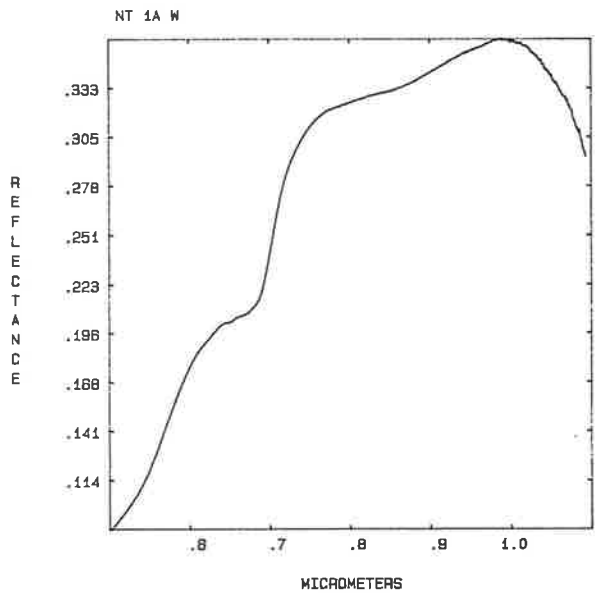


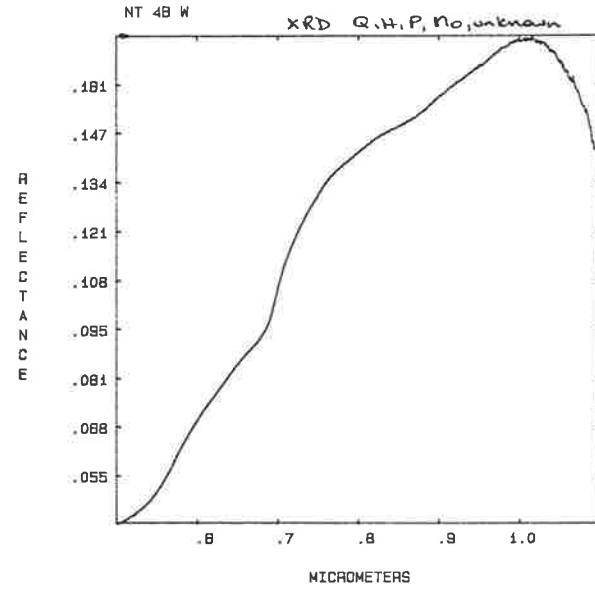
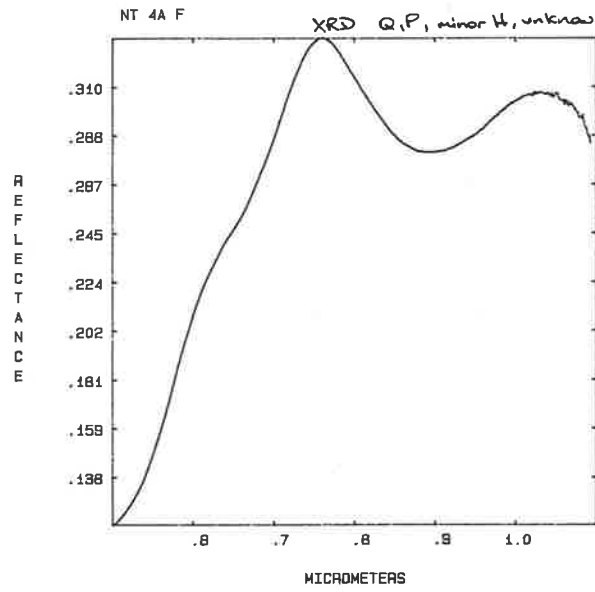
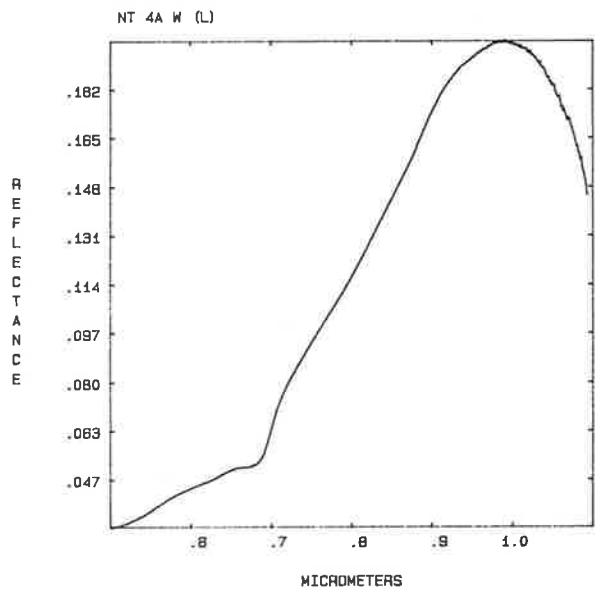
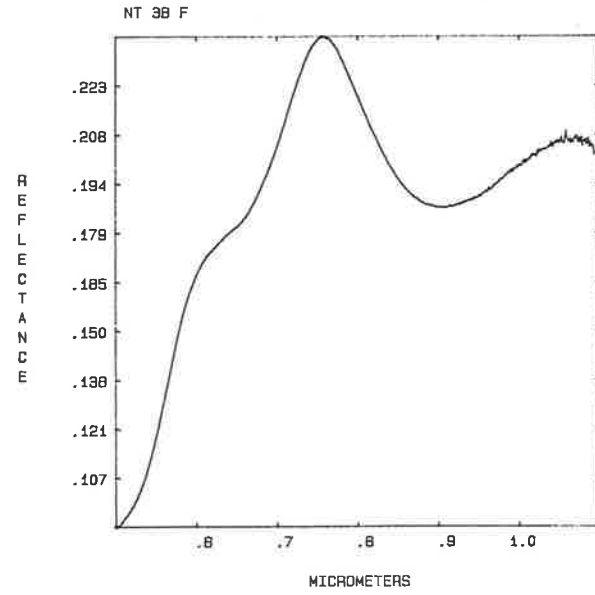
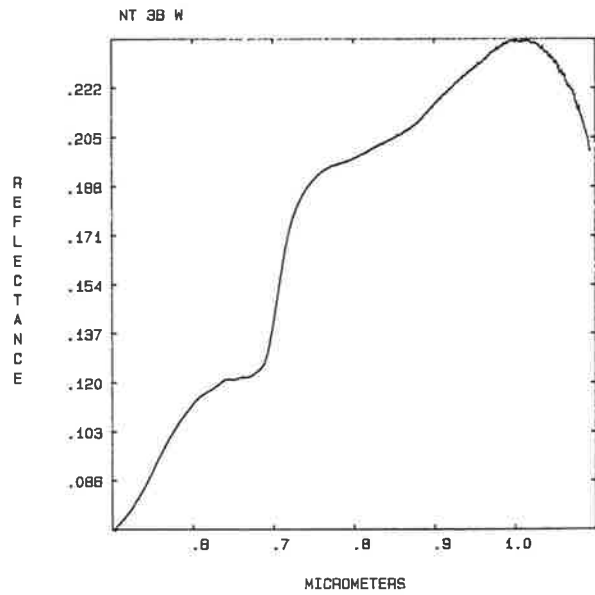
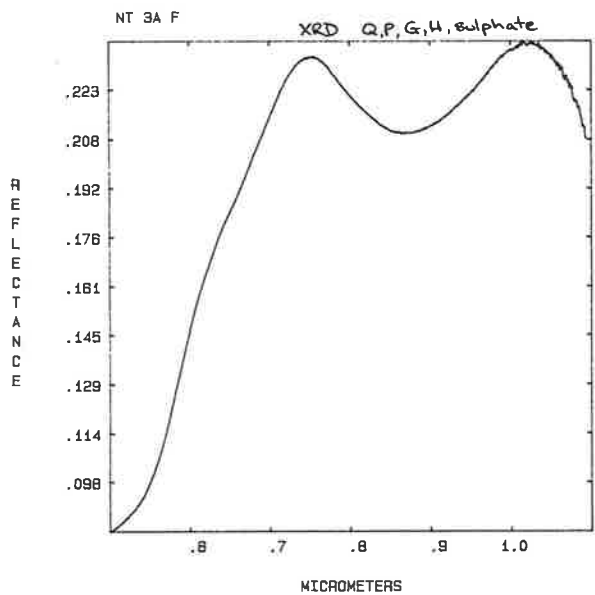


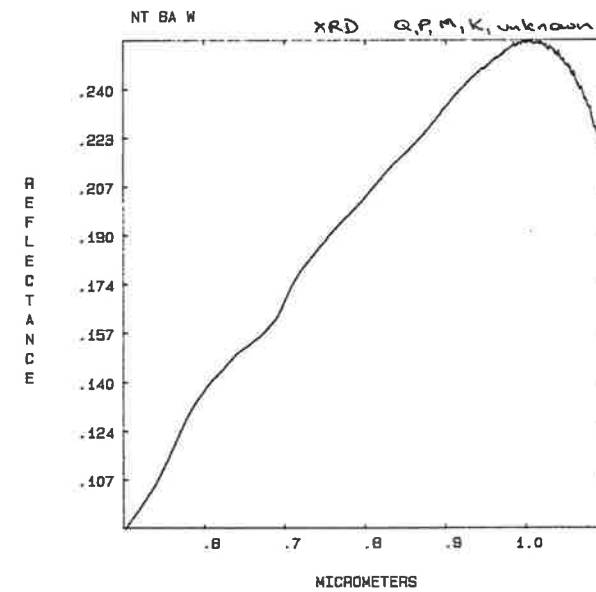
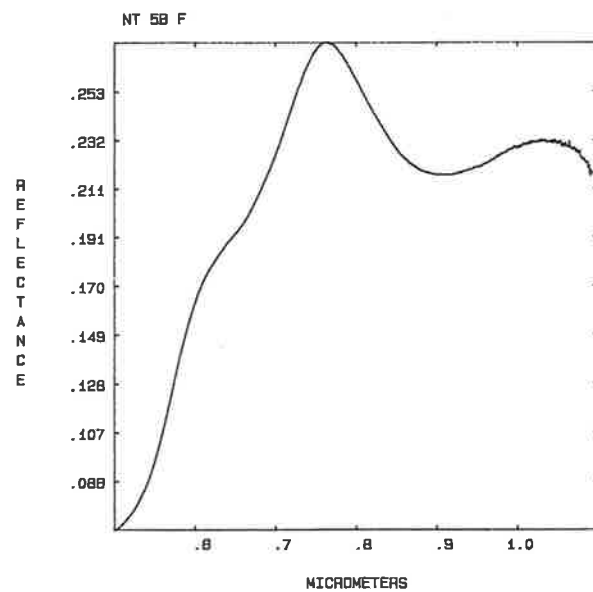
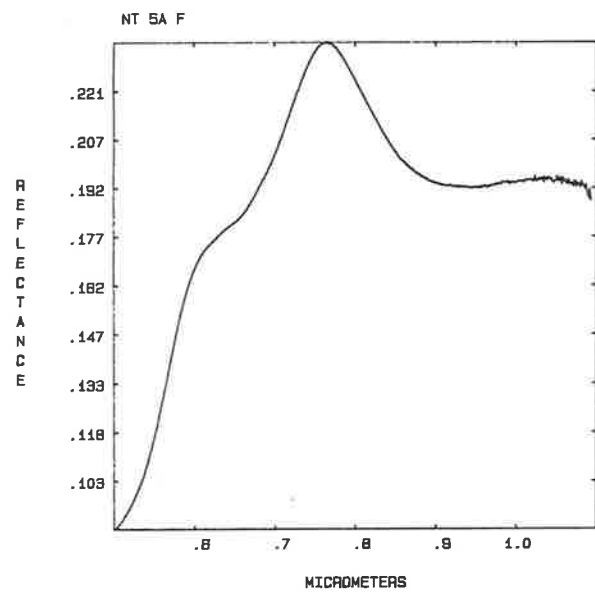
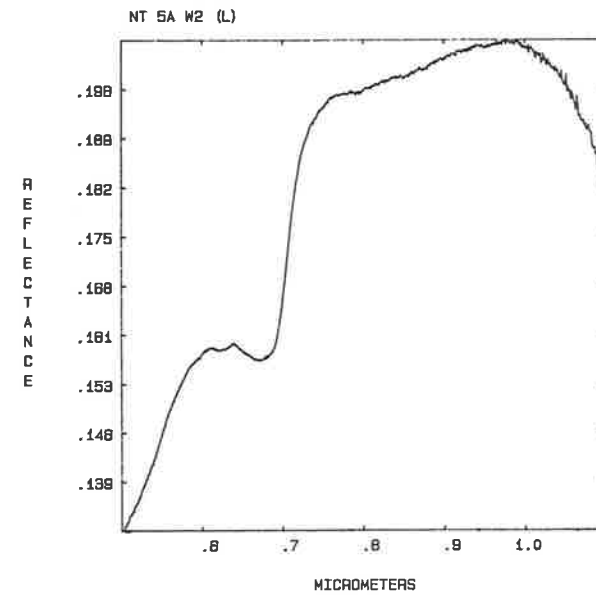
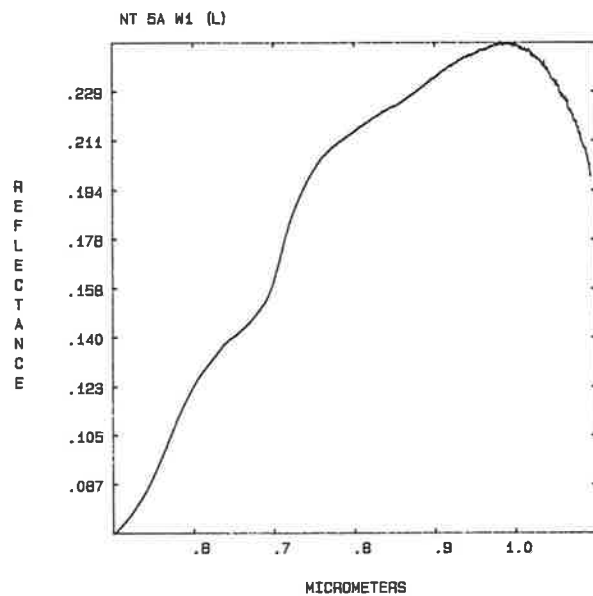
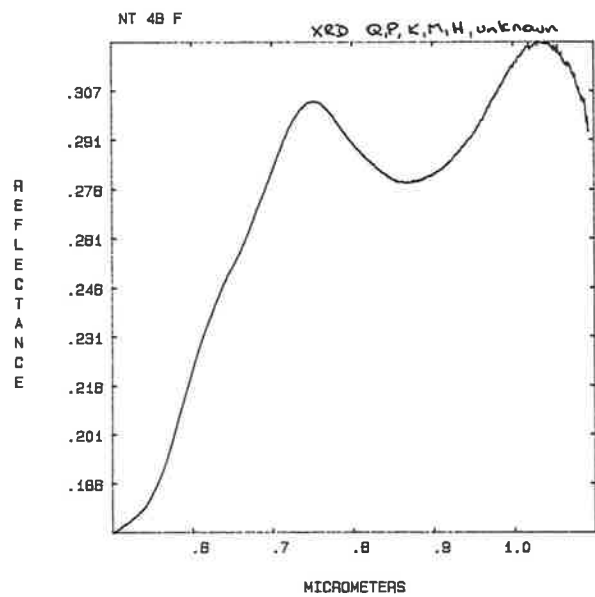


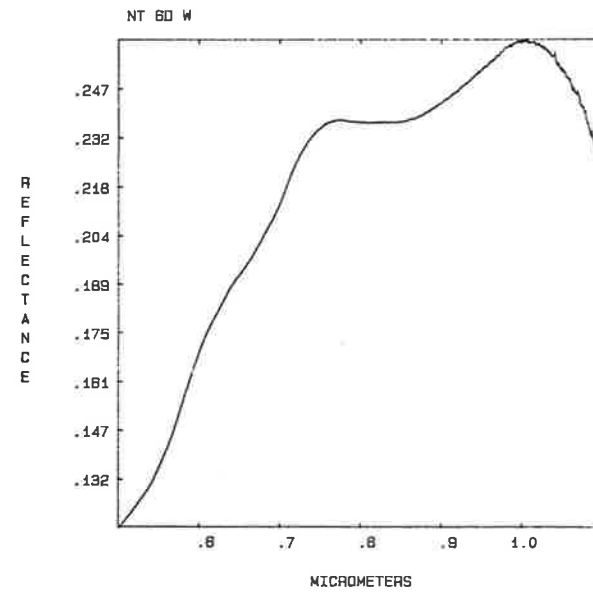
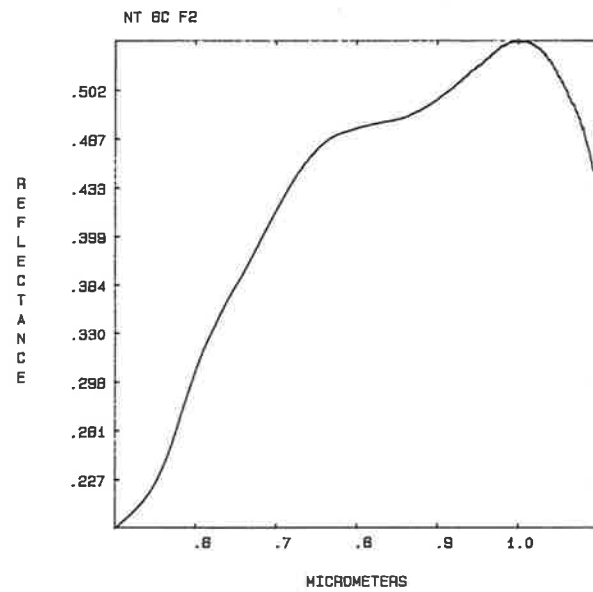
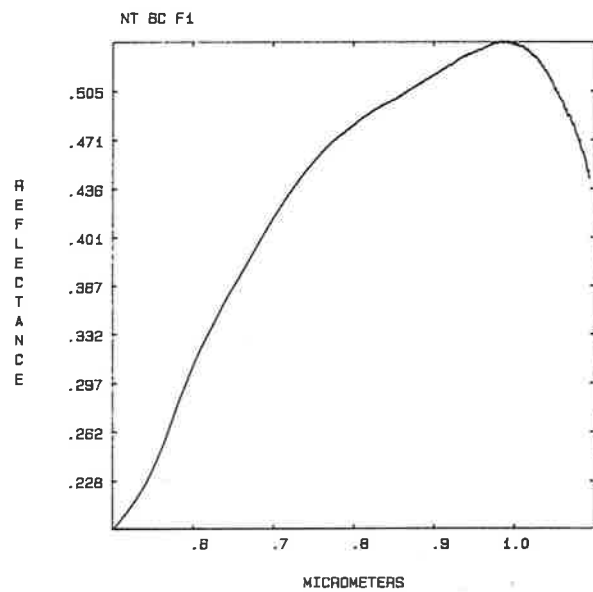
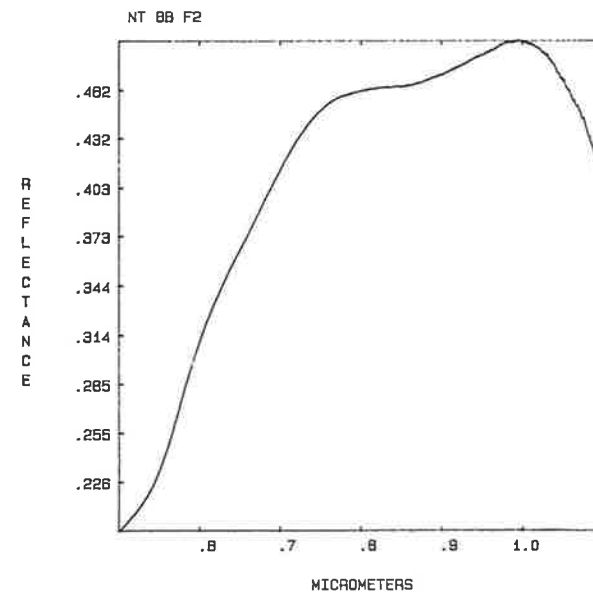
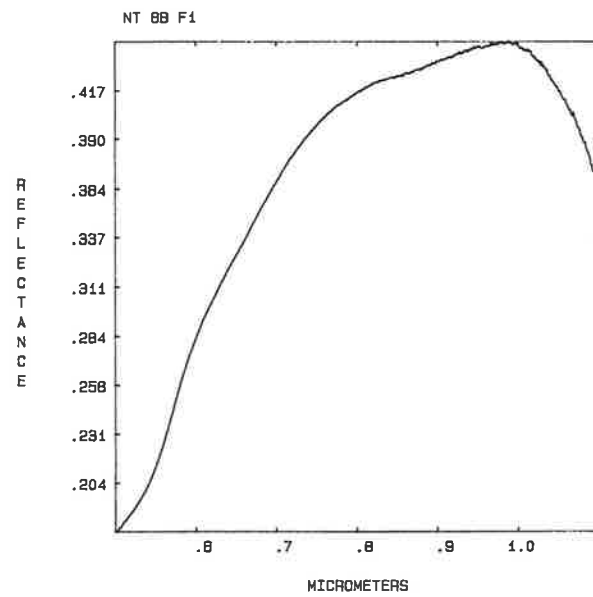
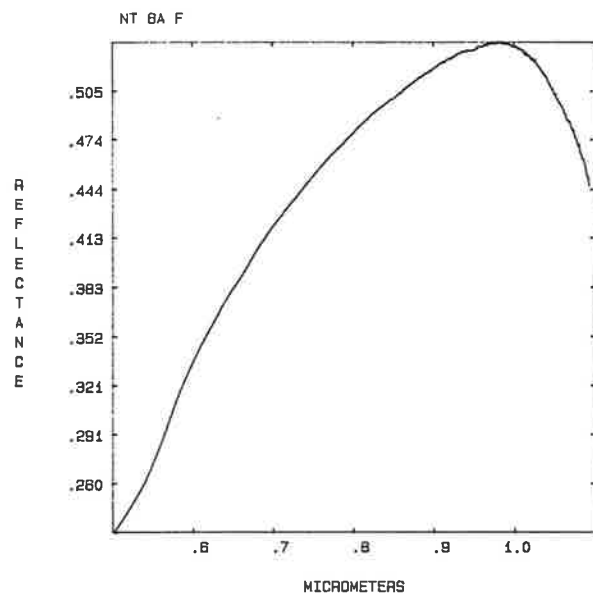
PH 11B F2

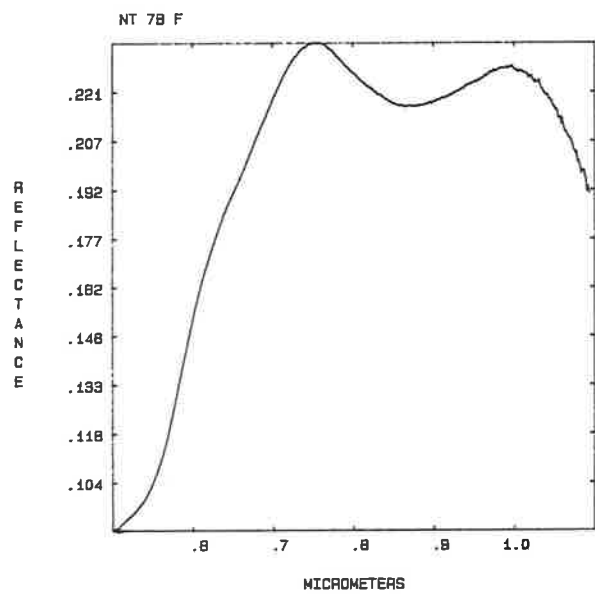
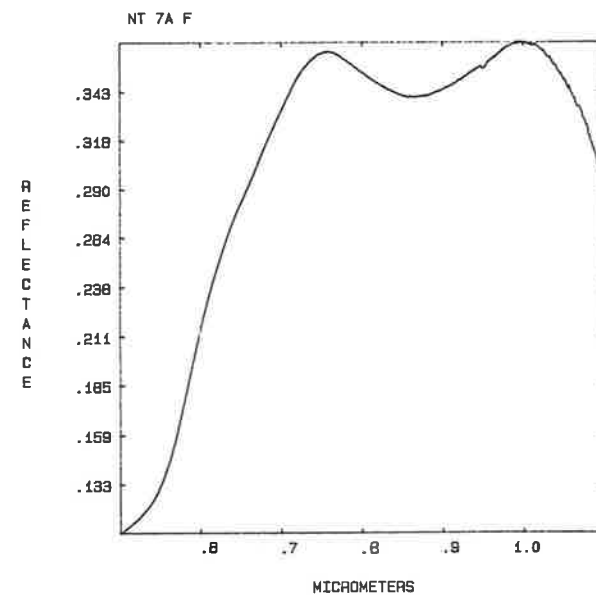
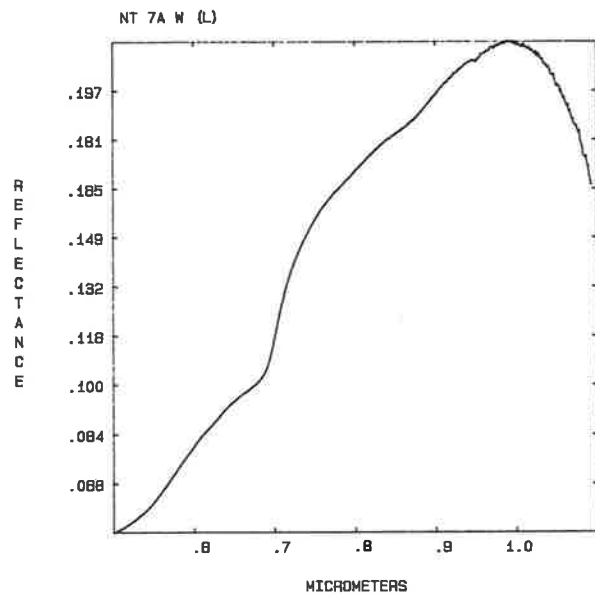
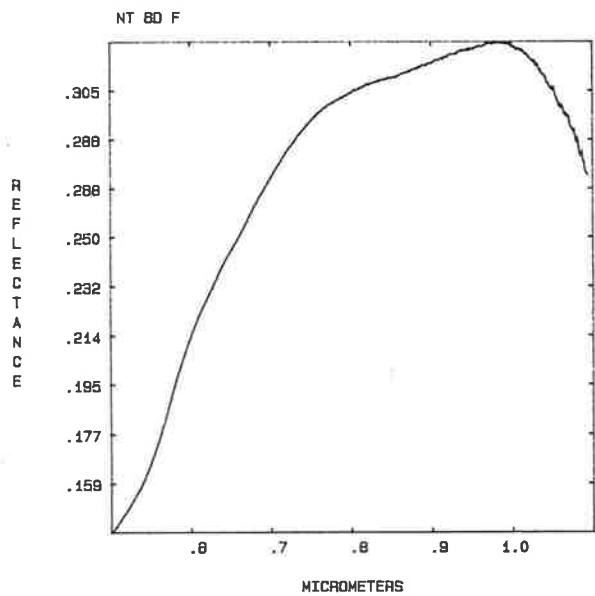


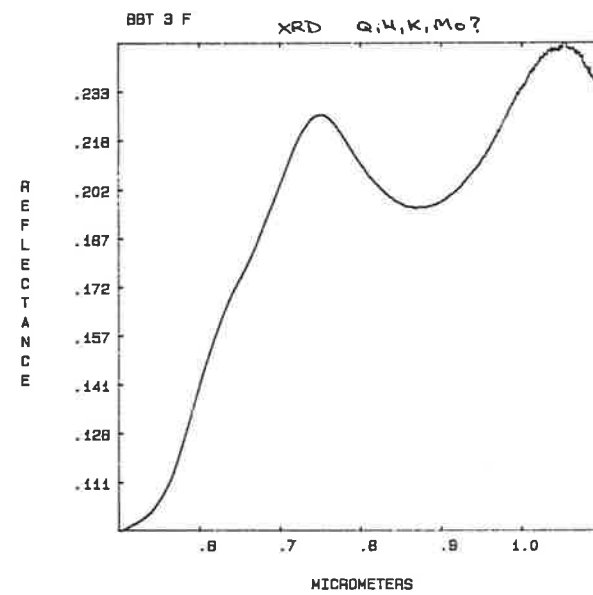
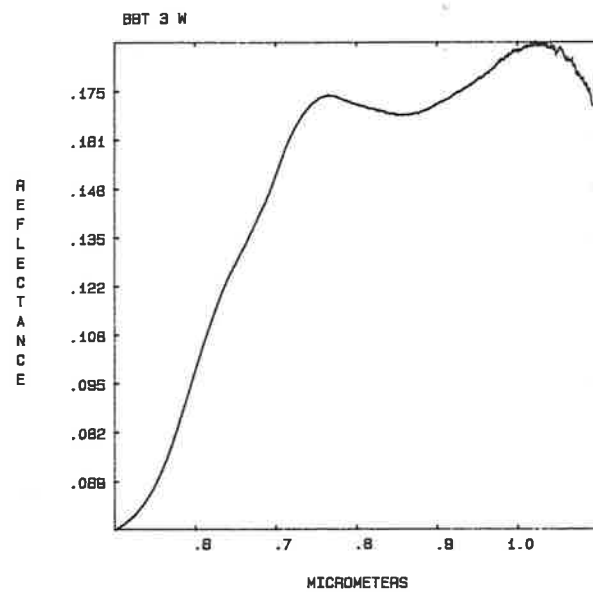
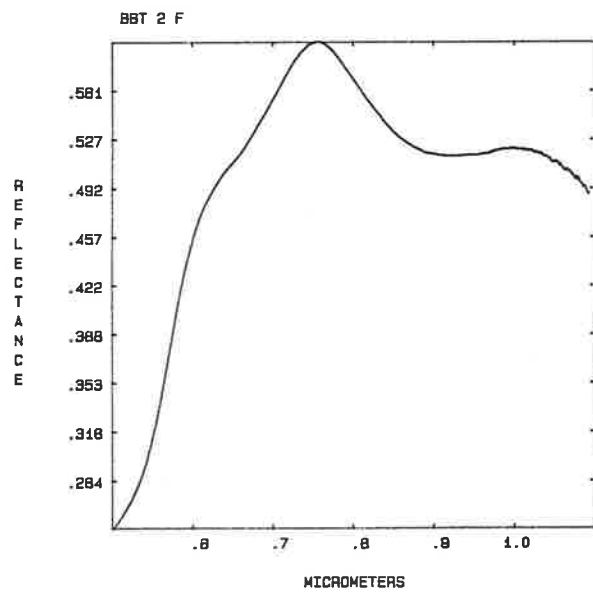
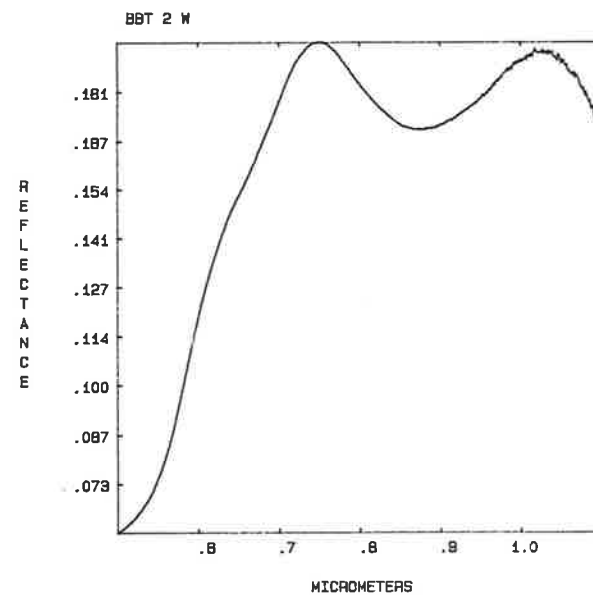
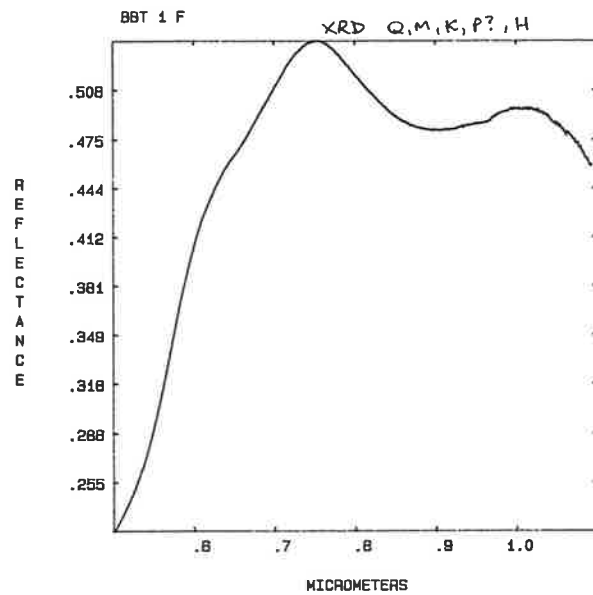
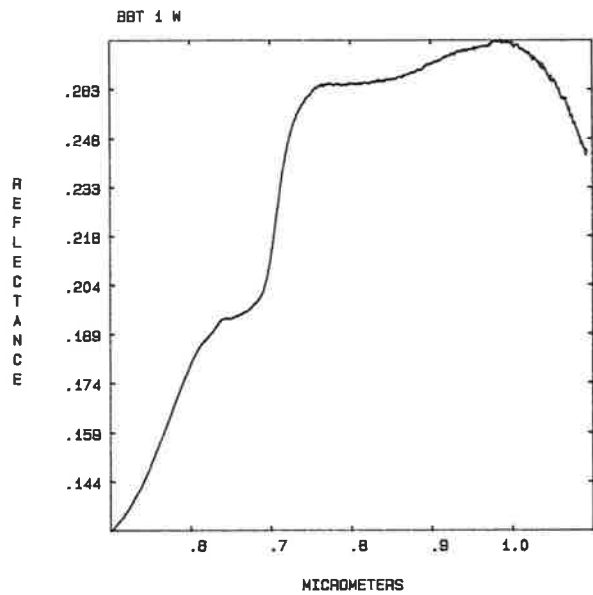


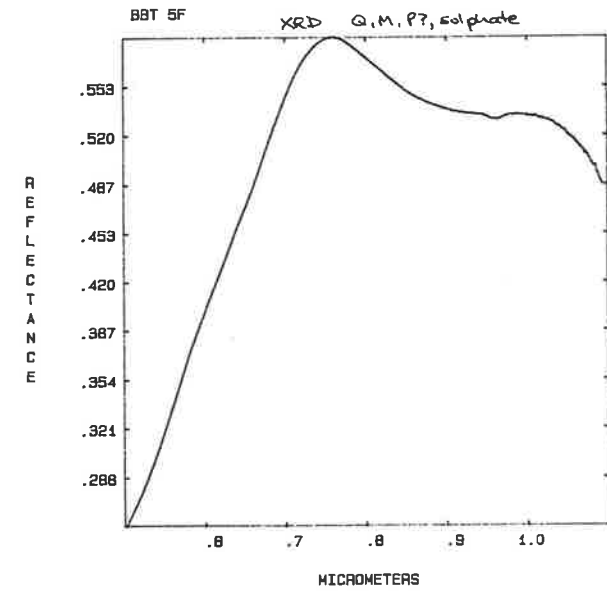
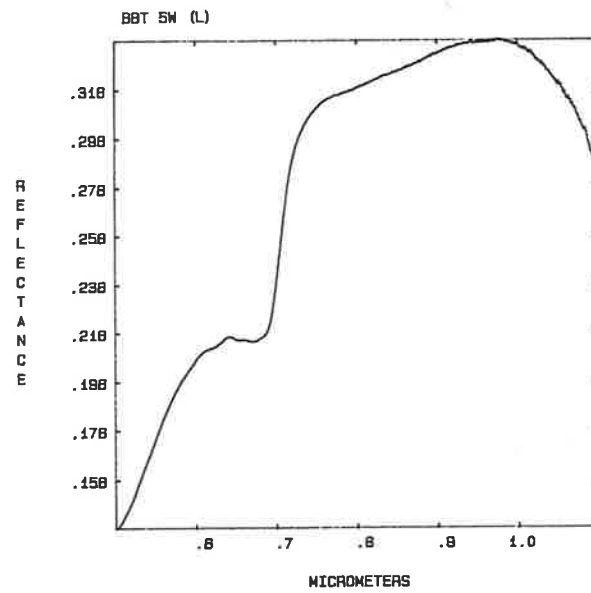
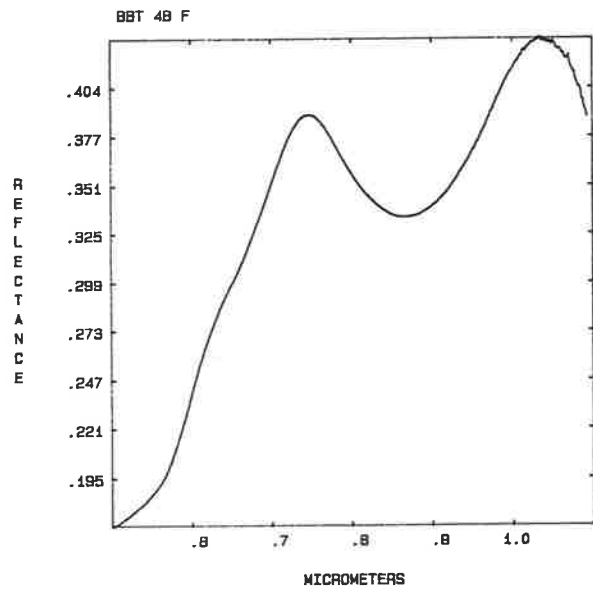
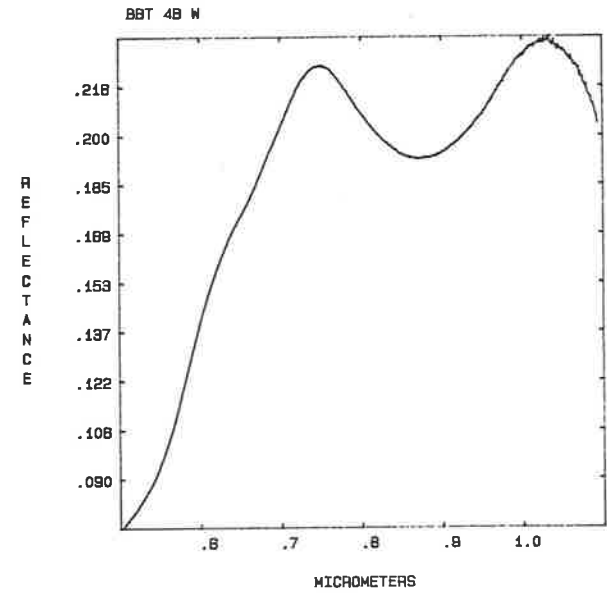
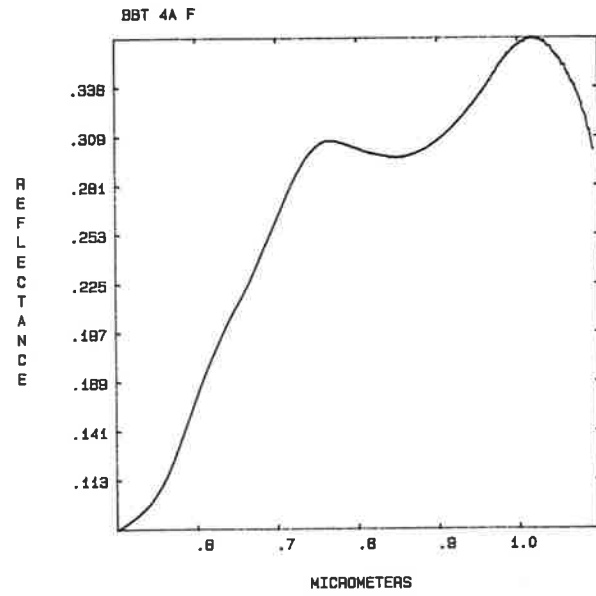
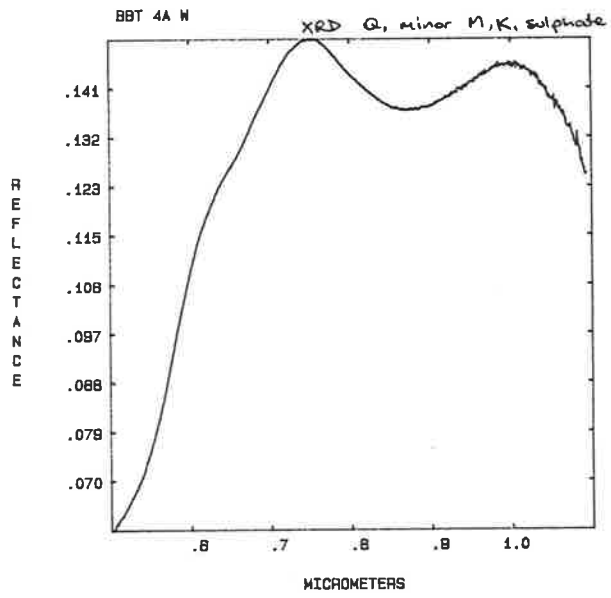


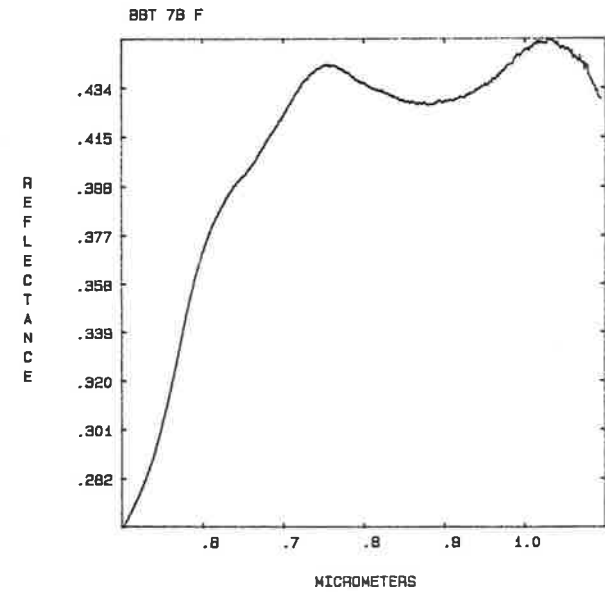
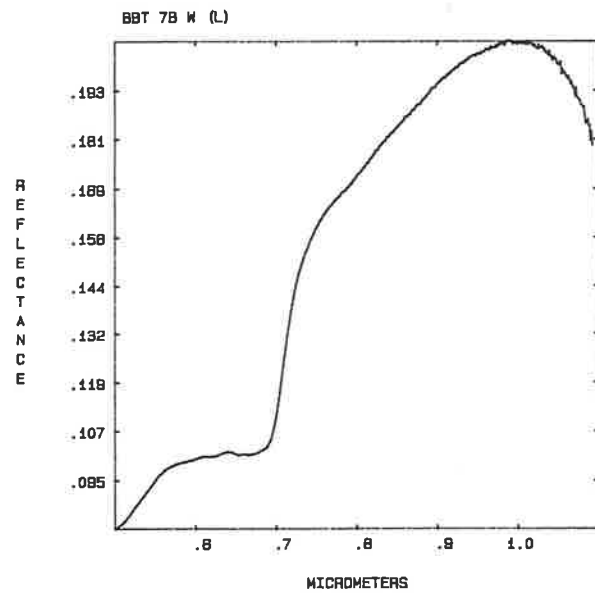
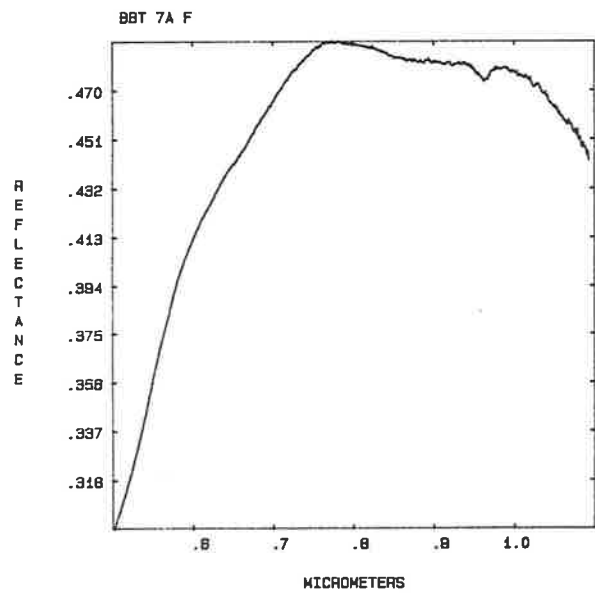
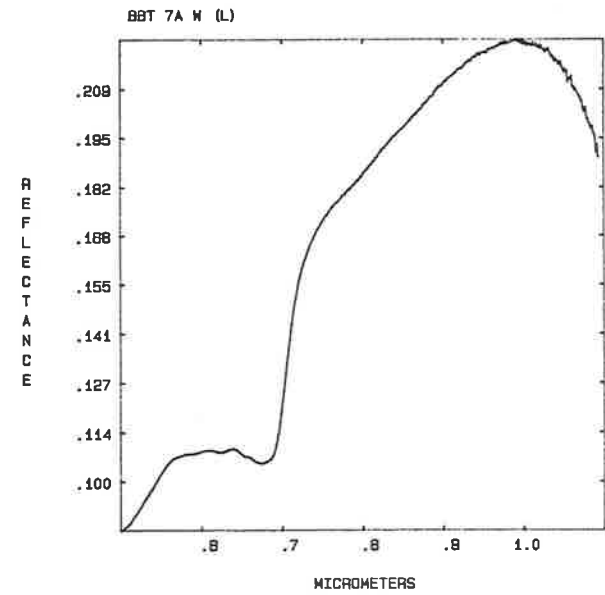
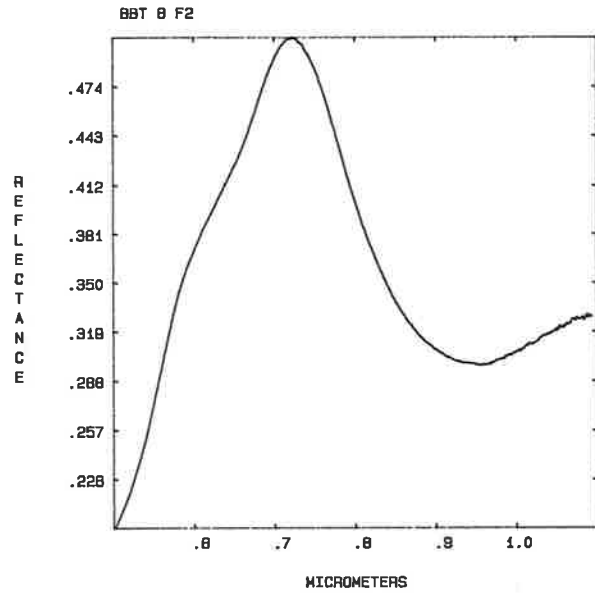
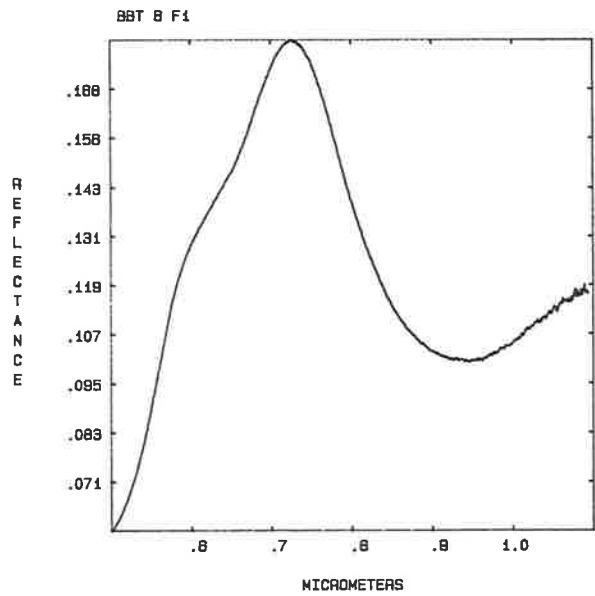


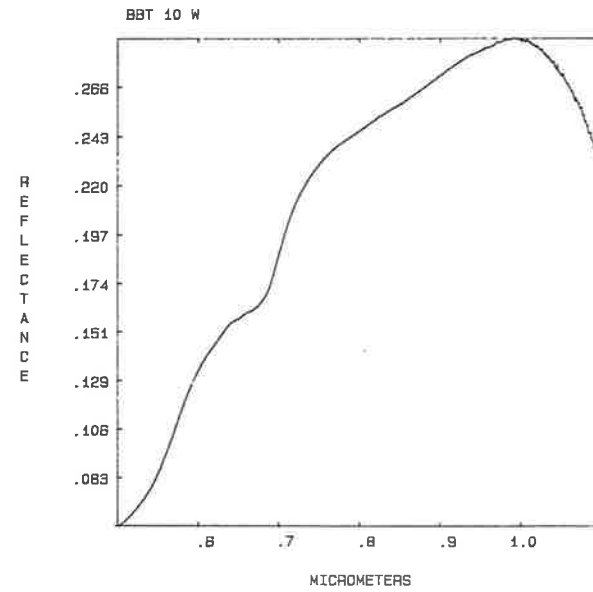
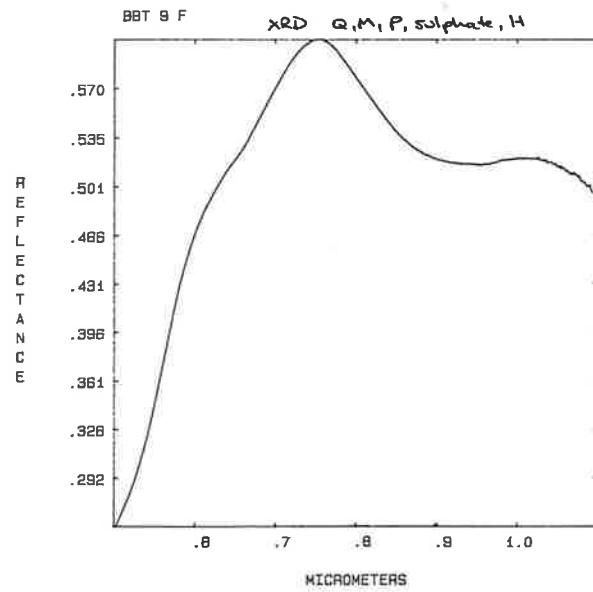
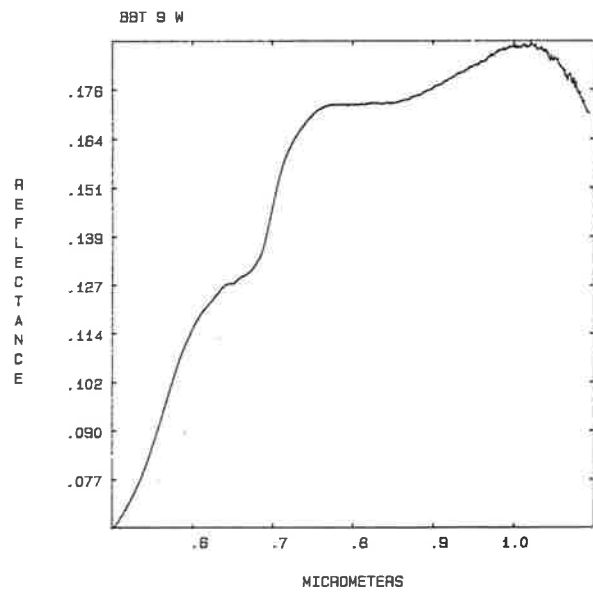
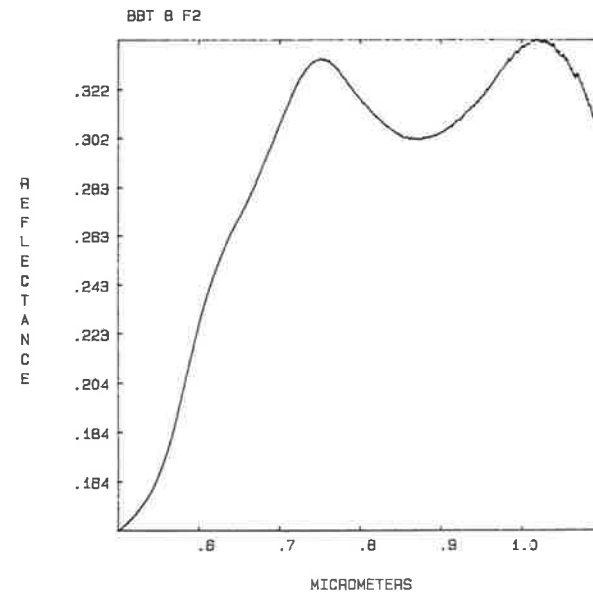
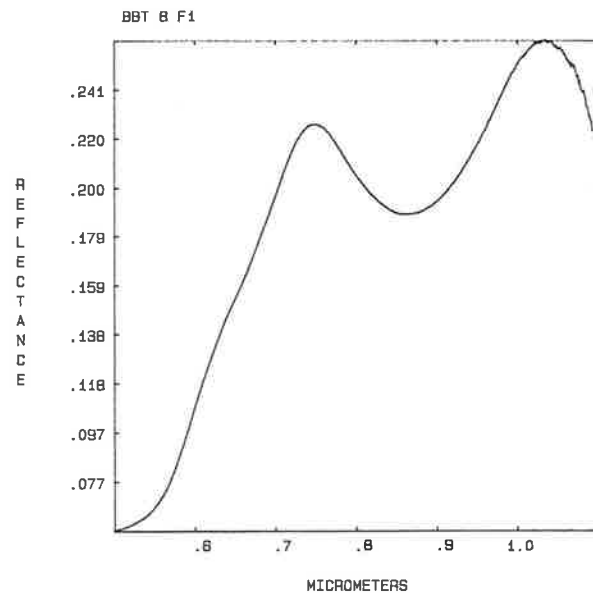
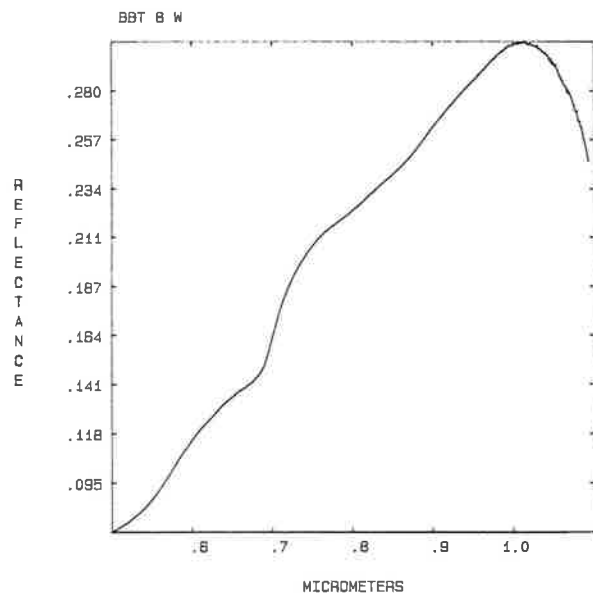


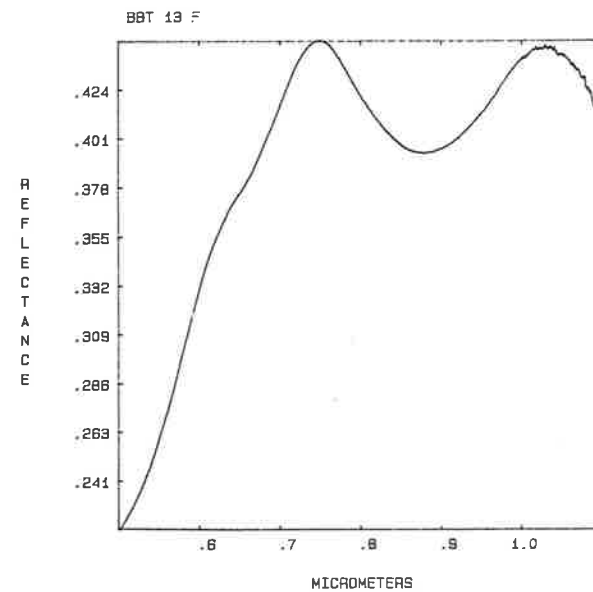
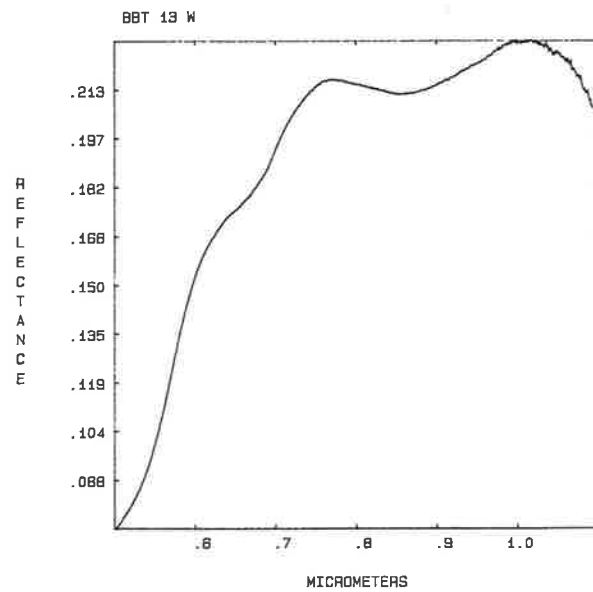
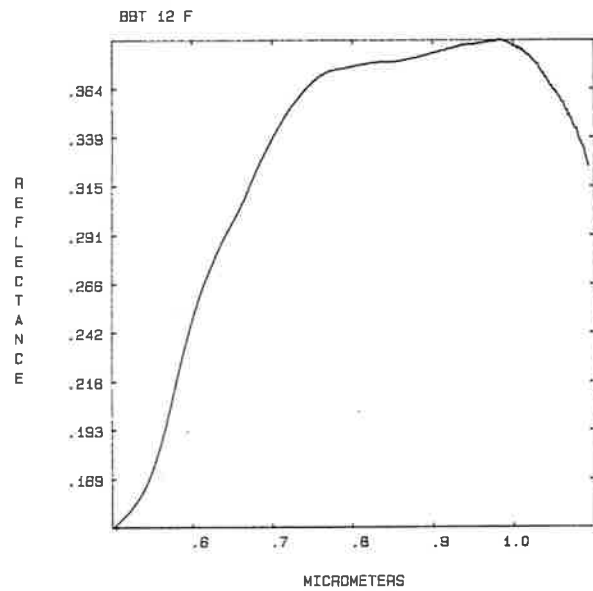
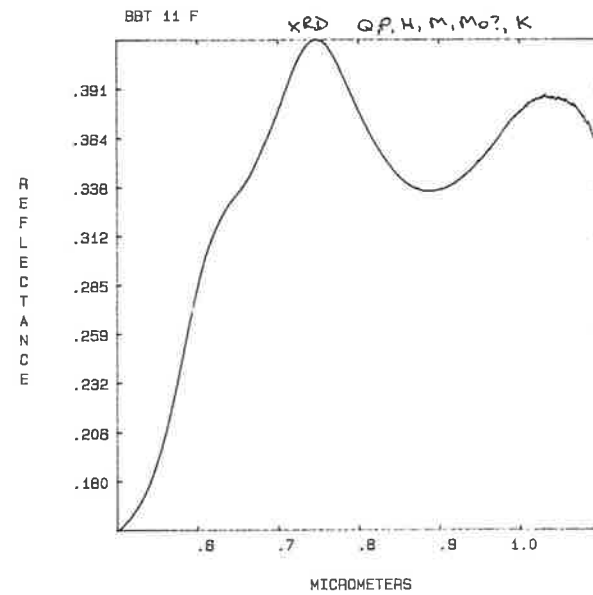
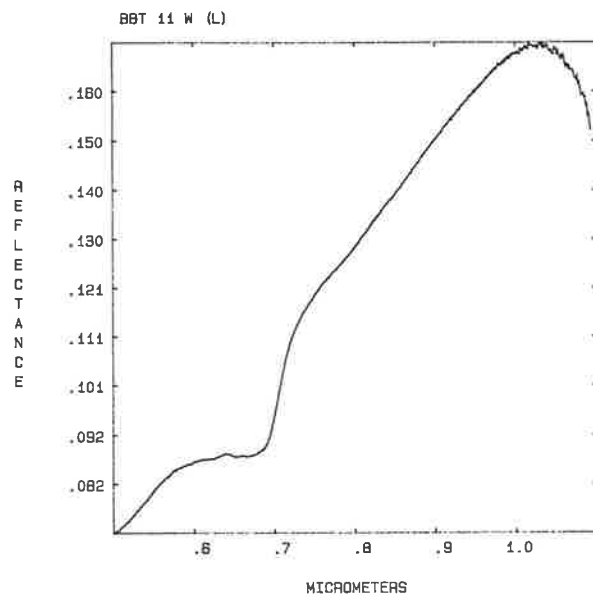
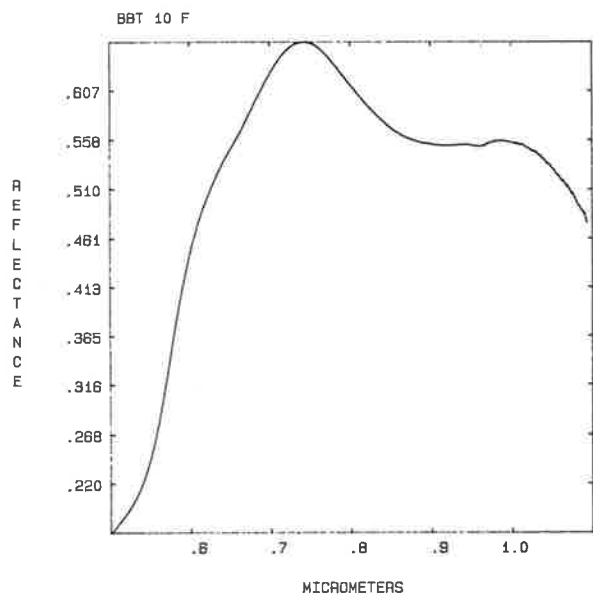












APPENDIX XVI SWIR laboratory reflectance spectra of surface samples
from Peak Hill.

The SWIR spectra of Peak Hill surface samples appear in this appendix in the same order as listed in Table 8.3, which should also be consulted for a summary of the interpretations. Spectra are also marked individually with their interpretation. Capital letters indicate the dominant mineral responsible for the absorption features in each plot. Any additional significant features are marked with a lower-case letter assigning their origin. Minerals detected by XRD analysis, where available appear at the top of each spectral plot, listed approximately in descending order of abundance. The key to the abbreviations is the same as that used in Table 8.3.

